Late Quaternary relative sea level change in the South Shetland Islands, Antarctica

WATCHAM, EMMA,PEARL

Late Quaternary relative sea level change in the South Shetland Islands, Antarctica

Emma Pearl Watcham

Thesis submitted for the degree of Doctor of Philosophy

Department of Geography
Durham University

June 2010

Late Quaternary relative sea level change in the South Shetland Islands, Antarctica

Emma Watcham

Models have been inconsistent in their prediction of ice sheet volumes and extent over the Antarctic Peninsula and sub-Antarctic islands during the Last Glacial Maximum (LGM), and their contribution to sea level rise during subsequent deglaciation remains uncertain. The use of precise relative sea level (RSL) data offers great potential for inferring regional ice sheet histories, as well as helping to validate numerical models predicting future ice sheet evolution and RSL change. This thesis aims to elucidate the RSL history of the South Shetland Islands (SSIs), a sub-Antarctic archipelago peripheral to the northern Antarctic Peninsula ice sheet, by integrating evidence from isolation basins with geomorphological evidence from raised beaches. This will extend the only previously reported RSL curve from the area (Bentley *et al*., 2005a), which reveals a complex but poorly chronologically constrained RSL history. In addition, this work also aims to improve the understanding of the long-term tectonic influence on RSL change.

Sediment cores were taken from five lakes on Fildes Peninsula, King George Island (eastern SSIs) at a range of altitudes above present sea level. Diatom, stable isotope ($\delta^{13}C$) and physical analyses of sediments revealed clear marine-lacustrine transitions in lakes below 16 m above mean sea level (amsl), with no marine signal above this altitude. Together with radiocarbon dates from raised beaches, a RSL curve was produced for the last 9500 ^{14}C yr BP. This curve shows a mid-Holocene RSL highstand at 15.5 m amsl between ca. 6150 and 6700 ^{14}C yr BP, preceded by a period of extremely rapid RSL rise and followed by more gradual RSL fall as a consequence of isostatic uplift in response to regional deglaciation.

In addition, regional GPS surveys of raised beaches were conducted to assess the spatial pattern of glacio-isostatic rebound following deglaciation. The centre of uplift was found to closely coincide with the centre of the LGM ice sheet reconstructed by John and Sugden (1971). Beaches were modelled using polynomial trend surface analysis to constrain the spatial variability of isostatic uplift across the SSIs, which has enabled the regional extrapolation of the RSL curve across the archipelago. Finally, two independent approaches were taken to constrain the long-term tectonic uplift rate of the SSIs as 0.22-0.48 m/ka. Tectonic uplift contributes between 1.4 and 2.9 m to the reconstructed RSL highstand.

Table of contents

CHAPTER 8: Conclusions

List of figures

CHAPTER 4

CHAPTER 5

CHAPTER 6

CHAPTER 7

CHAPTER 8

List of tables

List of appendices

Declaration

I confirm that no part of the material presented in this thesis has previously been submitted by me or any other person for a degree in this or any other institution. In all cases, where relevant, material from the work of others has been acknowledged.

Statement of copyright

Signed:

Dated:

Acknowledgements

I would firstly like to thank my supervisors, both at Durham and the British Antarctic Survey: Professor Mike Bentley, Dr Dominic Hodgson, Dr Rob Larter, Dr Jerry Lloyd and Dr Steve Roberts. They have all helped in different ways, but have all provided invaluable support and advice. A month into their PhD, most people are just acquainting themselves with the literature and settling into the life of a researcher, but not me; never one to take the 'normal' route, I was standing in the Antarctic! To say I was thrown in at the deep-end would be an understatement, but it is to Mike, Dom and Steve that I owe enormous thanks for making what could have been a very daunting prospect go as smoothly as possible and for providing much-needed guidance in the field. Particular thanks to Steve for putting up with me for the entire field season (everyone else had the sense to leave!).

On return from the field, all have been fantastic sources of knowledge and advice, from helping with lab work through to providing insightful comments as the chapters started to come together. Finally, my greatest thanks go to Mike. I'm not sure how you put up with me at times, particularly when everything was colour-coded and filed in alphabetical order! But it has been a privilege to work with you, and without your guidance and inspiration I would not have been able to complete this work.

This work is part of a wider research programme at the British Antarctic Survey, and I am extremely grateful to them for their generous financial support, which funded this project. I also acknowledge the role Rob has played in providing the link to this external research group, which has been a forum for interesting discussions.

Aside from my supervisory team, there is one other person to whom I owe enormous thanks – Peter Fretwell (British Antarctic Survey). Peter has been amazing throughout, from initial help in the field, to providing much of the GPS data used in Chapter 6. He has provided not only the data, but also support and has been brilliant at answering the bombardment of emails and questions I've hassled him with.

This research simply could not have been done without the fantastic field and logistical support I received. I gratefully acknowledge those who made my Antarctic field season possible, in particular the British Antarctic Survey's logistics division, and Captain Nick Lambert, crew and flight crew of HMS Endurance for their excellent and generous assistance. Particular thanks to Bruce Maltmann and Liz Homer for their invaluable help and support in the field (and no Bruce, I still can't tie knots). Also to the base commanders and all those at the Chinese Great Wall and Russian Bellingshausen Stations for their assistance with accommodation, use of base facilities, fieldwork support, and of course for providing entertainment and real food at Christmas! I never realised singing karaoke would be a pre-requisite of doing this PhD!

This research would also not have been possible without all those who assisted with laboratory work: Melanie Leng and staff at NIGL, Keyworth, for running the carbon isotope analyses; the Durham lab technicians, in particular Frank, Neil and Eddie; Andrea Balbo (BAS); the NERC radiocarbon facility and Beta Analytic for radiocarbon dates; the NERC Geophysical pool for the Leica GPS equipment; and the University of Edinburgh and SUERC cosmogenic laboratories. In particular, Steve Binnie (University of Edinburgh/Berkeley) has been brilliant in helping with the cosmogenic dating, and enormously patient with me and my constant stream of emails and questions. I am also grateful to the Quaternary Research Association for their financial contribution towards the cost of cosmogenic analyses. This work has also benefitted from useful discussions with members of QEC at Durham, particularly Ian Shennan, Pippa Whitehouse and Dave Evans.

On a personal level, thank you to my friends, fellow postgrads and office mates who have made my PhD years so enjoyable. I'm not going to mention you all by name, but you know who you are. Having said that, there are a few people who deserve special mention. To Tasha Barlow and Mark Smith, thanks for your support, wit and for keeping me organized; I have learnt a lot from both of you. To Caroline Jones for, well, generally being AMAZING! You are a brilliant friend, and thank you for being there through it all (sorry for all my geography-related rants!). And to Ed, for your love and support. There are also eight old men who've tried their best to stop me doing my PhD, but now I've finished my thesis, no that doesn't mean I have more time to cox for you!

Before I get to the end, there is just one more thing aside from acknowledging the people who have helped and contributed to this thesis. And that is I would like readers to be aware that the greatest achievement of my PhD is not this thesis. But in fact it is the pizza I made entirely from scratch in a tent in the Antarctic, with nothing more than a small camping stove and extreme resourcefulness. It even had bacon on.

This brings me full circle back to my time in the Antarctic. On a more serious note, there are two people who couldn't have been prouder at the time I found out I had this PhD place and was going South. They've supported me through everything and I will never forget that. Mum and Dad, this thesis is dedicated to you, from your little penguin.

CHAPTER 1

Introduction

1.1 Introduction

The Antarctic Ice Sheet is the largest glacial system on Earth, performing a critical role in the forcing and regulation of global atmospheric and oceanic circulation. Currently some sectors, notably of the West Antarctic and Antarctic Peninsula ice sheets, are losing mass rapidly, with potentially enormous consequences for climate change and sea level rise (Vaughan and Doake, 1996; Oppenheimer, 1998; Rignot *et al.*, 2002; Vaughan and Spouge, 2002; Thomas *et al.*, 2004; Cook *et al.*, 2005; Rignot, 2006; Meehl *et al.*, 2007; Rignot, 2008). Evidence exists of substantial ice sheet fluctuations during the Quaternary (Mercer, 1978; Scherer *et al.*, 1998), particularly since the Last Glacial Maximum (LGM), and it is recognized that the ice sheet has both responded to and contributed to global sea level in the past. At the LGM global sea level was ~120 m below present (Fairbanks, 1989), with subsequent deglaciation of the Antarctic ice sheet contributing significantly to rapid post-glacial sea level rise and the forcing of oceanic circulation. Estimates of the exact sea level contribution vary between as much as 37 m (Nakada and Lambeck, 1988) and 0.5-2.5 m (Colhoun *et al.*, 1992), although ice volume estimates are gradually converging in the range of 10-20 m sea level equivalent (Bentley, 1999; Ingólfsson and Hjort, 1999; Huybrechts, 2002). The lack of glacial geological or relative sea level (RSL) data from Antarctica to constrain former ice sheet volume, mean that currently many ice volume estimates are derived from global models of glacial isostatic adjustment where the Antarctic contribution is largely

unconstrained, and is calculated by subtraction of other ice sheets' volumes from a global total. Whilst this uncertainty is beginning to be addressed (e.g. Ivins and James, 2005), further field data are required, as until we have an improved understanding of past ice volumes and deglaciations, quantitative models of future sea level change and ice sheet evolution are limited (e.g. Nakada *et al.*, 2000; Bassett *et al.*, 2007).

1.2 Rationale

The ultimate rationale behind this research is the requirement for improved predictions of future sea level change. Currently ten million people worldwide suffer from coastal flooding annually and this is predicted to increase to 200 million by the 2080s (Meteorological Office, 1997). Global exposure to extreme sea level rise is also significant; it is estimated that around 400 million people (8% of the global population) are threatened by a 5 m rise in sea level (Nicholls *et al.*, 2008). Whilst the most recent Intergovernmental Panel on Climate Change report highlights the advances made in sea level research and prediction, ice dynamical processes of the polar ice sheets are not well enough understood to be captured by models, and therefore still limit sea level projections. For example, the full effects of rapidly changing ice sheet flow, especially in Greenland and West Antarctica, are excluded "because a basis in published literature is lacking" (Solomon *et al.*, 2007, p.70). Yet either of these ice sheets has the potential to raise sea level by at least tens of centimeters by the end of the century, and by a total of metres over longer timescales.

Similarly, models have not been consistent in their prediction of ice sheet volume and extent over the Antarctic Peninsula during the LGM and its contribution to sea level rise during subsequent deglaciation (Evans *et al.*, 2005). The modern-day Antarctic Peninsula ice sheet (APIS) system is thought to contain only 242 mm eustatic sea level equivalent (Pritchard and Vaughan, 2007), as compared to ~5 and 52 m of the West and East Antarctic Ice Sheets respectively (Lythe *et al.*, 2001). However, due to its potential instability under a warming climate regime, the Antarctic Peninsula area is still of particular interest and because of substantial expansion across broad continental shelves may well have been amongst Antarctica's largest contributors to post-LGM sea level rise (Nakada *et al.*, 2000).

Currently models of postglacial RSL change show poor agreement with observations of sea level change, particularly in the Antarctic Peninsula region (Nakada *et al.*, 2000; Bassett *et al.*, 2007). We therefore need to address these gaps in our current understanding of the dynamics of the APIS during late Quaternary deglaciations and collect further field data in order to test and refine current ice sheet models. This is essential in such a potentially unstable environment, as models of future deglaciation and sea level rise can only be robust if they accurately hindcast past behaviour.

1.3 The wider research context

The understanding of the last deglaciation in West Antarctica is a primary aim of the British Antarctic Survey's GRADES (Glacial Retreat in Antarctica and Deglaciation of the Earth System) research programme, to which this thesis contributes. Focussing on the West Antarctic and Antarctic Peninsula ice sheets, the GRADES programme aims to (1) improve understanding of ice sheet dynamics; (2) establish a well-dated deglaciation history since the LGM; and (3) develop techniques of data assimilation and improve numerical simulations of ice sheet evolution and sea level responses.

In order to achieve the second of these aims GRADES is integrating marine and terrestrial records to determine (1) the extent and elevation of the LGM ice sheet, (2) its thinning and retreat history, (3) RSL change, and (4) former ice sheet collapse. The third of these aims is the subject of this study, with RSL changes at locations peripheral to the ice sheet recording the response of the Earth's crust to glacial (un)loading and global sea level change. In this way RSL data can be used as an *independent* record of maximum ice volume changes and postglacial thinning. In this study a combination of raised beaches and isolation basins peripheral to the northern APIS is used to develop a RSL curve. This complements records of postglacial RSL change elsewhere in Antarctica (notably around the Ross Sea and East Antarctica, e.g. Zwartz *et al.*, 1998; Hall and Denton, 1999; Baroni and Hall, 2004; Hall *et al.*, 2004; Verleyen *et al.*, 2005), and addresses the gap in RSL data from the Antarctic Peninsula region.

1.4 Research aims and objectives

Although part of the British Antarctic Survey's GRADES programme, this thesis has a self-contained set of aims and objectives. The overall aim is to **reconstruct postglacial relative sea level change at a site in the South Shetland Islands, peripheral to the Antarctic Peninsula Ice Sheet**. This will help firstly in constraining former maximum ice volumes and subsequent deglaciation (both in terms of timing and changes in ice cover), and secondly in validating numerical models predicting future ice sheet evolution and sea level change.

In order to achieve these aims, the primary objectives were:

- To retrieve sediment cores from isolation basins at a range of altitudes on King George Island, South Shetland Islands, to form a series of sea level index points
- To use additional geomorphological evidence, such as raised beaches, to determine former marine limits and RSL history, both on King George Island and the broader area of the South Shetland Islands
- To quantify the long-term tectonic contribution to RSL change, through the study of high erosion surfaces and marine platforms
- To combine evidence from isolation basins, raised beaches and high platforms to produce a RSL curve for King George Island
- To assess spatial variations in the response to glacial unloading across the South Shetland Islands, using raised beaches

Secondary objectives included:

- To assess the potential for using $\delta^{13}C$ and C/N ratios as alternative indicators of palaeosalinity to biological proxies within isolation basin sediments in Antarctica
- To use cosmogenic isotope exposure age dating to determine a deglacial chronology.

1.5 Thesis structure

Chapter 2 provides the background to this thesis. The first section reviews Antarctic Peninsula glacial history and RSL change since the LGM. The second section reviews approaches to RSL reconstruction, including using evidence from raised marine features and isolation basins. The main body of the thesis is then divided between the different types of evidence used to reconstruct RSL. Chapters 3 to 5 describe the evidence from isolation basins. Chapter 3 describes the field sites in the South Shetland Islands and outlines the field and laboratory methods employed. Chapter 4 presents the results from multi-proxy analyses of sediment cores taken from isolation basins to reconstruct RSL. These results are interpreted in Chapter 5 and synthesized to develop a preliminary RSL curve from the isolation basin data. Chapter 6 presents additional geomorphological evidence for RSL change, focusing predominantly on raised beaches. This is used to refine and further constrain the RSL curve produced in the previous chapter. Chapter 7 assesses the tectonic contribution to RSL change, through the study of planated surfaces and raised marine deposits. Finally, Chapter 8 presents the conclusions of this thesis and synthesizes all the evidence to produce a RSL curve for the South Shetland Islands.

CHAPTER 2

Antarctic Peninsula glacial history and relative sea level change since the LGM, and approaches to its reconstruction

2.1 Introduction

As briefly outlined in Chapter 1, the extent and volume of the Antarctic ice sheet at the Last Glacial Maximum (LGM), as well as the timing of subsequent deglaciation and meltwater release remain contested. Here I briefly review the current literature on these subjects, including both field and modelling studies. Techniques of RSL reconstruction employed to constrain former ice volumes will be discussed, including geomorphological approaches and the use of evidence from isolation basins. This review focuses primarily on the Antarctic Peninsula and maritime Antarctic islands, relevant to the fieldwork locations in this study (Fig. 2.1). It compares these with similar studies from Arctic Canada and Fennoscandia.

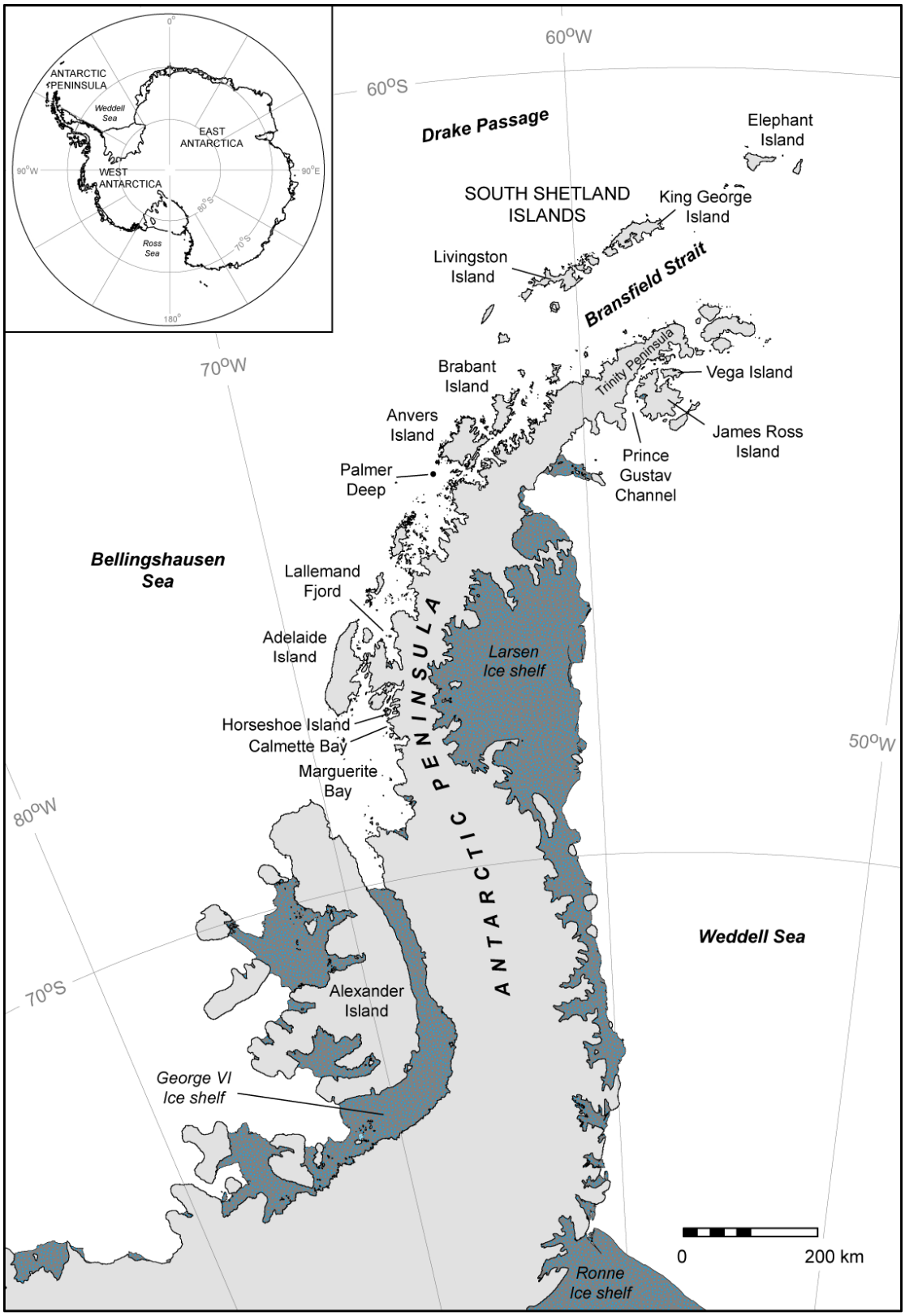

Fig. 2.1 Map of the Antarctic Peninsula

2.2 Quaternary glaciation

During the LGM, evidence from both offshore and onshore indicates the Antarctic Peninsula Ice Sheet (APIS) was more extensive than present (Fig. 2.2). Large glacial troughs extend across the continental shelf and geomorphological and sedimentary evidence from these troughs indicates they were occupied by grounded palaeo-ice streams (Pudsey *et al.*, 1994; Canals *et al.*, 2000; Anderson *et al.*, 2002; Heroy and Anderson, 2005). Terrestrial evidence of thicker ice cover than today exists in the form of erosional trimlines at high altitudes, striated bedrock on presently ice-free islands, erratics, and raised beach deposits (Ingólfsson *et al.*, 1998). The exact timing of the LGM remains contested, although many authors assume the maximum ice extent coincided with the period of lowest global sea levels during marine oxygen isotope stage (MIS) 2 between 20-18 ka BP (Ingólfsson, 2004).

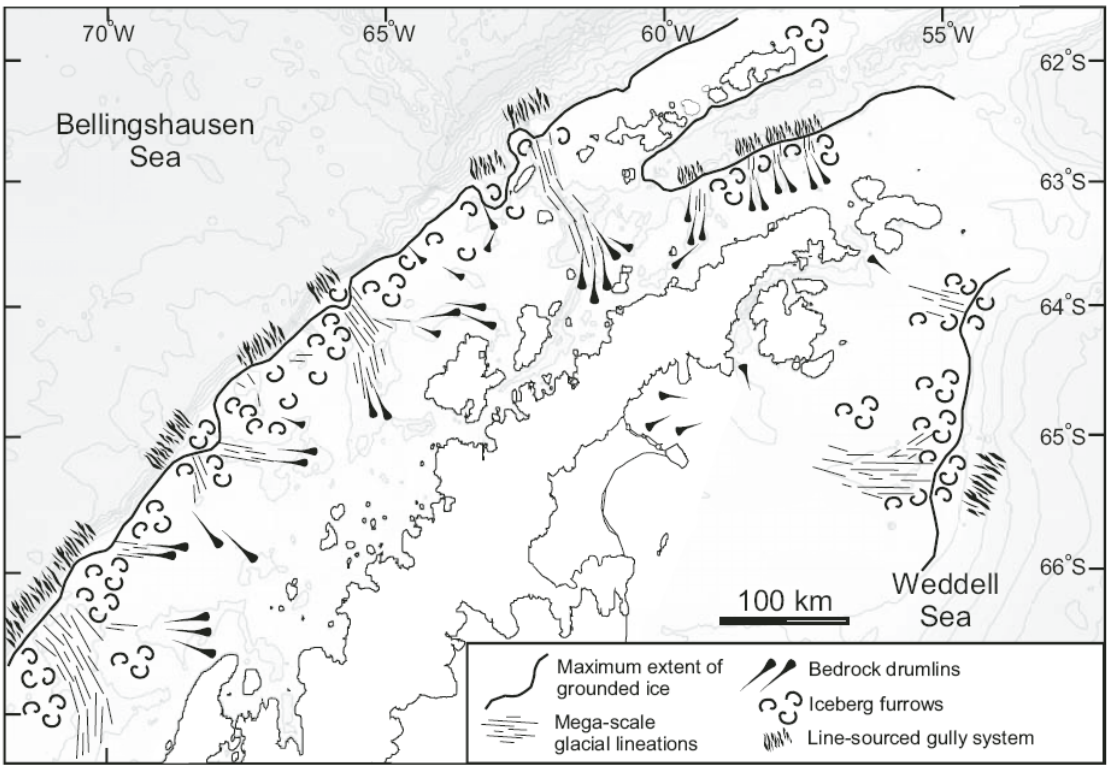

Fig. 2.2 Reconstruction of the geomorphic features mapped on the continental shelf and the resulting reconstruction of the maximum extent of grounded ice around the northern Antarctic Peninsula at the LGM (Source: Heroy and Anderson, 2005)

The South Shetland Islands (SSIs), situated to the north of the Antarctic Peninsula, do not appear to have been overridden by the APIS during the LGM. The islands remained separated from the APIS by the deep Bransfield Strait (Fig. 2.3; John and Sugden, 1971; Sugden and Clapperton, 1977; Anderson *et al*., 2002).

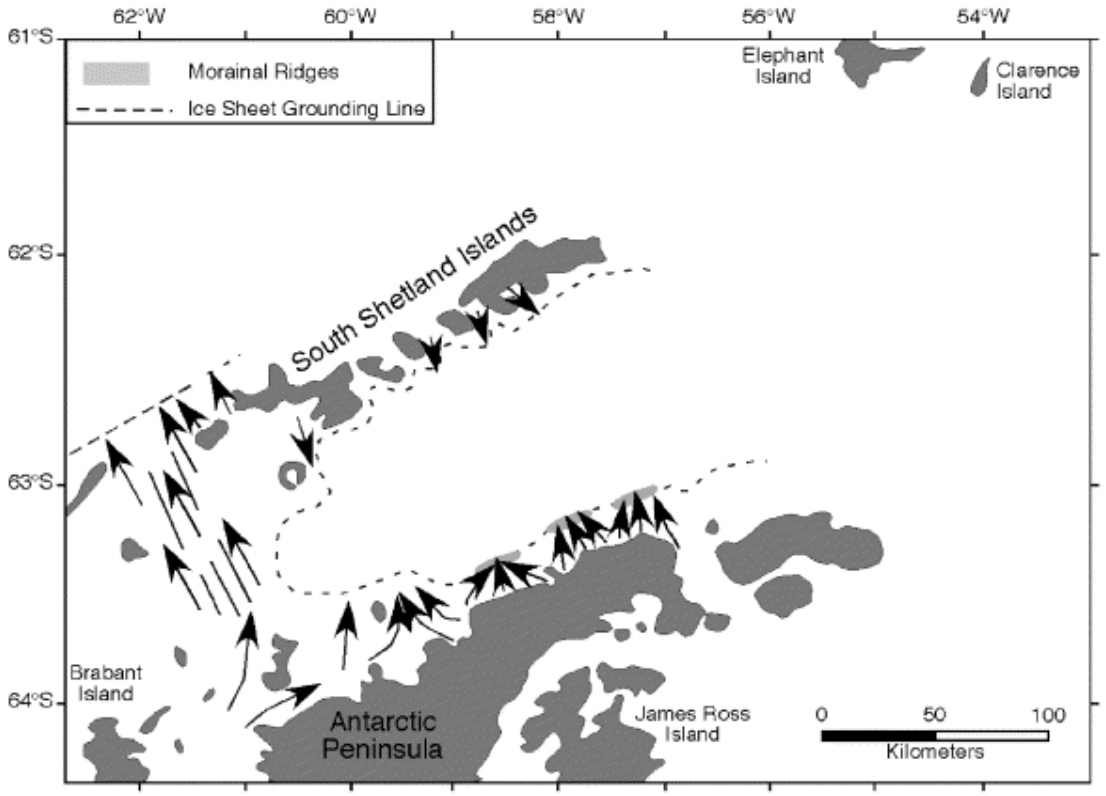

Fig. 2.3 Reconstruction of LGM ice extent and palaeodrainage for the Bransfield Strait region, showing the separation of the South Shetland Islands ice cap from the Antarctic Peninsula Ice Sheet. Arrows indicate direction of ice flow (Source: Anderson *et al*., 2002)

Our general understanding of the glacial history of the SSIs stems from a series of papers in the 1970s and 80s (John and Sugden, 1971; John, 1972; Sugden and John, 1973; Sugden and Clapperton, 1977; Curl, 1980). These identified two major phases of glaciation, with contrasting ice extents. During the first glacial phase, an ice cap measuring 65 by 250 km and up to 900 m thick covered the entire island chain, with its axis over the offshore platform to the northwest of the archipelago (Fig. 2.4; John and Sugden, 1971). The modern shallow (200 m) submarine platforms that surround the islands are assumed to represent this former ice extent (Sugden and Clapperton, 1977). Evidence of scouring on presently ice-free peninsulas, meltwater channels and

glacial troughs aligned north-west to south-east indicate ice movement transverse to the axis of the island group, with the ice dispersal centre to the northwest. Substantial glacial erosion and modification of the landscape occurred. Deglaciation is likely to have been rapid as the complex system of meltwater channels indicates the discharge of large volumes of meltwater (Curl, 1980).

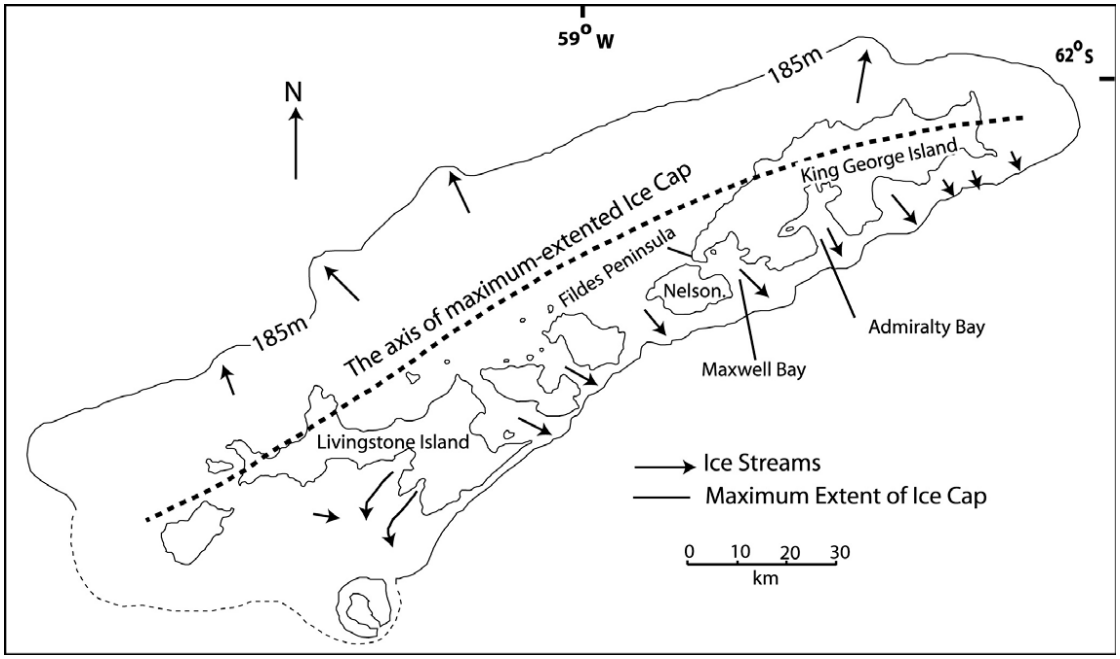

Fig. 2.4 Reconstruction of the maximum ice extent on the South Shetland Islands, based on erosional landforms. The water depth at the seaward limits of the ice cap is 185 m. Note the age of this glaciation is not well-constrained (Source: Seong *et al.*, 2006, after John and Sugden, 1971)

By contrast, the second glacial phase was characterized by less extensive ice cover, with small ice caps centred on individual islands (John and Sugden, 1971). Evidence for this more 'local' glaciation comes from erratics and glacial drift deposits. Separating the two glacial phases, John and Sugden proposed a non-glacial interval of high relative sea level and minimal ice cover. Marine inundation deposited beach sediments on glaciated rock surfaces, with pockets of *in situ* beach material preserved at altitudes between 55 and 275 m above sea level (asl). John (1972) proposed that their presence at such high altitudes was a function of rapid deglaciation from the early glacial phase, causing a marine transgression at a time when the island block was still isostatically depressed. However, whilst John and Sugden proposed an ice cap thick enough (~900 m in the axial zone) to cause 275 m of isostatic depression (assuming isostatic

equilibrium is reached and that the maximum amount of crustal depression is approximately one-third the thickness of the overlying ice), the deposits lie near the periphery of the former ice cap, where there would have been least isostatic depression. Therefore isostasy alone cannot account for their uplift, and highlights the importance of long-term tectonic uplift (see section 2.4.4).

Incorporation of the beach material in till suggests they pre-date the second glacial phase. Ubiquitous marine features, such as platforms, caves and sea-stacks are also inferred to pre-date the second glacial phase based on relative age techniques (such as height and weathering intensity). They are well-preserved and without evidence of glacial erosion. The terraces are very extensive, implying substantial periods of relative sea level stability. The predominance of a marine landscape rather than a glacial one suggests restricted ice during the second glacial phase, or at least thin, non-erosive, cold-based ice (Hall, 2003).

The studies of the 1970s interpreted this second glacial phase as corresponding to the LGM, with the earlier more extensive glacial event pre-dating the LGM. This interpretation was largely based on the altitudes of high and morphologically intact marine shorelines, preserved up to 250 m above present sea level across the archipelago (John and Sugden, 1971). These raised marine shorelines are likely to have been formed by marine planation and then subsequently uplifted either tectonically or isostatically. In the case of the latter they could indicate former heavy glacio-isostatic depression of the land. Based on relative age techniques (such as height and weathering intensity) these high shorelines, in combination with erratics found well above inferred LGM trimlines, were taken to represent a glacial event prior to the LGM, and therefore must have also pre-dated MIS 3, a well-documented circum-Antarctic interstadial period (Berkman *et al.*, 1998; Anderson and Andrews, 1999). An interpretation of early Wisconsinan/Weichselian age (MIS 4) therefore seemed favourable, although they could also be much older (Hjort *et al.*, 2003). This is supported by Bentley and Anderson (1998), who suggested that ice volumes were considerably greater before 35 ka compared to after, and also by Rabassa (1983), who dated a glacigenic drift deposit on James Ross Island to 34115 yr BP. Therefore on this evidence, the 1970s literature concluded that the Wisconsinan maximum ice extent on the SSIs did not coincide with the last global glacial maximum.

However, there is little chronological control on the geomorphological interpretations from the 1970s, and therefore reconstructions of LGM ice extent are debated and must still be considered as speculative (John Anderson, pers. comm.). Given our knowledge about the extent of LGM glaciation further south along the Antarctic Peninsula, it is difficult to account for why South Shetland glacial history would be out of phase with the rest of the Peninsula. Therefore it is possible that the extensive glacial event occurred during the LGM and the later more restricted advance occurred during a subsequent cold interval, such as the Antarctic Cold Reversal.

2.3 Deglaciation and Holocene RSL history

Based largely on the radiocarbon dating of glacial-marine sediments from the continental shelf it has been suggested that deglaciation of the Antarctic Peninsula began around 18000 cal yr BP (Heroy and Anderson, 2007). The APIS was close to its present configuration by the early Holocene, ca. 9500 cal yr BP (Sugden *et al.*, 2006). This is significantly earlier than suggested by global glacio-eustatic models, which predict Antarctic deglaciation began 12000 cal yr BP (Peltier, 1994; Nakada *et al.*, 2000) or 9000 cal yr BP (Tushingham and Peltier, 1991). It is also several thousand years earlier than predicted by one glaciological model, which suggested the onset of deglaciation of the northern Peninsula occurred 13000-14000 cal yr BP and progressed south by 6000 cal yr BP (Huybrechts, 2002).

Evans *et al*. (2005) highlighted regional differences in deglaciation histories, both in terms of timing and ice dynamics during retreat. Differences in timing are manifest between the east and west flanks of the Peninsula, as well as between the northern and southern regions (Fig. 2.5). Rapid deglaciation on the west side of the Peninsula contrasts markedly with more gradual ice stream retreat, interrupted by stillstands, in the Larsen A region of the eastern Antarctic Peninsula (Sugden *et al.*, 2006). In both cases, once ice fronts reached the present coastline, glaciers disintegrated slowly to their present margins, with some periods of local ice readvance (Mäusbacher, 1991; Hjort *et al.*, 1997; Ingólfsson *et al.*, 1998).

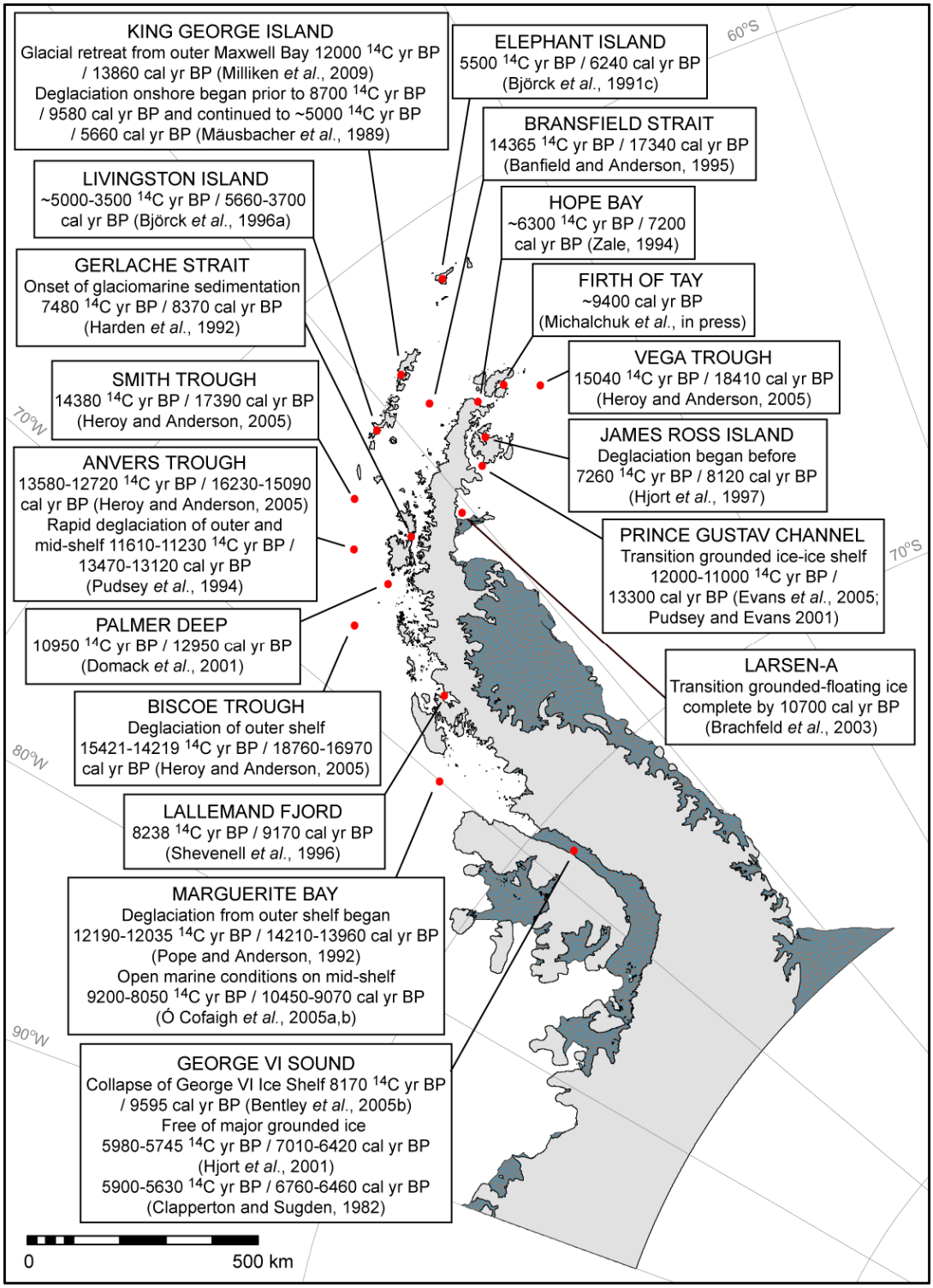

Fig. 2.5 Radiocarbon-based deglacial chronology of the Antarctic Peninsula. Unless otherwise stated, dates are minimum estimates of glacial retreat. Dates on calcareous material have been corrected using a reservoir age of 1300 yr (Berkman and Forman, 1996); Dates on acid insoluble organic carbon have been corrected using the local source corrections provided in the original studies.

The deglaciation of coastal areas that are presently ice-free is constrained by minimum ages obtained from radiocarbon dating of molluscs and bones in raised marine deposits, the onset of organic deposition in lake sediments, accumulation of moss bank peats, and the remains of abandoned penguin rookeries (e.g. Mäusbacher *et al.*, 1989; Björck *et al.*, 1991c; Zale, 1994b; Hjort *et al.*, 1997). In the SSIs, Seong *et al*. (2009) placed the maximum age of deglaciation at 15500 ± 2500 cal yr BP, and rapid glacial retreat occurred from Maxwell Bay between 10100 and 8200 cal yr BP (Milliken *et al.*, 2009). Mäusbacher (1991) placed the minimum age of deglaciation of King George Island at 9000 ^{14}C yr BP, with glaciers at or within their present limits by 5500 ^{14}C yr BP. However, there appear to be regional differences within the island group, with Byers Peninsula on Livingston Island deglaciated as late as 5000-3000 ^{14}C yr BP (Björck *et al.*, 1996a).

On the SSIs there are flights of raised beaches at numerous sites across the archipelago, extending laterally up to 8 km, which formed as a result of isostatic uplift following deglaciation (John and Sugden, 1971; Sugden and Clapperton, 1977; Del Valle *et al.*, 2002). Prominent beach ridges, traceable along many coastlines in the island group, at ~18.5 and 6 m asl represent RSL stillstands, suggesting that isostatic uplift was in equilibrium with RSL rise possibly due to minor glacial readvances. Undisturbed beaches occur up to altitudes of 54 m, although owing to frost shattering above 18.5-22 m compared to fresh weathering below, only deposits below 22 m are regarded as Holocene in age (Barsch and Mäusbacher, 1986b; Clapperton, 1990; Hall, 2003). Thus the prominent beach at ~18.5 m asl is regarded as the post-LGM marine limit. The age of this highest elevation Holocene beach also potentially provides a minimum age for deglaciation, however the exact age is not clear (Bentley *et al.*, 2005a). Previously reported ages of the SSI beaches are given in Table 2.1, along with inferences about ice extent and RSL from lake sediments.

Site	Feature	Altitude (m asl)	Conventional age (^{14}C yr BP)	Corrected age (^{14}C yr BP)	Calibrated age (cal yr BP)	Material dated and stratigraphic position	Laboratory code	Reference	Notes
King George Island - Fildes Peninsula									
Muschelbach, NW Fildes	Raised marine sediments	24	86000 ± 15000 (U/Th)			Shells (*Laternula*) contained in marine sediments, overlain by till	HD SCH2-1086	Barsch and Mäusbacher, 1986b	Date for interglacial
Muschelbach	Raised marine sediments	24	85000 ± 6000 (U/Th)			Shells (*Laternula*) contained in marine sediments, overlain by till	HD B42-1107	Barsch and Mäusbacher, 1986b	Date for interglacial
Muschelbach	Raised marine sediments	24	84000 ± 6500 (U/Th)			Shells (*Laternula*) contained in marine sediments, overlain by till	HD SCH1-1085	Barsch and Mäusbacher, 1986b	Date for interglacial
Wind Creek Valley (Windbachtal)	Raised beach	18	6650 ± 90	5520 ± 160[a]	6340 ± 160	Penguin bone	HD9425-9100	Barsch and Mäusbacher, 1986a	Minimum age for beach and deglaciation
Wind Creek Valley	Raised beach	18	6560 ± 55	5430 ± 140[a]	6240 ± 140	Penguin bone	HD9426-9106	Barsch and Mäusbacher, 1986a	Minimum age for beach and deglaciation
Hochlandsee	Freshwater lake	101	5410 ± 185	5410 ± 185	6120 ± 185	Freshwater moss (175-176 cm core depth)	HD11417-11148	Mäusbacher, 1991	Basal date – minimum age for deglaciation
Jurasee	Freshwater lake	47	8700 ± 300	8700 ± 300	9710 ± 300	Freshwater sediment (352-354 cm)	HD11166-11024	Mäusbacher *et al*., 1989	Basal date – minimum age for deglaciation
Mondsee	Freshwater lake	45	7200 ± 250	7200 ± 250	7980 ± 250	Freshwater sediment (317-319 cm)	HD11415-11133	Schmidt *et al*., 1990	Basal date – minimum age for deglaciation
Hotel Lake	Freshwater lake	40	6120 ± 120	6120 ± 120	6930 ± 120	Freshwater gyttja rich in moss (280-290 cm)	Gd-4413	Tatur *et al*., 1999	Minimum age for deglaciation
Ardley Lake	Freshwater lake	18	5410 ± 285	5410 ± 285	6130 ± 285	Freshwater sediment (390 cm)	HD11416-11147	Mäusbacher, 1991	Extrapolates to give basal age of 6380 yr BP (460 cm)
Profound Lake (Tiefersee)	Freshwater lake	17.5	5380 ± 165	5380 ± 165	6100 ± 165	Freshwater sediment (164-167 cm)	HD11420-11161	Mäusbacher *et al*., 1989	Basal date – minimum age for deglaciation
Kitezh Lake (Kiteschsee)	Isolation basin	15.5	6180 ± 150	6180 ± 150	7000 ± 150	Freshwater sediment (181-184 cm, above marine-fresh transition)	HD11163-10998	Mäusbacher *et al*., 1989	Minimum age of isolation
Kitezh Lake	Isolation basin	15.5	6950 ± 195	5650 ± 220[b]	6490 ± 220	Marine algae (190-195 cm, below m-f transtn)	HD11162-10997	Mäusbacher *et al*., 1989	Less accurate age of isolation date due to reservoir effect

Site	Feature	Altitude (m asl)	Conventional age (^{14}C yr BP)	Corrected age (^{14}C yr BP)	Calibrated age (cal yr BP)	Material dated and stratigraphic position	Laboratory code	Reference	Notes
Kitezh Lake	Isolation basin	15.5	3460 ± 140	3460 ± 140	3670 ± 140	Bulk freshwater sediment rich in moss (155-162 cm)	Lu 3679	Martinez-Macchiavello *et al*., 1996	Minimum age of isolation
Long Lake	Isolation basin	15	5723 ± 70	5723 ± 70	6460 ± 70	Bulk organic sediment (312 cm)	NZA13465	Yoon *et al*., 2006	Age of deglaciation, formation of postglacial limnic environment
Petrel Cave	Wave-cut palaeonotch	47	4620 ± 65	4620 ± 65	5210 ± 65	Bulk organic sediment	NIG-99050	Sun *et al*., 2005	Age for deglaciation
King George Island – Other									
Arctowski, Admiralty Bay	Peat bank	45.5	4950 ± 140	4950 ± 140	5640 ± 140	Subfossil peat overlying 45-50 m raised beach	U-4325	Birkenmajer *et al*., 1985	Glacial readvance
'Pingfo', Potter Peninsula	Raised beach	16.3	5750 ± 40	4620 ± 140[a]	5360 ± 140	Penguin bone	*Not given*	Del Valle *et al*., 2002	Minimum age of '12m beach'
'Pingfo', Potter Peninsula	Raised beach	15.4	5840 ± 40	4710 ± 140[a]	5460 ± 140	Penguin bone	*Not given*	Del Valle *et al*., 2002	Minimum age of '12m beach'
Penguin Ridge, Thomas Point	Raised beach	12	1610 ± 130	1610 ± 130	1470 ± 130	Base of peat (53-54 cm) overlying the 12 m raised beach	Gd-4636	Tatur *et al*., 1997	Minimum age for beach
Barton Peninsula	Raised beach	6-7	1390 ± 140	Modern[c]	Modern	Whalebone on beach surface	Birm-224	Sugden and John, 1973	Maximum age for beach
Three Brothers Hill	Raised beach	6	1360 ± 165	Modern[c]	Modern	Whalebone on beach surface	DIC-371	Curl, 1980	Maximum age for beach
Maxwell Bay	Raised beach	5.2	1440 ± 55	20 ± 210[c]	Modern	Whalebone on foreslope below 6 m beach	DIC-373	Curl, 1980	Maximum age for beach
Potter Cove	Exposed section	6	9670 ± 230	8370 ± 250[b]	9440 ± 250	Shells (*Laternula*) in raised marine sediments, overlain by till (3.5 m asl)	Birm-48	Sugden and John, 1973	Ice free by 8370 yr BP
Potter Cove	Exposed section	6	7683 ± 86	6380 ± 130[b]	7300 ± 130	Seaweed in raised marine sediments overlain by till (4 m asl)	Birm-23	Sugden and John, 1973	Subsequent glacial readvance after 6380 yr BP
Marian Cove	Coastal exposure	5.5	1223 ± 81	Modern[b]	Modern	Seaweed buried ~50 cm, overlying beach gravels	Birm-16	Sugden and John, 1973	Minimum age for beach
Marian Cove	Coastal exposure	3	1430 ± 470	130 ± 480[b]	360 ± 480	Seaweed buried ~2.5 m in beach gravels	Birm-17	Sugden and John, 1973	Minimum age for beach

Site	Feature	Altitude (m asl)	Conventional age (^{14}C yr BP)	Corrected age (^{14}C yr BP)	Calibrated age (cal yr BP)	Material dated and stratigraphic position	Laboratory code	Reference	Notes
Three Brothers Hill	Raised beach	2.1	1200 ± 110	Modern[c]	Modern	Whalebone in foreslope of 2.5-3 m beach	DIC-368	Curl, 1980	Maximum age for beach
Maxwell Bay	Raised beach	2	1210 ± 55	Modern[c]	Modern	Whalebone in foreslope of 2.5-3 m beach	DIC-369	Curl, 1980	Maximum age for beach
Keller Peninsula	Modern beach	1.8	1000 ± 45	Modern[c]	Modern	Whalebone on modern beach	DIC-367	Curl, 1980	Maximum age for beach
Potter Cove	Modern beach	0	850 ± 145	Modern[b]	Modern	Shells (*Laternula*) on modern beach	Birm-47a	Sugden and John, 1973	Maximum age for beach
Nelson Island									
Rip Point	Raised beach	6.5	802 ± 43	802 ± 43	700 ± 43	Tree trunk (*Austrocedrus chilensis*) buried 18 cm in beach	Birm-14	Sugden and John, 1973	Maximum age for beach
Livingston Island									
South Beaches, Byers	Raised beach	10.3	2823 ± 40	1400 ± 200[c]	1360 ± 200	Whalebone buried 30 cm in beach	SRR-1086	Hansom, 1979	Maximum age for beach
South Beaches	Raised beach	10.1	3121 ± 35	1700 ± 200[c]	1680 ± 200	Whalebone buried 40 cm in beach	SRR-1087	Hansom, 1979	Maximum age for beach
South Beaches	Raised beach	9	3115 ± 47	1690 ± 210[c]	1680 ± 210	Whalebone buried in beach crest	AA-45934	Hall and Perry, 2004	Maximum age for beach
South Beaches	Raised beach	7.6	2530 ± 85	1110 ± 220[c]	1060 ± 220	Whalebone from rear of 6 m beach	I-7870	Curl, 1980	Maximum age for beach
South Beaches	Raised beach	6	1692 ± 42	270 ± 200[c]	300 ± 200	Whalebone partially buried in beach (poor condition)	AA-45931	Hall and Perry, 2004	Maximum age for beach
South Beaches	Raised beach	6	1572 ± 42	150 ± 200[c]	220 ± 200	Whalebone partially buried in beach surface	AA-46816	Hall and Perry, 2004	Maximum age for beach
South Beaches	Raised beach	5	1625 ± 42	200 ± 200[c]	250 ± 200	Bone buried in beach foreslope	AA-45932	Hall and Perry, 2004	Maximum age for beach
South Beaches	Raised beach	4.5	1025 ± 80	Modern[c]	Modern	Whalebone on foreslope of 3.5-5 m beach	I-7869	Curl, 1980	Maximum age for beach
South Beaches	Raised beach	4	1715 ± 42	290 ± 200[c]	320 ± 200	Whalebone buried in beach foreslope	AA-45933	Hall and Perry, 2004	Maximum age for beach

Site	Feature	Altitude (m asl)	Conventional age (^{14}C yr BP)	Corrected age (^{14}C yr BP)	Calibrated age (cal yr BP)	Material dated and stratigraphic position	Laboratory code	Reference	Notes
South Beaches	Raised beach	4	1545 ± 46	120 ± 210[c]	210 ± 210	Whale vertebra partially buried in beach foreslope	AA-45936	Hall and Perry, 2004	Maximum age for beach
South Beaches	Raised beach	4	1431 ± 44	Modern[c]	Modern	Whale vertebra partially buried in beach foreslope	AA-45939	Hall and Perry, 2004	Maximum age for beach
South Beaches	Raised beach	3	1056 ± 130	Modern[c]	Modern	Whalebone embedded in beach gravel	Birm-50	Sugden and John, 1973	Maximum age for beach
South Beaches	Raised beach	2	1271 ± 47	Modern[c]	Modern	Whale vertebra on modern storm beach	AA-46815	Hall and Perry, 2004	Maximum age for beach
South Beaches	Raised beach	1.8	840 ± 75	Modern[c]	Modern	Whalebone on modern beach	DIC-372	Curl, 1980	Maximum age for beach
Barnard Point, False Bay	Raised beach	1.8	970 ± 50	Modern[c]	Modern	Seal bone on modern beach	DIC-370	Curl, 1980	Maximum age for beach
President Beaches, Start Point	Raised beach	1.8	4905 ± 100	3480 ± 220[c]	3870 ± 220	Whalebone on rear of storm beach	I-7872	Curl, 1980	Curl suggests specimen originally deposited at higher elevation, hence anomalously old age
Lake 48, Byers Peninsula	Freshwater lake	120-130	4570 ± 60	4570 ± 60	5160 ± 60	Freshwater moss (129-136 cm)	Ua-3923	Björck *et al*., 1996a	Basal date – minimum age for deglaciation
Lake 49, Byers Peninsula	Freshwater lake	80-90	3730 ± 400	3730 ± 400	4050 ± 400	Freshwater moss (93-100 cm)	Lu-3473	Björck *et al*., 1996a	Basal date – minimum age for deglaciation
Midge Lake, Byers	Freshwater lake	70	3735 ± 250	3735 ± 250	4040 ± 250	Freshwater moss (151 cm)	Ua-1220	Björck *et al*., 1991a	Basal date, age of deglaciation may be much older
Lake 30, Byers Peninsula	Freshwater lake	65	4480 ± 60	4480 ± 60	5040 ± 60	Freshwater moss (117-124 cm)	Ua-3925	Björck *et al*., 1996a	Basal date – minimum age for deglaciation
Lake Åsa, Byers	Freshwater lake	35	4600 ± 100	4600 ± 100	5190 ± 35	Freshwater moss (205-210 cm)	Lu-3088	Björck *et al*., 1993	Basal date – minimum age for deglaciation

Table 2.1 Radiocarbon dates on organic material from beaches, coastal exposures and isolation basins across the SSIs.
Radiocarbon dates have been corrected for the marine reservoir effect using (a) 1130 ± 134 yr for penguin bones, (b) 1300 ± 100 yr for marine sediment, shells and seaweed, and (c) 1424 ± 200 yr for whalebone and seal bone (Berkman and Forman, 1996); errors on the original date and on the ΔR value were combined in quadrature (Taylor, 1997). Dates were calibrated using Calib version 5.0.1 (Stuiver and Reimer, 1993) using the Marine04 calibration curve for marine dates (Hughen *et al.*, 2004) and SHCal04 calibration curve for terrestrial dates (McCormac *et al.*, 2004). The median of the calibrated age range is reported to 1-sigma. All corrected and calibrated dates and errors are rounded to the nearest 10 years.

More recently, a reconnaissance RSL curve developed by Bentley *et al*. (2005a) collated previously published evidence on the marine limit elevation and Holocene RSL history of the South Shetlands. They identified a RSL highstand at 14.5-16 m asl, reached sometime after 6180 ^{14}C yr BP. This is in contrast to Mäusbacher (1991), who placed the marine limit at 20 m asl. Such discrepancy highlights the need for further research, including more accurate surveying of the heights of key landforms. However, even allowing for the differences in range, a marine limit of 15-20 m asl around the SSIs is significantly lower than the 30 m asl reported further south on James Ross Island (dated to ca. 7500 ^{14}C yr BP; Hjort *et al*., 1997). The highest postglacial marine limit described on the Peninsula is at Calmette Bay in Marguerite Bay at 41 m asl (Bentley *et al.*, 2005a). This north-south gradient in marine limit elevation along the Peninsula is consistent with observations of Anderson *et al*. (2002) of greater LGM ice thicknesses in the southern and central sectors of the Antarctic Peninsula relative to further north.

2.3.1 Mid-Holocene and neo-glacial readvances

Following initial deglaciation from the LGM, the Antarctic Peninsula has undergone periods of glacial and climate oscillations (Fig. 2.6). Evidence of glacial readvance in the mid-Holocene comes from King George Island between 6000 and 4000 ^{14}C yr BP (Mäusbacher, 1991; Yoon *et al.*, 2000), James Ross Island between 5000 and 4500 ^{14}C yr BP (Hjort *et al.*, 1997), Brabant Island after 5,300 yr BP (Hansom and Flint, 1989) and George VI Sound (Clapperton and Sugden, 1982; Bentley *et al.*, 2005b). However, marine records from Palmer Deep (Domack *et al.*, 2001; Brachfeld *et al.*, 2002) show no evidence of local readvances, being situated too far offshore.

This brief period of mid-Holocene glacial readvance was followed immediately by the Holocene climatic optimum ('Mid-Holocene Hypsithermal') between 4000 and 2700 ^{14}C yr BP (4500-2800 cal yr BP) in the Antarctic Peninsula region (Hodgson *et al.*, 2004; Bentley *et al.*, 2009). Glaciers retreated rapidly and palaeoclimate records from lake sediments indicate a warmer and more humid climate than today during this time (Björck *et al.*, 1991a; 1993; 1996b). In marine sediments it is detected as a period of reduced sea-ice coverage and greater primary production (Shevenell *et al.*, 1996; Domack *et al.*, 2003). This period of warming on the Antarctic Peninsula is coincident with similar climatic optima reported from the maritime sub-Antarctic islands of Signy

and South Georgia (Jones *et al.*, 2000; Rosqvist and Schuber, 2003), the Ross Sea (Baroni and Orombelli, 1994) and Bunger Oasis of East Antarctica (Kulbe *et al.*, 2001).

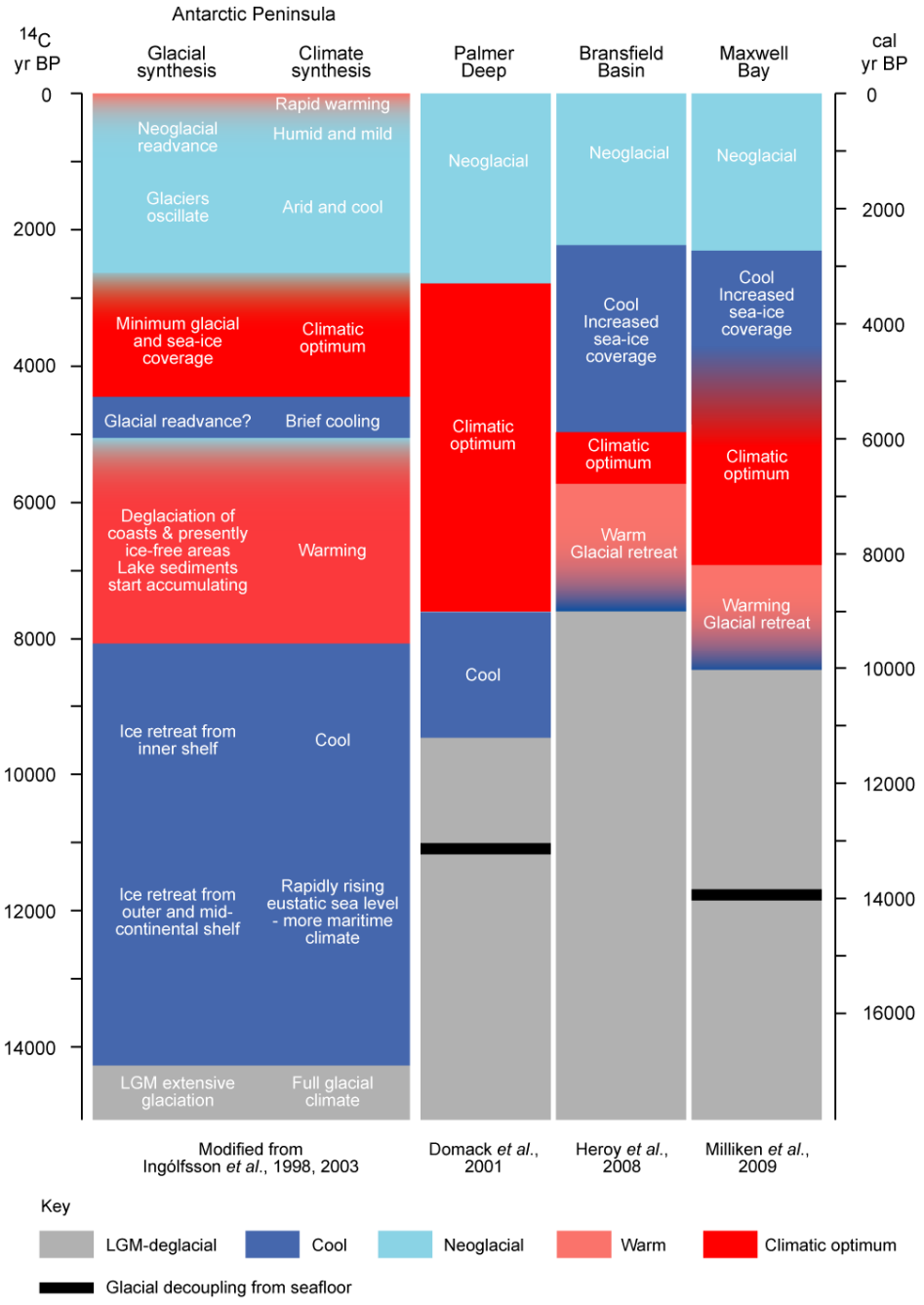

Fig. 2.6 Synthesis of Antarctic Peninsula glacial and climatic events throughout the Quaternary. The left column is based on a compilation of marine, lake and ice core palaeoclimate records from the Antarctic Peninsula, and provides a comparison with palaeoclimate studies from three specific locations based on marine sediment cores. Note there are discrepancies in the exact timings of phases in different locations, reflecting regional variations in atmospheric or oceanic circulation patterns (Based on Michalchuk *et al.*, 2009)

Around 2500 ^{14}C yr BP another climatic reversal occurred, with reports of neo-glacial expansion in the northern Antarctic Peninsula region (John and Sugden, 1971; Barsch and Mäusbacher, 1986a; Zale and Karlén, 1989; Clapperton, 1990; Mäusbacher, 1991; Björck *et al.*, 1993; Bárcena *et al.*, 1998; Fabres *et al.*, 2000; Domack *et al.*, 2001; Yoon *et al.*, 2002; Hall and Perry, 2004; Heroy *et al.*, 2008). Readvance moraines transgressing earlier Holocene raised beaches on the SSIs provide evidence for this, with an advance of 2-3 km in several fjords (Curl, 1980; Birkenmajer, 1981; Clapperton and Sugden, 1988; Björck *et al.*, 1996a). Dated to within the last 1000 years, they are broadly contemporaneous with Little Ice Age glacial advances in the northern hemisphere (Hall, 2007). Both these late and mid Holocene glacial readvances in the northern Antarctic Peninsula region appear synchronous with similar readvances on South Georgia around 3600 cal yr BP and 1100 cal yr BP respectively (Bentley *et al.*, 2007).

In conclusion, it is clear that constraining the LGM ice extent and subsequent deglaciation of the SSIs requires further research. This is largely a result of insufficient data rather than conflicting interpretations. Therefore the aim here is to advance our understanding of the SSIs. John and Sugden (1971) used raised marine features and other geomorphological observations to establish a detailed glacial history of the islands. This thesis aims to develop this study by providing new data from isolation basins. The following section discusses the techniques that can be employed to reconstruct past relative sea level changes, and thus former ice volumes and deglacial histories.

2.4 Approaches to the reconstruction of former ice volumes, deglaciation and RSL change

2.4.1 Introduction to relative sea level change

Relative sea level (RSL, $\Delta\zeta_{rsl}$) is defined as the vertical position of the ocean surface (geoid) relative to the solid land surface. It is the result of a complex interplay between eustasy (ocean volume changes, $\Delta\zeta_{esl}$), isostasy (crustal depression or rebound, $\Delta\zeta_{iso}$), tectonic activity ($\Delta\zeta_{tect}$) and local processes ($\Delta\zeta_{local}$), and can be expressed in terms of time τ and location σ as follows (Fleming *et al*., 1998; Lambeck *et al*., 1998; Shennan and Horton, 2002):

$$\Delta\zeta_{rsl}(\tau,\sigma) = \Delta\zeta_{esl}(\tau,\sigma) + \Delta\zeta_{iso}(\tau,\sigma) + \Delta\zeta_{tect}(\tau,\sigma) + \Delta\zeta_{local}(\tau,\sigma)$$

Eustasy $\Delta\zeta_{esl}(\tau,\sigma) = -\left(\frac{\rho_{ice}\Delta V_{ice}(\tau)}{\rho_{water} A_o(\tau)}\right)$

ρ_{ice} and ρ_{water} are the densities of ice and water respectively, ΔV_{ice} is the difference in the global land-based ice volume between time τ and the present, and A_o is the surface area of the ocean. $\Delta\zeta_{esl}$ therefore provides a measure of the change in ocean volume.

Local

$$\Delta\zeta_{local}(\tau,\sigma) = \Delta\zeta_{tide}(\tau,\sigma) + \Delta\zeta_{sed}(\tau,\sigma)$$

Total effect of local processes including changes in tidal regime and elevation of the sediment with reference to tide levels at the time of deposition ($\Delta\zeta_{tide}$) and sediment consolidation ($\Delta\zeta_{sed}$) since deposition.

Isostasy $\Delta\zeta_{iso}(\tau,\sigma) = \Delta\zeta_{ice}(\tau,\sigma) + \Delta\zeta_{water}(\tau,\sigma) + \Delta\zeta_{geoid}(\tau,\sigma)$

Total isostatic effect of the glacial rebound process including the ice (glacio-isostatic) and meltwater (hydro-isostatic) load contributions and geoid deformation to gravitational effects. $\Delta\zeta_{ice}$ includes the vertical movement of the earth's crust caused by changes in ice loading, and is therefore a function of the spatial and temporal history of global ice distribution and earth rheology. $\Delta\zeta_{water}$ includes the crustal displacement and gravitational effects associated with the redistribution of ocean waters and is a function of rheology, coastal geometry and eustatic sea level. $\Delta\zeta_{geoid}$ includes the deformation of the geoid due to changing gravitational potential of the surface load as mass is redistributed between land-based ice sheets and the oceans when ice sheets melt or expand; it is a function of ice sheet and ocean basin geometry.

At near-field sites (within, or close to, former ice sheet limits) postglacial RSL histories are dominated by local isostatic changes resulting from ice sheet unloading, although eustatic sea level rise is still important. By observing RSL change at a particular location, and correcting this for eustatic sea level variations and tectonic movements, it is possible to quantify glacio-isostasy (postglacial crustal rebound) through time. The former ice loading history required to produce the observed isostatic signature can then be calculated for a given value of mantle viscosity.

At present there is a paucity of RSL data from Antarctica. Only a few RSL curves are available, notably from Victoria Land (Baroni and Orombelli, 1991; Baroni and Hall, 2004; Hall *et al.*, 2004), the northern Antarctic Peninsula (Bentley *et al.*, 2005a), the Larsemann and Vestfold Hills, East Antarctica (Zwartz *et al.*, 1998; Verleyen *et al.*, 2005), and the Sôya Coast, East Antarctica (Miura *et al.*, 1998a). This is largely a reflection of the limited area of currently ice-free coastal locations where evidence of former sea levels can be preserved (<5% of the coastline consists of rock) and the lack of organic material available for radiocarbon dating. There are two main approaches to

the development of RSL curves, namely the use of morphological evidence such as raised marine features, and isolation basin sediments.

2.4.2 The morphological approach to RSL reconstruction

Early work from Arctic Canada and Fennoscandia provided the foundation for research on glacio-isostatic rebound and RSL change. Early workers identified suites of raised marine features and suggested these reflected postglacial changes in RSL. The highest marine deposits (including raised beaches and delta terraces) commonly define the marine limit (the maximum elevation attained by the sea along a glacio-isostatically-depressed coastline), with the elevation of the marine limit reflecting (1) the distance from the former ice margin and hence ice thickness and isostatic depression, (2) the date of deglaciation and (3) eustatic sea level rise. Therefore, regional measurement of its age and elevation led to the development of curves of postglacial RSL change (e.g. Andrews, 1968; Andrews, 1970; Blake, 1975; England, 1976a; Quinlan and Beaumont, 1981; England, 1983; Forman *et al.*, 1987; Dyke *et al.*, 1991; England, 1992; Forman *et al.*, 1997; Dyke, 1998; Ó Cofaigh, 1999). Important lessons can be learnt from the construction of these curves that are applicable to other near-field regions.

2.4.2.1 Lessons from the Arctic: geomorphology of the glacial-marine interface and styles of deglaciation

Central to the study of deglaciation in High Arctic Canada (Fig. 2.7) is the debate concerning the ice extent during the LGM, with two competing theories. The first favours extensive glaciation at the LGM whereby the Canadian Arctic archipelago was covered by the Innuitian Ice Sheet, confluent with the Laurentide and Greenland Ice Sheets (Blake, 1970, 1975; Tushingham, 1991; Blake, 1992). The second proposes restricted Late Wisconsinan glaciation, with limited expansion of highland and plateau ice masses only 5-60 km beyond present limits (England, 1976b, 1976a, 1983; Hodgson, 1985; Bednarski, 1986; Lemmen,

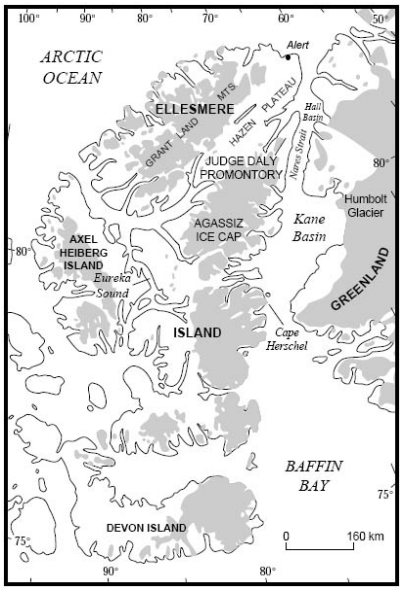

Fig. 2.7 The Queen Elizabeth Islands, High Arctic Canada; contemporary ice caps are shaded (Source: England, 1997)

1989; England, 1992; Lemmen and England, 1992; Lemmen *et al.*, 1994; Bell, 1996). Greenland ice remained separated from Ellesmere Island ice and England (1983) proposed a 'full glacial sea' transgressed into this ice-free corridor between the two ice sheets. Although in recent years this debate has been largely resolved by increased geomorphological evidence for an extensive LGM ice sheet (England, 1999; Ó Cofaigh, 1999), an examination of the changing interpretations of raised marine features demonstrates the complexity of RSL reconstruction in such environments.

Marked contrasts are observed across the High Arctic in the form of RSL curves and patterns of initial postglacial emergence. England (1976b) originally constructed a series of RSL curves for the Queen Elizabeth Islands of Arctic Canada, similar in form to curves from areas formerly covered by the Laurentide Ice Sheet in the central and southern Canadian Arctic, predicting continuous RSL fall since deglaciation and rapid initial postglacial emergence (Fig. 2.8a; Andrews, 1968, 1970). Similar rapid initial emergence rates of ≥ 5m/100 yr were observed by Blake (1975), Lemmen *et al*. (1994), Bednarski (1995), Dyke (1998) and Ó Cofaigh (1999). However, England (1983; 1992; 1997) reported evidence for a period of stable RSL at the marine limit followed by slow initial emergence of 1-2 m/100 yr (Fig. 2.8b).

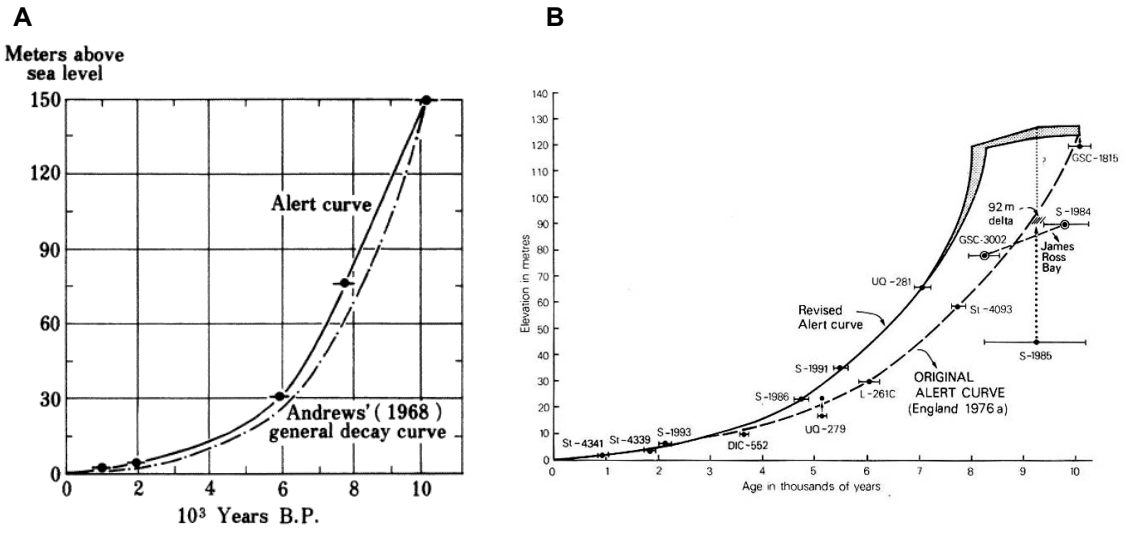

Fig. 2.8 Postglacial RSL curves from High Arctic Canada, showing marked differences in form and speed of initial emergence at different locations; (a) RSL curve from Alert, northern Ellesmere Island (England, 1976a), compared to Andrews' (1968) curve from Baffin Island, southern Arctic Canada; and (b) revised RSL curve, also from Alert, showing significantly slower initial emergence (England, 1983).

The lack of initial rapid emergence was originally considered by England to be a consequence of a limited LGM glacial cover, with glacio-isostatic uplift offset by global eustatic sea level rise. However, sites with slow initial emergence from Spitsbergen (Forman, 1990) and Franz Josef Land (Forman *et al.*, 1996; 1997) occupy areas formerly covered by relatively thick ice of the Barents Sea Ice Sheet (1500 m^2), and so slow initial emergence is not necessarily incompatible with extensive ice cover. This, coupled with geomorphological evidence from Nares Strait (separating Ellesmere Island and Greenland), led England (1999) to revise his earlier work, favouring a large Innuitian Ice Sheet with no full glacial sea. The prominent restricted ice margin within fjords of Ellesmere Island was re-interpreted as a regional stabilization of land-based ice following retreat of marine-based margins (England, 1999).

Such work from the Canadian Arctic provides a useful conceptual framework to consider in the Antarctic context. Changing interpretations of dated raised marine features demonstrates the complexities of RSL reconstruction in formerly glaciated areas. The concept of a full glacial sea is also significant. For example, it is possible that extensive platforms identified across the South Shetland Islands by John and Sugden (1971) may not in fact represent interglacials, but instead could respresent the full glacial marine limit.

2.4.2.2 The morphological approach to RSL reconstruction in the Antarctic

The majority of RSL curves from the Arctic have been chronologically constrained by the radiocarbon dating of driftwood, whalebone, seaweed, marine shells and molluscs incorporated in raised marine features. Using these curves to calculate the amount of emergence at a particular time period then enables the production of regional isobase maps, with isobases joining points of equal emergence. Similarly in the Antarctic, RSL reconstructions have largely relied upon chronologies developed from the radiocarbon dating of shells, bones, seal skin and penguin guano incorporated within raised marine deposits. Raised beaches are observed on numerous ice-free areas around Antarctica, including the Victoria Land coast of the Ross Sea (Baroni and Orombelli, 1991; Kirk, 1991; Hall and Denton, 1999; Baroni and Hall, 2004; Hall *et al.*, 2004), James Ross Island (Hjort *et al.*, 1997), ice-free oases of the East Antarctic coast (Colhoun *et al.*, 1992; Goodwin, 1993; Hayashi and Yoshida, 1994; Berkman *et al.*, 1998; Miura *et al.*,

1998a; 1998b; 1998c), and the sub-Antarctic islands (John and Sugden, 1971; Curl, 1980; Del Valle *et al.*, 2002).

Whilst the study of Antarctic raised beaches represents a major advance in the understanding of deglaciation, and ultimately RSL change and isostatic land uplift, large uncertainties surround the interpretation of the data and its associated RSL reconstructions. For example, (i) the indicative meaning of raised beaches is unclear; beaches may be storm ridges, formed above mean sea level, thus sea level curves may exaggerate total RSL change; (ii) individual beaches may vary in age and altitude between individual embayments; (iii) faunal remains such as penguin guano, bones or shells can be deposited at multiple altitudes both above and below mean sea level and so only provide constraining ages; penguins are also known to travel some distance from the coast and therefore the presence of guano or bones may be unrelated to RSL; and (iv) the assumption is made that the highest raised beach formation is contemporaneous with initial ice retreat. In addition, restrained rebound is likely to occur during the first stage of ice unloading and prior to the formation of beaches (Andrews, 1970), with the persistence of an ice shelf after the retreat of grounded ice preventing beach formation. In this way raised beaches frequently only record the latter stages of isostatic uplift and therefore underestimate former ice volumes (Bentley, 1999; Hall and Denton, 1999). In effect they record the passage of the calving line, not the grounding line.

2.4.3 Isolation basins and RSL reconstruction

In light of the uncertainties surrounding the use of raised marine features for RSL reconstruction, other independent approaches are needed. Isolation basins offer one powerful new method of producing high-resolution RSL data and regional ice sheet histories in Antarctica. Isolation basins are natural rock depressions that may, at various times in their history, be inundated by or isolated from the sea by changes in RSL (Long *et al.*, 1999). Elsewhere, they have been successfully used in sea level reconstruction for many decades, particularly in Scandinavia (Sundelin, 1919; Kjemperud, 1981), and in postglacial emergence studies from the Arctic (Retelle, 1986; Retelle *et al.*, 1989; Snyder *et al.*, 1997). The latter studies are of particular pertinence as they use isolation basins in a similar environmental setting to the SSIs, and make comparisons with isostatic uplift chronologies derived from radiocarbon-dated geomorphological features.

Fig. 2.9 provides a schematic representation of how isolation basins can be used to derive RSL curves.

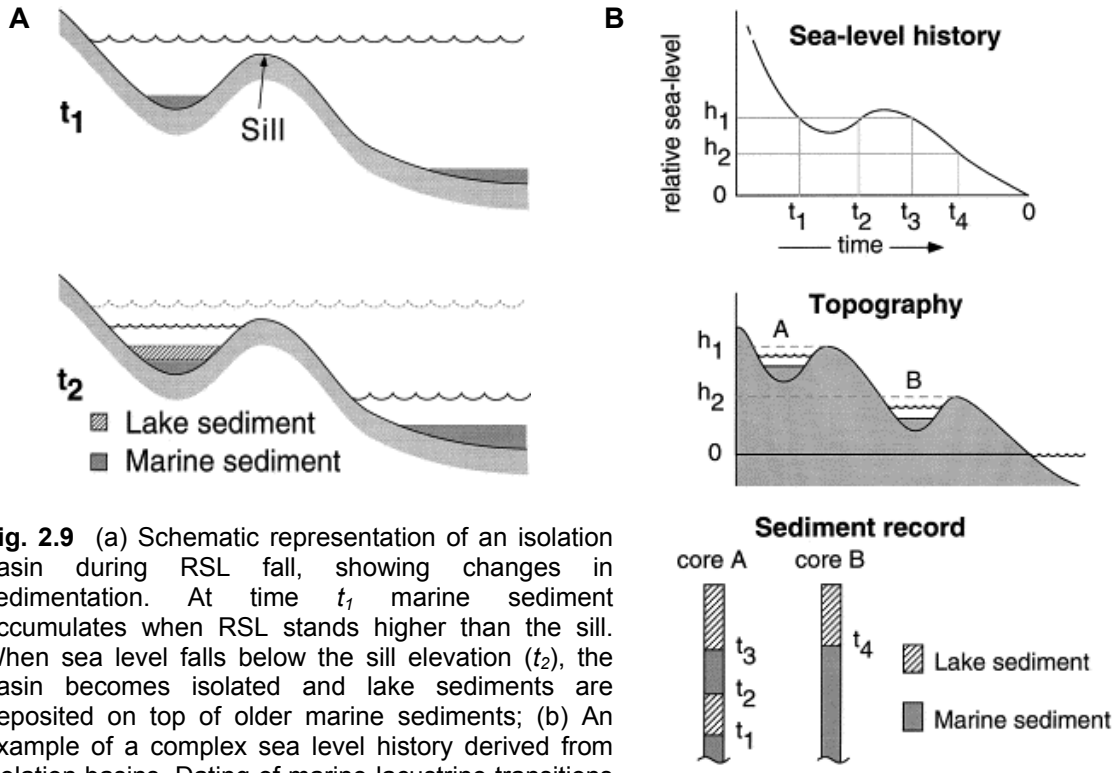

Fig. 2.9 (a) Schematic representation of an isolation basin during RSL fall, showing changes in sedimentation. At time t_1 marine sediment accumulates when RSL stands higher than the sill. When sea level falls below the sill elevation (t_2), the basin becomes isolated and lake sediments are deposited on top of older marine sediments; (b) An example of a complex sea level history derived from isolation basins. Dating of marine-lacustrine transitions at A and B constrain the elevations and ages of sea level highstands and lowstands. Each transition forms a point on the RSL curve (Source: Zwartz et al., 1998).

During sea level highstands, near-shore marine basins will accumulate marine sediment. As RSL falls, basins with submarine sills are progressively isolated from the sea. Initially the basin will be periodically connected to the sea at high tides, therefore allowing marine incursions, and a mix of freshwater, brackish and marine proxies can accumulate in the sediment. Brackish conditions predominate and a halocline may develop due to salinity differences between the fresh and marine water. As RSL falls further eventually the sill becomes raised above the highest tide and the basin becomes completely isolated from marine inundation, and so freshwater sediment accumulates. Consequently, three stratigraphical units are usually identified in isolation basin sequences: a clastic marine unit, transitional brackish unit, and freshwater unit. Three further non-synchronous isolation contacts are also observed: (i) the diatom inferred first isolation contact defining the point at which freshwater first appeared; (ii) the

hydrological isolation contact marking the point at which marine incursions ceased completely; and (iii) the sedimentological isolation contact marking the change from predominantly allochthonous minerogenic sediment of marine origin to autochthonous organic freshwater sediment (Long *et al.*, 1999). As isolation basins often have a rock sill impervious to seawater seepage, changes between marine, freshwater, and transitional environments are preserved in the sedimentology, geochemistry, flora and fauna of isolation basin sediments. By accurate dating of the marine-lacustrine transitions and measurement of the sill elevations, a series of precise RSL index points can be determined including the direction of RSL change. Depending on the rate of RSL change and the tidal range, the nature of marine-lacustrine transitions can vary. Basin isolation will occur fastest where the rate of RSL fall is high and tidal range low, and thus the transitional unit will be thinnest (Long *et al.*, 1999).

Following the early work on Scandinavian isolation basins by Kjemperud (1981; 1986), the isolation basin methodology has been extensively and successfully employed in the northern hemisphere in Scotland (Shennan *et al.*, 1994; 1996; Lloyd, 2000; Shennan *et al.*, 2005), Scandinavia (Eronen *et al.*, 2001; Westman and Hedenström, 2002; Miettinen, 2004; Lohne, 2005; Lohne *et al.*, 2007), Russia (Corner *et al.*, 1999; 2001; Dreßler *et al.*, 2009), and Greenland (Long *et al.*, 1999; 2003; Sparrenbom *et al.*, 2006a, 2006b; Long *et al.*, 2009). These latter studies have advanced the study of near-field RSL histories through the adoption of the sea level index point methodology (Tooley, 1978; Preuss, 1979; Shennan, 1982; van de Plassche, 1986). Using this approach, each sea level index point is ascribed an indicative meaning (vertical relationship between the local environment in which the sea-level indicator accumulated and its contemporaneous reference water level) and tendency (direction of change in water level in terms of an increase or decrease in marine influence). In this way, the isolation basin methodology has four major advantages over the morphological (raised beach) approach to RSL reconstruction in Antarctica, (i) firstly, the relationship between the dated transition and the sea level is clear through identification of the sill (Zwartz *et al.*, 1997); (ii) it provides a tendency of sea level change; (iii) dateable material is more abundant compared to that contained in raised beaches and is *in situ*; and (iv) the need to apply marine reservoir corrections to radiocarbon dates is avoided by the dating of freshwater material immediately above the transition, which is particularly pertinent to

the Antarctic where marine reservoir corrections can be large and often poorly known (Berkman *et al.*, 1998).

2.4.3.1 The Antarctic context

In Antarctica the only isolation basin studies to date are from the Vestfold Hills (Fulford-Smith and Sikes, 1996; Zwartz *et al.*, 1998; Cromer *et al.*, 2005) and Larsemann Hills (Verleyen *et al.*, 2005) in East Antarctica (Fig. 2.10). Isolation basins have also been recognized around the Marguerite Bay area of the Antarctic Peninsula and the South Shetland Islands, although until now have almost exclusively been used in palaeoenvironmental reconstructions (e.g. Schmidt *et al.*, 1990; Wasell and Håkansson, 1992; Björck *et al.*, 1993; Yang and Harwood, 1997; Khim *et al.*, 2004; Tatur *et al.*, 2004; Yoon *et al.*, 2006). The potential of these for sea level research was recognized by Bentley *et al*. (2005a). Using combined interpretation of isolation basin sediments supplemented by morphological evidence, they produced preliminary RSL curves for Marguerite Bay and the South Shetlands (Fig. 2.11; Bentley *et al*., 2005a).

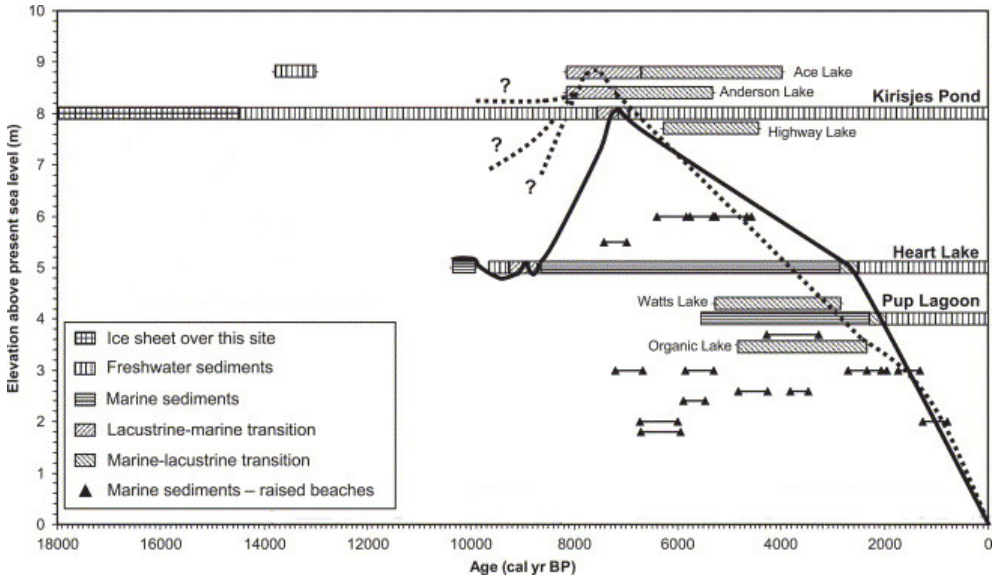

Fig. 2.10 RSL curves for the Larsemann Hills (solid line) and Vestfold Hills (dashed line), East Antarctica, derived from isolation basins. Note the Larsemann and Vestfold Hills are ~100 km apart. Horizontal bars beneath the curve represent marine sediments, and those above the curve represent lacustrine sediments. The Larsemann Hills curve is based on sediment sequences from the isolation basins marked in bold; all other basins contribute to the Vestfold Hills curve (Modified from Zwartz *et al.*, 1998; Verleyen *et al.*, 2005)

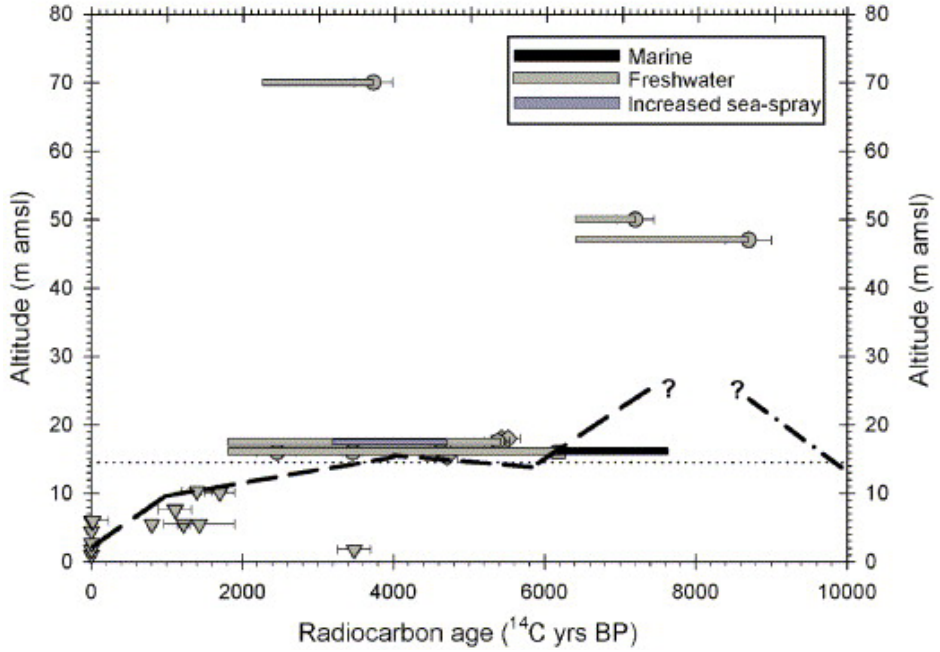

Fig. 2.11 Preliminary RSL curve for the South Shetland Islands derived from previously published data from isolation basins and ^{14}C dating of whalebone (grey triangles) and penguin bones (diamonds) preserved in raised beaches; minima for isolation are shown by grey circles. Data are plotted with 1-sigma error bars for ^{14}C ages and ±0.2 m for altitudes (Source: Bentley *et al.*, 2005a)

However, the preliminary South Shetlands curve revealed a complex and poorly chronologically constrained RSL history. Four general phases of RSL change are propsed: (i) early RSL rise, (ii) early-mid Holocene RSL fall, interrupted by (iii) a mid-Holocene RSL highstand, and (iv) late Holocene RSL fall. However, the date of deglaciation is poorly constrained and the period of early RSL rise remains speculative and undated. The timing and precise height of the mid-Holocene highstand is also unknown. Significantly the curve also differs substantially from the modelled RSL history of Bassett *et al*. (2007; Fig. 2.12). This study highlighted the misfit between sea-level observations from the SSIs and model-based predictions, with models under-predicting the isostatic component of the sea level response and hence maximum ice volume in this region. Likewise poor correlation between observed and predicted late Quaternary RSL changes reported for King George Island in the SSIs by Nakada *et al*. (2000) emphasize the need for further field data to help constrain the RSL history of the region and refine and extend these curves.

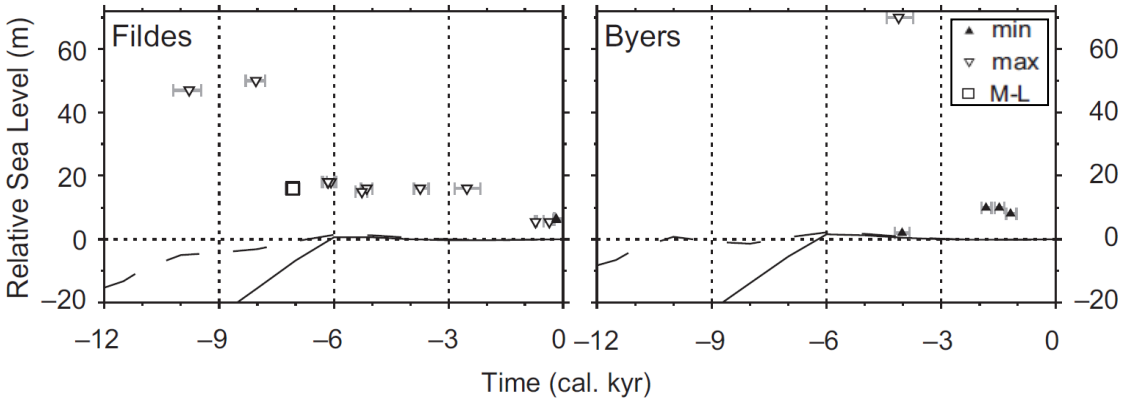

Fig. 2.12 Modelled sea level variations for Fildes Peninsula (King George Island) and Byers Peninsula (Livingston Island). Predictions are based on the reference earth model and two end member meltwater pulse-IA scenarios (both tuned to fit the Barbados sea level record): a sole northern hemisphere contribution (dashed line) and a dominant Antarctic contribution (solid line). Under either scenario the model predictions fail to match the observed RSL response to deglaciation. The symbols identify the type of sea level constraint; shells are interpreted as minimum sea level constraints, whereas seal hairs, penguin guano and remains in ornithogenic soils provide maximum sea level constraints. Isolation basins provide a 'fix' for sea level and are labeled as marine-lacustrine (M-L) (Source: Bassett *et al.*, 2007)

In addition to there being a need to provide field constraints for numerical models, a further part of the rationale for this work is to improve the quality of previously published data. Many of the previous studies on isolation basins do not describe coring methods or analyses in full, and do not present diatom or other data on which their conclusions are based. There are also disagreements in the literature between sill heights of the same basins. For these reasons, there is a need to improve the data quality.

2.4.4 Tectonics

An additional major uncertainty in the RSL curve for the SSIs (Fig. 2.11) is the potential contribution of tectonic uplift. Indeed RSL reconstruction in the SSIs is complicated by their location in a tectonically active region. The islands lie on the northwest flank of the actively-extending Bransfield Strait rift, within which there is active volcanism on Deception Island. The islands also lie close to a slowly-convergent plate boundary, and there are reports of neotectonic features on them (Pallàs *et al.*, 1995; González-Casado *et al.*, 1999). However, whilst the tectonic setting is not ideal for RSL reconstruction, there is an acute lack of ice-free areas around West Antarctica where evidence of changes in RSL can be preserved. Work from the Huon Peninsula, Papua New Guinea, also demonstrates that RSL reconstruction can be successful in tectonically active

areas (Chappell, 1974). Nonetheless, as the tectonic component is a key element of the RSL equation (section 2.4.1) it must not be overlooked. It is therefore necessary to understand the tectonic setting of the South Shetland Islands and to identify a means of quantifying the tectonic contribution to long term RSL change in this area.

2.4.4.1 Nature and importance of neotectonics in the Arctic

Another key outcome from Arctic research has been the recognition of the role of tectonics in postglacial emergence. Important lessons can be learnt from environments with similar styles of deglaciation and tectonic settings. High marine limits of up to 150 m asl on Ellesmere Island (High Arctic) have previously been attributed to late deglaciation (England, 1992). The Holocene onset of deglaciation would mean the countering effect of eustatic sea level rise would already be largely complete, allowing the emergence that followed to proceed with maximum effect, producing high marine limits (England, 1992). However, on Baffin Island (central Arctic) only 80-100 m of postglacial emergence is observed, despite a similar ice retreat history (Andrews, 1980). Therefore late deglaciation alone cannot account for the sizeable emergence observed in the High Arctic. As an alternative explanation, England (1992; 1997) highlighted the importance of tectonics.

Shorelines in glaciated regions rise towards the centres of maximum former ice thicknesses (Jamieson, 1865). Isobases (lines connecting points of equal uplift) therefore outline former centres of ice dispersal and reflect the glacio-isostatic response to glacial unloading. However, isobases drawn on the 8 ka shoreline of Ellesmere Island have an orientation and profile unlike those reported from other glaciated regions (England, 1992, 1997; Fig. 2.13). The isobase ridge of maximum emergence (area A, Fig. 2.13) parallels the regional geological structure and does not conform to the distribution of the last ice load, instead trending in the direction of least former ice cover. The gradient of isobases is also steep, not defining broad cells of uplift as described elsewhere (Andrews, 1970). This observation therefore makes it difficult to reconcile with a solely glacio-isostatic explanation of postglacial uplift, and instead suggests the possibility of a neotectonic component to postglacial emergence (England, 1992, 1997).

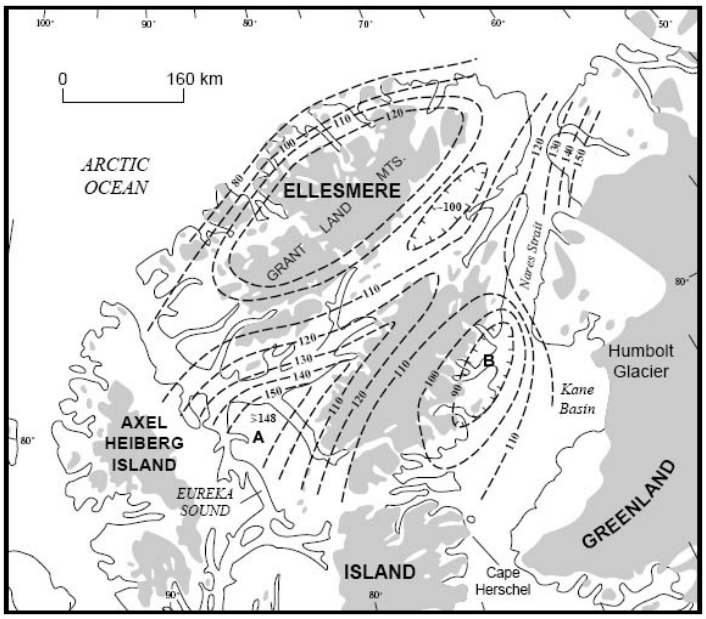

Fig. 2.13 Postglacial isobases drawn on the 8 ka BP marine limits in northern Ellesmere Island. Areas A and B are discussed in the text (Source: England, 1997)

Such a neotectonic component has been documented elsewhere during the deglaciation of central Arctic Canada, where reactivation of the Boothia Horst accounted for 60-120 m of local relief (offset) on the 9.3 ka shoreline (Dyke *et al.*, 1991). Dyke *et al*. (1991) also noted the emergence of Prince of Wales Island (central Arctic) without the delevelling (tilt) of shorelines, which is glacio-isostatically abnormal. They proposed a hypothesis of block tectonics, whereby postglacial rebound of the archipelago involved movement of a mosaic of island-sized blocks, some rebounding and tilting, others rebounding but not tilting. No evidence for similar abrupt displacement is observed on Ellesmere Island, but isobases could record epeirogenic warping (England, 1997). Similar tectonic complications have been reported from Lowther and Griffith Islands (central Arctic) where the spatial pattern of postglacial crustal deformation deviates from a normal glacio-isostatic pattern (Dyke, 1993). Ongoing tectonic uplift is also proposed in other formerly glaciated areas of Fennoscandia (Nesje and Dahl, 1990; Evans and Rea, 2005).

A further notable feature in the isobase pattern of High Arctic Canada is a depression in isobases on eastern Ellesmere Island (area B, Fig. 2.13), coincident with a prominent negative gravity anomaly (Jackson and Koppen, 1985; England, 1992). This gravity

anomaly has been attributed to changes in crustal density or mantle structure, and therefore its precise correlation with the isobase depression provides evidence for the structural influence on the magnitude and pattern of postglacial emergence. The apparent similarity between the proposed isobases and regional geologic structure may potentially be explained by the reactivation of old fault systems by glacial unloading in the Holocene, triggering renewed tectonic uplift (Dyke *et al.*, 1991; England, 1997).

As a consequence, England (1997) cautioned against the assumption that postglacial emergence and RSL change has a universally predictable signature solely portraying former ice loads. Instead, a consideration of tectonics and regional geological structure is necessary. In light of this, and the tectonic setting of the SSIs, a reassessment of raised marine features across the SSIs is required.

2.4.4.2 Tectonic setting of the South Shetland Islands

The South Shetland archipelago is an island arc located at the southwest end of the Scotia Arc (Fig. 2.14), an arcuate alignment of positive relief, mostly submerged, crustal fragments linking the southern South American continent, South Georgia, South Sandwich and South Orkney Islands and the northern Antarctic Peninsula (Dalziel, 1983; Pallàs *et al.*, 1995). The South Shetland archipelago is separated from the Antarctic Peninsula continental shelf by the Bransfield Strait (or Bransfield Basin), a NE-SW trending bathymetric trough (400 km long, 80 km wide, 2 km deep). The Bransfield Basin (BB) is a young and active elongated rift basin. Extension is focused close to the NW margin, giving the basin an asymmetric profile; the islands sit on the footwall of the fault zone that defines the NW margin (Barker and Dalziel, 1983; Barker *et al.*, 2003; Galindo-Zaldívar *et al.*, 2004).

To the northwest of the SSIs, a wide continental platform gives way to the 5 km deep South Shetland Trench (SST). This trench is a remnant of the subduction zone that was active along the entire Pacific margin of the Antarctic Peninsula during most of the past 200 Ma (Lawver *et al.*, 1995; Barker *et al.*, 2003). A series of ridge crest-trench collisions occurred progressively northeastward along the Antarctic Peninsula margin, and at the time of each collision subduction stopped along the part of the margin that was involved (Larter and Barker, 1991). The Hero Fracture Zone (to the south of the SST) marks the northeastern limit of collisions and the boundary between inactive and

active subduction. Slow convergence continues today at the SST (Robertson Maurice *et al.*, 2003), with roll-back of the hinge of subduction inducing extension in the overriding plate and forming the main mechanism of BB opening (Barker, 1982; Barker and Dalziel, 1983; Larter and Barker, 1991; Barker *et al.*, 2003). Seismic reflection data reveal normal faults within the BB are aligned with a NE-SW trend, providing evidence for crustal extension. In addition, multichannel seismic reflection profiles and multibeam swath bathymetry data showing typical convergent margin structures, striking lineated seafloor features and submarine volcanoes (Gambôa and Maldonado, 1990; Larter, 1991; Barker and Austin, 1994; Maldonado *et al.*, 1994; Kim *et al.*, 1995; Lawver *et al.*, 1996), as well as active seismicity (Pelayo and Wiens, 1989; Robertson Maurice *et al.*, 2003) and hydrothermal activity (Klinkhammer *et al.*, 2001) confirm ongoing extension of the BB and active subduction at the SST. The rate of convergence at the SST has varied over the last 30 Ma between 40-60 mm/yr prior to 6.7 Ma to less than 10 mm/yr in the late Pliocene and Quaternary, although precise estimates vary depending on the rate of extension in Bransfield Strait and the timing of the cessation of spreading on the Antarctic-Phoenix ridge (Maldonado *et al.*, 1994). GPS measurements indicate the current rate of extension across the central part of the Bransfield Strait to be 7 mm/yr in a NW-SE direction (Dietrich *et al.*, 2004; Taylor *et al.*, 2008).

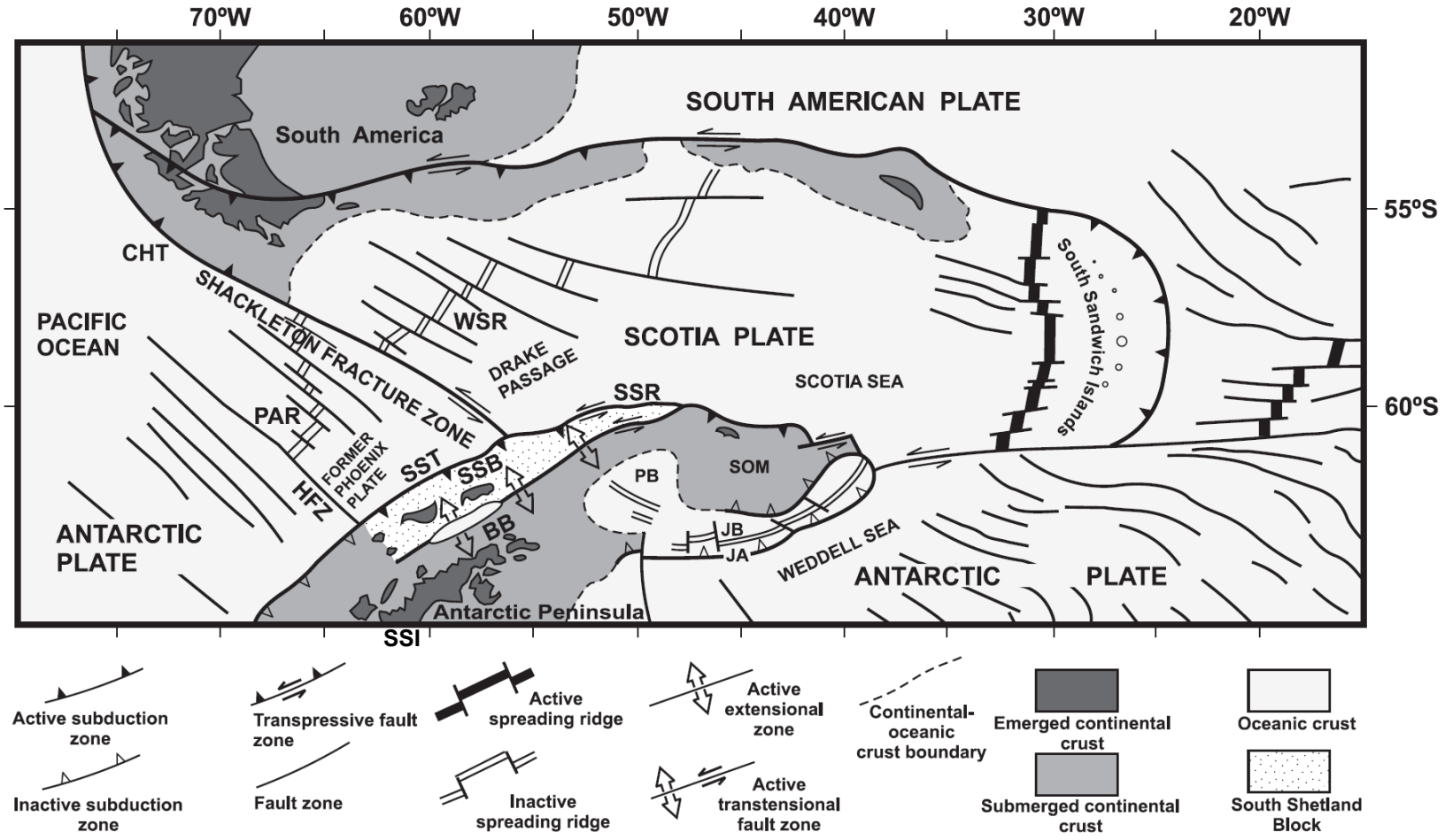

Fig. 2.14 Tectonic setting of the South Shetland Islands. BB - Bransfield Basin; CHT – Chile Trench; HFZ – Hero Fracture Zone; JA – Jane Arc; JB – Jane Bank; PAR – Phoenix-Antarctic Ridge; PB – Powell Basin; SOM – South Orkney microcontinent; SSB – South Shetland Block; SSI – South Shetland Islands; SSR – South Scotia Ridge; SST – South Shetland Trench; WSR – West Scotia Ridge (Source: Galindo-Zaldívar *et al.*, 2004)

2.4.4.3 Long-term tectonic history of the South Shetland Islands

John and Sugden (1971) noted the widespread occurrence of planated surfaces and platforms across the SSIs at altitudes up to 275 m asl. These are interpreted as marine in origin, cut during non-glacial periods (RSL highstands) and subsequently uplifted. They are therefore the product of both sea level changes and tectonic uplift. They are covered by tills corresponding to the last glaciation or earlier glaciations, and have a poorly constrained age of early Miocene to late Pleistocene. However, this age has been assigned purely on the basis of the relationship between the platforms and the geology they cut across (Adie, 1964; Barton, 1965). Attempts to date the formation of these platforms have not yet yielded quantitative chronologic data. For example, based on the principle that each marine terrace relates to one sea level highstand, Pallàs *et al*. (1997) tentatively assigned the ages of the most recent interglacials to increasingly higher platforms where a set of three or more occur at the same locality (Fig. 2.15).

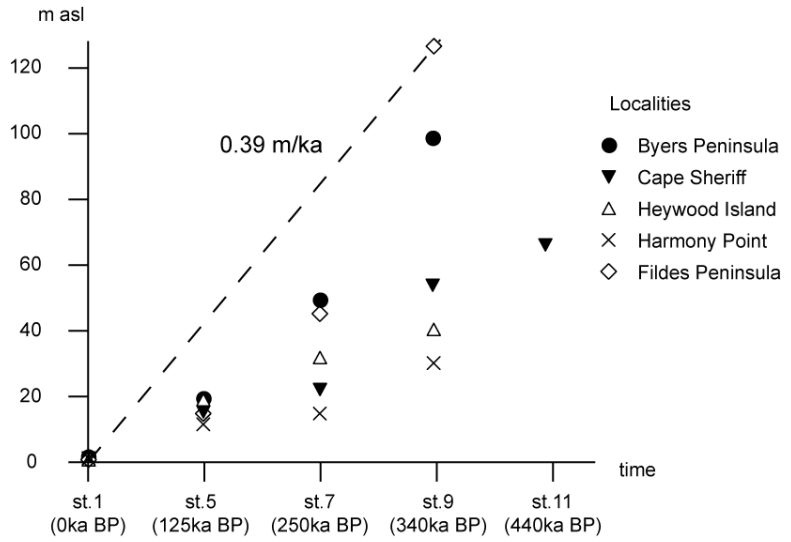

Fig. 2.15 Time/height diagram showing Pallàs *et al*.'s (1997) predicted maximum tectonic uplift rate for the SSIs. The ages of the most recent interglaciations (marine isotope stages 1, 5e, 7 and 9) have been assigned to sets of emerged platforms.

By this method they suggested that the platform at 120 m asl was from MIS 9, thus giving a maximum tectonic uplift rate for the SSIs of ~0.4 m/ka. If this is correct then this is encouraging for the reconstruction of Holocene RSL because it implies that the majority of RSL change in the South Shetlands can be attributed to glacio-hydro-isostatic processes and only a small proportion of uplift to tectonics. An assessment of emerged beach levels on Hurd Peninsula, Livingston Island by Pallàs *et al*. (1995) also

showed no vertical displacement of raised beaches along known fault outcrops and therefore refuted the idea of recent *differential* fault movement in this area. This is an important result as it suggests it is possible to take the broad-scale elevation of the platforms as proxies for long-term uplift. However, the assignment of platforms to interglacials is based purely on assumption, and therefore quantitative dates on platforms are necessary to constrain uplift and test the Pallàs *et al*. model.

A second potential source of error is the assumption that the uplift rate has remained constant through time. Saillard *et al*. (2009) identified similar sequences of marine terraces in the Chilean Andes, but demonstrated that uplift over the Pleistocene has been episodic. They also noted that sequences of preserved terraces did not always record all of the sea level highstands in the marine record. When the uplift rate was high, each sea level highstand resulted in the formation of a new platform at a lower elevation than older platforms; whereas during periods of lower uplift rate, marine erosion predominated and previously formed platforms may have been eroded. Similar variability has been observed at the Cascadia subduction zone (a close tectonic analogue to the South Shetland margin). Here variability in the uplift rate is likely to reflect local structures in the overriding plate (Muhs *et al.*, 1990). The abundance of strike-slip features around the SSIs mean that tectonic uplift here may be similarly episodic. An additional concern is that large earthquakes may have resulted in instantaneous vertical movements of up to several metres. There is evidence that the Cascadia subduction zone is subject to great earthquakes at intervals of several thousand years (Satake *et al.*, 1996), which may have resulted in vertical displacements similar to those associated with the 1964 earthquake in southern Alaska (Plafker, 1965; Shennan, 2009).

It is clear that the tectonic setting of the SSIs is complex and the long-term tectonic uplift history of the SSIs is poorly understood. This forms a key unknown in RSL reconstruction. Studies from the Arctic highlight the interplay between RSL and tectonics, and serve to demonstrate the complexities of reconstructing RSL histories in regions where glaciation interfaces with sea level evidence. Research in the Arctic regarding the potential genesis of high 'marine' features above the marine limit, as well as the recognition of neotectonics in RSL research both provide fundamental insights for Antarctic RSL reconstruction. The fact that the South Shetland crustal block overlies

a zone of magmatism, combined with the probability of continuing tectonic uplift, may well explain the unique assemblage of raised marine features on the SSIs, compared with the rest of the Antarctic Peninsula and sub-Antarctic region. They are unlikely to be explained by purely glaciological processes (Clapperton, 1990). Understanding the magnitude of tectonic uplift is essential for reconstructing the RSL history of the SSIs. The preliminary RSL curve presented in Fig. 2.11 is not corrected for any tectonic contribution to RSL change, but the effect of tectonic uplift could change the vertical height of the curve. In this study an assessment and quantification of the tectonic contribution to RSL change relative to isostatic processes forms a key objective. This will be achieved through the study of platforms and high raised beaches, in terms of their age, altitudinal correlation and possible displacement. A tectonic correction will lead to a more robust RSL curve that can be used to interpret former ice loads over the SSIs.

2.5 Summary

This chapter has reviewed the current literature on Antarctic Peninsula glacial and RSL history, as well as techniques of reconstructing RSL change. The following key conclusions can be drawn from this review:

- Reconstructions of LGM ice volumes and extents over the Antarctic Peninsula and sub-Antarctic islands are inconsistent. Assessments of their contribution to sea level rise during subsequent deglaciation are also frequently poorly constrained and only locally applicable.
- The use of precise RSL data offers great potential for inferring regional ice sheet histories, as well as helping to validate numerical models predicting future ice sheet evolution and RSL change.
- On the South Shetland Islands, John and Sugden (1971) used emerged marine features for isostatic fingerprinting of earlier expanded ice volumes. More recently, the potential of using isolation basin sediments to derive RSL curves as a means of reconstructing former ice volumes and isostatic uplift has been demonstrated by Bentley *et al*. (2005a) and Mäusbacher (1991). Therefore a combined approach is proposed.

- RSL reconstruction is complicated by tectonics. On active plate margins there are complex interactions between sea-level fluctuations and uplift. Consequently, it is important to assess morphological evidence such as marine platforms and high raised beaches in order to understand the 'background' long-term tectonic imprint. This is necessary to correct any new South Shetland RSL curve and assess its applicability on a regional scale.

CHAPTER 3

Isolation basins: field locations, field methods and laboratory techniques

3.1 Introduction

The previous two chapters have provided the background to this study and a review of changes in ice extent and RSL around the Antarctic Peninsula since the LGM. From this review the advantages of reconstructing RSL using a combination of evidence from isolation basin sediments and raised beaches are apparent. The application of both these methods will be presented in the next four chapters. This chapter introduces the work on isolation basins, and has three aims; (i) to describe the physical setting of the field sites and the isolation basins studied; (ii) to describe the field methods, and (iii) to describe and provide the rationale for the laboratory methods.

3.2 Field setting

Fieldwork was conducted between October 2006 and February 2007 across the South Shetland Islands archipelago (Fig. 3.1).

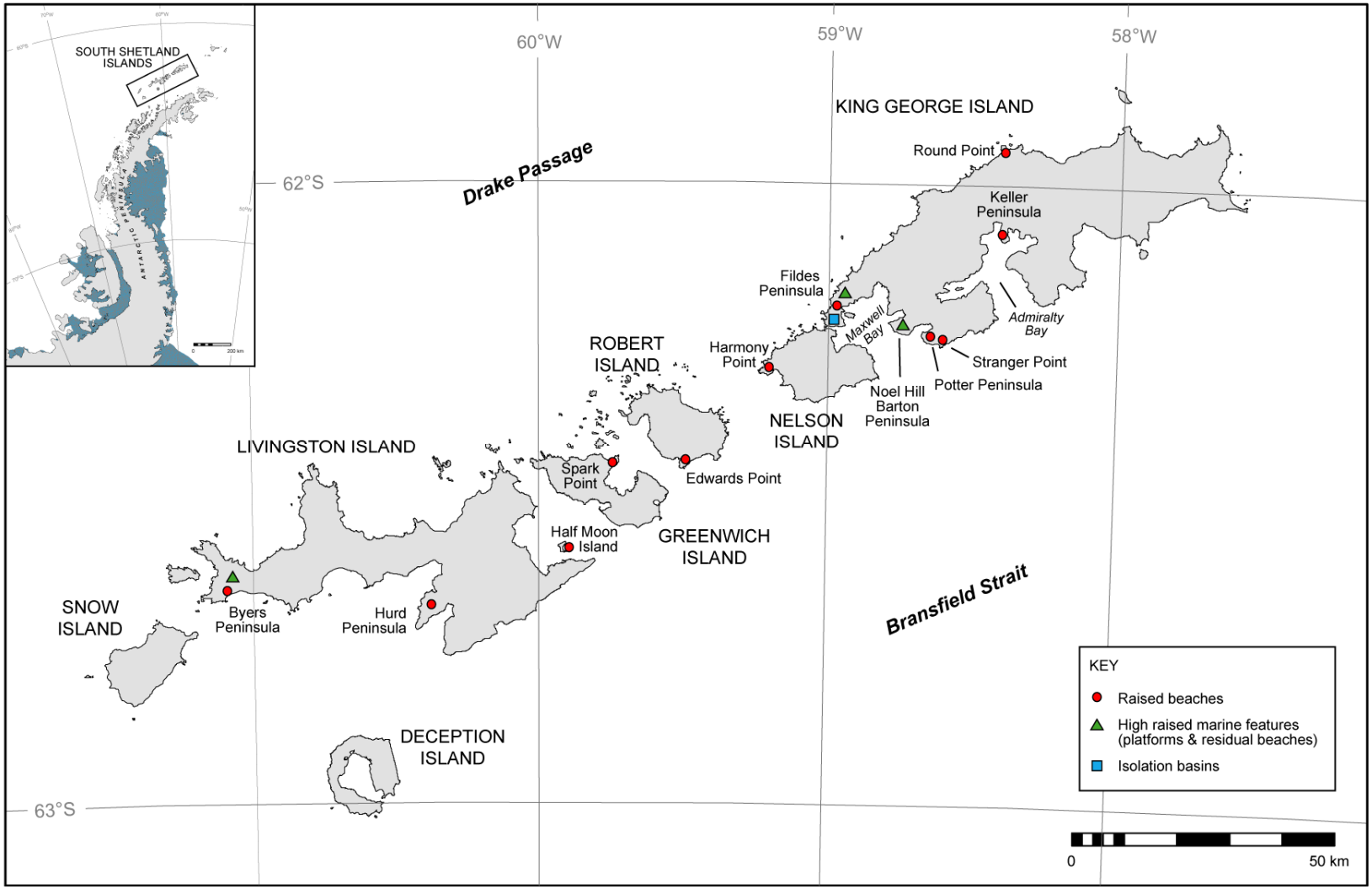

Fig. 3.1 Locations of field sites across the South Shetland Islands

The South Shetland Islands are situated in the maritime sub-Antarctic, around 160 km north of the Antarctic Peninsula, separated from it by the Bransfield Strait, and extending over 500 km. The main group of islands, including the two largest, King George and Livingston Islands, stretch in an arc around 230 km long, but never more than 35 km wide. The islands are extensively covered by ice caps and permanent snowfields, although some low-lying peninsulas are ice free. The largest ice-free area is Fildes Peninsula, King George Island, measuring 38 km^2. The islands rise above a shallow submarine platform. This is particularly extensive on the northern side of the archipelago, extending 40-60 km from the coast. Ice domes tend to drop steeply into ice cliffs with few rocky outcrops. By contrast the continental shelf to the south is much narrower, dropping in a series of faulted steps into the Bransfield Strait within 5 km of the south coasts of the islands (Clapperton, 1990).

As a site of former continental arc magmatism, the islands of the central part of the South Shetland archipelago are mainly composed of volcanic and plutonic rocks of Jurassic to Tertiary age. Older sedimentary rocks also crop out on Livingston Island (Adie, 1964). On King George Island, Jurassic volcanic rocks extend diagonally across the island from the south west to north east. They are flanked to the south by Upper Cretaceous to Tertiary lavas interbedded with plant-bearing sedimentary rocks, subdivided into the Dufayel Island, Ezcurra Inlet, Fildes Peninsula and Point Hennequin Groups and the Polonez Cove Formation (Barton, 1965; Birkenmajer, 1992). Volcanic rocks of Pliocene to recent age are also found along the south coast. These Pliocene lavas are interbedded with a fossiliferous marine conglomerate at Lions Rump. Fildes Peninsula is almost completely composed of andesitic and basaltic lavas, with a few interbedded terrestrial sediments including conglomerates and shales (Smellie *et al.*, 1984).

The islands have a maritime Antarctic climate. The mean annual temperature is -3^{o}C with extremes of 15^{o}C in summer and -30^{o}C in winter (Boyer and Haywood, 2006). Mean summer temperatures on King George Island average 2^{o}C (Anderson, 1999). Meteorological data from King Sejong Station on King George Island record mean annual precipitation of 437 mm, relative humidity of 89% and wind velocity of 7.9 m/s from a westerly direction (Lee *et al.*, 1997). By Antarctic standards, the islands are relatively rich in vegetation, which is dominated by mosses (e.g. *Sanionia uncinata*,

Andreaea spp., *Syntrichia* spp., *Bryum pseudotriquetrum*, *Polytrichastrum alpinum*, *Warnstorfia* spp., *Brachythecium* spp.), lichen (*Usnea* spp., *Caloplaca* spp., *Turgidosculum complicatum*), algae (*Prasiola crispa*) and two species of vascular plants (*Deschampsia antarctica* and *Colobanthus quitensis*) (Lindsay, 1971; Olech, 2002; Peter *et al.*, 2008). Several penguin species breed in large colonies; petrels, skuas, Antarctic shags and seals are also found.

The South Shetland Islands were chosen for study due to (i) their location peripheral to the modern APIS, and (ii) the relative abundance of isolation basins and raised marine features recording past changes in RSL. Very few, if any, other sites exist peripheral to the APIS with such potential for RSL reconstruction. A further advantage of the SSIs is that the geomorphology has been comprehensively described by John and Sugden (1971), and thus it was clear that a rich record of raised marine features is exposed on the islands. Lake coring was carried out on the ice-free Fildes Peninsula on King George Island (Fig. 3.2; Fig. 3.3), chosen primarily due to the cluster of accessible isolation basins at altitudes below 20 m asl (the height of the Holocene marine limit proposed by John and Sugden (1971) and Mäusbacher (1991)). In addition, some palaeolimnological work has previously been conducted on Fildes, meaning many lakes are reasonably well known. However, previous coring has almost exclusively been for palaeoclimatic reconstruction, despite the potential of many of the sites for deriving a RSL history (Bentley *et al.*, 2005a).

Sediment cores were extracted from five lakes on Fildes Peninsula, King George Island, at a range of altitudes above sea level: Yanou (14.5 m above mean sea level, amsl), Long (15 m amsl), Ardley (18 m amsl), Belén (19.9 m amsl), and Gaoshan (34.5 m amsl). Lakes were selected at such a range of altitudes to constrain the preliminary RSL curve produced by Bentley *et al*. (2005a; Fig. 2.11). The highest elevation lake, Gaoshan, is at an altitude significantly above the expected Holocene highstand, but was cored to provide a definite upper limit to RSL. Ardley and Belén were chosen as they are very close to the previously reported marine limit of 20 m amsl (Mäusbacher, 1991). Coring was limited to five basins due to time available. Table 3.1 provides a summary of the lakes cored.

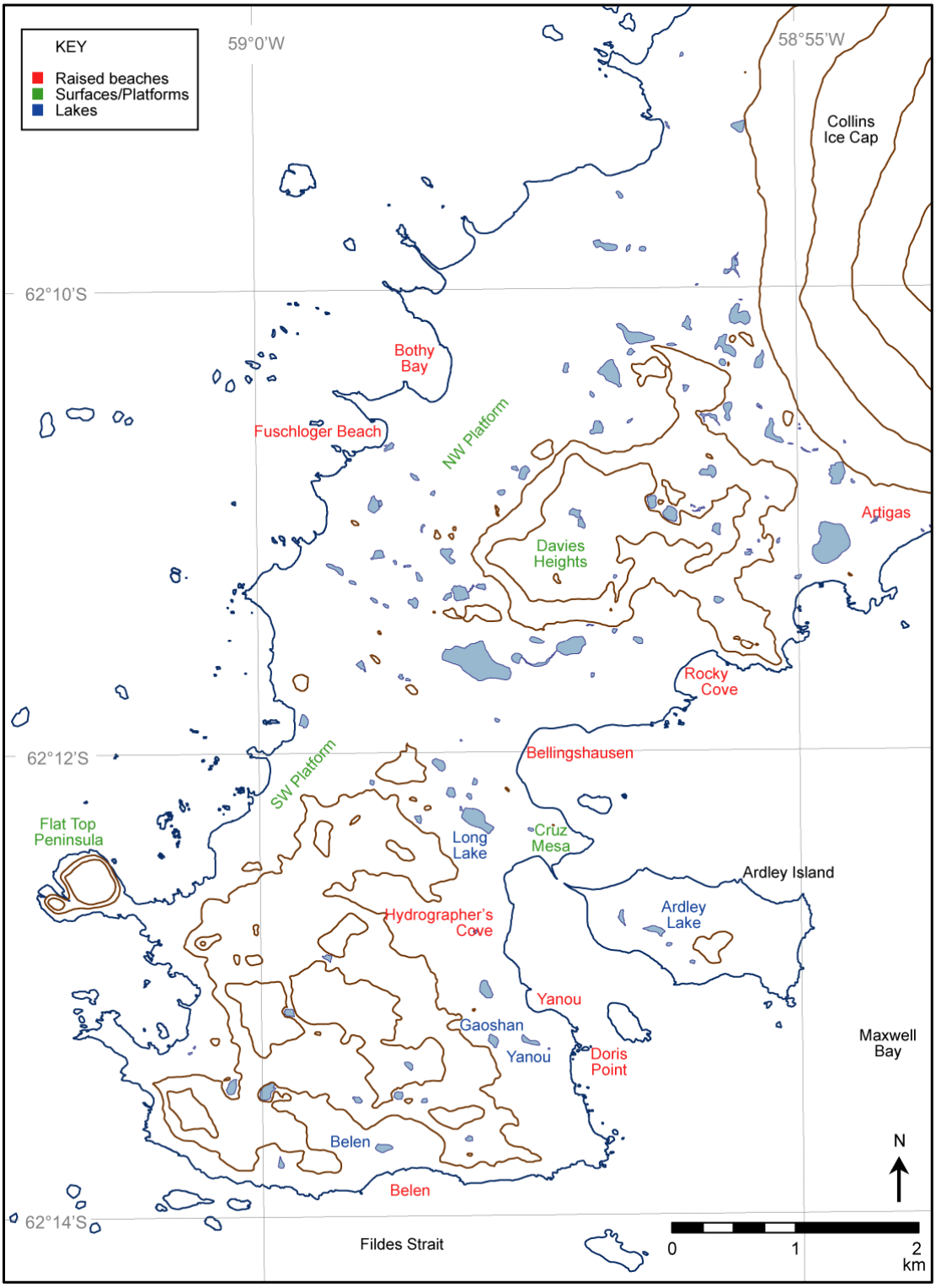

Fig. 3.2 Field sites on Fildes Peninsula, King George Island

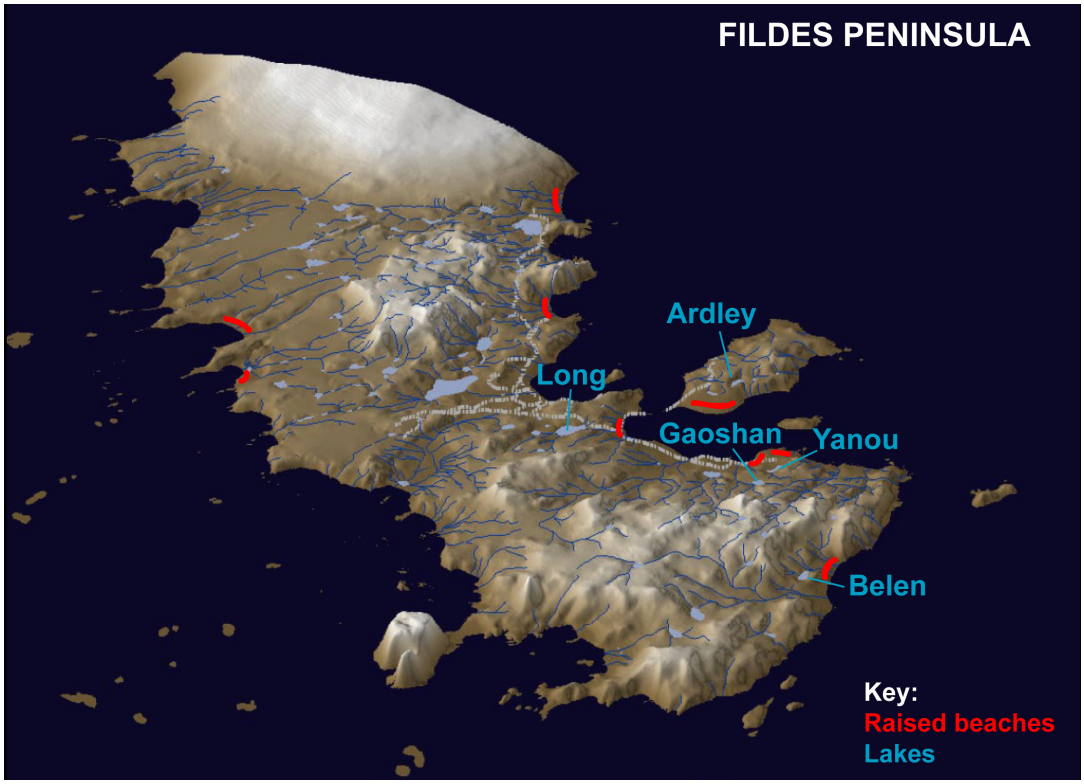

Fig. 3.3 3-D digital elevation model of Fildes Peninsula, showing locations of isolation basins and raised beaches

Lake	Core site location °S	°W	Sill height above mean sea level (m)	Sill height above mean higher high water (m)	Area (m^2)	Maximum water depth (m)	Water depth at core site (m)	Total core length (cm)
Yanou	62°13.243'	58°57.591'	14.5*	14.0*	6370 (4944^)	5.2	4.9	356
Long	62°12.298'	58°58.025'	15.0	14.5	29840	4.6	4.3	725
Ardley	62°12.774'	58°56.398'	18.0	17.5	8542	5.7	5.2	359
Belén	62°13.707'	58°58.917'	19.9	19.4	5898	5.8	4.4	275
Gaoshan	62°13.247'	58°57.881'	34.5	34.0	7173	6.3	6.1	355

Table 3.1 Summary of lakes cored. Sill heights were measured using a Leica kinematic GPS and expressed to the nearest 10 cm (section 3.3.2). Note the sill height of Yanou (*) is an estimated height, see explanation below in section 3.2.1 and Fig. 3.6. Areas were calculated from GPS lake edge tracks, measured using a Garmin 76CSx handheld GPS (the area of Yanou marked with ^ is the area at the end of summer when the lake became ice free and the water level dropped significantly, as described in section 3.2.1). Maximum water depths were measured with an echo sounder; water depths at core sites were also independently measured using a plumb line. Note the echo sounder overestimated the water depth by a constant of 20 cm compared to plumb line measurements, as the sound velocity used by the echo sounder to calculate depth was set to a fixed velocity that was significantly faster than actual velocity when temperatures are below 10°C.

3.2.1 Yanou Lake

Yanou Lake (62°13.243' S, 58°57.591' W, also called Laguna Tern by the Instituto Antartico Chileno (1996), Fig. 3.2, Fig. 3.4 and Fig. 3.5) is a freshwater lake on the southeast of Fildes Peninsula, situated ~500 m from the sea to the east and 400 m from Gaoshan Lake to the west. It measures ~165 m by 70 m, and is 5.2 m at its deepest point. It is bounded to the south and southwest by a steep scree-covered flat-topped bedrock ridge. To the north are a series of raised beaches, the highest at 16.8 m amsl. This highest raised beach was originally taken to be the sill, although the lake level does not reach the crest of the beach and water does not flow out over the top. Two dry 'channelled depressions' bisect the beach, which could mark the position of underground drainage or former lake overspill. The water level of the lake also fluctuates seasonally, with a marked fall observed during the field campaign from November to January as winter lake ice melted (Fig. 3.6c). The lake area decreased by ~1425 m^2 in this time. Such a significant drop in lake level was not observed at any of the other lakes across Fildes and therefore evaporation is ruled out as a cause of water level lowering. Instead this suggests the lake is draining by percolation through the raised beach. It is assumed that during the winter, the raised beach is impermeable due to frozen water in the pore spaces between the gravel; however, when temperatures rise in the summer the ice thaws and allows percolation through the gravel beach (Fig. 3.6b). For this reason the sill height was not taken as the elevation of the crest of the raised beach, but instead the elevation that the lake drained down to at the end of summer is taken to represent the base of the permeable barrier. This provides a maximum constraint as the lake level may have dropped further after the field campaign. The consistent sediment record preserved across the basin proves the lake does not drain completely.

Plotting the GPS data for lake water level reveals further complications in determining the precise sill height. Fig. 3.6a shows the GPS data points available to constrain the height of the lowest lake level. However, there are clearly some inconsistencies in the data, with the two measurements of high lake level taken from the same site differing by 1.15 m. The elevation of 'low' lake level also appears incorrect (too high) in relation to the heights obtained from the raised beach. Fig. 3.4, a photograph taken at low lake level, clearly shows the elevation of this low water level is significantly below the crest of the raised beach. The measurement of high lake level at 15.22 m amsl corresponds

to the elevation measured at the base of the boulder on Fig. 3.4, situated just above high lake level at 15.27 m. Therefore, assuming the highest lake level is ~15.2 m amsl, the lowest lake level must be at least 14.5 m amsl, given the clear elevation difference between the two on Fig. 3.6c. A difference of only 70 cm is a conservative estimate, and therefore 14.5 m amsl is a maximum constraint on the sill height. Given the lake level could also have lowered further after fieldwork was completed, a sill height of 14.5 m amsl is a maximum estimate. This agrees with elevation data from the online SCAR King George Island GIS Project (SCAR KGIS). The same elevation of 14.5 m amsl was also reported as the shore height of Yanou Lake by Yang and Harwood (1997), although they do not specify whether this is the lake shore at high or low water level. Either way, this helps confirm 14.5 m amsl as the maximum elevation of the sill at Yanou.

The lake catchment is dominated by a yellow-green carpet of moss (*Sanionia uncinata*) and cyanobacterial mat. There is human interference to the northwest in the form of vehicle tracks and a former terrestrial coring site ~ 2 m from the lake shore (Yang and Harwood, 1997); the lake is situated around 500 m from the Chinese Great Wall Station to the northwest. The geology of the catchment is dominated by dark green andesitic lavas along the western shore, which grade into lighter, phenocryst-rich bedrock on the eastern and southern shores. Large angular andesitic boulders are found on the northern shore. These have been sorted by frost action into a series of well-developed periglacial polygons approximately a metre in diameter.

Previous studies of Yanou Lake by Yang and Harwood (1997) and Shen *et al*. (1998) both identified a complex sequence of marine-freshwater and freshwater-marine transitions, but did not date these contacts.

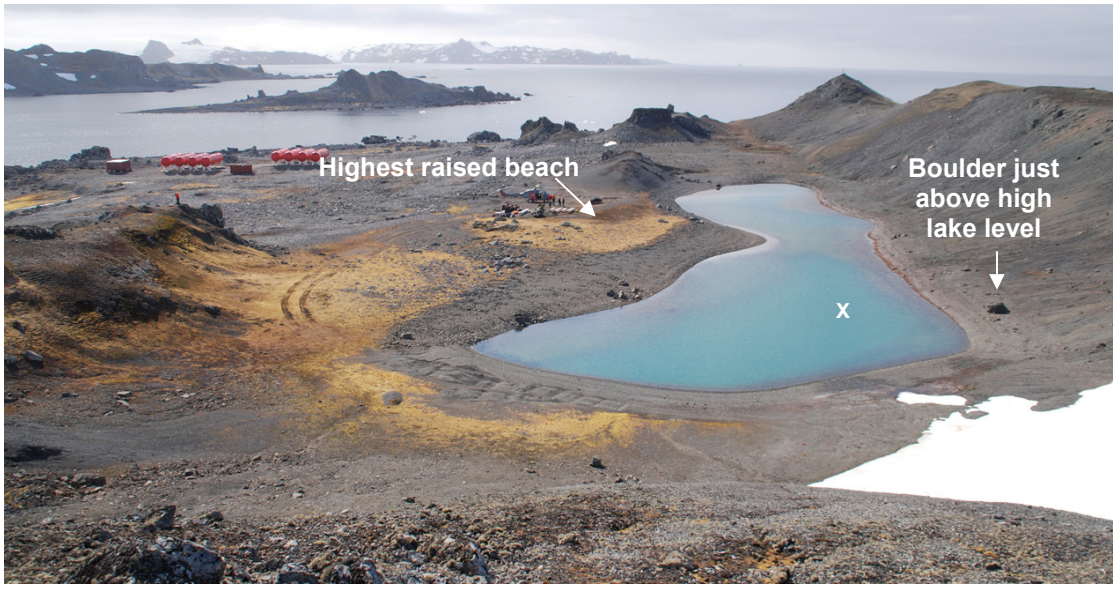

Fig. 3.4 Yanou Lake, looking east. The coring site is marked by the cross; note the brighter colour of the deepest areas of the lake. This is the lowest lake level observed during the field season.

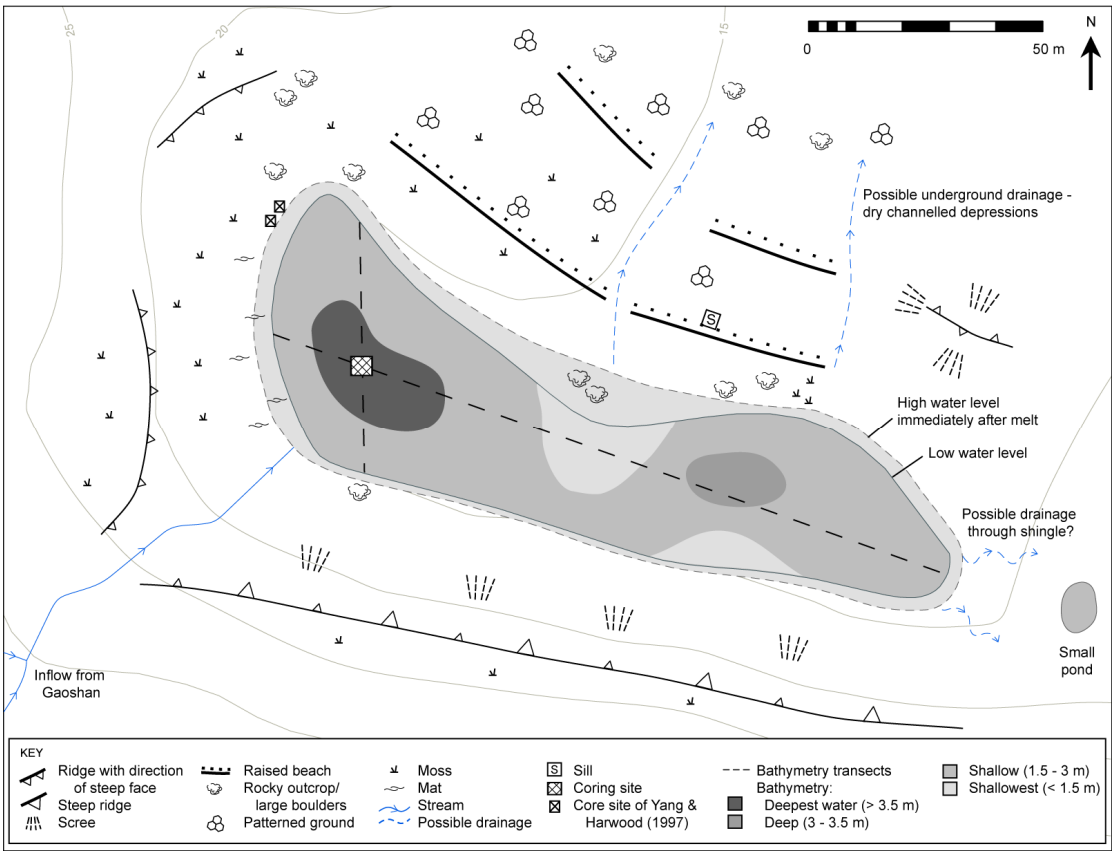

Fig. 3.5 Geomorphological map of the Yanou Lake catchment

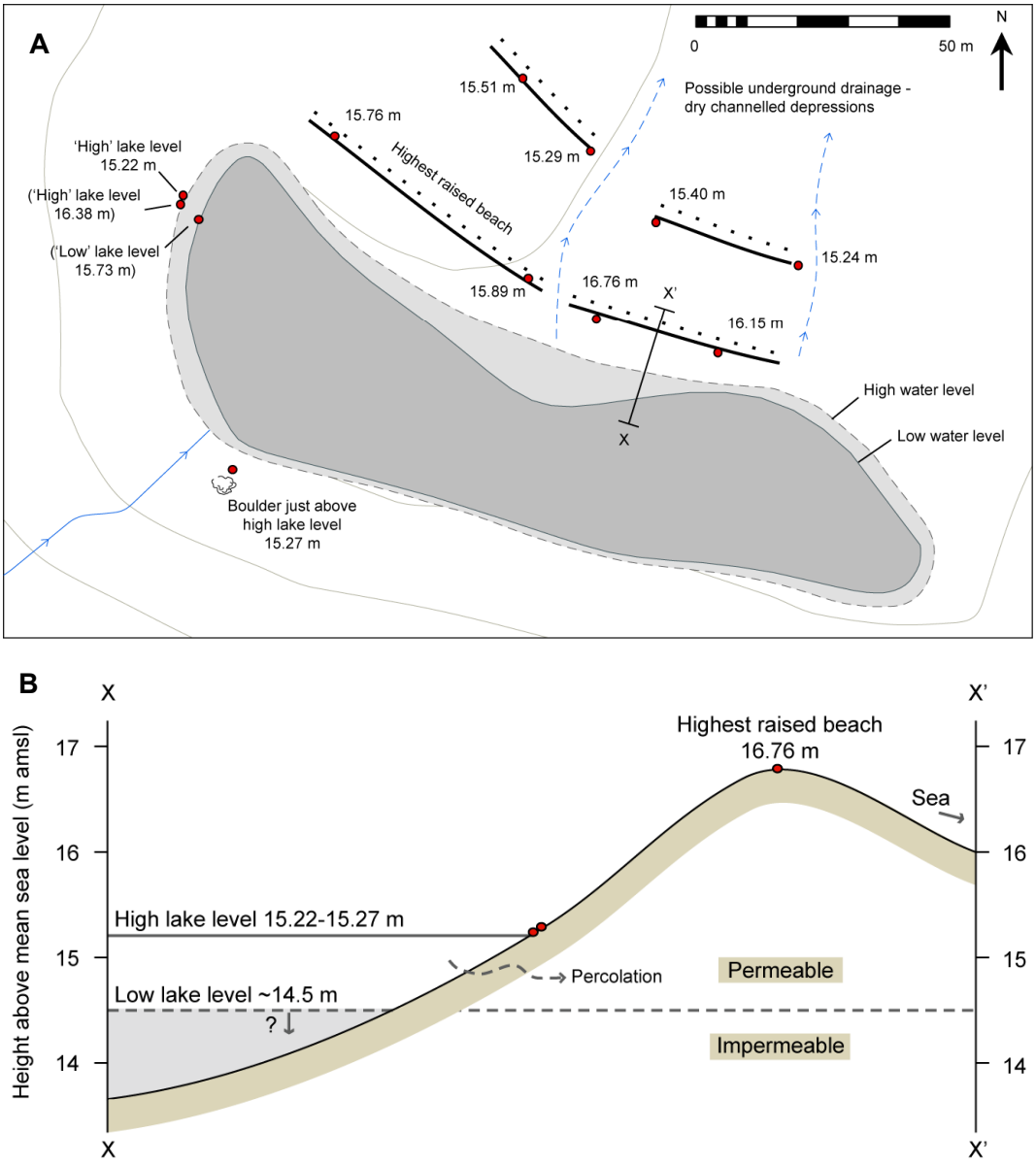

Fig. 3.6 Calculation of the sill height at Yanou, (a) GPS data from the catchment with implications on the sill height (all heights are metres above mean sea level; (b) schematic cross section across X-X' showing the high and low lake levels with respect to the height of the highest raised beach; (c) photograph showing the difference between high and low lake levels, taken at the site where the GPS lake level measurements were taken (rucksack on the high lake level for scale).

3.2.2 Long Lake

Long Lake (62°12.298' S, 58°58.025' W, also termed Langersee by Mäusbacher *et al*. (1991) and Ozero Dlinnoye by Govorukha and Simonov (1973), Fig. 3.2, Fig. 3.7 and Fig. 3.8) is a large freshwater lake situated on the eastern-central sector of Fildes Peninsula, 700 m from the sea to the southeast. It lies in the downstream end of a meltwater channel, which is a relic of a subglacial drainage system. It is the largest of the lakes studied, measuring 295 m long and 140 m wide at its maximum, 4.6 m at its deepest. During winter the lake is covered by 50 cm thick ice (Martinez-Macchiavello *et al.*, 1996); during summer, the ice-free lake is fed permanently by a small stream flowing in from the northwest along the relic meltwater channel. The outlet is across a bedrock sill at the southeast end of the lake at 15 m amsl (Fig. 3.7b).

Fig. 3.7 Long Lake, (a) looking north; the cross marks the core site; (b) outflow and sill.

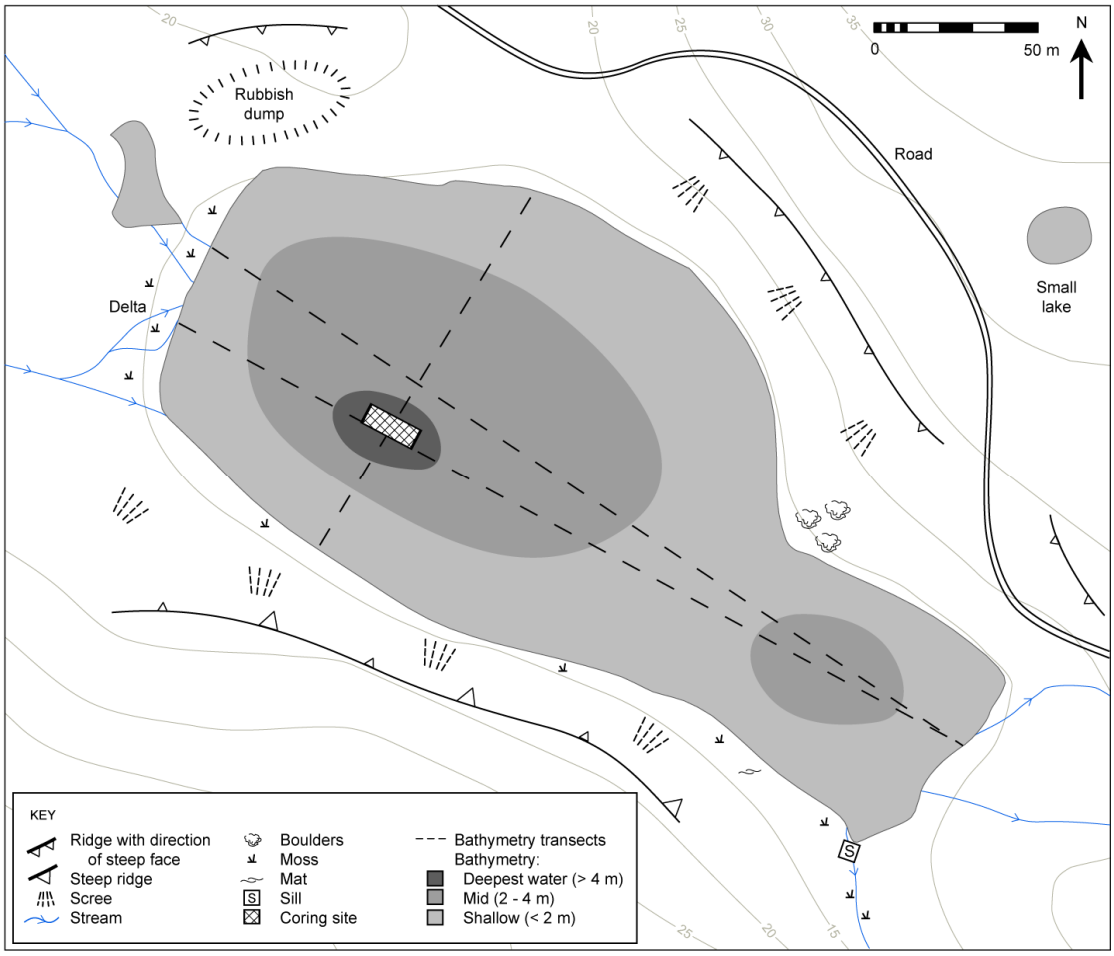

Fig. 3.8 Geomorphological map of the Long Lake catchment area

The catchment is heavily disturbed by human activity; the lake is situated 1 km from the Chilean Frei Base and a gravel road runs along the east side of the lake. The northeastern shore and bedrock ridge above it is littered with rubbish, including broken glass and building materials. Where there is less human influence, moss (*Sanionia uncinata*) and lichen (*Usnea antarctica*) grow on the shore. The geology of the catchment is varied, with heavily eroded andesitic volcanic lavas and agglomerate outcrops.

Previous studies of Long Lake come from Mäusbacher (1991), Martinez-Macchiavello *et al*. (1996) and Tatur *et al*. (2004), who all identified a marine-freshwater isolation contact. Khim *et al*. (2004), Yoon *et al*. (2006) and Lee *et al*. (2008) provided paleoproductivity and palaeoclimatic reconstructions for the Holocene.

3.2.3 Ardley Lake

Ardley Lake (62°12.774' S, 58°56.398' W, also called Ardleysee (Mäusbacher *et al.*, 1989), Laguna Ripamonti (Instituto Antartico Chileno, 1996), and Yue Ya Hu (SCAR, 2009), Fig. 3.2, Fig. 3.9 and Fig. 3.10) is a freshwater lake on the southwest of Ardley Island in Maxwell Bay. Ardley Island is connected to Fildes Peninsula in the west by a tombolo (~3 m wide) at low tide. The lake measures 160 m by 130 m, and is 5.7 m at its deepest. It is bounded to the north by a high steep scree-covered ridge, which shelves steeply into the lake basin, and a more subdued bedrock ridge to the east. To the south is a relatively steep mound, scree-covered with boulders at the base. During periods of high lake level, there is an outflow from the southeast, flowing over a narrow till-mantled bedrock sill at 18 m amsl. This outflow dries up around a month after the winter lake ice has completely melted. During very high water levels there is the possibility of an outflow from the west, although this was never observed during the fieldwork period. The lake receives no inflow, although a dry 'channelled depression' runs in to the east, possibly marking an underground inflow or former inflow stream. The lake is situated ~30 m inland from a well-defined flight of raised beaches, and the lake sill is 1.4 m higher than the highest beach level.

Fig. 3.9 Ardley Lake, looking northwest. The small boat marks the position of the core site (Photograph by S. Roberts)

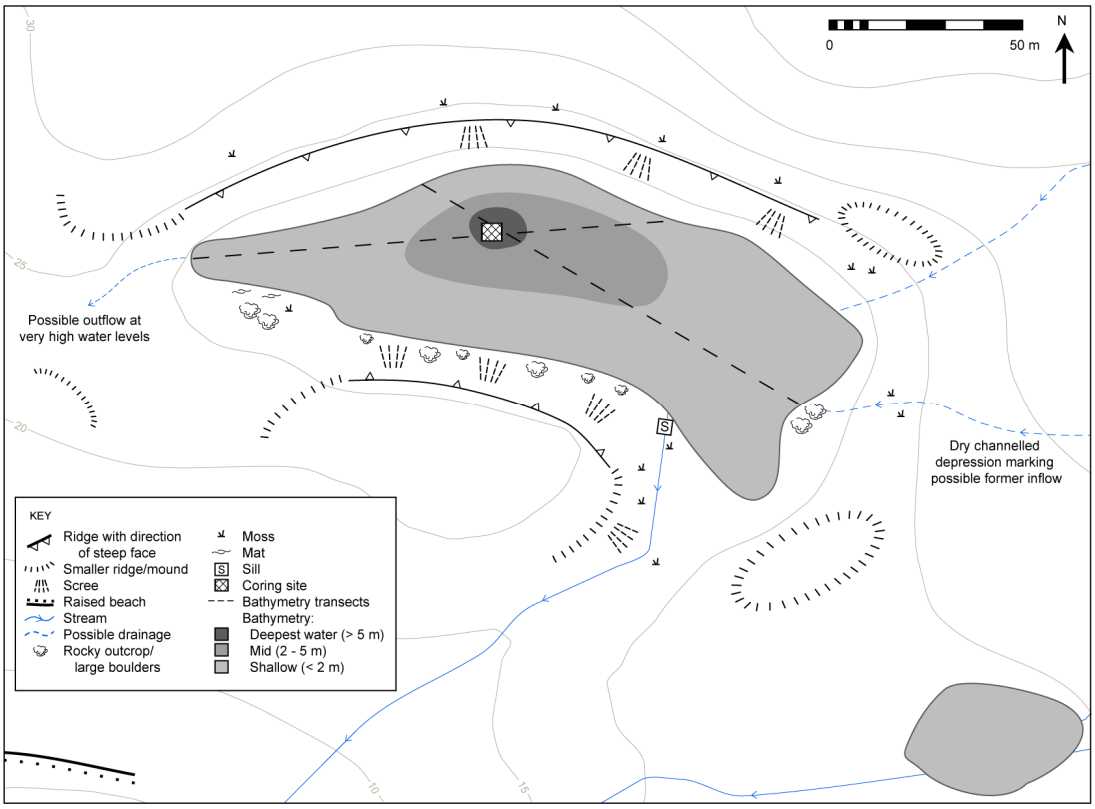

Fig. 3.10 Geomorphological map of the Ardley Lake catchment

The geology of the catchment is predominantly andesite and basalt-andesite bedrock, which has been heavily weathered in many places. Mosses (*Sanionia uncinata*, *Andreaea* spp.), lichens (*Usnea antarctica*, *Himantormia* spp.) and the vascular plant *Deschampsia antarctica* are present all around the catchment. There is no evidence of human activity.

Mäusbacher (1991) cored Ardley Lake and found an entirely freshwater sequence, and so concluded the elevation of the sill marked the postglacial marine limit (20 m). The only other sediment core studies from Ardley Island are from smaller lagoons on the island and have focused on reconstructing late Holocene penguin populations and bacterial communities to infer possible climate change and pollution (e.g. Sun *et al.*, 2000; Liu *et al.*, 2005; Li *et al.*, 2006; Liu *et al.*, 2006; Wang *et al.*, 2007).

3.2.4 Belén Lake

Belén Lake (62°13.707' S, 58°58.917' W, Fig. 3.2, Fig. 3.11 and Fig. 3.12) is a freshwater lake on the south of Fildes Peninsula, measuring ~170 m by 60 m, with a

maximum water depth of 5.8 m. It is situated behind a series of raised beaches and lies around 300 m from the sea to the south. It is bounded by a steep scree-covered ridge to the south and a steep mountain ridge lies 400 m to the north. The lake receives an inflow from the north, which forms a delta as it enters the lake. An outflow exists to the east, flowing over a clearly defined gravel-mantled bedrock sill at 19.9 m amsl (Fig. 3.12c) and down to the sea, cutting through the raised beaches. The sill is 1.6 m above the highest raised beach level. A braided stream flowing down from the mountains to the north joins the outflow, although does not actually enter the lake.

The geology of the catchment is predominantly andesite with several basaltic dykes present, some plagioclase phenocryst-rich. Yellow-green carpet moss (*Sanionia uncinata*) and cyanobacterial mat are present all around the catchment. There is no evidence of human activity. There are no records that this lake has been cored before.

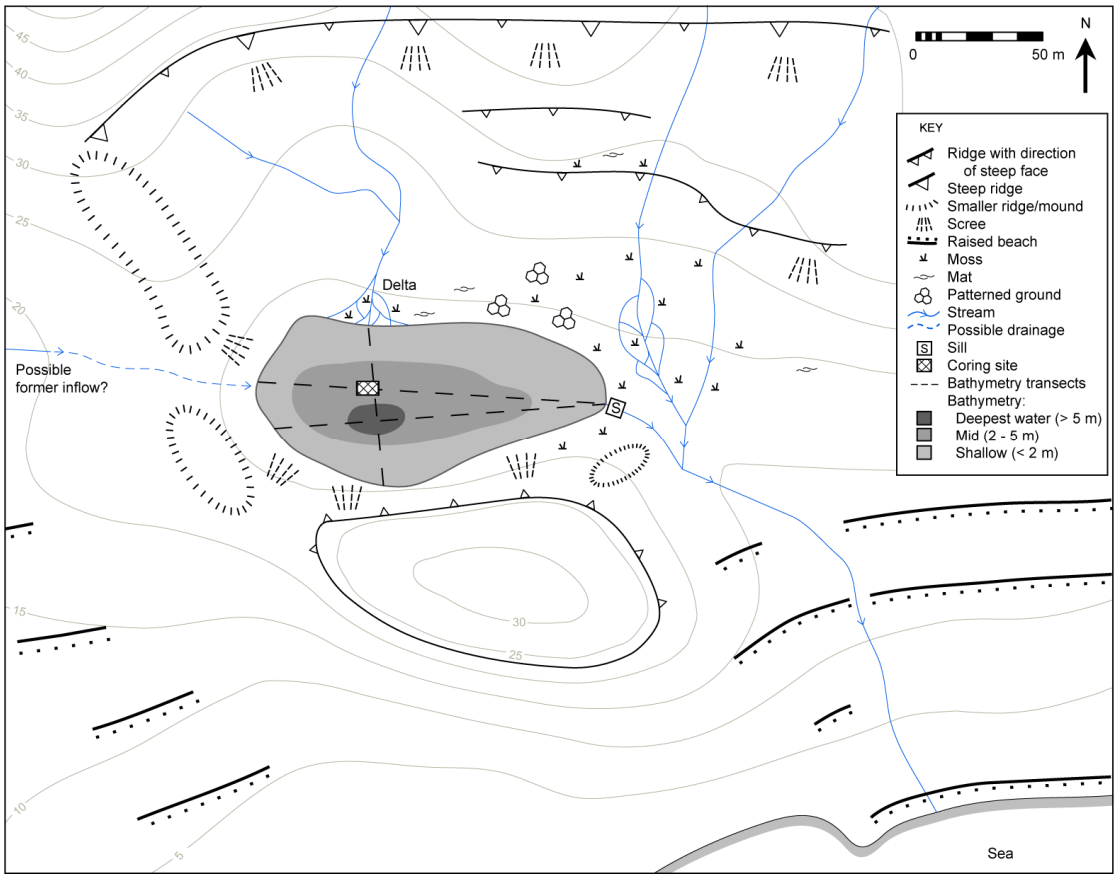

Fig. 3.11 Geomorphological map of the Belén Lake catchment

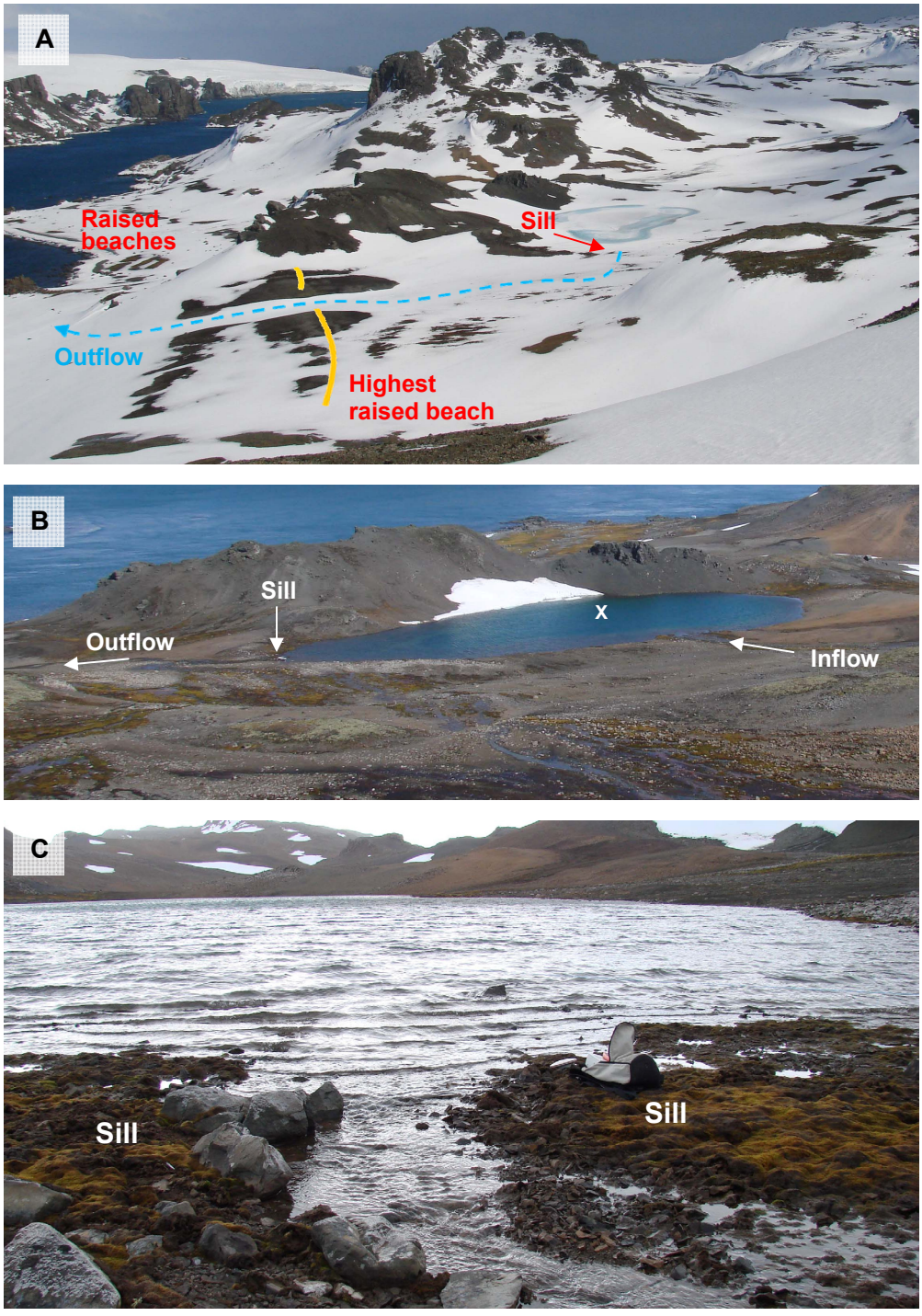

Fig. 3.12 Belén Lake (a) looking southwest showing its position behind a series of raised beaches; (b) looking south; the cross marks the core site; (c) outflow flowing out over the sill at 19.9 m amsl

3.2.5 Gaoshan Lake

Gaoshan Lake (62°13.247' S, 58°57.881' W, also called Lake Shanhaicuan by the Instituto Antartico Chileno (1996), Fig. 3.2, Fig. 3.13 and Fig. 3.14) is a freshwater lake on the southeast of Fildes Peninsula, situated ~1.3 km inland and 400 m from Yanou Lake to the east. Clement Hill (155 m amsl) lies to the west, with several smaller mounds to the south and northeast. The lake measures ~130 m by 70 m, and has a maximum water depth of 6.3 m. It is fed by two inflows from the northwest and south, and has an outflow to the sea across a till-mantled bedrock sill to the north at an elevation of 34.5 m amsl. The height of this sill could have changed slightly due to sediment movement as the sill is situated on a delta. However the change in sill height is assumed to be in the order of a few tens of centimetres and therefore will not affect the RSL reconstruction, as this altitude is well above the expected Holocene highstand. There is another till-mantled bedrock sill to the southeast at 39 m amsl, although the lake only overflows this sill during high lake levels and periods of thaw.

Carpet moss (*Sanionia uncinata*), lichen (*Turgidosculum complicatum*), and cyanobacterial mat are present around the inflow and outflow on the north shore. To the northeast the ground is periglacially reworked and overlain by soft till. The geology of the catchment is predominantly heavily weathered andesite and some basalt-andesite bedrock, covered by several metres of thick scree deposits. Human interference is observable in the form of small storage huts to the east, and the lake is situated 500 m from the Chinese Great Wall Base. There are no records that this lake has been cored before.

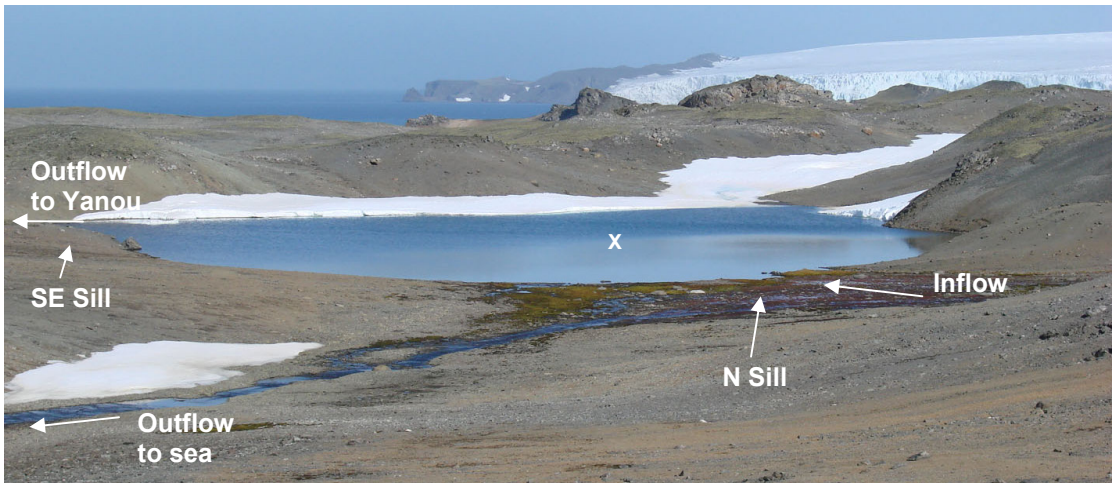

Fig. 3.13 Gaoshan Lake looking south. The coring site is marked by the cross.

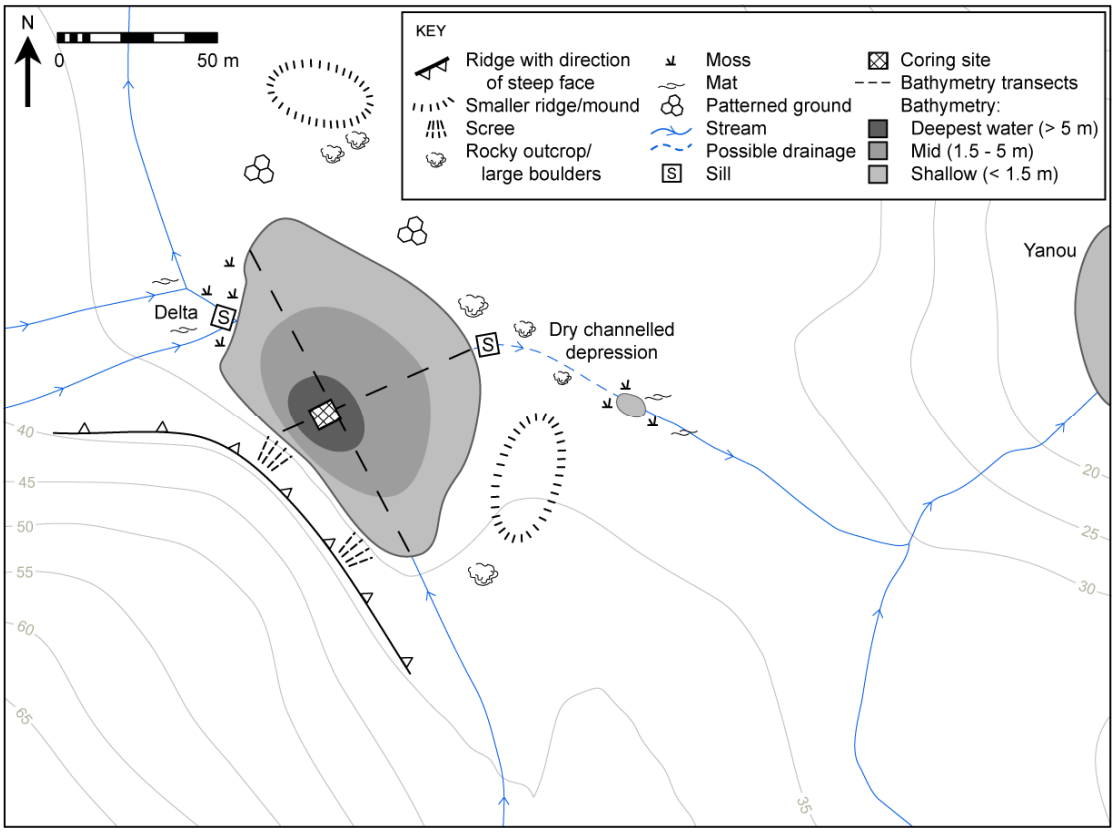

Fig. 3.14 Geomorphological map of the Gaoshan Lake catchment

3.3 Field methods

Fieldwork was conducted between October 2006 and February 2007 with colleagues from Durham University and the British Antarctic Survey (E. Watcham, S. Roberts, P. Fretwell, D. Hodgson, M. Bentley, B. Maltman, L. Homer). The following section describes the field methods employed.

3.3.1 Site survey

At each lake, core sites were identified from bathymetric surveys. Where lakes were ice free (Long, Belén) the deepest part of the basin was found using fixed lines, echo sounder and GPS. Where lakes were ice covered (Yanou, Ardley, Gaoshan), echo sounding was done along transects through holes drilled through the ice using a motorized Jiffy ice drill. Full bathymetric surveys from boats were then conducted later in the season when the lake ice had melted. Cores were drilled at the sites of deepest

water, with the exception of Belén, where the sediments in the deepest part of the basin contained coarse clasts that prevented core penetration. This is likely to be due to the close proximity to the steep scree slope to the south (Fig. 3.11, Fig. 3.12b).

3.3.2 GPS surveying of sill heights

The isolation basin technique for reconstructing RSL histories requires precise measurement of the altitude of the basin sill. As this is a remote area of Antarctica with poor map and benchmark control, a high-precision Leica kinematic GPS was used to precisely measure sill altitudes. Measured altitudes from the GPS were expressed relative to the WGS-84 ellipsoid, and then subsequently reduced to mean sea level using tidal height data for Ardley Cove obtained from TideWizard software (TideWizard, 2009). Timed tide readings were taken at six sites along the east coast of Fildes Peninsula in order to obtain an average measurement of the relationship between the ellipsoid and mean sea level, and account for any differences in tidal range or atmospheric pressure. Sill heights were also calculated relative to mean higher high water (MHHW), as the indicative meaning of isolation basins is taken to be MHHW, with the diatomological isolation contact assumed to equate to MHHW (Shennan *et al.*, 1994; Long *et al.*, 1999). MHHW is the equivalent to mean high water of spring tides (MHWST) as used in the UK.

The GPS unit was left running for a minimum of 30 minutes to ensure positional accuracy. The potential error associated with the GPS is ~2 cm, and since the sills are on bedrock (with the exception of Yanou) that has undergone negligible erosion since isolation, sill heights are assumed to be accurate to the nearest 10 cm. The situation at Yanou is more complex (as described in section 3.2.1) with the sill only impervious to seepage during the winter. Consequently a greater error is associated with this sill height measurement.

3.3.3 Sediment coring

Sediment cores were taken using either a UWITEC cable-operated piston corer at accessible sites or a Livingston corer (either off boats or standing on ice) at more inaccessible locations (Fig. 3.15). Coring stopped in consolidated sediment or coarse gravel, both preventing further penetration. Livingston cores were logged in the field immediately after extrusion, and were then frozen. UWITEC cores were sealed

immediately in the core barrel and frozen as soon as possible after recovery to prevent disturbance in transit. UWITEC cores were logged back in the laboratory when the core liners were cut open for sub-sampling.

Surface cores were also collected at each lake using a Russian or UWITEC short (1.2 m) gravity surface corer, in order to accurately capture the water-sediment interface. At Long and Belén a transect of surface cores was collected in order to determine the change in surface sediment characteristics with water depth, as well as distance from lake inflows/outflows. Surface cores were sectioned at 1 cm intervals in the field, stored in small Whirlpak sample bags and frozen. Table 3.2 provides a summary of all cores collected.

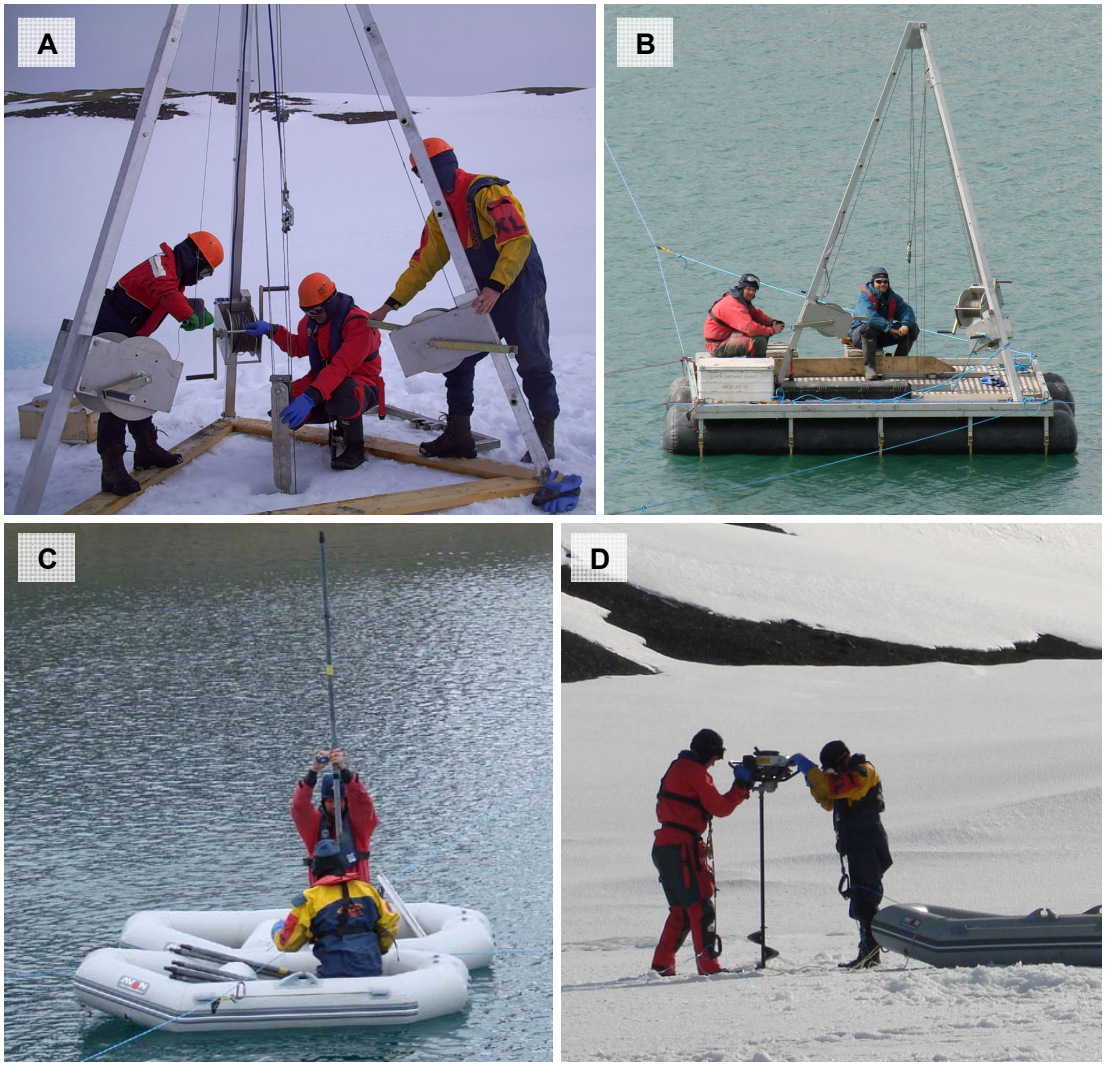

Fig. 3.15 Coring techniques (a) UWITEC coring on ice-covered Yanou Lake; (b) UWITEC coring on ice-free Long Lake; (c) Livingston coring from boats at Belén; (d) Jiffy ice drilling.

Lake	Core site location °S	°W	Coring type	Core code	Core length (cm)	Stratigraphic depth (cm)	Water depth at core site (cm)
Yanou	62°13.243'	58°57.591'	UWITEC	8A-I	100	0-100	490
			UWITEC	8A-II	85	100-185	
			UWITEC	9B-I	99	153-252	
			UWITEC	9B-II	87	252-339	
			UWITEC	8B-I	100	218-318	
			UWITEC	8B-II	38	318-356	
	62°13.241'	58°57.603'	Livingston	2A	59	0-59	459
			Livingston	3A	42	0-42	478
	62°13.241'	58°57.603'	Russian	1	32	0-32	459
			Russian	2	34	0-34	
Long	62°12.298'	58°58.025'	UWITEC	1A	75	0-75	417
			UWITEC	1B-I	95	60-155	
	62°12.294'	58°58.037'	UWITEC	1B-II	86	155-241	
			UWITEC	2A-I	100	0-100	423
			UWITEC	2A-II	73	100-173	
			UWITEC	2B-I	95	150-245	
			UWITEC	2B-II	48	245-293	
			UWITEC	2C-I	99	277-376	
			UWITEC	2C-II	87	376-463	
			UWITEC	2D-I	85	445-530	
			UWITEC	2D-II	100	530-630	
			UWITEC	3A-I	98	537-635	
			UWITEC	3A-II	90	635-725	
	62°12.294'	58°58.030'	U-surface		7.5	0-7.5	427
	62°12.336'	58°57.868'	Russian	S-A	23	0-23	60
	62°12.330'	58°57.891'	Russian	S-B	35	0-35	144
	62°12.337'	58°57.913'	Russian	S-C	17	0-17	143
	62°12.321'	58°57.936'	Russian	S-D	44	0-44	171
	62°12.317'	58°57.965'	Russian	S-E	49	0-49	241
	62°12.314'	58°57.981'	Russian	S-F	43	0-43	278
	62°12.309'	58°58.012'	Russian	S-G	41	0-41	409
	62°12.302'	58°58.033'	Russian	S-H	42	0-42	438
Ardley	62°12.774'	58°56.398'	Livingston	1A	86	0-86	519
			Livingston	1B	66	76-142	495
			Livingston	1C	96	110-206	485

Lake	Core site location °S	°W	Coring type	Core code	Core length (cm)	Stratigraphic depth (cm)	Water depth at core site (cm)
Ardley	62°12.774'	58°56.398'	Livingston	1D	100	189-289	485
			Livingston	1E	84	275-359	485
			U-surface		10	0-10	477
Belén	62°13.719'	58°58.922'	Livingston	1A	30	0-30	571
			Livingston	2A	52	0-52	560
	62°13.707'	58°58.917'	Livingston	3A	69	0-69	440
			Livingston	3B	89	67-156	440
			Livingston	3C	90	109-199	
			Livingston	3D	94	181-275	
			Livingston	3E	40	237-277	
	62°13.696'	58°58.918'	Livingston	4A	40	0-40	250
Gaoshan	62°13.247'	58°57.881'	Livingston	1A	44	15-59	582
			Livingston	1B	86	0-86	
			Livingston	1C	66	0-66	
			Livingston	1D	65	67-132	
			Livingston	1E	91	73-164	
			Livingston	1F	85	129-214	
			Livingston	1G	94	144-238	
			Livingston	1H	70	228-298	
			Livingston	1I	92	239-331	
			Livingston	1J	34	321-355	
			U-surface		14	0-14	566
	62°13.279'	58°57.841'	U-surface	A	1	0-1	50
	62°13.264'	58°57.857'	U-surface	B	1	0-1	232

Table 3.2 Details of the 59 cores collected (total length of cores collected = 38 m)

3.3.4 Limnology

Limnological variables were measured in order to understand contemporary analogues. Vertical profiling of lake water conductivity, temperature, oxygen saturation, pH and salinity were measured using a YSI MDS 600 water quality meter. Light penetration in the water column was measured using a Skye Spectrosense meter with UV-A, UV-B and PAR (Photosynthetically Available Radiation) sensors. Measurements were made both up and down the water column and light readings were taken until values fell to

approximately 1% of the irradiance measured directly below the water surface. The vertical light attenuation coefficient was calculated using standard methods (Kirk, 1994; Wetzel, 2001). This was calculated firstly to allow for variations in weather conditions between sampling days, and secondly as albedo is so large at polar latitudes that even small changes in solar angle with time of day will have a large influence on light received. Water samples for stable isotope analysis were also collected using a UWITEC water sampler.

3.3.5 Catchment reference data

Moss, cyanobacterial mat, algae, lichen, diatom specimens and characteristic rock samples were collected from each lake catchment. These were analysed for their elemental carbon (C_{org}), nitrogen (N_{org}) and isotopic carbon ($\delta^{13}C$) values. Duplicate biological specimens were collected, one preserved in ethanol for isotopic analysis and the other preserved in water for modern ^{14}C dating. In addition, water was sampled from a range of environments between the sea and lakes, including lake inflows, outflows, lagoons, brackish ponds and the sea, in order to assess the tolerances and habitats of the contemporary diatom flora.

3.4 Laboratory methods

Lake cores were analysed using a series of biological, geochemical and physical methods in order to provide a high-resolution reconstruction of palaeosalinity, from which to identify transitions between marine and freshwater environments. Surface cores were analysed in an identical way in order to provide a reference data set of the response of the proxies to a range of modern environmental parameters.

3.4.1 Physical analyses

Physical analyses of cores were performed initially as a rapid and non-destructive means of whole-core logging, and formed the initial basis of correlating overlapping core drives and identifying physical changes in the sediments that otherwise appear homogeneous to the naked eye. Physical analyses informed the selection of sediment sections for more detailed analyses, and highlighted sections of disturbance to avoid. These analyses were used to compile a continuous 'master core' for each lake (Appendix 1).

Prior to sub-sampling, cores were scanned using a Geotek multi-sensor core logger. Cores were then split, x-rayed, photographed, and described and logged in detail. Sediment type, structures, texture, water content, positions and nature of sedimentary boundaries, tephra layers, plant macro-fossils, and colours (using a Munsell colour chart) were recorded. All descriptions and sub-sampling were undertaken inside a Class 2 microbiological safety cabinet to avoid contamination.

3.4.1.1 Multi-sensor core logging

Cores were scanned intact using a Geotek multi-sensor core logger (MSCL; Fig. 3.16). Physical parameters including magnetic susceptibility (MS), gamma density and fractional porosity were measured at 2 mm resolution. Prior to logging, any gaps in cores, fractures, unconsolidated or crumbly materials were recorded, which might influence physical property data. The machine was also fully calibrated for each sensor, according to the Geotek MSCL Manual (Wetzel, 2001; 2008). Raw data were processed using Geotek software and data were cleaned to remove points related to core destruction (e.g. gaps in sediment) and 'end effects'.

Magnetic measurements provided an extremely rapid method of whole-core logging, and as the magnetic signal within a lake basin is largely homogenized, variations in MS were used to correlate multiple cores from the same lake (Dearing, 1999). Variations in magnetic mineral content were also used to identify tephra layers and increases in minerogenic sediment input. Details of the standard methods for measuring MS are described elsewhere (e.g. Thompson and Oldfield, 1986). Here MS was measured using a Bartington MS-2 loop sensor. It is recognized that the sensitivity level of loop sensors is lower than measuring the magnetic signal from individual pot samples (Sandgren and Snowball, 2001), however given the speed of whole-core scanning and the adequacy of results of core correlation, loop sensor data was deemed acceptable.

Gamma density was determined from attenuation of a gamma-ray beam transmitted from a radioactive source (^{137}Cs). It was used as a proxy for wet bulk density (Zolitschka *et al.*, 2001). Fractional porosity (the liquid content of fully saturated sediment) was calculated from the wet bulk density according to the formula in the Geotek Manual (2008).

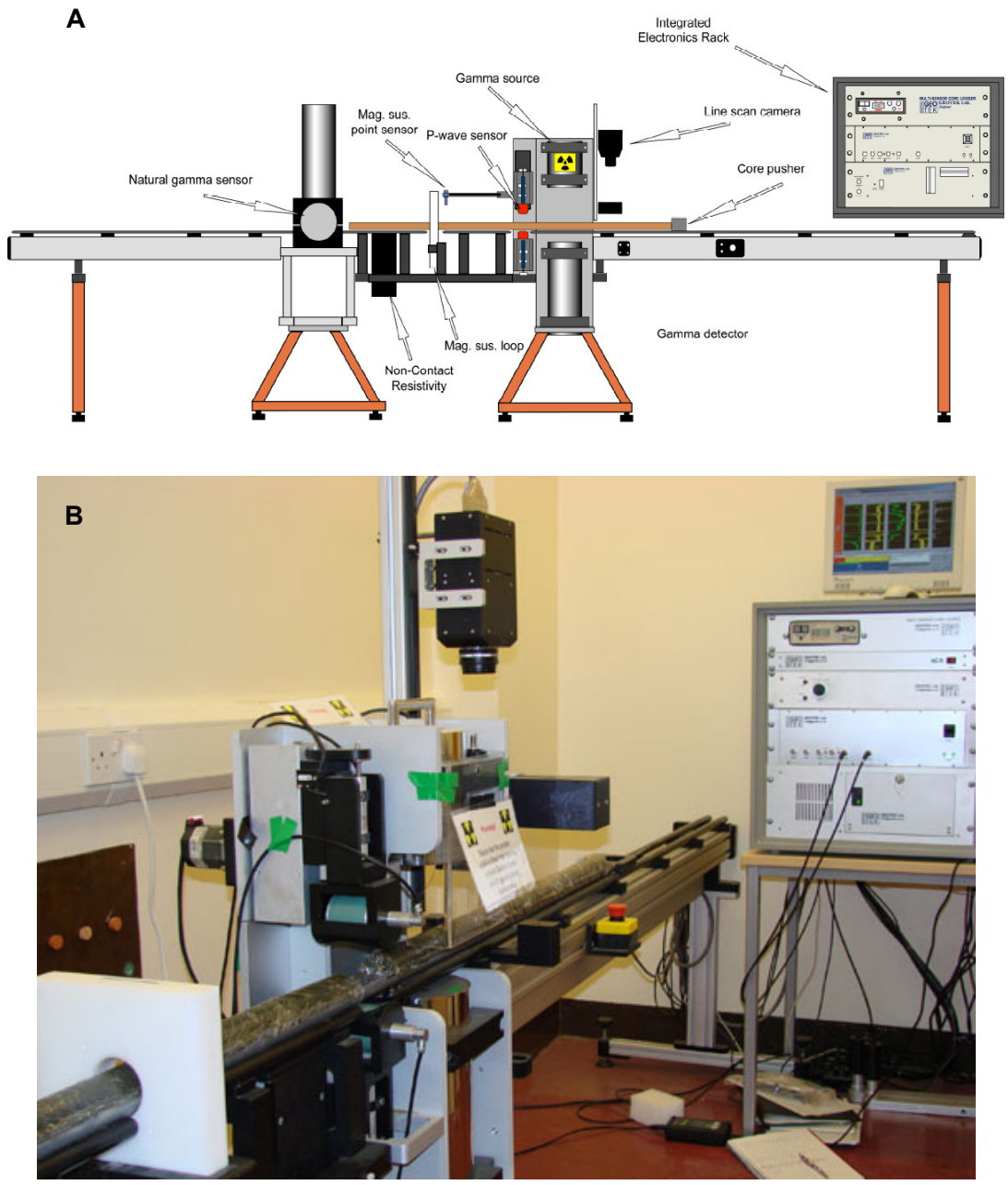

Fig. 3.16 (a) Geotek multi-sensor core logging unit (Source: Geotek Manual, 2008); (b) Photo of core scanning in progress

3.4.1.2 X-rays and core photographs

Cores were x-rayed at East Midlands Airport (by S. Roberts), again in order to identify contrasts in sediments that otherwise appear homogeneous to the naked eye, with variations in textural as well as chemical composition throughout the sediment causing differential attenuation of x-rays (Goudie, 1994). The x-ray camera was set to 70 kV,

with a 30 second exposure to radiation at 10 mA to provide good contrast between organic matter and mineral sediments. X-ray plates were subsequently photographed using a light board and Nikon D2x (12 mega pixel) camera. Split cores were also photographed using a Nikon MB-31 digital camera.

3.4.1.3 Loss-on-ignition

Sequential loss on ignition (LOI) is a widely used method for estimating the organic and carbonate contents of sediments (Dean, 1974; Heiri *et al.*, 2001). It was primarily used in this study as a fast and inexpensive means of estimating the organic matter content of core sediments, and in order to determine sample weights needed for carbon isotope analysis (section 3.4.3.2).

The determination of organic and carbonate content by LOI is based on sequential heating of samples in a muffle furnace, following Dean (1974) and Heiri *et al*. (2001). After oven-drying a sub-sample of wet sediment at 105°C for 12 hours, organic matter was combusted in a first reaction to carbon dioxide and ash at 550°C for 4 hours in a Carbolite ashing muffle furnace. Following cooling in a desiccator, the LOI was then calculated from the following equation:

$$LOI_{550} = ((DW_{105} - DW_{550}) / DW_{105}) * 100$$

where DW_{105} and DW_{550} are the dry weights of the sample prior to and after combustion respectively (in g). The weight loss should be proportional to the amount of organic carbon contained in the sample.

Samples were then returned to the furnace and heated to 950°C for 30 minutes. In this second reaction carbon dioxide was evolved from carbonate, and LOI was calculated by:

$$LOI_{950} = ((DW_{550} - DW_{950}) / DW_{105}) * 100$$

where DW_{550} and DW_{950} are the dry weights of the sample after heating to 550°C and 950°C respectively, and DW_{105} is the initial dry weight before organic carbon

combustion. Using the molar masses of carbon dioxide and carbonate, LOI_{950} can be used to calculate the weight of carbonate in the sample (Heiri *et al.*, 2001).

3.4.2 Biological analysis

3.4.2.1 Background to using diatoms to reconstruct RSL change

Diatoms (unicellular algae, class *Bacillariophyceae*) are one of the most commonly used indicators of palaeolimnological change, due to their specific habitat tolerances and sensitivity to changes in water chemistry and the physical environment (Hodgson *et al.*, 2004). Diatoms have been widely used in the reconstruction of relative sea level change as they are excellent indicators of salinity. In isolation basin settings, changes between freshwater, brackish, and marine taxa have been used to identify lake isolation from the sea and marine transgressions (e.g. Young and King, 1989; Pienitz *et al.*, 1991; Douglas *et al.*, 1996; Long *et al.*, 2003; Shennan *et al.*, 2005). In Antarctica, the relationship between diatoms and salinity has been examined by Fulford-Smith and Sikes (1996), Roberts and McMinn (1996; 1998), Roberts *et al*. (2000; 2004), Verleyen *et al*. (2004b) and Gibson *et al*. (2006). Dramatic and clear changes in both species composition and abundance have provided evidence of salinity changes that were not always picked out by other palaeolimnological proxies (Spaulding and McKnight, 1999). These studies from East Antarctica therefore demonstrate the potential that diatoms have in identifying lake isolation and marine incursions.

3.4.2.2 This study

Diatoms were used in this study primarily due to previously published evidence of the close control of salinity on the distribution of individual species, but also due to their resistance to post-burial silica dissolution and their ubiquity in these lake sediments. Cores were sub-sampled at a minimum of 8 cm intervals, with an increased resolution of 2 cm around transitions identified from physical analyses. Preparation of samples for diatom analysis followed the standard procedures of Battarbee (1986) and Battarbee *et al*. (2001). Sub-samples of 0.5-1.0 g bulk sediment were treated with 20 ml hydrogen peroxide (20% vol) and heated in a 100^{o}C water bath for 2-4 hours to remove all organic material. The digested samples were then rinsed with distilled water and centrifuged for 5 minutes at 3300 rpm. The supernatant liquid was decanted and the sediment pellet re-suspended. Slides were then prepared from this solution by settling

the diatoms onto a coverslip, which was then allowed to dry. The high refraction mountant Naphrax® was used for mounting cover slips on the slides. Diatom identification was carried out using a Leica DM LB2 microscope, fitted with a 100x/1.25 oil immersion objective. A minimum of 250 valves were counted per sample.

Freshwater species were identified using Patrick and Reimer (1966; 1975) Krammer and Lange-Bertalot (1991a; 1991b; 1997), Lange-Bertalot and Krammer (1989), Schmidt *et al.* (1990), Van de Vijver and Beyens (1996; 1997), Van de Vijver *et al.* (2002), Sabbe *et al.* (2003), Cremer *et al.* (2004), Ohtsuka *et al.* (2006), Sterken *et al.* (2009), and online databases (ANSP; Spaulding *et al*.; Kelly *et al*., 2005). Marine species were identified using Harwood and Maruyama (1992), Hasle *et al.* (1994), Hasle and Syvertsen (1997), Iwai and Winter (2002), Cremer *et al.* (2003), and Al-Handal and Wulff (2008). Both fresh and marine species were found in Wasell and Håkansson (1992), Wasell (1993), Hodgson *et al.* (2001b), and online databases (ADIAC). Developments in taxonomy (e.g. name changes and new species descriptions) are continually taking place and recent reviews of diatom systematics in Antarctica have highlighted that in the past species have often been mis-identified by force-fitting to European or North American names (Sabbe *et al*., 2003). In this study, the most up-to-date names have been used, following a thorough revision of sub-Antarctic diatom taxonomy by Van de Vijver *et al*. (2002) and Sterken *et al*. (2009). Synonyms and previous names have also been given to allow comparison with other studies. Where diatom species could not be distinguished by light microscopy, species were grouped (e.g. *Gomphonema angustatum/parvulum*). “cf.” was used where taxa did not exactly fit the formal type description.

Diatom species were classified according to the halobian classification system, Table 3.3 (Vos and de Wolf, 1993; Van Dam *et al.*, 1994). Note that as numerical salinity ranges are not often cited in the literature, particularly for Antarctic diatoms, the values cited in Table 3.3 were used as a rough guide only. Salinity preferences and ecological information were obtained from the literature above, as well as from Pienitz *et al*. (1991), Hemphill-Haley (1993), Jones (1996), and Lohne *et al*. (2004; 2007). Percentage data were plotted using C2, version 1.5.0 (Juggins, 2007).

Halobian group	Salinity tolerance
Polyhalobous	Marine (>30‰ salinity)
Mesohalobous	Brackish (30-0.2‰)
Oligohalobous-Halophilous	Brackish-freshwater; stimulated by small amounts of salt
Oligohalobous-Indifferent	Freshwater-brackish; tolerate small amounts of salt
Halophobous	Freshwater (<0.2‰); does not tolerate salt

Table 3.3 Halobian classification of diatoms according to salinity, after Hustedt (1957).

3.4.3 Geochemical analyses

3.4.3.1 Background to carbon isotopes and C/N ratios

Diatoms are influenced by a range of environmental variables in addition to salinity, and as a proxy can also suffer from variation in fossil abundance, poor preservation, and species assemblages for which there is no modern environmental analogue. Therefore a multi-proxy approach is recommended. A range of geochemical indicators of salinity have been successfully employed in combination with more established palaeosalinity proxies (e.g. diatoms or foraminifera) in estuarine environments, and more recently in isolation basin studies of RSL change (Müller and Voss, 1999; Chivas *et al.*, 2001; Westman and Hedenström, 2002; Mackie *et al.*, 2005; 2007). Such studies demonstrated that carbon isotope ($\delta^{13}C$) and carbon/nitrogen (C/N) ratios of bulk organic material can be reliable indicators of palaeosalinity trends associated with RSL change during the Holocene. Useful reviews of RSL reconstructions using carbon isotopes are provided by Leng *et al*. (2005) and Lamb *et al*. (2006).

When applied in tandem, $\delta^{13}C$ and C/N ratios can be used to identify the sources and composition of organic material, identifying changes in the dominant carbon source from marine to brackish then to terrestrial (or vice versa) in isolation basin sediments. Marine organic sediment is typically enriched in elemental ^{13}C relative to freshwater organic material, with marine algae having $\delta^{13}C$ values between -22 and -20‰ compared to values of -30 to -25‰ for freshwater algae (Meyers, 1994). This difference is explained by freshwater algae utilizing dissolved CO_2 in photosynthesis, which is in isotopic equilibrium with atmospheric CO_2 ($\delta^{13}C \approx -7‰$), whereas the source of

inorganic carbon for marine algae is dissolved bicarbonate ($\delta^{13}C \approx 0‰$). Terrestrial plants photosynthesizing using the C_3 Calvin pathway also have average $\delta^{13}C$ values of -27 ‰ (Meyers, 1994). This ~7‰ difference therefore means marine and continental sources of organic matter are distinguishable, and forms the rationale behind using carbon isotope ratios in this study. Furthermore, $\delta^{13}C$ values are not significantly influenced by grain size, making them useful in sites with changing depositional conditions (Meyers, 1997).

However, in lakes and coastal areas the isotopic signal is often complicated by the input of organic matter from not only algae and C_3 plants, but also from vascular plants using the C_4 Hatch-Slack photosynthetic pathway ($\delta^{13}C \sim -14‰$). Therefore carbon isotopic signals are best interpreted in combination with C/N ratios, to better discriminate between organic matter sources. Algae typically have atomic C/N ratios between 4 and 10, whereas vascular land plants have C/N ratios of ≥20 (Meyers, 1994). Fig. 3.17 shows the four distinctive suites of C/N and $\delta^{13}C$ values in plants.

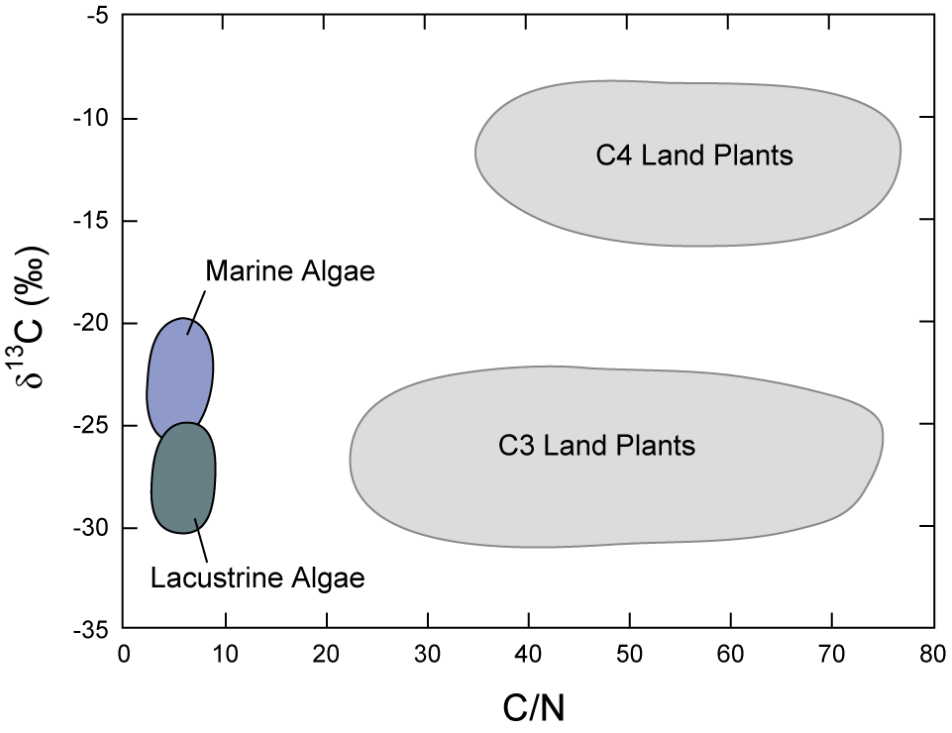

Fig. 3.17 Elemental (atomic C/N ratio) and isotopic ($\delta^{13}C$ value) identifiers of bulk organic matter produced by marine algae, lacustrine algae, C_3 and C_4 land plants (Redrawn from Meyers, 1997)

However, whilst this is characteristic of most sites, in the Antarctic there is an absence of vascular plants, with benthic cyanobacteria and diatoms dominating lake biomass, and aquatic mosses forming the highest form of plants (Hodgson *et al.*, 2003). All these have similar, and relatively low, C/N ratios (<10), and therefore the use of C/N ratios as a source discriminator is yet to be proven in Antarctica. Instead they have more commonly been used to reveal variations in lake productivity (e.g. McMinn, 2000; Kulbe *et al.*, 2001; Wagner *et al.*, 2004). Critically evaluating the use of C/N ratios, in combination with $\delta^{13}C$ analysis, as a palaeosalinity indicator forms one of the secondary objectives of this thesis.

There are also further possible complications to consider. For example, isotopic partitioning between marine and freshwater algae does not always occur in Antarctic sediments. Doran *et al*. (1994) reported a wide range of $\delta^{13}C$ values (-1.9 to -25.7‰) for sediments of Lake Hoare, Taylor Valley, East Antarctica. Similarly, sediments from the Ross Sea displayed wide ranging $\delta^{13}C$ values of -5 to -20‰ (Gibson *et al.*, 1999). Additionally, diagenetic alterations of ratios, in the form of selective degradation of organic matter components, must not be overlooked (Herczeg, 1988). However it is the direction of change in $\delta^{13}C$ and C/N, rather than absolute values, that is key for interpreting changes in RSL, and such changes are known to be preserved in some environmental settings (Lamb *et al.*, 2006).

To date $\delta^{13}C$ and C/N ratios have not been applied to RSL studies from isolation basins in Antarctica, although they have successfully been used successfully in the Antarctic to distinguish periods of freshwater and marine sedimentation in epishelf lakes (Smith *et al.*, 2007). Given this, and in addition to their promise in RSL reconstructions elsewhere (e.g. Chivas *et al.*, 2001; Westman and Hedenström, 2002), isotope analysis was used in this study.

3.4.3.2 This study

Cores were sub-sampled at minimum 8 cm resolution for $\delta^{13}C_{org}$, total organic carbon (TOC) and total organic nitrogen (TON), increasing the sampling resolution to 1 cm across transitional boundaries. C/N ratios were derived from TOC and TON. Surface sediments and catchment samples were also analysed for $\delta^{13}C_{org}$ and C/N; Lamb *et al*.

(2006) highlighted the importance of understanding organic matter sources in modern environments before palaeoenvironmental interpretations can be attempted.

Preparation of samples for geochemical analysis involved dry-sieving ~2 g of sediment and treating the <1 mm fraction with 50 ml 5% hydrochloric acid (HCl) to remove the carbonates. Samples were left in acid for 12 hours, and then filtered through Whatman No. 41 filter papers using a vacuum filter pump. Each sample was then rinsed three times with 200 ml de-ionised water. Samples were oven dried at 40^{o}C for 12 hours and crushed using an agate pestle and mortar.

Isotope analyses were then carried out at the NERC Isotope Geosciences Laboratory, Keyworth in collaboration with Professor Melanie Leng. In order to determine %C (and thus sample size required for δ^{13}C analysis) and %N, 10 ± 0.1 mg of each sample was accurately weighed into small tin capsules using a high-precision Sartorius microbalance. For contemporary samples (e.g. mosses and cyanobacterial mat collected from lake catchments) only 1 ± 0.1 mg was needed. $^{13}C/^{12}C$ analyses of bulk organic matter were performed by combustion in a Carlo Erba 1500 Elemental Combustion System on-line to a VG Triple Trap and Optima dual-inlet mass spectrometer. For samples of very low %C content (< 1%) a Carlo Erba/Triple Trap with coldfinger was used, in order to contain the CO_2 produced and concentrate it more effectively. Selected samples were analysed by both normal and coldfinger methods to check for consistency between methods. δ^{13}C values were calculated to the Vienna Peedee Belemnite (VPDB) scale using within-run laboratory standards (broccoli and soil) calibrated against reference materials NBS-19 and NBS-22. Replicate analysis of well-mixed samples indicated a precision of ± <0.1‰ (1 standard deviation). C/N ratios were determined by reference to an Acetanilide standard. Replicate analysis of well-mixed samples indicated a precision of ± <0.1.

3.4.4 Radiocarbon dating

3.4.4.1 Background to radiocarbon dating isolation basin sediments in Antarctica

As stated in Chapter 2, reconstruction of precise RSL histories from isolation basins relies on accurate dating of marine-lacustrine transitions. Radiocarbon dating (^{14}C) is the most widely used method, the background and basic principles of which are

discussed elsewhere (Bowman, 1990; Lowe, 1991; Björck and Wohlfarth, 2001). Studies focusing specifically on radiocarbon dating in the Antarctic highlight some challenges dating lake sediments from high latitudes, such as prolonged ice cover, low terrestrial and aquatic biological production, and slow rates of organic matter decomposition (Wolfe *et al.*, 2004). Therefore there is a need for careful sample selection and for interpreting ^{14}C dates with an understanding, and preferably independent measurements, of the potential contaminants (Björck *et al.*, 1991b; Jones *et al.*, 2000).

One of the greatest limitations to producing reliable radiocarbon chronologies in marine sediments is the Antarctic marine reservoir effect (AMRE). Radiocarbon ages on marine-derived material are often older than the conventional terrestrial radiocarbon timescale, due to upwelling of old bottom water depleted in ^{14}C (Omoto, 1983; Gordon and Harkness, 1992). Whilst all oceanic masses are depleted in ^{14}C relative to the surrounding atmosphere, in the Antarctic the marine reservoir effect is larger than elsewhere and regional differences in upwelling around the Southern Ocean lead to spatial variation in the AMRE (Berkman *et al.*, 1998). The mean residence time for a ^{14}C atom in the Southern Ocean has been estimated to be in excess of 1000 years, and therefore deep sea water has a radiocarbon age at least 1000 years older than the contemporary atmosphere (Björck *et al.*, 1991b). Consequently a variable reservoir correction must be applied to dates obtained from marine organisms. A widely used radiocarbon reservoir correction for the circum-Antarctic marine ecosystem is 1300 years (Berkman and Forman, 1996), but site-specific corrections can be more accurate and are therefore recommended.

However, radiocarbon ages of marine organisms from the Southern Ocean are not only influenced by the AMRE but also by 'vital effects', associated with species ecology and ^{14}C composition (Berkman *et al.*, 1998). There are significant differences in the radiocarbon ages of different marine organisms, such as calcareous invertebrates (1346 ± 104 yr), penguins (1130 ± 134 yr) and whales and seals (1424 ± 200 yr), partly due to feeding at different depths; consequently species-specific reservoir corrections must be used (Berkman and Forman, 1996). Bulk marine sediments are best avoided, because of mixtures of reworked organic components that may differ in age by as much as 10,000 years (Eglinton *et al.*, 1997). For example, in East Antarctica offsets of up to

7000 years were found between modern surface samples of bulk marine sediment due to contamination by reworked "old" carbon (Harris *et al.*, 1996). Similar contamination of radiocarbon dates on surface marine sediments by reworked "old" carbon has been observed elsewhere around Antarctica (Domack *et al.*, 1991; Andrews *et al.*, 1999; Evans *et al.*, 2005; Hillenbrand *et al.*, 2009).

Marine reservoir effects, caused by the disequilibrium between the atmosphere and the ocean water in which the organic carbon is produced, mean that in isolation basin sequences it is best to date the lacustrine side of marine-lacustrine sedimentary transitions (i.e. after isolation), where potential sources of error are greatly reduced. However, in some studies obtaining reliable ^{14}C chronologies from lacustrine sediments is not without challenges, as lacustrine reservoir effects can occur. Erroneously old ^{14}C ages have been reported from many studies of sediments from freshwater lakes in Antarctica (e.g. Zale and Karlén, 1989; Björck *et al.*, 1991b; Squyres *et al.*, 1991; Ingólfsson *et al.*, 1992; Doran *et al.*, 1999; Hall and Henderson, 2001), and are most commonly attributed to the input of ^{14}C depleted glacial meltwater, restricted gaseous exchange due to lake ice cover, and contamination by marine water or marine sediment (Moreton *et al.*, 2004). However, most of these can easily be identified by dating surface sediments. These potential sources of error will now be discussed in turn.

In some settings the interpretation of radiocarbon ages can be complicated by contamination from much older organic material. Because primary production in Antarctic lakes is generally low, the autochthonous carbon flux to sediments is also low. This increases the influence of contamination effects by ancient carbon derived from allochthonous sources, such as dissolved inorganic carbon from the weathering of carbonate-rich bedrock (Wolfe *et al.*, 2004). Examples of this come from Lake Boeckella, northern Antarctic Peninsula (Zale and Karlén, 1989) and Lake Åsa, Livingston Island (Björck *et al.*, 1991b). Likewise, "old" carbon can come from carbon dioxide contained in glacial meltwater. Whilst reservoir effects caused by old groundwater are not likely since the lakes lie in permafrost areas and are mainly fed by surface water and direct precipitation, meltwater from snowfields or glaciers can have a similar effect on the carbon reservoir and cause erroneously old ^{14}C ages (e.g. Björck *et al.*, 1991b; Doran *et al.*, 1999; Takahashi *et al.*, 1999; Hall and Henderson, 2001). This problem can be exacerbated if the lake is largely ice-covered during the growing

season of mosses. The lake water is sealed off from the atmosphere, and thus uptake of CO_2 is mainly restricted to the CO_2 of the glacially contaminated lake water, resulting in anomalously old ages for the dated moss material (Hall and Denton, 2000b; Björck and Wohlfarth, 2001). This "residence time effect" can be further enhanced where there is long-term water column stratification (Hodgson *et al.*, 2004). Whilst the lakes cored in this study lie at least 4 km from the nearest ice cap and do not presently receive glacial meltwater, it is possible that a supply of ^{14}C depleted CO_2 from glacier ice may have been significant in the past, during times of greater ice extent. Similarly, at present, summer melting of lake ice is likely to permit CO_2 exchange between lake water and the atmosphere and maintain a well-mixed carbon pool in equilibrium with atmospheric CO_2, but this may not always have occurred in the past. Therefore lacustrine reservoir effects must not be disregarded, and Doran *et al*. (1999) highlighted the need for surface dates in order to determine the magnitude of the reservoir correction.

Finally, the marine reservoir effect is not limited exclusively to the marine environment. Where lakes are situated near the sea, inwash of marine sediment or sea water can contaminate samples. For example, a study at Lake Boeckella in Hope Bay, northern Antarctic Peninsula, showed that ^{14}C dates from the lacustrine environment may also be contaminated by the marine reservoir effect, especially, in this case, because there is a penguin colony surrounding the lake (Zale, 1994a).

Despite the potential sources of error outlined above, recent studies have demonstrated that reliable chronologies can be obtained from Antarctic lacustrine sediments (Bird *et al.*, 1991; Melles *et al.*, 1994), especially where suitable macrofossils are preserved (Jones *et al.*, 2000; Hodgson *et al.*, 2001a). Terrestrial plant macrofossils are the most desirable targets for AMS ^{14}C dating as they are less susceptible to 'hard water effects' (i.e. uptake of 'old' carbon) than aquatic plants (Andrée *et al.*, 1986; Björck and Wohlfarth, 2001). The least reliable fraction for ^{14}C dating is undifferentiated organic matter from bulk sediment. This is because most bulk sediments comprise highly heterogeneous admixtures of organic carbon, both in age and composition (Colman *et al.*, 1996; Wolfe *et al.*, 2004). Distinct offsets between dates obtained from bulk sediment and plant macrofossils have led many authors to warn against using bulk sediment for ^{14}C dating (Barnekow *et al.*, 1998; Björck *et al.*, 1998). However, as the abundance of macrofossils in the Fildes Peninsula cores was frequently low, often in

key parts of cores, dating bulk sediment was unavoidable. In order to assess any possible offsets, paired dates of macrofossils and bulk sediment were done at several levels in the cores where macrofossils were found.

3.4.4.2 This study

A total of 49 samples were submitted for accelerator mass spectrometry (AMS) radiocarbon dating. AMS has the advantage over conventional methods of ^{14}C dating of enabling much smaller samples (by as much as six orders of magnitude, requiring less than 1 mg of carbon) to be analysed with precision (Wolfe *et al.*, 2004). Samples were submitted in three batches; the first 18 samples targetted key transitions, surface and basal ages, with the second and third batches (21 and 10 samples) aimed at producing robust age-depth models for each core. The second and third batches were submitted after the isotope and diatom analysis had been completed to enable additional transitions to be dated. Where samples in the first batch produced insufficient CO_2 for analysis, samples of higher %C content at similar depths were also re-submitted; this was common in the case of attempted basal dates. Analyses were undertaken at the NERC Radiocarbon Laboratory, East Kilbride (batches 1 and 2) and Beta Analytic (batch 3). Where possible, macrofossils (mosses and algae) were hand-picked for dating, as these have been shown to produce the most reliable chronologies (section 3.4.4.1). Bulk sediment was only dated in the absence of macrofossils. Three pairs of bulk sediment and macrofossil samples from the same depths were submitted to assess any possible offset. A summary of the material dated and justification for each date is given in Table 3.4.

Lake	Sample identifier	Stratigraphic depth (cm)	Material dated	*In situ* environment	Batch	Justification for dating
Ardley	SUR: 0	0-0.5	Surface moss (species A)	Matted moss on lake floor	2	Surface age (after 1A: 5 produced insufficient CO_2 for analysis in batch 1)
Ardley	1A: 5	5-6	Moss strands (A)	Fine organic mud	1	Surface age
Ardley	1A: 22	22-23	Bulk sediment	Fine organic mud	3	To establish (1) a robust age-depth model and (2) sedimentation rates in terrestrial environment
Ardley	1A: 42	42-43	Bulk sediment	Fine organic mud	3	To establish (1) a robust age-depth model and (2) sedimentation rates in terrestrial environment
Ardley	1A: 51	51-52	Moss strands (A)	Silt and clay	2	Paired date with bulk sediment
Ardley	1A: 51	51-52	Bulk sediment	Silt and clay	3	Paired bulk/moss age to establish possible bulk sediment terrestrial ^{14}C offset.
Ardley	1A: 74	74-75	Bulk sediment	Fine organic mud	3	Corresponds to LOI peak
Ardley	1B: 42	118-119	Bulk sediment	Fine organic mud	2	Transition brackish-fresh to fresh
Ardley	1C: 48	158-159	Bulk sediment	Fine organic mud	1	To establish a robust age-depth model. Also corresponds to peak in magnetic susceptibility
Ardley	1C: 77	180-181	Moss strands (B)	Fine organic mud	2	To establish (1) a robust age-depth model and (2) sedimentation rates in terrestrial environment
Ardley	1D: 63	252-253	Bulk sediment	Silt and clay	2	Paired date with seaweed (1D: 63.5) to determine possible reservoir effect
Ardley	1D: 63.5	252.5-253.5	Yellow-green algae	Silt and clay	2	To establish (1) a robust age-depth model and (2) sedimentation rates in brackish environment. Paired with bulk sediment (1D: 63)
Ardley	1D: 92	283-284	Yellow-green algae	Silt and clay	2	To establish (1) a robust age-depth model and (2) sedimentation rates in brackish environment
Ardley	1E: 33	308-309	Bulk sediment	Fine organic mud	1	Near basal age
Ardley	1E: 72	347-348	Bulk sediment	Silt and clay	2	Basal age (after 1E: 83 produced insufficient CO_2 for analysis in batch 1)

Lake	Sample identifier	Stratigraphic depth (cm)	Material dated	*In situ* environment	Batch	Justification for dating
Ardley	1E: 83	358-359	Bulk sediment	Massive inorganic clay-silt	1	Basal age
Belén	3A: 0	0-1	Moss strands (A)	Matted moss on lake floor	1	Surface age
Belén	3C: 20	129-130	Moss strands	Laminated clay-rich organic mud	1	Productivity transition, brackish to fresh
Belén	3D: 48	229-230	Bulk sediment	Silt and clay	2	Basal age (after 3D: 70 produced insufficient CO_2 for analysis in batch 1)
Belén	3D: 70	251-252	Bulk sediment	Massive inorganic silt-clay	1	Basal age
Gaoshan	1B: 0	0-1	Bulk sediment	Fine organic mud	1	Surface age
Gaoshan	1B: 24	24-25	Moss strands (A)	Massive organic mud and silt	1	To establish age-depth model
Gaoshan	1I: 75	314-315	Bulk sediment	Fine organic mud	1	Basal age
Long	1A: 0	0-1	Bulk sediment	Silt	3	Surface age
Long	1A: 24	24-25	Moss strands	Fine organic mud	1	Near surface age, no macros preserved nearer surface
Long	1B-I: 29	89-90	Bulk sediment	Silt and clay	2	Sharp transition in core scanning, isotopes and diatoms
Long	2C-I: 26	303-304	Bulk sediment	Fine organic mud	1	Above marine-fresh transition
Long	2C-I: 53	330-331	Bulk sediment	Fine organic mud	1	Immediately below marine-fresh transition
Long	2D-I: 67	512-513	Bulk sediment	Silt and clay	2	Freshwater/brackish spike in middle of marine section
Long	3A-I: 35	572-573	Shells (*Nacella consinna* and *N. mytilina*)	Marine silt and clay	2	To establish (1) a robust age-depth model and (2) sedimentation rates in marine environment
Long	3A-I: 35	572-573	Bulk sediment	Marine silt and clay	2	Paired with shells (3A-I: 35) to determine marine reservoir effect

Lake	Sample identifier	Stratigraphic depth (cm)	Material dated	*In situ* environment	Batch	Justification for dating
Long	3A-II: 68	697-698	Bulk sediment	Silt and clay	2	Basal age (after 3A-II: 84 produced insufficient CO_2 for analysis in batch 1)
Long	3A-II: 84	719-720	Bulk sediment	Inorganic clay	1	Basal age
Yanou	SUR: 1.5	1.5-3	Moss and organic-rich surface sediment	Flocculent organic-rich mud	2	Surface age
Yanou	8A-I: 5	5-6	Moss strands (A)	Matted moss on lake floor	1	Surface age
Yanou	8A-I: 14	14-15	Bulk sediment	Fine organic mud	3	To establish (1) a robust age-depth model and (2) sedimentation rates in terrestrial environment
Yanou	8A-I: 24	24-25	Bulk sediment	Fine organic mud	3	To establish (1) a robust age-depth model and (2) sedimentation rates in terrestrial environment
Yanou	8A-I: 32	32-33	Moss strands (A)	Fine organic mud	1	Productivity transition, possibly same as Belén 3C: 20
Yanou	9B-I: 37	190-191	Bulk sediment	Fine organic mud and silt	2	Paired date with moss below (9B-I: 37.5). To establish (1) a robust age-depth model and (2) sedimentation rates in terrestrial environment
Yanou	9B-I: 37.5	190.5-191	Moss strands (A)	Fine organic mud and silt	2	Paired bulk/moss age to establish possible bulk sediment terrestrial ^{14}C offset. Resubmitted in batch 2 after initial attempt produced insufficient CO_2 for analysis (9B-I: 38)
Yanou	9B-I: 38	191-192	Moss strands (A)	Fine organic mud and silt	1	To establish (1) a robust age-depth model and (2) sedimentation rates in terrestrial environment
Yanou	9B-I: 48	201-202	Moss strands (species C)	Fine organic mud and silt	2	To establish (1) a robust age-depth model and (2) sedimentation rates in terrestrial environment. 10cm above marine-fresh transition
Yanou	8B-I: 29	247-248	Bulk sediment	Silt and clay	2	Below fresh-marine transition
Yanou	8B-I: 42	260-261	Bulk sediment	Silt and clay	2	At lowermost marine-fresh transition

Lake	Sample identifier	Stratigraphic depth (cm)	Material dated	*In situ* environment	Batch	Justification for dating
Yanou	8B-I: 82	300-301	Bulk sediment	Inorganic silt and clay	3	To establish (1) a robust age-depth model and (2) sedimentation rates downcore
Yanou	8B-II: 22	340-341	Bulk sediment	Inorganic silt and clay	2	Basal age (after 8B-II: 24 produced insufficient CO_2 for analysis in batch 1)
Yanou	8B-II: 24	342-343	Bulk sediment	Coarse sand and gravel	1	Basal age
Yanou	8B-II: 24	342-343	Bulk sediment	Coarse sand and gravel	3	Basal age (resubmitted)
Yanou	8B-II: 32	350-351	Bulk sediment	Coarse sand and gravel	3	Basal age

Table 3.4 Samples submitted for AMS ^{14}C dating, with justifications. Notes on moss species: species A similar in morphology to *Andreaea depressinervis* (Ochyra, 1998, p.78), species B similar in morphology to *Andreaea regularis* (Ochyra, 1998, p.84-86), species C similar in morphology to *Holodontium strictum* (Ochyra, 1998, p.130-132). High Performance Liquid Chromatography (HPLC) analysis of samples ARD 1D: 63.5 and 1D: 92 (by Elie Verleyen, University of Ghent) confirmed the dominant pigment as vaucheriaxanthin, characteristic of yellow-green algae.

3.5 Summary

This chapter has provided the background to the first part of this thesis concerned with reconstructing RSL using evidence from isolation basin sediments. It has introduced the field sites located on the Fildes Peninsula of King George Island and described the physical setting of the five study lakes. This chapter also outlined the field methods employed and provided the rationale for the laboratory techniques used in this thesis. The results of this fieldwork and laboratory analysis will be described and interpreted over the next two chapters, with the aim of producing a preliminary RSL curve from the isolation basin data.

CHAPTER 4

Multi-proxy results from isolation basins

4.1 Introduction

This chapter presents the biological, isotopic and physical analyses of core material from the five lakes. Specifically this chapter has three aims; (i) to identify key transitions in each proxy record in each lake, associated with relative sea level change or other lake processes; (ii) to identify concurrent changes between different proxies within each lake; and (iii) to provide a chronology of transitions. The results are interpreted in Chapter 5, where records from each lake are compared and combined to develop a relative sea level curve.

4.2 Yanou Lake (14.5 m amsl)

Results of diatom, isotope and physical analyses, and radiocarbon dating are presented in turn. The diatom assemblage is presented in Fig. 4.1 and summary of all results in Fig. 4.2.

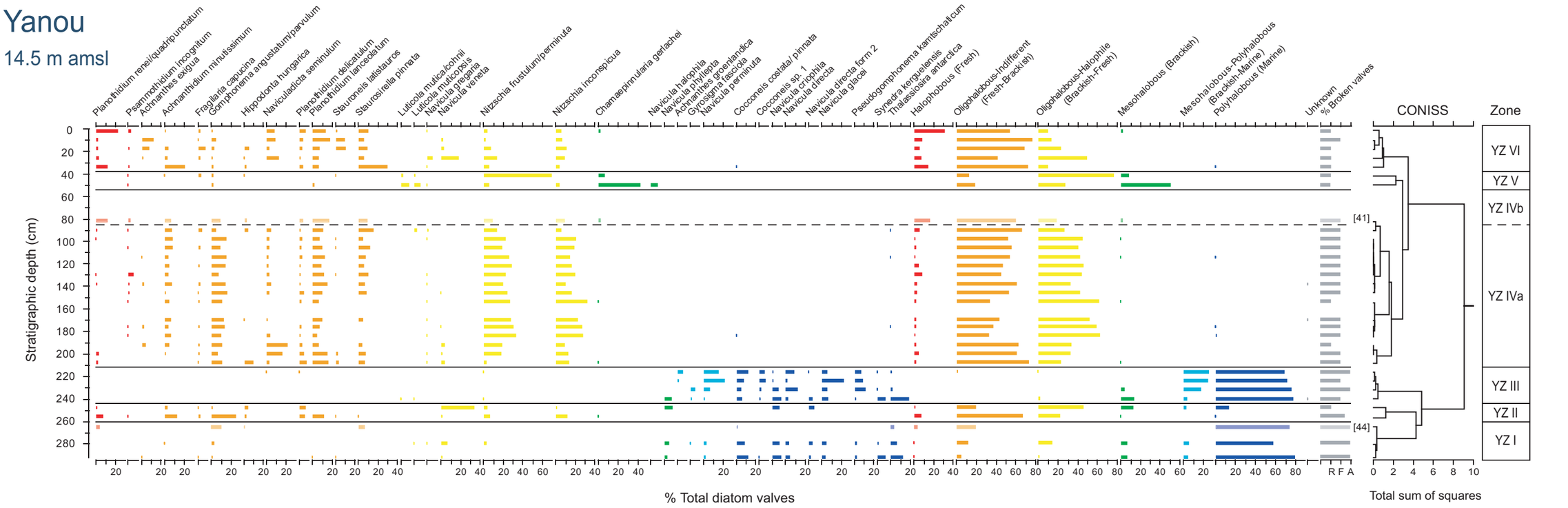

Fig. 4.1 Diatom assemblage of Yanou Lake. Species are grouped by salinity tolerance. Only species >5% of the total valves counted are shown. The percentage of broken valves is included, R = rare (0-20% of total count), F = frequent (20-40%), A = abundant (>40%). Where diatom concentrations were too low to achieve a full count of 250 valves, counts are shown as paler bars and the number of valves counted is shown in brackets (counts <25 are not shown)

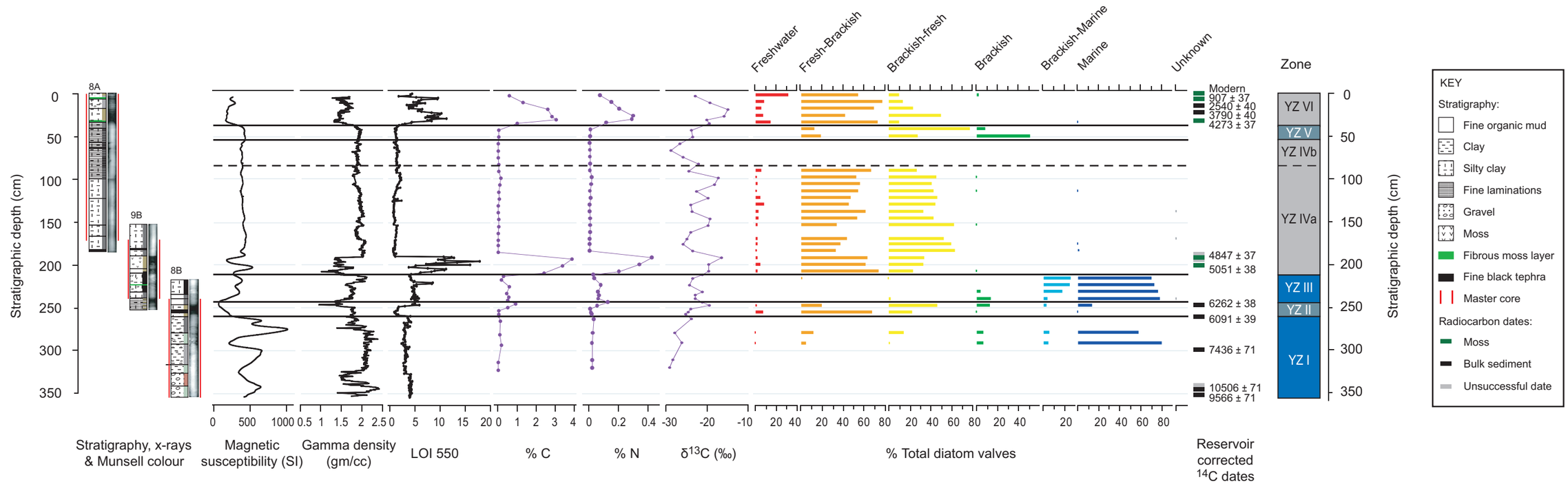

Fig. 4.2 Summary of physical, isotopic and diatom analyses from Yanou Lake, including core stratigraphy and radiocarbon dates. Samples below 300 cm were examined for diatoms, but produced counts <25 so are not shown.

4.2.1 Diatom analysis

Of the 43 samples prepared for diatom analysis, only 29 contained a high enough diatom concentration to count 250 valves. Taxa characteristic of the full salinity spectrum from fresh to brackish to marine are present. In total 118 diatom taxa were identified (of which only 5 could not be identified at species level). The full list of diatom species identified in all lakes, salinity tolerances, ecological preferences, and photographs are included in Appendices 2 and 3. The diatom stratigraphy can be divided into 6 zones based on cluster analysis performed using CONISS (Grimm, 1987, Fig. 4.1), hereafter referred to as Yanou Zones (YZ) I to VI.

Correspondence analysis also confirmed the zonation (Fig. 4.3). The unconstrained ordination method of detrended correspondence analysis (DCA) arranged samples along gradients based on species composition (Hill and Gauch, 1980). The unimodal species response between samples confirmed DCA was the most appropriate ordination technique (ter Braak and Prentice, 1988; ter Braak, 1995). DCA was performed using CANOCO (version 4.55, ter Braak and Šmilauer, 2006) on square-root-transformed diatom species percentage data. Rare species were downweighted to reduce their importance in the ordination. Samples were generally counted at 8 cm resolution, and so zone boundaries have been taken as the mid-point between transitional samples.

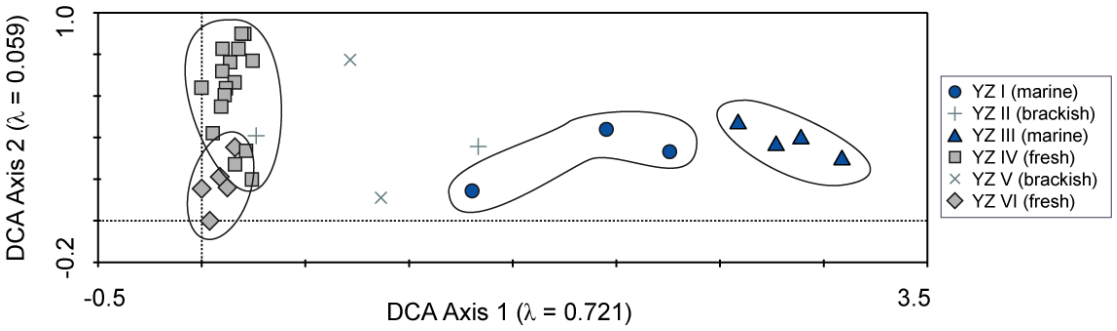

Fig. 4.3 Detrended correspondence analysis of samples from Yanou Lake. Samples plotting close to one another have similar diatom compositions. Eigenvalues (λ) are a measure of the importance of ordination axes.

4.2.1.1 YZ I (260-292 cm)

The lowest zone is dominated by polyhalobous species (>64%), although low concentrations of diatoms from all salinity classes are present. *Cocconeis*

costata/pinnata, *Thalassiosira antarctica*, *Navicula criophila*, and *Synedra kerguelensis* dominate the assemblage, and to a lesser extent *Navicula directa* and *N. glaciei*. There is a relatively high percentage of broken valves. Unfortunately low diatom abundance at the top of this zone prevents the upper boundary of the zone being placed with certainty.

4.2.1.2 YZ II (244-260 cm)

The base of this zone is a marked by the abrupt disappearance of polyhalobous and mesohalobous-polyhalobous taxa. They are replaced initially by the oligohalobous species *Gomphonema angustatum/parvulum*, *Achnanthidium minutissimum*, *Planothidium lanceolatum*, *Nitzschia inconspicua*, *Planothidium delicatulum*, as well as the halophobous species *Planothidium renei/quadripunctatum*. However the two samples which constitute this fresh-brackish spike are of contrasting species compositions. The upper sample is dominated by *Navicula veneta* (35%). Very low abundances of polyhalobous and mesohalobous species appear in the uppermost sample of this zone.

4.2.1.3 YZ III (212-244 cm)

This zone is characterized by a very similar species composition and diversity to YZ I. All species present are polyhalobous or mesohalobous; oligohalobous and halophobous species are completely absent. The zone starts with the appearance of *Thalassiosira antarctica*, *Synedra kerguelensis* and *Navicula criophila*. The species *Navicula perminuta*, *N. glaciei*, *Pseudogomphonema kamtschaticum* and *Cocconeis costata/pinnata* increase in abundance above 233 cm. This zone is marked by sharp changes in species composition at both the lower and upper boundaries.

4.2.1.4 YZ IV (54-212 cm)

The final transition from marine to freshwater conditions occurs between 208-216 cm. The transition is very sharp, with a complete change in the diatom assemblage from one sample to the next. However, this freshwater zone can be further subdivided into 2 sub-zones.

Sub-zone YZ IVa (86-212 cm) starts with the disappearance of polyhalobous and mesohalobous taxa, and the replacement with oligohalobous and halophobous species.

The species *Nitzschia inconspicua*, *N. frustulum/perminuta*, *Planothidium lanceolatum*, *Gomphonema angustatum/parvulum*, *Staurosirella pinnata*, *Achnanthidium minutissimum* dominate, with *Naviculadicta seminulum* and *Hippodonta hungarica* are abundant immediately following lake isolation.

There is a sharp decline in diatom concentration between 54-86 cm (*Sub-zone YZ IVb*). Six samples were prepared for diatom analysis in this sub-zone, but counts of 250 valves could not be achieved from any of these. However, where valves are preserved they are of the same species as those of sub-zone YZ IVa.

4.2.1.5 YZ V (38-54 cm)

This zone is marked by peaks in oligohalobous-halophilous and mesohalobous species, and suppressed abundances of oligohalobous-indifferent taxa. There is a peak in the mesohalobous species *Chamaepinnularia gerlachei* at 50 cm (43%), followed by a peak in the oligohalobous-halophilous species *Nitzschia frustulum/perminuta* (70%).

4.2.1.6 YZ VI (0-38 cm)

Finally, the uppermost section of the sequence is characterized by oligohalobous and halophobous species, and suppressed abundances of *Nitzschia frustulum/perminuta*. The species *Staurosirella pinnata*, *Planothidium lanceolatum*, *P. renei/quadripunctatum*, *Achnanthidium minutissimum*, *Naviculadicta seminulum* and *Nitzschia inconspicua* dominate the assemblage.

4.2.2 $\delta^{13}C_{org}$ and C/N ratios

The results of isotopic and physical analyses are presented in Fig. 4.2. In total, 44 samples were analysed for %C, %N and $\delta^{13}C$. There are two distinct peaks in %C values. The largest (3.9%) comes immediately after the main transition from marine to freshwater sediment (base of YZ IVa), with a similar magnitude peak in YZ VI after the transition from brackish to freshwater diatoms. There is a much smaller peak (0.9%) in YZ II, corresponding to the spike in freshwater diatoms. Nitrogen content is extremely low, with no sample >0.4% and only 6 samples >0.1%. Consequently C/N ratios could not be calculated. $\delta^{13}C$ values range between -15‰ and -29‰, but show no clear trends. There seems to be no correspondence between $\delta^{13}C$ values and diatom species, and the $\delta^{13}C$ profile is highly oscillatory.

4.2.3 Physical analyses

Physical analyses were primarily carried out to highlight major transitions and inform the selection of sediment sections to target for later analyses. However, there are some notable trends. The gamma density profile mirrors organic content, as does magnetic susceptibility (MS) with the exception of the basal metre of the core (Fig. 4.2). There are significant troughs in MS and gamma density at the marine/brackish-freshwater transitions. Fractional porosity was calculated from gamma density measurements, but the profile was exactly the inverse and therefore is not shown. LOI was also measured at high resolution, and as would be expected, the LOI profile exactly matches the %C record.

4.2.4 Core chronology

The chronology of the Yanou master core is based on 12 AMS ^{14}C dates (Table 4.2, Fig. 4.4). A moss and bulk sediment pair was dated from the same stratigraphic depth in order to determine any possible offset, but unfortunately the bulk sediment could not be dated due to a low organic content. The most significant dates are those on the two marine-freshwater transitions. A date of 5051 ± 38 ^{14}C yr BP (5730 cal yr BP) on freshwater moss from the base of YZ IVa provides a minimum age for the main marine-freshwater transition. The freshwater incursion (YZ II) in the middle of the marine section is constrained by two dates, 6262 ± 38 and 6091 ± 39 ^{14}C yr BP (7200-7000 cal yr BP). There is a slight age reversal, but this is just within the calibrated 2-sigma error range. The basal age of the core is constrained by two dates of 10506 ± 71 and 9566 ± 71 ^{14}C yr BP (12480-10930 cal yr BP). Again, these dates are reversed out of stratigraphic order.

Dates on marine material were corrected using a marine reservoir correction of 1064 ± 10 years, calculated from the ages of water samples reported from Maxwell Bay (Milliken *et al.*, 2009). This differs from the general circum-Antarctic radiocarbon marine reservoir correction of 1300 ± 100 years proposed by Berkman and Forman (1996), but is used here due to the known spatial variability of the Antarctic marine reservoir effect and the very close proximity of Maxwell Bay to Fildes Peninsula. The uppermost date from a marine core from Maxwell Bay of 1160 ± 40 ^{14}C yr BP at a core depth of 25 cm provides a minimum surface reservoir correction for this location of 1000-1100 years (Milliken *et al.*, 2009). The exact value of 1064 ± 10 years is based on the age range of

CO_2 in seawater samples collected from Maxwell Bay and Bransfield Strait just in front of Maxwell Bay (Table 4.1; Julia Smith Wellner, pers. comm.). A weighted average of the six samples and associated error term was calculated following Taylor (1997).

Sample location	Water sample depth (m)	^{14}C age (yr BP ± 1σ)
Maxwell Bay	150	1000 ± 25
Maxwell Bay	350	1060 ± 20
Maxwell Bay	477	1070 ± 30
Bransfield Strait	80	1130 ± 25
Bransfield Strait	251	1070 ± 25
Bransfield Strait	464	1060 ± 25

Table 4.1 Radiocarbon ages of water samples from Maxwell Bay, used to determine the local marine reservoir correction (Julia Smith Wellner, pers. comm.)

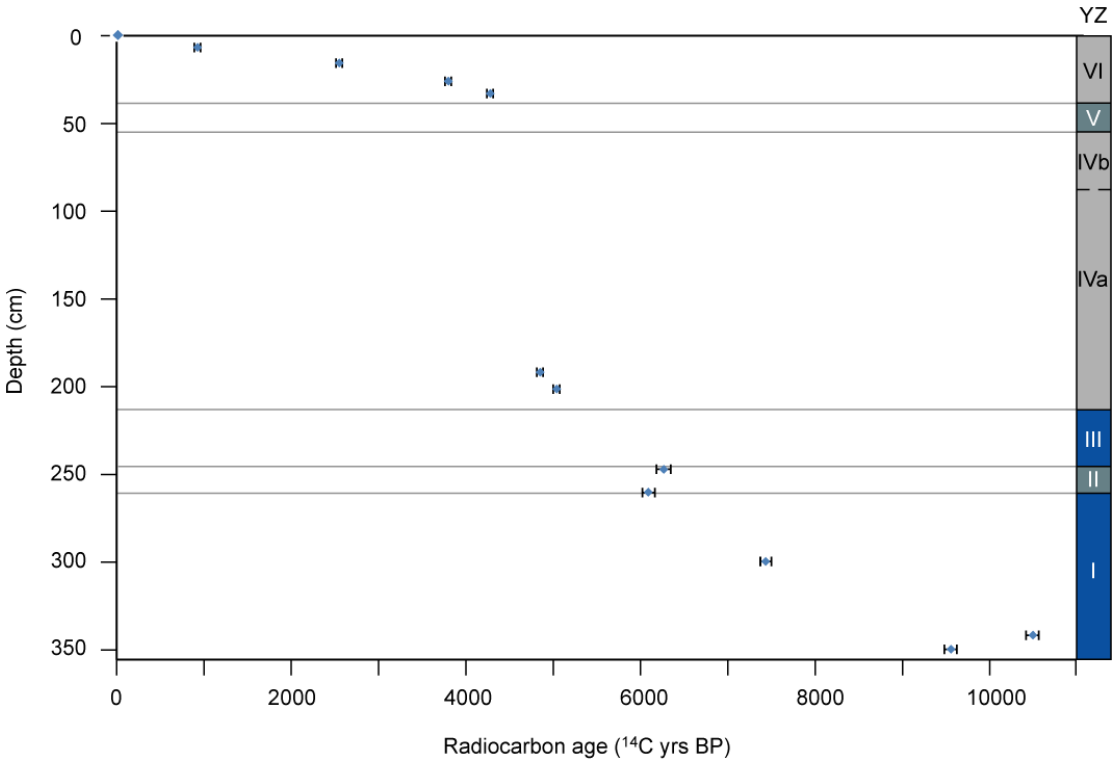

Fig. 4.4 Depth versus radiocarbon age (uncalibrated) for the Yanou core. Error bars are shown to 1-sigma. The five lowermost dates have been corrected using the marine reservoir correction of 1064 ± 10 yrs, reported for Maxwell Bay by Milliken *et al*. (2009) (details on reservoir correction are given in the caption to Table 4.2).

Sample	Material	Lab code	Conventional ^{14}C age	$\delta^{13}C_{VPDB}$ ± 0.1‰	Marine reservoir corrected ^{14}C age	Calibrated age range (cal yr BP)		
			(yr BP ± 1σ)		(yr BP ± 1σ)	1-sigma	2-sigma	Median
SUR: 1.5 (1.5)	Moss	SUERC-22325	Modern	-16.7	---	Modern		Modern
8A-I: 5 (5)	Moss	SUERC-18934	907 ± 37	-25.0*	---	730-797	683-818 (87%) 835-836 (0.1%) 866-904 (13%)	768
8A-I: 14 (14)	Bulk sediment	Beta-271289	2540 ± 40	-15.0	---	2487-2620 (66%) 2631-2645 (7%) 2651-2709 (27%)	2364-2415 (9%) 2432-2722 (91%)	2569
8A-I: 24 (24)	Bulk sediment	Beta-271290	3790 ± 40	-16.6	---	3990-4044 (39%) 4069-4150 (61%)	3932-3941 (1%) 3970-4236 (99%)	4086
8A-I: 32 (32)	Moss	SUERC-18935	4273 ± 37	-25.0*	---	4652-4669 (12%) 4704-4757 (50%) 4809-4845 (38%)	4589-4593 (0.5%) 4615-4766 (64%) 4784-4857 (36%)	4739
9B-I: 37 (190)	Bulk sediment	Produced insufficient CO_2 for AMS analysis						
9B-I: 37.5 (190.5)	Moss	SUERC-22310	4847 ± 37	-31.9	---	5475-5545 (84%) 5575-5589 (16%)	5332-5373 (7%) 5461-5602 (93%)	5518
9B-I: 38 (191)	Moss	Produced insufficient CO_2 for AMS analysis						
9B-I: 48 (201)	Moss	SUERC-22311	5051 ± 38	-26.5	---	5655-5750 (83%) 5829-5856 (17%)	5610-5634 (4%) 5641-5772 (67%) 5782-5794 (2%) 5805-5892 (27%)	5726
8B-I: 29 (247)	Bulk sediment	SUERC-22326	7326 ± 37	-20.7	6262 ± 38	7158-7238	7100-7289	7198
8B-I: 42 (260)	Bulk sediment	SUERC-22327	7155 ± 38	-27.1	6091 ± 39	6929-7063	6886-7133	6997
8B-I: 82 (300)	Bulk sediment	Beta-271291	8500 ± 70	-25.9	7436 ± 71	8224-8371	8151-8438	8300
8B-II: 22 (340)	Bulk sediment	Produced insufficient CO_2 for AMS analysis						
8B-II: 24 (342)	Bulk sediment	Beta-271292	11570 ± 70	-24.2	10506 ± 71	12353-12644	12187-12748	12481
8B-II: 32 (350)	Bulk sediment	Beta-271293	10630 ± 70	-25.3	9566 ± 71	10809-11081	10679-11129	10925

Table 4.2 Radiocarbon dates from Yanou Lake. Full caption on following page.

Table 4.2 cont. Radiocarbon dates from Yanou Lake. Stratigraphic depths of samples are given in brackets; * denotes estimated $\delta^{13}C$ value where there was insufficient material for an independent $\delta^{13}C$ measurement. ^{14}C ages have been normalized to $\delta^{13}C_{PDB}$‰ -25 using the $\delta^{13}C$ values shown. Three samples generated insufficient CO_2 to produce a graphite target and so could not be dated. Dates on marine bulk sediment have been corrected using a marine reservoir correction of 1064 ± 10 yrs (Milliken *et al.*, 2009); errors on the original date and ΔR value were combined in quadrature. Dates were calibrated using Calib (version 5.0.1, Stuiver and Reimer, 1993) using the SHCal04 calibration curve for terrestrial dates (McCormac *et al.*, 2004) and the Marine04 calibration curve for marine dates (Hughen *et al.*, 2004) with a ΔR value of 664 yrs (marine reservoir correction of 1064 yrs minus the global ocean reservoir correction of 400 yrs, Stuiver and Braziunas, 1993; Reimer, 2009). Where more than one calibrated range is given, the relative percentage area under the probability distribution is indicated in brackets; all other ranges constitute 100% of the probability distribution. Median ages are rounded to the nearest 10 years in all later discussions.

4.2.5 Summary

When the results of diatom, isotope and physical analyses from Yanou Lake are combined, six distinct zones are identifiable. The basal 1 m (YZ I) is fully marine (basal age of 10506-9566 ^{14}C yr BP, 12480-10930 cal yr BP), and terminates with the incursion of freshwater sediment between 6262 and 6091 ^{14}C yr BP (7200-7000 cal yr BP, YZ II). Above this, YZ III is fully marine once again, with polyhalobous diatoms, low organic content and high magnetic susceptibility and gamma density. The main isolation contact is between 208 and 216 cm and dates to around 5050 ^{14}C yr BP (5730 cal yr BP). There is an abrupt shift in diatom composition, organic content and physical parameters across the transition. The lake remains isolated to the present day, although there is a clear zone of brackish influence (YZ V) between 38-54 cm. There is a transition from this brackish-freshwater environment to a completely freshwater environment (YZ VI) around 4270 ^{14}C yr BP (4740 cal yr BP). The change in diatom assemblage is mirrored by an increase in %C and decrease in gamma density and magnetic susceptibility. $\delta^{13}C$ shows no clear relationship with the other proxies and so cannot be used as an indicator of palaeosalinity at this site.

4.3 Long Lake (15 m amsl)

Results of diatom, isotope and physical analyses, and radiocarbon dating are presented in turn. The diatom assemblage is presented in Fig. 4.5 and summary of all results in Fig. 4.6.

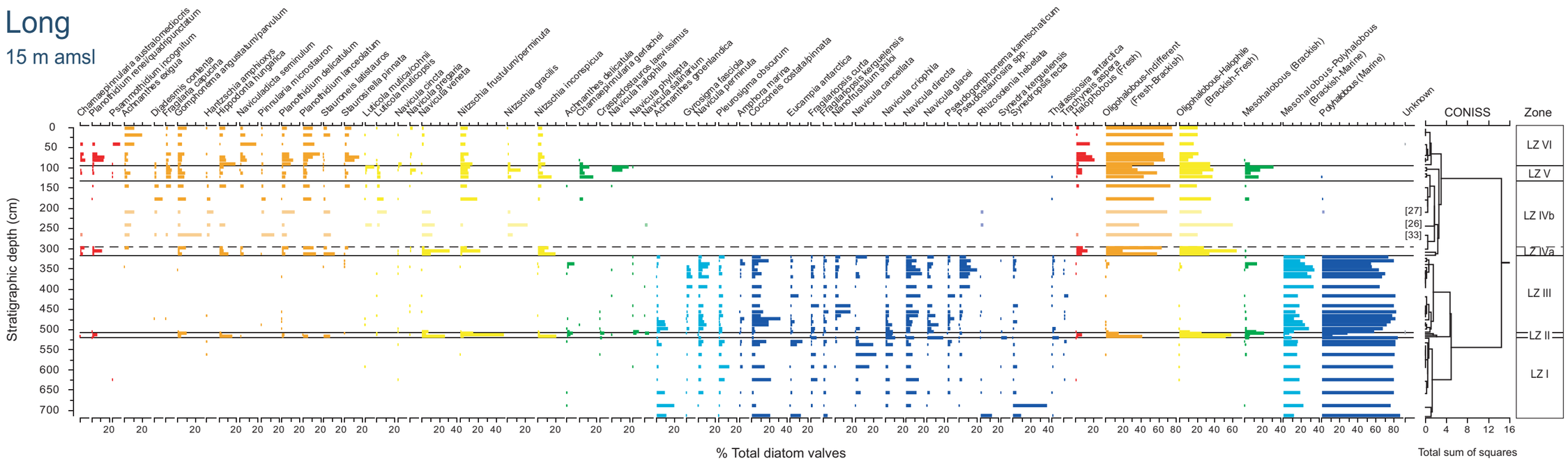

Fig. 4.5 Diatom assemblage of Long Lake. Species are grouped by salinity tolerance. Only species >5% of the total valves counted are shown. Where diatom concentrations were too low to achieve a full count of 250 valves, counts are shown as paler bars and the number of valves counted is shown in brackets

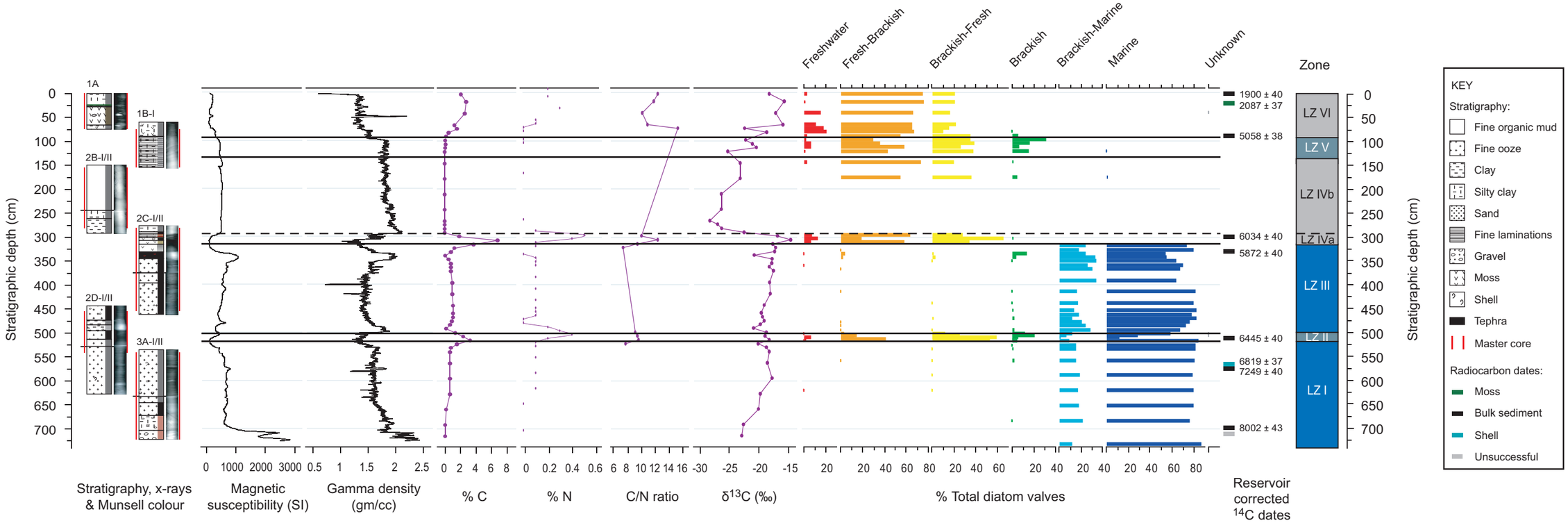

Fig. 4.6 Summary of physical, isotopic and diatom analyses from Long Lake, including core stratigraphy and radiocarbon dates

4.3.1 Diatom analysis

Of the 51 samples prepared for diatom analysis, 45 contained high enough diatom concentrations to achieve counts of a minimum of 250 valves. As in Yanou Lake, Long Lake contains taxa characteristic of the full salinity spectrum from fresh through brackish to marine. In total 135 diatom taxa were identified (of which only 5 could not be identified at species level). The diatom stratigraphy can be divided into 6 zones (Fig. 4.5), hereafter referred to as Long Zones (LZ) I to VI. Zonation was based on cluster analysis, with the exceptions of the lower boundary of LZ V and sub-zoning of LZ IV, which were established visually, since using CONISS resulted in over-complicated zonation. Zonation using CONISS was supported by DCA (Fig. 4.7).

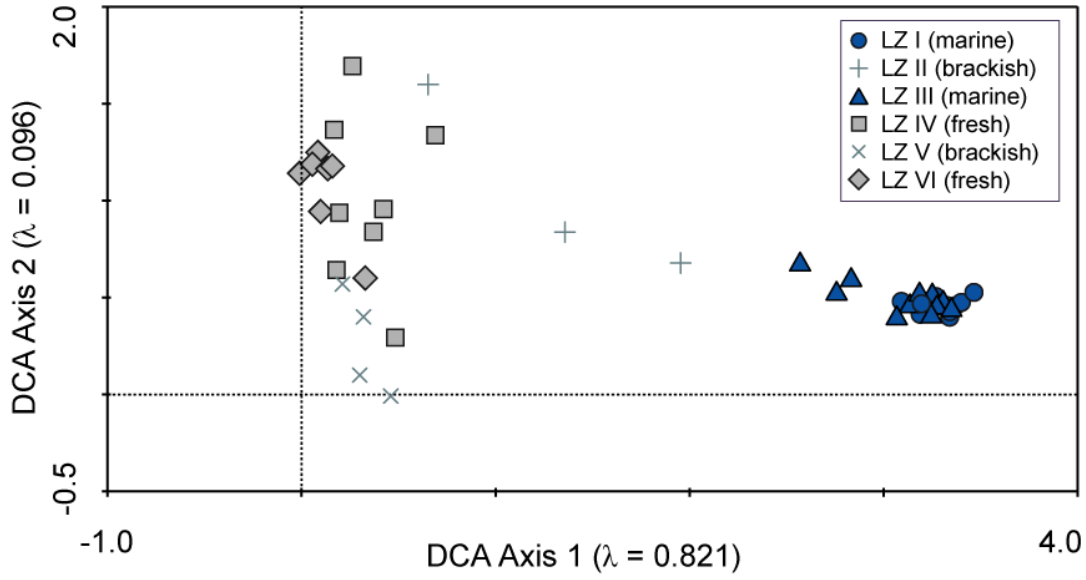

Fig. 4.7 Detrended correspondence analysis of samples from Long Lake. Samples plotting close to one another have similar diatom compositions. Eigenvalues (λ) are a measure of the importance of ordination axes.

4.3.1.1 LZ I (520-714 cm)

The lowest zone consists entirely of polyhalobous and mesohalobous-polyhalobous species. The basal 24 cm are dominated by *Synedropsis recta*, *Cocconeis costata/pinnata*, *Rhizosolenia hebetata*, *Eucampia antarctica* and *Achnanthes groenlandica*. *Navicula cancellata*, *Navicula directa* and *Pleurosigma obscurum* increase in abundance towards the top of the zone.

4.3.1.2 LZ II (508-520 cm)

Three samples form a distinct 'spike' in the diatom assemblage with the dominance of oligohalobous taxa and significant reduction in the abundance of polyhalobous species. This zone is dominated by *Nitzschia frustulum/perminuta*, with *Navicula veneta*, *Nitzschia inconspicua* and *Hippodonta hungarica* also present in large numbers. There is a significant, but low, concentration of mesohalobous species (*Achnanthes delicatula*, *Navicula phyllepta* and *Craspedostauros laevissimus*).

4.3.1.3 LZ III (318-508 cm)

This zone contains a very similar species composition to LZ I, with the dominance of polyhalobous species and disappearance of oligohalobous taxa. *Cocconeis costata/pinnata*, *Navicula glaciei*, *N. directa*, *N. perminuta* and *Nanofrustulum shiloi* dominate the assemblage. *Achnanthes groenlandica* is abundant at the base of this section, while *Pseudostaurosira* sp. and *Gyrosigma fasciola* increase in abundance towards the top. Lower concentrations of *Pleurosigma obscurum*, *Eucampia antarctica*, *Navicula cancellata*, *Synedropsis, Fragilariopsis* and *Thalassiosira* species occur throughout the zone.

4.3.1.4 LZ IV (134-318 cm)

The final transition from marine to freshwater diatoms occurs between 314-322 cm. The transition is very sharp, with a complete change in the diatom assemblage from one sample to the next. However, this freshwater zone can be further subdivided into 2 sub-zones.

Sub-zone LZ IVa (298-318 cm) represents the initial lake environment following isolation, and is dominated by oligohalobous species. There are no polyhalobous or mesohalobous species. The oligohalobous species which dominate the assemblage are the same as those of LZ II, namely *Navicula veneta*, *Nitzschia frustulum/perminuta*, *N. inconspicua*, *Planothidium lanceolatum*, *Stauroneis latistauros*, *Hippodonta hungarica*, *Gomphonema angustatum/parvulum* and *Planothidium renei/quadripunctatum*.

Between 134-298 cm (*Sub-zone LZ IVb*) there is a marked decline in diatom concentrations. Only two samples in this zone contained enough diatoms to obtain counts from, although species compositions are very similar to those found in sub-zone

IVa below. The three samples covering the section of lowest diatom concentrations from which full counts could not be achieved, also contain the same species.

4.3.1.5 LZ V (94-134 cm)

This zone sees a return to high diatom concentrations. Again the species composition is similar, although this zone is characterized by the appearance of mesohalobous species *Chamaepinnularia gerlachei* and *Navicula halophila*, and disappearance of *Navicula veneta*. Mesohalobous species constitute between 7 and 32% of the assemblage in this zone. Other species present in significant numbers include *Nitzschia gracilis*, *N. frustulum/perminuta*, *N. inconspicua*, *Fragilaria capucina* and *Gomphonema angustatum/parvulum*.

4.3.1.6 LZ VI (0-94 cm)

Finally, the uppermost zone is marked by the disappearance of mesohalobous taxa. As in sub-zone IVa and zone V, diatom species richness and concentration are high. It starts with peaks in *Hippodonta hungarica* and *Planothidium renei/quadripunctatum*. Significant concentrations of *Planothidium lanceolatum*, *P. delicatulum*, *Naviculadicta seminulum*, *Gomphonema angustatum/parvulum* and *Staurosirella pinnata* occur throughout, with *Achnanthes exigua* increasing in abundance towards the surface.

4.3.2 $\delta^{13}C_{org}$ and C/N ratios

The results of isotopic and physical analyses are presented in Fig. 4.6. In total, 49 samples were analysed for %C, %N (from which C/N ratios were calculated) and $\delta^{13}C$. There are two distinct peaks in %C values, corresponding to both transitions in the diatom record from marine to freshwater species. The lower peak (3.3%) occurs at the boundary between LZ I and LZ II, with values decreasing sharply at the upper limit of LZ II as marine diatoms dominate again. The upper peak (6.8%) occurs in LZ IVa, immediately after the main transition from marine to freshwater sediment. With the exception of these peaks and the uppermost 75 cm, organic content is low (<1.1%). Even in the uppermost 75 cm, carbon content does not exceed 3%. Likewise, %N is also low; only 13 of the 49 samples analysed contained a detectable level of nitrogen (>0.1%). Consequently it is not possible to assess trends from C/N ratios. Where %C and %N values are highest at the marine-freshwater transitions, C/N ratios are between 9 and 12.

$\delta^{13}C$ values range between -23‰ and -17‰ in the marine section, generally increasing upwards through the zone. There is no significant change in values in the lowermost freshwater section (LZ II). Values reach a peak at -14.9‰ immediately after the main marine-freshwater transition. There is a discernible lag between the diatom record and $\delta^{13}C$ profile, with $\delta^{13}C$ values relatively high in LZ IVa, then abruptly dropping at the boundary into sub-zone IVb. The abrupt shift in diatom species therefore occurs before the decrease in $\delta^{13}C$. $\delta^{13}C$ values decrease sharply to -28.4‰ in LZ IVb and values remain low until 114 cm depth. Below 114 cm freshwater sediments yield values below -23‰ and are therefore distinguishable from those of zones I to III. However, above this depth in LZ V and LZ VI, $\delta^{13}C$ values increase to between -23‰ and -16‰. Reasons for this will be explored in Chapter 5.

4.3.3 Physical analyses

As at Yanou Lake, both the magnetic susceptibility (MS) and gamma density profiles from Long Lake exactly mirror the $\delta^{13}C$ record (Fig. 4.6). There are significant troughs in MS and gamma density at the marine-freshwater transitions. Low MS and gamma density values correspond to periods of higher $\delta^{13}C$ values and vice versa. In the uppermost 114 cm where $\delta^{13}C$ values increase there is also a distinct drop in MS and gamma density.

4.3.4 Core chronology

The chronology of the Long Lake cores is based on 9 AMS ^{14}C dates (Table 4.3, Fig. 4.8). A shell and bulk sediment pair were dated from the same stratigraphic depth (572-573 cm) in order to determine any possible marine reservoir offset. Unfortunately the surface age (1900 ^{14}C yr) obtained is probably unreliable due to the human disturbance of the lake catchment contaminating the lake floor and preventing accurate radiocarbon dating. However, as the setting of Long is the same as the other lakes studied where reliable modern surface dates have been obtained, it is assumed that no surface correction is needed.

The most significant dates are those on the two marine-freshwater transitions. The lower transition (brief excursion from marine sediment above and below) is dated to 6445 ± 40 ^{14}C yr BP (7360 cal yr BP). The uppermost transition is constrained by two dates taken on either side of 5872 and 6034 ^{14}C yr BP (6730-6920 cal yr BP). There is

a slight age reversal, although this is within the 2-sigma error range. Note the conventional age obtained from just above the transition between LZ III and IVa (303 cm depth) is significantly older than that 27 cm below. It is likely that around the transition there would have been influences from both fresh and marine water and the carbon pool would still have been largely marine in origin immediately after the marine-lacustrine transition (Zwartz *et al.*, 1998). Therefore the date from 303 cm depth has been marine reservoir corrected even though it is on freshwater bulk sediment; correction is necessary to keep the dates in stratigraphic order.

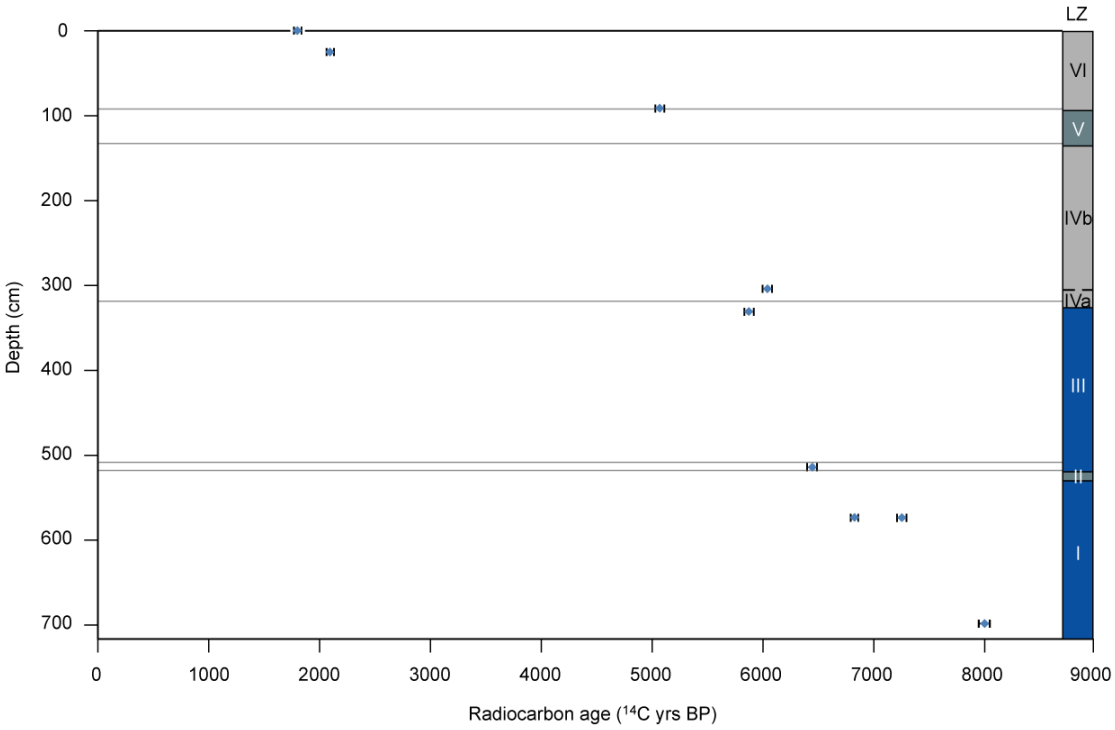

Fig. 4.8 Depth versus radiocarbon age (uncalibrated) for the Long Lake core. Error bars are shown to 1-sigma. Dates on marine material (all those below 300 cm) have been corrected using the Maxwell Bay marine reservoir correction of 1064 ± 10 yrs (details on reservoir correction are given in section 4.2.4 and in the caption to Table 4.2).

Sample	Material	Lab code	Conventional ^{14}C age	$\delta^{13}C_{VPDB}$ ± 0.1‰	Marine reservoir corrected ^{14}C age	Calibrated age range (cal yr BP)		
			(yr BP ± 1σ)		(yr BP ± 1σ)	1-sigma	2-sigma	Median
1A: 0 (0)	Bulk sediment	Beta-274128	1900 ± 40	-18.4	---	1718-1824	1634-1649 (2%) 1694-1882 (98%)	1779
1A: 24 (24)	Moss	SUERC-18933	2087 ± 37	-25.0*	---	1927-2041	1893-2072 (91%) 2076-2114 (9%)	1986
1B-I: 29 (89)	Bulk sediment	SUERC-22318	5058 ± 38	-22.4	---	5657-5752 (78%) 5827-5859 (22%)	5621-5626 (1%) 5644-5798 (67%) 5802-5893 (32%)	5735
2C-I: 26 (303)	Bulk sediment	SUERC-18924	7098 ± 39	-20.6	6034 ± 40	6860-6979	6787-7049	6920
2C-I: 53 (330)	Bulk sediment	SUERC-18925	6936 ± 39	-18.9	5872 ± 40	6666-6773	6625-6843	6725
2D-I: 67 (512)	Bulk sediment	SUERC-22319	7509 ± 39	-21.0	6445 ± 40	7325-7409	7269-7435	7364
3A-I: 35 (572)	Shell	SUERC-22301	7883 ± 36	1.5	6819 ± 37	7633-7726	7594-7777	7681
3A-I: 35 (572)	Bulk sediment	SUERC-22320	8313 ± 39	-18.0	7249 ± 40	8050-8158	7994-8202	8105
3A-II: 68 (697)	Bulk sediment	SUERC-22322	9066 ± 42	-20.6*	8002 ± 43	8957-9072	8852-9143 (99%) 9160-9170 (0.1%)	9007
3A-II: 84 (719)	Bulk sediment	Produced insufficient CO_2 for AMS analysis						

Table 4.3 Radiocarbon dates from Long Lake.
Stratigraphic depths of samples are given in brackets; * denotes estimated $\delta^{13}C$ value where there was insufficient material for an independent $\delta^{13}C$ measurement. ^{14}C ages have been normalized to $\delta^{13}C_{PDB}$‰ -25 using the $\delta^{13}C$ values shown. Details on reservoir correction and calibration are given in the caption to Table 4.2. Shell dates were corrected using the same reservoir correction as bulk marine sediment.

4.3.5 Summary

When the results of diatom, isotope and physical analyses from Long Lake are combined, six distinct zones are identifiable. The basal 4 m of the core (LZ I and III) from around 8000 to 6000 ^{14}C yr BP (9010-6900 cal yr BP) is marine, with high δ^{13}C values, low organic content and consists of polyhalobous diatoms. However, there is a distinct freshwater incursion between these zones (LZ II) around 6445 ^{14}C yr BP (7360 cal yr BP). At this time, freshwater diatom species dominate, organic content is high, and there are troughs in magnetic susceptibility and gamma density. The main isolation contact following the marine phase is placed between 314 and 322 cm, and dates to 5872-6034 ^{14}C yr BP (6730-6920 cal yr BP). There is an abrupt shift in all proxies, most notably in the diatom assemblage, but also troughs in magnetic susceptibility and gamma density. There is a significant decline in δ^{13}C immediately after the transition. The lake remains isolated to the present day, although as at Yanou there is a distinct period of brackish influence (LZ V) between 94 and 178 cm. This zone is not identifiable in the magnetic susceptibility, gamma density or %C records, but there is a marked increase in δ^{13}C upwards through the zone. There is a clear transition from this brackish-freshwater environment (LZ V) to a completely freshwater environment (LZ VI) around 5060 ^{14}C yr BP (5740 cal yr BP). The change in diatom assemblage is mirrored by an increase in δ^{13}C, %C and decrease in gamma density and magnetic susceptibility.

4.4 Ardley Lake (18 m amsl)

Results of diatom analysis are shown in Fig. 4.9, and a summary of all results is presented in Fig. 4.10.

4.4.1 Diatom analysis

Of the 44 samples prepared for diatom analysis, 40 contained a sufficient diatom concentration to count 250 valves per sample. Taxa characteristic of freshwater and brackish environments were identified, with only scattered polyhalobous diatoms (never more than 6% per sample, with the majority < 2%). In total 70 diatom taxa were identified (of which only two could not be identified at species level). The diatom stratigraphy can be divided into 3 zones based on cluster analysis (Fig. 4.9), hereafter referred to as Ardley Zones (AZ) I to III. Each zone coincides with the zonation suggested by the highest splits of CONISS.

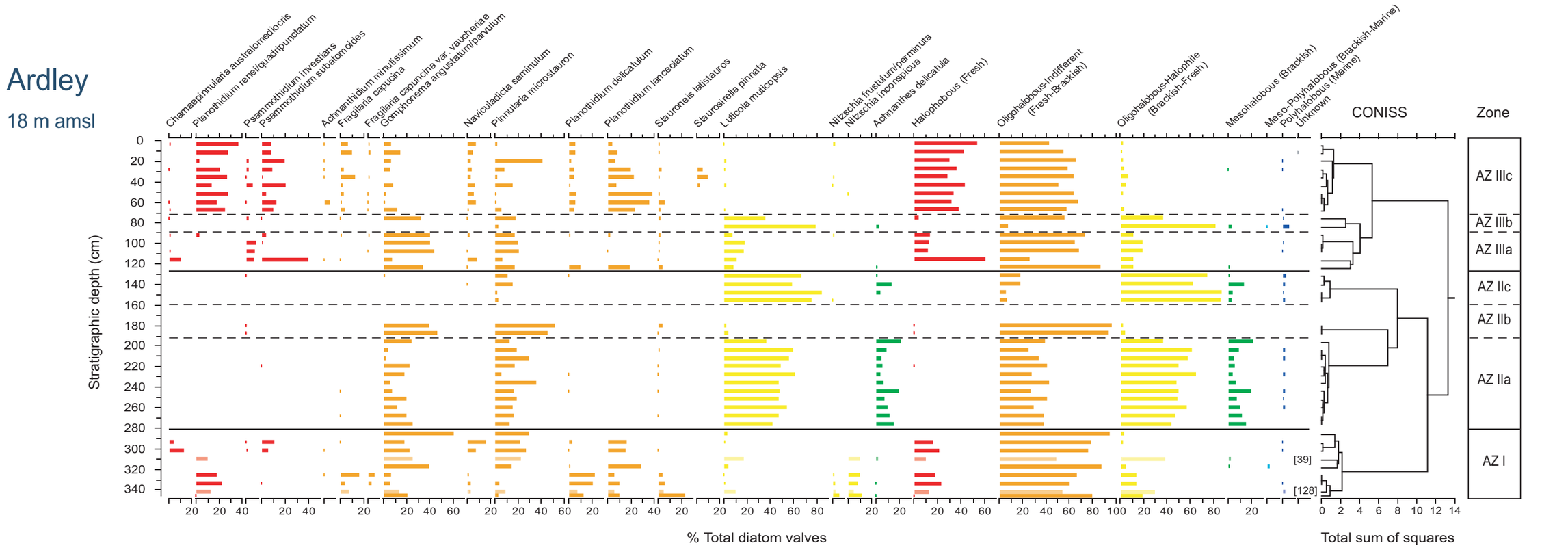

Fig. 4.9 Diatom assemblage of Ardley Lake. Species are grouped by salinity tolerance. Only species >5% of the total valves counted are shown. Where diatom concentrations were too low to achieve a full count of 250 valves, counts are shown as paler bars and the number of valves counted is shown in brackets

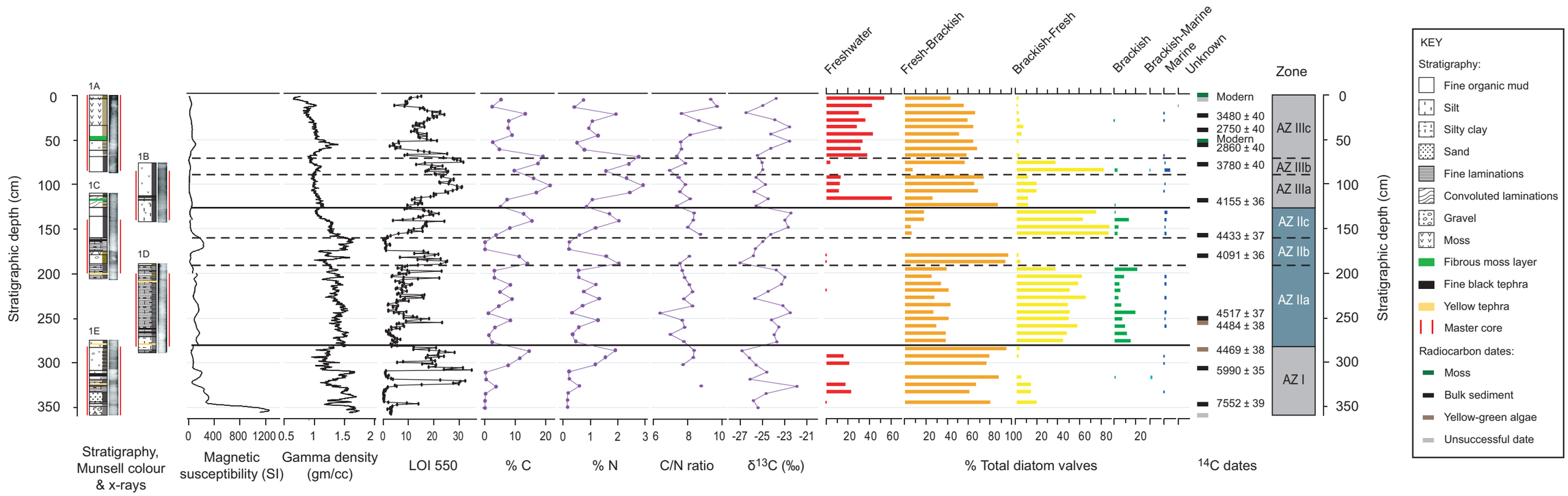

Fig. 4.10 Summary of physical, isotopic and diatom analyses from Ardley Lake, including core stratigraphy and radiocarbon dates

4.4.1.1 AZ I (281-346 cm)

The lowermost zone is dominated by oligohalobous-indifferent and halophobous species. *Stauroneis latistauros*, *Planothidium delicatulum*, *P. lanceolatum*, *Gomphonema angustatum/parvulum*, and *Planothidium renei/quadripunctatum* are the most abundant species at the base, with *Pinnularia microstauron*, *Naviculadicta seminulum*, *Chamaepinnularia australomediocris* and *Psammothidium subatomoides* increasing in relative abundance towards the top of the zone. There is a distinct peak in *Gomphonema angustatum/parvulum* at 286 cm (61%).

4.4.1.2 AZ II (128-281 cm)

This zone is marked by the absence of halophobous taxa, appearance of mesohalobous species (up to 22%) and increased relative abundances of oligohalobous-halophilous taxa. Polyhalobous species are present in very low relative abundances (<4%). Species diversity is also low, with four species constituting over 62% of the total diatom count per sample, and over 90% of total counts in 14 of the 18 samples. These four species are *Luticola muticopsis* (oligohalobous-halophilous), *Gomphonema angustatum/parvulum*, *Pinnularia microstauron* (oligohalobous-indifferent) and *Achnanthes delicatula* (mesohalobous).

This zone can be further sub-divided into 3 sub-zones, with *Sub-zone AZ IIa* (192-281 cm) and S*ub-zone AZ IIc* (128-160 cm) described as above, but an excursion between 160 and 192 cm (*Sub-zone AZ IIb*). The two lowermost samples of sub-zone AZ IIb are characterized by reduced abundances of the slightly brackish species *Luticola muticopsis* and *Achnanthes delicatula*, and increased concentrations of the fresh-brackish taxa *Pinnularia microstauron* and *Gomphonema angustatum/parvulum*. Above this (164-172 cm) there is a marked decrease in diatom concentrations, with two samples containing insufficient valves to achieve counts.

4.4.1.3 AZ III (0-128 cm)

The uppermost zone is characterized by the abrupt re-appearance of halophobous taxa and the disappearance of mesohalobous species. As with AZ II, this zone can be further divided into 3 sub-zones. The species composition of *Sub-zone AZ IIIa* (88-128 cm) is similar to that of AZ I. *Gomphonema angustatum/parvulum*, *Luticola muticopsis* and *Pinnularia microstauron* continue to dominate initially, although with significant

abundances of the halophobous species *Psammothidium subatomoides*, *P. investians* and *Chamaepinnularia australomediocris*.

Between 72 and 88 cm (*Sub-zone AZ IIIb*) there is a sharp peak in the oligohalobous-halophilous species *Luticola muticopsis*, which coincides with reduced abundances of halophobous species.

The top 70 cm (*Sub-zone AZ IIIc*) are dominated by *Planothidium renei/quadripunctatum*, *P. lanceolatum*, *Psammothidium subatomoides* and *Pinnularia microstauron*. *Gomphonema angustatum/parvulum*, *Planothidium delicatulum*, *Naviculadicta seminulum* and *Fragilaria capucina* are also present in low abundances.

4.4.2 $\delta^{13}C_{org}$ and C/N ratios

The results of isotopic and physical analyses are presented in Fig. 4.10. In total, 44 samples were analysed for %C, %N and $\delta^{13}C$. Ardley is much more organic than Long and Yanou, with sediments containing up to 22% carbon. A quarter of the samples analysed contain over 11% carbon. The %C profile is highly variable, although as expected corresponds perfectly to LOI. However, there are no clear trends associated with the diatom zones. Nitrogen levels are also higher, and so C/N ratios could be calculated; ratios are between 6.4 and 9.9. $\delta^{13}C$ values range between -21.8‰ and -27‰. However, again there seems to be no correspondence between $\delta^{13}C$ values and diatom species.

4.4.3 Physical analyses

Gamma density and magnetic susceptibility profiles show the same broad trends, with peaks and troughs aligned (Fig. 4.10). Peaks in both parameters relate to periods of very low diatom preservation and low organic content.

4.4.4 Core chronology

The chronology of the Ardley cores is based on 14 AMS ^{14}C dates (Table 4.4, Fig. 4.11). A freshwater algae and bulk sediment pair was dated from the same stratigraphic depth (252-253 cm) in order to determine any possible offset.

There are problems with age reversals amongst many of the dates from Ardley, which makes it difficult to place precise age constraints on the zone boundaries. The six dates obtained from a 165 cm section of AZ II all date to within 500 years (between 4091 and 4517 ^{14}C yr BP), with two age reversals in the sequence. Close agreement between the algae-bulk sediment pair towards the base of AZ II gives credence to this age being correct. An identical age on the yellow-green algae 30 cm below suggests this may in fact be the same macrofossil, which has been transported down core. This would place the boundary between AZ I and II somewhere between 5990 ^{14}C yr BP (28 cm below boundary) and ~4500 ^{14}C yr BP (28 cm above boundary). Assuming a constant sedimentation rate, the boundary dates to ~5245 ^{14}C yr BP (~5920 cal yr BP). The boundary between AZ II and AZ III dates to 4155 ± 36 ^{14}C yr BP (4620 cal yr BP).

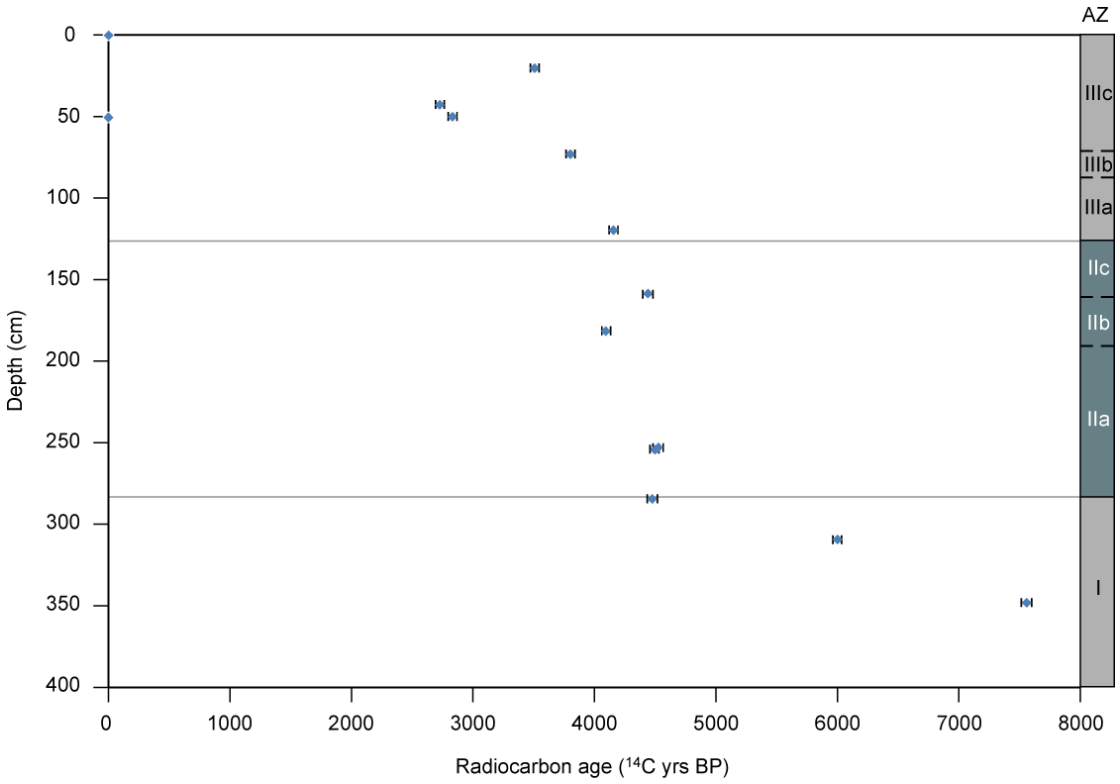

Fig. 4.11 Depth versus radiocarbon age (uncalibrated) for the Ardley core. Error bars are shown to 1-sigma.

Sample	Material	Lab code	Conventional ^{14}C age (yr BP ± 1σ)	$\delta^{13}C_{VPDB}$ ± 0.1‰	Calibrated age range (cal yr BP) 1-sigma	2-sigma	Median
SUR: 0 (0)	Moss	SUERC-22305	Modern	-23.8*	Modern		Modern
1A: 5 (5)	Moss	Produced insufficient CO_2 for AMS analysis					
1A: 22 (22)	Bulk sediment	Beta-271284	3480 ± 40	-25.7	3593-3597 (2%) 3613-3723 (88%) 3797-3816 (10%)	3572-3781 (87%) 3786-3828 (13%)	3680
1A: 42 (42)	Bulk sediment	Beta-271285	2750 ± 40	-23.6	2757-2803 (66%) 2816-2844 (34%)	2744-2877	2803
1A: 51 (51)	Moss	SUERC-22306	Modern	-23.8	Modern		Modern
1A: 51 (51)	Bulk sediment	Beta-271287	2860 ± 40	-24.0	2851-2961	2784-3006 (98%) 3014-3033 (2%) 3052-3059 (0.05%)	2908
1A: 74 (74)	Bulk sediment	Beta-271286	3780 ± 40	-25.8	3987-4048 (48%) 4064-4100 (27%) 4112-4147 (25%)	3927-3948 (3%) 3961-4181 (92%) 4197-4232 (5%)	4069
1B: 42 (118)	Bulk sediment	SUERC-22315	4155 ± 36	-26.4	4526-4629 (66%) 4634-4644 (4%) 4677-4691 (7%) 4762-4799 (23%)	4445-4474 (5%) 4478-4480 (0.1%) 4514-4729 (73%) 4740 (0.1%) 4750-4820 (22%)	4619
1C: 48 (158)	Bulk sediment	SUERC-18922	4433 ± 37	-25.9	4868-4974 (93%) 5019-5028 (7%)	4845-5052 (98%) 5191-5213 (2%)	4943
1C: 77 (180)	Moss	SUERC-22307	4091 ± 36	-23.9	4434-4533 (89%) 4543-4547 (3%) 4557-4567 (8%)	4416-4626 (95%) 4639-4641 (0.1%) 4763-4789 (5%) 4794-4796 (0.1%)	4506

Sample	Material	Lab code	Conventional ^{14}C age (yr BP ± 1σ)	$\delta^{13}C_{VPDB}$ ± 0.1‰	Calibrated age range (cal yr BP)		
					1-sigma	2-sigma	Median
1D: 63 (252)	Bulk sediment	SUERC-22316	4517 ± 37	-9.2	4977-5014 (17%) 5033-5071 (19%) 5108-5126 (8%) 5167-5277 (56%)	4890-4900 (1%) 4909-4928 (1%) 4959-5296 (98%)	5124
1D: 63.5 (252.5)	Yellow-green algae	SUERC-22308	4484 ± 38	-22.3	4880-4938 (23%) 4956-5054 (59%) 5189-5214 (12%) 5225-5232 (2%) 5245-5258 (4%)	4868-5078 (80%) 5104-5136 (5%) 5163-5280 (27%)	5025
1D: 92 (283)	Yellow-green algae	SUERC-22309	4469 ± 38	-20.5	4877-4944 (37%) 4947-5046 (63%) 5210 (0.1%)	4862-5071 (80%) 5108-5126 (2%) 5167-5276 (18%)	4997
1E: 33 (308)	Bulk sediment	SUERC-18951	5990 ± 35	-25.5	6677-6705 (20%) 6715-6796 (80%)	6666-6861 (98%) 6869-6881 (2%)	6759
1E: 72 (347)	Bulk sediment	SUERC-22317	7552 ± 39	-18.2	8215-8243 (21%) 8253-8256 (1%) 8303-8379 (78%)	8198-8270 (31%) 8272-8389 (69%)	8321
1E: 83 (358)	Bulk sediment	Produced insufficient CO_2 for AMS analysis					

Table 4.4 Radiocarbon dates from Ardley Lake.
Stratigraphic depths of samples are given in brackets; * denotes estimated $\delta^{13}C$ value where there was insufficient material for an independent $\delta^{13}C$ measurement. ^{14}C ages have been normalized to $\delta^{13}C_{PDB}$‰ -25 using the $\delta^{13}C$ values shown. Dates were calibrated using Calib (version 5.0.1, Stuiver and Reimer, 1993) using the SHCal04 calibration curve (McCormac *et al*., 2004). Where more than one calibrated range is given, the relative percentage area under the probability distribution is indicated in brackets.

4.4.5 Summary

The most significant outcome from Ardley Lake is the absence of a marine-freshwater isolation contact. There are three zones delimited from diatom analysis. AZ I and AZ III are fully freshwater, with salt intolerant diatoms dominating the record. AZ II is marked by the presence of brackish diatoms and absence of fully freshwater forms. There are also low, but significant numbers of marine diatoms (<3%). Physical and isotope profiles do not show the same zonation as the diatoms. %C and $\delta^{13}C$ values throughout the sequence are indicative of freshwater sediment.

4.5 Belén Lake (19.9 m amsl)

Results of diatom analysis are shown in Fig. 4.12, and a summary of all results is presented in Fig. 4.13.

4.5.1 Diatom analysis

Of the 34 samples prepared for diatom analysis, 31 contained a sufficient diatom concentration to count 250 valves per sample. Taxa characteristic of freshwater and brackish environments were identified. In total 72 diatom taxa were identified. The diatom stratigraphy can be divided into 3 zones based on cluster analysis (Fig. 4.12), hereafter referred to as Belén Zones (BZ) I to III. Each zone coincides with the zonation suggested by the highest splits of CONISS.

4.5.1.1 BZ I (206-266 cm)

The lowermost zone is dominated by oligohalobous and halophobous species. *Nitzschia frustulum/perminuta*, *Planothidium delicatulum* and *P. lanceolatum* dominate the assemblage throughout the zone, with *Staurosirella pinnata*, *Nitzschia inconspicua* and *Planothidium renei* to a lesser extent. There is also a notable 'spike' of polyhalobous diatoms (11%) at the top of the zone. Unfortunately diatom concentration was extremely low in this sample and a full count could not be achieved.

4.5.1.2 BZ II (134-206 cm)

This zone is marked by the appearance of the mesohalobous species *Chamaepinnularia gerlachei* (up to 78% at the base of the zone). *Nitzschia*

frustulum/perminuta continues to dominate, with *Fragilaria capucina* and *Gomphonema angustatum/parvulum* present in lower abundances.

4.5.1.3 BZ III (0-134 cm)

The uppermost zone is marked by increased abundances of halophobous and oligohalobous-indifferent species, which dominate the assemblage. Oligohalobous-halophilous taxa are present in reduced numbers and the mesohalobous species *Chamaepinnularia gerlachei* disappears. *Planothidium lanceolatum* and *Naviculadicta seminulum* dominate throughout, with *Chamaepinnularia australomediocris* abundant in the basal 80 cm of the zone, being replaced by *Psammothidium incognitum* and *Achnanthes exigua* towards the top.

4.5.2 $\delta^{13}C_{org}$ and C/N ratios

The results of isotopic and physical analyses are presented in Fig. 4.13. In total 37 samples were analysed for %C, %N and $\delta^{13}C$. The %C and $\delta^{13}C$ records can be divided into two zones, the boundary of which corresponds to the transition between BZ II and BZ III where brackish diatoms disappear. In the lower zone (equivalent to BZ I and BZ II), %C and %N values are extremely low (carbon <0.2%, nitrogen undetectable), and $\delta^{13}C$ values are highly oscillatory, fluctuating between -22‰ and -30.5‰. Whilst there is a significant decrease in $\delta^{13}C$ values across the transition observed in the diatom record between BZ I and BZ II where brackish diatoms appear, the $\delta^{13}C$ profile fluctuates too much for clear zones to be identified compared with the diatoms.

However, the transition in the diatom record between BZ II and BZ III is mirrored in the isotope record. Organic content is higher in the upper zone, with sediments containing between 2.5 and 9.3% carbon. C/N ratios are between 10 and 16. $\delta^{13}C$ values fluctuate over a smaller range than in the lower zone and are generally higher, between -19‰ and -24‰.

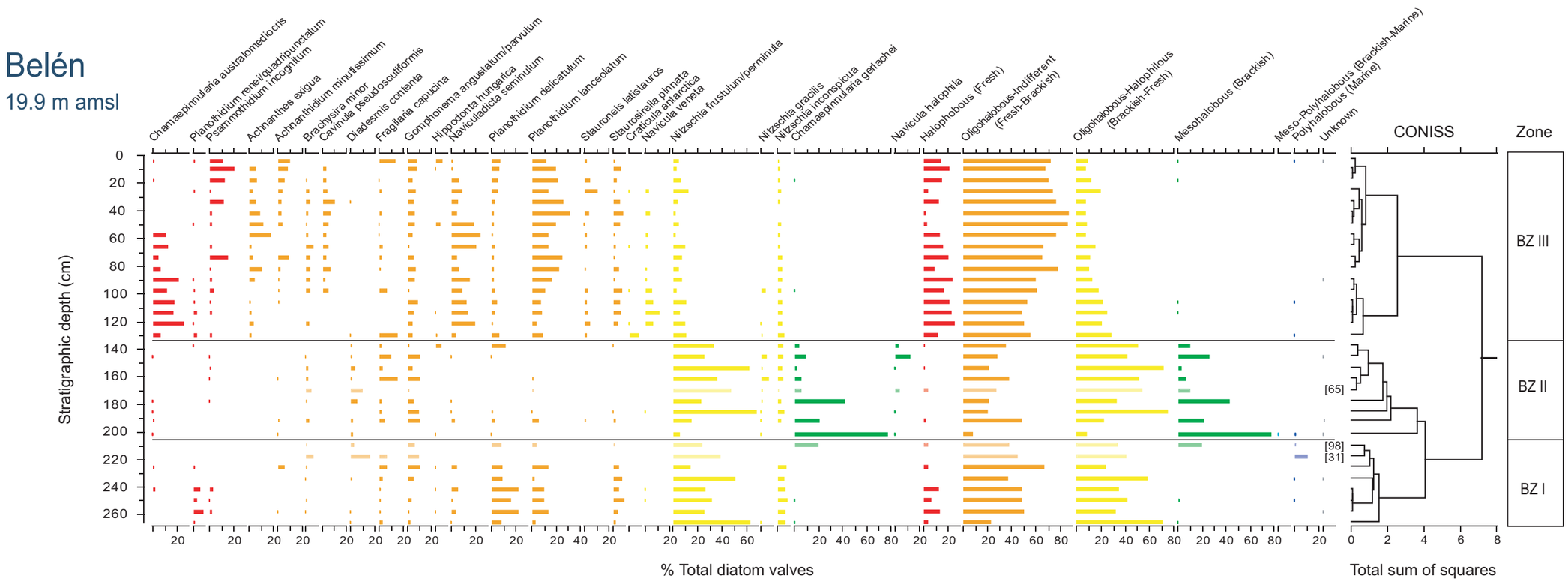

Fig. 4.12 Diatom assemblage of Belén Lake. Species are grouped by salinity tolerance. Only species >5% of the total valves counted are shown. Where diatom concentrations were too low to achieve a full count of 250 valves, counts are shown as paler bars and the number of valves counted is shown in brackets

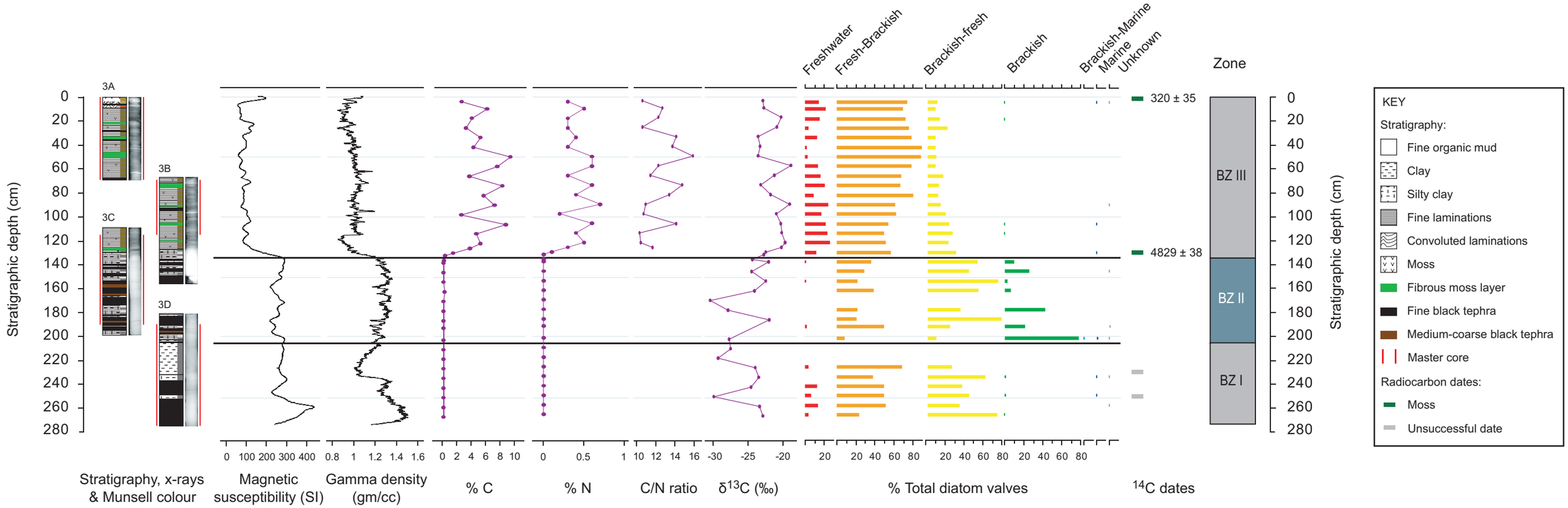

Fig. 4.13 Summary of physical, isotopic and diatom analyses from Belen Lake, including core stratigraphy and radiocarbon dates

4.5.3 Physical analyses

Profiles of physical parameters also divide into two zones. Gamma density and magnetic susceptibility are inversely related to organic content, being high throughout BZ I and BZ II, and sharply decreasing across the transition into BZ III (Fig. 4.13).

4.5.4 Core chronology

The chronology of the Belén cores is based on 2 AMS ^{14}C dates (Table 4.5, Fig. 4.13). Unfortunately the two attempts at obtaining a basal date were unsuccessful. The transition from a freshwater-brackish environment to fully freshwater (BZ II to BZ III) is dated to 4829 ± 38 ^{14}C yr BP (5510 cal yr BP).

Sample	Material	Lab code	Conventional ^{14}C age	$\delta^{13}C_{VPDB}$ ± 0.1‰	Calibrated age range (cal yr BP)		
			(yr BP ± 1σ)		1-sigma	2-sigma	Median
3A: 0 (0)	Moss	SUERC -18928	320 ± 35	-28.5	302-329 (35%) 376-394 (16%) 397-440 (49%)	284-453	382
3C: 20 (129)	Moss	SUERC -18931	4829 ± 38	-24.4	5471-5555 (85%) 5571-5586 (15%)	5329-5378 (12%) 5449-5595 (88%)	5514
3D: 48 (229)	Bulk sediment	Produced insufficient CO_2 for AMS analysis					
3D: 70 (251)	Bulk sediment	Produced insufficient CO_2 for AMS analysis					

Table 4.5 Radiocarbon dates from Belén Lake.
Stratigraphic depths of samples are given in brackets. ^{14}C ages have been normalized to $\delta^{13}C_{PDB}$‰ -25 using the δ^{13}C values shown. Details on calibration are given in the caption to Table 4.4.

4.5.5 Summary

As at Ardley, there is no marine-freshwater isolation contact at Belén. Three zones are identifiable from diatom analysis. BZ I and BZ III are fully freshwater, and BZ II is marked by the presence of brackish diatoms and reduced numbers of fully freshwater forms. However, only two zones are observable from isotopic and physical analyses. BZ I and BZ II appear the same, with a sharp transition in all isotopic and physical parameters between BZ II and BZ III. Finally, it is important to note that coring to the

glacial sediment interface was prevented by an impenetrable thick consolidated tephra layer.

4.6 Gaoshan Lake (34.5 m amsl)

Results of diatom analysis are shown in Fig. 4.14, and a summary of all results is presented in Fig. 4.15.

4.6.1 Diatom analysis

Of the 23 samples prepared for diatom analysis, 13 contained a sufficient diatom concentration to count 250 valves per sample. Taxa characteristic of freshwater and slightly brackish environments were identified. In total 51 diatom taxa were identified. Unlike the other lakes, the diatom stratigraphy has not been zoned as clear transitions are not visible (Fig. 4.14).

Gaoshan is dominated by oligohalobous-indifferent species, with oligohalobous-halophilous and halophobous taxa present in lower abundances. No polyhalobous species were identified, and only 17 valves of mesohalobous species were counted (0.7% of total counted). Species diversity is reasonably high, with no one species dominating the assemblage. *Achnanthidium minutissimum*, *Staurosirella pinnata*, *Planothidium delicatulum*, *P. lanceolatum*, *P. renei/quadripunctatum*, *Hippodonta hungarica*, *Naviculadicta seminulum*, *Gomphonema angustatum/parvulum* and *Nitzschia frustulum/perminuta* are the most dominant species throughout. There is a significant period of poor diatom preservation between 156 and 268 cm, where it was not possible to count 250 valves per sample.

4.6.2 $\delta^{13}C_{org}$ and physical analyses

The results of isotopic and physical analyses are presented in Fig. 4.15. 12 samples were analysed for %C, %N and $\delta^{13}C$. Organic content is generally low, with all samples containing <1.1% carbon and <0.1% nitrogen, with the exception of two samples at the base of the core of 4-4.7% carbon. $\delta^{13}C$ values are between -19‰ and -27.4‰.

Gamma density is broadly inverse to organic content, with the most organic samples having the lowest gamma density. The magnetic susceptibility profile shows no significant trends, with only two peaks at around 40 cm and at the very base of the core.

4.6.3 Core chronology

The chronology of the Gaoshan cores is based on 3 AMS ^{14}C dates (Table 4.6, Fig. 4.15).

Sample	Material	Lab code	Conventional ^{14}C age	$\delta^{13}C_{VPDB}$ ± 0.1‰	Calibrated age range (cal yr BP)		
			(yr BP ± 1σ)		1-sigma	2-sigma	Median
1B: 0 (0)	Bulk sediment	SUERC -18951	1223 ± 35	-21.3	1011-1027 (12%) 1054-1142 (80%) 1159-1169 (8%)	977-1176	1087
1B: 24 (24)	Moss	SUERC -18932	2215 ± 37	-25.0*	2066-2081 (8%) 2109-2164 (42%) 2166-2180 (7%) 2240-2305 (44%)	2009-2020 (1%) 2039-2214 (61%) 2217-2311 (38%)	2165
1I: 75 (314)	Bulk sediment	SUERC -18923	6366 ± 39	-20.9	7172-7224 (54%) 7230-7271 (46%)	7158-7329 (98%) 7358-7371 (1%) 7394-7413 (1%)	7236

Table 4.6 Radiocarbon dates from Gaoshan Lake.
Stratigraphic depths of samples are given in brackets; * denotes estimated $\delta^{13}C$ value where there was insufficient material for an independent $\delta^{13}C$ measurement. ^{14}C ages have been normalized to $\delta^{13}C_{PDB}$‰ -25 using the $\delta^{13}C$ values shown. Details on calibration are given in the caption to Table 4.4.

4.6.4 Summary

The analyses from Gaoshan confirm the lake to be an entirely freshwater basin for at least the last 6400 ^{14}C years. No distinct transitions are observable from the diatom, isotopic or physical analyses.

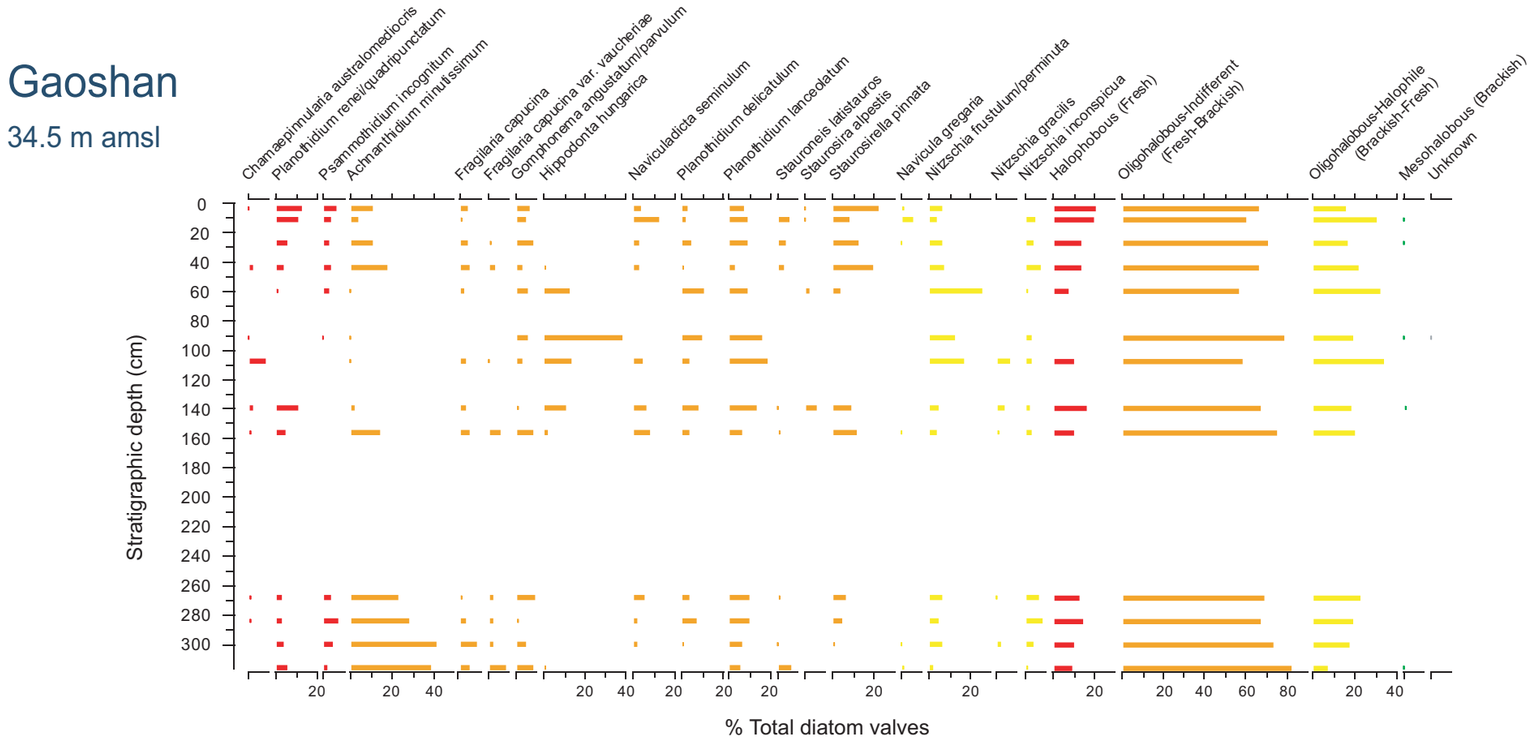

Fig. 4.14 Diatom assemblage of Gaoshan Lake. Species are grouped by salinity tolerance. Only species >5% of the total valves counted are shown.

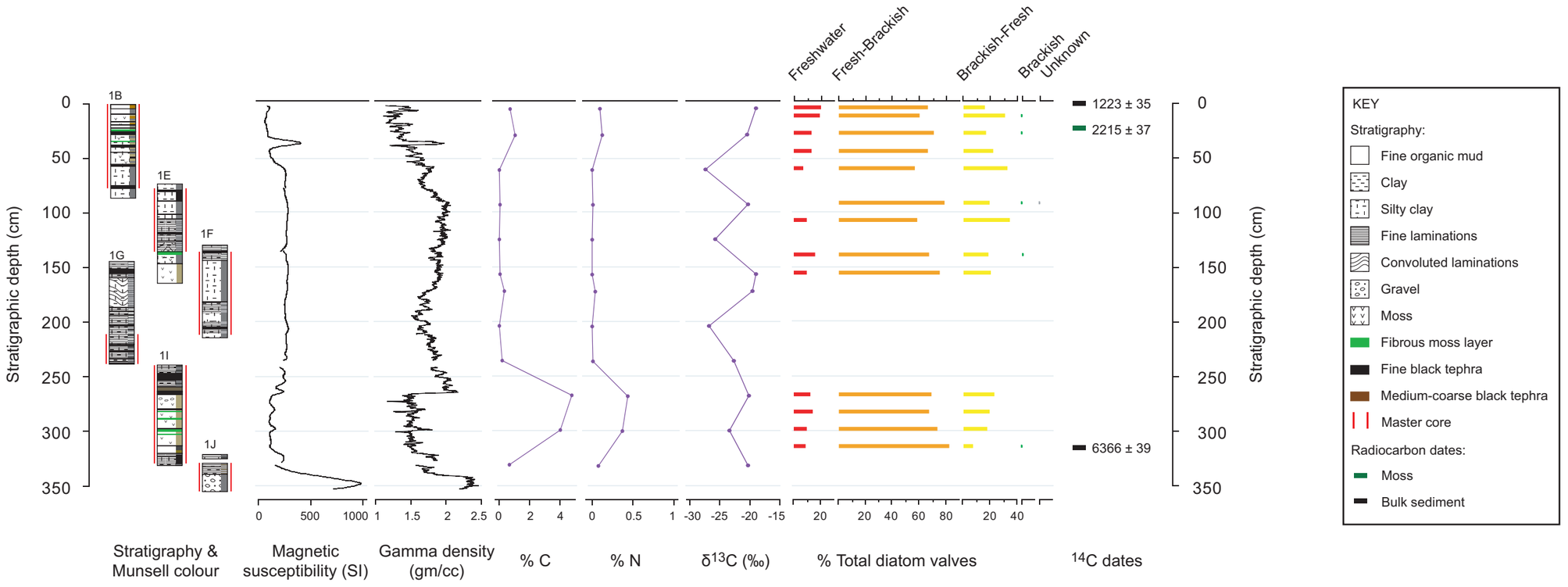

Fig. 4.15 Summary of physical, isotopic and diatom analyses from Gaoshan Lake, including core stratigraphy and radiocarbon dates

4.7 Summary

This chapter has presented the results of diatom, isotope and physical analyses of lake cores. Clear marine-freshwater transitions are present in Long and Yanou Lakes. Significantly there is not a marine signal in any of the three lakes above 15 m amsl, although there are brackish zones in both the Ardley and Belén records (18-20 m amsl). There are also notable freshwater incursions in between two marine sections in both Long and Yanou Lakes which require further explanation. In the next chapter, the biological zones identified in each lake are discussed in detail, and concurrent changes between lakes are explored. Specifically the implications for relative sea level are examined and a preliminary relative sea level curve developed based on the isolation basin data.

CHAPTER 5

Relative sea level reconstruction from isolation basins: interpretation of results

5.1 Introduction

This chapter discusses the results of diatom, isotope and physical analyses of lake cores which were presented in the previous chapter. Specifically this chapter has four aims; (i) to explain key transitions and trends in the proxy records in terms of relative sea level change and lake processes; (ii) to identify concurrent changes between lakes; (iii) to develop a relative sea level curve; and (iv) to place the results in context with other studies. The results are interpreted for each lake in turn, before being integrated to produce the RSL curve. The locations of all other sites referred to in this chapter are included on Fig. 5.1.

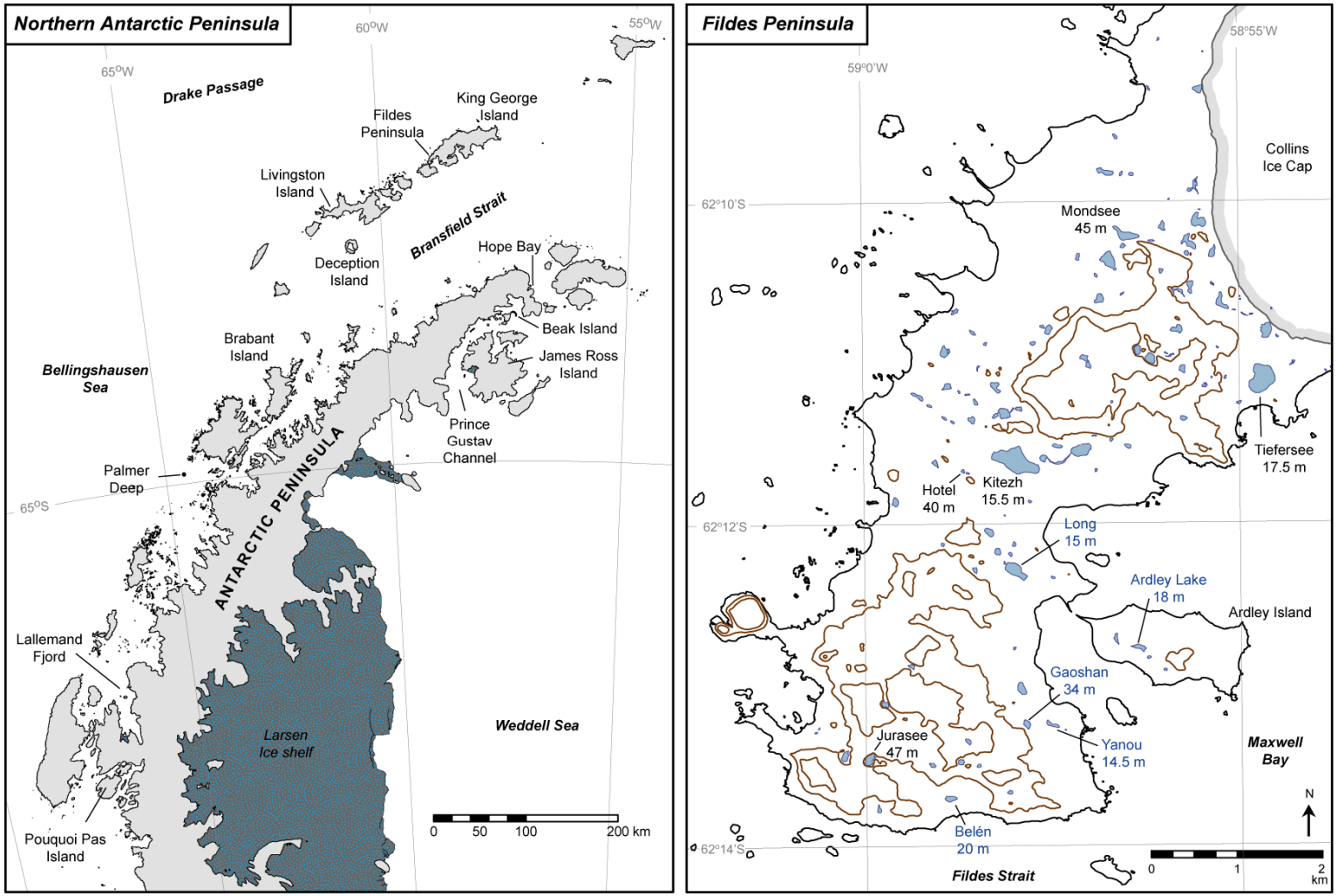

Fig. 5.1 Locations of sites referred to in this chapter on (a) the northern Antarctic Peninsula, and (b) Fildes Peninsula, King George Island. The lakes cored in this study are labelled in blue, and sill heights are quoted as metres above mean sea level. Sill heights of lakes not cored are taken from Mäusbacher *et al*. (1989), Mäusbacher (1991), and the SCAR King George Island GIS Project.

5.2 Yanou Lake (14.5 m amsl)

From diatom, isotope and physical analyses, there are six distinct zones identifiable in the Yanou Lake record (Fig. 4.2). There are two marine zones (YZ I and III), two freshwater zones (YZ IV and VI) and two fresh-brackish sections (YZ II and V). These will now be examined in turn.

5.2.1 YZ I: Marine

The basal zone of almost 1 m is dominated by marine diatoms, low organic content, and fluctuating (although generally high) magnetic susceptibility and gamma density (Fig. 4.2). It is characterized by low total diatom abundances and a relatively high percentage of broken valves. The diatom assemblage is composed of a mixture of marine (*Cocconeis costata/pinnata* and *Synedra kerguelensis*) and sea-ice related taxa (*Thalassiosira antarctica*, *Navicula criophila*, *N. directa* and *N. glaciei*). The dominance of sea-ice related species and low total abundances may reflect a period of sea-ice cover and cold climatic conditions. The poor preservation of the diatoms and the presence of coarse material in the marine organic mud matrix may be indicative of decaying icebergs and episodic melting (Sterken, 2009). The presence of a very few freshwater species reflects the nearshore position of the basin and suggests it was subject to dilution by freshwater run-off.

Two basal dates of 10506 ± 71 ^{14}C yr BP (12480 cal yr BP; note all calibrated dates reported are the median of the calibrated age range) and 9566 ± 71 ^{14}C yr BP (10925 cal yr BP) constrain the timing of deglaciation. To place these dates in context, the minimum age for ice retreat from Maxwell Bay (based on marine core and seismic data) is 13860 ± 140 cal yr BP, with a period of rapid glacial retreat between 10100 and 8200 cal yr BP (Milliken *et al.*, 2009). From the radiocarbon dating of lake sediments, Mäusbacher *et al*. (1989) proposed that Fildes Peninsula remained ice covered until 9000 ^{14}C yr BP, with subsequent glacial retreat occurring progressively from southwest to northeast across the peninsula until 5000 ^{14}C yr BP. The dates from Yanou therefore correspond with previous work, and it would appear that the base of YZ I marks the onset of deglaciation. The Yanou dates suggest deglaciation occurred slightly earlier than Mäusbacher *et al*. (1989) proposed, although as the ages of the two Yanou basal samples are reversed out of stratigraphic order there is potentially reworking of

sediment containing older carbon occurring, which suggests these should be interpreted as maximum ages.

As there is no freshwater sediment at the base of the core this implies that the sill of Yanou Lake (14.5 m amsl) was below sea level at the onset of deglaciation. This suggests that the Collins Ice Cap was grounded close to sea level around 9500-10500 ^{14}C yr BP, and as it retreated this part of Fildes Peninsula and other areas at the lowest altitudes were initially below sea level.

5.2.2 YZ II: Fresh-brackish

YZ I terminates with a brief interval of freshwater sedimentation between 6262 and 6091 ^{14}C yr BP (7200-7000 cal yr BP, but note the age reversal). This interval is only 16 cm thick but has entirely different characteristics to the zones above and below. %C and %N peak at the top of the zone and there are troughs in magnetic susceptibility and gamma density. Two samples were analysed for diatoms from this zone, interestingly with contrasting assemblages. The lowermost sample is dominated by diatom taxa with broad salinity tolerances that are characteristic of nutrient-rich waters, such as *Gomphonema angustatum/parvulum*, *Nitzschia frustulum/perminuta* and *N. inconspicua* (Jones *et al.*, 1993; Jones and Juggins, 1995; Sterken, 2009). The presence of these diatoms, together with the relative peak in organic content suggests high productivity conditions due to marine derived nutrients. Other relatively abundant taxa in the lowermost sample are *Achnanthidium minutissimum*, which is found to dominate shallow water lakes on Signy Island (Oppenheim and Ellis-Evans, 1989; Jones, 1996), and *Planothidium delicatulum*, an epilithic species found in low elevation lakes on Signy, Livingston and Beak Islands at sites associated with sea-spray and in meltwater streams (Jones *et al.*, 1993; Jones and Juggins, 1995; Sterken, 2009). The uppermost sample is dominated by *Navicula veneta*, which is also a eutrophic species, especially common in terrestrial habitats heavily influenced by sea-spray (Van de Vijver *et al.*, 2008; Sterken, 2009).

There are four possible explanations for this freshwater zone between marine intervals; it may be related to (i) relative sea level change and variations in the balance between eustasy and isostasy as a consequence of glacial retreat in two stages, or (ii) relative sea level change as a consequence of isostatic uplift followed by ice *readvance* and

isostatic depression, or (iii) relative sea level change as a consequence of peripheral forebulge migration or collapse, or (iv) an influx of glacial meltwater. In the case of the first three hypotheses that YZ II relates to a change in RSL, the lower contact of the unit represents isolation from the sea. Retreat of the Collins Ice Cap would have caused isostatic uplift and thus RSL fall throughout YZ I. Once RSL fell below the height of the sill at Yanou, the basin would have become disconnected from the sea and freshwater sediment would have accumulated (YZ II). Support for this hypothesis comes from the diatom species present, which were found in high relative abundances across the marine-freshwater transition zone of isolation basin cores from Beak Island, Prince Gustav Channel (Sterken, 2009) and Narrows Lake, Pourquoi Pas Island, Marguerite Bay (D. Hodgson, pers. comm., Roberts *et al.*, 2007). The transitional diatom assemblages rule out the possibility of this unit being re-deposited sediment. The presence of shallow water taxa, those associated with sea spray, and low abundances of marine diatoms in this zone suggest RSL did not fall much below the sill height of Yanou Lake. A similar unit of only 18 cm containing up to 80% lacustrine diatoms was observed within marine sediments in the Norwegian isolation basin Særvikmyra (Lohne *et al.*, 2004). This unit was also characterized by euryhaline diatom species, and interpreted as reflecting a period when sea level was very close to the basin threshold.

However, isostatic uplift and RSL fall cannot have continued as marine diatoms then dominate the assemblage again (YZ III). As global eustatic sea level is assumed to have risen throughout this period according to the widely accepted far-field curve (Fairbanks, 1989; Milne *et al.*, 2009) then isostatic uplift cannot have occurred linearly to cause the observed changes in RSL. Instead, the upper contact of YZ II may be explained by either glacial retreat in two stages (hypothesis 1) or a minor readvance of the ice cap (hypothesis 2), both affecting the rate of isostatic uplift. Alternatively, this may reflect the influence of the Antartic Peninsula ice sheet (hypothesis 3).

The first hypothesis that glacial retreat occurred in two stages is summarized in Fig. 5.2. These hypothetical graphs show the eustatic and isostatic components of RSL and demonstrate that a non-linear isostatic uplift rate could produce a RSL record like the one from Yanou Lake. During YZ I and the beginning of YZ II, glacial retreat would have caused isostatic uplift which outpaced eustatic sea level rise and produced the observed RSL fall and basin isolation. However if ice retreat temporarily stopped, and

so uplift slowed, then eustatic sea level rise would have dominated the RSL signal over the reduced rate of isostatic uplift, and caused ingression of the sea into Yanou (YZ III). A second phase of glacial retreat would then have had the same effect as the first, with isostatic uplift once again the dominant contributor to RSL fall, causing the second isolation of Yanou (YZ III to IV). This RSL curve shape is the same as that observed in northwest Scotland (Firth and Haggart, 1989; Boulton *et al.*, 1991; Shennan *et al.*, 1994; Lambeck, 1995; Shennan *et al.*, 2000; Shennan *et al.*, 2005), north Norway (Møller, 1986; Vorren *et al.*, 1988) and the Gulf of Finland (Miettinen, 2004), where isolation basin sediments show similar brief freshwater zones within a period of mid-Holocene marine dominance. Although it is interesting that the period of RSL rise occurs much later in the Yanou Lake record than in the northern hemisphere, where it is around 10000 cal yr BP.

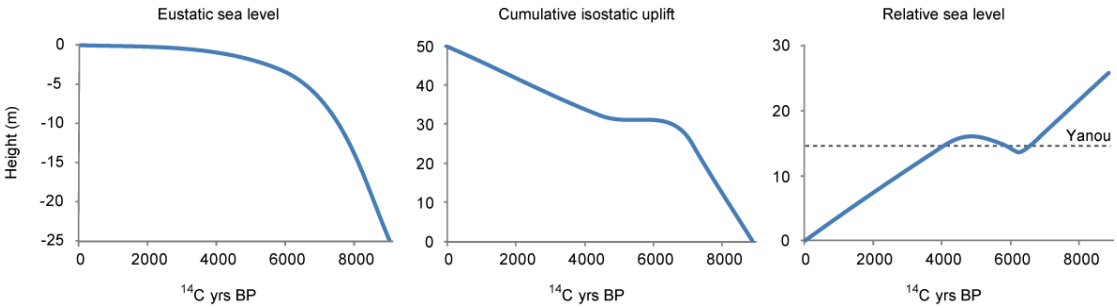

Fig. 5.2 Hypothetical sea level curves, showing the eustatic and potential isostatic components of relative sea level. The eustatic curve was constructed using data from Milne *et al*. (2009)

Alternatively isostatic uplift may have been interrupted by a minor glacial readvance. As suggested earlier, if sea level was close to the basin sill height then a slight glacial readvance may have depressed the land enough to cause a sea level incursion again. Similar reports of mid-Holocene RSL rise in a period otherwise characterized by RSL fall in response to deglaciation come from isolation basins of southern Greenland (Sparrenbom *et al.*, 2006a, 2006b). Here this RSL rise was interpreted as being partly due to reloading by advancing glaciers, although was of longer duration and the change in RSL was more gradual. Verleyen *et al*. (2005) also demonstrated that the RSL history of the Larsemann Hills region of East Antarctica was perturbed by readvance of the Lambert Glacier.

To assess the viability of a small glacial readvance causing the apparent sea level change, the possible magnitude of an elastic response to crustal loading was roughly calculated, based on the assumption of an infinite sheet of ice (P. Whitehouse, pers. comm., Watts, 2001). This equates to part a of Fig. 5.3.

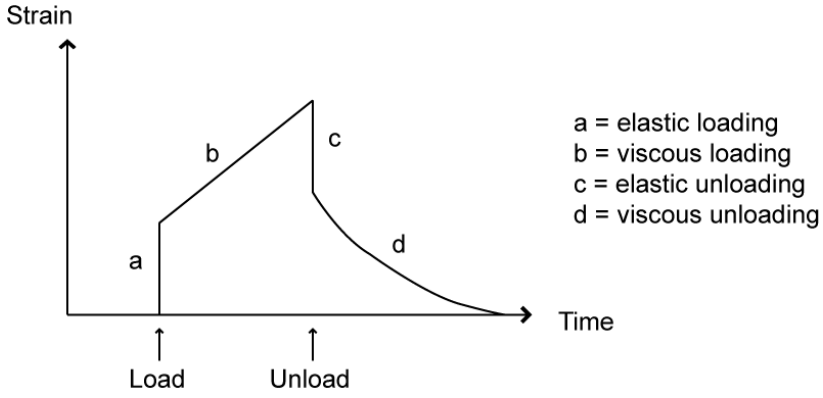

Fig. 5.3 Response of a viscoelastic material to loading

Deformation in response to an ice load ($\Delta\ell$) can be expressed as:

$$\Delta\ell = \varepsilon \times \ell$$

where **ε** is the strain and ℓ is the original lithosphere thickness (≈ 10^5 m). Strain includes both elastic (ε_e) and viscous (ε_v) components, expressed as:

$$\varepsilon_e = \frac{\sigma}{\mu} \qquad\qquad \varepsilon_v = \frac{\sigma \times t}{\eta}$$

where μ is the elastic modulus (≈ 6.7 x 10^{10} kg/ms^2), η is the mantle viscosity (≈ 5 x 10^{20} Pa s), *t* is time (in seconds), and σ is stress:

$$\sigma = \rho \times g \times h$$

where ρ is ice density (917 kg/m^3), *g* is acceleration due to gravity (9.81 m/s^2), and *h* is the thickness of the ice load applied (in metres).

Using the above equations the calculated total strain for an ice load of 100 m, loaded for 1000 years is 7 x 10^{-5} (of which ε_e equals 1.3 x 10^{-5}). This gives a value for $\Delta\ell$ of 7

m, of which the immediate elastic component is 1.3 m. Repeating the calculation using an ice load of 50 m thickness gives 3.5 m of deformation (0.67 m of elastic deformation). Therefore ice thickening of 50-100 m appears to give a reasonable elastic response (0.67-1.3 m), and suggests that the transition between YZ II and III could represent a RSL change caused by glacial readvance and thickening.

Support for a possible glacial readvance comes from Maxwell Bay, where Yoon *et al*. (2000) identified advanced glacier margins and extensive sea-ice cover between 6200 and 4000 ^{14}C yr BP (7070-4350 cal yr BP). Milliken *et al*. (2009) also reported low biological productivity and organic carbon content between ca. 7300 and 6000 cal yr BP from the SHALDRIL core from Maxwell Bay. The timing of YZ II also corresponds to cold events documented in marine sediments from Lallemand Fjord and Palmer Deep, eastern Antarctic Peninsula, between 6700-4900 ^{14}C yr BP (7500-5500 cal yr BP) and ca. 6000-4300 ^{14}C yr BP (6800-4800 cal yr BP) respectively (Shevenell *et al.*, 1996; Taylor and Sjunneskog, 2002). However, there does not appear to be further documented evidence of either a glacial readvance around 6000 yr BP or of climatic conditions favourable for an advance at this time. It pre-dates cold periods recorded on nearby Livingston Island and James Ross Island at ca. 5000-4000 ^{14}C yr BP (Björck *et al.*, 1996a; 1996b; Hjort *et al.*, 1997), and also precedes glacial readvances at Hope Bay ca. 4700 ^{14}C yr BP (Zale, 1994a) and on Brabant Island some time after 5000 ^{14}C yr BP (Hansom and Flint, 1989). Mäusbacher *et al*. (1989) dated the beginning of sedimentation in Tiefersee (situated 400 m from the present margin of Collins Ice Cap) to 5380 ^{14}C yr BP. Therefore there is no clear evidence of a glacial readvance and it is not possible to say where the ice margin was at the time of deposition of YZ II.

These two hypotheses focus on changes to the ice cap on the SSIs, however, it is possible that the Antarctic Peninsula ice sheet may influence the RSL record of the SSIs. RSL reconstructions in other areas peripheral to major ice sheets have highlighted the potential role of forebulge migration and collapse. Upon deglaciation, subsidence can occur around the periphery of ice sheets due to forebulge collapses, as observed at the periphery of the Laurentide (Dillon and Oldale, 1978; Barnhardt *et al*., 1995; Dyke and Peltier, 2000) and Fennoscandian (Vink *et al*., 2007) Ice Sheets. Therefore there may be a potential contribution from the Antarctic Peninsula to RSL which caused subsidence and a marine ingression into Yanou. However, subsidence at

Yanou is of an order of magnitude lower than observed due to forebulge collapse at the periphery of the Laurentide Ice Sheet (20-100 m), and whilst the influence would depend on distance away from the ice load centre, this difference in magnitude seems hard to explain. Unfortunately it is not possible to confirm or deny this hypothesis from the data available.

Finally, the alternative hypothesis that YZ II is related to an influx of freshwater into the Yanou basin must also be considered. If glacial retreat occurred relatively rapidly releasing a significant volume of meltwater, then a sudden influx of glacial meltwater could have washed into the basin, diluting the marine signal and also providing a shallow environment where freshwater diatoms could flourish. Similar meltwater input was observed at Watts and Ace Lakes, Vestfold Hills (East Antarctica), causing flushing of the lakes and a drop in salinity (Pickard *et al.*, 1986; Fulford-Smith and Sikes, 1996). A corresponding freshwater unit was also reported from Yanou by Yang and Harwood (1997), also with two layers of differing diatom species. They concluded that the alternation of diatoms may reflect periodic inflow of meltwater or local damming of lake drainage. The timing of the deposition of this unit corresponds to the onset of the Mid-Holocene climatic optimum identified from the western Bransfield Basin, which occurred between 6800 and 5900 cal yr BP (Heroy *et al.*, 2008), providing evidence for conditions favourable for a meltwater discharge event. There is the possibility that if this was a glacial meltwater event then the radiocarbon dates could be erroneously old as glacial meltwater contains relict dissolved inorganic carbon which is depleted in ^{14}C (Doran *et al.*, 1999; Takahashi *et al.*, 1999). However, they do seem to fit with respect to the other dates just above, and therefore correlation with the Mid-Holocene climatic optimum seems justified.

The deposition of YZ II also seems to have occurred around the same time as the isolation of Lake Kitezh ("Kiteschsee") on Fildes Peninsula at 6180 ± 150 ^{14}C yr BP (7000 cal yr BP, Mäusbacher *et al.*, 1989). Note Mäusbacher *et al*. reported the sill height of Kitezh as 16 m amsl, however the online King George Island GIS (SCAR KGIS) suggests the elevation is nearer 15 m amsl, and so the sill height should be revised to 15.5 m amsl. Being at the higher elevation, Lake Kitezh would be expected to isolate prior to Yanou Lake but, perhaps more significantly, Mäusbacher *et al*. (1989, p.227) reported that the "beginning of freshwater sedimentation in Kitezh seems to

reflect the meltwater of glacial retreat". Whilst this supports the hypothesis that this period on Fildes Peninsula was marked by significant volumes of glacial meltwater, the diatom assemblage contradicts this. Marine diatoms would still be expected to dominate the assemblage of a marine basin with inputs of glacial meltwater, however, the assemblage of YZ II is dominated by freshwater taxa and relatively low percentages of marine species.

On the basis of the evidence from Yanou Lake, the preferred initial interpretation is that the unit YZ II represents RSL change rather than the influx of glacial meltwater. It is proposed that initially isostatic uplift was the dominant contributor to RSL fall, causing the isolation of Yanou (YZ I-II). Subsequently the rate of eustatic sea level rise outpaced isostatic uplift to cause an ingression into Yanou, and the hypothesis of glacial retreat in two stages is favoured to explain this. Approximate calculations suggest a glacial readvance (thickening) of 50-100 m could cause an immediate elastic response of the required magnitude to also explain the ingression, however the absence of documented evidence of either a glacial readvance or climatic conditions favourable for an advance at this time add uncertainty to this interpretation. The hypothetical sea level curves of Fig. 5.2 also demonstrate that a glacial readvance is not necessary to produce the observed RSL record, but instead only a temporary pause in glacial retreat is required. The hypothesis that this unit reflects the influx of glacial meltwater can be discounted on the basis of the diatom assemblage, which suggests YZ II is a freshwater zone subject to weak marine influences. If the basin had not been isolated during YZ II, the diatom assemblage would be dominated by marine species with far lower percentages of salt-intolerant taxa. This interpretation will be re-examined when evidence from Long Lake is analysed.

5.2.3 YZ III: Marine

This zone documents a return to marine conditions. It is composed entirely of marine and brackish-marine diatoms, of which between 31 and 42% are sea-ice related taxa. The diatom assemblage is very similar to YZ I, although diatom concentrations are higher. Organic content is low, although higher than YZ I. The zone is marked by sharp lower and upper boundaries. Dates on freshwater sediment from YZ II and freshwater moss from the base of YZ IV constrain the deposition of this unit to between 6091 and

5051 ^{14}C yr BP (7000 to 5730 cal yr BP), although note the age reversal at the lower boundary.

5.2.4 YZ IV: Freshwater

There is a marked transition in all proxies between 208 and 216 cm, representing the transition from a marine to a freshwater environment, caused by regional isostatic uplift due to glacial unloading. The abrupt disappearance of marine diatoms coincides with a marked transition in lithology, an increase in organic content and troughs in magnetic susceptibility and gamma density. Marine diatoms are replaced by freshwater and fresh-brackish forms. The diatom species which dominate above the transition include *Nitzschia inconspicua*, *N. frustulum/perminuta*, *Planothidium lanceolatum*, *Gomphonema angustatum/parvulum* and *Naviculadicta seminulum*, which were all found in high relative abundances immediately following lake isolation on Beak Island (Sterken, 2009). The species are the same as those previously identified at Yanou above the marine-freshwater transition (Yang and Harwood, 1997).

In addition to the sharp contrast in diatom assemblages across the transition, there are also significant peaks in organic carbon and nitrogen content immediately after lake isolation. Similar peaks are observed at the top of YZ II after the transition from marine to freshwater conditions, although they are of greater amplitude in YZ IV. Similarly, peaks in organic content were observed in Holocene isolation basin sediments in northwest Scotland immediately after lake isolation (Mackie *et al.*, 2007). Here they were interpreted as reflecting a reduction in clastic material input at the end of marine inundation to the basin and an increase in *in situ* productivity. Zong (1997) also identified increased basin productivity close to the isolation contact in Scottish isolation basins based on substantial diatom blooms (*Paralia sulcata*) which are associated with high nutrient supply. The beginning of freshwater sedimentation in Yanou Lake is also comparable to that recorded immediately after isolation in Lake Kitezh (15.5 m amsl), with a similar peak in organic carbon and the presence of similar diatom species (Mäusbacher *et al.*, 1989; Mäusbacher, 1991).

However, in contrast to the marked differences in the diatom assemblages, organic content and physical properties of the marine and freshwater sediments, there is no consistent difference in δ^{13}C values. Marine sediment is typically enriched in elemental

^{13}C and is therefore normally characterized by higher $\delta^{13}C$ values, however the profile from Yanou is highly oscillatory and the marine and freshwater units cannot be distinguished on the basis of isotope values. This could be a function of the extremely low carbon content, and is explained in further detail in section 5.8.

Another significant feature of the transition between YZ III and IV is its sharpness and difference to the earlier marine to freshwater transition between YZ I and II. In isolation basin studies from both elsewhere in Antarctica and the northern hemisphere (Wasell and Håkansson, 1992; Verleyen *et al.*, 2004a; Lohne *et al.*, 2007; Dreßler *et al.*, 2009; Sterken, 2009) the isolation contacts are characterized by transitional diatom communities of brackish species and low abundances of marine taxa. However, brackish and marine diatom species are completely absent from the base of YZ IV. Whilst the general trend between YZ III and IV is of RSL fall, caused by regional isostatic uplift due to glacial unloading, one way for such a rapid isolation to have occurred is through the building of a storm beach seaward of the lake. A staircase of raised beaches is present between Yanou Lake and the sea (Fig. 3.4, Fig. 3.5, section 6.4.7.3), and therefore it is possible that the transition between YZ III and IV represents a beach building episode. However, the sampling resolution of 8 cm across the transition means this cannot be confirmed, as the sharpness of the transition may in fact be a function of this sampling resolution.

The minimum age for the isolation of Yanou Lake comes from the radiocarbon dating of freshwater moss immediately above the transition, and is placed at 5051 ± 38 ^{14}C yr BP (5730 cal yr BP). This is consistent with the date for isolation of Lake Kitezh (1 m higher, and therefore earlier isolation) at 6180 ^{14}C yr BP (Mäusbacher *et al.*, 1989).

So far this section has described the initial freshwater environment immediately after isolation. However, Fig. 4.2 shows that although the lake remains isolated, there are clear changes in all proxy records up to the present day. Indeed YZ IV can be sub-divided into two sub-zones based on productivity. Although there are no trends in the isotope and physical data, the top 32 cm of this zone is characterized by extremely low diatom concentrations. Unfortunately there are no dates on the zone boundaries, but dates at the base of YZ IVa and top of YZ V constrain the deposition of this unit to some time between 5051 and 4273 ^{14}C yr (5730-4740 cal yr BP). Assuming a constant rate of

sediment influx this represents a sedimentation rate of 2.2 mm/yr throughout this period (compared to 1.86 and 0.75 mm/yr before and after respectively).

Similar periods of low diatom abundance were identified at lakes across Fildes Peninsula, including Yanou (Yang and Harwood, 1997) and Lake Kitezh (Mäusbacher *et al.*, 1989). Mausbacher *et al*. (1989) correlated the Kitezh unit to an equivalent in Jurasee at 47 m amsl (dated to 5190-4320 ^{14}C yr BP) where organic content is also low, and is thought to reflect a high rate of sediment input. This zone could also correlate with minerogenic units containing few or no diatoms found in Mondsee (45 m amsl) and Tiefersee (17.5 m amsl) where sedimentation rates were calculated as being ten times greater than in the units above and below (Schmidt *et al.*, 1990). Dated to between 4700 and 3200 ^{14}C yr BP, these were interpreted as reflecting high allochthonous sediment influxes of fluvial or periglacial-fluvial origin, due to climate warming and extensive soil erosion by overland flow. Visual analysis of the sediments confirmed they were not tephra deposits. Likewise, Mäusbacher (1991) observed the highest sedimentation rates between 5000 and 3200 ^{14}C yr BP, due to meltwater from small snow-fields within lake catchments. High sediment inputs from glacial meltwater were excluded as no readvance of the Collins Ice Cap is evident in the sediments of Tiefersee, situated 400 m from the present ice margin.

Therefore YZ IVb is interpreted as representing a period of high sediment delivery after lake isolation, with high sediment influxes into the basin diluting the diatom abundance and creating a turbid and unstable environment which was unfavourable for the growth of diatoms. The correlation with similar units in cores from lakes across Fildes Peninsula suggests this was a regional event. It also correlates well with high ice-rafted debris fluxes recorded in the western Bransfield Basin around 4750 ^{14}C yr BP (5510 cal yr BP), when melting and calving in fjords occurred at an increased rate due to climate warming (Heroy *et al.*, 2008).

5.2.5 YZ V: Brackish-fresh

This zone of 16 cm is differentiated from those above and below on the basis of the diatom assemblage alone (Fig. 4.2). Organic content and physical parameters show no changes from YZ IV, however this zone is marked by peaks in brackish diatoms and lower abundances of freshwater taxa. Of the two samples forming this zone, the

lowermost (50 cm depth) is dominated by the mesohalobous species *Chamaepinnularia gerlachei* and the uppermost (42 cm) by the oligohalobous-halophilous species *Nitzschia frustulum/perminuta*. It is difficult to explain the dominance of different species, although it may be that the salinity changes within this zone and these two species lie very close on the salinity gradient. The salinity tolerance and ecological preferences of *Chamaepinnularia gerlachei* are not well documented as it is a new species only recently identified (Van de Vijver *et al.*, 2009). Its increased abundance at marine-freshwater transitions at Beak Island and near marine zones was used to suggest a preference for brackish to saline waters. However, at Beak Island it is found accompanied by the oligohalobous-halophilous species *Navicula cincta* and *Luticola cohnii*, and the oligohalobous-indifferent species *Achnanthes muelleri* and *Stauroneis latistauros*, suggesting it may not be a truly mesohalobous species. A date on freshwater moss immediately above the upper boundary of this zone constrains the termination of brackish conditions to 4273 ± 37 ^{14}C yr BP (4740 cal yr BP).

The key issue is whether this shift in the diatom assemblage is a response to real sea level change or whether it relates to changes in climate or lake processes. Support for the theory that the salinity fluctuation observed is related to a minor sea level rise that temporarily outpaces the rate of isostatic recovery comes from the organic carbon and nitrogen records. There are three distinct peaks in %C and %N values; the first two occurring in YZ II and YZ IV immediately after the transitions from marine to freshwater sediment. The uppermost peak occurs immediately after the 'spike' of brackish diatoms across the boundary of zones V and VI, which lends support to the idea of a brackish incursion around 4270 ^{14}C yr BP.

However, there are no marine diatoms present in this zone, which would be expected in the event of a RSL rise. For this reason it is unlikely that YZ V represents a RSL change, however this cannot be confirmed without analysis of the results from Long Lake at a close elevation above sea level. Possible explanations for this zone will therefore be discussed in detail in section 5.3.5.

5.2.6 YZ VI: Freshwater

The period from 4270 ^{14}C yr BP to present is characterized by freshwater diatoms, high organic content and troughs in magnetic susceptibility and gamma density. The

relatively high organic content throughout the zone indicates a reduction in inorganic inputs. The diatom assemblage is similar to that of YZ IVa, although with higher species diversity and increased relative abundances of truly freshwater halophobous species, such as *Planothidium renei/quadripunctatum*. This is likely to be an effect of isostatic uplift and the related availability of slightly different ecological niches, as well as longer term evolution (lake ontogeny).

Given the dates of 4270, 3790 and 2540 ^{14}C yr BP at 32, 24 and 14 cm depth respectively, the sediment accumulation rate is much lower in this zone than throughout the rest of the core, averaging between 0.075-0.166 mm/yr (compared to 2.2 mm/yr for YZ IV and V). This is interesting given the high organic production in the lake in the uppermost zone, and the coincidence with warmer and more humid conditions reported around 3000 yr BP from lake sediments of Livingston Island (Björck *et al.*, 1991a; 1993) and marine sediments from Maxwell Bay (Yoon *et al.*, 2000; Khim *et al.*, 2001; Yoon *et al.*, 2004). However, despite the extensive soil erosion and large allochthonous inputs detected on Livingston Island during this warmer period, no similar evidence is reported from King George Island (Mäusbacher *et al.*, 1989; Björck *et al.*, 1993).

5.3 Long Lake (15 m amsl)

Diatom, isotope and physical analyses from Long Lake show broadly similar trends to those discussed above from Yanou Lake. Again the record can be divided into six distinct zones (Fig. 4.6): two marine zones (LZ I and III), two freshwater zones (LZ IV and VI) and two brackish-fresh sections (LZ II and V). However there are some significant differences between the Long and Yanou results, which will be highlighted in the discussion below.

5.3.1 LZ I: Marine

The basal zone of almost 2 m is composed of sediment with entirely marine and marine-brackish diatoms, low organic content, relatively high δ^{13}C values, and relatively high magnetic susceptibility and gamma density. The diatom assemblage consists of a mixture of marine (*Cocconeis costata/pinnata*, *Rhizosolenia hebetata* and *Navicula cancellata*) and sea-ice related taxa (*Synedropsis recta*, *Navicula directa* and *Eucampia antarctica*). With the exception of the two basal samples, δ^{13}C values are between -18‰

and -21‰, which are characteristic of marine sediment (Meyers, 1994). The low values at the base of the zone may be explained by the effects of low temperatures on carbon fixation processes, with the solubility of CO_2, and hence availability to phytoplankton, higher at low temperatures, and thus fractionation is significantly increased to give lower $\delta^{13}C$ values (Wada *et al.*, 1987; Maslin and Swann, 2005; Yoon *et al.*, 2006).

As at Yanou Lake, this zone is interpreted as representing a period of sea-ice cover and cold climatic conditions immediately after glacial retreat. A date of 8002 ± 43 ^{14}C yr BP (9010 cal yr BP) near the base of the core provides a constraint on the timing of deglaciation. This corresponds well with Mäusbacher's (1991) evidence for glacial retreat across Fildes Peninsula both in terms of timing (9000-5000 ^{14}C yr BP) and direction of ice retreat, as an age ca. 1500-2000 yr younger than at Yanou supports the hypothesis that deglaciation occurred from southwest to northeast across Fildes Peninsula. Paired dates on shell and bulk sediment of 6819 ± 37 ^{14}C yr BP and 7249 ± 40 ^{14}C yr BP taken 125 cm above help confirm the reliability of this basal date, and also give confidence in bulk sediment dates. As these dates are reasonably close (although do not overlap) this suggests there are not problems of carbon reworking, but simply that slightly different marine reservoir corrections need to be applied to the two materials.

Although this zone is correlated to YZ I, there is one significant difference between the two, which relates to diatom abundances. Of the 10 samples prepared for diatom analysis from YZ I, only 2 contained high enough diatom concentrations to count 250 valves, compared to all 8 samples from LZ I. This may reflect the position of Long Lake closer to the ice cap margin. Diatom abundances are known to be relatively low under sea-ice, but increase by a factor of 4-5 adjacent to a receding ice edge (Burckle and Cirilli, 1987). Therefore as this peak in productivity is not observed at Yanou Lake, this suggests the ice margin did not remain at this site for as long and that glacial retreat was rapid until the margin was at least north of Long Lake.

5.3.2 LZ II: Fresh-brackish

As at Yanou Lake, the basal zone terminates with the deposition of freshwater sediment. This unit is only 12 cm thick but again is marked by distinct upper and lower boundaries in the proxy records. Organic content is high, with %C and %N peaking at

the lower and upper zone boundaries respectively. There are also troughs in magnetic susceptibility and gamma density. This zone consists of similar diatom species to YZ II, such as *Nitzschia frustulum/perminuta*, *Navicula veneta* and *Nitzschia inconspicua*, all brackish-freshwater species but with broad salinity tolerances. *Hippodonta hungarica* also co-dominates the assemblage, another species associated with high conductivity and high nutrient lakes, and previously reported from calcium-rich minerogenic sediments of lakes on King George Island (Schmidt *et al.*, 1990; Jones *et al.*, 2000). Such sediments commonly mark deglaciation in lakes in Greenland (Anderson *et al.*, 2004). As at Yanou, the presence of brackish diatoms and shallow-water taxa such as *Craspedostauros laevissimus*, albeit in low abundances, suggests a shallow basin with sea level close to the basin sill at this time.

The timing of the deposition of this zone is constrained by one radiocarbon date of 6445 ± 40 ^{14}C yr BP (7360 cal yr BP), taken from the mid-point of the zone. This is ca. 250 yrs earlier than YZ II, but confirms the two zones are (near) contemporaneous. As the same signature is observed in both lakes this rules out local catchment scale processes as a possible explanation, and suggests a regional forcing mechanism. Of the four hypotheses proposed in section 5.2.2, either (i) RSL change caused by two stage ice retreat, (ii) RSL change caused by ice readvance, (iii) RSL change caused by forebulge collapse, or (iv) an influx of glacial meltwater, the former is favoured by the results from Long Lake. The marine-freshwater transition occurs 250 years earlier in Long Lake than in Yanou Lake, which would be expected given the sill of Long is at least 50 cm above Yanou. Long Lake, at the higher elevation would also be expected to remain isolated for longer. Whilst the units in both lakes are of the same thickness, it is not possible to confirm the relative durations as this assumes the same sedimentation rate, and dating control is poor. The two dates on YZ II are reversed and only one is available to constrain LZ II. The timing of LZ II predates the isolation of Lake Kitezh by ca. 265 years (Mäusbacher *et al.*, 1989), which would not be expected given the sill height of Kitezh is around 50 cm higher than Long, but it is possible that this isolation contact in Kitezh corresponds to the LZ/YZ III-IV boundary. LZ II is only 12 cm thick and the corresponding freshwater unit of Lake Kitezh may have been missed due to the sampling resolution. Mäusbacher *et al*. (1989) do not present a diatom diagram and there is no mention of their sampling interval. Therefore it is not possible to use the Lake Kitezh record to inform the interpretation of LZ/YZ II. As the nature of the marine-

freshwater transitions in both Yanou and Long Lakes is indicative of genuine lake isolation (cf. Shennan *et al.*, 1994; Lohne *et al.*, 2004; Verleyen *et al.*, 2004b) and rough calculations of non-linear isostatic uplift caused by two stage ice retreat produce realistic RSL change, the initial interpretation proposed on the basis of results from Yanou is supported by data from Long to explain YZ/LZ II.

An interesting feature of this zone is the disagreement between the $\delta^{13}C$ record and all other proxies. Whereas $\delta^{13}C$ values would be expected to decrease with the input of freshwater sediment (typically depleted in ^{13}C relative to marine sediment), the average $\delta^{13}C$ values remain constant throughout LZ I, II and III. The only notable changes are in the two samples immediately outside this freshwater zone (uppermost sample of LZ I and lowermost of LZ III), which have slightly lower $\delta^{13}C$ values. The high values are likely to be a function of the short duration of this zone. $\delta^{13}C$ values across the other marine-freshwater transition (LZ III to IV) remain high initially as the marine carbon pool is still being utilized, and then decrease 28 cm above the zone boundary. Long Lake was not isolated for long enough around 6445 ^{14}C yr BP for the marine carbon pool to be depleted to cause a shift in the isotope signal.

5.3.3 LZ III: Marine

This zone has very similar characteristics to LZ I, with the dominance of marine diatoms, low organic content, and high $\delta^{13}C$ values indicative of marine sediment. Again the diatom assemblage is composed of a mixture of marine and sea-ice related taxa (between 20 and 36%). The deposition of this unit is constrained to between 6445-5872 ^{14}C yr BP (7360-6730 cal yr BP). There is a slight age reversal in the two dates taken immediately above and below the upper boundary of this zone, but this is within the 2-sigma error range.

The troughs in $\delta^{13}C$ values and organic content and peaks in magnetic susceptibility and gamma density at 338 cm relate to a tephra layer (Fig. 4.6). This is most likely derived from Deception Island (Björck *et al.*, 1991d). Unfortunately the tephrochronology of the region by Björck *et al*. (1991d) only extends back to 4700 ^{14}C yr BP, preventing firm correlation of this layer. However, it may correlate to a tephra layer reported from Hotel Lake on Fildes Peninsula, dated to ca. 6000 ^{14}C yr BP (Tatur *et al.*, 1999).

5.3.4 LZ IV: Freshwater

There is a clear transition from marine to freshwater sediment between 314 and 322 cm. Marine and sea-ice related diatoms are replaced by freshwater and fresh-brackish species, such as *Navicula veneta*, *Nitzschia frustulum/perminuta*, *Nitzschia inconspicua*, *Planothidium lanceolatum* and *Gomphonema angustatum/parvulum*. These species also dominate the assemblage of YZ IV and are widely reported as taxa associated with marine-freshwater transitions in isolation basins (Wasell and Håkansson, 1992; Sterken, 2009).

As at Yanou Lake, there are also significant peaks in organic carbon and nitrogen content immediately after lake isolation. These suggest a productivity bloom occurs at the end of marine inundation when the influx of clastic material is reduced and light and nutrient levels increase. However, unlike at Yanou Lake, there is a transition in $\delta^{13}C$ values after lake isolation. Significantly there is a lag between the decline in isotope values and change in diatom assemblages. $\delta^{13}C$ values are high in the lowermost 28 cm of the zone immediately above the marine-freshwater transition, peaking at -14.9‰. Above this, $\delta^{13}C$ values decrease to between -22.7‰ and -28.4‰, characteristic of freshwater sediment (Meyers, 1994). The occurrence of freshwater sediment with marine isotope values and the discernable lag between lake isolation and the change in $\delta^{13}C$ values may be explained by looking at the radiocarbon dates.

Two dates were taken either side of the isolation contact, one bulk marine sediment and one bulk freshwater sediment. Both conventional ^{14}C ages came out to be very similar (only 162 years apart), even though the uppermost date would not be expected to need correcting for the marine reservoir effect (1064 yrs). If uncorrected the uppermost 'freshwater' date would be 1226 years older than that immediately below the transition and 653 years older than the age of LZ II. This is clearly unrealistic so, based on the relative ages and the $\delta^{13}C$ data, the 'freshwater' date was considered to have been subject to contamination from marine carbon and has therefore been marine reservoir corrected. It suggests the marine carbon pool is still being utilized immediately after isolation. The sediment itself was not reworked around the isolation boundary because the shift in diatom species is abrupt. Instead, the zone boundary represents the inflow of freshwater, which brings in freshwater diatoms and causes marine species to die as they can no longer tolerate the reduced salinities. However, as the marine organic

carbon pool is still used initially (hence the marine $\delta^{13}C$ values and ^{14}C dates), the freshwater isotope signal does not return until the marine carbon pool is depleted. This also explains the peaks in carbon and nitrogen immediately after isolation, as when freshwater diatoms are put into a system of marine nutrients, productivity peaks. The peaks are shorter in Long Lake than in Yanou Lake as Long Lake is an open system with both inflows and outflows, and would therefore have been flushed out quicker than Yanou Lake, which receives only limited inflow and drains below the surface. Similar post-isolation productivity peaks have been reported from isolation basins in the Vestfold Hills (Zwartz *et al.*, 1998), Pourquoi Pas Island (Roberts *et al.*, 2007), and Scotland (Mackie *et al.*, 2007). In addition, this also suggests stratification of the lake, with the diatoms living in the surface freshwater layer, with a saline zone below the surface providing the heavier $\delta^{13}C$ source.

The second isolation of Long Lake is constrained by these two radiocarbon dates immediately above and below the diatom-defined marine-freshwater transition (LZ III to IV). There is a slight age reversal, but when corrected for the marine reservoir effect this is within the 2-sigma error range. Isolation is therefore placed around 5950 ^{14}C yr BP, specifically between 6034 ± 40 and 5872 ± 40 ^{14}C yr BP (6920-6730 cal yr BP). As would be expected from the relative sill heights, this is around 900 years earlier than Yanou Lake (50 cm lower) became isolated and 230 years later than Lake Kitezh (50 cm higher, Mäusbacher *et al.*, 1989). Unfortunately the marine-lacustrine transition also identified at Long Lake by Mäusbacher (1991) was not dated in that study and so cannot be compared.

As at Yanou, the transition between LZ III and IV is interpreted as representing isolation of the lake due to isostatic uplift in response to regional deglaciation. However, again the sharpness of the transition and absence of transitional diatom communities is hard to explain by isostatic uplift alone. At Yanou such rapid isolation was explained by the building of a storm beach during a period of continued RSL fall, which completely isolated the lake (near-)instantly. A staircase of raised beaches is present to the south of Long Lake at Hydrographers Cove (section 6.4.7.4), which although do not presently extend between Long Lake and the sea, may have done previously but have been destroyed by the building of the road which runs to the south of Long Lake. Therefore it is possible that the transition between LZ III and IV also represents a beach building

episode, although sub-sampling at higher resolution across the transition would be necessary to confirm this.

The similarities and differences between the upper and lower marine to freshwater transitions are also significant. Detrended correspondence analysis of samples from Long Lake shows the similarity in trajectories across the transitions (Fig. 5.4), supporting the hypothesis that both the LZ I-II and LZ III-IV boundaries are isolation contacts representing true RSL change. The difference in trajectories immediately after isolation reflects the relative durations of the freshwater zones LZ II and LZ IV. The relatively brief isolation of Long Lake represented by LZ II prevents the development of a completely freshwater diatom community.

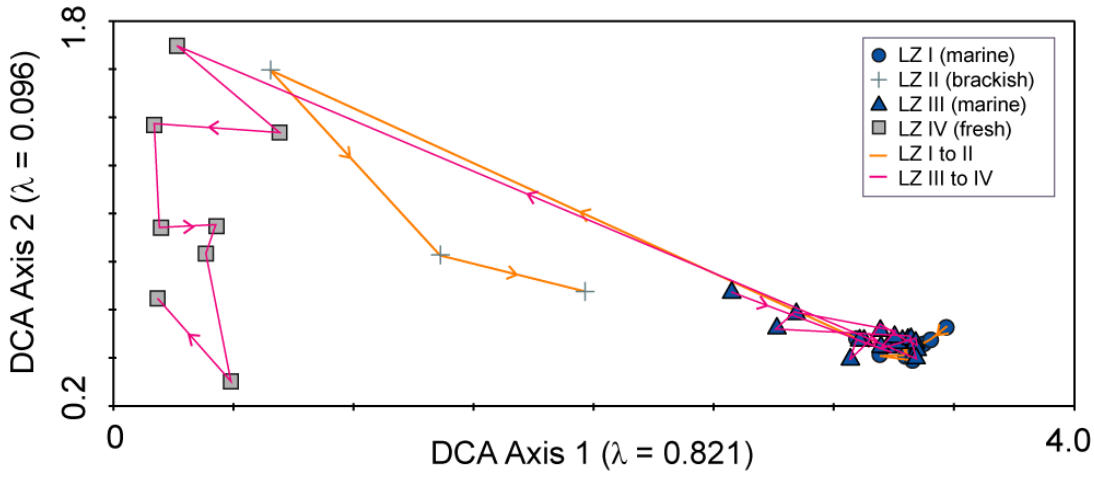

Fig. 5.4 Detrended correspondence analysis of samples across the marine-freshwater transitions in Long Lake. Samples plotting close to one another have similar diatom compositions. The lines connect samples in stratigraphic order and the arrows indicate the trajectory direction from core bottom to top (after Engstrom *et al.*, 2000).

This section has described the conditions across the marine-freshwater boundary and the environment immediately after isolation. However, as at Yanou Lake, zone IV can be sub-divided into two sub-zones based on diatom abundance and sediment delivery rates. The decline in $\delta^{13}C$ values described above coincides with the lower boundary of sub-zone LZ IVb. This zone is also characterized by very low organic content, high gamma density and very low diatom abundances. At Yanou Lake this was interpreted as representing a period of very high sediment influx, based on correlation with similar units preserved in other lakes across Fildes Peninsula (Mäusbacher *et al.*, 1989;

Schmidt *et al.*, 1990; Mäusbacher, 1991). However, at Long Lake this unit was deposited earlier than at Yanou Lake. Again there is no date on the upper boundary, but the dates on the base of YZ IVa and top of YZ V constrain the deposition of this unit to some time between ca. 5950 and 5058 ^{14}C yr BP (6820-5740 cal yr BP). This precedes the reported timing of high sedimentation rates and productivity in the region. An alternative explanation was proposed by Yoon *et al*. (2006), who observed the same unit at Long Lake, attributing low organic content and diatom production to tephra-fallout following an eruption of the Deception Island volcano, which shocked the lake biota (Björck *et al.*, 1991d). However, this hypothesis can be rejected as no tephra layers (either direct ashfall or reworked) are preserved in this section of the Long Lake core. Alternatively, lower productivity could be attributed to a change in lake ice-cover. An increase in annual ice-cover during this period would have limited the availability of carbon dioxide for photosynthesis and thus reduced diatom abundances (Douglas *et al.*, 2004).

Finally, comparisons should be made to other earlier studies of Long Lake. Although concentrated on palaeoenvironmental and palaeoproductivity reconstruction, they use many of the same proxies and therefore provide useful comparisons. Fig. 5.5 shows data from Khim *et al*. (2004) and Yoon *et al*. (2006). This shows a clear transition in geochemical and physical properties around 300 cm. Dated to 5723 ± 70 ^{14}C yr BP, this appears to be the same transition as observed at the same depth in this study between LZ III and IV. The TOC and TN profiles are very similar to those from this study with peaks at identical depths (Fig. 4.6); $CaCO_3$ also correlates well with the marine-freshwater transition. However, because these previous studies did not study the diatoms in this zone they mistakenly attributed this transition in physical and geochemical properties to a change between a glacial and lacustrine environment, rather than from a marine to freshwater environment (Khim *et al.*, 2004; Yoon *et al.*, 2006). They interpreted the basal 4.5 m of the core as a glacial diamicton and thus placed the onset of deglaciation of Fildes Peninsula much later at ca. 5000 ^{14}C yr BP with the formation of a postglacial lake at ca. 4000 ^{14}C yr BP. It is also interesting that the lower marine-freshwater transition between LZ I and II is not as apparent in Fig. 5.5 as in this study. There are peaks in TN and TOC at 500 cm, but there is not evidence of the transition in all proxies. However, no diatoms were analysed below 3 m in the two

other studies to obtain 7.5 m cores from Long Lake (Yoon *et al.*, 2006; Lee *et al.*, 2008), and it is the diatoms that are the strongest indicators of such a brief salinity change.

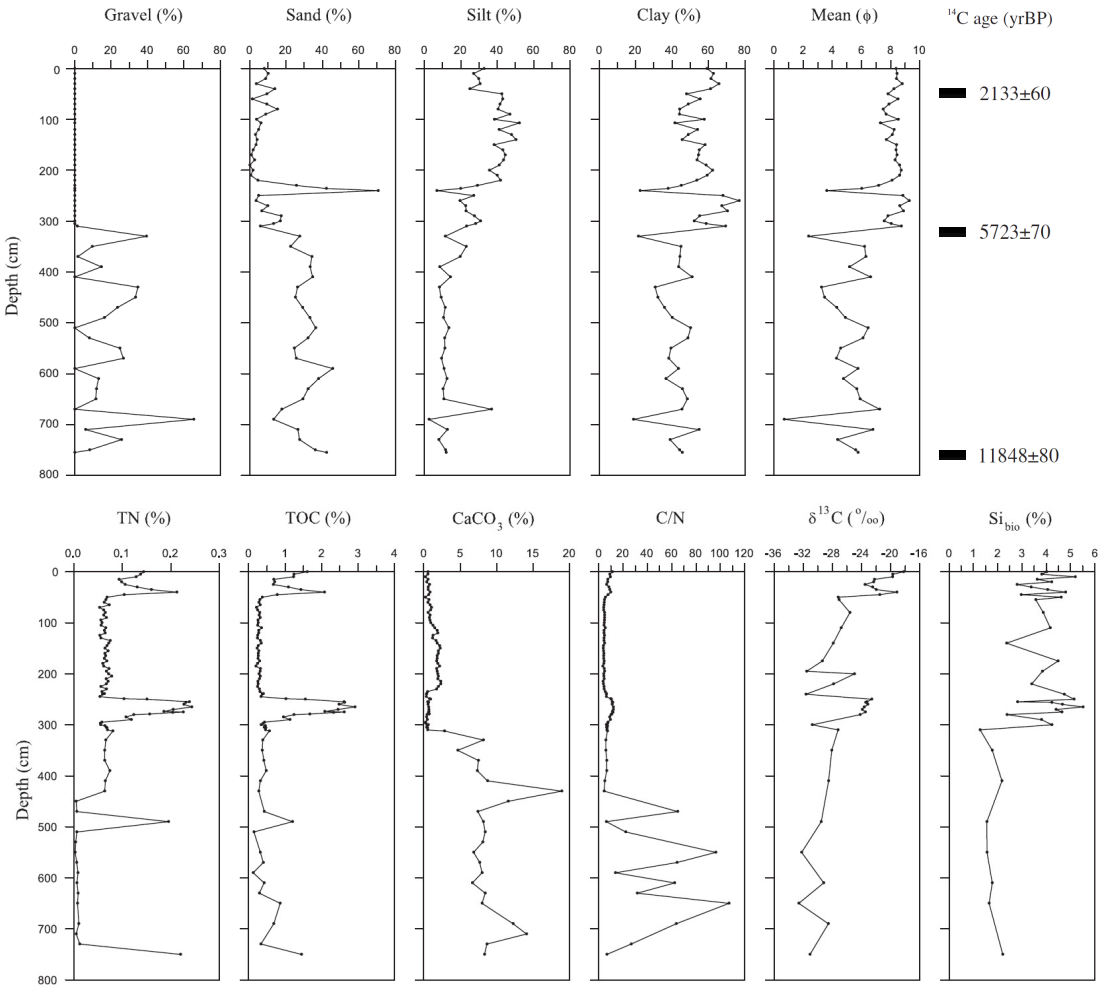

Fig. 5.5 Results of physical and geochemical analyses from previous studies of Long Lake by Khim *et al*. (2004) and Yoon *et al*. (2006)

5.3.5 LZ V: Brackish-fresh

As at Yanou Lake, this zone of 40 cm is differentiated from those above and below on the basis of the diatom assemblage alone (Fig. 4.6). $\delta^{13}C$ values do increase to levels more characteristic of marine sediment, but this appears to be part of a more general increasing trend from the top of LZ IV through to the top of the core. Organic content and physical parameters show no changes from LZ IV, however this zone is marked by peaks in brackish diatoms, such as *Chamaepinnularia gerlachei* and *Navicula halophila*.

A date on the upper boundary of this zone constrains the termination of brackish conditions to 5058 ± 38 ^{14}C yr BP (5740 cal yr BP).

This zone shows strong similarities to YZ V. It was tentatively suggested in section 5.2.5 that YZ V did not relate to a change in RSL. When LZ V is interpreted in parallel, there is strong evidence to suggest that LZ V and YZ V do not represent a response to real sea level change. The two zones are not synchronous, with the upper boundary of LZ V dating to 1000 cal years earlier than the termination at Yanou Lake. Whilst a minor RSL rise could have occurred to cause the brackish incursion at Long Lake (while Yanou was still inundated) and another minor sea level rise could have caused the same feature in Yanou, it seems highly coincidental that two such events occurred at virtually the same time after isolation of both lakes. There are also no marine diatoms found in either zone. Therefore, the interpretation of LZ V and YZ V will not affect the development of the RSL curve, although it is still interesting to explore some possible explanations.

The shift in diatom assemblages in LZ V and YZ V could be related to local events such as increased storm activities. This explanation was tentatively used to account for a similar brief marine/brackish incursion observed in Pup Lagoon, an isolation basin in the Larsemann Hills, East Antarctica (Verleyen *et al.*, 2004a). A period of increased storminess coupled with open water conditions in Maxwell Bay would cause incursions of sea spray into coastal lakes and may account for the peak in diatom species tolerant of higher salinities. Milliken *et al*. (2009) provide evidence for minimum sea ice cover in Maxwell Bay at this time to support this explanation.

Alternatively, this apparently rapid change in salinity could be a response to a sudden and rapid change in climate in the lake catchment area, which led to a negative water balance. A similar increased salinity event occurred in Beall Lake on the Windmill Islands, East Antarctica, and was attributed to a rapid increase in summer temperatures (Roberts *et al.*, 2004; Hodgson *et al.*, 2006). However, such an abrupt climate event is as yet undocumented for King George Island. This explanation also seems unlikely due to the large catchment inflows to Long Lake.

The coincidence in the timing of this brackish phase in both Yanou and Long Lakes at around the same time after isolation also suggests that it is possible that the salinity fluctuations of YZ V and LZ V are related to lake isolation and a change in the lake environment post-isolation. However, no other similar brackish phases are observed in isolation basins from other studies in the northern Hemisphere (e.g. Shennan *et al.*, 1994; Lohne *et al.*, 2004; Mackie, 2004). Therefore it is most likely that YZ/LZ V reflect a prolonged period of increased storminess and open water conditions in Maxwell Bay. This interpretation will be confirmed later by comparison with results from Ardley and Belén Lakes.

5.3.6 LZ VI: Freshwater

The uppermost zone is characterized by freshwater diatoms, high organic content, high $\delta^{13}C$ values, and low magnetic susceptibility and gamma density. The diatom assemblage is similar to that of LZ IV, dominated by species observed elsewhere in nutrient-rich isolated lakes (e.g. Sterken, 2009). Together with relatively high organic content and total diatom concentrations, the presence of these diatoms point to high productivity conditions. This zone is dated from 5058 ± 38 ^{14}C yr BP (5740 cal yr BP) to present. The surface date of 1900 ± 40 ^{14}C yr BP is surprisingly old, but Yoon *et al*. (2006) reported similarly 'old' dates of ca. 2100 ^{14}C yr BP from 8-37 cm core depth. This suggests contamination by older carbon derived from allochthonous sources, such as bedrock weathering, or an input of ^{14}C depleted meltwater from the Collins Ice Cap or local snowfields (Björck *et al.*, 1991b; Wolfe *et al.*, 2004). Alternatively this could be a function of contamination from catchment erosion from the building of the Chilean scientific base and road building nearby.

The other notable feature of this zone is the high $\delta^{13}C$ values. In LZ IV and V freshwater sediments yield values below -23‰, and are therefore distinguishable from the marine sediments of LZ I and III. However, in LZ VI $\delta^{13}C$ values increase to between -23‰ and -16‰. These values are typical of marine sediment (Fig. 5.6), thus contradicting the diatom results and more importantly the clear observation that the lake is currently isolated from the sea. The same trend was reported from Long Lake by other studies (Fig. 5.5; Khim *et al*., 2004; Yoon *et al*., 2006), suggesting this is a real result and not laboratory or sampling error.

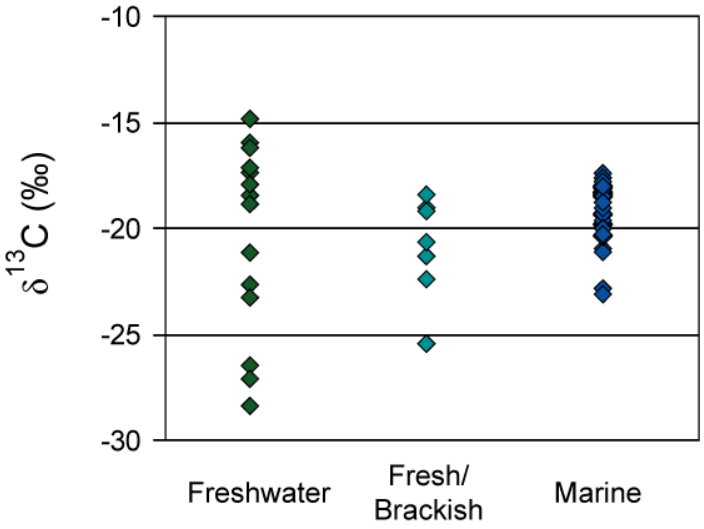

Fig. 5.6 $\delta^{13}C$ values for Long Lake, separated by the depositional environment inferred from diatom analysis

The same disagreement between isotope data and diatom flora was reported from Lateglacial sediments of Scottish isolation basins, with high $\delta^{13}C$ values coincident with freshwater diatoms (Mackie *et al.*, 2007). Here the isotope data were interpreted as responding to changes in the total dissolved inorganic carbon pool, related to increased basin productivity and changes in basin hydrodynamics. Meyers (1997) confirmed that organic $\delta^{13}C$ values are indicators not only of origins of organic matter but also of palaeoenvironmental conditions. Concentrations of CO_2 available to algae are affected by surface water temperatures, and concentrations of CO_2 in the photic zone can also be drawn down during times of elevated productivity. As lake waters have much smaller dissolved organic carbonate pools than marine waters, they are more sensitive to productivity-driven CO_2 depletion. Therefore an increase in productivity (as indicated by increased diatom abundances and relatively high organic content) could explain the higher than expected isotopic values in LZ VI and the wide range of values throughout the core. Bird *et al*. (1991) also reported widely varying isotopic values from lacustrine sediments of the Vestfold Hills, compared to more uniform values in marine sediments; freshwater sediments yielded $\delta^{13}C$ values ranging from -29.5‰ to -10.5‰.

There is also evidence from Alaska and Greenland of lake age being significantly related to algal communities, and therefore isotopic values (Engstrom *et al.*, 2000; McGowan *et al.*, 2008). Changes in lake productivity have been shown to guide

changes in isotopes, with plant communities (with differing isotopic signatures) changing through time after lake isolation. Evidence of the relationship between $\delta^{13}C$ values and lake productivity also comes from lakes of the Vestfold Hills, East Antarctica (Bird *et al.*, 1991). Here particularly high $\delta^{13}C$ values result during high levels of microbial activity in the lakes, due to high rates of photosynthetic CO_2 fixation which enrich the lake with respect to ^{13}C (Last and Slezak, 1986; Schidlowski *et al.*, 1994).

Finally, it is also possible that the increase in isotope values could be related to a period of increased lake ice-cover, possibly associated with the development of neoglacial conditions. Annual ice-cover limits the availability of CO_2 in the lake waters for photosynthesis, and therefore exerts a strong control on the abundance and diversity of plankton (Douglas and Smol, 1999; Douglas *et al.*, 2004; Hodgson and Smol, 2008). Therefore the onset of the upward trend in $\delta^{13}C$ values may coincide with a time when winter lake-ice no longer persisted all year round. An ice-free summer would result in increased evaporation, increased availability of CO_2 for photosynthesis in lake waters, and longer growing seasons for algae, thus causing the plankton population to increase. Consequently $\delta^{13}C$ values would increase as more ^{12}C is preferentially removed by the increased abundance of photosynthesizing organisms (Bird *et al.*, 1991; Hodgson *et al.*, 2006). This explanation also fits with the earlier interpretation that the low diatom abundances of LZ IVb may reflect increased lake ice-cover. As ice-cover reduced between LZ IVb and VI, productivity and $\delta^{13}C$ values increased.

5.3.7 Summary of results from Yanou and Long Lakes

Analysis of results from Yanou and Long shows the two lakes followed similar development trajectories through the mid- and late-Holocene. The similarities and differences between the two records can be used to inform the reconstruction of RSL change in the area at this time. A summary of RSL change and changing depositional environments, as interpreted from the results of Long and Yanou Lakes only, is presented schematically in Fig. 5.7 and described in the following section. This is a preliminary interpretation, which will be built upon with analyses from the other lakes.

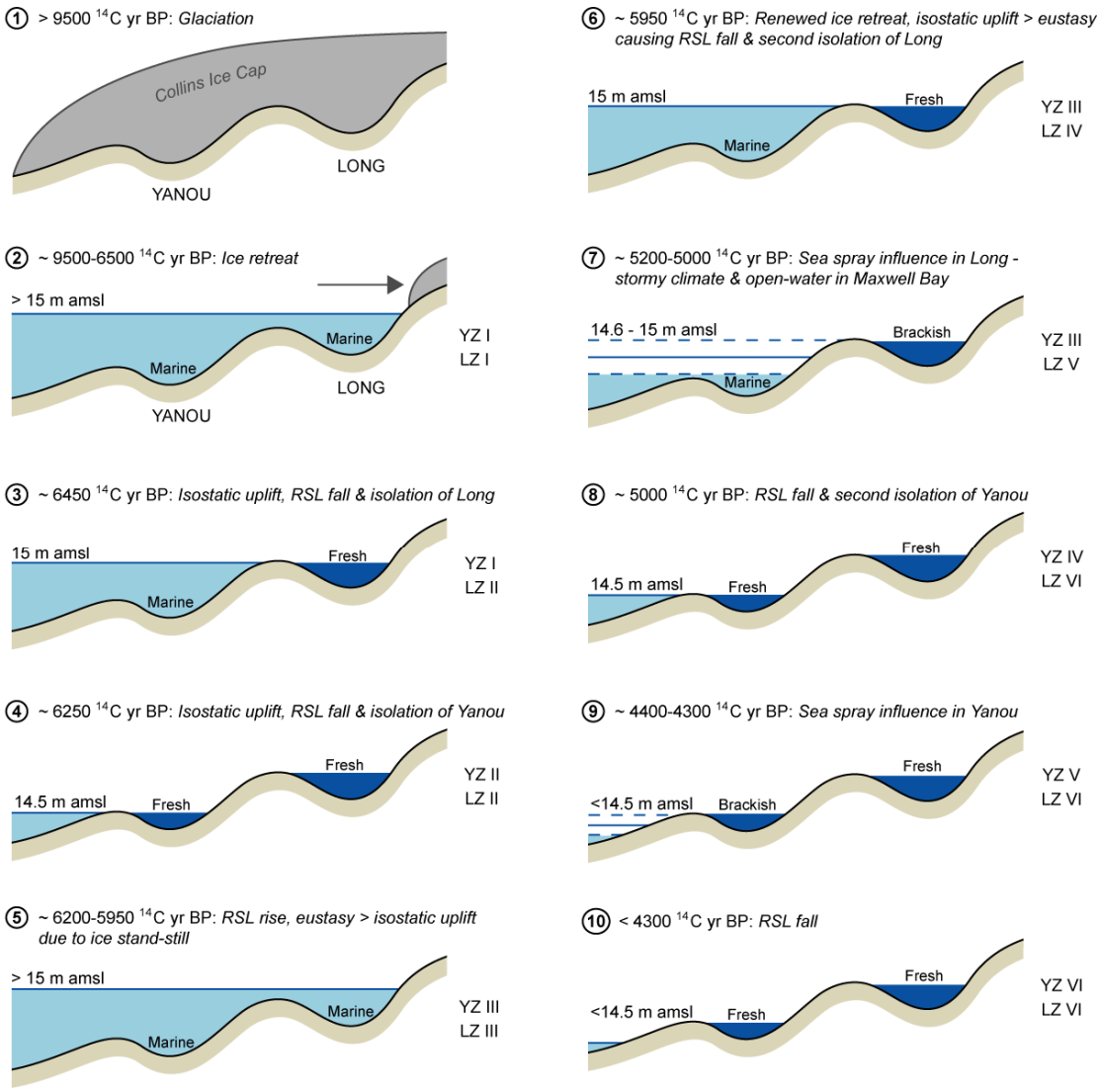

Fig. 5.7 Schematic representation of the isolation process at Long and Yanou lakes with RSL interpretations and the correspondence to the zones identified from diatom, isotope and physical analyses

The onset of deglaciation of Fildes Peninsula seems to have occurred prior to ca. 9500 ^{14}C yr BP. Ice retreated between the sites of the two lakes over the next ca. 1500 years, and the presence of marine and sea-ice related diatom species in YZ/LZ I confirm that areas of Fildes at the lowest altitudes were below sea level immediately after glacial retreat. Marine conditions continued until ca. 6450 ^{14}C yr BP at Long and ca. 6250 ^{14}C yr BP at Yanou. Isostatic uplift in response to regional deglaciation caused the isolation of both lakes. However isostatic uplift did not occur at a linear rate, and a temporary pause in the retreat of the Collins Ice Cap caused the rate of eustatic sea level rise to

exceed the reduced rate of isostatic uplift, leading to a marine ingression again into Yanou and Long (YZ/LZ III). Assuming sea level was close to the basin sill elevations at this time then it is possible that a small change in RSL could cause a significant shift in the proxy record. This interpretation of two stage glacial retreat to explain the observed RSL trends from Long and Yanou Lakes is favoured over alternative hypotheses that either the upper boundary of YZ/LZ II represents an ice readvance or the zone reflects an influx of glacial meltwater. In the case of the former, whilst rough calculations of the ice advance required to produce the observed RSL change seem realistic, there is an absence of previously documented evidence of a glacial readvance at this time. The latter glacial meltwater hypothesis is discounted on the basis of the diatom assemblage and the low abundances of marine species. The potential influence of the Antarctic Peninsula ice sheet on RSL in terms of forebulge collapse cannot be determined, but this would likely cause subsidence of a greater order of magnitude.

Isostatic uplift in response to the second stage of glacial retreat then predominates again, causing the second isolation of Long Lake at ca. 5950 ^{14}C yr BP and Yanou Lake at ca. 5050 ^{14}C yr BP. However, the absence of transitional diatom communities immediately after isolation and the sharpness of the transitions relative to the lower isolation contacts (YZ/LZ I-II) suggest this period between 5950 and 5050 ^{14}C yr BP was one of increased storminess when storm beaches were built, which resulted in rapid isolation. In both lakes a productivity bloom occurred immediately after isolation, followed by a period of very high sediment influxes and increased lake ice-cover (YZ/LZ IVb). A distinct brackish incursion subsequently occurred between ca. 5200-5000 ^{14}C yr BP in Long Lake and between ca. 4400-4300 ^{14}C yr BP in Yanou Lake. These salinity fluctuations are likely to reflect a prolonged period of increased storminess and open water conditions in Maxwell Bay which caused incursions of sea-spray into the lakes. Finally, high concentrations of salt-intolerant diatoms in YZ/LZ VI reflect the return to freshwater conditions, with continued isostatic uplift and RSL fall keeping both lakes isolated to the present day.

Multi-proxy analysis has highlighted the relative effectiveness of the different proxies as palaeosalinity indicators. The close control of salinity on diatom distribution is evident by the abrupt changes in assemblages, and there are also distinct peaks in organic content immediately after every marine/brackish to freshwater transition. However,

there are inconsistencies in the $\delta^{13}C$ record. Marine and freshwater sediments from Yanou are indistinguishable on the basis of $\delta^{13}C$ values alone. At Long Lake, whilst the second isolation transition is reflected in the isotope data, the $\delta^{13}C$ profile appears to be driven by palaeoenvironmental conditions as well as sources of organic matter. Therefore carbon isotopes are less reliable as a palaeosalinity proxy and must be analysed in conjunction with other proxies; diatoms remain the benchmark for identifying marine-freshwater transitions in Antarctic isolation basins.

5.4 Ardley Lake (18 m amsl)

In contrast to Yanou Lake and Long Lake, analyses from Ardley Lake show very different trends. This is significant for the interpretation of RSL changes. On the basis of the diatom assemblage, Ardley is divided into three zones (Fig. 4.10): two freshwater zones (AZ I and III), separated by a brackish-fresh section (AZ II). These will be interpreted in the following section, along with results of isotope and physical analyses.

5.4.1 AZ I: Freshwater

The basal zone of Ardley Lake is dominated by freshwater and fresh-brackish diatom species. The most abundant species are all commonly reported from freshwater lakes and pools around the South Shetland Islands (Schmidt *et al.*, 1990; Björck *et al.*, 1993; Jones *et al.*, 1993; Kawecka and Olech, 1993) and sub-Antarctic islands (Oppenheim and Greenwood, 1990; Jones and Juggins, 1995; Van de Vijver and Beyens, 1996; Jones *et al.*, 2000).

The basal core date of 7552 ± 39 ^{14}C yr BP (8320 cal yr BP) confirms sedimentation began in Ardley Lake at around the same time as in Yanou and Long Lakes, following ice removal. However, of most significance is the absence of any marine diatoms in AZ I, suggesting RSL was below the sill height of Ardley Lake when the Collins Ice Cap retreated from this site. As the nearby (< 2 km) basins of Yanou and Long Lakes were both occupied by marine sediments at this time, RSL is constrained to between 15 and 18 m above present immediately after deglaciation.

5.4.2 AZ II: Brackish-fresh

This zone is marked by a distinct change in the diatom species and diversity. Only four species account for over 90% of the total diatom counts in 14 of the 18 samples in this zone. *Gomphonema angustatum/parvulum* and *Pinnularia microstauron* are found in similar abundances to AZ I, with *Luticola muticopsis* and *Achnanthes delicatula* also dominating the assemblage of AZ II. These latter three species are commonly reported from coastal freshwater lakes that are influenced by sea spray (Oppenheim, 1990; Schmidt *et al.*, 1990; Van de Vijver and Beyens, 1997). The occurrence of very limited numbers of marine diatoms also suggests the influence of sea spray. Therefore AZ II could represent a period of increased storminess that caused an increase in sea spray reaching the lake. This would result in elevated salinity, the availability of marine-derived nutrients, and a different diatom species composition.

Unfortunately it is difficult to place an exact age constraint on the deposition of AZ II as there are two age reversals within the zone. All six dates from this zone are within 500 years, suggesting AZ II represents only a brief brackish event. However, the onset of brackish conditions may be earlier than the date on the lower boundary suggests. Close agreement between the algae-bulk sediment pair (29 cm above the AZ I-II boundary) suggests this age is correct, and an identical date on the algae fragment 30 cm below suggests this is in fact the same macrofossil which has been transported down core. Therefore assuming a constant sedimentation rate, the lower boundary dates to ca. 5250 ^{14}C yr BP. Nevertheless this still places the duration of the brackish incursion to around 1000 years.

AZ II is dated to between ca. 5250 and 4155 ^{14}C yr BP (5920-4620 cal yr BP), and is therefore too late to correspond to the RSL highstand associated with YZ/LZ I and III. The timing overlaps with the brackish zones of Yanou and Long Lakes, YZ/LZ V, and therefore despite the longer duration of AZ II relative to YZ/LZ V, these zones are likely to correspond to each other. When compared to the nearshore record from Maxwell Bay, the timing of AZ II correlates with a period of high biological productivity and significant seasonal variation in sea-ice cover (Milliken *et al.*, 2009). Therefore when sea-ice cover was low, increased wave activity and storminess over extensive open water would have brought in sea-spray associated diatoms. The interpretation that AZ II relates to a period of increased storminess therefore fits with the nearshore record.

In addition to this suggestion that AZ II relates to a period of increased sea spray influence, the diatom and isotope evidence also suggests a possible link related to the influence of penguins. The most abundant diatom species in AZ II, *Luticola muticopsis*, is commonly found near penguin rookeries (Van de Vijver and Beyens, 1997; Mataloni and Tell, 2002). Ardley Island is currently designated as an Antarctic Specially Protected Area (ASPA) due to its large penguin population. Therefore, AZ II may reflect a period of higher precipitation and consequently greater surface run-off from penguin rookeries (Tatur, 2002). Support for this hypothesis comes from the timing of this zone, which corresponds to periods of high sediment input recorded at Jurasee, Mondsee and Tiefersee between ca. 5000-3200 ^{14}C yr BP due to climate warming and extensive soil erosion by overland flow (Mäusbacher *et al.*, 1989; Schmidt *et al.*, 1990; Mäusbacher, 1991). The low diatom abundances of sub-zone AZ IIb may reflect a brief period of exceptionally high sediment influx, which diluted the diatom signal. Therefore, whilst the diatom species observed in AZ II can be used as sea-spray indicators, here they are also likely to reflect the increased run-off over ornithogenic soils.

Further evidence for the influence of penguins comes from isotope analysis. Whilst the %C, %N and δ^{13}C profiles show no clear trends, and do not correspond to changes in the diatom assemblage, they show that the sediments of Ardley Lake have a much higher organic content than Yanou and Long Lakes, containing up to 22% carbon (compared to <4% and <7% carbon for Yanou and Long Lakes). This is striking, and may reflect the role of penguins. Penguins feed on krill in the sea, but then moult and rest on land, depositing marine-derived carbon in their excreta, which not only fertilizes the terrestrial biota, but also adds marine carbon to the sediment. Therefore changing penguin populations could account for the oscillations in the δ^{13}C profile, as well as the age reversals in the radiocarbon dates. It is possible the dates have been contaminated by older marine carbon. Unfortunately, the influence of penguins cannot be verified by the δ^{13}C data, as Liu *et al*. (2006) found the range of δ^{13}C values of sediments associated with penguin guano overlap with those of freshwater sediments not influenced by marine animal activity.

Therefore AZ II appears to have been deposited during a period of high sediment delivery into the lake and enhanced sea spray influence. Both could be caused by a warmer/wetter stormier climate, with more sea spray reaching the lake and with

increased precipitation causing greater surface run-off (over ornithogenic soils) and sediment mobilization.

5.4.3 AZ III: Freshwater

The uppermost zone is characterized by freshwater and fresh-brackish diatoms again, with a similar species composition to AZ I. The diatom assemblage is also similar to that of YZ/LZ VI. There is a significant peak in *Luticola muticopsis* between 72-88 cm, which coincides with reduced abundances of truly freshwater diatom taxa (sub-zone AZ IIb). This may reflect a brief period of wetter conditions and increased run-off, as suggested to explain AZ II.

5.5 Belén Lake (19.9 m amsl)

The diatom profile from Belén Lake is broadly similar to that discussed above from Ardley Lake. Again the record can be divided into three distinct zones (Fig. 4.13): two freshwater zones (BZ I and III) and a brackish-fresh section (BZ II) in between. However, there are some significant differences between the records from Belén and Ardley Lakes, both in terms of diatom species and also physical properties and isotopic results, which are highlighted below.

5.5.1 BZ I: Freshwater

The basal zone consists of diatoms characteristic of freshwater through to brackish-fresh environments. The relatively wide salinity tolerances of the most abundant species (*Nitzschia frustulum/perminuta*, *Planothidium delicatulum* and *P. lanceolatum*) and the eutrophic nature of these taxa prevent detailed conclusions being drawn about the exact nature of the depositional environment at this time, beyond it being broadly freshwater. Organic content is very low (<0.05%), reflecting the high tephra content of this zone. The peaks in magnetic susceptibility and gamma density correspond to these tephra layers.

Unfortunately the two attempts to obtain a basal date were unsuccessful due to the very low organic content. This prevents possible correlation with AZ I. As at Ardley Lake there is an absence of marine diatoms, however, without a basal date it is not possible to conclude whether this means Belén Lake was never inundated, or whether the core

is not deep enough to cover the marine section. The latter is possible as the basal sediments of Belén are not glacial as at Yanou and Long Lakes; deeper coring at Belén was prevented by a thick impenetrable tephra layer. However, evidence from the other three basins suggests the mid-Holocene RSL highstand was between 16 and 18 m amsl, which implies the former hypothesis is true and Belén Lake is too high to have been a marine basin since deglaciation.

5.5.2 BZ II: Brackish-fresh

This zone is marked by the appearance of the brackish diatom species *Chamaepinnularia gerlachei*. Overall abundances of freshwater and fresh-brackish taxa remain similar to BZ I, although species composition changes slightly. As previously explained (section 5.2.5) the salinity and ecological preferences of this species are not well documented, but the presence of the true brackish species *Navicula halophila* and reduced abundances of salt intolerant taxa suggests this zone is indicative of brackish conditions.

Whilst there is a distinct change in the diatom assemblage between BZ I and II, this transition is not mirrored in the isotope record or physical properties of the sediments. Organic content remains very low and $\delta^{13}C$ values continue to fluctuate considerably. The low organic content is again a reflection of the abundance of tephra throughout the zone, and the $\delta^{13}C$ values are presumably highly oscillatory and less reliable due to the very low organic carbon content.

A date on freshwater moss immediately above the upper boundary of this zone constrains the termination of brackish conditions to 4829 ± 38 ^{14}C yr BP (5510 cal yr BP). This is later than the RSL highstand observed at Yanou and Long, and although it is earlier than the termination of AZ II, the zones do overlap and appear correlative. The low diatom concentrations of BZ II suggest this also correlates to the period of high allochthonous sediment influxes that are reported across Fildes Peninsula at this time (Mäusbacher *et al.*, 1989; Schmidt *et al.*, 1990). Diatom concentrations are lower than in AZ II, which is likely to be a function of the location of Ardley Lake in an area of high biological productivity. The similarity between the two zones in terms of the diatom composition (brackish taxa indicative of sea spray) supports the suggestion that this

was a period of stormier climate, causing increased sea spray influence in coastal lakes.

5.5.3 BZ III: Freshwater

The uppermost zone is dominated by freshwater and fresh-brackish diatom taxa, with higher species diversity and overall concentrations. The species composition is similar to AZ III, YZ VI and LZ VI. The reduced abundances of brackish-fresh and brackish species suggests the boundary between BZ II and III reflects a decrease in salinity. The transition in the diatom record also corresponds to a marked increase in organic content. There is a clear stratigraphic contact between inorganic silty clay and fine organic mud containing freshwater moss. Carbon content increases from <0.2% below this boundary to between 2.5 and 9.3% above it. There is also a shift in the $\delta^{13}C$ profile, with values fluctuating over a smaller range in BZ III and increasing to between -19‰ and -24‰. These values are typical of marine sediment (Meyers, 1994), thus contradicting the diatom results and the clear observation that Belén is currently a freshwater lake. However, a similar trend was observed at Long Lake in the uppermost zone, and attributed to a change in palaeoenvironmental conditions (section 5.3.6). Warmer temperatures may have caused the melting of lake-ice in summer and consequently a change in the algal community, enhanced productivity, and a shift in isotopic composition. Alternatively the isotope record may reflect the development of vegetation in the catchment.

5.6 Gaoshan Lake (34.5 m amsl)

Gaoshan Lake was analysed at lower resolution due to the higher altitude of the lake, which was not expected to be influenced by changes in Holocene RSL as the other lakes at lower elevation have been. At 34 m amsl Gaoshan shows the typical diatom species, isotope values and physical properties of a true freshwater lake (Fig. 4.15). However, there are still three significant conclusions from the study of Gaoshan Lake.

Firstly, the basal date of 6366 ± 39 ^{14}C yr BP (7240 cal yr BP) provides a minimum age on deglaciation. It is possible that the onset of lake formation was not captured at the base of the core as very compacted sediments at depth could not be penetrated by manual Livingston coring. This is confirmed by the older basal dates obtained from

Long and Ardley Lakes of >7500 ^{14}C yr BP, both also deglaciated later due to their more northerly position on Fildes Peninsula, closer to the present ice margin. However, the date still forms a minimum constraint and gives support to the other basal dates being correct.

Secondly, assuming Gaoshan Lake is significantly above the marine limit then it is interesting that between 7% and 33% of the total diatom count consists of oligohalobous-halophobous (brackish-fresh) species (Fig. 4.14). As Gaoshan Lake is less exposed to sea spray than the other lakes due to its position further inland, this is significant for the interpretation of the diatom results from other lakes. Where there are peaks in brackish-freshwater diatoms in other lakes, such as YZ/LZ V and AZ/BZ II, this suggests these may not be entirely related to sea spray reaching the lakes, but instead induced by climate or lake productivity changes. The presence of brackish species in Gaoshan suggests that there is a 'background' level of brackish-fresh diatoms even in essentially freshwater lakes in this area. This is plausible given all lakes studied are within 350 m of the coast.

Finally, δ^{13}C values fluctuate widely between -19‰ and -27.4‰ (Fig. 4.15). This covers the ranges characteristic of both freshwater and marine sediment, and therefore there is the same disagreement between isotope data and diatom flora as observed in LZ VI and BZ III. Again this highlights the role of changing palaeoenvironmental conditions in driving the carbon isotope signal, and suggests they have limited use as a palaeosalinity proxy in Antarctic lake sediments.

5.7 Synthesis

Following analysis of results from all lakes, the interpretations are integrated here to provide an overall summary of the Holocene RSL history of Fildes Peninsula. The preliminary interpretation presented in section 5.3.7 is expanded upon with the results from the higher altitude lakes. A summary of RSL and changing depositional environments is presented schematically in Fig. 5.8.

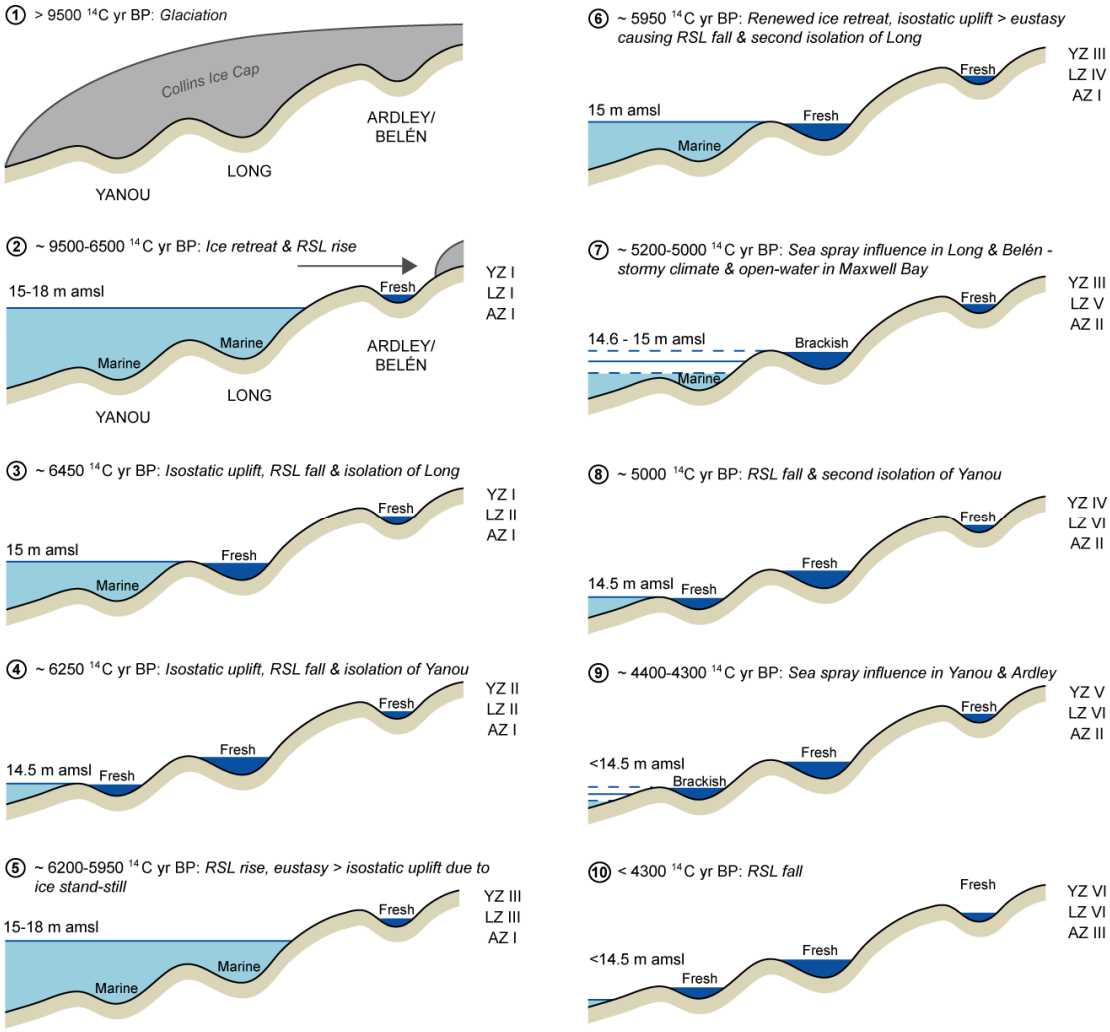

Fig. 5.8 Schematic representation of RSL change on Fildes Peninsula, with correspondence to the zones identified from diatom, isotope and physical analyses. As the results from Ardley and Belén Lakes are very similar, Belén is not included on the diagram for simplicity. Gaoshan is also not included as results from this lake do not further constrain RSL change.

The onset of deglaciation of Fildes Peninsula seems to have occurred prior to ca. 9500 ^{14}C yr BP. Once the ice margin was grounded on the peninsula, it retreated from the south to central peninsula, with lakes formed by meltwater or marine water occupying depressions. Marine sediments at the base of Yanou and Long, and the absence of a marine component at Ardley and Belén Lakes confirm that immediately after glacial retreat RSL was between 15-18 m above present. On the basis of isolation basin data alone it is not known whether RSL rose to this highstand. Models suggest RSL did rise to the highstand (Bassett *et al.*, 2007, Fig. 2.12), but this still needs to be confirmed

from additional evidence, and will be discussed in chapter 6. From the time of the highstand to ca. 6450 ^{14}C yr BP, RSL fell to 15 m amsl as a consequence of isostatic uplift in response to regional deglaciation, causing the isolation of Long Lake. By ca. 6250 ^{14}C yr BP RSL had fallen to 14.5 m amsl, causing the isolation of Yanou Lake. Ice retreat then temporarily stopped, causing the rate of isostatic uplift to slow significantly and be outpaced by eustatic sea level rise. Consequently RSL rose to cause a marine ingression into Yanou and Long. Again the absence of a marine component at Ardley and Belén Lakes confirm that RSL did not rise above 18 m amsl.

Subsequent renewed glacial retreat caused the rate of isostatic uplift to increase again and became the dominant contributor to RSL fall prior to 5950 ^{14}C yr BP. At this time Long Lake became isolated, meaning RSL stood at 15 m amsl. Between ca. 5950 and 5050 ^{14}C yr BP marine sedimentation continued in Yanou and all other basins were freshwater, suggesting RSL was between 14.5 and 15 m amsl. At ca. 5050 ^{14}C yr BP Yanou became isolated for the second time following continued isostatic uplift, and therefore RSL stood at 14.5 m amsl. Subsequently, isostatic land uplift and RSL fall has continued to the present day.

However there are significant shifts in the proxy records after 5000 ^{14}C yr BP, which are interpreted to reflect changes in palaeoclimate. A period of increased surface run-off, either due to climate warming and/or increased precipitation, causing high allochthonous sediment influxes into the lakes, was observed between ca. 5100 and 4200 ^{14}C yr BP at Yanou and Ardley, and slightly earlier at Long and Belén. At Ardley and Belén this period of high sediment delivery into the lakes is also characterized by enhanced sea spray, with short-lived brackish incursions also observed in Yanou and Long Lakes around 500-750 years after isolation. It is therefore proposed that this was a period of stormier climate and open water conditions in Maxwell Bay, with storms causing increased sea spray in coastal lakes, and the increased precipitation causing greater surface run-off. Such changes in palaeoenvironmental conditions also appear to drive the isotopic profile, with high δ^{13}C values characterizing freshwater sediment, which would not be expected from the source of organic matter. The potential use of carbon isotopes as a palaeosalinity proxy is discussed is section 5.8.

The relative sea level history of Fildes Peninsula described above is summarized on the RSL curve (Fig. 5.9) by plotting the ages of marine-lacustrine transitions in the lake cored against the sill height of each lake (note this represents the altitude of MHHW, the indicative meaning of the isolation basin diatomological contact).

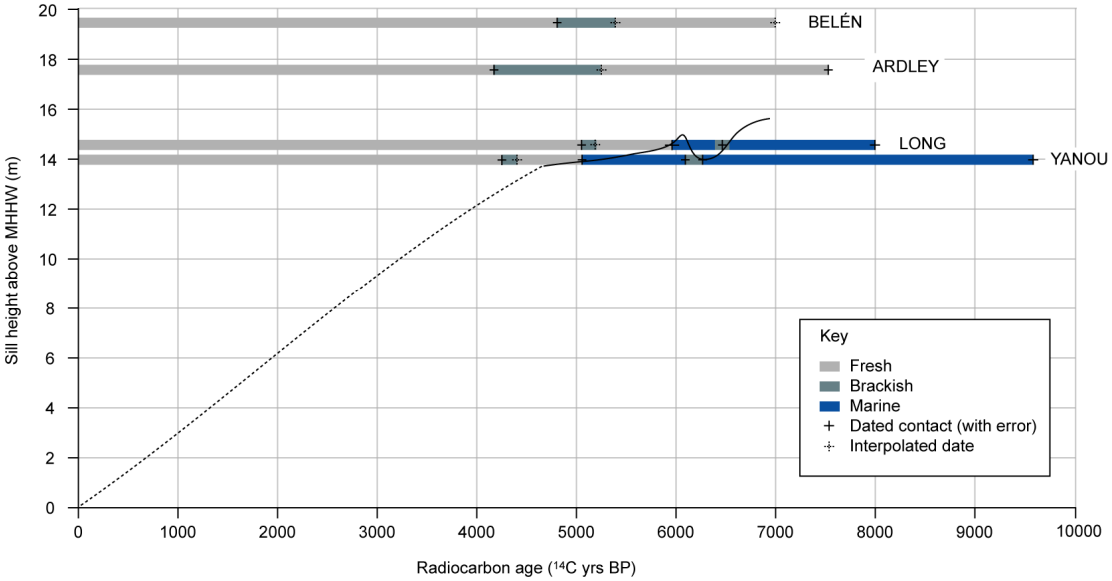

Fig. 5.9 Preliminary relative sea level curve for Fildes Peninsula based on isolation basin data from this study only. Sill heights are plotted above mean higher high water, as this is the assumed indicative meaning of isolation basins.

Note the RSL curve around 6400-6200 ^{14}C yr BP does not precisely go through the isolation and ingression contacts of both Yanou and Long Lakes, due to the poor dating control on these contacts. Also note that the precise form of the curve after ca. 4500 ^{14}C yr BP cannot be constrained by isolation basin data alone, and so is represented by a dotted line. The direction of RSL change prior to ca. 7000 ^{14}C yr BP is also unknown so has not been shown. This preliminary curve will be built upon and refined in the subsequent chapters with additional data from raised beaches and raised marine features, but the isolation basin data clearly provide strong constraints on the mid-Holocene highstand of RSL.

5.7.1 Placing the results in a regional context

The date for the onset of deglaciation of Fildes Peninsula prior to ca. 9500 ^{14}C yr BP fits with previously reported dates for glacial retreat from Maxwell Bay. Milliken *et al*. (2009) placed the minimum age of glacial retreat from the outer portion of Maxwell Bay at

13100 ± 60 ^{14}C yr BP (13860 ± 140 cal yr BP), with a period of rapid retreat between 10100 and 8200 cal yr BP. From onshore evidence, Mäusbacher *et al*. (1989) proposed that deglaciation of Fildes Peninsula began after 9000 ^{14}C yr BP.

When compared to other lake records from around Fildes Peninsula there are significant similarities and differences. Results from previously published work are integrated with results from this study and presented in Fig. 5.10, a modified RSL curve from Fig. 5.9.

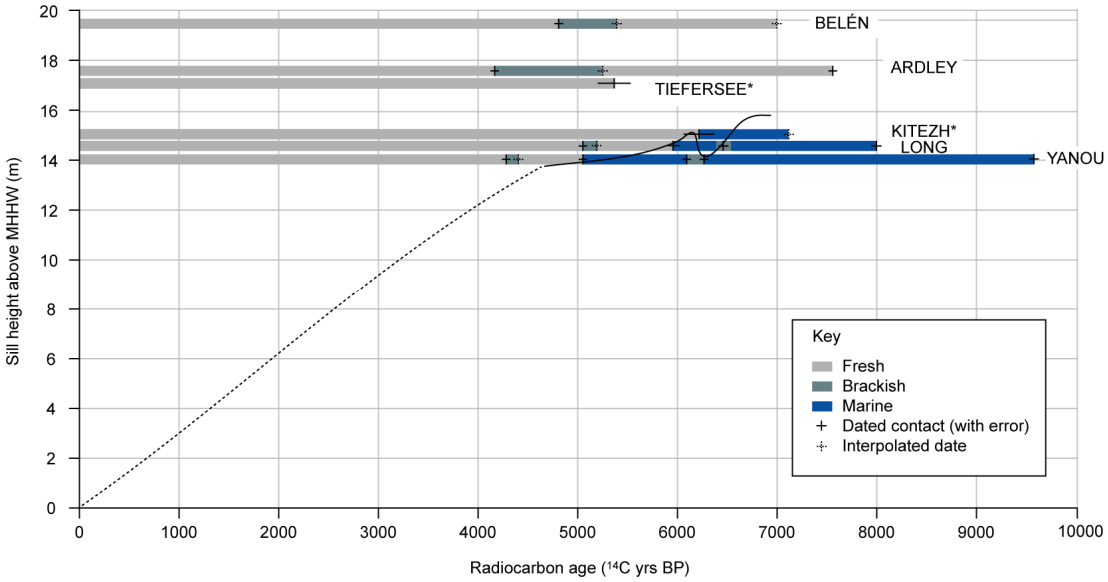

Fig. 5.10 Preliminary relative sea level curve for Fildes Peninsula, produced from results from this study and previously published work (*). As in Fig. 5.9, sill heights are plotted above mean higher high water, as this is the assumed indicative meaning of isolation basins. The results from Lake Kitezh come from Mäusbacher *et al*. (1989) and Tiefersee from Schmidt *et al*. (1990). The previously published results from Ardley and Long (Mäusbacher, 1991) are very similar to those in this study, so have not been shown.

Of most significance is the disagreement between the Long/Yanou and Kitezh records. Only one isolation contact is reported from Lake Kitezh, with a sill elevation 50 cm amsl higher than Long Lake, by Mäusbacher *et al*. (1989). This was dated to around 270 years later than this study suggests Long Lake was isolated the first time and 230 years earlier than the second. This would not be expected given the relative sill heights of the two lakes. However, it is possible that the first isolation event observed in Long and Yanou Lakes was missed in Lake Kitezh due to the sampling resolution of the Mäusbacher *et al*. (1989) study. There is also a larger error on the sill height of Lake

Kitezh as the height reported by Mäusbacher *et al*. (1989) does not agree with the SCAR King George Island GIS (section 5.2.2) and they do not report details of surveying of the lake sill. For this reason the RSL curve drawn in Fig. 5.10 does not completely follow the results from Lake Kitezh.

By contrast, the records from Ardley and Belén Lakes are very similar to that from Tiefersee at 17.5 m amsl (Mäusbacher *et al.*, 1989; Schmidt *et al.*, 1990), with a marine component absent from all three lakes. At Tiefersee the brackish section of low diatom abundance was also attributed to high sediment influxes. However, due to the position of the Tiefersee basin very close to the present ice margin and the basal date on the core of 5380 ± 165 ^{14}C yr BP, it is not possible to conclude whether the absence of a marine component reflects the altitude of the sill height above the Holocene RSL highstand or the occupation of the basin by glacier ice at the time of the marine transgression. Either way, it is very unlikely that the Ardley and Belén basins were still occupied by ice during the marine transgression shown in the Yanou and Long records, given their southerly location on Fildes Peninsula and the evidence of ice margin retreat from south to north (Mäusbacher, 1991). This therefore constrains the height of the Holocene marine limit to below 18 m amsl.

5.8 Carbon isotope and C/N ratios as potential palaeosalinity proxies for isolation basin sediments

This study has highlighted the disagreement between diatom and carbon isotope records, and demonstrated the relative unreliability of using carbon isotopes as a palaeosalinity proxy. At Yanou and Long, marine and freshwater sediments are indistinguishable on the basis of δ^{13}C values alone (Fig. 5.6). In the freshwater lakes of Ardley, Belén and Gaoshan, freshwater sediments have isotopic signatures normally characteristic of marine sediments. It also appears that the isotopic profiles are frequently driven not only by changes in the source of organic matter and thus RSL, but also by palaeoenvironmental and productivity changes.

Previous studies have used C/N ratios in tandem with carbon isotopes to help distinguish between marine and terrestrial carbon sources. However, the sediments of the Fildes Peninsula lakes have exceptionally low nitrogen content, which has

prevented the calculation of C/N ratios for whole cores. When combined with the overlap of $\delta^{13}C$ values between marine and freshwater sediment, conventional C/N and isotopic partitioning between marine and freshwater algae is not always possible in the Fildes lake sediments (Fig. 5.11). Similar problems of lacustrine sediments yielding wide ranging $\delta^{13}C$ values have been reported from the Vestfold Hills and Taylor Valley, East Antarctica (Bird *et al.*, 1991; Doran *et al.*, 1994). Rau *et al*. (1989) have also shown that organic matter produced by marine algae living in cold polar water can have $\delta^{13}C$ values as low as -28‰, which is in the range of lacustrine algae.

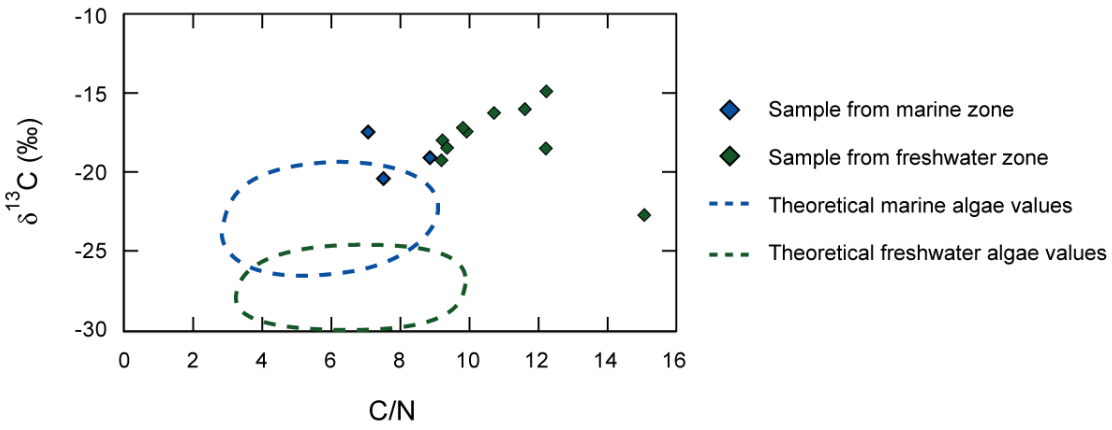

Fig. 5.11 Biplot of C/N ratio versus $\delta^{13}C$ values for Long Lake. Only three samples are plotted from the marine zones due to all other samples having %N concentrations of <0.1% which prevented C/N ratios being calculated

Useful reviews of the potential limitations of using carbon isotopes as salinity indicators are provided by Mackie *et al*. (2005; 2007) and Lamb *et al*. (2006), with further discussion of stable isotopes in lacustrine organic matter by Bird *et al*. (1991), Leng and Marshall (2004), Leng *et al*. (2005) and Smith *et al*. (2006b). These highlight several possible reasons for the failure of carbon isotopes to function as a palaeosalinity proxy, some of which were introduced in section 5.3.6 to explain the unexpectedly high $\delta^{13}C$ values in a zone of freshwater sediment. Firstly, the isotope data appear to be responding not only to changes in the origins of organic matter but also to changes in lake basin productivity. Increased aquatic productivity has been shown to enrich the dissolved carbon pool in ^{13}C owing to high rates of photosynthesis and preferential uptake of ^{12}C (Bird *et al.*, 1991; Leng *et al.*, 2005; Mackie *et al.*, 2007). Secondly, the influence of palaeosalinity may be partly masked by changes in lake ice cover. Lawson

et al. (2004) attributed ^{13}C enrichment of nearshore organic matter relative to deep water samples from lakes of the McMurdo Dry Valleys (East Antarctica) to lake ice cover, with the lake edges seasonally ice-free. Increased growth rates in response to light availability in the ice-free areas resulted in greater competition for CO_2 by microbial autotrophs and consequently higher $\delta^{13}C$ values.

In addition, Lamb *et al*. (2006) demonstrated the difficulties in interpreting $\delta^{13}C$ in terms of RSL change in environments where phytoplankton dominates the input to the sediments. Where there is more of a balance between organic material derived from terrestrial plants and phytoplankton, variations in their relative proportions can be more successfully deduced using C/N and $\delta^{13}C$. This may therefore be a problem in this study.

Therefore unlike in Scottish isolation basins where $\delta^{13}C$ values and C/N ratios were successfully used to distinguish between Holocene marine and freshwater sediments (Mackie, 2004; Mackie *et al.*, 2007), this study has highlighted the potential limitations of carbon isotopes as a potential proxy for reconstructing palaeosalinity in Antarctic environments.

5.9 Summary

This chapter has discussed the results of diatom, isotope and physical analyses of lake cores. Long and Yanou Lakes provide the longest records of RSL change and are key for understanding the deglacial RSL history of Fildes Peninsula. When integrated with the results from lakes at higher elevations, it has been possible to produce a RSL curve, which is well-constrained for the period between ca. 7000 and 4500 ^{14}C yr BP. The overall trend throughout the Holocene is of RSL fall, caused by isostatic uplift in response to regional deglaciation. However, superimposed on the signal of RSL change are changes in palaeoclimate and palaeoproductivity. The lakes are sensitive to small local environmental changes, which are frequently translated into significant ecological changes within the lakes. Possible explanations for such changes have been proposed here, but remain secondary to the overall aim of reconstructing RSL change.

The RSL curve developed in this chapter still needs further refinement, particularly for the period prior to ca. 7000 ^{14}C yr BP. In the next chapter, morphological evidence of RSL change is analysed. Specifically the aim is to integrate evidence of RSL change from raised beaches with the isolation basin data presented here to develop a more robust RSL curve.

CHAPTER 6

Determination of isostatic uplift from raised beaches

6.1 Introduction

The benefits of reconstructing RSL using a combination of evidence from isolation basins and raised beaches were discussed in Chapter 2. The previous three chapters have dealt with the former, and the interpretation of data from isolation basin sediments has allowed the production of a preliminary RSL curve. However, one key question is the area of the SSIs over which this curve is applicable. An understanding of this can be gained from a study of spatial distribution of raised beaches. This chapter introduces the work on raised beaches, and has three aims; (i) to describe the geomorphology of raised beaches at key sites across the SSIs; (ii) to determine the spatial variability of RSL change across the SSIs by quantifying the pattern, extent and magnitude of differential isostatic uplift along the island chain, and (iii) to refine the RSL curve produced from isolation basin data.

There are flights of raised beaches at numerous sites across the South Shetlands archipelago (Fig. 6.1), extending laterally up to 8 km, which formed as a result of isostatic land uplift following deglaciation (John and Sugden, 1971; Curl, 1980; Hall, 2003). Depending on location and local factors, raised beaches across the SSIs vary from staircases of terraces, with up to ten beach crests, to single beach levels. As

described in Chapter 2 (section 2.3), undisturbed beaches occur up to altitudes of 54 m above mean sea level (amsl). However, there are marked differences between the beaches above and below 18.5-22 m amsl. The beach at ~18.5 m amsl is laterally continuous over distances up to 8 km and is characterized by the following features (John and Sugden, 1971):

- Well-defined backslope of up to 6 m, convex in form
- Composed of well-rounded and rounded pebbles and cobbles
- Inland the ground surface is covered with till, striated rock surfaces and solifluction debris. At the foot of the backslope, the contrast between till and beach material is often remarkably abrupt
- Much fresher form than higher beaches (John and Sugden reported ~84% rounded and well-rounded pebbles below 18 m amsl compared to ~82% angular and sub-angular pebbles on higher beaches due to frost shattering)
- Aligned roughly parallel to present coast

On the basis of these characteristics, John and Sugden proposed the ~18.5 m beach is a transgressive feature. Above this altitude beach remnants are poorly preserved, showing modification by erosion and frost shattering. They are composed of well-rounded cobbles like the lower beaches, but also with angular fragments that have been derived from the rounded cobbles by frost splitting (John and Sugden, 1971). Therefore only freshly weathered beaches below 18.5-22 m amsl are regarded as Holocene in age, and the prominent beach at ~18.5 m amsl is regarded as the post-LGM marine limit (Barsch and Mäusbacher, 1986b; Hall, 2003). However, the altitude of the highest Holocene beaches varies across the archipelago, from 20 m amsl at Mitchell Cove (Robert Island) and Hurd Peninsula (Livingston Island) to 17.3 m amsl on Fildes Peninsula (King George Island), to as low as 8.7 m amsl at Williams Point (Livingston Island) (John and Sugden, 1971). Previous studies have also reported variable beach morphology, both locally and across the island chain.

Work on SSIs beaches has been piecemeal, with a few early studies describing the whole area (John and Sugden, 1971; John, 1972; Curl, 1980), but most subsequent work has been more localized (e.g. López-Martínez *et al.*, 1992; Pallàs *et al.*, 1995; Arche *et al.*, 1996; Del Valle *et al.*, 2002). Differential isostatic uplift is frequently ignored, and beach levels are normally measured from sea level rather than equated to modern day equivalent heights, such as contemporary storm beaches. Therefore an

opportunity exists to re-examine the heights and distribution of beaches across the SSIs in more detail and with a focus on the spatial pattern of glacio-isostasy.

6.2 Field locations

Areas of raised shorelines were initially identified using remote sensing. Aerial photographs of the South Shetland Islands from the 1956/57 Falkland Islands Dependency Survey (FIDASE) and UK Royal Navy photography from the 1970s and 80s were used to identify suites of raised beaches. In some areas satellite imagery (Landsat TM or Aster) was also employed and proved useful at a regional level. Previous studies from the area provided extremely useful background on site locations and descriptions of beaches (John and Sugden, 1971; John, 1972; Sugden and John, 1973; Curl, 1980; Hansom, 1983; López-Martínez *et al.*, 1992; Arche *et al.*, 1996; Birkenmajer, 1998). Existing topographic and geomorphological maps were also used to locate field sites (Instituto Antartico Chileno, 1996; López-Martínez *et al.*, 1996; Braun, 2001). Finally, helicopter reconnaissance from *HMS Endurance* confirmed possible features. Fig. 6.1 shows the distribution of raised shorelines in the central part of the SSIs archipelago. From these, 15 survey areas were selected for fieldwork. Areas were selected to give as broad as possible geographic distribution of sites, although some sites could not be visited due to logistical difficulties or the lack of suitable helicopter landing sites.

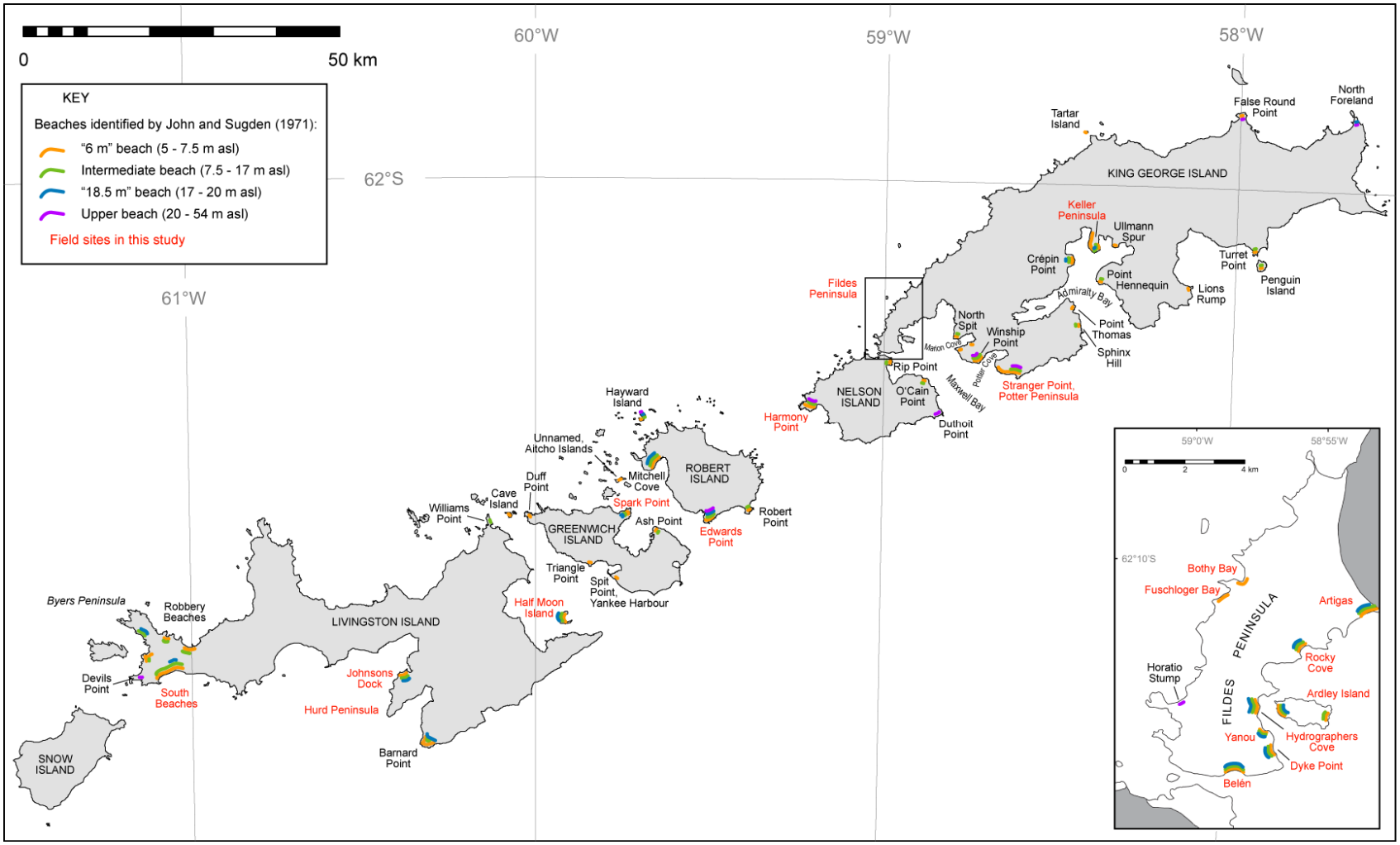

Fig. 6.1 Raised beaches across the South Shetland Islands. Sites surveyed in this study are in red.

6.3 Field and analytical methods

Fieldwork was conducted over two successive field seasons: November 2006 to January 2007 (P. Fretwell, M. Bentley, E. Watcham, S. Roberts) and January 2008 (P. Fretwell), using the logistical support of *HMS Endurance*. During the first fieldwork period much of the data were collected from the more accessible sites including Fildes Peninsula. During the second fieldwork period helicopter deployment from *HMS Endurance* allowed access to more remote localities, and enabled additional sites to be surveyed to achieve greater spatial coverage across the archipelago. As this study forms part of a much wider British Antarctic Survey research programme (section 1.3) the fieldwork was divided between personnel, and consequently I did not visit those raised beach sites outside of Fildes Peninsula. However, as the results from this ongoing work are critical for informing the RSL history, the field methods and full set of sites are described here. For this I acknowledge Fretwell *et al*. (2010) and the British Antarctic Survey field report (Hodgson *et al.*, 2007), from which site descriptions are taken, as well as personal communications with Peter Fretwell.

6.3.1 Geomorphological mapping

Raised beaches were mapped firstly to determine the relationship between different shoreline levels, and secondly to confirm their preservation and suitability for subsequent GPS surveying. Suitable beach ridges were defined as those with level, well-defined crests and composed of well-sorted clasts of similar sizes to the present day beach (indicative of a constant wave environment). Beach ridges with irregular or undulating crests, different clast sizes to the present day beach (indicating a change in the wave environment), and/or evidence of solifluction, overwash by fluvial processes, or other post-depositional modification were regarded as unsuitable for GPS surveying. Clast sizes were noted as beaches with pebble to cobble sized clasts were preferred for surveying. Beaches of smaller sand or silt sized particles were prone to deformation, and where clasts were larger than cobble sized difficulties were encountered in ascertaining an indicative level. At some sites mapping was limited by the amount of time available at the site due to helicopter support (Harmony Point, Edwards Point) or by snow cover (Spark Point).

6.3.2 GPS surveying

High precision GPS data were required to provide the most accurate positioning of features (particularly vertical) and to relate features from different field sites to each other within a GIS. Beach ridge crest altitudes were measured using a Leica kinematic GPS system, consisting of a fixed tripod-mounted high-definition dual frequency GPS receiver linked to a roving stake-mounted GPS unit (Fig. 6.2).

Beaches deemed 'suitable' from initial mapping were surveyed by walking along the beach crest with the roving GPS (Fig. 6.2b). Measurements were taken along the crests at ~10 m intervals, although shorter intervals were used where the beach ridges were less than 100 m in length. This technique is similar to that used in the UK by Smith *et al*. (2000), and enabled mean heights to be calculated for each section. This is important given the maximum potential error in the GPS survey was the inconsistency of beach height (Table 6.1); calculating mean altitudes helped to minimize this error. GPS readings were only taken where the level was considered to be indicative of the overall beach level (avoiding stream cuttings or human interference), and when the roving unit was in contact with the static GPS and displayed less than 5 cm error between itself and the static unit. The static GPS unit was always left running for a minimum of one hour before survey to ensure positional accuracy.

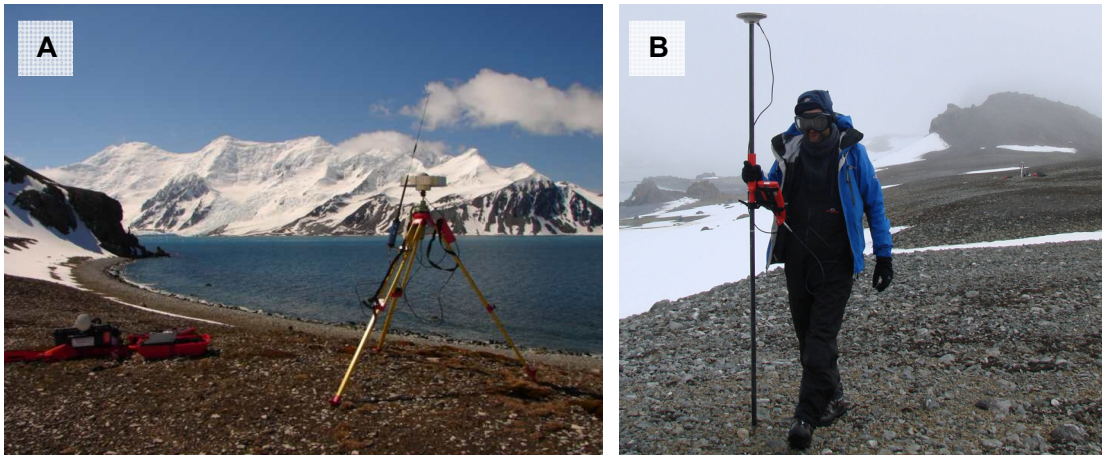

Fig. 6.2 GPS equipment used for surveying of raised beaches (a) static GPS receiver; (b) roving GPS (Photograph A by P. Fretwell)

Potential vertical error	Maximum error (cm)
Variation of beach level	~ 200
GPS rover error	< 5
GPS static error	~ 2

Table 6.1 Potential survey errors. The estimate of variation in the elevation of a single beach ridge comes from John and Sugden (1971), and reflects variations in fetch, offshore topography and availability of material.

At each site it was important to survey the present day storm beach (PDB) as well as palaeo-beach levels, as observations of modern beaches are important for informing the interpretation of palaeo-beaches (Hall and Denton, 2000a). The elevations of palaeo-beaches are given here as the height above the PDB, which is considered to be the modern analogue. The indicative meaning of the raised beaches is therefore taken as the PDB, which forms during summer at storm tide level. The PDB varies in altitude above mean sea level and geoidal height, and therefore by analyzing palaeo-beach levels with reference to the height of the PDB rather than height above sea level, sites can be compared. Sutherland (1981) suggested variability of up to 2.4 m in height of the PDB when related to mean high water spring tide. A discussion of how the raised beach data will be combined with isolation basin data is given in section 6.7.3.

At many sites the PDB is a composite feature comprising a lower fresher ridge and an older storm ridge behind. The higher ridge represents the most recent large storm event, whereas the lower ridge formed at current high tide. At such sites, the higher storm ridge was considered to be the contemporary analogue of Holocene palaeo-beach ridges. Similarly, at sites surveyed early in the Antarctic summer two contemporary beaches were frequently observed. The lower elevation beach of the two was often ice cored, as small bergs had been incorporated into the beach during the winter months. This ice cored “winter beach” formed in a shielded environment, as sea ice dampens the power of wave energy reaching the beach, and so normally formed slightly lower and closer to the shoreline than the “summer beach”. By mid-summer the ice in the lower beach melted and, as the feature was no longer shielded, the beach material was gradually reworked into the “summer beach”. Therefore, when levelling to the present day beach, the “summer beach” was considered as the modern day analogue of the palaeo-beach ridges, and showed much less variability in height than

the lower “winter beach”. Similarly the palaeo-beaches were always surveyed at their highest crest.

6.3.3 Dating the shorelines

One of the major problems associated with the study of raised beaches elsewhere has been the determination of their age. Particularly in Antarctica there are often problems associated firstly with a lack of organic material preserved within the beach sediments for radiocarbon dating, and secondly with associating the dateable material to relative sea level (e.g. Hall and Denton, 1999; Baroni and Hall, 2004; Hall *et al.*, 2004). For example, shells that occur in situ within raised beaches afford maximum ages for the beaches because they live below coeval sea level. Conversely, seaweed and sealskin on beach surfaces yield minimum ages because occupation occurred after beach formation. Similarly dates on penguin bones form minimum ages as penguins today generally live above the storm beach (Hall *et al.*, 2004).

To establish an absolute chronology for the formation of the highest raised beach, trenches were excavated through the backslopes of the highest surveyed beaches (Fig. 6.3) at several sites across Fildes Peninsula (Belen, Dyke Point, Hydrographers Cove and Ardley) in order to find organic macrofossils suitable for radiocarbon dating, such as penguin bones or shells. Time did not allow sections to be dug behind intermediate beach levels or at other sites.

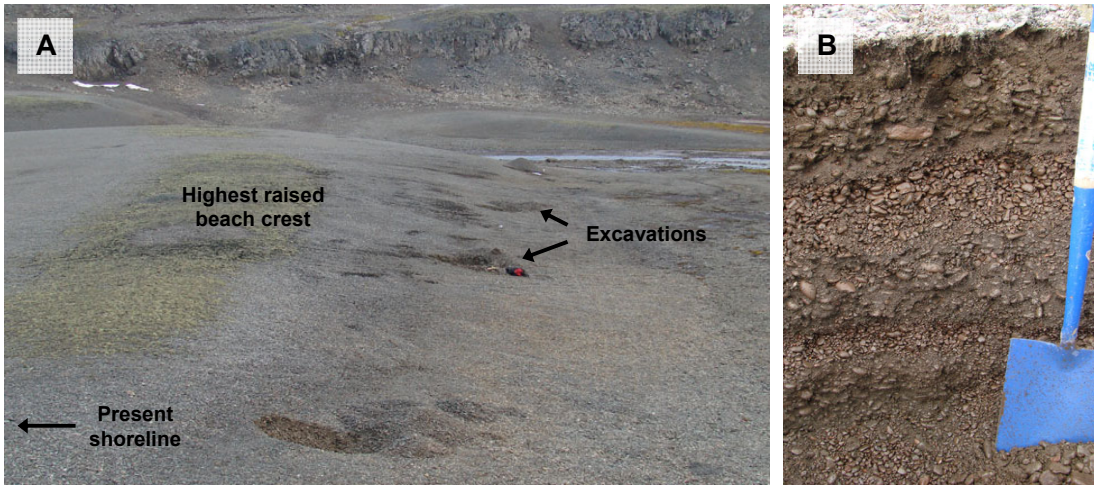

Fig. 6.3 Sampling of raised beaches for organic macrofossils for radiocarbon dating (a) sites of excavation behind the highest raised beach at Hydrographers Cove; (b) example of the highest raised beach profile at Belén.

Unfortunately, no datable material was found preserved in the raised beach sections excavated, which appears to be a common problem across the SSIs (Brenda Hall, pers. comm.). Therefore the formation of the highest beaches was instead constrained using dates from several isolation basins on Fildes Peninsula, which are situated immediately behind the highest beach. Long Lake, Yanou Lake (this study), and Lake Kitezh (Mäusbacher *et al.*, 1989) are isolation basins formed during a period of storm beach construction and RSL fall, and occupy depressions immediately behind, or in close proximity to, the steep back-slope of the highest raised beach. This suggests they formed contemporaneously with the highest raised beach, and are analogous to palaeo-lagoons observed to be actively forming in depressions behind retaining sills and the PDB at Hydrographers Cove and Fuschloger Bay (Fig. 6.18). These three lakes are the highest altitude isolation basins on Fildes Peninsula, with sill heights of 15.5 m amsl (Lake Kitezh, measured from SCAR King George Island GIS data), 15 m amsl (Long Lake, measured by kinematic GPS), and 14.5 m amsl (Yanou Lake, measured from GIS data and kinematic GPS). Dates of the isolation contacts (marine-freshwater transitions) will provide minimum ages to constrain the formation of the highest raised beach.

6.3.4 GIS and isostatic uplift analysis

GPS data on raised shorelines were input into a high-resolution GIS of the study area. This enabled beach levels to be defined from which isobase maps were constructed. The mean height of both the PDB and highest raised beach were calculated at each site. From plots of the GPS data (Fig. 6.4), beach heights not indicative of the general beach level were identified and not used in analysis. The mean height of the PDB was then subtracted from the mean height of the corresponding palaeo-beach to give a value indicating the difference in height, and hence the amount of uplift since the formation of the palaeo-beach. Presenting the height of the palaeo-beaches in this way has the advantage of negating the need for either geoidal correction or knowledge of local tides, both of which would have been difficult to assess at many of the sites visited without a much greater outlay of fieldwork and logistics, and which would have introduced greater errors. This means that survey errors can be kept to the 5 cm accuracy of the GPS.

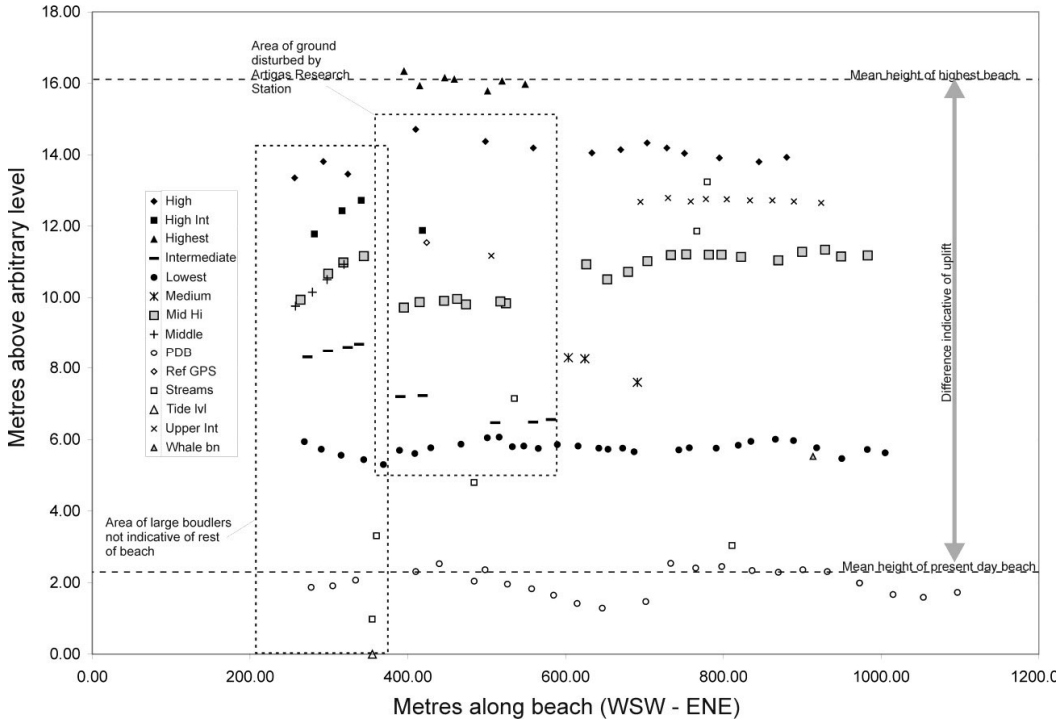

Fig. 6.4 Example of GPS data from raised beaches at Artigas, Fildes Peninsula. Such plots were used to identify points not indicative of the general beach level. This is representative of the amount and type of data collected at each beach location.

The spatial pattern of isostatic uplift in the SSIs region was then modelled by trend surface (polynomial regression) analysis using the indicative height of the highest raised beach at each site. This technique has been widely used to determine patterns of glacio-isostatic uplift in Scotland (Cullingford *et al.*, 1991; Firth *et al.*, 1993; Smith *et al.*, 2000; Smith *et al.*, 2006a). It is recognized that there are considerable weaknesses to this approach of fitting the data to a trend surface (Fretwell *et al.*, 2004; Smith *et al.*, 2006a). Firstly, trend surface models do not account for localized ice loading effects, and as they trend to infinity beyond the data, the predicted pattern of uplift beyond the area of the measured data must be interpreted with caution. The accuracy of land uplift estimates is therefore limited to a restricted geographical area. Secondly, shoreline formation in glacio-isostatically affected areas is believed to be diachronous and therefore the measured altitudes along a given shoreline do not represent an instant in time, but a period of up to several hundred years (Fretwell *et al.*, 2004). Consequently, displaced shorelines could conceal changes in the pattern of uplift. However, with these criticisms in mind, trend surface analysis is used here as an independent means of

assessing the applicability of the RSL curve developed for Fildes Peninsula over the wider area of the SSIs.

Recent advances in the technique of trend surface analysis have favoured a Gaussian approach (Fretwell *et al.*, 2004), which provides a better fit to shoreline altitude data in glacio-isostatically uplifting areas than polynomial trend surface analysis. However, this proved unviable for the SSIs due to the near-linear orientation of the island chain, which limits the geographic spread of data in a north-south direction. The quality of the data collected also did not justify calculating a fit to any function more complicated than a second-order polynomial. The trend surface analysis was carried out in ArcGIS by Peter Fretwell, but again is fundamental to the RSL interpretation and is therefore included here.

6.4 Results: Raised beach heights and geomorphology

The following section describes the field sites across the SSIs in terms of raised beach heights and geomorphology. Table 6.2 provides a summary of the heights of the highest raised beaches and number of beach levels at each location, as well as indicating which sites I worked at and those surveyed by Peter Fretwell and colleagues. Fig. 6.4 shows an example of the GPS data collected from each site.

Site	Latitude (°S)	Longitude (°W)	Height of highest raised beach above PDB (m)	No. of palaeo-beach ridges	Notes
Livingston Island					
Byers Peninsula	62°40’	61°06’	11.7	4	Central South Beaches post-depositionally modified by fluvial action. No modification to west.
North Hurd Peninsula	62°39’	60°23’	17.7	4	Human disturbance
South Hurd Peninsula	62°42’	60°24’	16.9	2	
Half Moon Island	62°35’	59°55’	16.8	4	
Greenwich Island					
Spark Point	62°27’	59°43’	16.2	4	Extensive snow cover
Robert Island					
Edwards Point	62°27’	59°30’	17.2	8	
Nelson Island					
Harmony Point	62°24’	59°14’	20.0	6	Lower beaches modified by penguins
King George Island					
Belén, Fildes Peninsula*	62°13’	58°58’	15.5	4	
Dyke Point, Fildes*	62°13’	58°57’	15.4	4	
Yanou, Fildes*	62°13’	58°57’	13.1	5	Some human disturbance
Hydrographers Cove, Fildes*	62°13’	58°58’	15.7	6	
Ardley Island*	62°12’	58°55’	15.0	7	
Rocky Cove, Fildes*	62°11’	58°55’	12.7	5	Highest beach absent
Artigas, Fildes*	62°10’	58°53’	13.8	6	
Stranger Point	62°15’	58°36’	12.2		Modified by penguins
Keller Peninsula	62°05’	58°23’	n/a	3	No GPS data taken, snow covered

Table 6.2 Summary of locations and heights of the highest raised beaches at field sites across the South Shetland Islands. * denotes sites I worked at.

6.4.1 South Beaches, Byers Peninsula, Livingston Island

The raised beach levels on Byers Peninsula, Livingston Island, are well documented (López-Martínez *et al.*, 1992; Arche *et al.*, 1996; Hall and Perry, 2004), with several raised sequences on the north, west and south of the peninsula. The beaches are generally lower than those further to the east on the South Shetland archipelago. The Holocene raised beaches are flanked inland by pre-Holocene raised marine platforms, between 30 and 140 m amsl, which often form small steep cliffs on the landward side of the beaches (John and Sugden, 1971).

Fieldwork concentrated on the South Beaches, the longest sequence of beaches on Byers Peninsula, extending ~ 10 km. The western end of the South Beaches was chosen for detailed surveying as much of the central area was unsuitable due to beaches being fragmented and dissected by numerous drainage channels. Beach ridges are poorly defined and composed of poorly sorted angular clasts in a sandy gravel matrix. There is also evidence of modification by fluvial action. By contrast, a flight of well-defined raised beaches exists to the west, extending ~ 500 m (Fig. 6.5a). Here four beach levels are identifiable, the highest of which is 11.7 m above the PDB. Beaches consist of rounded pebbles and cobbles. Although a carpet of moss and algae covers the crest of the highest beach (Fig. 6.5b), this was only a few centimeters thick and so did not compromise the accuracy of the GPS survey.

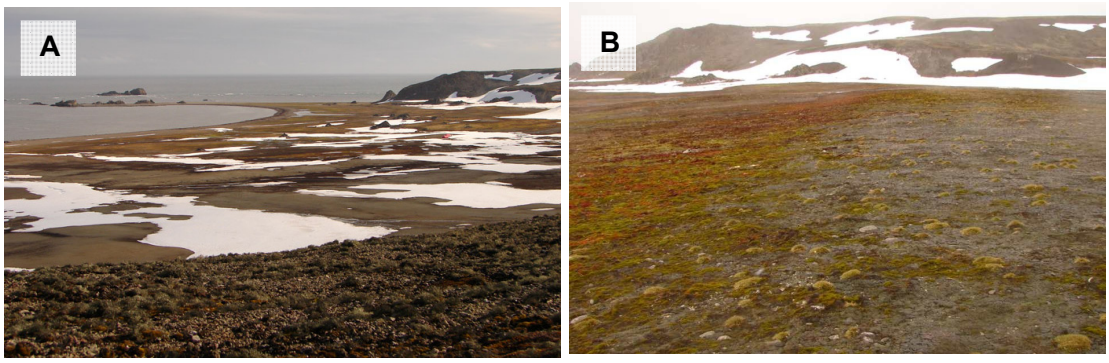

Fig. 6.5 South Beaches, Byers Peninsula (a) flight of raised beaches; (b) typical vegetation cover of palaeo-beaches on Byers Peninsula (Photographs by P. Fretwell)

6.4.2 Hurd Peninsula, Livingston Island

6.4.2.1 North

A sequence of raised beaches exists near Johnsons Dock on the northern side of Hurd Peninsula (Fig. 6.6a). There are four beach levels, with the highest 17.7 m above the PDB. However, due to the proximity to the Spanish Juan Carlos research base, access to the site was limited. Consequently it was not possible to conduct a full GPS survey. Combined with the observed human modification of the beaches and the poorly defined nature of the present-day beach, data from this site was excluded from analysis.

6.4.2.2 South

An unnamed bay on the south side of Hurd Peninsula was also surveyed. In contrast to the north, there are only two beach levels above the present-day beach. The highest beach ridge (16.9 m above the PDB, Fig. 6.6b) is well-defined, with a sizeable and steep backslope. A much lower and less well-defined beach ridge is also evident at ~2-3 m above the PDB.

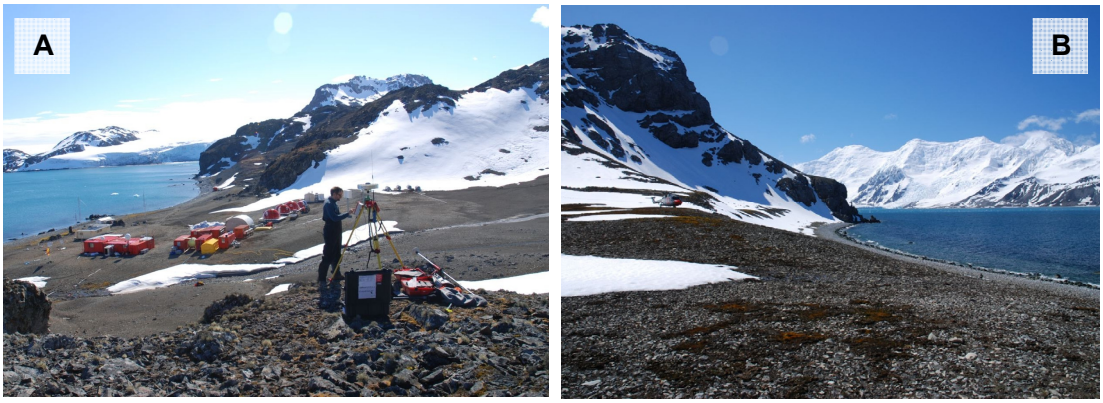

Fig. 6.6 Raised beaches on Hurd Peninsula (a) North Hurd, with human modification clearly visible; (b) South Hurd (helicopter for scale) (Photographs by P. Fretwell)

6.4.3 Half Moon Island

Half Moon Island lies to the east of Livingston Island in McFarlane Strait. The island is dominated by two craggy hills ~100 m high, joined by a shingle tombolo consisting of a series of raised beaches. The highest beach ridges are 16.8 m above the PDB, and are symmetrical on the east and west sides of the tombolo (Fig. 6.7). These highest beaches also coincide with the altitude of an erosional notch cut into the cliffs and talus slope on the flank of the craggy knoll to the northwest.

With the exception of the highest beaches, the beach sequences on either side of the tombolo differ (Fig. 6.7). The most prominent beach ridges do not occur at the same altitudes, with four levels on the western side and only two on the east. Notable differences include a 'double' beach ridge at ~ 6 m amsl on the west side (compared to only a single ridge on the east), and a prominent intermediate beach on the west side (not seen at all on the east). The swale/depression behind the 6 m beach is also more pronounced on the east side.

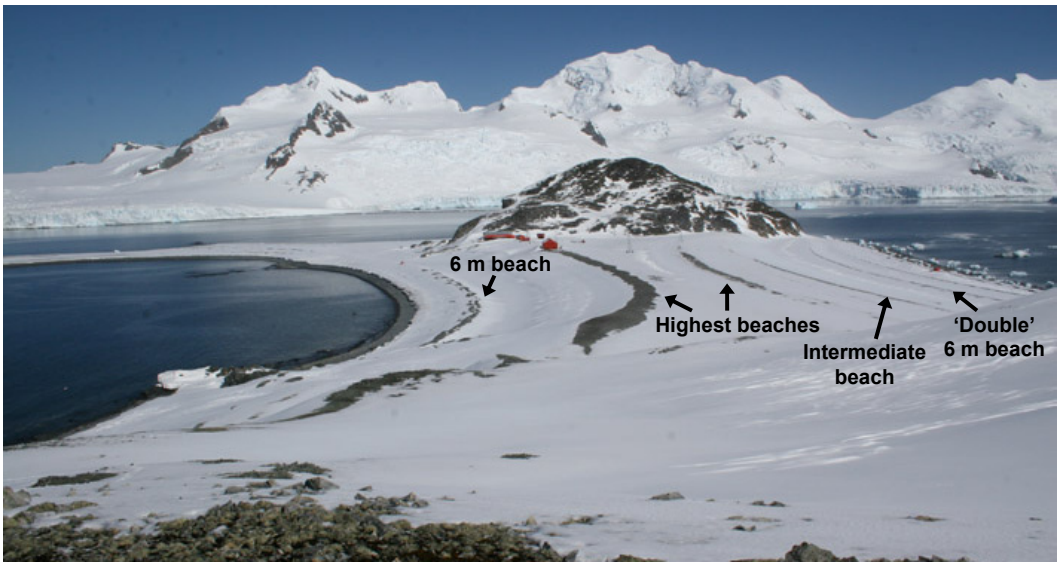

Fig. 6.7 Raised beaches on the central part of Half Moon Island, looking south. The crests of the highest beaches are clearly visible as well as the differences in beach sequences on either side of the tombolo (Photograph by M. Bentley)

6.4.4 Spark Point, Greenwich Island

Spark Point is an ice-free peninsula on the northeast of Greenwich Island, extending over 1 km into English Strait between Greenwich and Robert Islands. Unfortunately fieldwork at this site took place early in the season when most of the beaches were still covered in thick snow, and therefore only the most prominent beach crests were exposed. However, a series of raised beaches were visible on the northern and eastern side of the Point, divided by four mesas (Fig. 6.8a). The mesas display concordant surfaces, which cut across folded rocks, and are therefore likely to reflect marine planation rather than being original geological structures (Fig. 6.8b). There is also a prominent palaeonotch in these mesas at ~15 m asl (Fig. 6.8c), approximately the same height as the highest raised beach further inland. There are a maximum of four palaeo-

beach levels, the oldest and highest of which is 850 m inland from the present shoreline and 16.2 m above the height of the PDB. The surface of this highest beach shows patterned ground, with platy clasts orientated end-on in polygons around areas of flat-lying platy clasts. The relatively high altitude of this beach and the realignment of clasts by periglacial reworking suggest this beach may be older than many of the raised beaches seen in the region.

Fig. 6.8 Spark Point (a) oblique view from the air of raised beaches, with beach crests exposed above the snow, and mesas to the right; (b) mesas with concordant surfaces (dashed lines). Note surfaces only appear tilted due to the perspective of the photo; (c) palaeonotch at ~15 m amsl (person for scale is 1.7 m tall) (Photographs by M. Bentley)

6.4.5 Edwards Point, Robert Island

A sequence of eight raised beaches occupies a small embayment on the eastern side of Edwards Point, on the south of Robert Island (Fig. 6.9). The beach ridges are well-defined and level, well vegetated and often with shallow ephemeral lagoons behind. The highest beach is 17.2 m above the present-day storm beach. During fieldwork skuas were observed nesting on the beaches, but unlike at Stranger Point (section 6.4.8), there is no evidence of significant modification to the beach levels by the birds.

Fig. 6.9 Raised beaches at Edwards Point, oblique aerial view looking northeast (Photograph by P. Fretwell)

6.4.6 Harmony Point, Nelson Island

John and Sugden (1971) reported extensive flights of raised beaches at Harmony Point, an ice-free peninsula on the western side of Nelson Island. Fieldwork concentrated on a prominent sequence of beaches on the western side of the point, as time did not allow a full survey of the whole peninsula. There are six well-defined beach ridges, with the highest 20 m above the height of the PDB (Fig. 6.10).

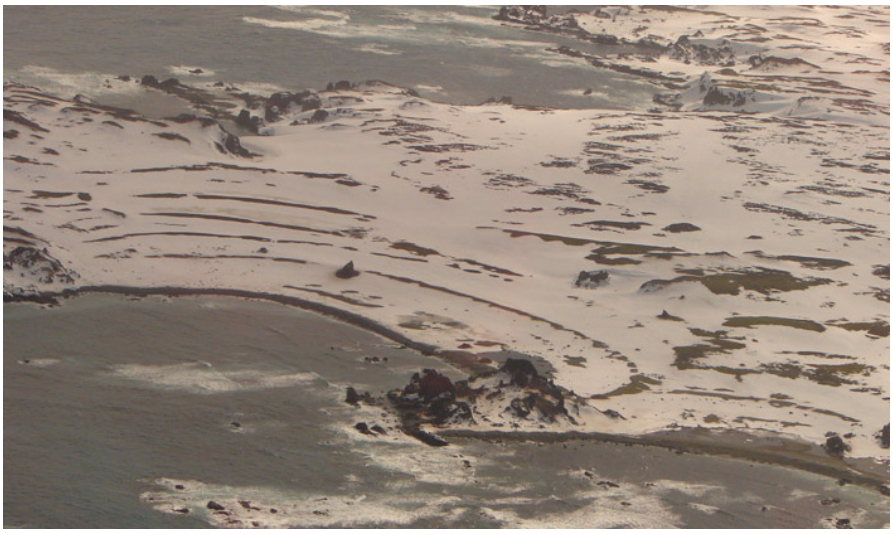

Fig. 6.10 Raised beaches at Harmony Point, oblique aerial view looking northwest (Photograph by P. Fretwell)

6.4.7 Fildes Peninsula, King George Island

Fildes Peninsula, the largest ice-free area of King George Island, has extensive raised beach sequences on the eastern and southern coasts. All flights of raised beaches occupy enclosed bays, each less than a kilometre in length. Most of the sequences are well-defined and consist of well-sorted pebble to cobble sized andesitic and basaltic clasts. The beach sediments vary in angularity and degree of sorting depending upon the wave energy of each bay and the duration of each RSL stand. Several research stations on the eastern side of the peninsula are sited on or near raised beaches (Frei, Bellingshausen, Artigas and Great Wall stations). Around these stations the beaches have been heavily modified and in two cases, near Frei and Bellingshausen, human interference meant they were unsuitable for survey. Fig. 6.11 provides a summary of the beaches we surveyed on Fildes Peninsula.

6.4.7.1 Belén

A distinctive flight of raised beaches exists on the south coast of Fildes Peninsula (Fig. 6.12). The beaches extend around 600 m in an east-west direction, divided by a rocky knoll in the middle. There are four palaeo-beach levels, although one does not exist on the eastern side of the knoll. The highest beach level is 15.5 m above the PDB, with a distinct steep backslope of ~ 2 m. This highest raised beach represents a marker for the Holocene RSL highstand in the area, as there is no evidence of a marine incursion in the depression behind this highest beach (no rounded clasts or sorting of clasts). There are also no marine sediments in Belén Lake, which lies behind the highest raised beach and knoll, approximately 100 m inland and 1.7 m higher than the highest raised beach (Fig. 6.12a).

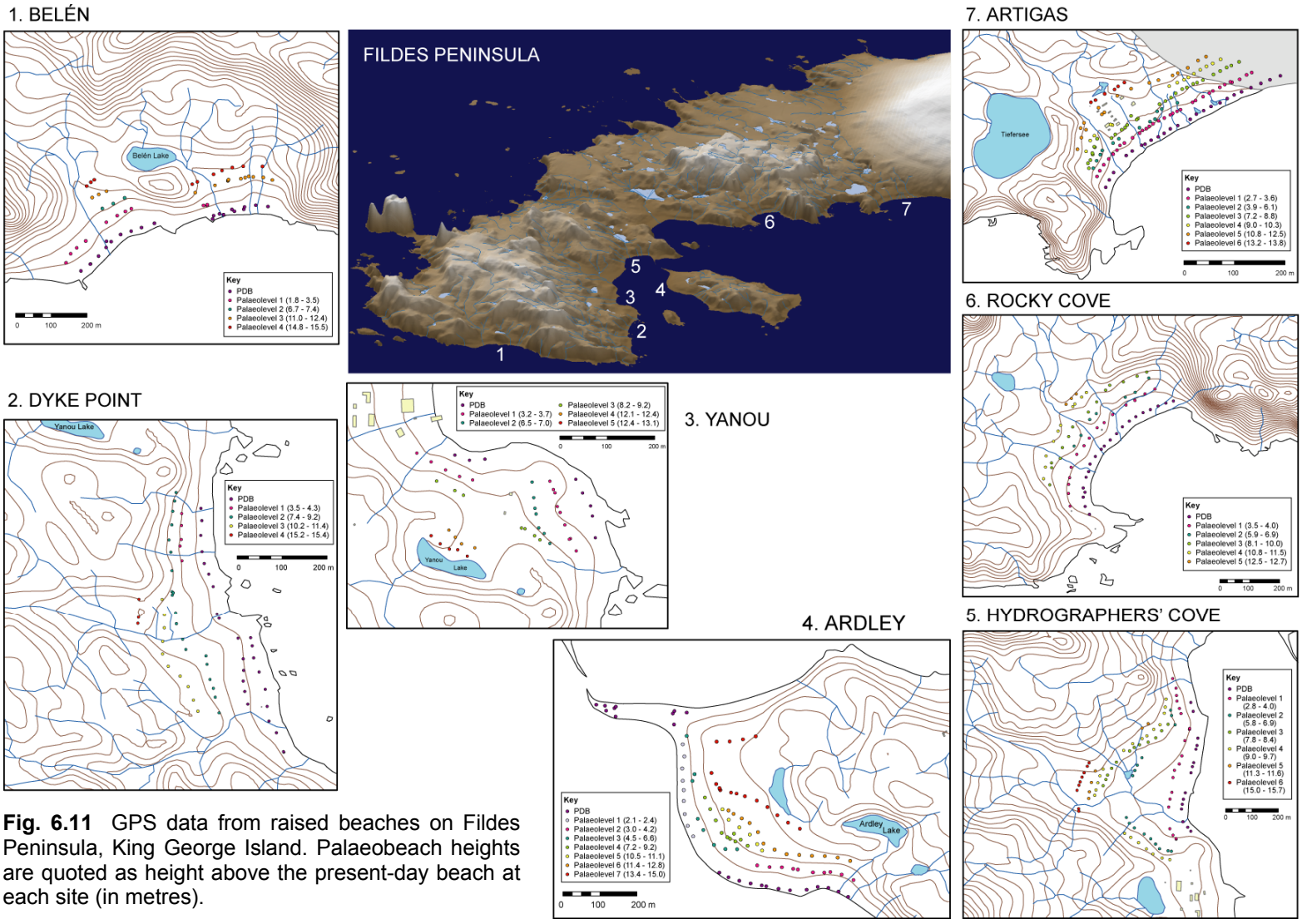

Fig. 6.11 GPS data from raised beaches on Fildes Peninsula, King George Island. Palaeobeach heights are quoted as height above the present-day beach at each site (in metres).

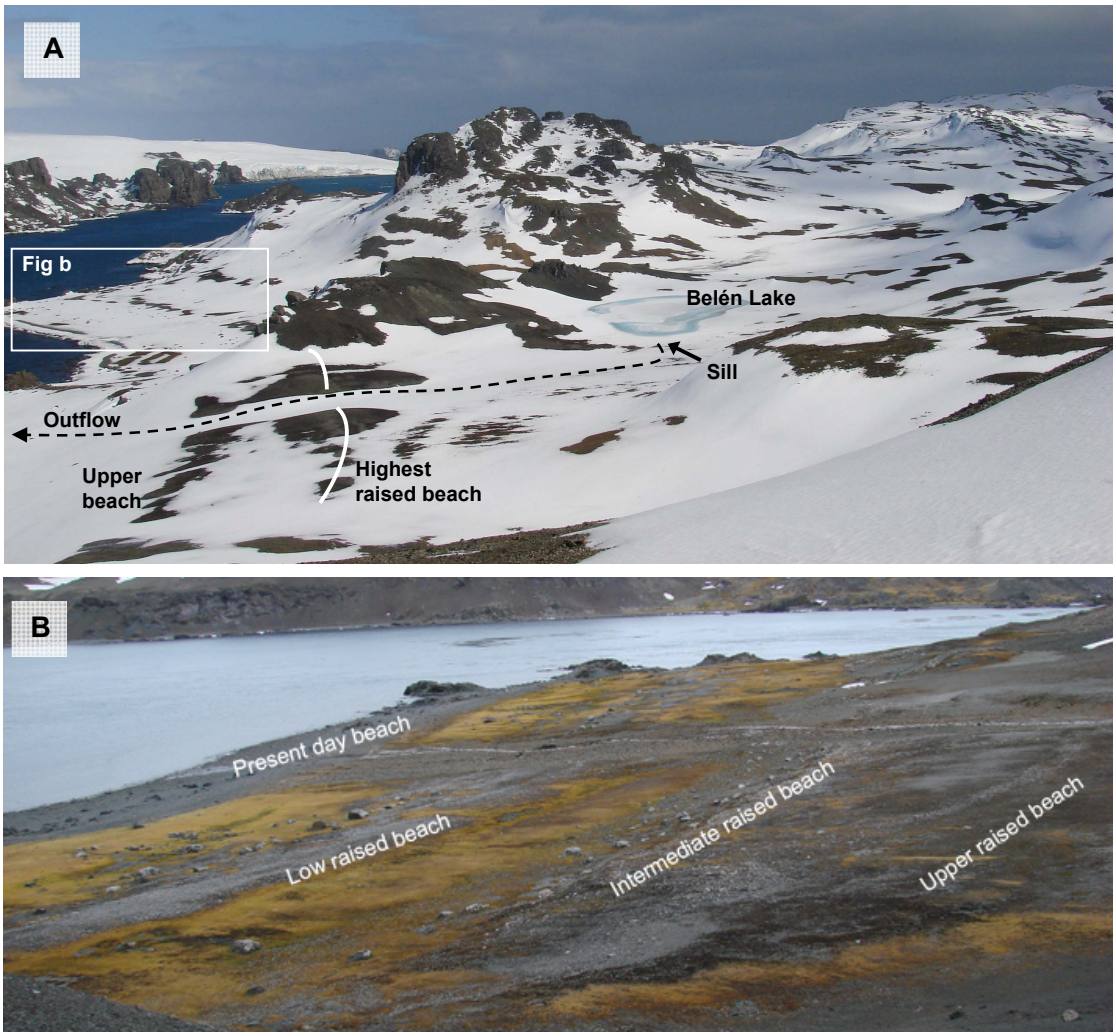

Fig. 6.12 Raised beaches at Belén, south coast of Fildes Peninsula. (a) The location of the raised beaches in front of Belén Lake; (b) close-up of beaches showing the carpet of moss and lichen between beach crests, which is characteristic of sites on the southeast of Fildes Peninsula.

6.4.7.2 Dyke Point

Along the southern-most part of the east coast, a flight of raised beaches extends for 600 m either side of Dyke Point (also called Doris Point). As at Belén, there are four palaeo-beach levels. An igneous dyke bisects the lower beach levels, but the higher beach levels are continuous. The highest beach is well-defined, with a steep backslope and fluvial depression behind. It is 15.4 m above the height of the PDB. It is cut by a stream channel to the south. The beach heights immediately next to the channel are markedly 50 cm higher than the rest of the beach, and therefore these points were not used in analysis.

6.4.7.3 Yanou

A flight of beaches exists to the east of Yanou Lake, 250 m north of Dyke Point. Five palaeo-beach ridges are evident (Fig. 6.13a), although some deformation of the middle beach has occurred by the construction of a road from Great Wall station 300 m to the north. Yanou Lake lies immediately behind the highest raised beach. This highest beach is not as well-defined as the highest raised beach at other sites on Fildes Peninsula, with no steep backslope, and is also lower, being only 13.1 m above the PDB.

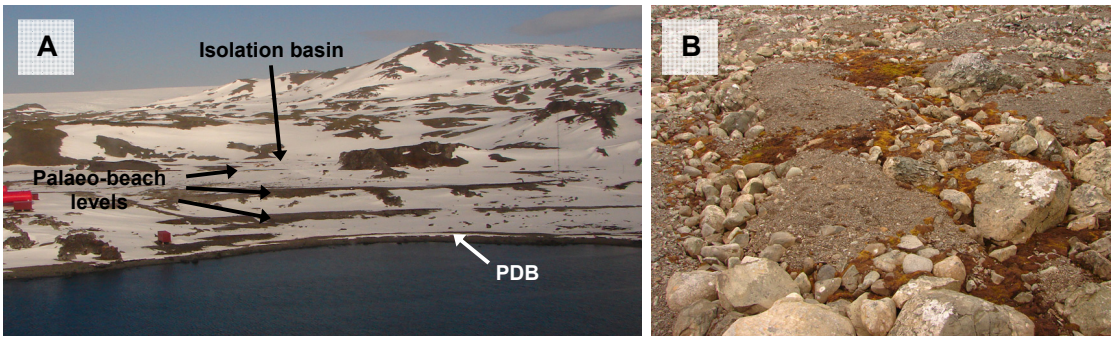

Fig. 6.13 Raised beaches at Yanou. (a) Raised beaches highlighted by the snow. The isolation basin studied in the previous chapters lies immediately behind the highest raised beach. Evidence of human disturbance is visible on the left of the photo; (b) beach surface, showing angular boulders (drop stones) and periglacial reworking by freeze-thaw (Photographs by P. Fretwell)

The beaches are characterized by angular boulders both on the beach crests, and in troughs between crests (Fig. 6.13b). These are interpreted as iceberg drop stones, and are commonly observed in the present day intertidal zone around the SSIs (Hall and Perry, 2004). However, no drop stones were found on the highest beach crests elsewhere, as the waves do not have the energy to transport them to the required height. Therefore, both the presence of drop stones on the highest beach at Yanou and the absence of the steep backslope suggest this highest preserved beach was not formed at the highest Holocene sea level (Hall and Perry, 2004). This is also supported by isolation basin data from Yanou Lake, which shows the Holocene RSL highstand was above 14.5 m amsl. Consequently as this beach was not a reliable constraint on the altitude of the highest Holocene beach, data from this site were not used in analysis.

6.4.7.4 Hydrographers Cove

A broad plain in the eastern-central part of Fildes Peninsula borders onto Hydrographers Cove (also called Playa Grande, Windbachtal and Wind Creek Valley), around 500 m north of Yanou. There are six well-defined palaeo-beach levels. The highest beach is 15.7 m above the PDB, 450 m inland from the coast. It has a steep backslope with silty fluvial sediments occupying the depression behind, suggesting this beach is associated with the Holocene RSL highstand (Fig. 6.14).

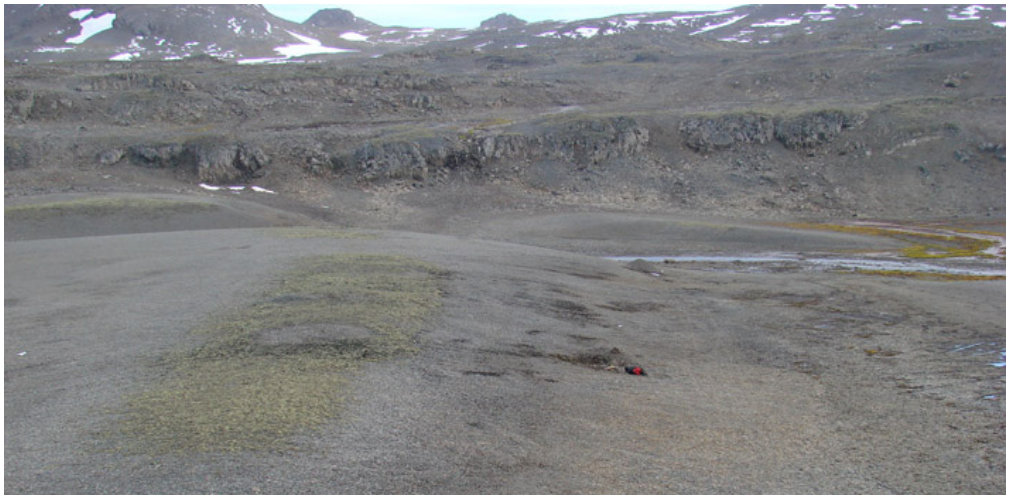

Fig. 6.14 Highest raised beach at Hydrographers Cove, showing the steep backslope characteristic of the highest shorelines across Fildes Peninsula

6.4.7.5 Ardley Island

Ardley Island is situated in Maxwell Bay and is connected to Fildes Peninsula in the west by a tombolo (~3 m wide at low tide). There are seven well-defined beach levels on the southwest of the island, extending up to 850 m from the coast (Fig. 6.15). At other sites on Fildes Peninsula the clast sizes of the beaches are similar at each level, when studied in a transect perpendicular to the shoreline, suggesting a similar wave environment existed as each raised beach formed. However, in the west of Ardley Island, the PDB is composed of much larger (gravel-pebble size), poorly sorted, and more angular clasts than the higher beaches (well-sorted, rounded cobbles). There is also evidence of erosion, and consequently analysis was confined to beaches in the east, where clast sizes were consistent between beach levels. Here the highest beach is 15.0 m above the PDB.

There are two lakes behind the highest beach; an ephemeral lagoon in the west that drains in summer, and Ardley Lake to the east. The lagoon is enclosed by the highest beach, but Ardley Lake has a rock sill 1.4 m above the highest beach and ~30 m inland.

Fig. 6.15 Raised beaches on Ardley Island

6.4.7.6 Rocky Cove

North of Ardley Island, another well-defined flight of raised beaches exists in Rocky Cove (also called Pedregosa Bay). There are five palaeo-beach levels, the highest of which is 12.7 m above the PDB (Fig. 6.16). However, this highest beach does not have the steep backslope characteristic of the other highest Holocene raised beaches in the area. Instead there is a clean contact between the Holocene beach deposits and the talus of the older bedrock and till behind. This high beach is also ~80 cm lower than the highest beaches on Fildes Peninsula, suggesting the sea level highstand associated with these beaches did not form the highest beach at Rocky Cove. It is possible that the topography of the bay prevented the formation of a beach at the time of the Holocene sea level highstand; if the sea level highstand reached the backing cliff, then beach formation would not have been possible until isostatic uplift had occurred. As it was not possible to confirm that the highest preserved beach represented the Holocene sea level highstand due to the absence of the steep backslope typical of the highest beaches elsewhere, the Rocky Cove data were not used in analysis.

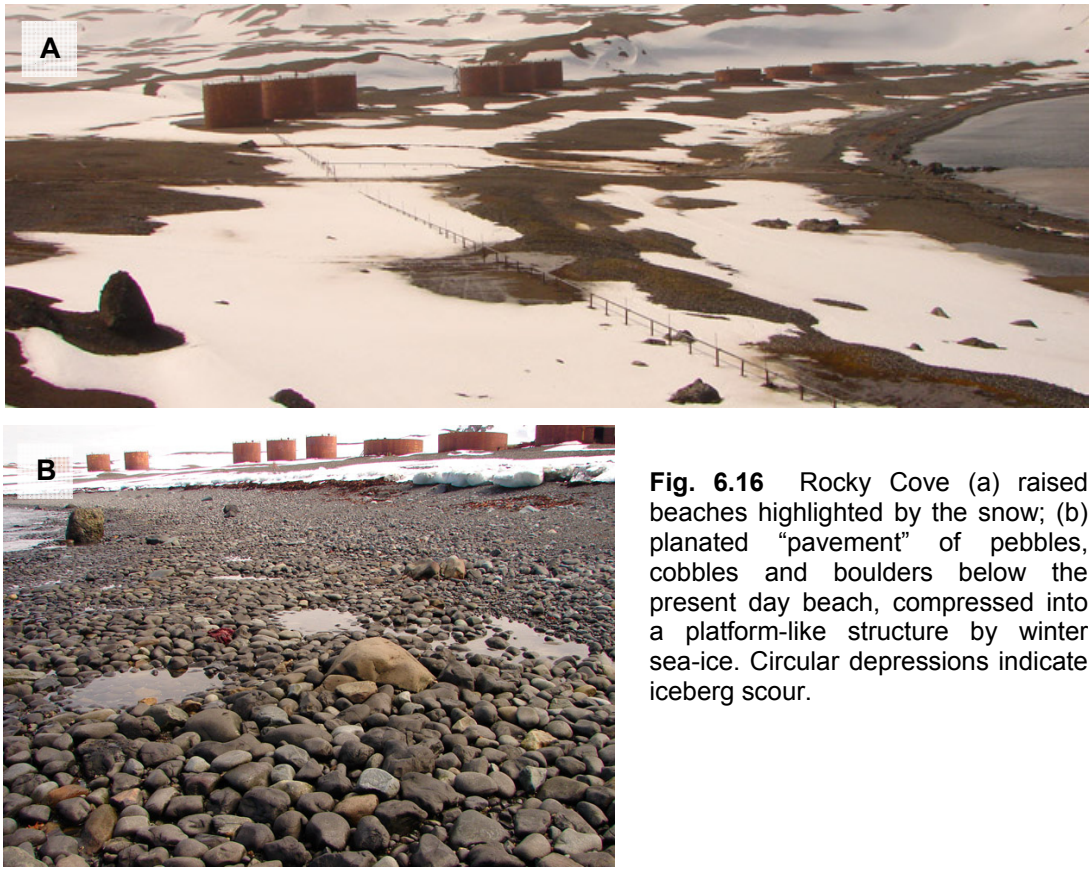

Fig. 6.16 Rocky Cove (a) raised beaches highlighted by the snow; (b) planated "pavement" of pebbles, cobbles and boulders below the present day beach, compressed into a platform-like structure by winter sea-ice. Circular depressions indicate iceberg scour.

6.4.7.7 Artigas

Artigas is the most northerly site of raised beaches on Fildes Peninsula, around 1.5 km northeast of Rocky Cove. The beaches extend 850 m inland and occupy a small embayment from the rocky promontory of Jasper Point in the southwest to Collins Ice Cap in the northeast (Fig. 6.17a). There are six palaeo-beach levels, the highest at 13.8 m above the PDB. Notably all the beaches, with the exception of the highest beach, extend up to and under the ice cap (as also noted by John and Sugden (1971), Fig. 6.17b), suggesting reduced ice cover at the time of beach formation. Aerial photographs from 1957 (FIDASE) show the ice margin was 300-500 m southwest of its present position, and has since retreated. As the beaches are well-defined, this suggests the shorelines can survive relatively unmodified under permanent ice cover, suggesting cold-based ice.

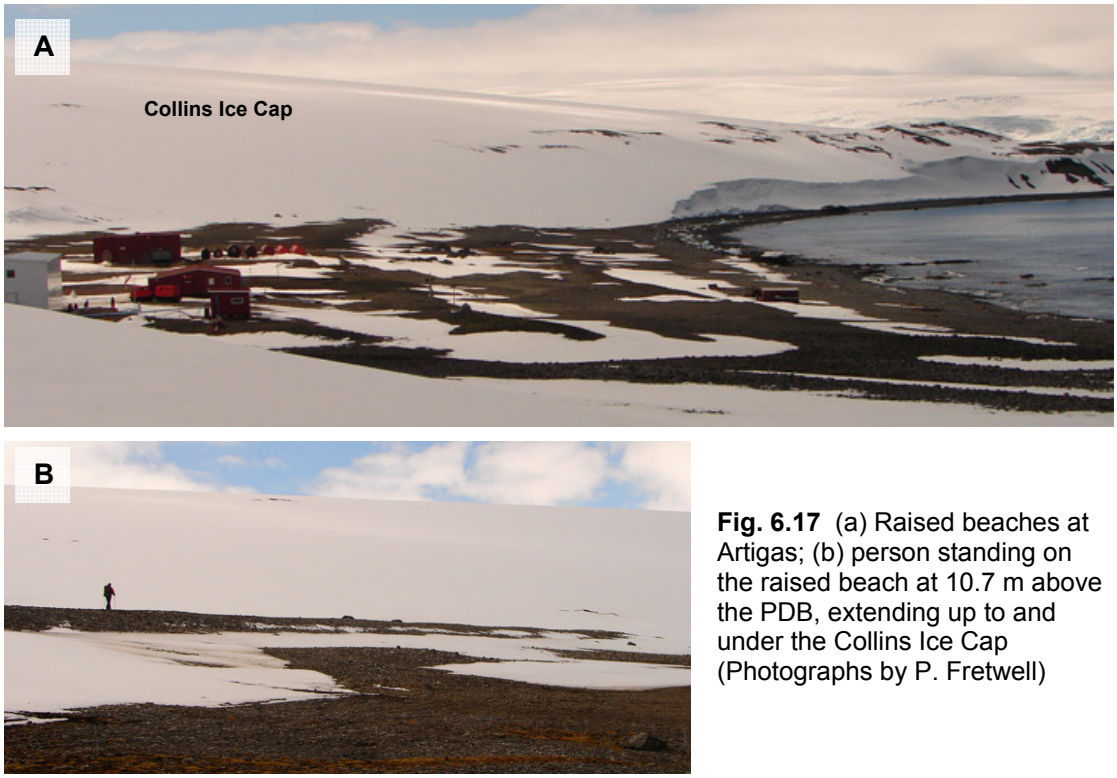

Fig. 6.17 (a) Raised beaches at Artigas; (b) person standing on the raised beach at 10.7 m above the PDB, extending up to and under the Collins Ice Cap (Photographs by P. Fretwell)

The Uruguayan research station of Artigas is built on the higher beach levels, with some deformation in the area immediately surrounding the base. However, the highest level is of consistent height with no evidence of human modification. The beaches are composed of well-rounded clasts and have a "fresher" appearance compared to the southern beaches of Fildes Peninsula. This is also a feature of the Rocky Cove beaches, and suggests the beaches formed in higher energy wave environments. This is likely given their location on the north of the Peninsula where the fetch is greater than in the south.

6.4.7.8 Western Fildes Peninsula

In contrast to the eastern side of the peninsula, few palaeo-shorelines exist on the west coast facing Drake Passage. Well-defined present day beaches are observed in four bays, but a low palaeo-beach exists in only two of these bays (Fuschloger and Bothy Bays), 4 m above the PDB (Fig. 6.18). No higher levels are preserved. Similarly, at Tartar Point on the northern coast of King George Island there are no raised beaches preserved higher than 5 m above the PDB.

Reasons for the lack of raised beaches on the west coast of Fildes Peninsula remain speculative. Firstly, the wave energy during the mid- to late-Holocene may have been more erosional than depositional, meaning beaches were not deposited. This is supported by the presence of an extensive submarine wave-cut platform, which extends 40-60 km from the coast (John and Sugden, 1971) and is suggestive of high wave energy. Secondly, it is possible that deglaciation of the western side of the Peninsula occurred much later than in the east, with ice cover preventing beach formation. However, this would seem unlikely as raised beaches are well preserved at Artigas, directly in front of the present day ice margin.

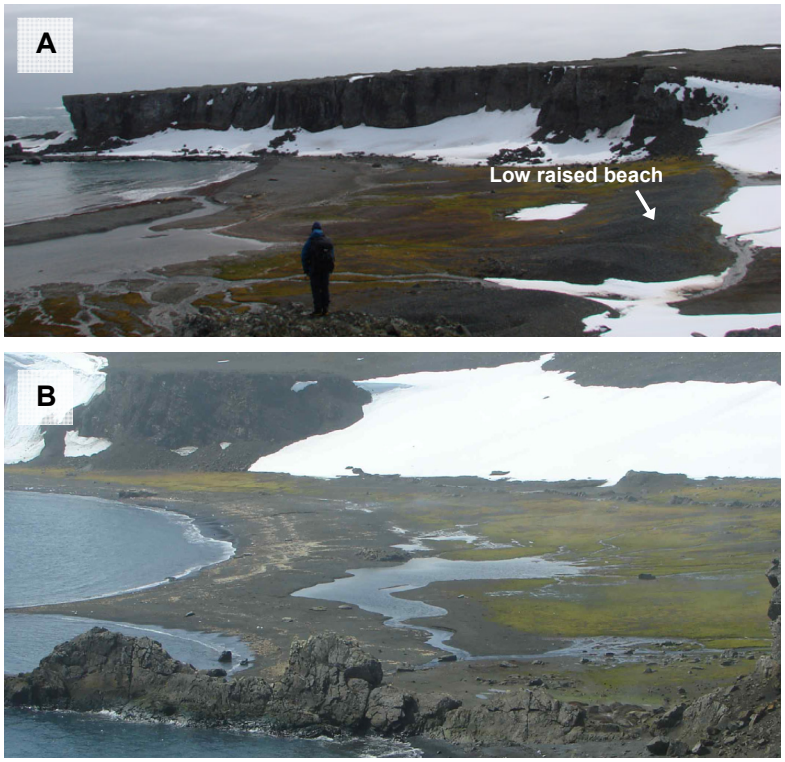

Fig. 6.18 Beaches on the western coast of Fildes Peninsula (a) Fuschloger Bay with a single palaeo-beach 4 m above the PDB (the person is standing on a cliff in the foreground, not down on the beach level); (b) Elephant Bay with no raised beaches. The saltwater lagoon behind the present day beach is characteristic of the western coast. There are several lakes on the eastern peninsula at the elevation of the highest raised beach or just above, but correspondingly there are no lakes at a similar height on the western peninsula. The lagoons of the west coast may be analogues for the older Holocene lakes in the east. (Photograph B by P. Fretwell)

6.4.8 Stranger Point, King George Island

Stranger Point, on the south side of Potter Peninsula, has a prominent set of raised beaches. There are a few well-defined beach levels including the present day beach,

and a beach at ~4 m above the PDB. However, the most striking, and highest, raised beach level exists as a series of low mounds rather than continuous beach crests, 12.2 m above the PDB (Fig. 6.19a). These mounds are approximately circular, 20-25 m in diameter with a 2.5-3 m height difference between crest and trough. They consist of very well-sorted and well-rounded gravel and pebble-sized clasts, suggesting they were originally from a well-sorted marine beach. By analogy to similar features found closer to present-day sea level (Fig. 6.19b), these mounds are interpreted as former shorelines modified by penguins into their present shape. A large colony of Gentoo penguins breeds on the PDB and observation of breeding pairs confirmed that the penguins construct shallow rock nests around their eggs from nearby beach material, and in doing so deform the beach crest. The penguins prefer to nest on the beach closest to the present sea level, but as glacio-isostatic land uplift has occurred and this beach has been superseded by a new beach closer to the shore, the penguins have left the older beach for the newer and more favourable nesting place (Tatur *et al.*, 1997). Therefore higher beaches have become redundant penguin rookeries and a checkerboard of mounds and depressions has formed, creating an ornithogenic landscape (Tatur, 2002).

Stranger Point forms a crucial site in the trend surface analysis as it is the most easterly site on the SSIs that was surveyed. However, as a consequence of the observed modification of raised beaches, two isobase models were developed, one including and one excluding the Stranger Point data.

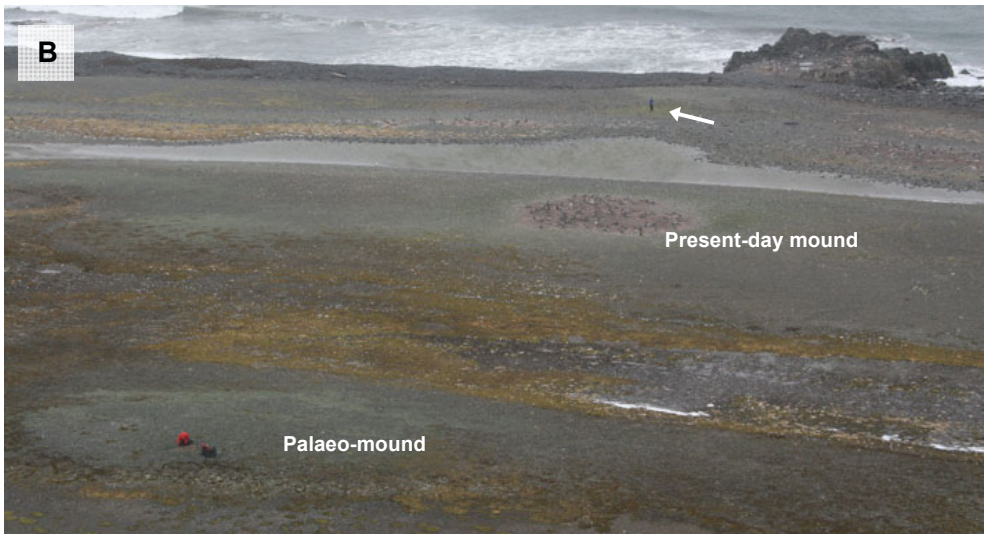

Fig. 6.19 Raised beaches at Stranger Point. (a) Circular mounds on the highest raised beach, interpreted as former penguin colonies; (b) a present-day mound with penguins, and a palaeo-mound (rucksacks for scale). The presently inhabited nest forms a dark 'dotted' circle surrounded by white bands of dry guano and phosphatic clay, whereas the abandoned colonies form entirely white circles. The person (arrowed) is standing on the prominent beach 4 m above the PDB (Photographs by M. Bentley)

6.4.9 Keller Peninsula, Admiralty Bay, King George Island

Keller Peninsula stretches 3.5 km southwards from King George Island into Admiralty Bay. On the west side of Keller Peninsula there are raised beaches preserved up to ~8 m above the PDB. A prominent beach at ~4 m above the PDB extends along most of the west side of the peninsula, grading into a small lateral/frontal moraine to the north. In places there is also a higher ridge (6-8 m above PDB) above this. A second inner moraine ridge extends into, and has deformed the contemporary beach. On the south of the peninsula, there are beaches up to 12-14 m above the PDB, occurring as a series of linked fragments, and best-preserved in the back of small embayments. However, these highest beaches, although displaying rounded clasts typical of beach material, are generally poorly defined and do not have the steep backslope typical of the highest transgressive shorelines across the rest of the island chain. For this reason this higher beach was not deemed suitable for use in analysis and not surveyed in detail.

In addition, in some places the raised beaches are inter-fingered with rockfall or talus deposits. This complicated the mapping of beaches as false marine limits could be created where apparently fresh beaches are deposited over 'old' talus, or talus buries

young beaches. This also means there are likely to be buried higher beaches and thus a higher marine limit than observed. This, and problems with equipment at this site, led to exclusion of data from this area.

6.5 Chronology of raised beaches

Two isolation basins on Fildes Peninsula, King George Island, were formed contemporaneously with the highest raised beach. Dates on the isolation contacts in these lakes therefore accurately constrain the minimum age of the highest raised beach. As presented in the previous chapter, the first isolation of Long Lake occurred at 6445 ± 40 ^{14}C yr BP (7360 cal yr BP). Mäusbacher *et al*. (1989) dated the isolation of Lake Kitezh at 6180 ± 150 ^{14}C yr BP (7000 cal yr BP).

In addition, the date of isolation of Yanou Lake can be used as a limiting age to constrain the formation of the highest raised beach, even though data from the raised beaches at Yanou were excluded from the trend surface analysis due to uncertainty over the height of the highest raised beach relative to the Holocene sea level highstand. The first isolation of Yanou Lake occurred ca. 6250 ^{14}C yr BP (7100 cal yr BP).

Therefore, together these dates on isolation contacts constrain the formation of the highest raised beaches on Fildes Peninsula to between 6485 and 6030 ^{14}C yr BP. This is slightly older than ages previously reported for the highest raised beach at Hydrographers Cove by Barsch and Mäusbacher (1986a). Penguin bones from this beach yielded uncorrected radiocarbon ages of 6650 ± 90 and 6560 ± 55 ^{14}C yr BP. Using the marine reservoir correction for penguin bones of 1130 ± 134 yrs (Berkman and Forman, 1996), this places the formation of the beach between 5520 ± 160 and 5430 ± 140 ^{14}C yr BP (ca. 6300 cal yr BP). However, the dates presented here are consistent with the age of ca. 7300 cal yr BP for the highest raised beaches of Fildes Peninsula reported by Hall (2007), calculated by extrapolation of unpublished dates from lower beaches (Brenda Hall, pers. comm.).

6.6 Isostatic uplift analysis and spatial variations in the response to glacial unloading across the SSIs

A polynomial trend surface based upon the altitudes of the highest Holocene shoreline fits the data closely (Fig. 6.20a). The surface is orientated with the major axis running southwest to northeast, following the axis of the archipelago. The correlation coefficient of the polynomial trend surface is 0.82, and the maximum residual for the surface is 2.88 m at Harmony Point (Fig. 6.21), with other residuals generally < 1 m. The main centre of uplift is situated over Greenwich Island and eastern Livingston Island, centred on the north of MacFarlane Strait. Maximum uplift since the formation of the highest Holocene raised beach is 20.37 m.

The lack of data from the east and north of King George Island means isobases are less accurate in this area. In order to improve the isostatic uplift model, a second polynomial trend surface was calculated including the data from Stranger Point (Fig. 6.20b), which was originally excluded due to disturbance of the beaches by penguins, but is located in this poorly-constrained area.

The altitude of the highest raised beach at Stranger Point was derived from the midpoint between the highest point of adjacent mounds and the level of the intervening beach crest. With Stranger Point included, the correlation coefficient of the polynomial trend surface (0.80) and the maximum residual (2.8 m, also at Harmony Point) are both lower. The orientation of the trend surface remains similar, although is broader in a north-south direction and the centre of uplift shifts slightly further northeast over English Strait, between Robert and Greenwich Islands. Maximum uplift since the formation of the highest Holocene raised beach is reduced to 18.67 m with the inclusion of Stranger Point data.

Although the correlation coefficient of the second trend surface is reduced very slightly (only by 0.02), the improved spatial distribution of data by including Stranger Point means the second isobase model (Fig. 6.20b) is chosen as the most realistic model of isostatic uplift. Significantly, the two models do not differ in the Fildes Peninsula area, where the isolation basin data used to construct the RSL curve comes from.

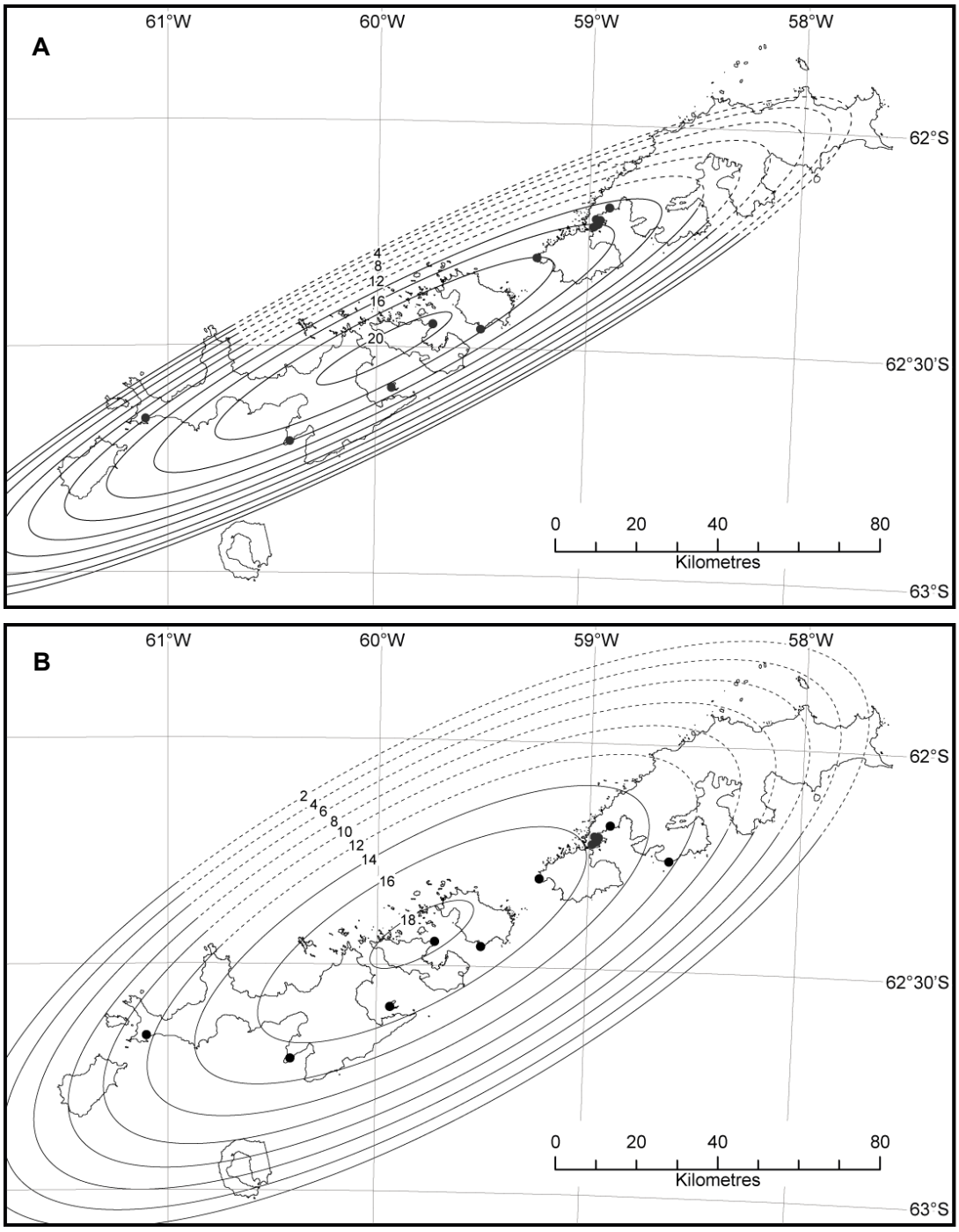

Fig. 6.20 Isobases of isostatic uplift computed by second-order polynomial trend surface analysis of the highest Holocene raised beaches on the South Shetland Islands, (a) excluding Stranger Point; (b) including Stranger Point. The numbers represent the amount of isostatic uplift (in metres) since the formation of the highest raised beach. The uplift model has been cropped to a minimum uplift isobase of 2 m, as an uplift pattern lower than 2 m is unrepresentative due to the tendency of polynomial models to trend to infinity (Fretwell *et al.*, 2004).

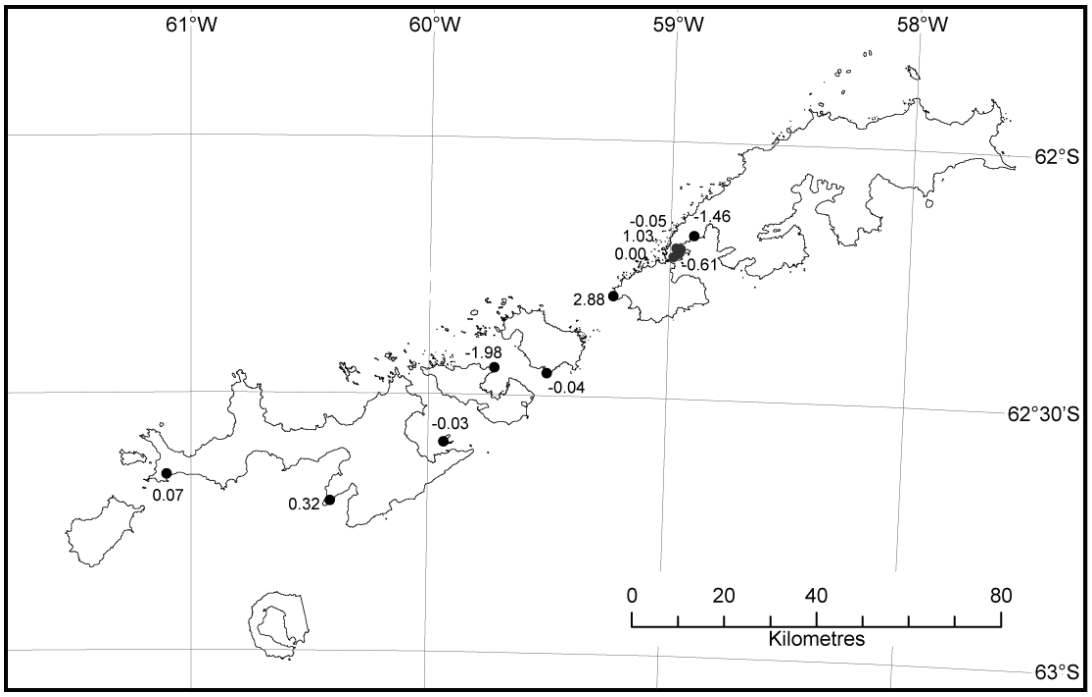

Fig. 6.21 Residuals of the trend surface fit to the measured beach heights at each site (in metres), excluding Stranger Point data

As with all polynomial models, the accuracy of the reconstructed isobases depends upon the number of data points, their spread, and the accuracy of the data. The relatively small number of data points used in the SSI model means the correlation coefficients are low in comparison to those from polynomial models of isostatic uplift elsewhere with better spatial distribution of data, for example in Scotland where correlation coefficients of 0.92-0.96 are reported (Smith *et al.*, 2000). Even including Stranger Point, the lack of GPS data in this study from the east of King George Island results in a poor fit between previously published field measurements and modelled reconstructions of the altitude of the highest raised beaches in this area. For example, beach crests from Turret Point, southeast King George Island, have been measured at ca. 11.7 m amsl by John and Sugden (1971), but the isobase model predicts 7 m of isostatic uplift for this site. Isobases in eastern King George Island are therefore considered conjectural and have been dashed in Fig. 6.20 to reflect this. Additional data collection from this area and from other peripheral areas of the island chain would be useful in refining the isobase models.

However, despite these limitations and the sensitivity of the isobase model to isolated data points, the cluster of data from the centre of the island chain makes the model more robust here, and enables three main conclusions can be drawn. Firstly, isostatic uplift across the SSIs is spatially variable. Secondly, a maximum of 18.7 m of uplift has occurred since the formation of the highest Holocene raised beach. Thirdly, isostatic uplift is centred near Greenwich Island, north of the main east-west axis of the archipelago, suggesting that most ice has been removed from the centre of the SSI archipelago. This is consistent with previous reconstructions of maximum ice extent on the SSIs from John and Sugden (1971; Fig. 6.22), originally interpreted as pre-dating the LGM, but subsequently revised to be the LGM ice extent (section 2.2). This therefore suggests that the uplift history of the SSIs is dominated by the SSIs ice cap and was not significantly affected by Antarctic Peninsula ice (un)loading, although the spatial distribution of data points is such that the shape of the isobases would be the same even if there was an influence from the Antarctic Peninsula.

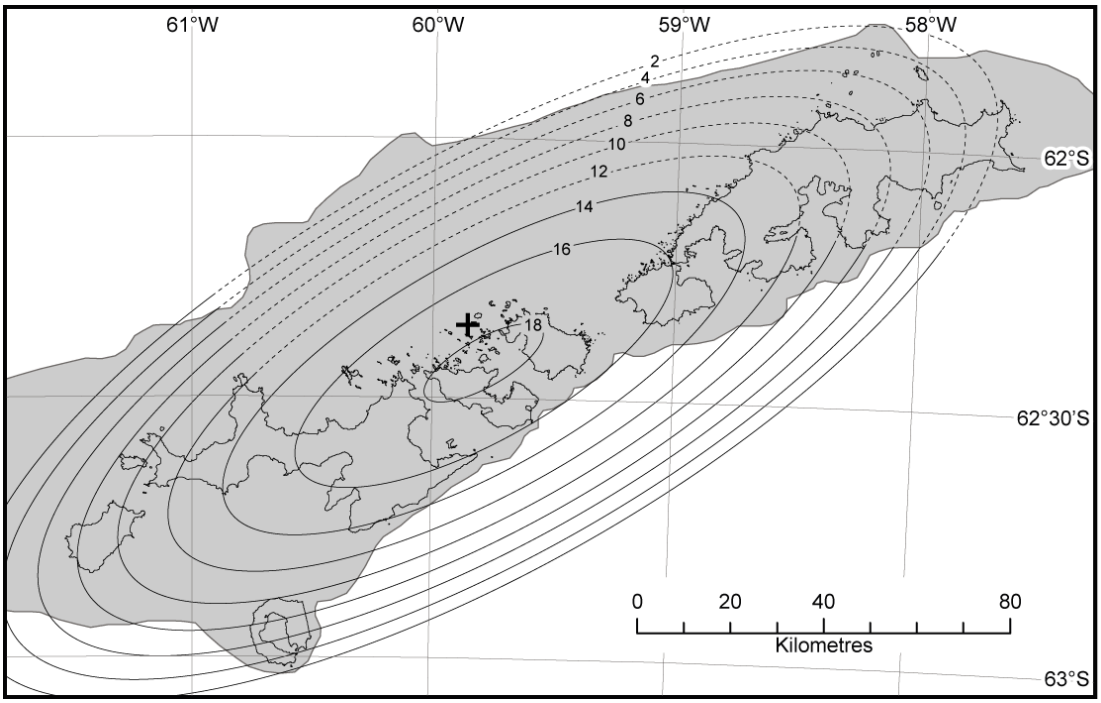

Fig. 6.22 Ice extent at the Last Glacial Maximum (shaded grey) from John and Sugden (1971), compared with new isobases (dotted lines). The "mean centre of gravity" of the reconstructed LGM ice sheet of John and Sugden is marked by the black cross, and closely coincides with the centre of uplift in the isobase model of this study (Source: Peter Fretwell).

6.7 Further chronological control on RSL from late Holocene raised beaches and morphological evidence

The above isobase models constrain the spatial variability of glacio-isostatic uplift since the formation of the highest Holocene raised beach and Holocene RSL highstand. The isobase plots show how the RSL curve presented in the previous chapter, which was developed from isolation basins on Fildes Peninsula, relates to the rest of the SSIs. However, as well as providing this spatial control, the raised beaches can also be used to further constrain this RSL curve. Whilst the age of the highest Holocene raised beach was constrained by dates on isolation basin contacts, there are previously published dates on the lower Holocene beaches available in the literature, which can help to refine the period of late Holocene RSL change. In addition, two sedimentary sections were sampled during fieldwork to help provide further constraints.

6.7.1 Potter Cove, King George Island

Organic deposits from a section on the south shore of Potter Cove (62°14'S 58°48'W) were sampled to help constrain the timing of glacier advances and RSL change. Till forming part of a small moraine (~1.5 m thick) overlies marine deposits consisting of well-sorted sand with a continuous 1-2 cm thick layer of seaweed debris, surveyed at 5.1 m amsl (Fig. 6.23). Beneath this is a massive silty sand containing shell fragments (~1.2 m thick). Observations of the contemporary beaches ~ 1-2 km along the coast from Potter Cove provide a modern analogue for the depositional environment recorded in the section. In the modern beaches there are accumulations of seaweed that are being actively deposited into swales and elongate back-beach lagoons behind beach bars. Such seaweed was being washed over the main beach ridge into a swale on a windy day during fieldwork, with 2-3 m high waves overtopping the main seaward ridge. This depositional environment was within an estimated 1-2 m of mean sea level. Interestingly the seaweed accumulating had the same morphology - flat 3-5 mm wide strands dark brown-green - as the material in the section. The Potter Cove seaweed probably accumulated in a beach swale environment and thus provides a constraint of sea level being below this point (perhaps by only 1-2 m) at the time of deposition.

Two samples of seaweed and two shell fragments were radiocarbon dated from this section (Fig. 6.23). All four samples yield ages ~7850 ^{14}C yr BP, within the 1-sigma

error range (Table 6.3). Initially this appears a robust result, however there are complications regarding the exact marine reservoir correction to apply. If all dates are corrected with the same marine reservoir correction of 1064 ± 10 yrs as applied to marine sediments and shells from isolation basins, then the ages become ca. 6790 ^{14}C yr BP. As RSL must have been below 5.1 m amsl at the time of deposition, an age of 6790 ^{14}C yrs conflicts with results from isolation basins in the previous chapter. The isolation of Long Lake (15 m amsl) occurred at 6445 ± 40 ^{14}C yr BP, with the isolation of Yanou Lake (14.5 m amsl) around 6250 ^{14}C yr BP. This means if the Potter Cove ages are truly 6790 ^{14}C yr BP, then RSL must have risen over 10 m (from 5.1 m above present to over 15 m amsl) in around 350 years, which would be an extremely rapid and unrealistic rate of RSL rise. The maximum sea level rise associated with the 8.2 ka climate cooling event has been quoted as only 4 m (Kendall *et al.*, 2008; Hijma and Cohen, 2010), which would leave 6 m to be accounted for by land subsidence, equating to an unrealistic rate of ~17 mm/yr. This therefore suggests that the either the full marine reservoir correction should not be applied, or the elevation of the sample is incorrect.

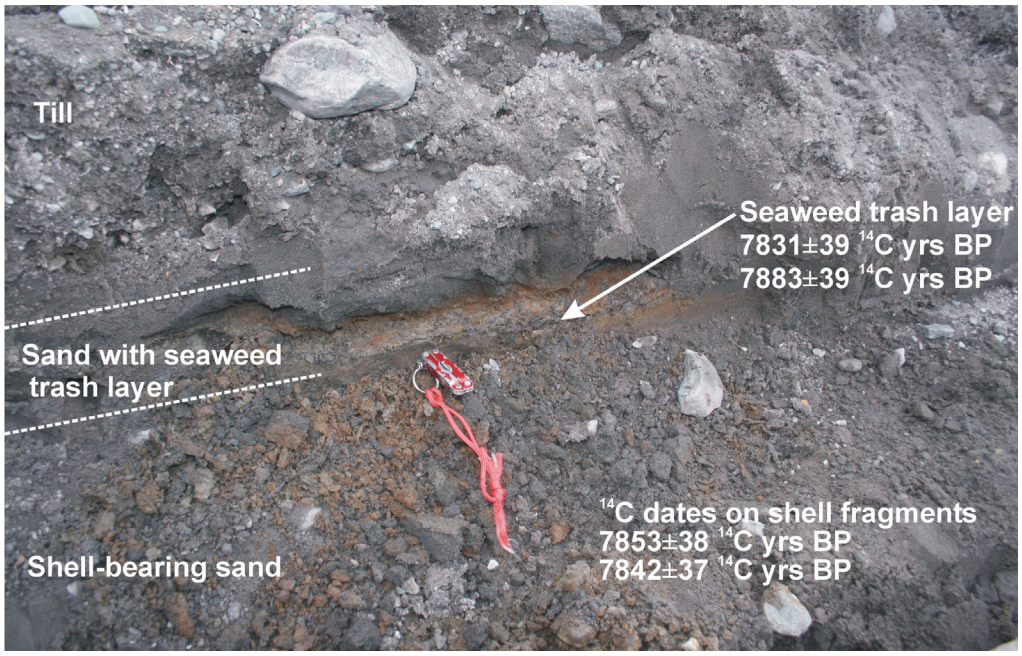

Fig. 6.23 Potter Cove section, showing the positions of the seaweed and shells sampled for radiocarbon dating. The seaweed trash layer is at 5.1 m amsl. The dates presented are conventional radiocarbon ages with 1-sigma errors, uncorrected for the marine reservoir effect (Photograph by M. Bentley)

Sample	Lab code	Conventional ^{14}C age (yr BP ± 1σ)	$\delta^{13}C_{VPDB}$ ± 0.1‰	Calibrated age (cal yr BP) 1-sigma age range	Median
Seaweed - 1	SUERC-14413	7831 ± 39	-25.3	8480-8494 (10%) 8516-8598 (90%)	8550
Seaweed - 2	SUERC-14414	7883 ± 39	-25.6	8546-8643	8610
Shell - 1	SUERC-14416	7853 ± 38	1.4	8540-8629	8570
Shell - 2	SUERC-14417	7842 ± 37	0.2	8482-8492 (5%) 8518-8532 (8%) 8536-8605 (86%)	8560

Table 6.3 Radiocarbon dates from Potter Cove. ^{14}C ages have been normalized to $\delta^{13}C_{PDB}$‰ -25 using the $\delta^{13}C$ values shown. Dates were calibrated using Calib (version 5.0.1, Stuiver and Reimer, 1993) using the SHCal04 calibration curve (McCormac *et al.*, 2004). Where more than one calibrated range is given, the relative percentage area under the probability distribution is indicated in brackets. A marine reservoir correction has not been applied (see text for full explanation).

Support for not applying the full reservoir correction comes from paired dates from isolation basin sediment cores. There is a 430 year offset between dates on a shell fragment and bulk marine sediment from the same stratigraphic depth at Long Lake. This suggests these particular shells do not require the full reservoir correction needed for marine sediments, and therefore nearshore organisms living in the intertidal zone, where the water column is well-mixed (so incorporating atmospheric rather than deep water carbon), may not require the full 1064 yr marine reservoir correction.

The literature is also inconclusive as to the appropriate reservoir correction that should be applied to seaweed, mainly due to most modern samples post-dating the 1957-62 nuclear testing and therefore being contaminated by 'bomb ^{14}C'. 'Modern' seaweed samples from the South Shetland Islands reported by Gordon and Harkness (1992) yielded ages ranging from 225 ± 50 to 900 ± 55 ^{14}C yr BP, with seaweed collected from South Georgia and the Antarctic Peninsula giving ages ranging from modern to 835 ± 45 ^{14}C yr BP. As it is uncertain to what extent these samples have been affected by the incorporation of 'bomb ^{14}C', it is not possible to determine the reservoir effect. Gordon and Harkness (1992) tentatively suggested, on the basis of one seaweed sample paired with a date on a tree trunk incorporated into the same beach, that seaweed requires a reservoir correction of ca. 700 years. However, this should be viewed with caution on the basis of a single dating pair.

With regards to the shell dates, shallow marine fossils elsewhere have given dates as young as 687 ± 40 and 850 ± 50 ^{14}C yr BP (Harkness, 1979; Stuiver and Braziunas, 1985). Interestingly, the fraction of the shell that is dated also appears to be critical. The inner and outer fractions of modern bivalve shells collected from Potter Cove reported in Sugden and John (1973) and Shotton *et al*. (1968) yielded ages of 850 ± 145 and 586 ± 113 ^{14}C yr BP respectively (Birm-47a and 47b). Additionally, there is disparity between the shell ages obtained in this study and those previously reported from the same section by Sugden and John (1973). They dated a seaweed sample from the same stratigraphic layer of the section to 7683 ± 230 ^{14}C yr BP, but a sample of shell fragments yielded an age of 9670 ± 230 ^{14}C yr BP. The difference in age between this latter date and the dates on shell fragments from this study may reflect the position of the shell sample collected by Sugden and John, lower down in the silty sand unit.

This discussion demonstrates the problems with interpreting the dates obtained from Potter Cove. It would be surprising if seaweed did not require any marine reservoir correction, given it is found to grow down to water depths of 30 m in Potter Cove (Gómez *et al.*, 1997; Wiencke *et al.*, 2007), and even more surprising if the shells did not require reservoir correcting. The best approach is therefore to report a range of possible dates depending on the reservoir correction applied. The shells are likely to require a reservoir correction of between 1064 yrs and 634 yrs (1064 minus the 430 yr offset from Long Lake), placing the corrected ages between ca. 6780 and 7210 ^{14}C yr BP. Correcting the seaweed dates by the Gordon and Harkness (1992) correction of 700 years gives an average age of 7160 ^{14}C yr BP. As the layer of seaweed overlies the shell-bearing sand unit, the seaweed dates should be younger than those of the shells. Consequently, the shells can be assumed to date to the older end of the proposed age range, around 7210 ^{14}C yr BP.

On this basis, these radiocarbon dates from Potter Cove suggest that at ca. 7200 ^{14}C yr BP RSL was < 5.1 m amsl (Fig. 6.27) and the section also illustrates that a glacier advance occurred at some time after 7200 ^{14}C yr BP. However, this interpretation contradicts evidence from isolation basins. Yanou Lake (14.5 m amsl) was fully marine from ca. 10000 to 6200 ^{14}C yr BP, and Long Lake (15 m amsl) was fully marine from ca. 8000 to 6445 ^{14}C yr BP, which means RSL cannot have been < 5.1 m amsl at 7200 ^{14}C yr BP. Given the consistency of the four dates from Potter Cove (even allowing for

differences in the marine reservoir correction, they are clearly within this period of marine sedimentation in isolation basins), an alternative explanation is the interpretation of the indicative meaning of the seaweed may be wrong. The indicative meaning of the seaweed layer was originally assumed to be 1-2 m amsl on the basis of comparison to contemporary beaches. However, if the indicative meaning is instead taken to be the growth position of the seaweed rather than a depositional position on the beach, then the Potter Cove dates and isolation basin data become reconcilable. As noted above, seaweed grows to water depths of 30 m in Potter Cove (Gómez *et al.*, 1997; Wiencke *et al.*, 2007), and it is possible that an advance of a marine-terminating glacier "bulldozed" over the seaweed in its growth position, leaving a compacted seaweed layer overlain by till (Fig. 6.23). After subsequent ice retreat and RSL change the site was exposed at its current elevation. This would place an elevation error on the Potter Cove dates of up to 30 m, which unfortunately means they cannot be used as a constraint on the RSL curve.

6.7.2 Spark Point, Greenwich Island

The section is located under the seaward-terminating margin of an unnamed glacier in the bay immediately west of the Spark Point beaches. Here the glacier terminates on a broad wave-cut platform, extending several hundred metres, and which exposes a possible moraine at low tide ~200-400 m in front of the margin (Fig. 6.24).

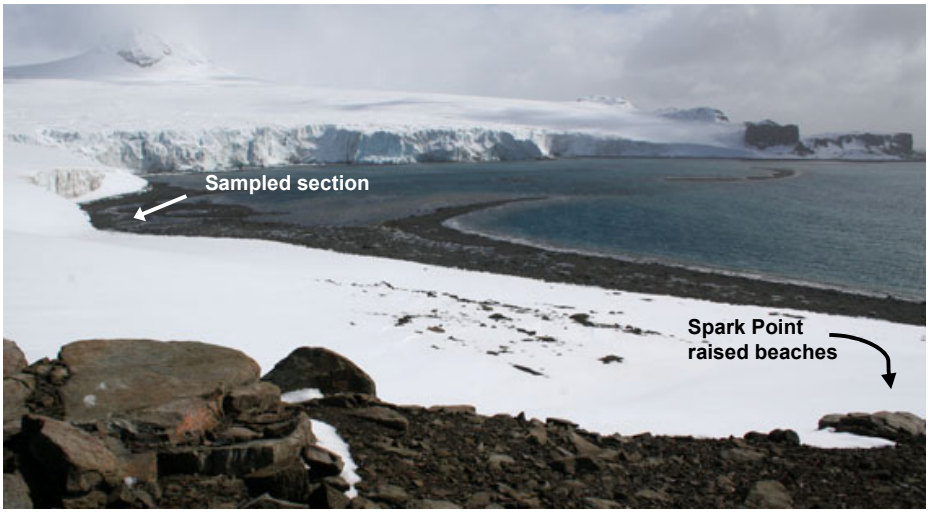

Fig. 6.24 Location of the Spark Point section (indicated by the white arrow), also showing the wave-cut platform in front of the glacier margin and possible sinuous moraine (Photograph by M. Bentley)

High tide reaches the lower part of the calving front. The glacier overlies a diamict, at least 50-80 cm thick and extending discontinuously across the glacier front (Fig. 6.25a). The diamict is sandy, matrix-supported, and massive in its lower part (40-50 cm) with occasional stringers of silty material showing intense deformation. In places the lower massive diamict is overlain by an upper fissile diamict (10-30 cm) with abundant partings parallel to the glacier sole. The upper diamict is directly overlain by glacier ice. Below the diamict is the pebbly sand that constitutes the local cover of the wave-cut platform. At the time of the field visit, this was covered with an extensive layer of brash ice blocks.

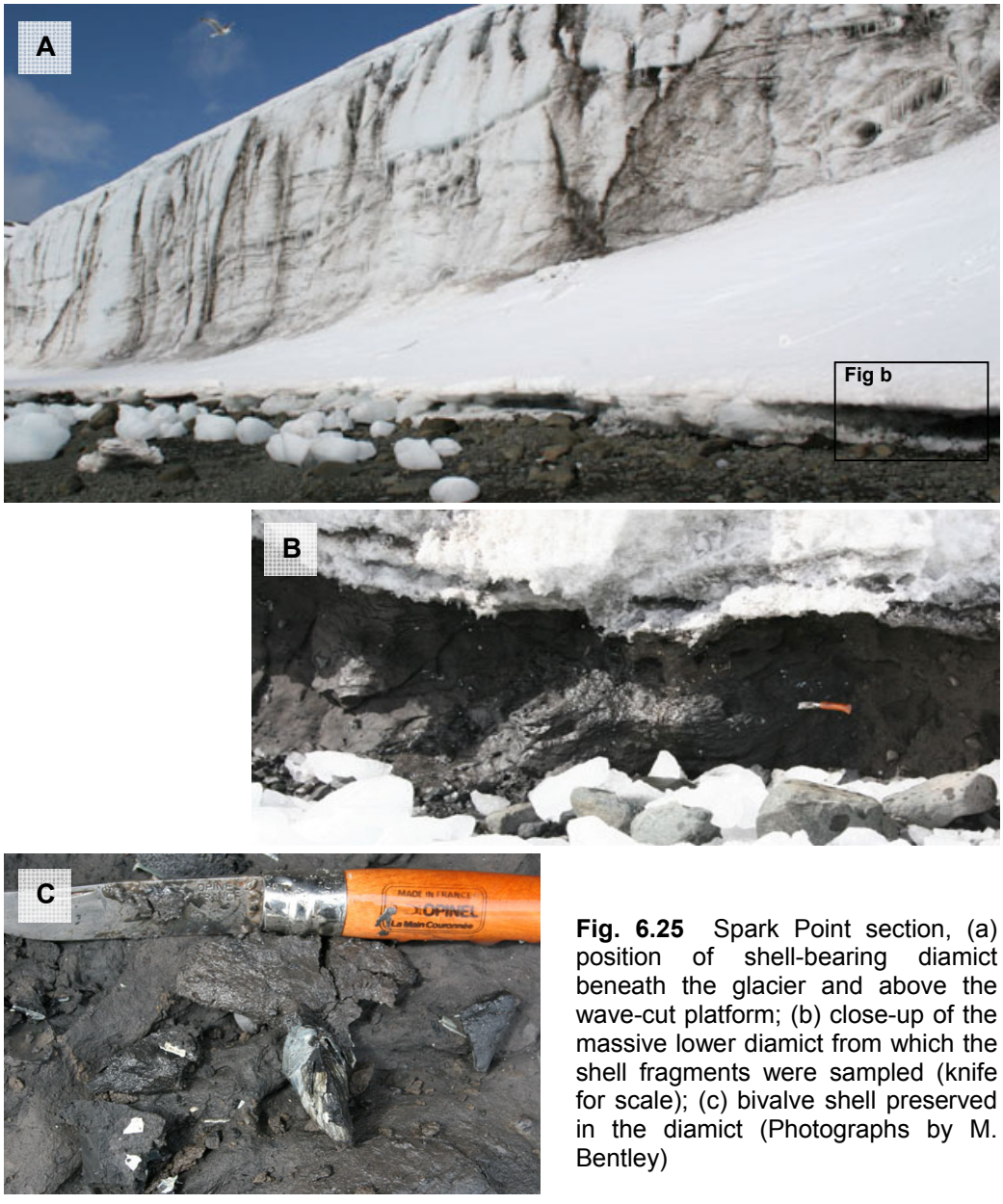

Fig. 6.25 Spark Point section, (a) position of shell-bearing diamict beneath the glacier and above the wave-cut platform; (b) close-up of the massive lower diamict from which the shell fragments were sampled (knife for scale); (c) bivalve shell preserved in the diamict (Photographs by M. Bentley)

The lower diamict contains abundant shell material (Fig. 6.25). These are mostly articulated valve pairs of a bivalve, probably *Laternula elliptica*, along with valves and fragments from a smaller species that resembles *Mya truncata*. The *Laternula* valves reach 8 cm in length, whilst the smaller species is 2-3 cm in length. Mother-of-pearl translucent lining is retained in the *Laternula* shells, along with detailed growth lines and radial structures.

The interpretation of this section is that the glacier is advancing across a former sub-tidal beach deposit (massive sand). The fissility of the diamict and deformation of silty layers show that the glacier has deformed the underlying material but the abundance of articulated shells and preservation of mother-of-pearl and delicate growth structures on shells suggests that material has not been transported far, and that the shells may even be in situ, or very close to it. This would imply that the deposit provides a minimum for a former sea level that would have occupied a position slightly above the sand. The shells yield uncorrected ^{14}C ages of 1552 ± 37 and 1557 ± 37 yr BP, which are 504 ± 38 and 506 ± 38 yr BP when corrected using the marine reservoir correction of 1064 ± 10 yr BP (Milliken *et al.*, 2009). These provide a maximum age for the timing of glacier advance and also show that RSL must have been above present at this location at ca. 500 yr BP.

6.7.3 Previously published radiocarbon dates on raised beaches

As stated in the introduction to this section, there are previously published dates on the lower Holocene raised beaches in the SSIs which can help to refine the RSL curve. These dates were used by Bentley *et al*. (2005a) to produce the preliminary RSL curve for the SSIs (Fig. 2.11). All previously published dates on SSI raised beaches are given in Table 2.1, however here only sites within the 12-18 m isobases (as inferred from trend surface analysis in Fig. 6.20b) are used. As the RSL curve from Chapter 5 has been produced from isolation basins on Fildes Peninsula (between the 14-16 m isobases), this will minimize the error that would be introduced by using sites of significantly different uplift. All samples that yield 'modern' ages have also been excluded as they will not help in constraining the shape of the RSL curve.

The dates are presented in Table 6.4 and come from whalebone, penguin bone, and wood. Penguin bones provide only minimum limiting dates for RSL as penguin

rookeries may be located tens of metres above mean sea level. Conversely, most of the whalebone samples were reported as being buried several tens of centimetres in the beaches, and as the bones are large, it seems likely that wave activity would be required to bury the bones in the beach. Therefore the bones are likely to be older than the beaches in which they are embedded and so their ages are interpreted as maximum ages. The exception to this is where bones are not embedded in the beach sediments, but instead are found on beach surfaces. In this case bones are assumed to have been deposited in either the final stages of beach formation or subsequently, and therefore afford a minimum age for the beach. The dates are plotted on the RSL curve at the end of the chapter (Fig. 6.27).

The curve combines data from both isolation basins and raised beaches, and so it was necessary to apply vertical error bars to the beach data to reflect the different indicative meanings of each type of index point. The beach dates in Table 6.4 were reported in the literature relative to mean sea level, however as the indicative meaning of raised beaches is the PDB, which forms at an average altitude in the SSIs of ~2 m amsl (calculated from GPS heights of the PDB measured in this study), vertical error bars of 2 m are plotted on the RSL curve to account for the height of the PDB relative to mean sea level. This ensures that the isolation basin and raised beach data can be compared on the same reference frame.

Site	Published altitude (m amsl)	Height above PDB (m)	Conventional age (^{14}C yr BP)	Corrected age (^{14}C yr BP)	Material dated and stratigraphic position	Laboratory code	Reference	Age constraint for beach
Wind Creek Valley, Fildes, King George Island	18	16	6650 ± 90	5520 ± 160	Penguin bone	HD9425-9100	Barsch and Mäusbacher, 1986a	Minimum
Wind Creek Valley	18	16	6560 ± 55	5430 ± 140	Penguin bone	HD9426-9106	Barsch and Mäusbacher, 1986a	Minimum
'Pingfo', Potter Peninsula, King George Island	16.3	14.3	5750 ± 40	4620 ± 140	Penguin bone	*Not given*	Del Valle *et al*., 2002	Minimum
'Pingfo', Potter Peninsula	15.4	13.4	5840 ± 40	4710 ± 140	Penguin bone	*Not given*	Del Valle *et al*., 2002	Minimum
Penguin Ridge, Thomas Point, King George Island	12	10	1610 ± 130	1610 ± 130	Moss bank at base of peat overlying the 12 m raised beach	Gd-4636	Tatur *et al*., 1997	Minimum
Rip Point, Nelson Island	6.5	4.5	802 ± 43	802 ± 43	Tree trunk (*Austrocedrus chilensis*) buried 18 cm in beach	Birm-14	Sugden and John, 1973	Maximum
South Beaches, Byers Peninsula, Livingston Island	10.3	8.3	2823 ± 40	1400 ± 200	Whalebone buried 30 cm in beach	SRR-1086	Hansom, 1979	Maximum
South Beaches	10.1	8.1	3121 ± 35	1700 ± 200	Whalebone buried 40 cm in beach	SRR-1087	Hansom, 1979	Maximum
South Beaches	9	7	3115 ± 47	1690 ± 210	Whalebone buried in beach crest	AA-45934	Hall and Perry, 2004	Maximum
South Beaches	7.6	5.6	2530 ± 85	1110 ± 220	Whalebone from rear of beach	I-7870	Curl, 1980	Maximum
South Beaches	6	4	1692 ± 42	270 ± 200	Whalebone partially buried in beach (poor condition)	AA-45931	Hall and Perry, 2004	Minimum
South Beaches	6	4	1572 ± 42	150 ± 200	Whalebone partially buried in beach surface	AA-46816	Hall and Perry, 2004	Minimum
South Beaches	5	3	1625 ± 42	200 ± 200	Whalebone buried in beach foreslope	AA-45932	Hall and Perry, 2004	Maximum
South Beaches	4	2	1715 ± 42	290 ± 200	Whalebone buried in beach foreslope	AA-45933	Hall and Perry, 2004	Maximum
South Beaches	4	2	1545 ± 46	120 ± 210	Whale vertebra buried in beach foreslope	AA-45936	Hall and Perry, 2004	Maximum

Table 6.4 Radiocarbon dates on organic material from raised beaches at selected sites across the SSIs situated between the 12-18 m isobases (as predicted by trend surface analysis, Fig. 6.20b). Instead of using the original authors' reservoir corrections, different corrections have been applied depending the type of material dated, 1130 ± 134 yr for penguin bone and 1424 ± 200 yr for whalebone (Berkman and Forman, 1996). Errors on the original date and on the ΔR value were combined in quadrature; corrected dates and errors are rounded to the nearest 10 years.

6.8 Synthesis: integrating evidence from raised beaches and isolation basins

Having described the raised beaches of the SSIs and reconstructed the spatial pattern and magnitude of Holocene isostatic uplift, these results must be integrated with the interpretations drawn from the isolation basin data that were presented in the previous chapter. This synthesis is divided into four key themes.

6.8.1 General agreement between the isobase model and isolation basin data

The performance of the isobase model against isolation basin data can only be tested at Fildes Peninsula. For this area, the isobase model predicts 14-16 m of uplift since the formation of the highest raised beach. From the isolation basin data (relative to MSL) it was concluded that RSL was between 15-18 m above present immediately after glacial retreat. Therefore, given eustatic sea level rise at this time, and assuming (i) that raised beach formation occurred contemporaneously with ice retreat, and (ii) the indicative meaning of raised beaches is the PDB height of ~ 2 m amsl, this places the Holocene RSL highstand immediately after deglaciation towards the lower end of the 15-18 m amsl proposed from the isolation basin data. For example, if MSL was 15 m above present immediately after deglaciation, then the beach at that time would have formed at 17 m above present (indicative meaning of 2 m amsl). The difference in height between this highest Holocene beach and the PDB would then be 15 m, which fits with the isobase model prediction of 14-16 m of uplift. Conversely, if MSL was 18 m above present immediately after deglaciation, the beach at that time would have formed at 20 m above present, which is 18 m higher than the PDB and exceeds the isobase-derived estimate of 14-16 m of uplift.

6.8.2 Constraining deglacial retreat and the glacial still-stand identified from isolation basins

The raised beaches at Artigas, Fildes Peninsula, are critical for expanding upon the interpretation of RSL change from isolation basin data. As described in section 6.4.7.7, all the beach levels at Artigas, with the exception of the highest raised beach, extend up to and beneath the present ice cap. This not only provides evidence for glacial readvance since the time of raised beach formation, but also the much shorter length of the highest beach and its position to the west relative to the lower levels provide key evidence for Holocene glacier fluctuations (Fig. 6.26).

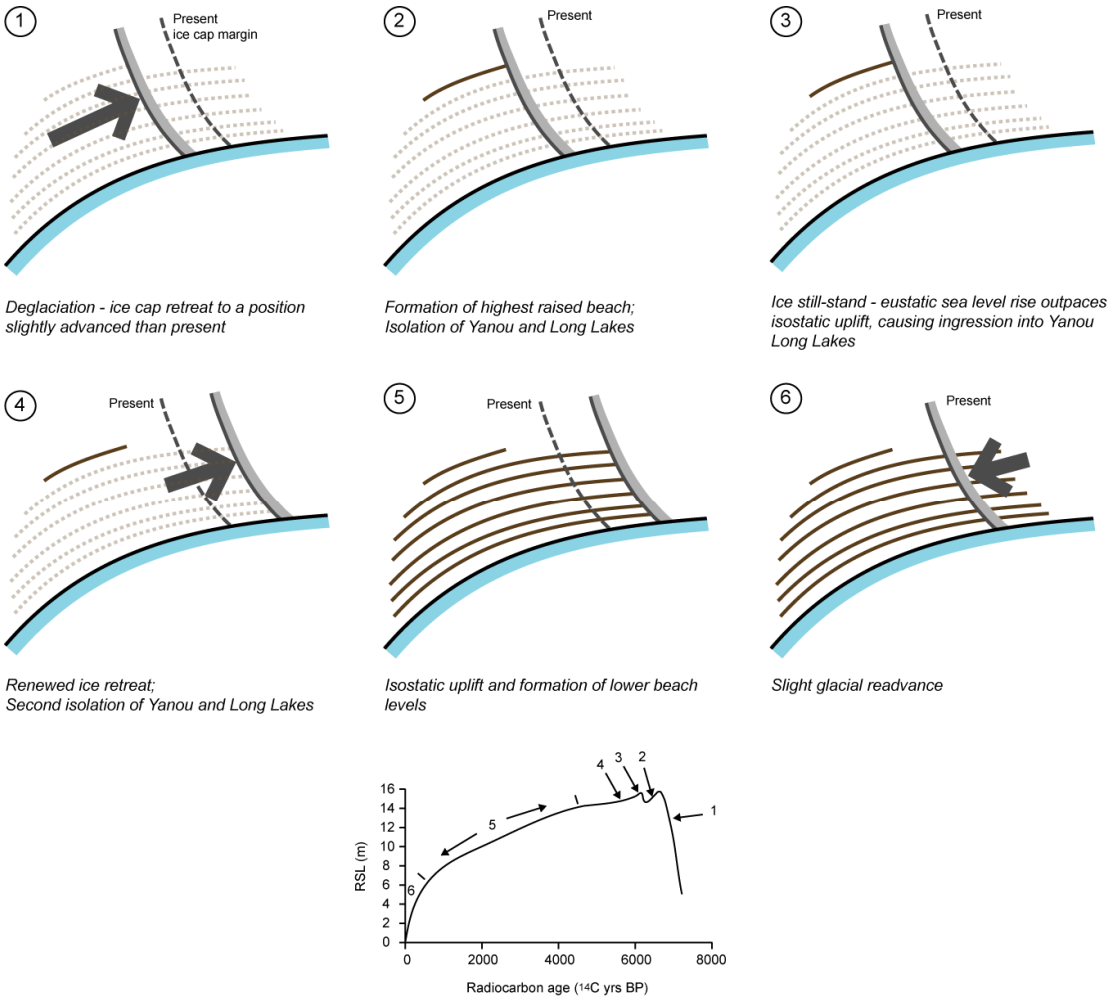

Fig. 6.26 Schematic representation of the retreat and advance of the Collins Ice Cap on Fildes Peninsula, and formation of the raised beaches at Artigas. Note the position of the coast has been drawn in the same place on each time-slice for simplicity. The approximate timing of the stages 1-6 are shown on a simplified version of the RSL curve.

Evidence for the glacial readvance proposed in the final stage of Fig. 6.26 also comes from Hall (2007). Radiocarbon dates of moss incorporated in moraines up to 500 m from the present-day margin of the Collins Ice Cap indicate the ice cap advanced after 650 cal yr BP. Further radiocarbon data indicate that this was the most extensive advance of the last 3500 years. Such a late Holocene ice readvance would explain why the raised beaches extend under the present ice margin; preservation of beaches beneath the ice cap suggests non-erosive cold-based ice. This readvance is not identified in the isolation basin record as it would have been of insufficient magnitude to cause inundation of lakes over 14 m amsl.

6.8.3 Refinement of the RSL curve

The GPS surveying of raised beaches across the SSIs revealed no discontinuities in the uplift pattern or horizontal displacement of shorelines. This is consistent with more detailed analyses of neotectonic faulting from Hurd Peninsula (Pallàs, 1993; Pallàs *et al.*, 1995). These studies mapped the neotectonic faults and raised beaches of Hurd Peninsula from aerial photographs and ground surveys and found no evidence of beaches cut by faults or vertical displacement of beaches due to tectonic movements. Consequently, the RSL curve presented in the previous chapter from isolation basin evidence (Fig. 5.10) is applicable over a wider area of the SSIs beyond Fildes Peninsula (where the isostatic response is similar).

In addition, dates reported from previous studies on late Holocene raised beaches help constrain the falling limb of the curve (Fig. 6.27). Unfortunately it has still not been possible to fully constrain the direction of RSL change prior to 7000 ^{14}C yr BP from field evidence. Models suggest RSL rose to the highstand (Bassett *et al.*, 2007, Fig. 2.12), and the geomorphology of the highest raised beaches suggests they are transgressive features. John and Sugden (1971) proposed that the highest Holocene raised beach was associated with a RSL transgression, and the characteristics they suggested as being indicative of these beaches (section 6.1) were observed during fieldwork. The steep backslope and abrupt contact between this backslope and older weathered material inland provide evidence for a RSL transgression. If the beaches had been formed in contact with the ice margin, they would be expected to be more diffuse. Therefore based on evidence from modelling and beach geomorphology, the preferred interpretation of RSL change in the early Holocene is gradual rise. Rapid RSL rise (Potter Cove scenario) is discounted for the reasons discussed in section 6.7.1.

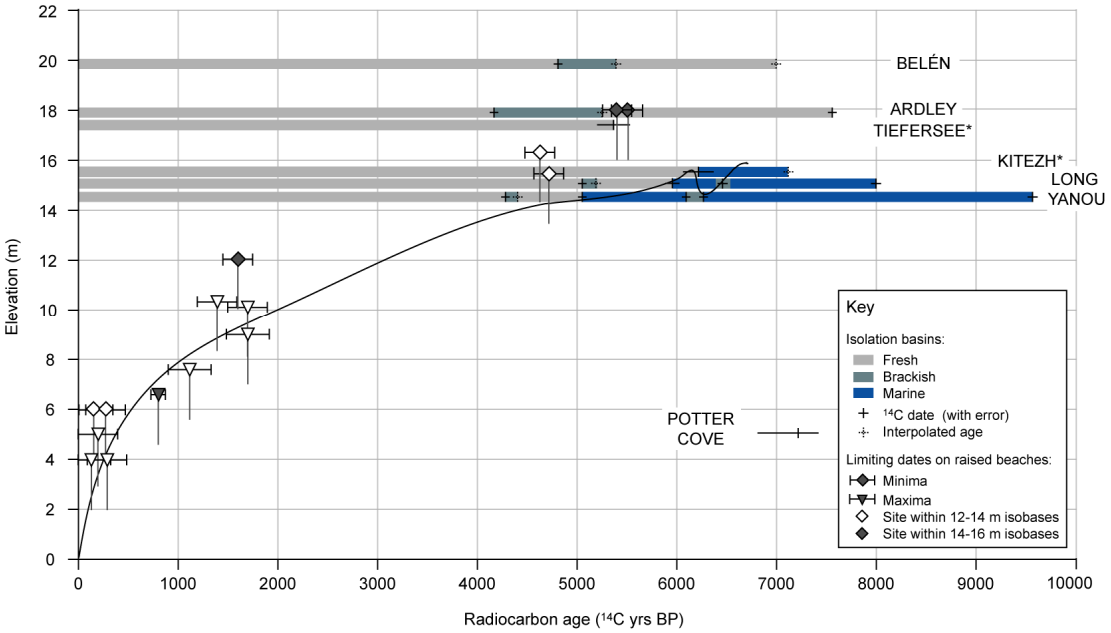

Fig. 6.27 Relative sea level curve for the South Shetland Islands, produced from raised beaches and isolation basin evidence from this study and previously published work (lakes marked by * and raised beach dates). The results from Lake Kitezh come from Mäusbacher *et al*. (1989) and Tiefersee from Schmidt *et al*. (1990). Limiting dates on raised beaches come from penguin bones and whalebones that have previously been published (Table 6.4). To account for the different indicative meanings of isolation basins and raised beaches, isolation basin sill altitudes have been corrected by subtracting 1.5 m (difference in height between mean higher high water and mean sea level for Ardley Cove); beach dates are plotted at their reported altitudes with 2 m vertical error bars to reflect the height of the present day beach (assumed indicative meaning) above mean sea level. As these are limiting dates, the RSL curve should pass beneath the samples forming minimum ages, and above those which form maxima. The line of the curve itself is an inferred curve only. Note the vertical error associated with the Potter Cove dates is not shown for simplicity, but is interpreted to be ~30 m (section 6.7.1). Early Holocene RSL change is not shown due to uncertainty, but evidence from modelling and beach geomorphology favours gradual RSL rise.

One of the main aims of this thesis was to refine and extend the preliminary RSL curve produced for the SSIs by Bentley *et al*. (2005a) from a review of previously published data (Fig. 2.11). The overall form of this new curve (Fig. 6.27) is similar, but significant advances have been made in constraining the mid-Holocene highstand. The Bentley curve predicted only a single peak in mid-Holocene RSL at ca. 4000 ^{14}C yr BP, compared to the double peak much later between 6000 and 7000 ^{14}C yr BP. Early Holocene RSL change has also been further constrained from the original curve.

The form of this new curve is consistent with the conclusions of John and Sugden (1971) from their study of raised beaches across the SSIs. The re-inundation of

isolation basins after initial isolation observed in this study concurs with evidence from John and Sugden (1971) of a rapid eustatic surge following rapid isostatic uplift in the early stages of deglaciation. They proposed that a readvance of glaciers was necessary for eustatic sea level rise to outpace isostatic uplift, and whilst this study has re-interpreted the evidence to suggest only a glacial still-stand would have been necessary, the shape of the proposed RSL curve is the same. John and Sugden (1971) proposed that the highest Holocene raised beach was associated with this RSL transgression. In addition, the curve also agrees with the more recent observations of Hall (2009), who referred to the Holocene RSL history of the SSIs as complex and involving short-lived transgressions, rather than being a simple exponential emergence curve.

Comparison to the postglacial RSL curves characteristic of the six global sea level zones of Clark *et al*. (1978) is problematic. Although the shape of the SSIs curve most closely corresponds to zone V (covering the southern oceans and characterized by postglacial sea level change that is initially controlled by eustatic submergence, and once meltwater stops flowing into the oceans, slight emergence takes over owing to hydroisostatic effects), there are significant differences between the two curves. Most notably, zone V curves are typically characterized by emergence of ~2 m. The differences are likely to reflect the influence of local factors as well as the division of the globe into just six zones, meaning fitting the curve to a broad sea level zone is inappropriate. Instead comparison with sites of similar glacial and deglacial histories is more applicable. Based on isolation basins, Zwartz *et al*. (1998) produced a RSL curve of the same shape from the Vestfold Hills, East Antarctica, with initial RSL rise to a highstand around 6200 ka BP, followed by RSL fall to present. There is also agreement with RSL interpretations from raised beaches in Lützow-Holm Bay, East Antarctica, which suggest RSL rose to a highstand in this area of ~16 m at 6000-7000 yr BP before falling monotonically to present (Yoshida and Moriwaki, 1979; Hayashi and Yoshida, 1994; Zwartz *et al*., 1997).

6.8.4 Implications of the uplift rate for assessing the tectonic contribution to RSL change

Taking the age of the highest raised beaches as ~6300 ^{14}C yr BP, then 20 m of uplift in the centre of the archipelago since this time is equivalent to an uplift rate of ca. 3

mm/yr. This rate is an order of magnitude greater than the maximum rate of tectonic uplift for the SSIs of 0.4 mm/yr proposed by Pallàs *et al*. (1997). This therefore strongly suggests that the uplift rate of 3 mm/yr represents glacio-isostatic rebound rather than tectonic uplift, and supports Pallàs *et al*.'s assertion that tectonic uplift only plays a minor role in the crustal movements of the SSIs. This will be examined in more detail in the next chapter.

6.9 Summary

This chapter has presented data on raised beaches across the SSI archipelago. Although the raised beaches of the SSIs may be indicative of small-scale events such as individual storms, the broad-scale surveys across the archipelago demonstrate that there are clearly prominent beach levels across the island chain, reflecting large-scale isostatic uplift and RSL fall. Surveyed beaches were modelled using second-order polynomial trend surface analysis to produce an isobase plot of isostatic uplift since the Holocene sea level highstand. These isobase models constrain the spatial variability of glacio-isostatic uplift across the SSIs since the formation of the highest Holocene raised beach, and enable the regional extrapolation of RSL age constraints across the SSIs. A maximum of 18.7 m uplift, centred between Greenwich and Robert Islands, has occurred since the formation of the highest Holocene raised beach at around 6300 ^{14}C yr BP (7200 cal yr BP).

The RSL curve produced in the previous chapter from isolation basin data has also been updated. Previously published radiocarbon dates on organic material preserved in lower raised beaches have been used to constrain the falling limb of the curve. The highest Holocene raised beach has also been interpreted as representing a RSL transgression, which is consistent with numerical models of sea level change on Fildes Peninsula from Bassett *et al*. (2007), and together this evidence has been used to infer RSL rose to the mid-Holocene highstand.

However, despite the developments made in this chapter in refining the RSL curve, the precise tectonic contribution to RSL must still be examined. There is no evidence of displacement of beach levels and the uplift rate is suggestive of isostatic uplift rather than tectonic activity, which is promising, but does not mean the possible tectonic

contribution can be ignored. The long-term tectonic uplift history of the SSIs will be examined in the next chapter in order to finalise the RSL curve.

CHAPTER 7

Assessment of the tectonic contribution to relative sea level change

7.1 Introduction

Using evidence from isolation basins it has been possible to develop a RSL curve for Fildes Peninsula, King George Island, with regional GPS surveys providing spatial patterns of Holocene uplift. However, section 2.4.4 demonstrated the complex tectonic setting of the SSIs and highlighted that the long-term tectonic uplift history of the islands is not well understood. Therefore, due to the location of the SSIs in a tectonically active region, a significant uncertainty in the RSL curve is the potential contribution of long-term tectonic uplift relative to glacio-isostatic and eustatic processes. This chapter therefore aims to (i) constrain the long-term uplift rate of the SSIs, and (ii) quantify the tectonic contribution to the RSL curve developed in the previous chapters.

7.2 Assessment of the long-term tectonic uplift rate using residual beach deposits

Previous geomorphological studies of the SSIs (John and Sugden, 1971; John, 1972; Curl, 1980; Hall, 2003) described a landscape dominated by marine features, with

planated surfaces, sea stacks, raised beaches (both Holocene and older) preserved up to over 200 m amsl. The latter were sampled in this study in an attempt to quantify the long-term uplift rate. John and Sugden (1971) defined these “residual beaches” as pockets of *in situ* beach material deposited by marine action in a non-glacial interval and subsequently overridden by ice. The beaches consist of well-rounded and well-sorted shingle deposits interbedded with sands and gravels, in ridge forms, located in sheltered sites below cliffs. Individual deposits can extend for tens of metres laterally and are >1 m thick. John and Sugden considered possible alternative origins, including formation by subaerial river action, glaciofluvial deposition or weathering, but all were ruled out on the basis of the deposit locations, composition, form, and similarity to present day beaches.

Residual beach deposits were reported at 134 m amsl on Noel Hill, Barton Peninsula, King George Island, which have previously been *estimated* to be > 250 ka (Pallàs *et al.*, 1997). However, there are no dates published on any of the deposits, and there is independent evidence that all of the raised marine features have been overridden by (largely) cold-based ice several times during the Quaternary (John and Sugden, 1971). For this reason simple exposure dating of bedrock features poses some challenges. These residual beaches provide a potential alternative solution if it is possible to obtain an estimate of the time taken for the beaches to be uplifted to 134 m amsl.

7.2.1 Field location

The ‘residual beach’ deposit on Noel Hill, Barton Peninsula, described by John and Sugden (1971) and mapped by López-Martínez *et al*. (2002), formed the study location. The deposit is at an altitude of 134 m amsl on the northwest flank of an ice-moulded hill, ~1.5 km southwest of Noel Hill (62^{o}13.583’ S, 58^{o}46.266’ W, Fig. 7.1).

The ‘residual beach’ deposit occupies a broad embayment, between two possible palaeo-promontories, forming a terrace-like surface ~10 m by 25 m in extent (Fig. 7.2). It lies at the base of a ~15 m cliff, where the back of the deposit is clearly delimited by a distinct break of slope; preservation decreases with distance away from the hill. The deposit consists of rounded and well-rounded pebbles and cobbles (Fig. 7.3a), in parts supported in a sandy-gravel matrix, and in parts clast-supported. There is a strong

resemblance to the present-day storm beaches of the SSIs (Fig. 7.3b). Some periglacial sorting of beach material into polygons is present.

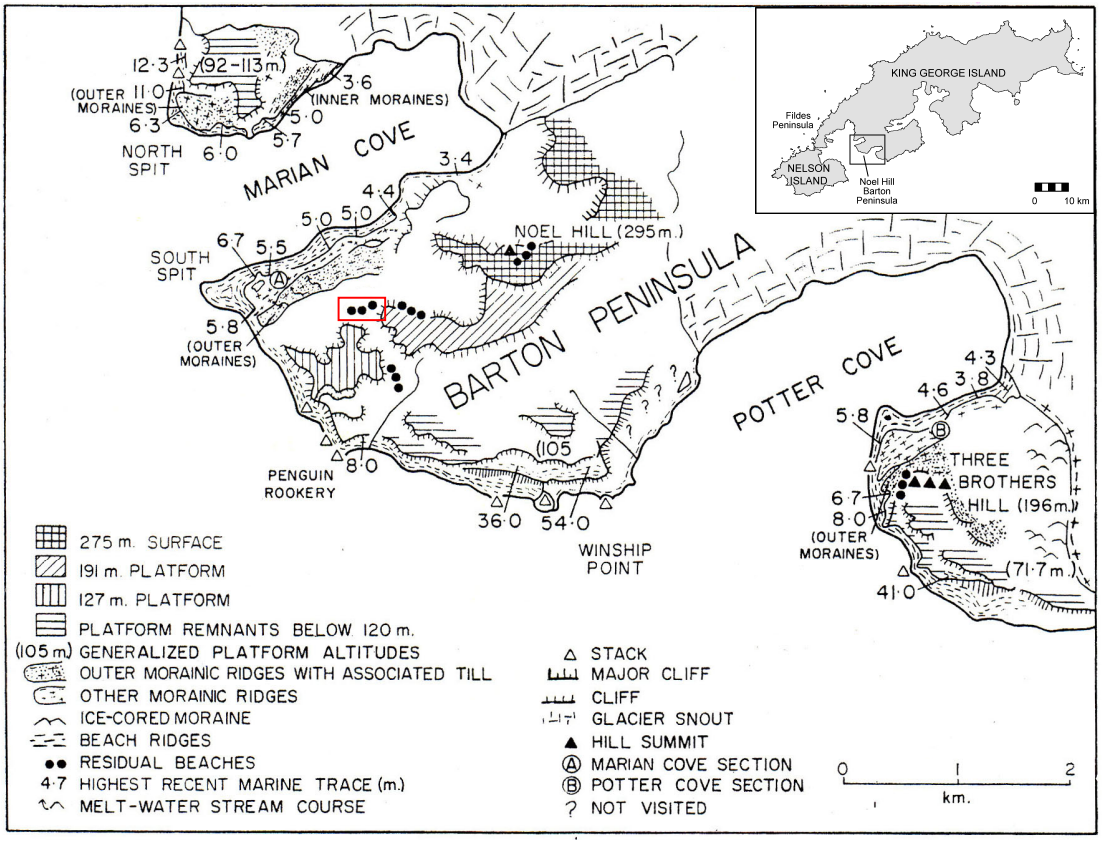

Fig. 7.1 Morphological map of the Marian Cove-Barton Peninsula-Potter Cove area of King George Island, showing the raised marine features identified by John and Sugden (1971). The 'residual beach' sampled in this study is highlighted by the red box. The location of the Potter Cove sedimentary section described in the previous chapter (section 6.4.10) is also shown (labeled B) (Source: John and Sugden, 1971)

The hillslopes surrounding the deposit are generally covered with talus and solifluction material, although scattered rounded pebbles and cobbles are found continuing around the base of the ice-moulded hill and downhill in the direction of Noel Hill. Some less well-defined deposits were observed nearby at higher elevation (164 m amsl), but with only 1-2 rounded cobbles per 10 sq. m. It is hypothesized that 'residual beaches' may have also previously occupied these areas but are much less well preserved today due to an absence of protection from overriding ice, such as this ice-moulded hill provides.

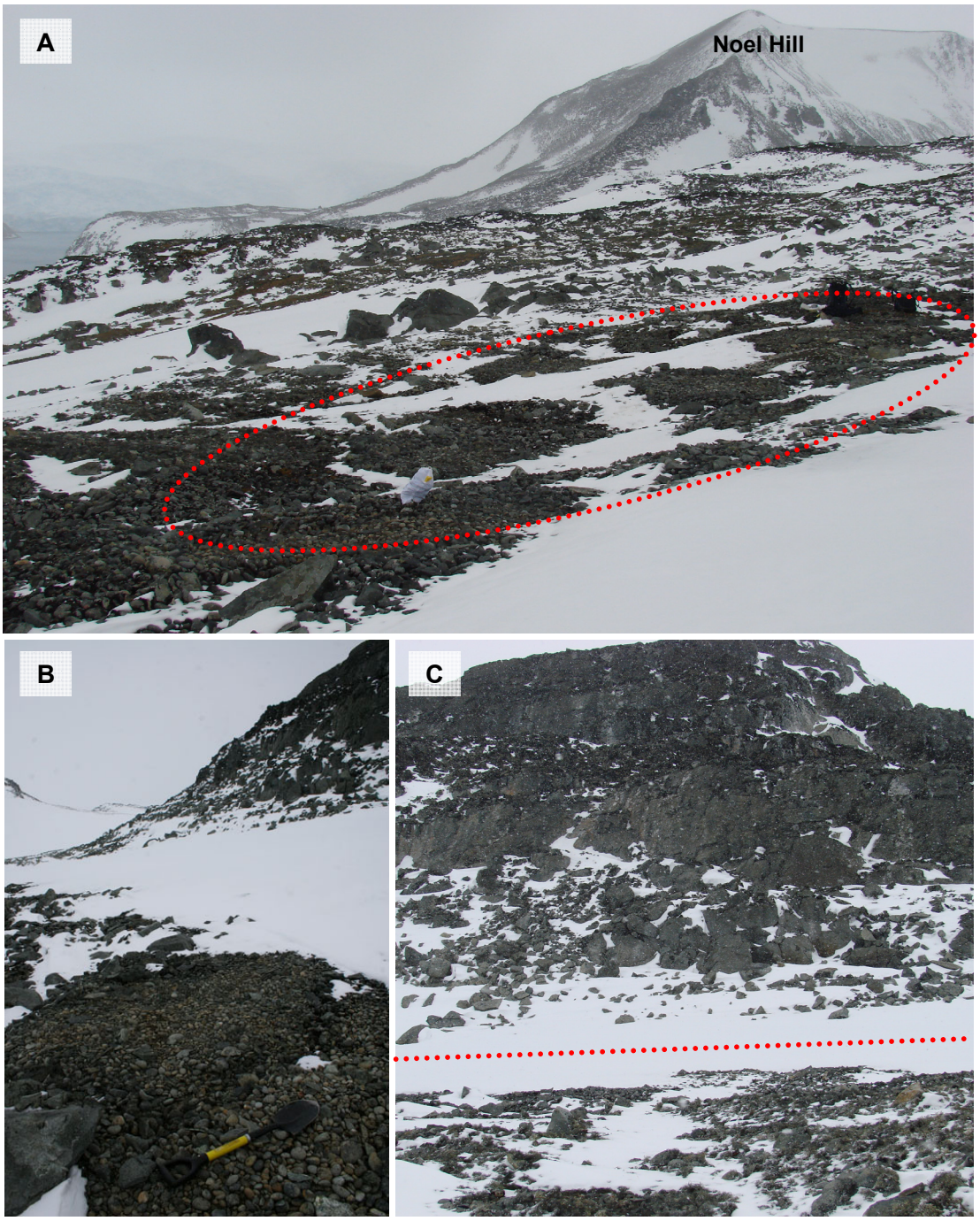

Fig. 7.2 'Residual beach' deposits at 134 m amsl on the side of Noel Hill, Barton Peninsula, King George Island, (a) beach terrace below a small cliff face (off the photo to the right), looking NW; (b) terrace wrapped around the base of an ice-moulded hill; (c) backing cliff with talus visible behind and above the deposit. The limit of 'residual beach' terrace is marked by distinct break of slope. (Photograph B by M. Bentley)

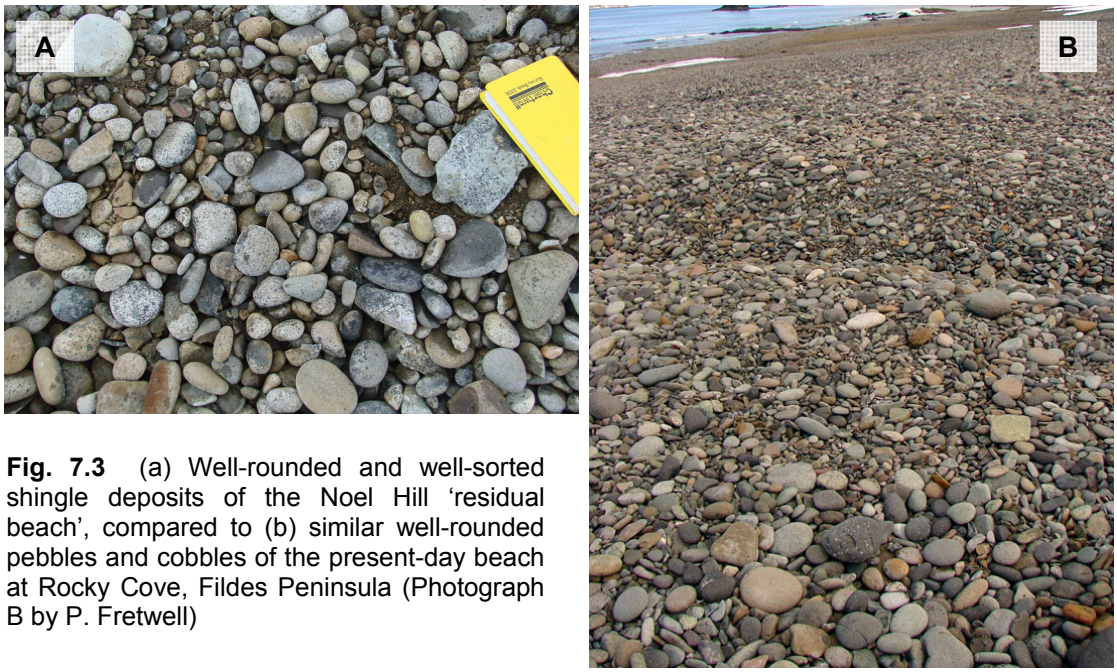

Fig. 7.3 (a) Well-rounded and well-sorted shingle deposits of the Noel Hill 'residual beach', compared to (b) similar well-rounded pebbles and cobbles of the present-day beach at Rocky Cove, Fildes Peninsula (Photograph B by P. Fretwell)

7.2.2 Analytical methods

7.2.2.1 Dating strategy

Cobbles from the 134 m 'residual beach' were sampled for cosmogenic exposure age dating. Where possible the cosmogenic sampling protocol of Gosse and Phillips (2001) was followed. Approximately 30 clasts were collected from three locations along the terrace (~5 m apart), of which 8 were selected for dating. The clasts were distinctly more weathered on the upper surface (Fig. 7.4), suggesting they were preserved *in situ* and had not rolled.

Originally the proposed strategy was to date the clasts using multiple cosmogenic isotope analysis (beryllium-10, aluminium-26 and neon-21), to allow consideration of the complications associated with multiple periods of ice cover. The ^{10}Be-^{26}Al co-isotopic analysis would give the relative balance between exposure and burial by ice (Bierman *et al.*, 1999), with ^{21}Ne giving the *total* accumulated exposure time of a particular clast (Codilean *et al.*, 2008). With the three isotopes it was hoped that it would be possible to infer a reasonable exposure history, or small set of exposure histories, and therefore obtain an estimate for the time taken to uplift the 'residual beach' to 134 m amsl.

However, there were no quartz-bearing clasts found and therefore the ^{10}Be-^{26}Al analysis would not be possible. As the available clasts were feldspar-rich, the dating strategy was revised to using chlorine-36 alone, to provide a measure of exposure. Along with a set of realistic exposure history scenarios the ^{36}Cl data could potentially provide constraints on the likely age of the deposit.

Fig. 7.4 Clasts sampled from Noel Hill for cosmogenic exposure age dating, (a) showing the difference in the surface of the exposed and buried parts of the clast; (b) inside of clast; (c) upper exposed surface of clast; (d) lower buried surface of clast

7.2.2.2 Sample preparation for ^{36}Cl analysis

Samples were prepared for whole-rock ^{36}Cl analysis at the University of Edinburgh Cosmogenic Nuclide Laboratory following the method of Stone *et al*. (1996), as outlined below. The ^{36}Cl/^{37}Cl and ^{35}Cl/^{37}Cl concentrations were measured using accelerator mass spectrometry (AMS) at the Scottish Universities Environmental Research Centre (SUERC). I carried out the sample preparation, with the final stages of target preparation and AMS measurements carried out by Steve Binnie (University of

Edinburgh). Unfortunately, of the eight samples selected for analysis, the masses of the non-magnetic fraction of three samples were too small to prepare targets from, and the sulphur content of another sample was too high. As sulphur is the isobar of ^{36}Cl, the AMS struggles to distinguish between the two isotopes and hence the interference would be too great to get a reliable measurement. Consequently only four samples were dated.

Samples were crushed using a Fritsch P13 disk mill and sieved to the 250-710 μm size fraction. A split of the whole rock was taken from one sample (NH1) for whole rock chemistry measurements by prompt-gamma neutron activation analysis (PGNAA), using standard separation techniques to avoid any grain size differences between the whole rock sample and the PGNAA splits. The remainder of the sample processing and target preparation was undertaken at the University of Edinburgh Cosmogenic Isotope Laboratory.

Magnetic separation was used to remove mafic minerals. The feldspar separates were etched by shaking for several days in a mixture of HF and HNO_3 (1.5ml 48% HF plus 6ml 2M HNO_3 per gram of sample), dissolving approximately 40% of the sample mass. After etching, splits from each of the pure feldspar separates were collected for major element analysis by x-ray fluorescence.

The etched feldspar sample was weighed into plastic (Perfluoroethylene-propylene) bottles, slurried with 18 MΩ water, and spiked with a known amount of Cl (approximately ~1.3mg) from a ^{35}Cl enriched carrier. This carrier, prepared at the Edinburgh laboratory, is a binary mixture of ^{35}Cl enriched NaCl, purchased from Oak Ridge National Laboratory, and commercial NaCl (Fisher Scientific) with a natural ratio of ^{37}Cl to ^{35}Cl. Samples were dissolved on a shaker table in a mixture of concentrated HF and 2M HNO_3. The dissolved sample solutions were centrifuged to remove any insoluble fluorides, heated on a hotplate and, under low light conditions, 10% $AgNO_3$ was added in order to precipitate AgCl. The samples were cooled overnight to allow the AgCl precipitate to collect on the base of the bottles. After settling, the supernatant above the AgCl flocculate was removed and the AgCl was extracted by centrifugation and rinsed with 18 MΩ water. To reduce isobaric interference from sulphur in the accelerator mass spectrometer (AMS), the AgCl was dissolved in NH_3 and $BaNO_3$ was

added to each sample. The samples were refrigerated for 48 hours to promote precipitation of $BaSO_4$ and were then syringed through an Anatop-10, inorganic membrane filter to remove any precipitated crystals of $BaSO_4$. AgCl was re-precipitated with HNO_3 and the precipitates were centrifuged and rinsed in 18 MΩ water before oven drying at 70 °C overnight.

AMS targets were prepared by priming the copper cathode holders of the type used by SUERC with an AgBr substrate, into which the sample AgCl was pressed. A full process laboratory blank was prepared and measured in tandem with the samples. Samples and laboratory blanks were measured at the AMS laboratory at SUERC, alongside targets containing ^{35}Cl enriched carrier and targets of "natural" ratio Cl. The pure carrier and "natural" Cl targets allow direct measurement of stable Cl in the samples on the accelerator. AMS measurements of $^{36}Cl/^{35}Cl$, $^{36}Cl/^{37}Cl$ and $^{37}Cl/^{35}Cl$ were normalized to the Purdue Z93-0005 standard with an assumed R/S (radioactive Cl/stable Cl) ratio of 1.2E-12 and corrected for isobaric interference from sulphur.

The amount of stable chlorine and the ^{36}Cl concentrations of the samples were calculated according to Desilets *et al*. (2006) using both the $^{36}Cl/^{35}Cl$ and $^{36}Cl/^{37}Cl$ AMS results. The concentrations derived using these different R/S (radioactive Cl/stable Cl) ratios agree to within 2%, and so the ^{36}Cl concentration results were derived using the mean of the two. In addition, the ^{36}Cl concentrations reported include a laboratory blank subtraction that varies between 65% and 10% of the total ^{36}Cl concentration measured. Relative to typical ^{36}Cl blank measurements from Edinburgh/SUERC this subtraction is large and due to the low concentrations of ^{36}Cl in the samples, and not likely to be contamination during sample processing. The size of the blank correction is represented in the large uncertainties reported on the concentrations. Propagated errors on the 1σ ^{36}Cl concentrations include the AMS uncertainty, an assumed 1% uncertainty in the dissolved sample mass and 2% on the Cl carrier mass, plus the uncertainty associated with the blank subtraction. Stable Cl in each sample aliquot was derived from the $^{37}Cl/^{35}Cl$ ratios, measured by Faraday cup detectors on the AMS synchronously with the ^{36}Cl determinations. Stable Cl contamination during target preparation was estimated using the difference between the average stable Cl values of the full process laboratory blanks and that measured in pure carrier targets and was found to be negligible.

7.2.3 Results of cosmogenic dating

The concentrations of cosmogenic ^{36}Cl atoms were used to calculate ages using the spreadsheet of Schimmelpfennig *et al*. (2009). The full calculations of the ages are included in Appendix 4, and summarized in Table 7.1. Details on the derivation of ages are outlined below, including the assumptions made in the calculations.

The whole rock chemistry of sample NH1 was used to estimate the neutron flux through the sampled lithologies, in order to estimate production of ^{36}Cl on ^{35}Cl by thermal neutron capture. The sample lithologies are assumed to be consistent enough that the PGNAA results of NH1 are representative of the other samples. Accounting for the neutron flux is complicated by the fact that, unlike the whole rock, the 'residual beach' deposit will have void spaces and the moisture content in this setting will have varied through time. As such there is a significant uncertainty associated with the thermal neutron attenuation. To investigate the potential effect of changing moisture over time, the water content of the samples was varied by 100% and the results show that the differences made to the exposure ages is within their one sigma uncertainties.

Spallogenic production rates are scaled for elevation and latitude according to Stone (2000), incorporating the influence of a stable Antarctic high-pressure system, and variations in the geomagnetic field as discussed in Balco *et al*. (2008). High latitude, sea level spallogenic production rates on Ca and K are taken from Phillips *et al*. (2001); other production rate values are those given in Schimmelpfennig *et al*. (2009) taken from Fabrya-Martin (1988), Phillips and Plumber (1996), Evans *et al*. (1997), Fink *et al*. (2000), Gosse and Phillips (2001), and Heisinger *et al*. (2002). Radiogenic production of ^{36}Cl by thermal neutrons is estimated based on an assumed age of 48 Ma for the sampled lithology. This is based on potassium-argon ages of 46-52 Ma on the granodiorite intrusion of Barton Peninsula immediately NE from where the samples are derived (Watts, 1982; Pankhurst and Smellie, 1983; Smellie *et al.*, 1984), and fits with the broader estimation of late Palaeocene-Eocene for the exact site from which the samples were taken (Chun *et al.*, 1994; Lee *et al.*, 2002). The spreadsheet shows the final dates are highly insensitive to changing the lithology age above 10 Ma, and therefore as the previously reported ages are well above this, an average was used of 48 ± 3 Ma. Topographic shielding is estimated following Dunne *et al*. (1999) and a value of 2.5 g/cm^3 is used for the rock density. Snow cover and the change in elevation with

time remain potential sources of uncertainty in the age determinations. The influence of snow cover on ^{36}Cl exposure ages is complicated by the different production mechanisms of ^{36}Cl; while snow cover will reduce ^{36}Cl production by fast neutrons and, to a lesser degree, muons, it may cause an increase in thermal neutron production (Gosse and Phillips, 2001). In order to account for snow cover and potential variations in thickness over time a minimum uncertainty of 20% is applied to individual exposure ages. The effect of a variable snow cover on the ages is most probably within this value (Tibor Dunai, pers. comm.).

Sample	Target element concentrations (ppm)					^{36}Cl	1σ error	Age	Age
	Ca	K	Fe	Ti	Cl	(atoms/g)	^{36}Cl (atoms/g)	(yr)	uncertainty (yr)
NH1	22087	10659	2238	216	46	47000	48200	**5497**	6979
NH2	12284	22801	2389	187	35	51500	9490	**5764**	1440
NH3	20729	19459	2797	258	41	77300	84100	**8764**	10823
NH8	6362	35514	1538	354	50	108000	9260	**7849**	1337

Table 7.1 ^{36}Cl ages from Noel Hill. For full calculations of ages see Appendix 3. Note ages assume no erosion.

The overall age of the deposit is taken as the error weighted mean and 1-sigma standard deviation of the four exposure age measurements (equations in Taylor, 1997). Two of the ages have large uncertainties and therefore the weighted mean reduces their influence on the overall result. The large uncertainties are likely to be for two reasons. Firstly, the samples have low concentrations of the target elements for ^{36}Cl production, calcium and potassium, which results in lower quantities of measureable ^{36}Cl and hence greater uncertainties. Secondly, due to the low ^{36}Cl concentrations of the samples, they were close to the background concentration (measured by laboratory blank targets), and therefore a significant background correction produced a large error.

With this in mind, the weighted mean age of the deposit on Noel Hill is 6872 ± 966 yr BP, assuming zero erosion of the samples.

7.2.4 Interpretation of results

An exposure age of ca. 7 ka differs enormously from the estimated age of ca. 250 ka, and suggests the original hypothesis that the dated deposits are beach sediments

deposited at sea level and subsequently uplifted needs revising. Even accounting for the large uncertainties associated with the measured ages, this result is significantly younger than the previous estimate, and therefore is an important result irrespective of the large error bars. There are at least three possible explanations for this significantly younger result.

The first explanation that the deposits are Holocene raised beach sediments that have been uplifted and therefore mark the Holocene marine limit can be quickly discounted. This would not fit with either the evidence from isolation basins presented earlier (marine-freshwater transitions would not be present in basins below 15 m at 6.5-6 ka BP if RSL was 134 m above present at 7 ka BP) or with numerical models (Bassett *et al.*, 2007).

The second possibility is that this deposit is a residual beach that is much older than the dates suggest and has only been exposed during the last deglaciation. This assumes the 'beach' was covered by ice almost immediately after deposition during a previous interglacial and then remained ice-covered until the final deglaciation. This scenario would seem unlikely as it is difficult to explain why the deposit would *only* have been exposed during the current interglacial. Whilst this fits with cosmogenic ^{3}He analyses of Pliocene lava surfaces on James Ross Island, which showed they were covered by ice almost continuously from when they were formed (~4.69 Ma BP) until the most recent deglaciation (Johnson *et al.*, 2009), it is not consistent with the extensive wave-cut platforms on Fildes Peninsula and elsewhere across the SSIs at elevations up to 290 m amsl (section 7.3), which were cut during non-glacial intervals.

A third possible interpretation is that the deposit is not a residual beach but is of glaciofluvial origin. It could be a kame terrace, a glaciofluvial ice-marginal landform, defined as a gently sloping depositional terrace perched on a valley side, and deposited by a meltwater stream flowing between the glacier margin and the adjacent valley wall (Benn and Evans, 1998). The only previous report of kame terraces on the SSIs is at Potter Cove (Birkenmajer, 1998), although here they are below the marine limit and date to within the last 500 years. The deposit on Noel Hill appears to closely resemble the description of "well-rounded stones in a sandy to gravelly matrix forming a small terrace-like step in the valley side" at 160 m asl in the Tumbledown Cliffs area of James

Ross Island (Lundqvist *et al.*, 1995). Aside from this, there are limited observations of kame terraces elsewhere in Antarctica in the McMurdo Dry Valleys (Healy, 1975) and Bunger Hills, East Antarctica (Gore *et al.*, 2001).

Whilst kame terraces appear to be uncommon in Antarctica, the deposit closely resembles kame terraces found around polythermal glacier margins elsewhere. For example, kame terraces have been reported on Ellesmere Island in the Canadian High Arctic, in very similar environmental settings well above the marine limit in a landscape where glaciation interfaces with sea level evidence (Evans, 1988, 1990a, 1990b; Bednarski, 1995; England *et al.*, 2000), as well as in Iceland (Evans, 2005). In Arctic Canada they are associated with extensive lateral moraines and normally occur perched on valley sides (Fig. 7.5). Given this resemblance, it is reasonable to re-interpret the Noel Hill deposit as a kame terrace. Of course it is possible that the other similar deposits on Three Brothers Hill, southwest Fildes Peninsula, and elsewhere on Barton Peninsula, which John and Sugden also interpreted as residual beaches, may also be kame terraces. However, this interpretation must remain purely speculative without further field examination and dating.

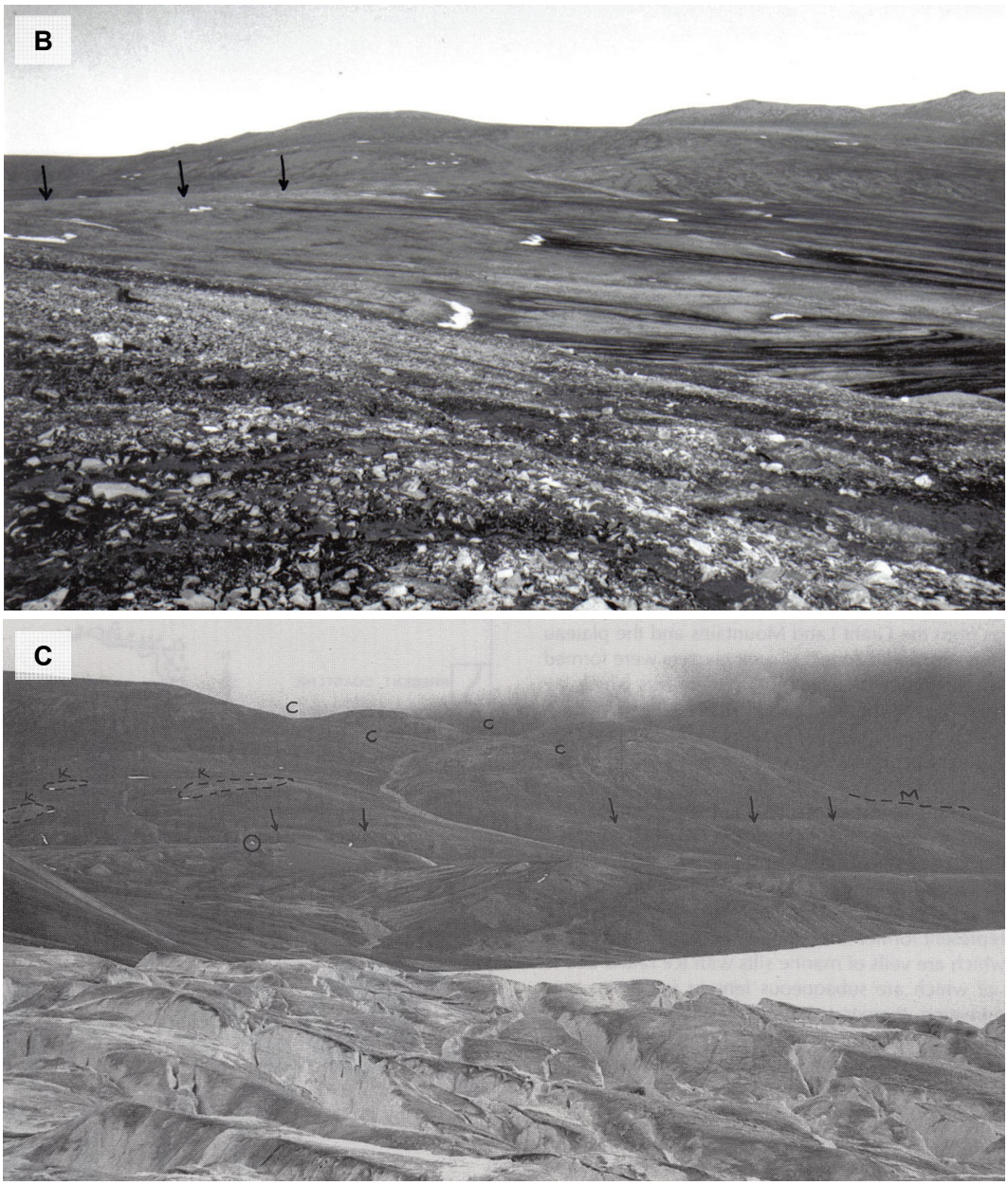

Fig. 7.5 Kame terraces in Phillips Inlet, Ellesmere Island, Canada, (a) aerial photograph of Bushmill Pass showing a lateral moraine (beaded line) grading into a kame terrace (k) at 222 m asl (numbers are marine limits and lake shorelines in m asl); (b) photograph of same kame terrace (arrowed) as in (a) at 222 m asl, with lateral moraine in foreground; (c) kame terraces (k) on Wootton Peninsula, Ellesmere Island, above the marine limit (arrowed) at 91 m asl (c = meltwater channels, circle = ice contact delta, M = moraine) (Fig. a and c: Evans, 1990a; Fig. b: Evans, 1988)

Although this does not yield any information on RSL history or aid in the determination of the long-term uplift rate of the SSIs, the discovery of a relatively rare glaciofluvial feature in the Antarctic is still interesting. In addition, the date of 6872 ± 966 yr BP fits

extremely well with the deglacial history of Barton Peninsula from Seong *et al*. (2009). They used ^{36}Cl ages on glacially eroded bedrock surfaces at a range of elevations on Barton Peninsula to constrain the timing and rate of deglaciation (Fig. 7.6). The age proposed for the kame terrace in this study fits closely to their ice thinning rate. This also further supports the exclusion of repeatedly exposed beach deposits by suggesting the exposure relates to the current interglacial.

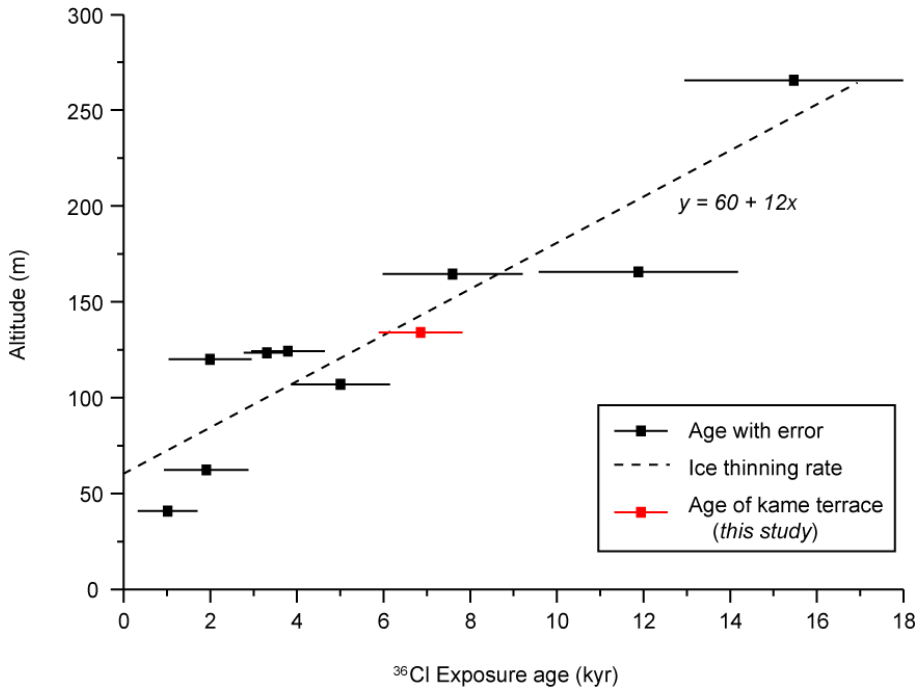

Fig. 7.6 ^{36}Cl exposure ages of glacially striated surfaces on Barton Peninsula, King George Island, from Seong *et al*. (2009). The oldest exposure age of 15.5 ± 2.5 ka BP forms a minimum date for deglaciation, and consistent decreasing of ages with altitude suggest ice progressively downwasted at an apparent rate of 12 mm/yr on Barton Peninsula. The date on the kame terrace deposit from this study fits closely with the proposed ice thinning rate of Seong *et al*.

7.3 Assessment of the long-term tectonic uplift rate using surfaces and platforms

Unfortunately, due to the re-interpretation of the deposits previously assumed to be "old" residual beaches as recent glaciofluvial features, the problem of constraining the long-term uplift rate of the SSIs remains. One alternative is to use the planated surfaces observed across the ice-free areas of the islands.

John and Sugden (1971) reported the widespread occurrence of planated surfaces and platforms across the SSIs at altitudes up to 290 m amsl (Fig. 7.7). These are thought to result from marine planation, cut during non-glacial periods and subsequently uplifted, although the uppermost may have formed subaerially. The platforms included in Fig. 7.7 are those reported by John and Sugden (1971); field evidence for this thesis supports their work, with extensive platforms observed on Fildes Peninsula, Barton Peninsula and Byers Peninsula. On Fildes Peninsula, platforms occur up to 155 m amsl (Fig. 7.8) and are gently undulating, seaward sloping and marked by distinct fronting cliffs. The most extensive platform lies in the northwest of the peninsula at 35-40 m amsl (Fig. 7.9). It is ~2 km wide, laterally continuous over ~7 km, and truncated by vertical cliffs of ~30 m and backed by steep ~60 m cliffs. The flat topography of this platform is demonstrated by the hypsometric profile shown in Fig. 7.10. Similar well-preserved platforms were observed on Byers Peninsula (Livingston Island) separated by spectacular shore-parallel cliffs (Hall, 2003).

By combining platform levels reported by John and Sugden (1971) with fieldwork at a limited number of sites (mapping and GPS surveying), it is possible to define sequences of platform levels (Fig. 7.7). No vertical offsets of platforms was observed, which is consistent with results from Chapter 6 and a previous assessment of raised beach levels by Pallàs *et al*. (1995), which suggest there has been no horizontal displacement of Holocene shorelines. Lateral continuity of surfaces confirms that uplift has been relatively uniform across the area, as opposed to differential movement of fault-bounded blocks, thus making it possible to take the broad-scale elevation of the platforms as proxies for long-term uplift.

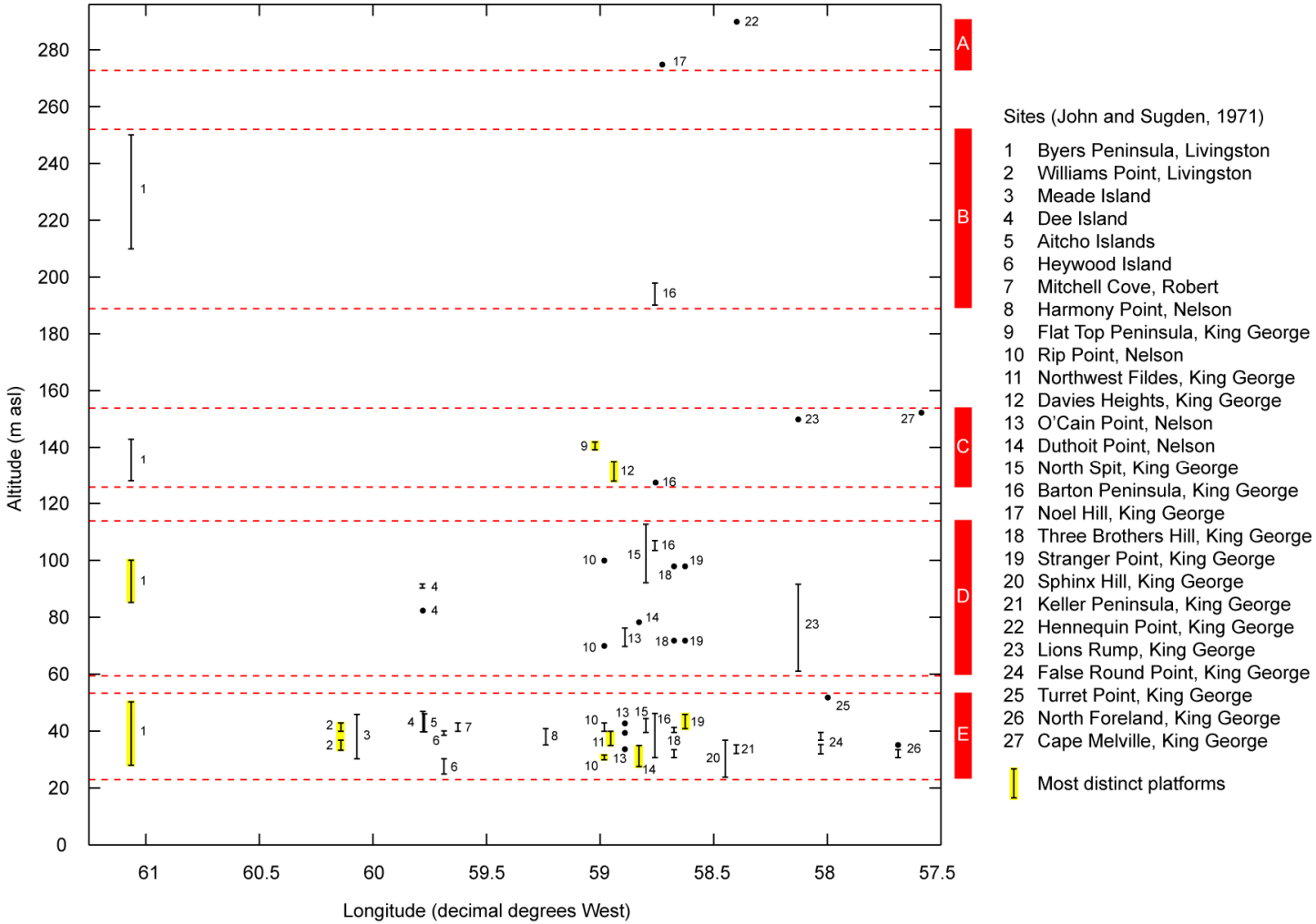

Fig. 7.7 Platforms reported across the SSIs, taken from Table I of John and Sugden (1971). For this work, platforms of similar altitudes have been grouped into five levels (A-E).

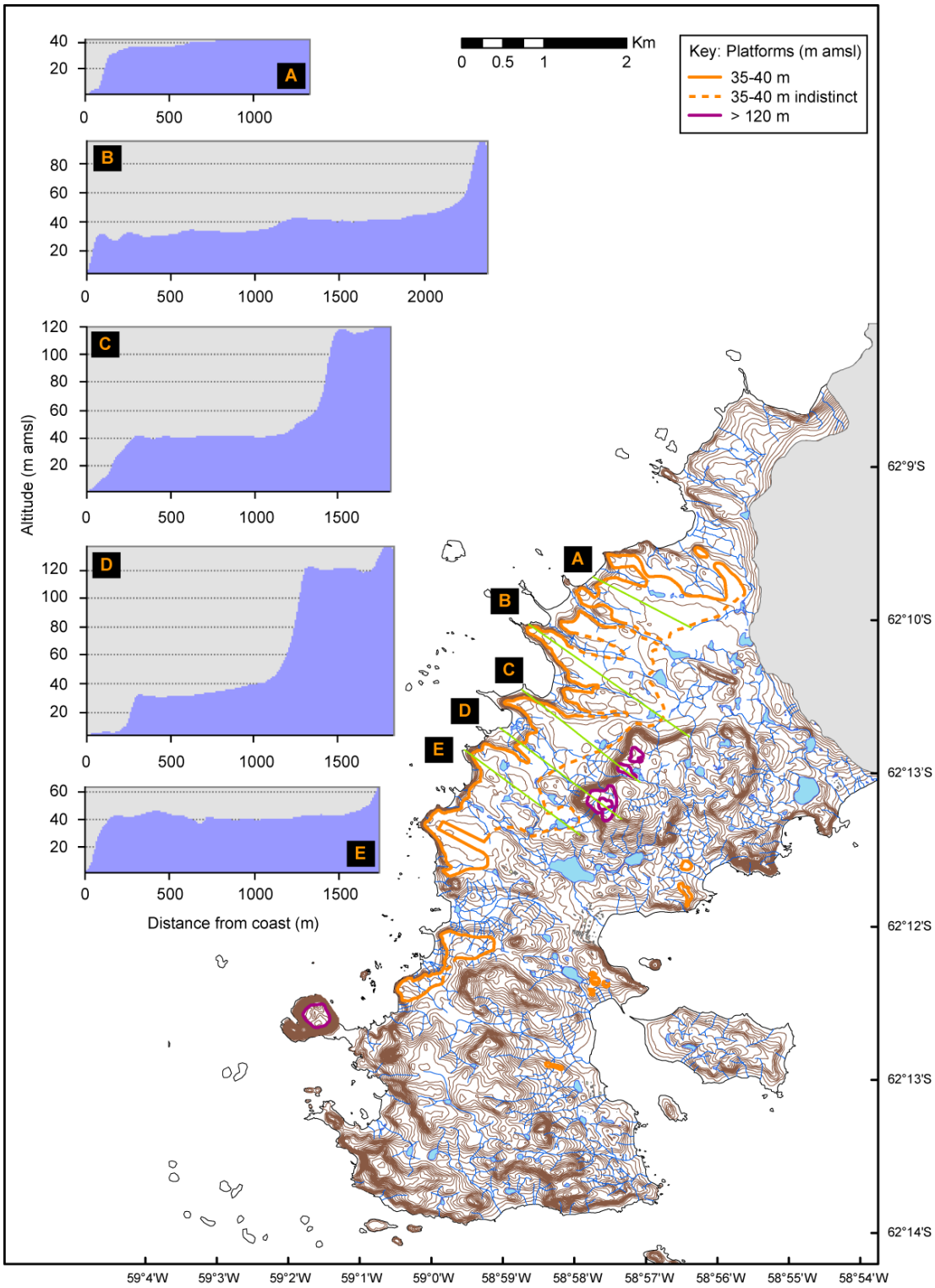

Fig. 7.8 Platform levels on Fildes Peninsula, King George Island. Cross-sections of platforms were constructed from contour data from the SCAR King George Island GIS project (SCAR KGIS).

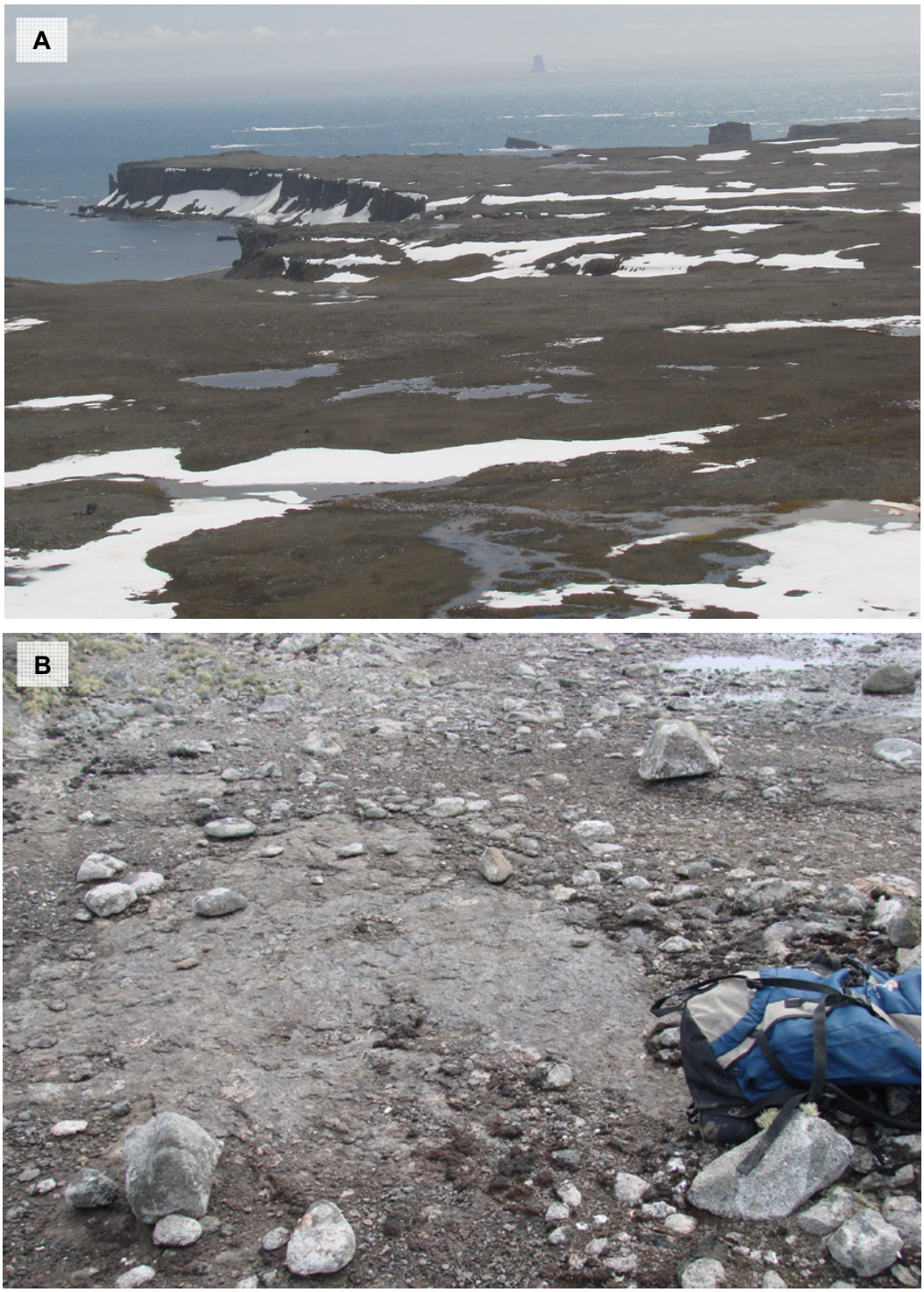

Fig. 7.9 Marine platform on the northwest of Fildes Peninsula at 35-40 m amsl, (a) extent of the platform showing the bounding vertical cliffs. The photo is taken looking perpendicular to transects A-E in Fig. 7.8; (b) surface cover showing exposed planated bedrock and sub-angular cobbles and boulders, some resting on the surface and others supported in a sandy gravel matrix

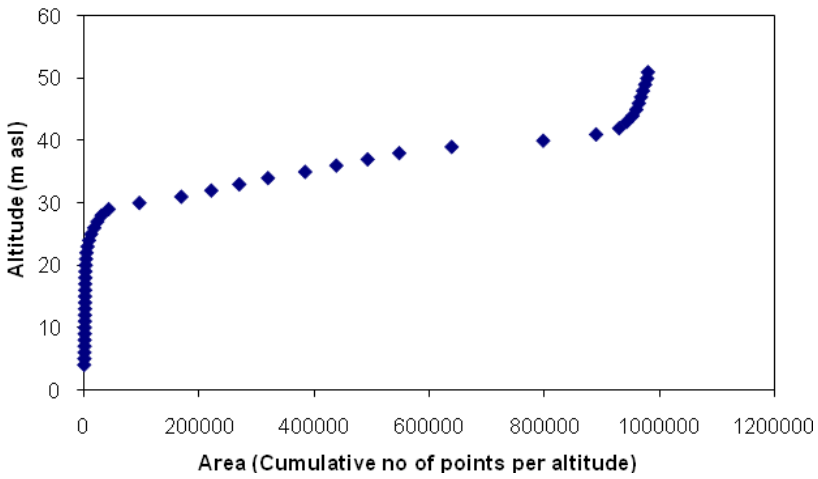

Fig. 7.10 Hypsometry of the Northwest platform of Fildes Peninsula. Calculated in ArcGIS from a digital elevation model created from contour data from the SCAR KGIS. The hypsometry shows the extensive nature of the 35-40 m platform.

Attempts to date the formation of these platforms observed across the SSIs have not yielded quantitative chronologic data; relative ages have only been assigned on the basis of the relationship between the platforms and the geology they cut across or associated marine conglomerates on the platform surfaces (Adie, 1964; Barton, 1965; John and Sugden, 1971). Pallàs *et al*. (1997) provided an alternative means of estimating the platform ages, by assuming that each platform level relates to one sea level highstand. They tentatively assigned the ages of the most recent interglacials to increasingly higher platforms (where a set of three or more occur at the same locality). Then based on the principle that eustatic sea level during marine isotope stages (MIS) 5e, 9 and 11 was close to present, they assumed that platforms cut during these interglacials would record no eustatic oscillations, but instead the tectonic uplift of the islands. By this method they suggested that platforms at 120 m amsl were from MIS 11, thus giving a tectonic uplift rate of 0.27 m/ka (Fig. 7.11a). However, there is an alternative possibility that platforms were also formed during MIS 7. Pallàs *et al*. (1997) assumed that eustatic sea level during MIS 7 was lower than present (Shackleton, 1987), and therefore the height of platforms cut during MIS 7 relative to the other interglacials is uncertain. Assuming the platform of stage 7 is above that of stage 5e, this gives a tectonic uplift rate of 0.39 m/ka (Fig. 7.11b). If the platform of stage 7 is in fact lower, then the rate becomes 0.4 m/ka (Fig. 7.11c).

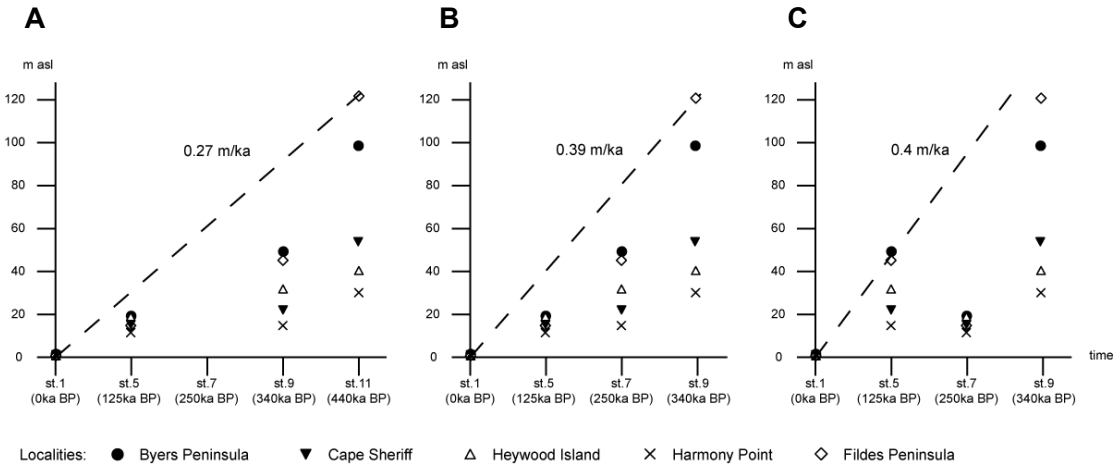

Fig. 7.11 Predicted tectonic uplift rates for the SSIs according to Pallàs *et al*. (1997), based on the assignment of the ages of the most recent interglacials to sets of emerged platforms, (a) assuming platforms formed during marine isotope stages (MIS) 1, 5e, 9 and 11; (b) assuming MIS 7 was also a time of platform formation; (c) assuming platforms of MIS 7 are below those of MIS 5e.

However, the subsequently published sea level record from corals of Thompson and Goldstein (2005) suggested the eustatic sea level of MIS 7 equated to that of MIS 5e. This therefore has implications on Pallàs *et al*.'s estimations, disproving their first and third scenarios (Fig. 7.11a,c), and meaning the uplift rate of the SSIs estimated using the heights of marine platforms is 0.39 m/ka (Pallàs *et al*., 1997).

The approach of Pallàs *et al*. (1997) was repeated here using the platform levels defined in Fig. 7.7 from John and Sugden (1971) and the revised marine isotope stage timescale for Antarctica of Jouzel *et al*. (2007) (Table 7.2, Fig. 7.12). The former is particularly necessary as the highest platform that Pallàs *et al*. (1997) used was at 120 m amsl, which was not recorded by John and Sugden (1971). By assignment of platform levels E, D, C and B to marine isotope stages 5, 7, 9 and 11 respectively, this gives a maximum uplift rate of 0.61 m/ka (250 m in 410 ka). However, this is likely to be an over-estimate as the platform at 210-250 m amsl on Byers Peninsula, which marks the upper limit of 'level' B, is described by John and Sugden as only a "possible summit surface" which may not have been formed by marine planation. The highest definite platform reported is on Barton Peninsula at 191-198 m amsl. Recalculating the uplift rate based on a maximum platform elevation of 198 m amsl reduces the uplift rate to 0.48 m/ka.

Platform level	Height range (m amsl)	Marine isotope stage	MIS age (ka BP)
A	275-290		
B	191-250	11.3	410
C	127-155	9.3	335
D	61-113	7.5	240
E	24-52	5.5	130
		Uplift rate	**0.48 m/ka**

Table 7.2 Platform levels of the SSIs based on heights reported from John and Sugden (1971) and defined in Fig. 7.7 and their assignment to previous interglacials. The timings of the marine isotope stages are as defined by Jouzel *et al*. (2007).

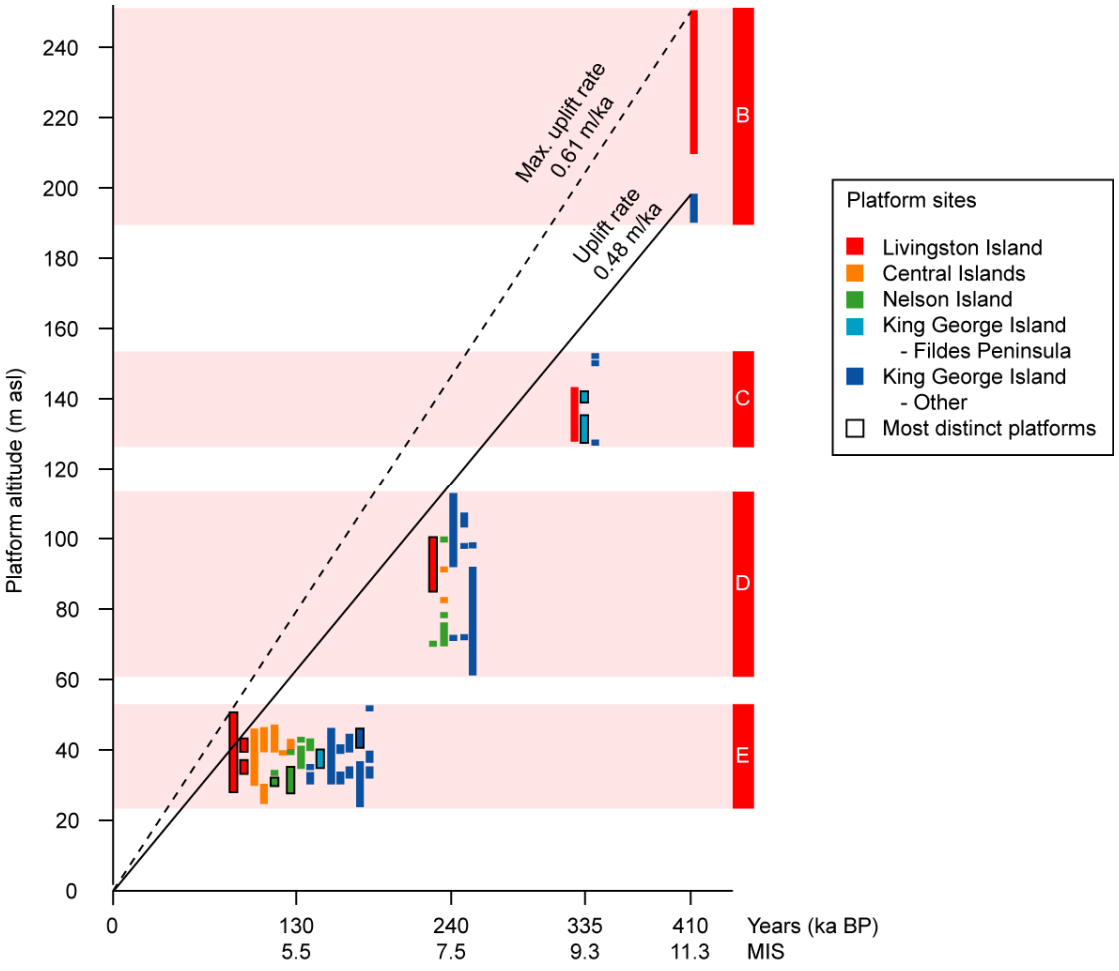

Fig. 7.12 Predicted tectonic uplift rate for the SSIs, calculated by assigning the ages of the most recent interglacials to emerged platforms, based on the method of Pallàs *et al*. (1997) but using the platform levels defined in Fig. 7.7 from John and Sugden (1971) and the revised marine isotope stage timescale for Antarctica of Jouzel *et al*. (2007)

In addition, the same approach was adopted using only the platform levels on Fildes Peninsula, where a suite of platforms were observed at distinct heights above sea level (Fig. 7.8). Platform levels are shown in Table 7.3, which were measured using the high precision Leica GPS (as used for raised beach surveys). Repeating the calculations above using these heights gives an uplift rate of 0.43 m/ka. Therefore it is clear that the estimation of Pallàs *et al*. (1997) is repeatable using the revised heights and timescale outlined above, and gives an overall long-term uplift rate in the range of 0.43 m/ka (based on Fildes platforms only) to 0.48 m/ka (based on all platforms).

Platform height (m amsl)	Marine isotope stage	MIS age (ka BP)
130-145	9.3	335
115-120	7.5	240
35-40	5.5	130
	Uplift rate	**0.43 m/ka**

Table 7.3 Platform levels on Fildes Peninsula. Heights were measured with the Leica GPS system, as used for the raised beach surveys in Chapter 6. The timings of the marine isotope stages are as in Table 7.2.

Whilst the surfaces and beaches are observed to be laterally continuous with no evidence of horizontal displacement, which suggests the platform elevations can be used to assess the uplift rate, there are several criticisms of this method, besides its 'count-back' nature. Firstly, a potential source of error in Pallàs *et al*.'s approach is the assumption that the uplift rate has remained constant through time. Saillard *et al*. (2009) identified similar sequences of marine terraces in the Chilean Andes, but demonstrated that uplift over the Pleistocene has been episodic. Similar variability has been observed along the southern Oregon coast (Muhs *et al*., 1990), which forms part of the Cascadia subduction zone, a close tectonic analogue to the South Shetland margin. Muhs *et al*. (1990) demonstrated that whilst the type of convergent margin may place an upper limit on the possible uplift rate, local structures play a large role in uplift rate variability. The abundance of strike-slip features around the SSIs mean that tectonic uplift here may be similarly episodic.

Secondly, Saillard *et al*. (2009) also noted that sequences of preserved terraces do not always record all the sea level highstands. Therefore assignment of the platforms to interglacials may be problematic. It does however mean that the uplift rates are maxima. Similarly, the Pallàs *et al*. approach also assumes there has been no degradation of platforms, which may be unrealistic (Anderson *et al.*, 1999). Consequently, the accuracy of Pallàs *et al*.'s approach of estimating of the long-term uplift rate of the SSIs remains uncertain, and an alternative method of constraining the uplift rate must still be sought.

7.4 Alternative methods of assessing the long-term tectonic uplift rate

A possible alternative means of quantifying the long-term uplift rate of the SSIs is to consider the throw on the fault system that defines the boundary between the islands and the deep Bransfield Basin (Rob Larter, pers. comm.). The central Bransfield Basin has a maximum water depth of 1950 m (Gràcia *et al.*, 1997), and considering the elevations of the headlands along the southeast coast of King George Island and the fact there are several hundred metres of sediments in the basin, the overall throw must be around 3000 m. If it is assumed that Bransfield Basin opening started when spreading stopped on the Antarctic-Phoenix ridge (at magnetic chron C2A, 3.3 ± 0.2 Ma BP, Livermore *et al.*, 2000), and that displacement has been over this period, split equally between the basin going down and the islands going up, then this gives an average uplift rate of 0.45 m/ka.

A possible criticism of this approach is that geodetic GPS data (e.g. Dietrich *et al.*, 2004) show the current rate of extension across the Bransfield Strait is 7 mm/yr, yet the deep central Bransfield Basin (>1500 m) is ~50 km wide (Gràcia *et al.*, 1997). At this rate it would have taken 7 Ma to open. Therefore either (i) extension started earlier than assumed, (ii) extension occurred at a faster rate initially, or (iii) some fraction of the deep basin is the result of subsidence of stretched continental crust rather than extension. The first explanation is a possibility, as the opening of the Bransfield Basin may have started at the time of abrupt slowing of Antarctic-Phoenix spreading, rather than at its cessation. Spreading slowed abruptly from ~70 mm/yr to ~40 mm/yr at around 6.9 Ma (on magnetic reversal timescale CK95) (Larter and Barker, 1991; Maldonado *et al.*, 1994). If this is correct, then this gives a lower long-term uplift of 0.22

m/ka. Assuming either a longer history of displacement or faster early opening, would both result in a slower average displacement rate over the past few 100 ka.

Whilst there are many uncertainties associated with this approach, it provides an initial estimate of the long-term uplift rate, of between 0.22-0.45 m/ka. This therefore agrees remarkably well with Pallàs *et al*.'s (1997) estimation of the uplift rate of ~0.39 m/ka, and the revised version of Pallàs *et al*.'s approach of 0.43-0.48 m/ka. Thus an assessment of marine platforms and consideration of the fault system around the SSIs, has placed a constraint on the long-term tectonic uplift rate of the islands in the range of ~0.22-0.48 m/ka (Table 7.4). This range incorporates the estimates based on (i) Pallàs *et al*.'s assessment of platform levels (0.39 m/ka), (ii) revised calculations using updated platform heights and timescales (0.43-0.48 m/ka), and (iii) consideration of the throw on the fault system (0.22-0.45 m/ka). Neither method is without its limitations, as discussed, but the strong agreement between the outcomes of the two completely different methods gives us some degree of confidence in the values.

	Method	Uplift rate (m/ka)
1	Cosmogenic dating of previously reported "residual beaches"	N/A
2	Platforms – Original Pallàs *et al*. (1997) method	0.39
3	Platforms – Revised calculations of Pallàs *et al*. using more sites, elevations of John and Sugden (1971), and updated timescale	0.48
4	Platforms – Fildes Peninsula only	0.43
5	Fault system and opening of the Bransfield Basin	0.22-0.45
	Overall	**0.22-0.48**

Table 7.4 Summary of uplift rates calculated by each different method

7.5 Implications of the long-term uplift rate for the RSL curve

The RSL curve developed from isolation basins and raised beaches includes the combined effects of both isostatic and tectonic uplift. As there is no evidence of displacement of beach levels, the shape of the RSL curve is not altered by tectonic uplift, but instead quantification of the tectonic uplift rate enables an assessment of the relative contributions of the two processes. Assuming that tectonic uplift has been

constant throughout the Holocene at a rate of 0.22-0.48 m/ka, then based on the two end-members of this range, the tectonic uplift component of the RSL highstand (15.5 m amsl) is between 1.4 m and 2.9 m. Glacio-isostatic rebound therefore dominates the RSL curve.

7.6 Summary

This chapter has examined the tectonic contribution to RSL change in the SSIs. Bentley *et al*. (2005a) identified the need for consideration of long-term tectonic uplift, which is particularly important in a region known to be tectonically active. Unfortunately, the originally proposed method of dating what was assumed to be high altitude pre-Holocene beach deposits, was unsuccessful in estimating the long-term tectonic uplift rate due to their unexpected young age. This in itself was an interesting discovery, with glaciofluvial kame terraces rarely reported in the region. An age for the kame terrace of ca. 7 ka BP also helps further constrain the deglacial history of Barton Peninsula.

The re-interpretation of these deposits required a re-assessment of how the tectonic uplift rate could be estimated. Using marine platforms as proxies for long-term uplift, a rate in the range of 0.39-0.48 m/ka was proposed. An alternative method of quantifying the rate by considering the throw on the fault system that forms the boundary between the SSIs and the Bransfield Basin, also gave similar uplift rates of 0.22-0.45 m/ka. As both methods are based on broad assumptions, the full range of 0.22-0.48 m/ka was used to define the tectonic component of RSL change. Tectonic uplift contributes between 1.4 and 2.9 m to the reconstructed RSL highstand of 15.5 m amsl.

CHAPTER 8

Conclusions

8.1 Introduction

This chapter concludes this thesis by reviewing the major findings of the work in the context of the original aims and objectives outlined in Chapter 1. It also makes recommendations for potential future research on relative sea level change in the South Shetland Islands.

The overall aim of this thesis was to *reconstruct postglacial relative sea level change at a site in the South Shetland Islands, peripheral to the Antarctic Peninsula Ice Sheet.* In order to achieve this aim, this thesis sought to:

- Retrieve sediment cores from isolation basins at a range of altitudes on King George Island, South Shetland Islands, to form a series of sea level index points
- Use additional geomorphological evidence, such as raised beaches, to determine former marine limits and RSL history, both on King George Island and the broader area of the South Shetland Islands
- Quantify the long-term tectonic contribution to RSL change, through the study of high erosion surfaces and marine platforms
- Combine evidence from isolation basins, raised beaches and high platforms to produce a RSL curve for King George Island
- Assess spatial variations in the response to glacial unloading across the South Shetland Islands, using raised beaches

Secondary objectives were to:

- Assess the potential for using $\delta^{13}C$ and C/N ratios as alternative indicators of palaeosalinity to biological proxies within isolation basin sediments in Antarctica
- Use cosmogenic isotope exposure age dating to determine a deglacial chronology.

The following section discusses the ways in which these objectives were addressed and the key conclusions from this work.

8.2 Key findings

To retrieve sediment cores from isolation basins at a range of altitudes on King George Island, to form a series of RSL tie points

Five lakes were cored on Fildes Peninsula, King George Island, at a range of altitudes above present sea level. Lakes were selected between 14.5 m amsl and 34.5 m amsl in order to constrain the preliminary RSL curve produced for the SSIs by Bentley *et al*. (2005a). The results of diatom, isotope and physical analyses of these lake cores are presented in Chapters 4 and 5. Yanou and Long Lakes (14.5 and 15 m amsl respectively) provide the longest records of RSL change, with two clear marine-freshwater transitions. By contrast, no marine signal is present in the three lakes above 16 m amsl (Ardley, Belen and Gaoshan Lakes). By integrating the results from all lakes, it has been possible to produce a RSL curve, which is well-constrained for the period between ca. 7000 and 4500 ^{14}C yr BP (Fig. 8.1a), and shows an overall trend throughout the Holocene of RSL fall, interpreted to be caused by isostatic uplift in response to regional deglaciation. However, superimposed on the signal of RSL change are changes in palaeoclimate and palaeoproductivity.

To assess the potential for using $\delta^{13}C$ and C/N ratios as alternative indicators of palaeosalinity to biological proxies within isolation basin sediments in Antarctica

This study demonstrated the unreliability of using carbon isotopes as a palaeosalinity proxy, especially relative to diatoms. The isotopic profiles appear to be driven not only by changes in the source of organic matter and thus RSL, but also by palaeoenvironmental and productivity changes. Marine and freshwater sediments were

indistinguishable on the basis of $\delta^{13}C$ values alone and freshwater sediments had isotopic signatures normally characteristic of marine sediments. Unfortunately it was not possible to use C/N ratios in tandem with carbon isotopes to help distinguish between marine and terrestrial carbon sources, as the sediments of the Fildes Peninsula lakes have exceptionally low nitrogen content.

To use geomorphological evidence, such as raised beaches, to determine former marine limits and RSL history, both on King George Island and the broader area of the SSIs

There are flights of raised beaches preserved across the SSIs, and although the beaches may be indicative of small-scale events such as individual storms, the broad-scale GPS surveys across the archipelago demonstrate that there are clearly prominent beach levels, reflecting large-scale isostatic uplift (and long-term tectonic uplift) and RSL fall. Unfortunately it was not possible to establish an absolute chronology for the formation of the beaches, as originally intended, due to a lack of dateable material preserved. Instead the formation of the highest beaches was constrained using dates from isolation basins immediately behind them, and the RSL curve was refined from previously published radiocarbon dates (Fig. 8.1b). The highest Holocene raised beach was interpreted as being associated with a RSL transgression.

To assess spatial variations in the response to glacial unloading across the SSIs, using raised beaches

More significantly than constraining the RSL curve itself, the work on raised beaches has been critical in providing an assessment of the spatial patterns of Holocene isostatic uplift and therefore the applicability of the curve over the area beyond Fildes Peninsula. The beaches were modelled using polynomial trend surface analysis to produce an isobase plot of isostatic uplift since the Holocene RSL highstand, and a key outcome of this thesis is the use of this isobase model to constrain the spatial variability of glacio-isostatic uplift across the SSIs since the formation of the highest Holocene raised beach, which has enabled the regional extrapolation of RSL age constraints across the SSIs. The isobase model shows a maximum of 18.7 m of uplift has occurred since the formation of the highest Holocene raised beach at around 6300 ^{14}C yr BP,

centred between Greenwich and Robert Islands, with Fildes Peninsula uplifted by 15-16 m during this time. It is recognized that the trend surface analysis does not preclude the influence of the Antarctic Peninsula ice sheet on RSL change.

To quantify the long-term tectonic contribution to RSL change

In a region known to be tectonically active, it is essential to consider the potential contribution of long-term tectonic uplift to the RSL curve. Two independent approaches of (i) using marine platforms as proxies for long-term uplift and (ii) considering the fault system around the SSIs, were taken to quantify the tectonic uplift rate, both giving very similar estimates in the range of 0.22-0.48 m/ka. The reconstructed RSL highstand of 15.5 m amsl includes the combined effects of both isostatic and tectonic uplift. Assuming a tectonic uplift rate of 0.22-0.48 m/ka, this places the tectonic uplift component of the RSL highstand between 1.4 m and 2.9 m.

To use cosmogenic isotope exposure age dating to determine a deglacial chronology

Originally it was proposed to use cosmogenic dating of previously reported high altitude pre-Holocene 'residual beach' deposits to estimate the long-term tectonic uplift rate of the SSIs. However, this was unsuccessful due to the unexpectedly young age of the deposits, and instead they were re-interpreted as glaciofluvial kame terraces. This was an interesting discovery as kame terraces are rarely reported in the region. An age for the kame terrace on Noel Hill of ca. 7 ka BP also helps further constrain the deglacial history of Barton Peninsula, and agrees extremely well with previous work (Seong *et al.*, 2009).

To combine evidence from isolation basins, raised beaches and high platforms to produce a RSL curve for King George Island

The overall output of this thesis is a new RSL curve for Fildes Peninsula, King George Island, which has been produced by combining evidence from isolation basins and raised beaches, and takes into account long-term tectonic uplift (Fig. 8.1b). It shows a period of RSL rise in the early Holocene prior to 6700 ^{14}C yr BP, on the basis of the

transgressive nature of the highest Holocene raised beaches and numerical models. RSL rises to a mid-Holocene highstand of 15.5 m amsl between ca. 6150 and 6700 ^{14}C yr BP. RSL then falls initially after 6700 ^{14}C yr BP as a consequence of isostatic uplift in response to regional deglaciation. However isostatic uplift appears not to have occurred at a linear rate, and a temporary pause in ice retreat ca. 6300 ^{14}C yr BP caused the rate of eustatic sea level rise to exceed the rate of isostatic uplift, leading to a slight RSL rise of ~1 m and a double peak to the mid-Holocene highstand. RSL then falls from 6150 ^{14}C yr BP to present in response to continued glacial unloading and isostatic rebound. Dates from late Holocene raised beaches suggest RSL fall has possibly accelerated in the last 700 years.

The isobase model of isostatic uplift since the Holocene RSL highstand, presented in Chapter 6, suggests Fildes Peninsula has been subject to similar rates of isostatic uplift (± 3 m) to Livingston Island, central islands (e.g. Greenwich, Robert, Nelson) and eastern King George Island. This isobase model therefore defines the degree to which the RSL curve is applicable across the SSIs. This combined approach of using isolation basin and raised beach data is therefore very powerful, as it yields not only a Holocene RSL curve but also the spatial pattern of how this RSL change occurred across the archipelago.

Fig. 8.1 (Following page) Development of the relative sea level curve for the South Shetland Islands, produced by integrating data from isolation basins and raised beaches
(a) Stage 1, based on isolation basin data from Fildes Peninsula, both from this study and previously published work (*). The results from Lake Kitezh come from Mäusbacher *et al*. (1989) and Tiefersee from Schmidt *et al*. (1990). Sill heights are plotted above mean higher high water, as this is the assumed indicative meaning of isolation basins.
(b) Stage 2, final relative sea level curve for the South Shetland Islands, produced from isolation basin data (as above) and raised beaches. Limiting dates on raised beaches come from penguin bones and whalebones that have previously been published. To account for the different indicative meanings of isolation basins and raised beaches, isolation basin sill altitudes have been corrected by subtracting 1.5 m (difference in height between mean higher high water and mean sea level for Ardley Cove); beach dates are plotted at their reported altitudes with 2 m vertical error bars to reflect the height of the present day beach (assumed indicative meaning) above mean sea level. As these are limiting dates, the RSL curve should pass beneath the samples forming minimum ages, and above those which form maxima. The line of the curve itself is an inferred curve only. There is evidence for early Holocene RSL rise from modelling and beach geomorphology, but this has not been shown due to the element of uncertainty. Assuming a tectonic uplift rate of 0.22-0.48 m/ka, the RSL highstand includes a tectonic component of between 1.4 and 2.9 m.

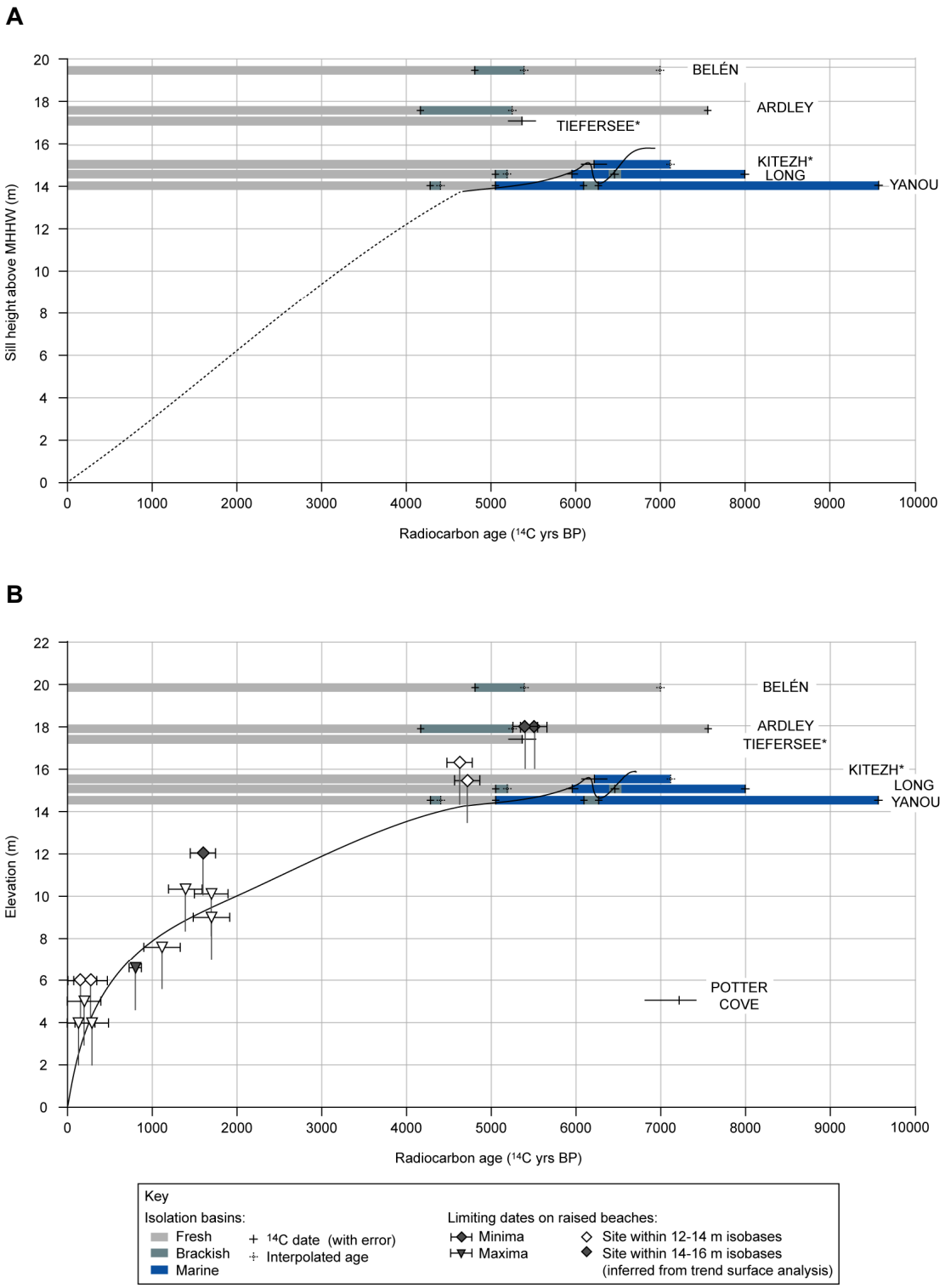
A
Sill height above MHHW (m)
Radiocarbon age (14C yrs BP)
BELÉN
ARDLEY
TIEFERSEE*
KITEZH*
LONG
YANOU
B
Elevation (m)
Radiocarbon age (14C yrs BP)
BELÉN
ARDLEY
TIEFERSEE*
KITEZH*
LONG
YANOU
POTTER
COVE
Key
Isolation basins:
Fresh
Brackish
Marine
14C date (with error)
Interpolated age
Limiting dates on raised beaches:
Minima
Maxima
Site within 12-14 m isobases
Site within 14-16 m isobases
(inferred from trend surface analysis)

A further outcome of this work, although not one of the explicit original aims, has been providing new evidence constraining the deglacial history of Fildes Peninsula. With the recent publication of the SHALDRILL marine core from Maxwell Bay (Milliken *et al.*, 2009) and papers of Yoon *et al*. (Yoon *et al.*, 2000; Khim and Yoon, 2003; Yoon *et al.*, 2004), understanding of the postglacial history of the SSIs from the marine geological record has advanced significantly. This study is complementary and has helped provide constraints on deglaciation from terrestrial evidence.

The two most significant constraints on the deglacial history of Fildes Peninsula are minimum dates of deglaciation from Fildes Peninsula, and the identification of a period of glacial stillstand in the mid-Holocene. Basal dates from isolation basins indicate that the onset of deglaciation of Fildes Peninsula occurred prior to ca. 9500 ^{14}C yr BP, when the south of Peninsula deglaciated. Once the ice margin was grounded on land, it retreated from the south to north, and ice had retreated from the central Peninsula by 8000 ^{14}C yr BP. This is consistent with the evidence from the marine record, with the minimum age of glacial retreat from the outer portion of Maxwell Bay reported to be ca. 13100 ^{14}C yr BP (Milliken *et al.*, 2009). In addition, evidence from isolation basins has been used to suggest that ice retreat did not occur continuously. Following the isolation of both Long and Yanou Lakes by 6250 ^{14}C yr BP, subsequent marine ingressions into both basins suggest ice retreat temporarily stopped causing eustatic sea level rise to outpace the significantly slower rate of isostatic uplift. The glacial stillstand seems to only have been of short duration, with the second isolation of Long Lake at 5950 ^{14}C yr BP indicative of increased rates of isostatic uplift and renewed glacial retreat.

8.3 Wider implications

As stated in the introduction, a large part of the rationale behind this work was to provide field constraints which help to validate numerical models predicting future ice sheet evolution and sea level change. This thesis contributes to the British Antarctic Survey's GRADES research programme (section 1.3), and the RSL curve will be used as an independent record of maximum ice volume changes and postglacial thinning. It helps to address the gap in RSL data from the Antarctic Peninsula region, and the new curve will provide a constraint for glacial isostatic adjustment (GIA) modelling both by GRADES and others. It also feeds directly into the work of Whitehouse, Bentley *et al*.,

who are currently developing a new GIA correction for Antarctic satellite gravity data, and the new RSL curve will be incorporated into this work.

8.4 Recommendations for future work

As with all work in remote, complex and challenging environments, with limited baseline data, there are limitations to this work. These have been discussed in each chapter. Here, I outline how to address some of these limitations in the future and ways to extend this research.

8.4.1 Isolation basins at different elevations and locations

The RSL curve could be constrained further by coring additional isolation basins, covering both a greater range of elevations and sites across the SSIs. Coring was limited to only five basins in this study due to the time available, however it would be useful to get data from additional basins at elevations between 15 and 18 m amsl (the altitudes of Long and Ardley respectively) to further constrain the precise height of the RSL highstand. On Fildes Peninsula, Petrel Lake (400 m northwest of Yanou) and Laguna Hidrógrafos (100 m northwest of Long) were identified during fieldwork as potential isolation basins, at elevations between 15-20 m amsl (SCAR KGIS), but time constraints prevented coring at these sites. It would also be useful to obtain records from lakes outside Fildes Peninsula; there are potential isolation basins on Byers Peninsula (López-Martínez *et al.*, 1996) and the glacier foreland around Jubany Base on Potter Peninsula in front of the Warszawa Icefield.

8.4.2 Additional diatom baseline data

One of the main limitations encountered during analysis of sediment cores was the lack of diatom reference material. A lack of taxonomic precision and consistency, coupled with insufficient data from the sub-Antarctic, meant species were often identified using keys from European or North American sites. Salinity preferences of species were also not always published. Advances have been made in this area (e.g. Van de Vijver *et al.*, 2002; Sterken, 2009), but further work is needed. In particular, the study of contemporary diatom distributions and the sampling of diatoms across the full range of salinities at sites in the SSIs to establish salinity optima of species, like that undertaken

elsewhere (e.g. Jones *et al.*, 1993; Sabbe *et al.*, 2003; Gibson *et al.*, 2006; Smith *et al.*, 2006b).

8.4.3 Further investigation of carbon isotopes as palaeosalinity proxies

This study has demonstrated that carbon isotopes are not always reliable palaeosalinity proxies, especially relative to diatoms. Transitions between marine and freshwater sediments that were identifiable by changes in the diatom assemblage were not distinguishable on the basis of carbon isotope values. Previous studies have shown that it is possible to use stable isotopes to track the presence of fresh and marine water in epishelf lakes (Smith *et al.*, 2006b) and to distinguish between marine and freshwater sediments of Holocene age from isolation basins in Scotland (Mackie *et al.*, 2007). However, this study has demonstrated that this is not always possible, and it would be interesting to investigate further the possible reasons for this by conducting similar isotope analyses elsewhere.

8.4.4 Raised beaches surveys at additional sites across the SSIs

The relatively small number of sites used in the trend surface analysis of raised beaches meant the correlation coefficients of isobase models were low in comparison to polynomial models of isostatic uplift elsewhere with better spatial distribution of data. Time constraints did not allow any more sites to be surveyed during the fieldwork period, but GPS data from additional sites in peripheral areas of the island chain, particularly in the east of King George Island, would improve the accuracy of the isobase model. Key sites to survey would be North Foreland and Turret Point (King George Island), and Barnard Point and northwest Byers Peninsula (Livingston Island), where raised beaches up to 18.5 m amsl have previously been described by John and Sugden (1971).

8.4.5 Further attempts to date the raised beaches

It was not possible in this study to establish an absolute chronology for the formation of the highest Holocene raised beaches, as no dateable material was found preserved in the beaches. However, time only allowed excavations of beach sections at four sites on Fildes Peninsula. If sections could be dug through the highest beaches surveyed elsewhere, then it may be possible to provide dates to constrain the age of beach

formation. There are still problems in associating any dateable material found to RSL (e.g. Hall and Denton, 1999; Hall *et al.*, 2004), but any dates would still afford minimum and maximum age constraints.

Alternatively, it may be possible to date the beaches using optically stimulated luminescence (OSL) dating. Promising results from preliminary studies suggest it is possible to isolate quartz grains from the underside of cobbles from raised beaches and boulder pavements for OSL measurements, to give the time elapsed since the cobbles were last exposed to sunlight when they were turned over in the swash zone at sea level (Kouremenos, 2008; DeWitt *et al.*, 2009; Kouremenos *et al.*, 2009). These studies obtained OSL ages from samples on Ardley Island, Potter Cove and Suffield Point (King George Island) that were internally consistent, with a "zero" age for the modern beach, multiple ages from the same beach ridge agreeing within error limits, and higher beaches dating older than lower beaches from the same site. The OSL technique has the advantages over radiocarbon dating of material being prevalent, longer age ranges, and being unaffected by marine reservoir effects. Therefore, preliminary studies suggest OSL is a robust method for dating raised beaches in areas where material for radiocarbon dating is problematic or unavailable.

8.4.6 Investigate alternative methods of dating platforms to help constrain the long-term tectonic uplift rate

Marine platforms were used as proxies for long-term tectonic uplift, however as no absolute ages have been obtained either in this study or in previously published literature, ages were based purely on assumption. This is a significant limitation in the estimation of the long-term tectonic uplift rate. Elsewhere marine terrace ages have been determined by uranium-series and amino acid dating of fossils associated with them (e.g. Muhs *et al.*, 1990; Bishop, 1991), however no similar dateable fossils were observed on the platforms of the SSIs. Instead it may be possible to follow the methodology adopted by Saillard *et al*. (2009) of using cosmogenic radionuclides (^{10}Be) to date marine platforms in the Chilean Andes (Perg *et al.*, 2001; Kim and Sutherland, 2004). The situation in the SSIs is complicated by multiple periods of ice cover, however if ^{21}Ne was measured as well to give the total exposure time (Alvarez-Marrón *et al.*, 2008), it may be possible to obtain a small set of possible exposure histories and hence uplift rates.

References

ADIAC. *Automatic Diatom Identification and Classification: Diatom Image Database*. <http://rbg-web2.rbge.org.uk/ADIAC/db/Adiacgen.htm>

Adie, R.J. 1964. Geological history. In: Priestley, R.E., Adie, R.J. and Robin, G.D.Q. (Eds.) *Antarctic Research*. Butterworths: London, pp. 118-162.

Al-Handal, A.Y. and Wulff, A. 2008. Marine benthic diatoms from Potter Cove, King George Island, Antarctica. *Botanica Marina*, **51**: 51-68.

Alvarez-Marrón, J., Hetzel, R., Niedennann, S., Menéndez, R. and Marquínez, J. 2008. Origin, structure and exposure history of a wave-cut platform more than 1 Ma in age at the coast of northern Spain: a multiple cosmogenic nuclide approach. *Geomorphology*, **93**: 316-334.

Anderson, J.B. 1999. *Antarctic Marine Geology*. Cambridge Univeristy Press: Cambridge, 289 pp.

Anderson, J.B. and Andrews, J.T. 1999. Radiocarbon constraints on ice sheet advance and retreat in the Weddell Sea, Antarctica. *Geology*, **27**: 179-182.

Anderson, J.B., Shipp, S.S., Lowe, A.L., Wellner, J.S. and Mosola, A.B. 2002. The Antarctic Ice Sheet during the Last Glacial Maximum and its subsequent retreat history: a review. *Quaternary Science Reviews*, **21**: 49-70.

Anderson, N.J., Ryves, D.B., Grauert, M. and McGowan, S. 2004. Holocene paleolimnology of Greenland and the North Atlantic Islands (North of 60^{o}N). In: Pienitz, R., Douglas, M.S.V. and Smol, J.P. (Eds.) *Long-term Environmental Change in Arctic and Antarctic Lakes*. Springer: Dordrecht, pp. 319-347.

Anderson, R.S., Densmore, A.L. and Ellis, M.A. 1999. The generation and degradation of marine terraces. *Basin Research*, **11**: 7-19.

Andrée, M., Oeschger, H., Siegenthaler, U., Riesen, T., Moell, M., Ammann, B. and Tobolski, K. 1986. ^{14}C dating of plant macrofossils in lake sediment. *Radiocarbon*, **28**: 411-416.

Andrews, J.T. 1968. Postglacial rebound in Arctic Canada: similarity and prediction of uplift curves. *Canadian Journal of Earth Sciences*, **5**: 39-47.

Andrews, J.T. 1970. *A Geomorphological study of post-glacial uplift with particular reference to Arctic Canada*. Institute of British Geographers: London, 156 pp.

Andrews, J.T. 1980. Progress in relative sea level and ice sheet reconstructions Baffin Island N.W.T. for the last 125,000 years. In: Mörner, N.-A. (Ed.) *Earth Rheology, Isostasy and Eustasy*. Wiley: Chichester, pp. 175-200.

Andrews, J.T., Domack, E.W., Cunningham, W.L., Leventer, A., Licht, K.J., Jull, A.J.T., DeMaster, D.J. and Jennings, A.E. 1999. Problems and possible solutions concerning radiocarbon dating of surface marine sediments, Ross Sea, Antarctica. *Quaternary Research*, **52**: 206-216.

ANSP. *Algae Image Database, Phycology Section, Patrick Centre for Environmental Research, The Academy of Natural Sciences*. <http://diatom.acnatsci.org/AlgaeImage/>

Arche, A., López-Martínez, J., Serrano, E. and Martínez de Píson, E. 1996. Marine landforms and deposits. In: López-Martínez, J., Thomson, M.R.A., Arche, A., Björck, S., Ellis-Evans, J.C., Hathway, B., Hernández-Cifuentes, F., Hjort, C.,

Ingólfsson, Ó., Ising, J., Lomas, S., Martínez de Píson, E., Serrano, E., Zale, R. and King, S. (Eds.) *Geomorphological map of Byers Peninsula, Livingston Island*. British Antarctic Survey: Cambridge, pp. 35-42, Sheet 5-A, 1:25 000 with supplementary text.

Balco, G., Stone, J.O., Lifton, N.A. and Dunai, T.J. 2008. A complete and easily accessible means of calculating surface exposure ages or erosion rates from ^{10}Be and ^{26}Al measurements. *Quaternary Geochronology*, **3**: 174-195.

Banfield, L.A. and Anderson, J.B. 1995. Seismic facies investigation of the late Quaternary glacial history of Bransfield Basin, Antarctica. In: Cooper, A.K., Barker, P.F. and Brancolini, G. (Eds.) *Geology and Seismic Stratigraphy of the Antarctic Margin. Antarctic Research Series, Volume 68*. American Geophysical Union: Washington, pp. 123-140.

Bárcena, M.A., Gersonde, R., Ledesma, S., Fabrés, J., Calafat, A.M., Canals, M., Sierro, F.J. and Flores, J.A. 1998. Record of Holocene glacial oscillations in Bransfield Basin as revealed by siliceous microfossil assemblages. *Antarctic Science*, **10**: 269-285.

Barker, D.H.N. and Austin, J.A. 1994. Crustal diapirism in Bransfield Strait, West Antarctica: Evidence for distributed extension in marginal-basin formation. *Geology*, **22**: 657-660.

Barker, D.H.N., Christeson, G.L., Austin, J.A. and Dalziel, I.W.D. 2003. Backarc basin evolution and cordilleran orogenesis: Insights from new ocean-bottom seismograph refraction profiling in Bransfield Strait, Antarctica. *Geology*, **31**: 107-110.

Barker, P.F. 1982. The Cenozoic subduction history of the Pacific margin of the Antarctic Peninsula: ridge crest-trench interactions. *Journal of the Geological Society of London*, **139**: 787-801.

Barker, P.F. and Dalziel, I.W.D. 1983. Progress in geodynamics in the Scotia Arc region. In: Cabré, R. (Ed.) *Geodynamics of the eastern Pacific region, Caribbean and Scotia Arcs*. AGU: Washington, pp. 137-170.

Barnekow, L., Possnert, G. and Sandgren, P. 1998. AMS ^{14}C chronologies of Holocene lake sediments in the Abisko area, northern Sweden - a comparison between dated bulk sediment and macrofossil samples. *GFF*, **120**: 59-67.

Barnhardt, W.A., Gehrels, W.R., Belknap, D.F. and Kelley, J.T. 1995. Late Quaternary relative sea-level change in the western Gulf of Maine: Evidence for a migrating glacial forebulge. *Geology*, **23**: 317-320.

Baroni, C. and Orombelli, G. 1991. Holocene raised beaches at Terra Nova Bay, Victoria Land, Antarctica. *Quaternary Research*, **36**: 157-177.

Baroni, C. and Orombelli, G. 1994. Abandoned penguin rookeries as Holocene paleoclimatic indicators in Antarctica. *Geology*, **22**: 23-26.

Baroni, C. and Hall, B.L. 2004. A new Holocene relative sea-level curve for Terra Nova Bay, Victoria Land, Antarctica. *Journal of Quaternary Science*, **19**: 377-396.

Barsch, D. and Mäusbacher, R. 1986a. Beiträge zur Vergletscherungsgeschichte und zur reliefentwicklung der Südshetland Inseln. *Zeitschrift für Geomorphologie Supplement*, **61**: 25-37.

Barsch, D. and Mäusbacher, R. 1986b. New data on the relief development of the South Shetland Islands, Antarctica. *Interdisciplinary Science Reviews*, **11**: 211-218.

Barton, C.M. 1965. The Geology of the South Shetland Islands: III. The stratigraphy of King George Island. *British Antarctic Survey Scientific Reports, No. 44*. 33 pp.

Bassett, S.E., Milne, G.A., Bentley, M.J. and Huybrechts, P. 2007. Modelling Antarctic sea-level data to explore the possibility of a dominant Antarctic contribution to meltwater pulse IA. *Quaternary Science Reviews*, **26**: 2113-2127.

Battarbee, R.W. 1986. Diatom analysis. In: Berglund, B.E. (Ed.) *Handbook of Holocene Palaeoecology and Palaeohydrology*. John Wiley: Chichester, pp. 527-557.

Battarbee, R.W., Carvalho, L., Jones, V.J., Flower, R.J., Cameron, N.G., Bennion, H. and Juggins, S. 2001. Diatoms. In: Smol, J.P., Birks, H.J.B. and Last, W.M. (Eds.) *Tracking Environmental Change Using Lake Sediments. Volume 3: Terrestrial, Algal, and Siliceous Indicators*. Kluwer: Dordrecht, pp. 155-202.

Bednarski, J. 1986. Late Quaternary glacial and sea-level events, Clements Markham Inlet, Northern Ellesmere Island, Arctic Canada. *Canadian Journal of Earth Sciences*, **23**: 1343-1355.

Bednarski, J. 1995. Glacial advances and stratigraphy in Otto Fjord and adjacent areas, Ellesmere Island, Northwest Territories. *Canadian Journal of Earth Sciences*, **32**: 52-64.

Bell, T. 1996. The last glaciation and sea level history of Fosheim peninsula, Ellesmere island, Canadian High Arctic. *Canadian Journal of Earth Sciences*, **33**: 1075-1086.

Benn, D.I. and Evans, D.J.A. 1998. *Glaciers and Glaciation*. Arnold: London, 734 pp.

Bentley, M.J. and Anderson, J.B. 1998. Glacial and marine geological evidence for the ice sheet configuration in the Weddell Sea Antarctic Peninsula region during the Last Glacial Maximum. *Antarctic Science*, **10**: 309-325.

Bentley, M.J. 1999. Volume of Antarctic Ice at the Last Glacial Maximum, and its impact on global sea level change. *Quaternary Science Reviews*, **18**: 1569-1595.

Bentley, M.J., Hodgson, D.A., Smith, J.A. and Cox, N.J. 2005a. Relative sea level curves for the South Shetland Islands and Marguerite Bay, Antarctic Peninsula. *Quaternary Science Reviews*, **24**: 1203-1216.

Bentley, M.J., Hodgson, D.A., Sugden, D.E., Roberts, S.J., Smith, J.A., Leng, M.J. and Bryant, C. 2005b. Early Holocene retreat of the George VI Ice Shelf, Antarctic Peninsula. *Geology*, **33**: 173-176.

Bentley, M.J., Evans, D.J.A., Fogwill, C.J., Hansom, J.D., Sugden, D.E. and Kubik, P.W. 2007. Glacial geomorphology and chronology of deglaciation, South Georgia, sub-Antarctic. *Quaternary Science Reviews*, **26**: 644-677.

Bentley, M.J., Hodgson, D.A., Smith, J.A., Ó Cofaigh, C., Domack, E.W., Larter, R.D., Roberts, S.J., Brachfeld, S., Leventer, A., Hjort, C., Hillenbrand, C.-D. and Evans, J. 2009. Mechanisms of Holocene palaeoenvironmental change in the Antarctic Peninsula region. *Holocene*, **19**: 51-69.

Berkman, P.A. and Forman, S.L. 1996. Pre-bomb radiocarbon and the reservoir correction for calcareous marine species in the Southern Ocean. *Geophysical Research Letters*, **23**: 363-366.

Berkman, P.A., Andrews, J.T., Björck, S., Colhoun, E.A., Emslie, S.D., Goodwin, I.D., Hall, B.L., Hart, C.P., Hirakawa, K., Igarashi, A., Ingólfsson, Ó., López-Martínez, J., Lyons, W.B., Mabin, M.C.G., Quilty, P.G., Taviani, M. and Yoshida, Y. 1998. Circum-Antarctic coastal environmental shifts during the Late Quaternary reflected by emerged marine deposits. *Antarctic Science*, **10**: 345-362.

Bierman, P.R., Marsella, K.A., Patterson, C., Davis, P.T. and Caffee, M. 1999. Mid-Pleistocene cosmogenic minimum-age limits for pre- Wisconsinan glacial surfaces in southwestern Minnesota and southern Baffin island: a multiple nuclide approach. *Geomorphology*, **27**: 25-39.

Bird, M.I., Chivas, A.R., Radnell, C.J. and Burton, H.R. 1991. Sedimentological and stable isotope evolution of lakes in the Vestfold Hills, Antarctica. *Palaeogeography Palaeoclimatology Palaeoecology*, **84**: 109-130.

Birkenmajer, K. 1981. Lichenometric dating of raised marine beaches at Admiralty Bay, King George Island (South Shetland Islands, West Antarctica). *Bulletin de l'Academie Polonaise des Sciences*, **29**: 119-127.

Birkenmajer, K., Ochyra, R., Olsson, I.U. and Stuchlik, L. 1985. Mid-Holocene radiocarbon-date peat at Admiralty Bay, King George Island (South Shetland Islands, West Antarctica). *Bulletin of the Polish Academy of Sciences, Earth Sciences*, **33**: 7-13.

Birkenmajer, K. 1992. Cenozoic glacial history of the South Shetland Islands and northern Antarctic Peninsula. *III Congreso Geológico de España y VIII Congreso Latinoamericano de Geologia*, Salamanca, Spain: pp. 251-260.

Birkenmajer, K. 1998. Quaternary geology at Potter Peninsula, King George Island (South Shetland Islands, West Antarctica). *Bulletin of the Polish Academy of Sciences, Earth Sciences*, **46**: 9-20.

Bishop, D.G. 1991. High-level marine terraces in western and southern New Zealand: indicators of the tectonic tempo of an active continental margin. In: Macdonald, D.I.M. (Ed.) *Sedimentation, Tectonics and Eustasy: Sea-level Changes at Active Margins*. Blackwell: Oxford, pp. 69-78.

Björck, S., Håkansson, H., Zale, R., Karlén, W. and Jönsson, B.L. 1991a. A late Holocene lake sediment sequence from Livingston Island, South Shetland Islands, with paleoclimatic implications. *Antarctic Science*, **3**: 61-72.

Björck, S., Hjort, C., Ingólfsson, Ó. and Skog, G. 1991b. Radiocarbon dates from the Antarctic Peninsula region - problems and potential. *Quaternary Proceedings*, **1**: 55-65.

Björck, S., Malmer, N., Hjort, C., Sandgren, P., Ingólfsson, Ó., Wallen, B., Smith, R.I.L. and Jönsson, B.L. 1991c. Stratigraphic and paleoclimatic studies of a 5500-year-old moss bank on Elephant Island, Antarctica. *Arctic and Alpine Research*, **23**: 361-374.

Björck, S., Sandgren, P. and Zale, R. 1991d. Late Holocene tephrochronology of the northern Antarctic Peninsula. *Quaternary Research*, **36**: 322-328.

Björck, S., Håkansson, H., Olsson, S., Barnekow, L. and Janssens, J. 1993. Palaeoclimatic studies in South Shetland Islands, Antarctica, based on numerous stratigraphic variables in lake sediments. *Journal of Paleolimnology*, **8**: 233-272.

Björck, S., Hjort, C., Ingólfsson, Ó., Zale, R. and Ising, J. 1996a. Holocene deglaciation chronology from lake sediments. In: López-Martínez, J., Thomson, M.R.A., Arche, A., Björck, S., Ellis-Evans, J.C., Hathway, B., Hernández-Cifuentes, F., Hjort, C., Ingólfsson, Ó., Ising, J., Lomas, S., Martínez de Píson, E., Serrano, E., Zale, R. and King, S. (Eds.) *Geomorphological map of Byers Peninsula, Livingston Island*. British Antarctic Survey: Cambridge, pp. 49-51, Sheet 5-A, 1:25 000 with supplementary text.

Björck, S., Olsson, S., Ellis-Evans, C., Håkansson, H., Humlum, O. and deLirio, J.M. 1996b. Late Holocene palaeoclimatic records from lake sediments on James Ross Island, Antarctica. *Palaeogeography Palaeoclimatology Palaeoecology*, **121**: 195-220.

Björck, S., Bennike, O., Possnert, G., Wohlfarth, B. and Digerfeldt, G. 1998. A high-resolution ^{14}C dated sediment sequence from southwest Sweden: age comparisons between different components of the sediment. *Journal of Quaternary Science*, **13**: 85-89.

Björck, S. and Wohlfarth, B. 2001. ^{14}C chronostratigraphic techniques in paleolimnology. In: Last, W.M. and Smol, J.P. (Eds.) *Tracking Environmental Change Using Lake Sediments. Volume 1: Basin Analysis, Coring, and Chronological Techniques*. Kluwer: Dordrecht, pp. 205-245.

Blake, W. 1970. Studies of glacial history in Arctic Canada. I. Pumice, radiocarbon dates, and differential postglacial uplift in the eastern Queen Elizabeth Islands. *Canadian Journal of Earth Sciences*, **7**: 634-664.

Blake, W. 1975. Radiocarbon age determinations and postglacial emergence at Cape Storm, southern Ellesmere Island, Arctic Canada. *Geografiska Annaler*, **57A**: 1-71.

Blake, W. 1992. Holocene emergence at Cape Herschel, East-Central Ellesmere Island, Arctic Canada: Implications for ice sheet configuration. *Canadian Journal of Earth Sciences*, **29**: 1958-1980.

Boulton, G.S., Peacock, J.D. and Sutherland, D.G. 1991. Quaternary. In: Craig, G.Y. (Ed.) *Geology of Scotland* (3rd Edn). The Geological Society: London, pp. 503-543.

Bowman, S. 1990. *Interpreting the Past: Radiocarbon Dating*. British Museum Publications: London, 64 pp.

Boyer, P. and Haywood, E. 2006. Islands of the Southern Ocean. *International Forum on the Sub-Antarctic*, Hobart, July 2006.

Brachfeld, S., Domack, E., Kissel, C., Laj, C., Leventer, A., Ishman, S., Gilbert, R., Camerlenghi, A. and Eglinton, L.B. 2003. Holocene history of the Larsen-A Ice Shelf constrained by geomagnetic paleointensity dating. *Geology*, **31**: 749-752.

Brachfeld, S.A., Banerjee, S.K., Guyodo, Y. and Acton, G.D. 2002. A 13 200 year history of century to millennial-scale paleoenvironmental change magnetically recorded in the Palmer Deep, western Antarctic Peninsula. *Earth and Planetary Science Letters*, **194**: 311-326.

Braun, M. 2001. King George Island, South Shetland Islands, Antarctica: Topographic Map (Satellite Image Map), 1:100 000. Institut für Physische Geographie, Universität Freiburg, Germany and Laboratório de Pesquisas Antárticas e Glaciológicas, Universidade Federal do Rio Grande do Sul, Brazil.

Burckle, L.H. and Cirilli, J. 1987. Origin of diatom ooze belt in the Southern Ocean: implications for late Quaternary paleoceanography. *Micropaleontology*, **33**: 82-86.

Canals, M., Urgeles, R. and Calafat, A.M. 2000. Deep sea-floor evidence of past ice streams off the Antarctic Peninsula. *Geology*, **28**: 31-34.

Chappell, J. 1974. Geology of coral terraces, Huon Peninsula, New Guinea: a study of Quaternary tectonic movements and sea-level changes. *Geological Society of America Bulletin*, **85**: 553-570.

Chivas, A.R., García, A., van der Kaars, S., Couapel, M.J.J., Holt, S., Reeves, J.M., Wheeler, D.J., Switzer, A.D., Murray-Wallace, C.V., Banerjee, D., Price, D.M., Wang, S.X., Pearson, G., Edgar, N.T., Beaufort, L., De Deckker, P., Lawson, E. and Cecil, C.B. 2001. Sea-level and environmental changes since the last interglacial in the Gulf of Carpentaria, Australia: an overview. *Quaternary International*, **83-5**: 19-46.

Chun, H.Y., Chang, S.K. and Lee, J.I. 1994. Biostratigraphic study on the plant fossils from Barton Peninsula and adjacent area. *Journal of the Paleontological Society of Korea*, **10**: 69-84.

Clapperton, C.M. and Sugden, D.E. 1982. Late Quaternary glacial history of George VI Sound area, West Antarctica. *Quaternary Research*, **18**: 243-267.

Clapperton, C.M. and Sugden, D.E. 1988. Holocene glacier fluctuations in South America and Antarctica. *Quaternary Science Reviews*, **7**: 185-198.
Clapperton, C.M. 1990. Quaternary glaciations in the Southern Ocean and Antarctic Peninsula area. *Quaternary Science Reviews*, **9**: 229-252.
Clark, J.A., Farrell, W.E. and Peltier, W.R. 1978. Global changes in postglacial sea level: a numerical calculation. *Quaternary Research*, **9**: 265-287.
Codilean, A.T., Bishop, P., Stuart, F.M., Hoey, T.B., Fabel, D. and Freeman, S.P.H.T. 2008. Single-grain cosmogenic ^{21}Ne concentrations in fluvial sediments reveal spatially variable erosion rates. *Geology*, **36**: 159-162.
Colhoun, E.A., Mabin, M.C.G., Adamson, D.A. and Kirk, R.M. 1992. Antarctic ice volume and contribution to sea-level fall at 20,000 yr BP from raised beaches. *Nature*, **358**: 316-319.
Colman, S.M., Jones, G.A., Rubin, M., King, J.W., Peck, J.A. and Orem, W.H. 1996. AMS radiocarbon analyses from Lake Baikal, Siberia: challenges of dating sediments from a large, oligotrophic lake. *Quaternary Science Reviews*, **15**: 669-684.
Cook, A.J., Fox, A.J., Vaughan, D.G. and Ferrigno, J.G. 2005. Retreating glacier fronts on the Antarctic Peninsula over the past half-century. *Science*, **308**: 541-544.
Corner, G.D., Yevzerov, V.Y., Kolka, V.V. and Moller, J.J. 1999. Isolation basin stratigraphy and Holocene relative sea-level change at the Norwegian-Russian border north of Nikel, northwest Russia. *Boreas*, **28**: 146-166.
Corner, G.D., Kolka, V.V., Yevzerov, V.Y. and Moller, J.J. 2001. Postglacial relative sea-level change and stratigraphy of raised coastal basins on Kola Peninsula, northwest Russia. *Global and Planetary Change*, **31**: 155-177.
Cremer, H., Gore, D., Melles, M. and Roberts, D. 2003a. Palaeoclimatic significance of late Quaternary diatom assemblages from southern Windmill Islands, East Antarctica. *Palaeogeography Palaeoclimatology Palaeoecology*, **195**: 261-280.
Cremer, H., Roberts, D., McMinn, A., Gore, D. and Melles, M. 2003b. The Holocene diatom flora of marine bays in the Windmill Islands, East Antarctica. *Botanica Marina*, **46**: 82-106.
Cremer, H., Gore, D., Hultzsch, N., Melles, M. and Wagner, B. 2004. The diatom flora and limnology of lakes in the Amery Oasis, East Antarctica. *Polar Biology*, **27**: 513-531.
Cromer, L., Gibson, J.A.E., Swadling, K.M. and Ritz, D.A. 2005. Faunal microfossils: Indicators of Holocene ecological change in a saline Antarctic lake. *Palaeogeography, Palaeoclimatology, Palaeoecology*, **221**: 83-97.
Cullingford, R.A., Smith, D.E. and Firth, C.R. 1991. The altitude of the Main Postglacial Shoreline in Eastern Scotland. *Quaternary International*, **9**: 39-52.
Curl, J. 1980. A glacial history of the South Shetland Islands, Antarctica. *Institute of Polar Studies Report 63*. Ohio State University: Columbus.
Dalziel, I.W.D. 1983. The evolution of the Scotia Arc: a review. In: Oliver, R.L., James, P.R. and Jago, J.B. (Eds.) *Antarctic Earth Science*. Cambridge University Press: Cambridge, pp. 283-288.
Dean, W.E. 1974. Determination of carbonate and organic matter in calcareous sediments and sedimentary rocks by loss on ignition: comparison with other methods. *Journal of Sedimentary Petrology*, **44**: 242-248.
Dearing, J.A. 1999. Holocene environmental change from magnetic proxies in lake sediments. In: Maher, B.A. and Thompson, R. (Eds.) *Quaternary Climates, Environments and Magnetism*. Cambridge University Press: Cambridge, pp. 231-278.

Del Valle, R.A., Montalti, D. and Inbar, M. 2002. Mid-Holocene macrofossil-bearing raised marine beaches at Potter Peninsula, King George Island, South Shetland Islands. *Antarctic Science*, **14**: 263-269.

Desilets, D., Zreda, M., Almasi, P.F. and Elmore, D. 2006. Determination of cosmogenic ^{36}Cl in rocks by isotope dilution: innovations, validation and error propagation. *Chemical Geology*, **233**: 185-195.

DeWitt, R., Kouremenos, P., Drewry, A.M. and Simms, A.R. 2009. Dating the light shielded surface of cobbles to reconstruct past sea levels in Antarctica. *Conference on Micro-Raman Spectroscopy and Luminescence Studies in the Earth and Planetary Sciences*, Mainz, Germany.

Dietrich, R., Rulke, A., Ihde, J., Lindner, K., Miller, H., Niemeier, W., Schenke, H.W. and Seeber, G. 2004. Plate kinematics and deformation status of the Antarctic Peninsula based on GPS. *Global and Planetary Change*, **42**: 313-321.

Dillon, W.P. and Oldale, R.N. 1978. Late Quaternary sea-level curve: Reinterpretation based on glaciotectonic influence. *Geology*, **6**: 56-60.

Domack, E., Leventer, A., Dunbar, R., Taylor, F., Brachfeld, S. and Sjunneskog, C. 2001. Chronology of the Palmer Deep site, Antarctic Peninsula: a Holocene palaeoenvironmental reference for the circum-Antarctic. *The Holocene*, **11**: 1-9.

Domack, E.W., Jull, A.J.T. and Nakao, S. 1991. Advance of East Antarctic outlet glaciers during the Hypsithermal: Implications for the volume state of the Antarctic ice sheet under global warming. *Geology*, **19**: 1059-1062.

Domack, E.W., Leventer, A., Root, S., Ring, J., Williams, E., Carlson, D., Hirshorn, E., Wright, W., Gilbert, R. and Burr, G. 2003. Marine sedimentary record of natural environmental variability and recent warming in the Antarctic Peninsula. In: Domack, E., Leventer, A., Burnett, A., Bindschadler, R., Convey, P. and Kirby, M. (Eds.) *Antarctic Peninsula Climate Variability: A Historical and Palaeoenvironmental Perspective. Antarctic Research Series, Volume 79*. American Geophysical Union: Washington, pp. 205-222.

Doran, P.T., Wharton, R.A., Spaulding, S.A. and Foster, J.S. 1994. McMurdo LTER: Paleolimnology of Taylor Valley, Antarctica. *Antarctic Journal of the United States*, **29**: 234-237.

Doran, P.T., Berger, G.W., Lyons, W.B., Wharton, R.A., Davisson, M.L., Southon, J. and Dibb, J.E. 1999. Dating Quaternary lacustrine sediments in the McMurdo Dry Valleys, Antarctica. *Palaeogeography Palaeoclimatology Palaeoecology*, **147**: 223-239.

Douglas, M.S.V., Ludlam, S. and Feeney, S. 1996. Changes in diatom assemblages in Lake C2 (Ellesmere Island, Arctic Canada): response to basin isolation from the sea and to other environmental changes. *Journal of Paleolimnology*, **26**: 217-226.

Douglas, M.S.V. and Smol, J.P. 1999. Freshwater diatoms as indicators of environmental change in the high Arctic. In: Stoermer, E.F. and Smol, J.P. (Eds.) *The Diatoms: Applications for the Environmental and Earth Sciences*. Cambridge University Press: Cambridge, pp. 227-244.

Douglas, M.S.V., Hamilton, P.B., Pienitz, R. and Smol, J.P. 2004. Algal indicators of environmental change in Arctic and Antarctic lakes and ponds. In: Pienitz, R., Douglas, M.S.V. and Smol, J.P. (Eds.) *Long-term Environmental Change in Arctic and Antarctic Lakes*. Springer: Dordrecht, pp. 117-157.

Dreßler, M., Schult, M., Schubert, M. and Buck, J. 2009. Basin elevation and salinity changes: late Holocene development of two freshwater lakes at the Karelian White Sea coast, northwest Russia as reflected in their sediments. *Hydrobiologia*, **631**: 247-266.

Dunne, J., Elmore, D. and Muzikar, P. 1999. Scaling factors for the rates of production of cosmogenic nuclides for geometric shielding and attenuation at depth on sloped surfaces. *Geomorphology*, **27**: 3-11.

Dyke, A.S., Morris, T.F. and Green, D.E.C. 1991. Postglacial tectonic and sea level history of the central Canadian Arctic. *Geological Society of Canada Bulletin*, **397**: 56.

Dyke, A.S. 1993. Glacial and sea level history of Lowther and Griffith Islands, Northwest Territories: a hint of tectonics. *Geographie Physique et Quaternaire*, **47**: 133-145.

Dyke, A.S. 1998. Holocene delevelling of Devon Island, Arctic Canada: implications for ice sheet geometry and crustal response. *Canadian Journal of Earth Sciences*, **35**: 885-904.

Dyke, A.S. and Peltier, W.R. 2000. Forms, response times and variability of relative sea-level curves, glaciated North America. *Geomorphology*, **32**: 315-333.

Eglinton, T.I., Benitez-Nelson, B.C., Pearson, A., McNichol, A.P., Bauer, J.E. and Druffel, E.R.M. 1997. Variability in radiocarbon ages of individual organic compounds from marine sediments. *Science*, **277**: 796-799.

England, J. 1976a. Postglacial isobases and uplift curves from the Canadian and Greenland High Arctic. *Arctic and Alpine Research*, **8**: 61-78.

England, J. 1976b. Late Quaternary glaciation of eastern Queen Elizabeth Islands, N.W.T., Canada: alternative models. *Quaternary Research*, **6**: 185-202.

England, J. 1983. Isostatic adjustments in a full glacial sea. *Canadian Journal of Earth Sciences*, **20**: 895-917.

England, J. 1992. Postglacial emergence in the Canadian High Arctic: integrating glacioisostasy, eustasy, and late deglaciation. *Canadian Journal of Earth Sciences*, **29**: 984-999.

England, J. 1997. Unusual rates and patterns of Holocene emergence, Ellesmere Island, Arctic Canada. *Journal of the Geological Society*, **154**: 781-792.

England, J. 1999. Coalescent Greenland and Innuitian ice during the Last Glacial Maximum: revising the Quaternary of the Canadian High Arctic. *Quaternary Science Reviews*, **18**: 421-456.

England, J., Smith, I.R. and Evans, D.J.A. 2000. The last glaciation of east-central Ellesmere Island, Nunavut: ice dynamics, deglacial chronology, and sea level change. *Canadian Journal of Earth Sciences*, **37**: 1355-1371.

Engstrom, D.R., Fritz, S.C., Almendinger, J.E. and Juggins, S. 2000. Chemical and biological trends during lake evolution in recently deglaciated terrain. *Nature*, **408**: 161-166.

Eronen, M., Glückert, G., Hatakka, L., van de Plassche, O., van der Plicht, J. and Rantala, P. 2001. Rates of Holocene isostatic uplift and relative sea-level lowering of the Baltic in SW Finland based on studies of isolation contacts. *Boreas*, **30**: 17-30.

Evans, D.J.A. 1988. *Glacial geomorphology and late Quaternary history of Phillips Inlet and the Wootton Peninsula, Northwest Ellesmere Island, Canada*. Unpublished PhD Thesis, University of Alberta: 281 pp.

Evans, D.J.A. 1990a. The effect of glacier morphology on surficial geology and glacial stratigraphy in a high arctic mountainous terrain. *Zeitschrift für Geomorphologie*, **34**: 481-503.

Evans, D.J.A. 1990b. The last glaciation and relative sea level history of Northwest Ellesmere Island, Canadian high arctic. *Journal of Quaternary Science*, **5**: 67-82.

Evans, D.J.A. 2005. Ice-marginal terrestrial landsystems: active temperate glacier margins. In: Evans, D.J.A. (Ed.) *Glacial Landsystems*. Hodder Arnold: London, pp. 12-43.

Evans, D.J.A. and Rea, B.R. 2005. Late Weichselian deglaciation and sea level history of St Jonsfjorden, Spitsbergen: a contribution to ice sheet reconstruction. *Scottish Geographical Journal*, **121**: 175-202.

Evans, J., Pudsey, C.J., Ó Cofaigh, C., Morris, P. and Domack, E. 2005. Late Quaternary glacial history, flow dynamics and sedimentation along the eastern margin of the Antarctic Peninsula Ice Sheet. *Quaternary Science Reviews*, **24**: 741-774.

Evans, J.M., Stone, J.O.H., Fifield, L.K. and Cresswell, R.G. 1997. Cosmogenic chlorine-36 production in K-feldspar. *Nuclear Instruments and Methods in Physics Research Section B*, **123**: 334-340.

Fabres, J., Calafat, A., Canals, M., Barcena, M.A. and Flores, J.A. 2000. Bransfield Basin fine-grained sediments: late-Holocene sedimentary processes and Antarctic oceanographic conditions. *Holocene*, **10**: 703-718.

Fabryka-Martin, J.T. 1988. *Production of radionuclides in the earth and their hydrogeologic significance, with emphasis on chlorine-36 and iodine-129*. Unpublished PhD Thesis, University of Arizona.

Fairbanks, R.G. 1989. A 17,000-year glacio-eustatic sea-level record: influence of glacial melting rates on the Younger Dryas event and deep-ocean circulation. *Nature*, **342**: 637-642.

Fanuko, N. 1989. Possible relation between a bloom of *Distephanus speculum* (Silicoflagellata) and anoxia in bottom waters in the Northern Adraitic, 1983. *Journal of Plankton Research*, **11**: 75-84.

Fink, D., Vogt, S. and Hotchkis, M. 2000. Cross-sections for ^{36}Cl from Ti at Ep=35-150 MeV: Applications to in-situ exposure dating. *Nuclear Instruments & Methods in Physics Research Section B*, **172**: 861-866.

Firth, C.R. and Haggart, B.A. 1989. Loch Lomond Stadial and Flandrian shorelines in the inner Moray Firth area, Scotland. *Journal of Quaternary Science*, **4**: 37-50.

Firth, C.R., Smith, D.E. and Cullingford, R.A. 1993. Late Devensian and Holocene glacio-isostatic uplift patterns in Scotland. *Quaternary Proceedings*, **3**: 1-14.

Fleming, K., Johnston, P., Zwartz, D., Yokoyama, Y., Lambeck, K. and Chappell, J. 1998. Refining the eustatic sea-level curve since the last glacial maximum using far- and intermediate-field sites. *Earth and Planetary Science Letters*, **163**: 327-342.

Forman, S.L., Mann, D.H. and Miller, G.H. 1987. Late Weichselian and Holocene relative sea-level history of Bröggerhalvöya, Spitsbergen. *Quaternary Research*, **27**: 41-50.

Forman, S.L. 1990. Postglacial relative sea-level history of northwestern Spitsbergen, Svalbard. *Geological Society of America Bulletin*, **102**: 1580-1590.

Forman, S.L., Lubinski, D., Miller, G.H., Matishov, G.G., Korsun, S., Snyder, J., Herlihy, F., Weihe, R. and Myslivets, V. 1996. Postglacial emergence of western Franz Josef Land, Russia, and retreat of the Barents Sea ice sheet. *Quaternary Science Reviews*, **15**: 77-90.

Forman, S.L., Weihe, R., Lubinski, D., Tarasov, G., Korsun, S. and Matishov, G. 1997. Holocene relative sea-level history of Franz Josef Land, Russia. *Geological Society of America Bulletin*, **109**: 1116-1133.

Fretwell, P.T., Peterson, I.R. and Smith, D.E. 2004. The use of Gaussian trend surfaces for modelling glacio-isostatic crustal rebound. *Scottish Journal of Geology*, **40**: 175-179.

Fretwell, P.T., Hodgson, D.A., Watcham, E.P., Bentley, M.J. and Roberts, S.J. 2010. Holocene isostatic uplift of the South Shetland Islands, Antarctic Peninsula, modelled from raised beaches. *Quaternary Science Reviews*, in press, doi: 10.1016/j.quascirev.2010.04.006.

Fulford-Smith, S.P. and Sikes, E.L. 1996. The evolution of Ace Lake, Antarctica, determined from sedimentary diatom assemblages. *Palaeogeography, Palaeoclimatology, Palaeoecology*, **124**: 73-86.

Galindo-Zaldívar, J., Gamboa, L., Maldonado, A., Nakao, S. and Bochu, Y. 2004. Tectonic development of the Bransfield Basin and its prolongation to the South Scotia Ridge, northern Antarctic Peninsula. *Marine Geology*, **206**: 267-282.

Gambôa, L.A.P. and Maldonado, P.R. 1990. Geophysical Investigations in the Bransfield Strait and in the Bellingshausen Sea - Antarctica. In: St. John, B. (Ed.) *Antarctica as an Exploration Frontier - Hydrocarbon Potential, Geology and Hazards*. American Association of Petroleum Geologists: Tulsa, USA, pp. 127-141.

Geotek Manual. 2008. *Multi-Sensor Core Logger*. <www.geotek.co.uk/ftp/manual.pdf>

Gibson, J.A.E., Trull, T., Nichols, P.D., Summons, R.E. and McMinn, A. 1999. Sedimentation of ^{13}C-rich organic matter from Antarctic sea-ice algae: A potential indicator of past sea-ice extent. *Geology*, **27**: 331-334.

Gibson, J.A.E., Roberts, D. and Van de Vijver, B. 2006. Salinity control of the distribution of diatoms in lakes of the Bunger Hills, East Antarctica. *Polar Biology*, **29**: 694-704.

Gómez, I., Weykam, G., Klöser, H. and Wiencke, C. 1997. Photosynthetic light requirements, metabolic carbon balance and zonation of sublittoral macroalgae from King George Island (Antarctica). *Marine Ecology Progress Series*, **148**: 281-293.

González-Casado, J.M., López-Martínez, J. and Durán, J.J. 1999. Active tectonics and morphostructure at the northern margin of central Bransfield Basin, Hurd Peninsula, Livingston Island (South Shetland Islands). *Antarctic Science*, **11**: 323-331.

Goodwin, I.D. 1993. Holocene deglaciation, sea-level change, and the emergence of the Windmill Islands, Budd Coast, Antarctica. *Quaternary Research*, **40**: 70-80.

Gordon, J.E. and Harkness, D.D. 1992. Magnitude and geographic variation of the radiocarbon content in Antarctic marine life: implications for reservoir corrections in radiocarbon dating. *Quaternary Science Reviews*, **11**: 697-708.

Gore, D.B., Rhodes, E.J., Augustinus, P.C., Leishman, M.R., Colhoun, E.A. and Rees-Jones, J. 2001. Bunger Hills, East Antarctica: Ice free at the Last Glacial Maximum. *Geology*, **29**: 1103-1106.

Gosse, J.C. and Phillips, F.M. 2001. Terrestrial in situ cosmogenic nuclides: theory and application. *Quaternary Science Reviews*, **20**: 1475-1560.

Goudie, A. 1994. *Geomorphological Techniques* (2nd Edn). Routledge: London, 570 pp.

Govorukha, L.S. and Simonov, I.M. 1973. Geograficheskiye issledovaniya na ostrove King-Dzhordzh (vaterloo) [Geographical investigations on King George (Waterloo) Island]. *Infromatsionnyy byulleten Sovetskoy Antarkticheskoy Ekspeditsee [Information Bulletin of the Soviet Antarctic Expedition]*, **85**: 8-15.

Gràcia, E., Canals, M., Farràn, M.L., Sorribas, J. and Pallàs, R. 1997. Central and eastern Bransfield basins (Antarctica) from high-resolution swath-bathymetry data. *Antarctic Science*, **9**: 168-180.

Grimm, E.C. 1987. CONISS: a FORTRAN 77 program for straigraphically constrained cluster analysis by the method of incremental sum of squares. *Computers and Geosciences*, **13**: 13-35.

Hall, B.L. and Denton, G.H. 1999. New relative sea-level curves for the southern Scott Coast, Antarctica: evidence for Holocene deglaciation of the western Ross Sea. *Journal of Quaternary Science*, **14**: 641-650.

Hall, B.L. and Denton, G.H. 2000a. Extent and chronology of the Ross Sea ice sheet and the Wilson Piedmont Glacier along the Scott Coast at and since the last glacial maximum. *Geografiska Annaler*, **82A**: 337-363.

Hall, B.L. and Denton, G.H. 2000b. Radiocarbon chronology of Ross Sea drift, Eastern Taylor Valley, Antarctica: Evidence for a grounded ice sheet in the Ross Sea at the Last Glacial Maximum. *Geografiska Annaler*, **82A**: 305-336.

Hall, B.L. and Henderson, G.M. 2001. Use of uranium-thorium dating to determine past ^{14}C reservoir effects in lakes: examples from Antarctica. *Earth and Planetary Science Letters*, **193**: 565-577.

Hall, B.L. 2003. An overview of late Pleistocene glaciation in the South Shetland Islands. In: Domack, E., Leventer, A., Burnett, A., Bindschadler, R., Convey, P. and Kirby, M. (Eds.) *Antarctic Peninsula Climate Variability. Antarctic Research Series, Volume 79*. American Geophysical Union: Washington, pp. 103-113.

Hall, B.L., Baroni, C. and Denton, G.H. 2004. Holocene relative sea-level history of the Southern Victoria Land Coast, Antarctica. *Global and Planetary Change*, **42**: 241-263.

Hall, B.L. and Perry, E.R. 2004. Variations in ice rafted detritus on beaches in the South Shetland Islands: a possible climate proxy. *Antarctic Science*, **16**: 339-344.

Hall, B.L. 2007. Late-Holocene advance of the Collins Ice Cap, King George Island, South Shetland Islands. *The Holocene*, **17**: 1253-1258.

Hall, B.L. 2009. Holocene glacial history of Antarctica and the sub-Antarctic islands. *Quaternary Science Reviews*, **28**: 2213-2230.

Hansom, J.D. 1979. Radiocarbon dating of a raised beach at 10 m in the South Shetlands. *British Antarctic Survey Bulletin*, **49**: 287-288.

Hansom, J.D. 1983. Shore-platform development in the South Shetland Islands, Antarctica. *Marine Geology*, **53**: 211-229.

Hansom, J.D. and Flint, C.P. 1989. Holocene ice fluctuations on Brabant Island, Antarctic Peninsula. *Antarctic Science*, **1**: 165-166.

Harden, S.L., Demaster, D.J. and Nittrouer, C.A. 1992. Developing sediment geochronologies for high-latitude continental shelf deposits: a radiochemical approach. *Marine Geology*, **103**: 69-97.

Harkness, D.D. 1979. Radiocarbon dates from Antarctica. *British Antarctic Survey Bulletin*, **47**: 43-59.

Harris, P.T., O'Brien, P.E., Sedwick, P. and Truswell, E.M. 1996. Late Quaternary history of sedimentation on the Mac Robertson Shelf, East Antarctica: problems with 14C dating of marine sediment cores. *Papers and Proceedings of the Royal Society of Tasmania*, **130**: 47-53.

Harwood, D.M. and Maruyama, T. 1992. Middle Eocene to Pleistocene diatom biostratigraphy of Southern Ocean sediments from the Kerguelen Plateau, Leg 120. In: Wise, S.W., Schlich, R. and others (Eds.). *Proceedings of the Ocean Drilling Program, Scientific Results, Volume 120*. 683-733 pp.

Hasle, G.R., Medlin, L.K. and Syvertsen, E.E. 1994. *Synedropsis* gen. nov., a genus of araphid diatoms associated with sea ice. *Phycologia*, **33**: 248-270.

Hasle, G.R. and Syvertsen, E.E. 1997. Marine Diatoms. In: Tomas, C.R. (Ed.) *Identifying Marine Phytoplankton*. Academic Press: San Diego, pp. 5-385.

Hayashi, M. and Yoshida, Y. 1994. Holocene raised beaches in the Lützow-Holm Bay region, East Antarctica. *Memoirs of the National Institute of Polar Research, Special Issue*, **50**: 49-84.

Healy, T.R. 1975. Thermokarst - a mechanism of de-icing ice-cored moraines. *Boreas*, **4**: 19-23.

Heiri, O., Lotter, A.F. and Lemcke, G. 2001. Loss on ignition as a method for estimating organic and carbonate content in sediments: reproducibility and comparability of results. *Journal of Paleolimnology*, **25**: 101-110.

Heisinger, B., Lal, D., Jull, A.J.T., Kubik, P., Ivy-Ochs, S., Knie, K. and Nolte, E. 2002. Production of selected cosmogenic radionuclides by muons: 2. Capture of negative muons. *Earth and Planetary Science Letters*, **200**: 357-369.

Hemphill-Haley, E. 1993. Taxonomy of recent and fossil (Holocene) diatoms (Bacillariophyta) from northern Willapa Bay, Washington. *USGS Open File Report 93-289*. 151 pp.

Herczeg, A.L. 1988. Early diagenesis of organic matter in lake sediments: a stable carbon isotope study of pore waters. *Chemical Geology*, **72**: 199-209.

Heroy, D.C. and Anderson, J.B. 2005. Ice-sheet extent of the Antarctic Peninsula region during the Last Glacial Maximum (LGM) - Insights from glacial geomorphology. *Geological Society of America Bulletin*, **117**: 1497-1512.

Heroy, D.C. and Anderson, J.B. 2007. Radiocarbon constraints on Antarctic Peninsula Ice Sheet retreat following the Last Glacial Maximum (LGM). *Quaternary Science Reviews*, **26**: 3286-3297.

Heroy, D.C., Sjunneskog, C. and Anderson, J.B. 2008. Holocene climate change in the Bransfield Basin, Antarctic Peninsula: evidence from sediment and diatom analysis. *Antarctic Science*, **20**: 69-87.

Hijma, M.P. and Cohen, K.M. 2010. Timing and magnitude of the sea-level jump preluding the 8200 yr event. *Geology*, **38**: 275-278.

Hill, M.O. and Gauch, H.G. 1980. Detrended correspondence analysis: an improved ordination technique. *Vegetatio*, **42**: 47-58.

Hillenbrand, C.D., Kuhn, G. and Frederichs, T. 2009. Record of a Mid-Pleistocene depositional anomaly in West Antarctic continental margin sediments: an indicator for ice-sheet collapse? *Quaternary Science Reviews*, **28**: 1147-1159.

Hjort, C., Ingólfsson, Ó., Möller, P. and Lirio, J.M. 1997. Holocene glacial history and sea-level changes on James Ross Island, Antarctic Peninsula. *Journal of Quaternary Science*, **12**: 259-273.

Hjort, C., Bentley, M.J. and Ingolfsson, O. 2001. Holocene and pre-Holocene temporary disappearance of the George VI Ice Shelf, Antarctic Peninsula. *Antarctic Science*, **13**: 296-301.

Hjort, C., Ingólfsson, O., Bentley, M.J. and Björck, S. 2003. The late Pleistocene and Holocene glacial and climate history of the Antarctic Peninsula region as documented by the land and lake sediments - a review. In: Domack, E., Leventer, A., Burnett, A., Bindschadler, R., Convey, P. and Kirby, M. (Eds.) *Antarctic Peninsula Climate Variability. Antarctic Research Series, Volume 79*. American Geophysical Union: Washington, pp. 95-101.

Hodgson, D.A. 1985. The last glaciation of west-central Ellesmere Island, Arctic Archipelago, Canada. *Canadian Journal of Earth Sciences*, **22**: 347-368.

Hodgson, D.A., Noon, P.E., Vyverman, W., Bryant, C.L., Gore, D.B., Appleby, P., Gilmour, M., Verleyen, E., Sabbe, K., Jones, V.J., Ellis-Evans, J.C. and Wood, P.B. 2001a. Were the Larsemann Hills ice-free through the Last Glacial Maximum? *Antarctic Science*, **13**: 440-454.

Hodgson, D.A., Vyverman, W. and Sabbe, K. 2001b. Limnology and biology of saline lakes in the Rauer Islands, eastern Antarctica. *Antarctic Science*, **13**: 255-270.

Hodgson, D.A., McMinn, A., Kirkup, H., Cremer, H., Gore, D., Melles, M., Roberts, D. and Montiel, P. 2003. Colonization, succession, and extinction of marine floras during a glacial cycle: A case study from the Windmill Islands (east Antarctica) using biomarkers. *Paleoceanography*, **18**: 1067, doi:10.1029/2002PA000775.

Hodgson, D.A., Doran, P.T., Roberts, D. and McMinn, A. 2004. Paleolimnological studies from the Antarctic and Subantarctic Islands. In: Pienitz, R., Douglas, M.S.V. and Smol, J.P. (Eds.) *Long-term Environmental Change in Arctic and Antarctic Lakes*. Springer: Dordrecht, pp. 419-474.

Hodgson, D.A., Roberts, D., McMinn, A., Verleyen, E., Terry, B., Corbett, C. and Vyverman, W. 2006. Recent rapid salinity rise in three East Antarctic lakes. *Journal of Paleolimnology*, **36**: 385-406.

Hodgson, D.A., Bentley, M.J., Roberts, S.J., Fretwell, P.T., Watcham, E.P. and Others. 2007. Field Report - Sledge Bravo. British Antarctic Survey: Cambridge: 85 pp.

Hodgson, D.A. and Smol, J.P. 2008. High-latitude paleolimnology. In: Vincent, W.F. and Laybourn-Parry, J. (Eds.) *Polar Lakes and Rivers*. Oxford University Press: New York, pp. 43-64.

Horton, B.P., Corbett, R., Culver, S.J., Edwards, R.J. and Hillier, C. 2006. Modern saltmarsh diatom distributions of the Outer Banks, North Carolina, and the development of a transfer function for high resolution reconstructions of sea level. *Estuarine Coastal and Shelf Science*, **69**: 381-394.

Hughen, K.A., Baillie, M.G.L., Bard, E., Bayliss, A., Beck, J.W., Bertrand, C.J.H., Blackwell, P.G., Buck, C.E., Burr, G.S., Cutler, K.B., Damon, P.E., Edwards, R.L., Fairbanks, R.G., Friedrich, M., Guilderson, T.P., Kromer, B., McCormac, F.G., Manning, S.W., Bronk Ramsey, C., Reimer, P.J., Reimer, R.W., Remmele, S., Southon, J.R., Stuiver, M., Talamo, S., Taylor, F.W., Van Der Plicht, J. and Weyhenmeyer, C.E. 2004. Marine04 marine radiocarbon age calibration, 26-0 ka BP. *Radiocarbon*, **46**: 1059-1086.

Hustedt, F. 1957. Die Diatomeenflora des Flußsystems der Weser im Gebiet der Hansestadt Bremen. *Abhandlungen Herausgegeben vom Naturwissenschaftlicher Verein zu Bremen*, **34**: 181-440.

Huybrechts, P. 2002. Sea-level changes at the LGM from ice-dynamic reconstructions of the Greenland and Antarctic ice sheets during the glacial cycles. *Quaternary Science Reviews*, **21**: 203-231.

Ingólfsson, Ó., Hjort, C., Björck, S. and Smith, R.I.L. 1992. Late Pleistocene and Holocene glacial history of James Ross Island, Antarctic Peninsula. *Boreas*, **21**: 209-222.

Ingólfsson, Ó., Hjort, C., Berkman, P.A., Björck, S., Colhoun, E.A., Goodwin, I.D., Hall, B., Hirakawa, K., Melles, M., Moller, P. and Prentice, M.L. 1998. Antarctic glacial history since the Last Glacial Maximum: an overview of the record on land. *Antarctic Science*, **10**: 326-344.

Ingólfsson, Ó. and Hjort, C. 1999. The Antarctic contribution to Holocene global sea level rise. *Polar Research*, **18**: 323-330.

Ingólfsson, Ó., Hjort, C. and Humlum, O. 2003. Glacial and climate history of the Antarctic Peninsula since the Last Glacial Maximum. *Arctic Antarctic and Alpine Research*, **35**: 175-186.

Ingólfsson, Ó. 2004. Quaternary glacial and climate history of Antarctica. In: Ehlers, J. and Gibbard, P.L. (Eds.) *Quaternary Glaciations: Extent and Chronology, Part III*. Elsevier: Amsterdam, pp. 3-43.

Instituto Antartico Chileno. 1996. Republica de Chile: Isla Rey Jorge-Peninsula Fildes, Islas Shetland del Sur (Fildes Peninsula / King George Island), 1:10 000 topographic map.

Ivins, E.R. and James, T.S. 2005. Antarctic glacial isostatic adjustment: a new assessment. *Antarctic Science*, **17**: 541-553.

Iwai, M. and Winter, D. 2002. Data Report: Taxonomic notes of Neogene diatoms from the western Antarctic Peninsula: Ocean Drilling Program Leg 178. In: Barker, P.F., Camerlenghi, A., Acton, G.D. and Ramsay, A.T.S. (Eds.). *Proceedings of the Ocean Drilling Program, Scientific Results, Volume 178*. 1-57 pp.

Jackson, H.R. and Koppen, L. 1985. The Nares Strait gravity anomaly and its implications for crustal structure. *Canadian Journal of Earth Sciences*, **22**: 1322-1328.

Jamieson, T.F. 1865. On the history of the last geological changes in Scotland. *Quarterly Journal of the Geological Society of London*, **21**: 161-203.

John, B.S. and Sugden, D.E. 1971. Raised marine features and phases of glaciation in the South Shetland Islands. *British Antarctic Survey Bulletin*, **24**: 45-111.

John, B.S. 1972. Evidence from the South Shetland Islands towards a glacial history of West Antarctica. In: Price, R.J. and Sugden, D.E. (Eds.) *Polar Geomorphology*. Institute of British Geographers, Special Publication 4, pp. 75-92.

Johnson, J.S., Smellie, J.L., Nelson, A.E. and Stuart, F.M. 2009. History of the Antarctic Peninsula Ice Sheet since the early Pliocene - Evidence from cosmogenic dating of Pliocene lavas on James Ross Island, Antarctica. *Global and Planetary Change*, **69**: 205-213.

Jones, V.J., Juggins, S. and Ellis-Evans, J.C. 1993. The relationship between water chemistry and surface sediment diatom assemblages in maritime Antarctic lakes. *Antarctic Science*, **5**: 339-348.

Jones, V.J. and Juggins, S. 1995. The construction of a diatom-based chlorophyll a transfer function and its application at three lakes on Signy Island (maritime Antarctic) subject to differing degrees of nutrient enrichment. *Freshwater Biology*, **34**: 433-445.

Jones, V.J. 1996. The diversity, distribution and ecology of diatoms from Antarctic inland waters. *Biodiversity and Conservation*, **5**: 1433-1499.

Jones, V.J., Hodgson, D.A. and Chepstow-Lusty, A. 2000. Palaeolimnological evidence for marked Holocene environmental changes on Signy Island, Antarctica. *Holocene*, **10**: 43-60.

Jouzel, J., Masson-Delmotte, V., Cattani, O., Dreyfus, G., Falourd, S., Hoffmann, G., Minster, B., Nouet, J., Barnola, J.M., Chappellaz, J., Fischer, H., Gallet, J.C., Johnsen, S., Leuenberger, M., Loulergue, L., Luethi, D., Oerter, H., Parrenin, F., Raisbeck, G., Raynaud, D., Schilt, A., Schwander, J., Selmo, E., Souchez, R., Spahni, R., Stauffer, B., Steffensen, J.P., Stenni, B., Stocker, T.F., Tison, J.L., Werner, M. and Wolff, E.W. 2007. Orbital and millennial Antarctic climate variability over the past 800,000 years. *Science*, **317**: 793-796.

Juggins, S. 2007. *C2 Version 1.5: Software for ecological and palaeoecological data analysis and visualisation*.

Kawecka, B. and Olech, M. 1993. Diatom communities in the Vanishing and Ornithologist Creek, King George Island, South Shetland, Antarctica. *Hydrobiologia*, **269/270**: 327-333.

Kawecka, B., Olech, M., Nowogrodzka-Zagórska, M. and Wojtun, B. 1998. Diatom communities in small water bodies at H. Arctowski Polish Antarctic Station (King George Island, South Shetland Islands, Antarctica). *Polar Biology*, **19**: 183-192.

Kelly, M.G., Bennion, H., Cox, E.J., Goldsmith, B., Jamieson, J., Juggins, S., Mann, D.G. and Telford, R.J. 2005. *Common freshwater diatoms of Britain and Ireland: an interactive key*. <http://craticula.ncl.ac.uk/EADiatomKey/html/>

Kendall, R.A., Mitrovica, J.X., Milne, G.A., Tornqvist, T.E. and Li, Y.X. 2008. The sea-level fingerprint of the 8.2 ka climate event. *Geology*, **36**: 423-426.

Khim, B.K., Yoon, H.I., Kim, Y. and Shin, I.C. 2001. Late Holocene stable isotope chronology and meltwater discharge event in Maxwell and Admiralty bays, King George Island, Antarctica. *Antarctic Science*, **13**: 167-173.

Khim, B.K. and Yoon, H.I. 2003. Postglacial marine environmental changes in Maxwell Bay, King George Island, West Antarctica. *Polar Research*, **22**: 341-353.

Khim, B.K., Yoon, H.I., Kang, C.Y. and Zhao, J. 2004. Holocene variations of organic carbon contents in Lake Langer of King George Island, South Shetland Islands, West Antarctica. *Ocean and Polar Research*, **26**: 507-514.

Kim, K.J. and Sutherland, R. 2004. Uplift rate and landscape development in southwest Fiordland, New Zealand, determined using ^{10}Be and ^{26}Al exposure dating of marine terraces. *Geochimica et Cosmochimica Acta*, **68**: 2313-2319.

Kim, Y., Kim, H.-S., Larter, R.D., Camerlenghi, A., Gambôa, L.A.P. and Rudowski, S. 1995. Tectonic deformation in the upper crust and sediments at the South Shetland Trench. In: Cooper, A.K., Barker, P.F. and Brancolini, G. (Eds.) *Geology and Seismic Stratigraphy of the Antarctic Margin, Antarctic Research Series Volume 68*. AGU: Washington, pp. 157-166.

Kirk, J.T.O. 1994. *Light and photosynthesis in aquatic ecosystems* (2nd Edn). Cambridge University Press: Cambridge, 401 pp.

Kirk, R.M. 1991. Raised beaches, late Quaternary sea-levels and deglacial sequences on the Victoria Land coast, Ross Sea, Antarctica. In: Gillieson, D.S. and Fitzsimons, S. (Eds.) *Quaternary Research in Australian Antarctica: Future directions*. Department of Geography and Oceanography, University College, Australia Defence Force Academy: Canberra, pp. 85-105.

Kjemperud, A. 1981. Diatom changes in sediments of basins possessing marine/lacustrine transitions in Frosta, Nord-Trøndelag, Norway. *Boreas*, **10**: 27-38.

Kjemperud, A. 1986. Late Weichselian and Holocene shoreline displacement in the Trondheimsfjord area, central Norway. *Boreas*, **15**: 61-82.

Klinkhammer, G.P., Chin, C.S., Keller, R.A., Dahlmann, A., Sahling, H., Sarthou, G., Petersen, S. and Smith, F. 2001. Discovery of new hydrothermal vent sites in Bransfield Strait, Antarctica. *Earth and Planetary Science Letters*, **193**: 395-407.

Kohly, A. 1998. Diatom flux and species composition in the Greenland Sea and the Norwegian Sea in 1991-1992. *Marine Geology*, **145**: 293-312.

Kouremenos, P. 2008. *Testing the use of OSL on cobbles from the raised beaches of King George Island, Antarctica*. Unpublished MSc Thesis, Oklahoma State University: 68 pp.

Kouremenos, P., Simms, A. and DeWitt, R. 2009. Using OSL to create sea-level curves in Antarctica. *GSA Annual Meeting*, Portland, USA.

Krammer, K. and Lange-Bertalot, H. 1991a. Bacillariophyceae 4. Teil: Achnanthaceae, Kritische Ergänzungen zu Navicula (Lineolate) und Gomphonema. In: Ettl, H., Gärtner, G., Gerloff, J., Heynig, H. and Mollenhauer, D. (Eds.) *Süßwasserflora von Mitteleuropa, Band 2/4*. Gustav Fischer Verlag: Stuttgart, pp. 437.

Krammer, K. and Lange-Bertalot, H. 1991b. Bacillariophyceae 3. Teil: Centrales, Fragilariaceae, Eunotiaceae. In: Ettl, H., Gerloff, J., Heynig, H. and Mollenhauer, D. (Eds.) *Süßwasserflora von Mitteleuropa, Band 2/3*. Gustav Fischer Verlag: Stuttgart, pp. 576.

Krammer, K. and Lange-Bertalot, H. 1997. Bacillariophyceae 1. Teil: Naviculaceae. In: Ettl, H., Gerloff, J., Heynig, H. and Mollenhauer, D. (Eds.) *Süßwasserflora von Mitteleuropa, Band 2/1*. Gustav Fischer Verlag: Jena, pp. 876.

Kulbe, T., Melles, M., Verkulich, S.R. and Pushina, Z.V. 2001. East Antarctic climate and environmental variability over the last 9400 years inferred from marine sediments of the Bunger Oasis. *Arctic Antarctic and Alpine Research*, **33**: 223-230.

Lamb, A.L., Wilson, G.P. and Leng, M.J. 2006. A review of coastal palaeoclimate and relative sea-level reconstructions using $\delta^{13}C$ and C/N ratios in organic material. *Earth Science Reviews*, **75**: 29-57.

Lambeck, K., Smither, C. and Johnston, P. 1998. Sea-level change, glacial rebound and mantle viscosity for northern Europe. *Geophysical Journal International*, **134**: 102-144

Lambeck, K. 1995. Late Devensian and Holocene shorelines of the British Isles and North Sea from models of glacio-hydro-isostatic rebound. *Journal of the Geological Society*, **152**: 437-448.

Lange-Bertalot, H. and Krammer, K. 1989. *Achnanthes: eine Monographie der Gattung mit Definition der Gattung Cocconeis und Nachträgen zu den Naviculaceae*, Bibliotheca Diatomologica, Volume 18. J Cramer: Berlin, 393 pp.

Larter, R.D. 1991. Debate: Preliminary results of seismic reflection investigations and associated geophysical studies in the area of the Antarctic Peninsula. *Antarctic Science*, **3**: 217-222.

Larter, R.D. and Barker, P.F. 1991. Effects of ridge crest-trench interaction on Antarctic-Phoenix spreading: forces on a young subducting plate. *Journal of Geophysical Research*, **96**: 19583-19607.

Last, W.M. and Slezak, L.A. 1986. Paleohydrology, sedimentology, and geochemistry of two meromictic saline lakes in southern Saskatchewan. *Géographie Physique et Quaternaire*, **40**: 5-15.

Lawson, J., Doran, P.T., Kenig, F., Des Marais, D.J. and Priscu, J.C. 2004. Stable carbon and nitrogen isotopic composition of benthic and pelagic organic matter in lakes of the McMurdo Dry Valleys, Antarctica. *Aquatic Geochemistry*, **10**: 269-301.

Lawver, L.A., Keller, R.A., Fisk, M.R. and Strelin, J.A. 1995. Bransfield Strait, Antarctic Peninsula: Active extension behind a dead arc. In: Taylor, B. (Ed.) *Backarc Basins: Tectonics and Magmatism*. Plenum Press: New York, pp. 315-342.

Lawver, L.A., Sloan, B.J., Barker, D.H.N., Ghidella, M., Von Herzen, R.P., Keller, R.A., Klinkhammer, G.P. and Chin, C.S. 1996. Distributed, active extension in Bransfield Basin, Antarctic Peninsula: evidence from multibeam bathymetry. *GSA Today*, **6**: 1-6.

Lee, B.Y., Won, Y. and Oh, S.N. 1997. Meteorological characteristics at King Sejong Station, Antarctica (1988-1996). *Korea Ocean Research and Development Institute Report BSPE*, pp. 571-599.

Lee, J.I., Hur, S.D., Yoo, C.M., Yeo, J.P., Kim, H., Hwang, J., Choe, M.Y., Nam, S.H., Kim, Y., Park, B.K., Zheng, X. and López-Martínez, J. 2002. Explanatory Text of the Geological Map of Barton and Weaver Peninsulas, King George Island, Antarctica. Korea Ocean Research and Development Institute: Seoul, South Korea: 30 pp.

Lee, K., Yoon, S.-K. and Yoon, H.I. 2008. Holocene paleoclimate changes determined using diatom assemblages from Lake Long, King George Island, Antarctica. *Journal of Paleolimnology*, doi: 10.1007/s10933-008-9243-1.

Lemmen, D.S. 1989. The last glaciation of Marvin Peninsula, northern Ellesmere Island, High Arctic Canada. *Canadian Journal of Earth Sciences*, **26**: 2578-2590.

Lemmen, D.S. and England, J. 1992. Multiple glaciations and sea level changes, northern Ellesmere Island, High Arctic Canada. *Boreas*, **21**: 137-152.

Lemmen, D.S., Aitken, A.E. and Gilbert, R. 1994. Early Holocene deglaciation of Expedition and Strand Fjords, Canadian High Arctic. *Canadian Journal of Earth Sciences*, **31**: 943-958.

Leng, M.J. and Marshall, J.D. 2004. Palaeoclimate interpretation of stable isotope data from lake sediment archives. *Quaternary Science Reviews*, **23**: 811-831.

Leng, M.J., Lamb, A.L., Heaton, T.H.E., Marshall, J.D., Wolfe, B.B., Jones, M.D., Holmes, J.A. and Arrowsmith, C. 2005. Isotopes in lake sediments. In: Leng, M.J. (Ed.) *Isotopes in Palaeoenvironmental Research*. Springer: Dordrecht, pp. 147-184.

Li, S.K., Xiao, X., Yin, X.B. and Wang, F.P. 2006. Bacterial community along a historic lake sediment core of Ardley Island, west Antarctica. *Extremophiles*, **10**: 461-467.

Lindsay, D.C. 1971. Vegetation of the South Shetland Islands. *British Antarctic Survey Bulletin*, **25**: 59-83.

Liu, X.D., Sun, L.G., Xie, Z.Q., Yin, X.B. and Wang, Y.H. 2005. A 1300-year record of penguin populations at Ardley Island in the Antarctic, as deduced from the geochemical data in the ornithogenic lake sediments. *Arctic Antarctic and Alpine Research*, **37**: 490-498.

Liu, X.D., Li, H.C., Sun, L.G., Yin, X.B., Zhao, S.P. and Wang, Y.H. 2006. $\delta^{13}C$ and $\delta^{15}N$ in the ornithogenic sediments from the Antarctic maritime as palaeoecological proxies during the past 2000 yr. *Earth and Planetary Science Letters*, **243**: 424-438.

Livermore, R., Balanyá, J.C., Maldonado, A., Martínez, J.M., Rodríguez-Fernández, J., de Galdeano, C.S., Galindo Zaldívar, J., Jabaloy, A., Barnolas, A., Somoza, L., Hernández-Molina, J., Suriñach, E. and Viseras, C. 2000. Autopsy on a dead spreading center: The Phoenix Ridge, Drake Passage, Antarctica. *Geology*, **28**: 607-610.

Lloyd, J. 2000. Combined foraminiferal and thecamoebian environmental reconstruction from an isolation basin in NW Scotland: Implications for sea-level studies. *Journal of Foraminiferal Research*, **30**: 294-305.

Lohne, Ø.S., Bondevik, S., Mangerud, J. and Schrader, H. 2004. Calendar year age estimates of Allerod-Younger Dryas sea-level oscillations at Os, western Norway. *Journal of Quaternary Science*, **19**: 443-464.

Lohne, Ø.S. 2005. *Late Weichselian relative sea-level changes and glacial history in Hordaland, western Norway*. Unpublished PhD Thesis, University of Bergen, Norway.

Lohne, Ø.S., Bondevik, S., Mangerud, J. and Svendsen, J.I. 2007. Sea-level fluctuations imply that the Younger Dryas ice-sheet expansion in western Norway commenced during the Allerød. *Quaternary Science Reviews*, **26**: 2128-2151.

Long, A.J., Roberts, D.H. and Wright, M.R. 1999. Isolation basin stratigraphy and Holocene relative sea-level change on Arveprinsen Ejland, Disko Bugt, West Greenland. *Journal of Quaternary Science*, **14**: 323-345.

Long, A.J., Roberts, D.H. and Rasch, M. 2003. New observations on the relative sea level and deglacial history of Greenland from Innaarsuit, Disko Bugt. *Quaternary Research*, **60**: 162-171.

Long, A.J., Woodroffe, S.A., Dawson, S., Roberts, D.H. and Bryant, C.L. 2009. Late Holocene relative sea level rise and the Neoglacial history of the Greenland ice sheet. *Journal of Quaternary Science*, **24**: 345-359.

López-Martínez, J., Vilaplana, J.M., Martinez de Pisón, E., Calvet, J., Arche, A., Serrat, D. and Pallàs, R. 1992. Geomorphology of selected areas in Livingston Island, South Shetland Islands. *III Congreso Geológico de España y VIII Congreso Latinoamericano de Geologia*, Salamanca, Spain: pp. 271-281.

López-Martínez, J., Thomson, M.R.A., Arche, A., Björck, S., Ellis-Evans, J.C., Hathway, B., Hernández-Cifuentes, F., Hjort, C., Ingólfsson, Ó., Ising, J., Lomas, S., Martínez de Píson, E., Serrano, E., Zale, R. and King, S. 1996. Geomorphological map of Byers Peninsula, Livingston Island. BAS Geomap Series, Sheet 5-A, 1:25 000 with supplementary text, 65 pp. British Antarctic Survey: Cambridge.

López-Martínez, J., Serrano, E. and Lee, J.I. 2002. Geomorphological map of Barton and Weaver Peninsulas, King George Island, Antarctica, 1:10 000. Korea Ocean Research and Development Institute: Seoul, Korea.

Lowe, J.J. 1991. Radiocarbon dating: recent applications and future potential. *Quaternary Proceedings*, **1**: 1-89.

Lundqvist, J., Lilliesköld, M. and Östmark, K. 1995. Glacial and periglacial deposits of the Tumbledown Cliffs area, James Ross Island, West Antarctica. *Geomorphology*, **11**: 205-214.

Lythe, M.B., Vaughan, D.G. and BEDMAP Consortium. 2001. BEDMAP: A new ice thickness and subglacial topographic model of Antarctica. *Journal of Geophysical Research-Solid Earth*, **106**: 11335-11351.

Mackie, E.A.V. 2004. *Environmental and relative sea-level reconstruction from isolation basins in NW Scotland using geochemical techniques*. Unpublished PhD Thesis, University of Durham.

Mackie, E.A.V., Leng, M.J., Lloyd, J.M. and Arrowsmith, C. 2005. Bulk organic $\delta^{13}C$ and C/N ratios as palaeosalinity indicators within a Scottish isolation basin. *Journal of Quaternary Science*, **20**: 303-312.

Mackie, E.A.V., Lloyd, J.M., Leng, M., Bentley, M.J. and Arrowsmith, C. 2007. Assessment of $\delta^{13}C$ and C/N ratios in bulk organic matter as palaeosalinity indicators in Holocene and Lateglacial isolation basin sediments, northwest Scotland. *Journal of Quaternary Science*, **22**: 579-591.

Maldonado, A., Larter, R.D. and Aldaya, F. 1994. Forearc tectonic evolution of the South Shetland Margin, Antarctic Peninsula. *Tectonics*, **13**: 1345-1370.

Martinez-Macchiavello, J.C., Tatur, A., Servant-Vildary, S. and Del Valle, R. 1996. Holocene environmental change in a marine-estuarine-lacustrine sediment sequence, King George Island, South Shetland Islands. *Antarctic Science*, **8**: 313-322.

Maslin, M.A. and Swann, G.E.A. 2005. Isotopes in marine sediments. In: Leng, M.J. (Ed.) *Isotopes in Palaeoenvironmental Research*. Springer: Dordrecht, pp. 227-290.

Mataloni, G. and Tell, G. 2002. Microalgal communities from ornithogenic soils at Cierva Point, Antarctic Peninsula. *Polar Biology*, **25**: 488-491.

Mäusbacher, R., Müller, J. and Schmidt, R. 1989. Evolution of postglacial sedimentation in Antarctic lakes (King George Island). *Zeitschrift für Geomorphologie*, **33**: 219-234.

Mäusbacher, R. 1991. *Die jungquartäre Relief- und Klimageschichte im Bereich der Fildeshalbinsel Süd-Shetland-Inseln, Antartktis*. Unpublished PhD Thesis, Universität Heidelberg: 211 pp.

McCormac, F.G., Hogg, A.G., Blackwell, P.G., Buck, C.E., Higham, T.F.G. and Reimer, P.J. 2004. SHCal04 Southern Hemisphere Calibration 0-11.0 cal Kyr BP. *Radiocarbon*, **46**: 1087-1092.

McGowan, S., Juhler, R.K. and Anderson, N.J. 2008. Autotrophic response to lake age, conductivity and temperature in two West Greenland lakes. *Journal of Paleolimnology*, **39**: 301-317.

McMinn, A. 2000. Late Holocene increase in sea ice extent in fjords of the Vestfold Hills, eastern Antarctica. *Antarctic Science*, **12**: 80-88.

Meehl, G.A., Stocker, T.F., Collins, W.D., Friedlingstein, P., Gaye, A.T., Gregory, J.M., Kitoh, A., Knutti, R., Murphy, J.M., Noda, A., Raper, S.C.B., Watterson, I.G., Weaver, A.J. and Zhao, Z.C. 2007. Global Climate Projections. In: Solomon, S., Qin, D., Manning, M., Chen, Z., Marquis, M., Averyt, K.B., Tignor, M. and Miller, H.L. (Eds.). *Climate Change 2007: The Physical Science Basis. Contribution of Working Group I to the Fourth Assessment Report of the Intergovernmental Panel on Climate Change*. Cambridge University Press: Cambridge: 747-845 pp.

Melles, M., Verkulich, S.R. and Hermichen, W.D. 1994. Radiocarbon dating of lacustrine and marine sediments from the Bunger Hills, East Antarctica. *Antarctic Science*, **6**: 375-378.

Mercer, J.H. 1978. West Antarctic ice sheet and CO_2 greenhouse effect: a threat of disaster. *Nature*, **271**: 321-325.

Meteorological Office. 1997. *Climate Change and its impacts: a global perspective*. <http://www.metoffice.gov.uk/research/hadleycentre/pubs/brochures/COP3.pdf>

Meyers, P.A. 1994. Preservation of elemental and isotopic source identification of sedimentary organic matter. *Chemical Geology*, **114**: 289-302.

Meyers, P.A. 1997. Organic geochemical proxies of paleoceanographic, paleolimnologic, and paleoclimatic processes. *Organic Geochemistry*, **27**: 213-250.

Michalchuk, B.R., Anderson, J.B., Wellner, J.S., Manley, P.L., Majewski, W. and Bohaty, S. 2009. Holocene climate and glacial history of the northeastern Antarctic Peninsula: the marine sedimentary record from a long SHALDRIL core. *Quaternary Science Reviews*, **28**: 3049-3065.

Miettinen, A. 2004. Holocene sea-level changes and glacio-isostasy in the Gulf of Finland, Baltic Sea. *Quaternary International*, **120**: 91-104.

Milliken, K.T., Anderson, J.B., Wellner, J.S., Bohaty, S.M. and Manley, P.L. 2009. High-resolution climate record from Maxwell Bay, South Shetland Islands, Antarctica. *Geological Society of America Bulletin*, **121**: 1711-1725.

Milne, G., Bradley, S., Mitrovica, J., Zong, Y. and Horton, B. 2009. Interpreting far-field Holocene sea-level records: constraining the eustatic signal. *IGCP Project 495 Conference*, South Carolina.

Miura, H., Maemoku, H., Igarashi, A. and Moriwaki, K. 1998a. *Late Quaternary raised beach deposits and radiocarbon dates of marine fossils around Lutzow-Holm Bay*, Special Map Series of National Institute of Polar Research No. 6. National Institute of Polar Research: Tokyo, 46 pp.

Miura, H., Maemoku, H., Seto, K. and Moriwaki, K. 1998b. Late Quaternary East Antarctic melting event in the Sôya Coast region based on stratigraphy and oxygen isotopic ratio of fossil molluscs. *Polar Geoscience*, **11**: 260-274.

Miura, H., Moriwaki, K., Maemoku, H. and Hirakawa, K. 1998c. Fluctuations of the East Antarctic ice-sheet margin since the last glaciation from the stratigraphy of raised beach deposits along the Sôya Coast. *Annals of Glaciology*, **27**: 297-301.

Møller, J.J. 1986. Holocene transgression maximum about 6000 years BP at Ramså, Vesterålen, North Norway. *Norsk Geografisk Tidsskrift*, **40**: 77-87.

Moreton, S.G., Rosqvist, G.C., Davies, S.J. and Bentley, M.J. 2004. Radiocarbon reservoir ages from freshwater lakes, South Georgia, sub-Antarctic: modern analogues from particulate organic matter and surface sediments. *Radiocarbon*, **46**: 621-626.

Muhs, D.R., Kelsey, H.M., Miller, G.H., Kennedy, G.L., Whelan, J.F. and Mcinelly, G.W. 1990. Age estimates and uplift rates for late Pleistocene marine terraces: southern Oregon portion of the Cascadia Forearc. *Journal of Geophysical Research*, **95**: 6685-6698.

Müller, A. and Voss, M. 1999. The palaeoenvironments of coastal lagoons in the southern Baltic Sea, II. $\delta^{13}C$ and $\delta^{15}N$ ratios of organic matter - sources and sediments. *Palaeogeography, Palaeoclimatology, Palaeoecology*, **145**: 17-32.

Nakada, M. and Lambeck, K. 1988. The melting history of the late Pleistocene Antarctic ice sheet. *Nature*, **333**: 36-40.

Nakada, M., Kimura, R., Okuno, J., Moriwaki, K., Miura, H. and Maemoku, H. 2000. Late Pleistocene and Holocene melting history of the Antarctic ice sheet derived from sea-level variations. *Marine Geology*, **167**: 85-103.

Nesje, A. and Dahl, S.O. 1990. Autochthonous block fields in southern Norway: implications for the geometry, thickness, and isostatic loading of the late Weichselian Scandinavian Ice Sheet. *Journal of Quaternary Science*, **5**: 225-234.

Nicholls, R.J., Tol, R.S.J. and Vafeidis, A.T. 2008. Global estimates of the impact of a collapse of the West Antarctic ice sheet: an application of FUND. *Climatic Change*, **91**: 171-191.

Ó Cofaigh, C. 1999. Holocene emergence and shoreline delevelling, southern Eureka Sound, High Arctic Canada. *Géographie Physique et Quaternaire*, **53**: 235-247.

Ó Cofaigh, C., Dowdeswell, J.A., Allen, C.S., Hiemstra, J.F., Pudsey, C.J., Evans, J. and Evans, D.J.A. 2005a. Flow dynamics and till genesis associated with a marine-based Antarctic palaeo-ice stream. *Quaternary Science Reviews*, **24**: 709-740.

Ó Cofaigh, C., Larter, R.D., Dowdeswell, J.A., Hillenbrand, C.D., Pudsey, C.J., Evans, J. and Morris, P. 2005b. Flow of the West Antarctic Ice Sheet on the continental margin of the Bellingshausen Sea at the Last Glacial Maximum. *Journal of Geophysical Research*, **110**: 1-13.

Ochyra, R. 1998. *The Moss Flora of King George Island, Antarctica*. Polish Academy of Sciences: Cracow, 278 pp.

Ohtsuka, T., Kudoh, S., Imura, S. and Ohtani, S. 2006. Diatoms composing benthic microbial mats in freshwater lakes of Skarvsnes ice-free area, East Antarctica. *Polar Bioscience*, **20**: 113-130.

Olech, M. 2002. Plant communities on King George Island. In: Beyer, L. and Bölter, M. (Eds.) *Geoecology of Antarctic Ice-Free Coastal Landscapes*. Springer-Verlag: Berlin, pp. 215-231.

Omoto, K. 1983. The problem and significance of radiocarbon geochronology in Antarctica. In: Oliver, R.L., James, P.R. and Jago, J.B. (Eds.) *Antarctic Earth Science*. Australian Academy of Science: Canberra, pp. 450-452.

Oppenheim, D.R. and Ellis-Evans, J.C. 1989. Depth-related changes in benthic diatom assemblages of a maritime Antarctic lake. *Polar Biology*, **9**: 525-532.

Oppenheim, D.R. 1990. A preliminary study of benthic diatoms in contrasting lake environments. In: Kerry, K.R. and Hempel, G. (Eds.) *Antarctic Ecosystems: Ecological Change and Conservation*. Springer-Verlag: Berlin, pp. 91-99.

Oppenheim, D.R. and Greenwood, R. 1990. Epiphytic diatoms in two freshwater maritime Antarctic lakes. *Freshwater Biology*, **24**: 303-314.

Oppenheimer, M. 1998. Global warming and the stability of the West Antarctic Ice Sheet. *Nature*, **393**: 325-332.

Pallàs, R. 1993. *Evolució geològica recent de la Península Hurd (Illa Livingston, Shetland del Sud, Antàrtida): Anàlisi estructural i geomorfològica*. Unpublished MSc Thesis, Universitat de Barcelona: 120 pp.

Pallàs, R., Vilaplana, J.M. and Sàbat, F. 1995. Geomorphological and neotectonic features of Hurd Peninsula, Livingston Island, South Shetland Islands. *Antarctic Science*, **7**: 395-406.

Pallàs, R., James, T.S., Sàbat, F., Vilaplana, J.M. and Grant, D.R. 1997. Holocene uplift in the South Shetland Islands: evaluation of tectonics and glacio-isostasy. In: Ricci, C.A. (Ed.) *The Antarctic Region: Geological Evolution and Processes*. Terra Antarctica Publication: Siena, pp. 861-868.

Pankhurst, R.J. and Smellie, J.L. 1983. K-Ar geochronology of the South Shetland Islands, Lesser Antarctica: Apparent lateral migration of Jurassic to Quaternary island arc volcanism. *Earth and Planetary Science Letters*, **66**: 214-222.

Patrick, R. and Reimer, C.W. 1966. *The Diatoms of the United States, Volume 1*. The Academy of Natural Sciences of Philadelphia: Pennsylvania, 688 pp.

Patrick, R. and Reimer, C.W. 1975. *The Diatoms of the United States, Volume 2*. The Academy of Natural Sciences of Philadelphia: Pennsylvania, 213 pp.

Patterson, R.T., Dalby, A.P., Roe, H.M., Guilbault, J.P., Hutchinson, I. and Clague, J.J. 2005. Relative utility of foraminifera, diatoms and macrophytes as high resolution indicators of paleo-sea level in coastal British Columbia, Canada. *Quaternary Science Reviews*, **24**: 2002-2014.

Pelayo, A.M. and Wiens, D.A. 1989. Seismotectonics and relative plate motions in the Scotia Sea region. *Journal of Geophysical Research*, **94**: 7293-7320.

Peltier, W.R. 1994. Ice age paleotopography. *Science*, **265**: 195-201.

Perg, L.A., Anderson, R.S. and Finkel, R.C. 2001. Use of a new ^{10}Be and ^{26}Al inventory method to date marine terraces, Santa Cruz, California, USA. *Geology*, **29**: 879-882.

Peter, H.-U., Buesser, C., Mustafa, O. and Pfeiffer, S. 2008. Risk assessment for the Fildes Peninsula and Ardley Island, and development of management plans for their designation as Specially Protected or Specially Managed Areas. Federal Environmental Agency: 508 pp.

Phillips, F.M. and Plummer, M.A. 1996. CHLOE: A program for interpreting in-situ cosmogenic nuclide data for surface exposure dating and erosion studies. *Abstracts of the 7th International Conference on Accelerator Mass Spectrometry*, Tucson, Arizona: pp. 98-99.

Phillips, F.M., Stone, W.D. and Fabryka-Martin, J.T. 2001. An improved approach to calculating low-energy cosmic-ray neutron fluxes near the land/atmosphere interface. *Chemical Geology*, **175**: 689-701.

Pickard, J., Adamson, D.A. and Heath, C.W. 1986. The evolution of Watts Lake, Vestfold Hills, East Antarctica, from marine inlet to freshwater lake. *Palaeogeography, Palaeoclimatology, Palaeoecology*, **53**: 271-288.

Pienitz, R., Lortie, G. and Allard, M. 1991. Isolation of lacustrine basins and marine regression in the Kuujjuaq Area (northern Quebec), as inferred from diatom analysis. *Géographie Physique et Quaternaire*, **45**: 155-174.

Plafker, G. 1965. Tectonic deformation associated with the 1964 Alaska earthquake. *Science*, **148**: 1675-1687.

Pope, P.G. and Anderson, J.B. 1992. Late Quaternary glacial history of the northern Antarctic Peninsula's western continental shelf. In: Elliot, D.H. (Ed.) *Evidence from the Marine Record, Contributions to Antarctic Research III. Antarctic Research Series, Volume 57*. American Geophysical Union: Washington DC, pp. 63-91.

Preuss, H. 1979. Progress in computer evaluation of sea level data within the IGCP Project no. 61. *Proceedings of the 1978 International Symposium of Coastal Evolution in the Quaternary*, pp.104-134.

Pritchard, H.D. and Vaughan, D.G. 2007. Widespread acceleration of tidewater glaciers on the Antarctic Peninsula. *Journal of Geophysical Research-Earth Surface*, **112**: F03S29.

Pudsey, C.J., Barker, P.F. and Larter, R.D. 1994. Ice sheet retreat from the Antarctic Peninsula shelf. *Continental Shelf Research*, **14**: 1647-1675.

Pudsey, C.J. and Evans, J. 2001. First survey of Antarctic sub-ice shelf sediments reveals mid-Holocene ice shelf retreat. *Geology*, **29**: 787-790.

Quinlan, G. and Beaumont, C. 1981. A comparison of observed and theoretical post-glacial relative sea-level in Atlantic Canada. *Canadian Journal of Earth Sciences*, **18**: 1146-1163.

Rabassa, J. 1983. Stratigraphy of the glacigenic deposits in James Ross Island, Antarctic Peninsula. In: Evenson, E., Schlüchter, C. and Rabassa, J. (Eds.) *Tills and Related Deposits*. A. A. Balkema: Rotterdam, pp. 329-340.

Rau, G.H., Takahashi, T. and Marais, D.J.D. 1989. Latitudinal variations in plankton $\delta^{13}C$: Implications for CO_2 and productivity in past oceans. *Nature*, **341**: 516-518.

Reimer, P.J. 2009. *Marine Reservoir Correction Database*. <http://www.calib.qub.ac.uk/marine>

Retelle, M.J. 1986. Stratigraphy and sedimentology of high arctic coastal lacustrine basins, northeastern Ellesmere Island, Northwest Territories. *Géographie Physique et Quaternaire*, **40**: 117-128.

Retelle, M.J., Bradley, R.S. and Stuckenrath, R. 1989. Relative sea level chronology determined from raised marine sediments and coastal isolation basins, northeastern Ellesmere Island, Arctic Canada. *Arctic and Alpine Research*, **21**: 113-125.

Rignot, E., Vaughan, D.G., Schmeltz, M., Dupont, T. and MacAyeal, D. 2002. Acceleration of Pine Island and Thwaites Glaciers, West Antarctica. *Annals of Glaciology*, **34**: 189-194.

Rignot, E. 2006. Changes in ice dynamics and mass balance of the Antarctic ice sheet. *Philosophical Transactions of the Royal Society A-Mathematical Physical and Engineering Sciences*, **364**: 1637-1655.

Rignot, E. 2008. Changes in West Antarctic ice stream dynamics observed with ALOS PALSAR data. *Geophysical Research Letters*, **35**: L12505, doi:10.1029/2008GL033365.

Roberts, D. and McMinn, A. 1996. Relationships between surface sediment diatom assemblages and water chemistry gradients in saline lakes of the Vestfold Hills, Antarctica. *Antarctic Science*, **8**: 331-341.

Roberts, D. and McMinn, A. 1998. A weighted-averaging regression and calibration model for inferring lakewater salinity from fossil diatom assemblages in saline lakes of the Vestfold hills: a new tool for interpreting Holocene lake histories in Antarctica. *Journal of Paleolimnology*, **19**: 99-113.

Roberts, D. and McMinn, A. 1999. A diatom-based palaeosalinity history of Ace Lake, Vestfold Hills, Antarctica. *Holocene*, **9**: 401-408.

Roberts, D., McMinn, A. and Zwartz, D. 2000. An initial palaeosalinity history of Jaw Lake, Bunger Hills based on a diatom-salinity transfer function applied to sediment cores. *Antarctic Science*, **12**: 172-176.

Roberts, D., McMinn, A., Cremer, H., Gore, D.B. and Melles, M. 2004. The Holocene evolution and palaeosalinity history of Beall Lake, Windmill Islands (East Antarctica) using an expanded diatom-based weighted averaging model. *Palaeogeography Palaeoclimatology Palaeoecology*, **208**: 121-140.

Roberts, S.J., Hodgson, D.A., Balbo, A., Vyverman, W., Verleyen, E., Sterken, M., Vanwichelen, J., Heirman, K., Diaz, C., Bentley, M.J., Smith, J.A., Watcham, E.P., Fox, A. and Fretwell, P.T. 2007. Palaeoenvironmental change on the Antarctic Peninsula from lake sediments. *INQUA Congress*, Cairns, Australia.

Robertson Maurice, S.D., Wiens, D.A., Shore, P.J., Vera, E. and Dorman, L.M. 2003. Seismicity and tectonics of the South Shetland Islands and Bransfield Strait from a regional broadband seismograph deployment. *Journal of Geophysical Research*, **108**: doi:10.1029/2003JB002416.

Rosqvist, G.C. and Schuber, P. 2003. Millennial-scale climate changes on South Georgia, Southern Ocean. *Quaternary Research*, **59**: 470-475.

Sabbe, K. and Vyverman, W. 1995. Taxonomy, morphology and ecology of some widespread representatives of the diatom genus *Opephora*. *European Journal of Phycology*, **30**: 235-249.

Sabbe, K., Verleyen, E., Hodgson, D.A., Vanhoutte, K. and Vyverman, W. 2003. Benthic diatom flora of freshwater and saline lakes in the Larsemann Hills and Rauer Islands, East Antarctica. *Antarctic Science*, **15**: 227-248.

Saillard, M., Hall, S.R., Audin, L., Farber, D.L., Herail, G., Martinod, J., Regard, V., Finkel, R.C. and Bondoux, F. 2009. Non-steady long-term uplift rates and Pleistocene marine terrace development along the Andean margin of Chile (31°S) inferred from ^{10}Be dating. *Earth and Planetary Science Letters*, **277**: 50-63.

Sandgren, P. and Snowball, I. 2001. Application of mineral magnetic techniques to paleolimnology. In: Last, W.M. and Smol, J.P. (Eds.) *Tracking Environmental Change Using Lake Sediments. Volume 2: Physical and Geochemical Methods*. Kluwer: Dordrecht, pp. 217-237.

Satake, K., Shimazaki, K., Tsuji, Y. and Ueda, K. 1996. Time and size of a giant earthquake in Cascadia inferred from Japanese tsunami records of January 1700. *Nature*, **379**: 246-249.

SCAR. 2009. *Composite Gazetteer of Antarctica*. <http://data.add.gov.au/aadc/gaz/scar>

SCAR KGIS. *King George Island GIS Project*. <http://www.kgis.scar.org/>

Scherer, R.P., Aldahan, A., Tulaczyk, S., Possnert, G., Engelhardt, H. and Kamb, B. 1998. Pleistocene collapse of the West Antarctic ice sheet. *Science*, **281**: 82-85.

Schidlowski, M., Gorzawski, H. and Dor, I. 1994. Carbon isotope variations in a solar pond microbial mat: Role of environmental gradients as steering variables. *Geochimica et Cosmochimica Acta*, **58**: 2289-2298.

Schimmelpfennig, I., Benedetti, L., Finkel, R., Pik, R., Blard, P.H., Bourlès, D., Burnard, P. and Williams, A. 2009. Sources of in-situ ^{36}Cl in basaltic rocks. Implications for calibration of production rates. *Quaternary Geochronology*, **4**: 441-461.

Schmidt, R., Mäusbacher, R. and Muller, J. 1990. Holocene diatom flora and stratigraphy from sediment cores of two Antarctic lakes (King George Island). *Journal of Paleolimnology*, **3**: 55-74.

Seong, Y.B., Lim, H.S., Yoon, H.I., Lee, Y.I., Kim, Y. and Owen, L.A. 2006. A preliminary geomorphic overview of late Quaternary glacier fluctuations in the

South Shetland Islands, West Antarctica. *Journal of the Korean Geographical Society*, **41**: 513-526.
Seong, Y.B., Owen, L.A., Lim, H.S., Yoon, H.I., Kim, Y., Lee, Y.I. and Caffee, M.W. 2009. Rate of late Quaternary ice-cap thinning on King George Island, South Shetland Islands, West Antarctica defined by cosmogenic ^{36}Cl surface exposure dating. *Boreas*, **38**: 207-213.
Shackleton, N.J. 1987. Oxygen isotopes, ice volume and sea level. *Quaternary Science Reviews*, **6**: 183-190.
Shen, Y.B., Chen, X.B., Yang, S.R., Sun, X.C., Gou, Y.X., Lan, X., Lin, Q.B. and Pan, H.Z. 1998. Late Quaternary biotic assemblages and their environments of core A from Yan'ou Lake on King George Island, Antarctica. *Acta Palaeontologica Sinica*, **37**: 261-268.
Shennan, I. 1982. Interpretation of Flandrian sea-level data from Fenland, England. *Proceedings of the Geologists' Association*, **98**: 53-63.
Shennan, I., Innes, J.B., Long, A.J. and Zong, Y.Q. 1994. Late Devensian and Holocene relative sea-level changes at Loch nan Eala, near Arisaig, Northwest Scotland. *Journal of Quaternary Science*, **9**: 261-283.
Shennan, I., Green, F., Innes, J., Lloyd, J., Rutherford, M. and Walker, K. 1996. Evaluation of rapid relative sea-level changes in north-west Scotland during the last glacial-interglacial transition: evidence from Ardtoe and other isolation basins. *Journal of Coastal Research*, **12**: 862-874.
Shennan, I., Lambeck, K., Horton, B., Innes, J., Lloyd, J., McArthur, J., Purcell, T. and Rutherford, M. 2000. Late Devensian and Holocene records of relative sea-level changes in northwest Scotland and their implications for glacio-hydro-isostatic modelling. *Quaternary Science Reviews*, **19**: 1103-1135.
Shennan, I. and Horton, B. 2002. Holocene land- and sea-level changes in Great Britain. *Journal of Quaternary Science*, **17**: 511-526.
Shennan, I., Hamilton, S., Hillier, C. and Woodroffe, S. 2005. A 16,000-year record of near-field relative sea-level changes, northwest Scotland, United Kingdom. *Quaternary International*, **133-34**: 95-106.
Shennan, I. 2009. Late Quaternary sea-level changes and palaeoseismology of the Bering Glacier region, Alaska. *Quaternary Science Reviews*, **28**: 1762-1773.
Shevenell, A.E., Domack, E.W. and Kernan, G.M. 1996. Record of Holocene palaeoclimate change along the Antarctic Peninsula: evidence from glacial-marine sediments, Lallemand Fjord. *Papers and Proceedings of the Royal Society of Tasmania*, **130**: 55-64.
Shotton, F.W., Blundell, D.J. and Williams, R.E.G. 1968. Birmingham University radiocarbon dates II. *Radiocarbon*, **10**: 200-206.
Smellie, J.L., Pankhurst, R.J., Thomson, M.R.A. and Davies, R.E.S. 1984. The geology of the South Shetland Islands: VI. Stratigraphy, geochemistry and evolution. *British Antarctic Survey Scientific Reports, No. 87*. 85 pp.
Smith, D.E., Cullingford, R.A. and Firth, C.R. 2000. Patterns of isostatic land uplift during the Holocene: evidence from mainland Scotland. *Holocene*, **10**: 489-501.
Smith, D.E., Fretwell, P.T., Cullingford, R.A. and Firth, C.R. 2006a. Towards improved empirical isobase models of Holocene land uplift for mainland Scotland, UK. *Philosophical Transactions of the Royal Society A*, **364**: 949-972.
Smith, J.A., Hodgson, D.A., Bentley, M.J., Verleyen, E., Leng, M.J. and Roberts, S.J. 2006b. Limnology of two Antarctic epishelf lakes and their potential to record periods of ice shelf loss. *Journal of Paleolimnology*, **35**: 373-394.
Smith, J.A., Bentley, M.J., Hodgson, D.A., Roberts, S.J., Leng, M.J., Lloyd, J.M., Barrett, M.S., Bryant, C. and Sugden, D.E. 2007. Oceanic and atmospheric

forcing of early Holocene ice shelf retreat, George VI Ice Shelf, Antarctica Peninsula. *Quaternary Science Reviews*, **26**: 500-516.

Snyder, J.A., Forman, S.L., Mode, W.N. and Tarasov, G.A. 1997. Postglacial relative sea-level history: sediment and diatom records of emerged coastal lakes, north-central Kola Peninsula, Russia. *Boreas*, **26**: 329-346.

Solomon, S., Qin, D., Manning, M., Alley, R.B., Berntsen, T., Bindoff, N.L., Chen, Z., Chidhaisong, A., Gregory, J.M., Hegerl, G.C., Heimann, B., Hewitson, B., Hoskins, B.J., Joos, F., Jouzel, J., Kattsov, V., Lohmann, U., Matsuno, T., Molina, M., Nicholls, N., Overpeck, J., Raga, G., Ramaswamy, V., Ren, J., Rusticucci, M., Somerville, R., Stocker, T.F., Whetton, P., Wood, R.A. and Wratt, D. 2007. Technical Summary. In: Solomon, S., Qin, D., Manning, M., Chen, Z., Marquis, M., Averyt, K.B., Tignor, M. and Miller, H.L. (Eds.). *Climate Change 2007: The Physical Science Basis. Contribution of Working Group I to the Fourth Assessment Report of the Intergovernmental Panel on Climate Change*. Cambridge University Press: Cambridge: 19-91 pp.

Sparrenbom, C.J., Bennike, O., Björck, S. and Lambeck, K. 2006a. Relative sea-level changes since 15 000 cal. yr BP in the Nanortalik area, southern Greenland. *Journal of Quaternary Science*, **21**: 29-48.

Sparrenbom, C.J., Bennike, O., Björck, S. and Lambeck, K. 2006b. Holocene relative sea-level changes in the Qaqortoq area, southern Greenland. *Boreas*, **35**: 171-187.

Spaulding, S., Esposito, R., Lubinski, D., Horn, S., Cox, M., McKnight, D., Alger, A., Hall, B., Mayernick, M., Whittaker, T. and Yang, C. *Antarctic Freshwater Diatoms, McMurdo Dry Valleys Long-Term Ecological Research*. <http://huey.colorado.edu/diatoms/>

Spaulding, S.A. and McKnight, D.M. 1999. Diatoms as indicators of environmental change in antarctic freshwaters. In: Stoermer, E.F. and Smol, J.P. (Eds.) *The Diatoms: Applications for the Environmental and Earth Sciences*. Cambridge University Press: Cambridge, pp. 245-263.

Squyres, S.W., Andersen, D.W., Nedell, S.S. and Wharton, R.A. 1991. Lake Hoare, Antarctica: sedimentation through a thick perennial ice cover. *Sedimentology*, **38**: 363-379.

Sterken, M. 2009. *A paleolimnological reconstruction of Late-Quaternary environmental change along a transect from South America to the Antarctic Peninsula*. Unpublished PhD Thesis, University of Ghent: 215 pp.

Sterken, M., Van de Vijver, B., Jones, V., Verleyen, E., Hodgson, D.A., Vyverman, W. and Sabbe, K. 2009. An illustrated and annotated checklist of freshwater diatoms (Bacillariophyta) from Maritime Antarctica (Livingston, Signy and Beak Island). In: Sterken, M. (Ed.) *A paleolimnological reconstruction of Late-Quaternary environmental change along a transect from South America to the Antarctic Peninsula*. Unpublished PhD Thesis: University of Ghent, pp. 69-113.

Stone, J.O., Allan, G.L., Fifield, L.K. and Cresswell, R.G. 1996. Cosmogenic chlorine-36 from calcium spallation. *Geochimica et Cosmochimica Acta*, **60**: 679-692.

Stone, J.O. 2000. Air pressure and cosmogenic isotope production. *Journal of Geophysical Research-Solid Earth*, **105**: B10, 23753-23759.

Stuiver, M. and Braziunas, T.F. 1985. Compilation of isotopic dates from Antarctica. *Radiocarbon*, **27**: 117-304.

Stuiver, M. and Braziunas, T.F. 1993. Modeling atmospheric ^{14}C influences and ^{14}C ages of marine samples back to 10,000 BC. *Radiocarbon*, **35**: 137-189.

Stuiver, M. and Reimer, P.J. 1993. Extended ^{14}C database and revised CALIB radiocarbon calibration program. *Radiocarbon*, **35**: 215-230.

Sugden, D.E. and John, B.S. 1973. The ages of glacier fluctuations in the South Shetland Islands, Antarctica. In: van Zinderen Bakker, E.M. (Ed.) *Palaeoecology of Africa of the Surrounding Islands and Antarctica*. International Council of Scientific Unions Scientific Committee on Antarctic Research Conference on Quaternary Studies, A.A. Balkema: Cape Town, pp. 139-159.

Sugden, D.E. and Clapperton, C.M. 1977. The maximum ice extent on island groups in the Scotia Sea, Antarctica. *Quaternary Research*, **7**: 268-282.

Sugden, D.E., Bentley, M.J. and Ó Cofaigh, C. 2006. Geological and geomorphological insights into Antarctic ice sheet evolution. *Philosophical Transactions of the Royal Society A*, **364**: 1607-1625.

Sun, L.G., Xie, Z.Q. and Zhao, J.L. 2000. A 3,000-year record of penguin populations. *Nature*, **407**: 858-858.

Sun, L.G., Liu, X.D., Yin, X.B., Xie, Z.Q. and Zhao, J.L. 2005. Sediments in palaeo-notches: potential proxy records for palaeoclimatic changes in Antarctica. *Palaeogeography, Palaeoclimatology, Palaeoecology*, **218**: 175-193.

Sundelin, U. 1919. Uber die spätquartäre Geschichte der kustengegenden Östergötlands und Smålands. *Bulletin Geological Insitut Upsala*, **16**: 195-242.

Sutherland, D.G. 1981. The high-level marine shell beds of Scotland and the buildup of the last Scottish ice sheet. *Boreas*, **10**: 247-254.

Takahashi, H.A., Wada, H., Nakamura, T. and Miura, H. 1999. ^{14}C anomaly of freshwater algae in Antarctic coastal ponds and lakes. *Polar Geoscience*, **12**: 248-257.

Tatur, A., Myrcha, A. and Niegodzisz, J. 1997. Formation of abandoned penguin rookery ecosystems in the maritime Antarctic. *Polar Biology*, **17**: 405-417.

Tatur, A., del Valle, R. and Barczuk, A. 1999. Discussion on the uniform pattern of Holocene tephrochronology in South Shetland Islands, Antarctica. *Polish Polar Studies 26th International Symposium*, Lublin: pp. 303-321.

Tatur, A. 2002. Ornithogenic ecosystems in the Maritime Antarctic - formation, development and disintegration. In: Beyer, L. and Bölter, M. (Eds.) *Geoecology of Antarctic Ice-Free Coastal Landscapes*. Springer: Berlin, pp. 161-184.

Tatur, A., del Valle, R.A., Barczuk, A. and Martinez-Macchiavello, J. 2004. Records of Holocene environmental changes in terrestrial sedimentary deposits on King George Island, Antarctica; a critical review. *Ocean and Polar Research*, **26**: 531-537.

Taylor, F. and Sjunneskog, C. 2002. Postglacial marine diatom record of the Palmer Deep, Antarctic Peninsula (ODP Leg 178, Site 1098) 2. Diatom assemblages. *Paleoceanography*, **17**: (3) 8001, doi:10.1029/2000PA000564.

Taylor, F.W., Bevis, M.G., Dalziel, I.W.D., Smalley, R., Frohlich, C., Kendrick, E., Foster, J., Phillips, D. and Gudipati, K. 2008. Kinematics and segmentation of the South Shetland Islands-Bransfield Basin system, northern Antarctic Peninsula. *Geochemistry Geophysics Geosystems*, **9**: doi: 10.1029/2007GC001873.

Taylor, J.R. 1997. *An Introduction to Error Analysis: The Study of Uncertainties in Physical Measurements* (2nd Edn). University Science Books: Sausalito, California, 327 pp.

ter Braak, C.J.F. and Prentice, I.C. 1988. A theory of gradient analysis. *Advances in Ecological Research*, **18**: 271-317.

ter Braak, C.J.F. 1995. Ordination. In: Jongman, R.H.G., ter Braak, C.J.F. and van Tongeren, O.F.R. (Eds.) *Data Analysis in Community and Landscape Ecology*. Cambridge University Press: Cambridge, pp. 91-173.

ter Braak, C.J.F. and Šmilauer, P. 2006. *CANOCO for Windows, version 4.55*. Plant Research International: Wageningen,

Thomas, R., Rignot, E., Casassa, G., Kanagaratnam, P., Acũna, C., Akins, T., Brecher, H., Frederick, E., Gogineni, P., Krabill, W., Manizade, S., Ramamoorthy, H., Rivera, A., Russell, R., Sonntag, J., Swift, R., Yungel, J. and Zwally, J. 2004. Accelerated sea-level rise from West Antarctica. *Science*, **306**: 255-258.

Thompson, R. and Oldfield, F. 1986. *Environmental Magnetism*. Allen and Unwin: London, 227 pp.

Thompson, W.G. and Goldstein, S.L. 2005. Open-system coral ages reveal persistent suborbital sea-level cycles. *Science*, **308**: 401-404.

TideWizard. 2009. *Tide Height Prediction Software, Smartcom Software*. <www.tidewizard.com>

Tooley, M.J. 1978. *Sea-Level Changes: North-West England during the Flandrian Stage*. Clarendon Press: Oxford, 232 pp.

Tushingham, A.M. 1991. On the extent and thickness of the Innuitian Ice Sheet: a postglacial-adjustment approach. *Canadian Journal of Earth Sciences*, **28**: 231-239.

Tushingham, A.M. and Peltier, W.R. 1991. Ice-3G: a new global model of late Pleistocene deglaciation based upon geophysical predictions of post-glacial relative sea level change. *Journal of Geophysical Research*, **96**: 4497-4523.

Underwood, G.J.C. and Provot, L. 2000. Determining the environmental preferences of four estuarine epipelic diatom taxa: growth across a range of salinity, nitrate and ammonium conditions. *European Journal of Phycology*, **35**: 173-182.

Van Dam, H., Mertens, A. and Sinkeldam, J. 1994. A coded checklist and ecological indicator values of freshwater diatoms from the Netherlands. *Netherlands Journal of Aquatic Ecology*, **28**: 117-133.

van de Plassche, O. 1986. *Sea-level research: a manual for the collection and evaluation of data*. Geobooks: Norwich, 617 pp.

Van de Vijver, B. and Beyens, L. 1996. Freshwater diatom communities of the Strømness Bay area, South Georgia. *Antarctic Science*, **8**: 359-368.

Van de Vijver, B. and Beyens, L. 1997. Freshwater diatoms from some islands in the maritime Antarctic region. *Antarctic Science*, **9**: 418-425.

Van de Vijver, B., Frenot, Y. and Beyens, L. 2002. *Freshwater diatoms from Ile de la Possession (Crozet Archipelago, Subantarctica)*, Bibliotheca Diatomologica, Volume 46. J Cramer: Berlin, 412 pp.

Van de Vijver, B., Gremmen, N. and Smith, V. 2008. Diatom communities from the sub-Antarctic Prince Edward Islands: diversity and distribution patterns. *Polar Biology*, **31**: 795-808.

Van de Vijver, B., Sterken, M., Vyverman, W., Mataloni, G., Nedbaloca, L., Kopalova, K., Verleyen, E. and Sabbe, K. 2009. Five new non-marine diatom taxa from islands in the Southern Atlantic Ocean. In: Sterken, M. (Ed.) *A paleolimnological reconstruction of Late-Quaternary environmental change along a transect from South America to the Antarctic Peninsula*. Unpublished PhD Thesis: University of Ghent, pp. 119-134.

Vaughan, D.G. and Doake, C.S.M. 1996. Recent atmospheric warming and retreat of ice shelves on the Antarctic Peninsula. *Nature*, **379**: 328-331.

Vaughan, D.G. and Spouge, J.R. 2002. Risk estimation of collapse of the West Antarctic Ice Sheet. *Climatic Change*, **52**: 65-91.

Verleyen, E., Hodgson, D.A., Sabbe, K., Vanhoutte, K. and Vyverman, W. 2004a. Coastal oceanographic conditions in the Prydz Bay region (East Antarctica) during the Holocene recorded in an isolation basin. *Holocene*, **14**: 246-257.

Verleyen, E., Hodgson, D.A., Sabbe, K. and Vyverman, W. 2004b. Late Quaternary deglaciation and climate history of the Larsemann Hills (East Antarctica). *Journal of Quaternary Science*, **19**: 361-375.

Verleyen, E., Hodgson, D.A., Milne, G.A., Sabbe, K. and Vyverman, W. 2005. Relative sea-level history from the Lambert Glacier region, East Antarctica, and its relation to deglaciation and Holocene glacier readvance. *Quaternary Research*, **63**: 45-52.

Vink, A., Steffen, H., Reinhardt, L. and Kaufmann, G. 2007. Holocene relative sea-level change, isostatic subsidence and the radial viscosity structure of the mantle of northwest Europe (Belgium, the Netherlands, Germany, southern North Sea). *Quaternary Science Reviews*, **26**: 3249-3275.

Vinocur, A. and Unrein, F. 2000. Typology of lentic water bodies at Potter Peninsula (King George Island, Antarctica) based on physical-chemical characteristics and phytoplankton communities. *Polar Biology*, **23**: 858-870.

Vorren, T.O., Vorren, K.D., Alm, T., Gulliksen, S. and Lovlie, R. 1988. The last deglaciation (20,000 to 11,000 BP) on Andøya, northern Norway. *Boreas*, **17**: 41-77.

Vos, P.C. and de Wolf, H. 1993. Diatoms as a tool for reconstructing sedimentary environments in coastal wetlands; methodological aspects. *Hydrobiologia*, **269/270**: 285-296.

Wada, E., Terazaki, M., Kabaya, Y. and Nemoto, T. 1987. ^{15}N and ^{13}C abundances in the Antarctic Ocean with emphasis on the biogeochemical structure of the food web. *Deep-Sea Research*, **34**: 829-841.

Wagner, B., Cremer, H., Hultzsch, N., Gore, D.B. and Melles, M. 2004. Late Pleistocene and Holocene history of Lake Terrasovoje, Amery Oasis, East Antarctica, and its climatic and environmental implications *Journal of Paleolimnology*, **32**: 321-339.

Wang, J.J., Wang, Y.H., Wang, X.M. and Sun, L.G. 2007. Penguins and vegetations on Ardley Island, Antarctica: evolution in the past 2,400 years. *Polar Biology*, **30**: 1475-1481.

Wasell, A. and Håkansson, H. 1992. Diatom stratigraphy in a lake on Horseshoe Island, Antarctica: a marine-brackish-fresh water transition, with comments on the systematics and ecology of the most common diatoms. *Diatom Research*, **7**: 157-194.

Wasell, A. 1993. Diatom stratigraphy and evidence of Holocene environmental changes in selected lake basins in the Antarctic and South Georgia. *Stockholm University, Department of Quaternary Research, Report 23*.

Watts, A.B. 2001. *Isostasy and Flexure of the Lithosphere*. Cambridge University Press: Cambridge, 458 pp.

Watts, D.R. 1982. Potassium-argon ages and paleomagnetic results from King George Island, South Shetland Islands. In: Craddock, C. (Ed.) *Antarctic Geoscience*. University of Wisconsin Press: Madison, pp. 255-261.

Westman, P. and Hedenström, A. 2002. Environmental changes during isolation processes from the Litorina Sea as reflected by diatoms and geochemical parameters - a case study. *Holocene*, **12**: 531-540.

Wetzel, R.G. 2001. *Limnology: Lakes and River Ecosystems*. Academic Press: London, 1006 pp.

Wiencke, C., Clayton, M.N., Gómez, I., Iken, K., Lüder, U.H., Amsler, C.D., Karsten, U., Hanelt, D., Bischof, K. and Dunton, K. 2007. Life strategy, ecophysiology and ecology of seaweeds in polar waters. *Reviews in Environmental Science and Biotechnology*, **6**: 95-126.

Wolfe, A.P., Miller, G.H., Olsen, C.A., Forman, S.L., Doran, P.T. and Holmgren, S.U. 2004. Geochronology of high latitude lake sediments. In: Pienitz, R., Douglas, M.S.V. and Smol, J.P. (Eds.) *Long-term Environmental Change in Arctic and Antarctic Lakes*. Springer: Dordrecht, pp. 19-52.

Yang, S. and Harwood, D.M. 1997. Late Quaternary environmental fluctuations based on diatoms from Yanou Lake, King George Island, Fildes Peninsula, Antarctica. In: Ricci, C.A. (Ed.) *The Antarctic Region: Geological Evolution and Processes*. Terra Antarctica: Siena, pp. 853-859.

Yoon, H.I., Park, B.K., Kim, Y. and Kim, D. 2000. Glaciomarine sedimentation and its paleoceanographic implications along the fjord margins in the South Shetland Islands, Antarctica during the last 6000 years. *Palaeogeography, Palaeoclimatology, Palaeoecology*, **157**: 189-211.

Yoon, H.I., Park, B.K., Kim, Y. and Kang, C.Y. 2002. Glaciomarine sedimentation and its paleoclimatic implications on the Antarctic Peninsula shelf over the last 15 000 years. *Palaeogeography, Palaeoclimatology, Palaeoecology*, **185**: 235-254.

Yoon, H.I., Yoo, K.C., Park, B.K., Kim, Y., Khim, B.K. and Kang, C.Y. 2004. The origin of massive diamicton in Marian and Potter coves, King George Island, West Antarctica. *Geosciences Journal*, **8**: 1-10.

Yoon, H.I., Khim, B.K., Lee, K., Park, Y.H. and Yoo, K.C. 2006. Reconstruction of postglacial paleoproductivity in Long Lake, King George Island, West Antarctica. *Polish Polar Research*, **27**: 189-206.

Yoshida, Y. and Moriwaki, K. 1979. Some consideration on elevated coastal features and their dates around Syowa Station, Antarctica. *Memoirs of the National Institute of Polar Research, Special Issue*, **13**: 220-226.

Young, R.B. and King, R.H. 1989. Sediment chemistry and diatom stratigraphy of two high arctic isolation lakes, Truelove Lowland, Devon Island, N.W.T., Canada. *Journal of Paleolimnology*, **2**: 207-225.

Zale, R. and Karlén, W. 1989. Lake sediment cores from the Antarctic Peninsula and surrounding islands. *Geografiska Annaler*, **71A**: 211-220.

Zale, R. 1994a. Changes in size of the Hope Bay Adélie penguin rookery as inferred from Lake Boeckella sediment. *Ecography*, **17**: 297-304.

Zale, R. 1994b. ^{14}C age corrections in Antarctic lake sediments inferred from geochemistry. *Radiocarbon*, **36**: 173-185.

Zolitschka, B., Mingram, J., Van Der Gaast, S., Jansen, J.H.F. and Naumann, R. 2001. Sediment logging techniques. In: Last, W.M. and Smol, J.P. (Eds.) *Tracking Environmental Change Using Lake Sediments. Volume 1: Basin Analysis, Coring, and Chronological Techniques*. Kluwer: Dordrecht, pp. 137-153.

Zong, Y.Q. 1997. Implications of *Paralia sulcata* abundance in Scottish isolation basins. *Diatom Research*, **12**: 125-150.

Zwartz, D., Lambeck, K., Bird, M. and Stone, J. 1997. Constraints on the former Antarctic Ice Sheet from sea-level observations and geodynamic modelling. In: Ricci, C.A. (Ed.) *The Antarctic Region: Geological Evolution and Processes*. Terra Antarctica Publication: Siena, pp. 821-828.

Zwartz, D., Bird, M., Stone, J. and Lambeck, K. 1998. Holocene sea-level change and ice-sheet history in the Vestfold Hills, East Antarctica. *Earth and Planetary Science Letters*, **155**: 131-145.

Appendices

Appendix 1 Development of master cores

This appendix shows the lithological and physical core data used to splice the multiple-core records together to form the 'master cores' presented in this study

KEY (for all Appendix 1)

- Fine organic mud
- Fine ooze
- Clay
- Silt
- Silty clay
- Sand
- Fine laminations
- Convoluted laminations
- Gravel
- Moss
- Shell
- Master core
- Fibrous moss layer
- Fine black tephra
- Yellow tephra
- Medium-coarse black tephra

Appendix 1.1 Yanou 'master core'

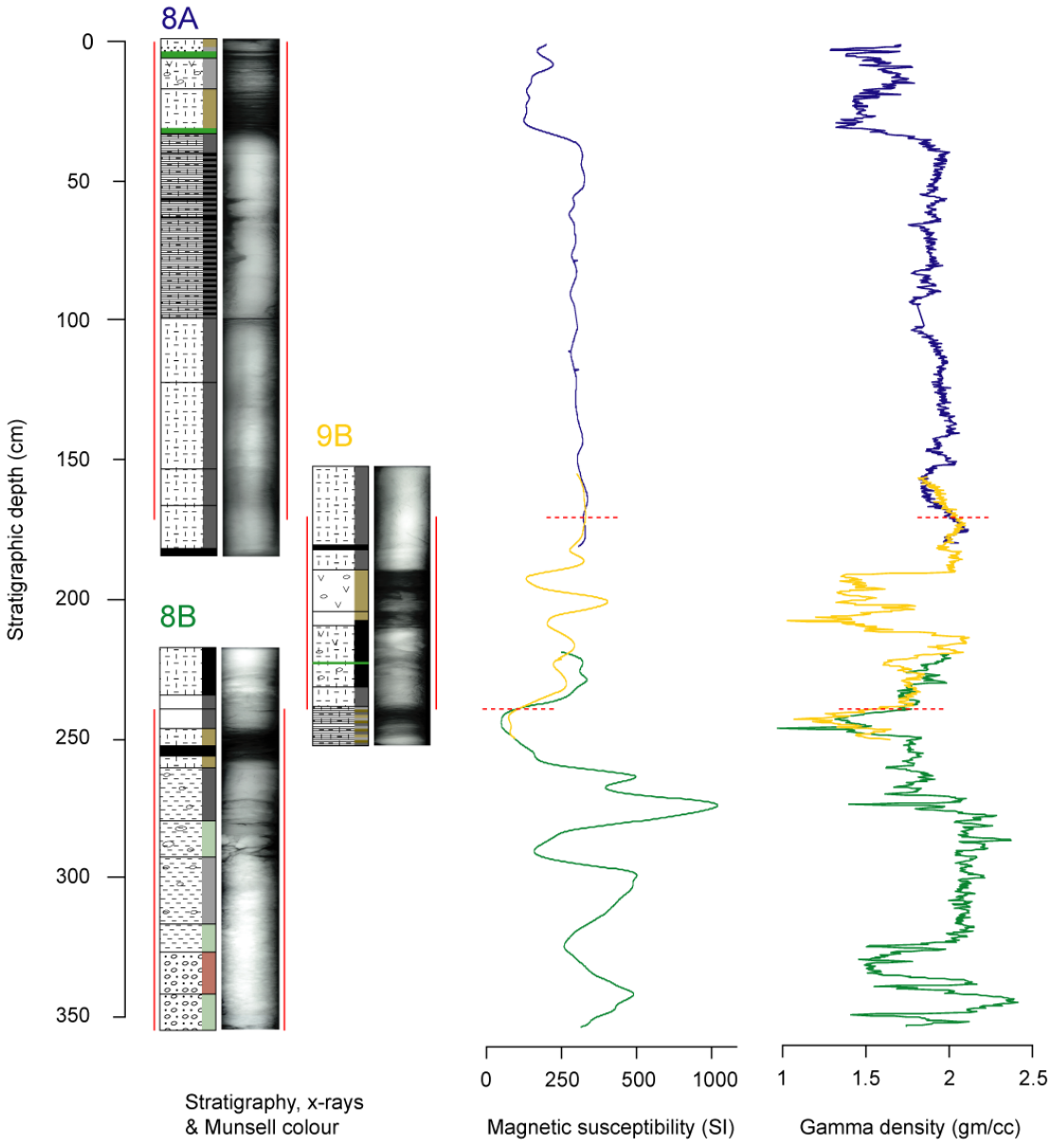

Appendix 1.2 Long 'master core'

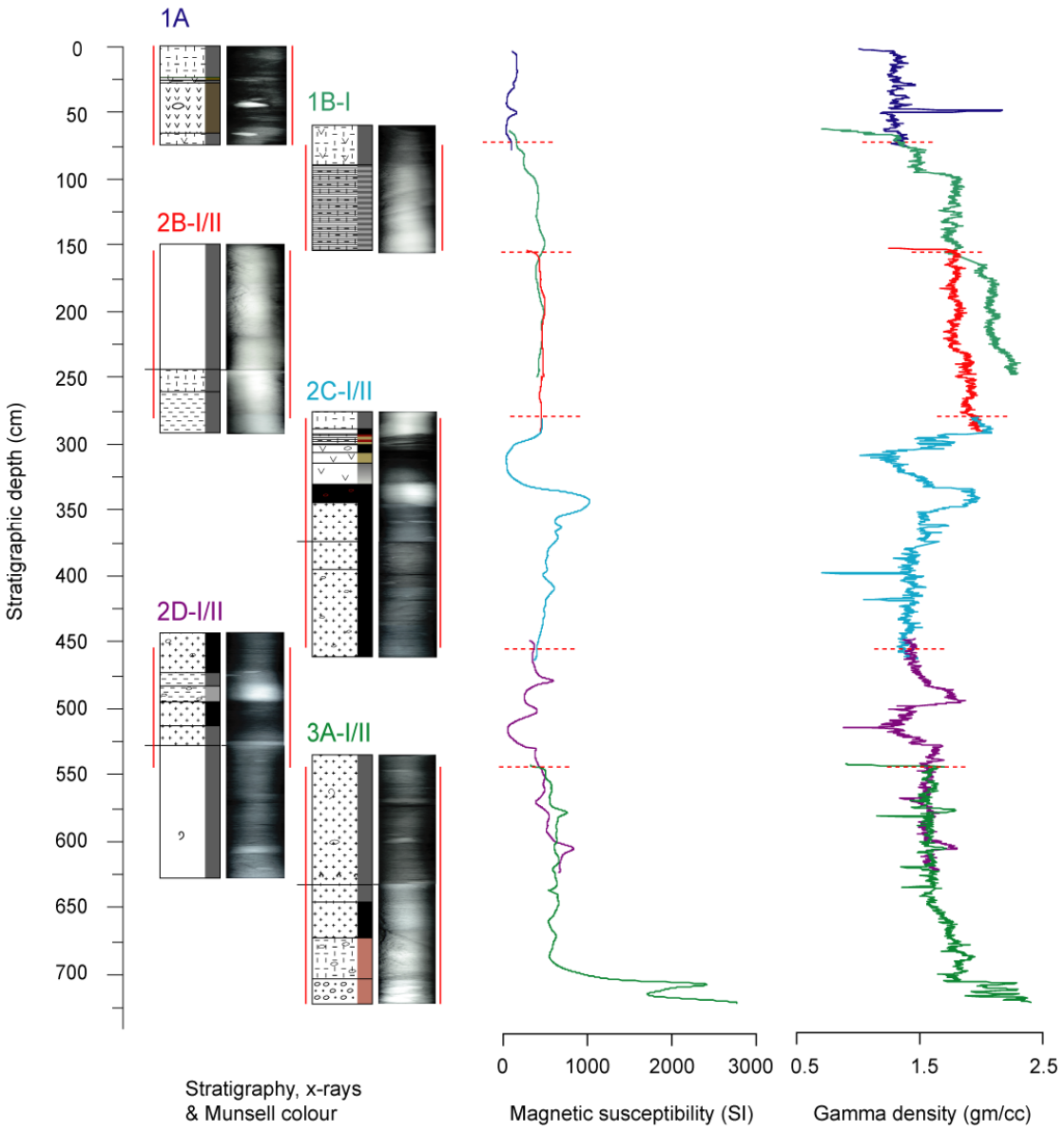

Appendix 1.3 Ardley 'master core'

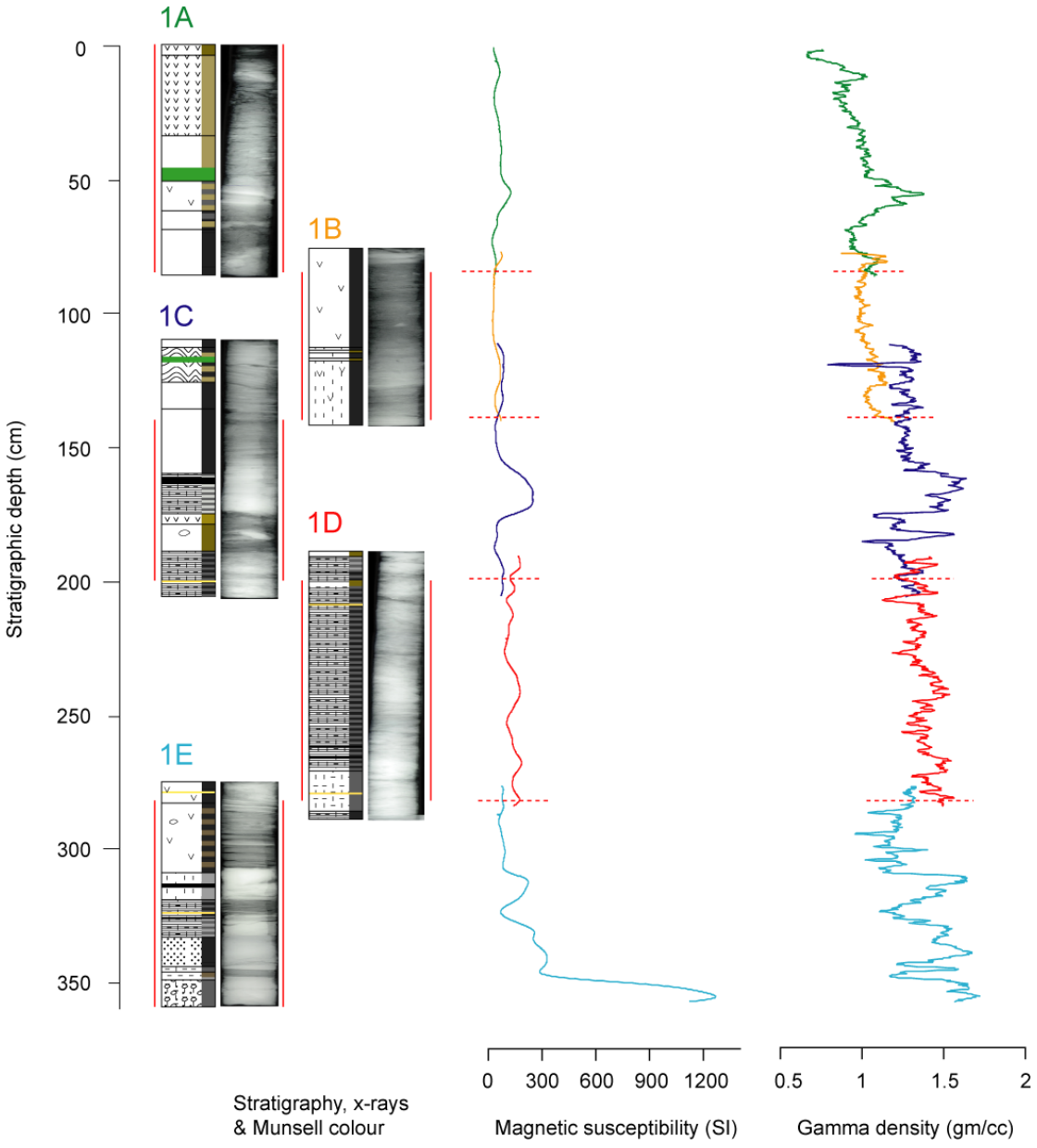

Appendix 1.4 Belén 'master core'

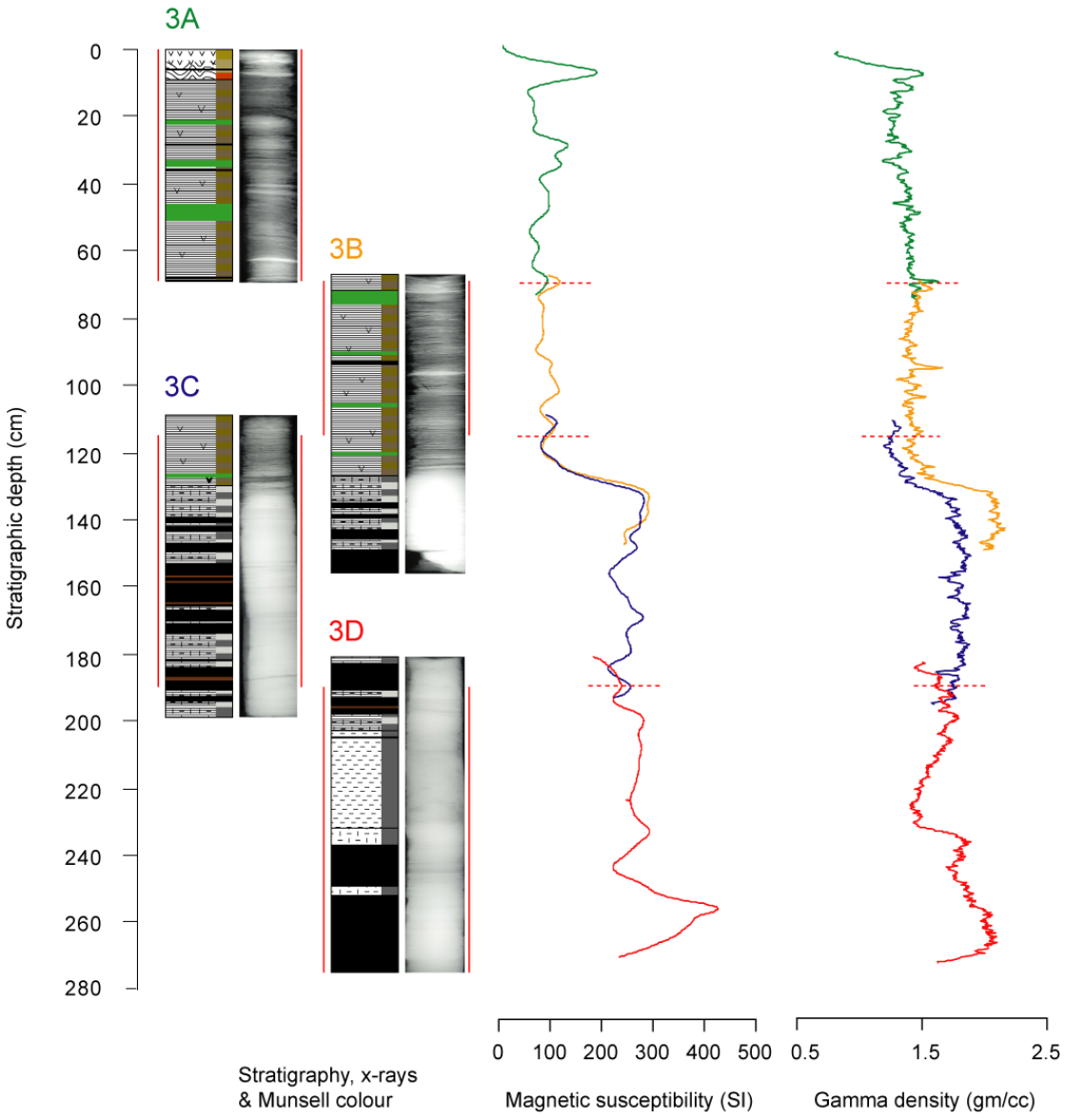

Appendix 1.5 Gaoshan 'master core'

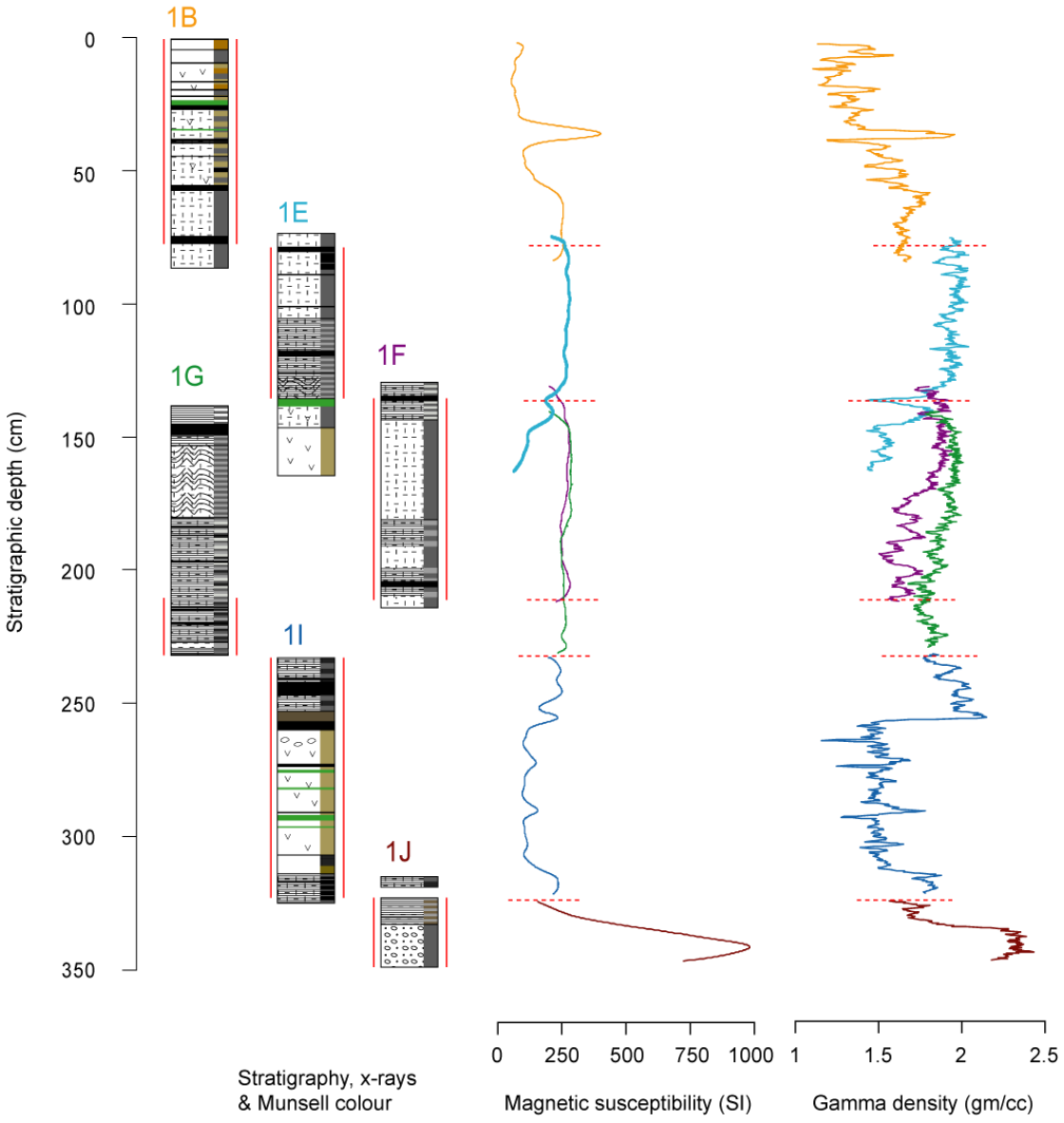

Appendix 2. Diatom species

Diatom species	Alternate name	Nomenclature comments	Morphology comments	Authority	Source photo	Salinity classification	Source salinity	Ecology	Source ecology	Figure (Appx 3)
Achnanthes delicatula		Cr03b identify as *Planothidium delicatulum*		(Kützing) Grunow	Cr03b f.22-23 (plan); LK89 p.83 f.17,22	M, eury	VD94; VW93; HH93	be, ss	Cr03b; WH92; VB97; Sc90	1: 4-5
Achnanthes exigua				Grunow	KL91b p.23 f.4-19; LK89 p.45 f.4-23	O-I	VD94; VW93; Pz91	peri	Pz91	
Achnanthes groenlandica			Similar to *A.brevipes* var. *intermedia* of Cr03b f.8-10	(Cleve) Grunow	WH92 f.8-9	M-P	Cr03b; WH92	be, epilit	Ka02; Pa05	1: 2-3
Achnanthes cf. muelleri	*Achnanthes taylorensis*	WH92 identify as *A. brevipes* var. *intermedia*	Similar to *A. taylorensis* (Sa03) but narrower fascia and more rhombic valve outline. Also similar to *A. coarctata* but without central valve constriction	Carlson	VV02 p.19 f.1-11; St09 f.1-5; VB96 f.2:18-19	O-I	Sa03; WH92			1: 1
Achnanthidium minutissimum	*Achnanthes minutissima*			(Kützing) Czarnecki	VV02 p.22 f.1-9; KL91b p.32 f.1-24; LK89 p.51 f.1-20	O-I	VD94; Pz91; Lo04	peri, epipel	Pz91; HH93	1: 6
Actinocyclus actinochilus				(Ehrenberg) Simonsen	Cr03b f.24; AH08 f.11; IW02 p.33 f.1	P	Cr03b; AH08	pl	Cr03b	3: 120
Actinocyclus curvatulus	*Coscinodiscus curvatulus*			Janisch	AH08 f.4	P	AH08; HH93	pl	HH93	3: 121-122
Amphora coffeaeformis				(Agardh) Kützing	Cr03b f.13; KL97 f.151: 1-5	M	Cr03b; Pz91; PR75	be, peri, epi	Cr03b; Pz91; HH93	1: 47
Amphora holsatica				Hustedt	AH08 f.110	M	AH08; Pz91			1: 48
Amphora marina				Smith	AH08 f.112-115	P	AH08			1: 49
Amphora veneta			Similar to *A. oligotraphenta* (St09 f.6-13)	Lange-Bertalot	KL97 f.151:7-17; Cr04 f. 3a-o; Hg01 f.7:17; Sa03 f.30	O-H, eury	VD94; Hr06; Sa03; Oh06; Ve04	be, peri, lit	Ro04; Hr06; Wa93	1: 46
Asteromphalus hookeri				Ehrenberg	Cr03b f.29	P	Cr03b	pl	Cr03b	3: 134
Asteromphalus hyalinus				Karsten	Cr03b f.27-28	P	Cr03b	pl	Cr03b	3: 135
Aulacoseira distans				(Ehrenberg) Simonsen	VV02 p.1 f.1-9	H	VD94			2: 97
Bacillaria paradoxa	*Bacillaria paxillifer*			Gmelin	Wa93 f.8-9	M	VD94; Lo04; Wa93	epi, epipel	HH93	
Brachysira minor				(Krasske) Lange-Bertalot	St09 f.14-16	O-I?	St09	bryo	St09; VB97	2: 78-79
Caloneis bacillum				(Grunow) Cleve	KL97 f.173:9-20; St09 f.17-21; VV02 p.82 f.1-9	O-I	VD94; VW93; Pz91; Lo07	peri, epipel	Pz91; HH93	2: 74
Cavinula pseudoscutiformis	*Navicula pseudoscutiformis*			(Hustedt) Mann and Stickle	St09 f.44-45; KL97 f.59:12-15 (Nav)	O-I	VD94; Pz91; PR66	peri, be	Pz91	
Chamaepinnularia australomediocris	*Navicula australomediocris*			(Lange-Bertalot and Schmidt) Van de Vijver	St09 f.37-39; VV02 p.86 f.7-13; Sc90 f.7k (Nv); VB96 f.2:9 (Nv)	H?	St09; Sc90; VV08			1: 36-37
Chamaepinnularia gerlachei				Van de Vijver and Sterken	St09 f.59-66; VV09 f.1-16	M, eury	St09; VV09			1: 31-34
Chamaepinnularia gracilistriata				Van de Vijver and Beyens	VV02 p.87 f.1-5	?				1: 35
Chamaepinnularia krookiformis				(Krammer) Lange-Bertalot and Krammer	St09 f.81-90	?				1: 39
Chamaepinnularia krookii			Similar to *Navicula soehrensis var. hassiaca* (Sc90 f.7l)	(Grunow) Lange-Bertalot and Krammer	St09 f.70-73	?		aero, epi	VB97; VV02	1: 38
Cocconeis californica var. kerguelensis				Heiden	Cr03b f.48-49; AH08 f.45	P	Cr03b; Pz91; AH08	be	Cr03b	3: 117
Cocconeis costata/pinnata		Grouped *C. costata* and *C. pinnata*		Gregory	AH08 f.38; WH92 f.24-27; IW02 p.6 f.16	P	Cr03b; Pz91; AH08	lit, be	WH92	3: 113-114

Diatom species	Alternate name	Nomenclature comments	Morphology comments	Authority	Source photo	Salinity classification	Source salinity	Ecology	Source ecology	Figure (Appx 3)
Cocconeis fasciolata				(Ehrenberg) Brown	Cr03b f.45; AH08 f.37	P	Cr03b; AH08	be, pl	Cr03b	3: 115
Cocconeis schuettii				Van Heurck	Cr03b f.43-44; AH08 f.34,36,42-43	P	Cr03b; AH08	be	Cr03b	3: 116
Cocconeis scutellum				Ehrenberg	AH08 f.62-63	P	VW93; Pz91; Lo04	epi	VW93; HH93	3: 119
Cocconeis sp.1				Manguin	Cr03b f.46-47; AH08 f.54-55	P	AH08; Cr03b	pl	Cr03b	3: 118
Craspedostauros laevissimus	*Tropodoneis laevissimus*			(West and West) Sabbe	Sa03 f.35-37; Wa93 f.26; Gi06 f.2x	M	Sa03	be	Hg06; Wa93	
Craticula antarctica			Very similar to *C.molesta* and *submolesta* (Sa03 f.64-65, Cr04 f.4a-k, Gi06)	Van de Vijver and Sabbe	St09 f.67-69; VV09 f.49-58	O-H	St09; Sa03; VV09			
Craticula subpampeana	*Navicula cuspidata*	Name revised by St09		Van de Vijver and Sterken	St09 f.110-111; VV09 f.43-48	O-I	VD94; Pz91; St09	peri	Pz91	2: 72
Dactyliosolen antarcticus				Castracane	IW02 p.7 f.14	P	Cr03b	pl	Cr03b	
Denticulopsis sp.					IW02 p.1-2	P	IW02			
Diadesmis australis			Very similar to *D. perpusilla* (as incorrectly identified by Sa03 f.26-29 and Cr04 f.5a-k)	Van de Vijver and Sabbe	St09 f.123-129; VV09 f.19-28	O-I	PR66; Sa03	aero	Cr04; Ro04	
Diadesmis contenta	*Navicula contenta*			(Grunow) Mann	KL97 f.75:1-5; AFD; VV02 p.61 f.1-4	O-I	VD94; PR66; HH93	aero, epipel	VW93; VB97; HH93	2: 80
Diadesmis tabellariaeformis	*Navicula tabellariaeformis*			(Krasske) Lange-Bertalot and Wojtal	VB97 f.8; St09 f.378-382; Sc90 f.7r	H	Sc90	bryo	VB97; Sc90	
Diploneis smithii				(Brebisson) Cleve	AH08 f.96	P	AH08; VW93; Pz91; Lo07	peri, epipel	Pz91; HH93	
Distephanus speculum				(Ehrenberg) Haeckel	Fa89 f.3	P	Ve04			3: 151
Encyonema minutum	*Cymbella minuta*			(Hilse in Rabenhorst) Mann	KL97 f.119:1-13; St09 f.92-98	O-I	VD94	epipel, peri	HH93	1: 50
Entomoneis gigantea				Grunow	AH08 f.117,119	P	AH08			2: 95-96
Entomoneis paludosa	*Amphiprora paludosa*			(Smith) Reimer	AH08 f.116	M	AH08; PR75			
Eucampia antarctica				(Castracane) Manguin	Cr03b f.53-55; WH92 f.129; IW02 p.27 f.6	P	Cr03a; Cr03b	pl	Cr03b	3: 150
Eunotia praerupta				Ehrenberg	KL91a p.148 f.1-17; AH08 f.60	H	VD94; Pz91; AH08	peri, aero	Pz91	2: 99
Fallacia marnierii	*Navicula marnierii*			(Manguin) Witkowski, Lange-Bertalot and Metzeltin	Cr03b f.100; IW02 p.27 f.11 (Nv)	P	Cr03b	be	Cr03b	2: 82
Fragilaria capucina				Desmazières	VV02 p.7 f.1-13,19-31; St09 f.154-168; KL91a p.108 f.1-8	O-I	VD94; Lo04	pl	We02	2: 101
Fragilaria capucina var. *vaucheriae*	*Fragilaria intermedia*			(Kützing) Lange-Bertalot	KL91a p.108 f.10-15 p.109 f.7-15; VV02 p.7 f.14-18	O-I	Pz91	peri	HH93	2: 102
Fragilaria crotonensis				Kitton	KL91a p.116 f.1-4	O-I	VD94			
Fragilariopsis curta	*Nitzschia curta*			(Van Heurck) Hustedt	Cr03b f.61-66; WH92 f.60	P	Cr03a,b	pl, cryo	Cr03b; Ro04	2: 108
Fragilariopsis cylindriformis				(Hasle) Hasle	Hg01 f.7:21	P	Cr03b	pl	Cr03b	2: 110
Fragilariopsis kerguelensis	*Nitzschia kerguelensis*			(O'Meara) Hustedt	Cr03b f.77-78; IW02 p.3 f.1-3	P	Cr03b	pl, cryo	Cr03b	
Fragilariopsis rhombica	*Fragilariopsis angulata*			(O'Meara) Hustedt	Cr03b f.67-68; Hg01 f.7:18; AH08 f.124	P	AH08	pl	Cr03b	2: 109
Fragilariopsis ritscheri				(Hustedt) Hasle	Hg01 f.7:6; Cr03b f.81-82	P	Cr03b	pl	Cr03b	2: 112
Fragilariopsis sublinearis				(Van Heurck) Heiden	Cr03b f.91-92	P	Cr03b	pl	Cr03b	2: 111
Gomphonema acuminatum				Ehrenberg	KL97 f.160:1-12	O-I	VD94; Pz91; Lo07	be	We02	

Diatom species	Alternate name	Nomenclature comments	Morphology comments	Authority	Source photo	Salinity classification	Source salinity	Ecology	Source ecology	Figure (Appx 3)
Gomphonema angustatum/parvulum		Grouped *G. angustatum* and *G. parvulum* (as WH92)		(Kützing) Rabenhorst (Kützing) Kützing	WH92 f.28-36; St09 f.169-226; KL91b p.76 f.1-7 p.84 f.9-14	O-I	VD94; VW93; Pz91; HH93	epi	VW93; HH93; WH92	1: 41
Gomphonema gracile				Ehrenberg	KL91b p.79 f.1-7	O-I	VD94; Pz91	epi	Ta99	1: 40
Gomphonema olivaceum				(Hornemann) Brebisson	KL97 f.165: 1-7	O-I	HH93; VD94	epi, epipel	HH93	1: 42
Gyrosigma fasciola				(Ehrenberg) Griffith and Henfrey	AH08 f.101	M-P	HH93; AH08; PR66	pl; lit	HH93	3: 140
Hantzschia amphioxys				(Ehrenberg) Grunow	St09 f.263-265; VV02 p.123 f.11-16; Cr04 f.8a-b	O-I	VD94; VW93; Pz91; HH93	aero, epipel	VW93; Pz91; HH93	2: 85
Hippodonta hungarica	*Navicula capitata var. hungarica*			(Grunow) Lange-Bertalot, Metzeltin and Witkowski	St09 f.227-230; VV02 p.42 f.29-31; KL97 f.42:5-9	O-I	VD94; Pz91	peri, epi	Pz91; HH93	2: 63
Licmophora antarctica				Carlson	AH08 f.8	P	AH08	epi	AH08	3: 141
Licmophora decora				Heiden and Kolbe	Cr03b f.97; AH08 f.7,9	P	Cr03b; AH08	pl, be	Cr03b	3: 142
Licmophora gracilis				(Kützing) Peragallo	Cr03b f.98-99; AH08 f.29-30	P	Cr03b; AH08	be, epi	Cr03b; AH08	3: 143
Luticola mutica/cohnii	*Navicula mutica*			(Kützing) Mann (mutica) (Hilse) Mann (cohnii)	St09 f.235-236,238-239; KL97 f.61:1-7; VV02 p.56 f.1-4	O-H	VD94; VW93; WH92; VV02	be, peri, aero	Cr03b; Hg06; WH92	2: 75-76
Luticola muticopsis	*Navicula muticopsis*			(Van Heurck) Mann	Sa03 f.41-44; St09 f.240-253; KL97 f.61:12-15; VV02 p.56 f.7-10, p.57 f.1-6	O-H	Sa03	be, peri, ss	Ro04; Hg06; WH92	2: 77
Mayamaea atomus var. permitis				(Kützing) Lange-Bertalot	VV02 p.42 f.12-37; St09 f.266-269	O-I?	St09; VV08	aero	St09	2: 81
Muelleria				Van de Vijver and Spaulding	St09 f.509-510	?				1: 45
Nanofrustulum shiloi	*Fragilaria construens* var. *venter*	Name revised by Hg06	Similar to *Staurosira circula* (VV02 p.11 f.1-18) and *Staurosira* cf. *circula* (St09 f.99-103)	(Lee, Reimer and McEnery) Round, Hallsteinsen and Paasche	Sa03 f.16-17; Hg01 f.14	P, eury	St09; Hg01; Sa03; Hg06			2: 103
Navicula australoshetlandica				Van de Vijver and Sabbe	St09 f.371-377; VV09 f.30-42	O-H?	St09; VV09			2: 51
Navicula cancellata				Donkin	AH08 f.58; WH92 f.39, 50	P	VW93; AH08	lit	WH92	2: 60
Navicula cincta				(Ehrenberg) Ralfs	KL97 f.28:8-15; St09 f.385-387; AFD	O-H	VW93; Lo07; PR66; Hr06; HH93	epi, epipel	Hr06; HH93	2: 52
Navicula criophila				(Castracane) De Toni	Cr03b f.106-107	P	Cr03b	pl, be	Cr03b	2: 59
Navicula directa				(Smith) Ralfs	AH08 f.64-65; WH92 f.37	P	Cr03a,b; AH08; RM99	be, cryo	Cr03b	2: 70
Navicula directa form *2*				(Smith) Ralfs	Cr03b f.103-104	P	Cr03b	cryo	Cr03b	2: 71
Navicula glaciei				Van Heurck	St09 f.277-279; WH92 f.43; Cr03b f.110-112	P	Cr03a,b	be, cryo	Cr03b; Ro04	2: 68
Navicula gregaria				Donkin	KL97 f.38:10-15; St09 f.291-295; Oh06 f.26-28; VV02 p.35 f.9-18	O-H	VD94; PR66; HH93	peri, epipel	Pz91; HH93	2: 54-55
Navicula halophila				(Grunow) Cleve	KL97 f.44:1-11,14-18	M	VD94; Pz91; PR66; HH93	peri, epipel	Pz91; HH93	2: 67
Navicula imperfecta var. antarctica				Heiden	Cr03b f.105	P	Cr03b	be, cryo	Cr03b	2: 69
Navicula perminuta				Grunow	KL97 f.35:14-20; WH92 f.45-47; Cr03b f.116-117	P-M, eury	AH08; Cr03b; St09; UP00; RM98	be, peri, epipel	Cr03b; UP00	2: 61-62
Navicula phyllepta				Kützing	KL97 f.32:5-11; WH92 f.41,44; Sa03 f.68-69	M, eury	Sa03; Ve04; HH93; UP00	epipel	HH93; UP00	2: 56-57
Navicula salinarium				Grunow	Wa93 f.21	M, eury	VD94; Wa93; UP00; VW93; Pz91; HH93	peri, epipel	Pz91; HH93; UP00	

Diatom species	Alternate name	Nomenclature comments	Morphology comments	Authority	Source photo	Salinity classification	Source salinity	Ecology	Source ecology	Figure (Appx 3)
Navicula senonquei				Peragallo	Cr03b f.108	P	Cr03b	be	Cr03b	2: 58
Navicula veneta		Grouped with *N. cryptocephala* var. *veneta*		(Kützing) Rabenhorst	KL97 f.31: 8-14, 32:1-4; VV02 p.35 f.29-35	O-H	VD94 (v); VW93; PR66	epipel	HH93	2: 53
Naviculadicta seminulum			Morphologically similar to *Eolimna minima* and *Sellaphora seminulum*	(Grunow) Lange-Bertalot	VV02 p.39 f.1-8; St09 f.331-342	O-I	VD94			2: 64-66
Nitzschia australis				(Peragallo) Mann	AH08 f.81-82	P?	AH08			2: 88
Nitzschia commutata				Grunow	LK87 p.22 f.1-9; Cr04 f.8d-f; Oh06 f.29-30; Sa03 f.54-55	M	VD94; HH93; Cr04; Sa03; Gi06	epipel	HH93	2: 87
Nitzschia frustulum/perminuta/ acidoclinata		Too similar to distinguish species		(Kützing) Grunow (frust)	St09 f.388-424; VV02 p.130 f.21-36; WH92 f.55-56; LK87 p.33 f.28-29; VB96 f.2:11-12	O-H	VD94; Pz91; Lo04; HH93	peri, be	Pz91; HH93	2: 92
				(Kützing) Peragallo (per)						
Nitzschia gracilis				Hantzsch	VV02 p.129 f.19-30; St09 f.486-504	O-H	Kw98			2: 90-91
Nitzschia inconspicua				Grunow	VV02 p.130 f.15-20; St09 f.425-438	O-H	VD94; Hr06			2: 93
Nitzschia lecointei				Van Heurck	Cr03b f.119-120	P	Cr03b; RM99; Hg06	pl, be, cryo	Cr03b; RM99; Hg06	2: 89
Nitzschia medioconstricta				Hustedt	Cr03b f.123-124	P	Cr03b	pl	Cr03b	2: 86
Odontella litigiosa				(Van Heurck) Hoban	AH08 f.2,25-27,32	P	Cr03b; AH08	pl	Cr03b	3: 125
Opephora naveana			Morphologically similar to *Fragilaria elliptica* (KL91a p.130 f.31-42)	Le Cohu	VV02 p.10 f.23-31; SV95 f.43-44	O-I	VD94; SV95; Cr03a	pl, peri	Cr03a	2: 106
Orthoseira roeseana	*Melosira roseana*			(Rabenhorst) O'Meara	KL91a p.10 f.1-11; St09 f.30-34; VV02 p.3 f.1-12	H	VU00	tycho	VU00	2: 98
Parlibellus delognei	*Navicula delognei*			(Van Heurck) Cox	Cr03b f.150-151; AH08 f.78-80	P	Cr03b; AH08	be	Cr03b	2: 83
Petroneis plagiostoma				(Grunow) Mann	AH08 f.87-89	P	AH08			2: 84
Pinnularia borealis				Ehrenberg	Sa03 f.32-33; St09 f.544-545; KL97 f.177:1-4,6-7	O-I	VD94; VW93; Pz91; HH93	aero, epipel, pl	VW93; Pz91; HH93; Ko98	1: 23
Pinnularia bottnica	*Pinnularia lundii var. baltica*			Krammer	VV02 p.102 f.1-11; Wa93 f.22 (lundii)	M? (Sea spray)	VV02	lit	Wa93	1: 24
						O-H/P	Wa93			
Pinnularia gemella			Morphologically similar to *P. dulcicola* & *P. quadratarea* var. *dulcicola* (VV02 p.96 f.16-20)	Van de Vijver	St09 f.540-543	?				1: 27
Pinnularia kolbei				Manguin	St09 f.681-683; VV02 p.103 f.1-9	O-H	VV02; VV08	Common in penguin rookeries	VV02	1: 29
Pinnularia microstauron				(Ehrenberg) Cleve	Sa03 f.34; WH92 f.54; St09 f.516-522; KL97 f.191:1-6, 192:1-16	O-I	VD94; Pz91; RM98	peri	Pz91	1: 26
Pinnularia obscura				Krasske	St09 f.546-547; VV02 p.111 f.17-24	O-I	VD94	aero	VB97; Kw98	1: 25
Pinnularia quadratarea				(Schmidt) Cleve	AH08 f.76-77; WH92 f.52	P	Cr03b; AH08; Pz91; Lo04	be, cryo	Cr03b	1: 30
Pinnularia subantarctica var. *elongata*				(Manguin) Van de Vijver and Le Cohu	VV02 p.114 f.1-9; St09 f.548-551	O-H?	VV02	Common in penguin rookeries	VV02	1: 28
Placoneis elginensis	*Navicula elginensis/dicephala*			(Gregory) Cox	St09 f.296-300; WH92 f.48; KL97 f.46:1-9	O-I	VD94; Pz91	peri	Pz91	2: 73
Planothidium delicatulum	*A. delicatula* aff. *linkei/ A. delicatula* ssp. *delicatula*		Morphologically similar to *Achnanthes delicatula* (Sc90 and WH92)	(Kützing) Round and Bukhtiyarova	St09 f.577-581; KL91b p.39 f.6-14 (Ach)	O-I	WH92; Sc90	epilit, meltwater streams	St09	1: 7-8
Planothidium lanceolatum	*Achnanthes lanceolata*			(Brebisson) Lange-Bertalot	St09 f.567-568; VV02 p.23 f.7-14; LK89 p.84 f.1-16 (Ach); VB96 f.2:20-21 (Ach)	O-I	VD94; VW93; Pz91	epilit	St09; VW93; Ta99	1: 9-10

Diatom species	Alternate name	Nomenclature comments	Morphology comments	Authority	Source photo	Salinity classification	Source salinity	Ecology	Source ecology	Figure (Appx 3)
Planothidium renei/ quadripunctatum	*Achnanthes renei*	Too morphologically similar to distinguish species		(Lange-Bertalot and Schmidt) Van de Vijver (Oppenheim) Sabbe (quad)	St09 f.582-592; VV02 p.23 f.35-49; Sc90 f.6s-t; Sa03 f.13-14; WH92 f.14-17	H?	WH92; Sa03; Sc90			1: 11-12
Pleurosigma eudon var. kerguelensis				Heiden et Kolbe	AH08 f.99-100	P	AH08			3: 136-137
Pleurosigma obscurum	*Gyrosigma obscurum*			Smith	AH08 f.102	P/M, eury	AH08; PR66			3: 138-139
Porosira glacialis				(Grunow) Jorgensen	Cr03b f.152-153	P	Cr03b	pl, cryo	Cr03b	3: 123-124
Psammothidium abundans	*Achnanthes abundans*	Name revised by Hg06		(Manguin) Bukhtiyarova and Round	St09 f.599-605; Sa03 f.7-8; LK89 p.61 f.18-29; VV02 p.31 f.1-13	O-I	Hg01; Sa03	be, peri	Hg06	1: 13
Psammothidium germainii	*Achnanthes germainii*			(Manguin) Sabbe	VV02 p.27 f.26-33; St09 f.635-637; Sa03 f.11-12	H	Sa03	tycho	VU00	1: 22
Psammothidium incognitum	*Achnanthes incognita*		Morphologically very similar to *P. stauroneioides* , but has more rhombic central area	(Krasske) Van de Vijver	St09 f.593-598; LK89 p.68 f.6-15 (Ach); VV02 p.29 f.1-11	H?	Sa03	bryo	VB97	1: 19-21
Psammothidium investians	*Achnanthes investians*		Similar to *Achnanthes laevis*	(Carter) Bukhtiyarova	St09 f.610-612; VV02 p.29 f.12-19; LK89 p.18 f.27-29 (Ach)	H?	VV08			1: 14-15
Psammothidium manguinii	*Achnanthes manguinii*			(Germain) Van de Vijver	VV02 p.29 f.20-33; VB96 f.2:26-27	H?	Sa03			1: 18
Psammothidium metakryophilum	*Achnanthes metakryophilum*			(Lange-Bertalot and Schmidt) Sabbe	Sc90 f.6f-l; Sa03 f.3-6; Cr04 f.5d'-n'; Oh06 f.31-36; St09 f.613-618	H	Sa03; Oh06			1: 16
Psammothidium subatomoides	*Achnanthes/Navicula subatomoides*			(Hustedt) Bukhtiyarova and Round	St09 f.619-624; LK89 p.21 f.1-18; WH92 f.12-13 (Ach); VV02 p.29 f.42-52	H	VD94			1: 17
Pseudogomphonema kamtschaticum				(Grunow) Medlin	Cr03b f.143-144	P	Cr03b; AH08	epi, cryo, be	Cr03b; Ka02	1: 43
Pseudonitzschia turgiduloides				(Hasle) Hasle	Cr03b f.133-134	P	Cr03b	pl	Cr03b	2: 94
Pseudostaurosira sp.			Resembles *Pseudostaurosira perminuta* of SV95 and sp.1 of	(Grunow) Sabbe and Vyverman	Sa03 f.18-21; Hg01 f.7:15-16; SV95 f.1-44	P-M	Sa03; SV95	be, epipsam	SV95	2: 107
Rhizosolenia antennata				(Ehrenberg) Brown	HS97 p.27	P	HS97			
Rhizosolenia hebetata				Bailey	IW02 p.7 f.4-5	P	HS97	pl	Ko98	
Rhizosolenia styliformis				Brightwell	IW02 p.7 f.1-2, p.28 f.18-19	P	HS97	pl	Ko98	3: 148
Stauroforma exiguiformis			Very similar to *S. inermis* (Sa03 f.24-25) - grouped by VV02	(Lange-Bertalot) Flower, Jones and Round	VV02 p.15 f.12-23	O-H	St09; Sa03; VV08			2: 104
Stauroneis latistauros	*Stauroneis anceps*	Name revised by VV04		Van de Vijver et Lange-Bertalot	Oh06 f.43-45; St09 f.667-668,675-680; Sa03 f.31; KL97 f.87:3-9; Cr04 f.4l-q	O-I	VD94; Pz91; Lo07	peri, be	Pz91; HH93	1: 44
Stauroneis phoenicenteron				(Nitzsch) Ehrenberg	KL97 f.85:1-6; VB96 f.2:10	O-I	VD94; Pz91	peri	Pz91	
Staurosira alpestris				(Krasske) Van de Vijver	VV02 p.14 f.1-11; St09 f.149-153	O-I	St09; Le08			
Staurosirella pinnata	*Fragilaria pinnata*			(Ehrenberg) Williams and Round	KL91a p.133 f.1-18 (Frg); St09 f.641-644	O-I	VD94; VW93; Pz91	tycho, peri	VW93; Hr06; HH93; St09	2: 105
Stellarima microtias				(Ehrenberg) Hasle and Sims	IW02 p.10 f.4	P	Cr03b	pl, cryo	Cr03b	3: 126-128
Stephanopyxis sp.					IW02 p.9, p.25	P	IW02			3: 133
Surirella sp. 1			Same as unidentified *Surirella* of St09		St09 f.684-685					2: 100
Synedra kerguelensis				Heiden	Cr03b f.154-155; AH08 f.19	P	Cr03b; AH08	lit	Cr03b	3: 144

Diatom species	Alternate name	Nomenclature comments	Morphology comments	Authority	Source photo	Salinity classification	Source salinity	Ecology	Source ecology	Figure (Appx 3)
Synedropsis fragilis				(Manguin) Hasle, Syvertsen and Medlin	Cr03b f.161-163; AH08 f.20; Ha94 f.125-128	P	Cr03a,b; AH08	epi, cryo	Cr03b	
Synedropsis laevis				(Heiden) Hasle, Syvertsen and Medlin	Cr03b f.159; Ha94 f.61-67	P	Cr03a,b; AH08	cryo	Cr03b	
Synedropsis recta				Hasle, Syvertsen and Medlin	Cr03b f.164-165; AH08 f.21-22; Ha94 f.51-55, 57-60	P	Cr03a,b; AH08	cryo	Cr03b	3: 145
Thalassionema nitzschoides				(Grunow) Mereschkowsky	Cr03b f.169; AH08 f.93; IW02 p.5 f.18	P	Cr03b; AH08; VW93	pl	Cr03b	3: 146
Thalassiosira antarctica				Comber	Cr03b f.174-175; IW02 p.24 f.1	P	Cr03a,b	pl, cryo	Cr03b; Ka02	3: 130
Thalassiosira gracilis				(Karsten) Hustedt	Cr03b f.180; AH08 f.49; IW02 p.24 f.2	P	Cr03b; AH08	pl	Cr03b; Ka02	3: 131
Thalassiosira lentiginosa				(Janisch) Fryxell	AH08 f.3; IW02 p.20 f.1,4, p.24 f.4	P	Cr03b; AH08	pl	Cr03b	3: 129
Thalassiosira tumida				(Janisch) Hasle	Cr03b f.190-191; AH08 f.12	P	Cr03b; AH08	pl	Cr03b	3: 132
Thalassiothrix antarctica				Schimper ex Karsten	IW02 p.5 f.19, p.24 f.9, p.28 f.16	P	Cr03b	pl	Cr03b	3: 147
Trachyneis aspera				(Ehrenberg) Cleve	AH08 f.83-85	P	Cr03b; AH08; VW93	be, epi, epipel	Cr03b; HH93	3: 149

Key to authors: AFD: Spaulding *et al*.; **AH08**: Al-Handal and Wulff 2008; **Cr03a**: Cremer *et al*. 2003a; **Cr03b**: Cremer *et al*. 2003b; **Cr04**: Cremer *et al*. 2004; **Fa89**: Fanuko 1989; **Gi06**: Gibson *et al*. 2006; **Ha94**: Hasle *et al*. 1994; **Hg01**: Hodgson *et al*. 2001b; **Hg06**: Hodgson *et al*. 2006; **HH93**: Hemphill-Haley 1993; **Hr06**: Horton *et al*. 2006; **HS97**: Hasle and Syvertsen 1997; **IW02**: Iwai and Winter 2002; **Ka02**: Kang *et al*. 2002; **KL91a**: Krammer and Lange-Bertalot 1991a; **KL91b**: Krammer and Lange-Bertalot 1991b; **KL97**: Krammer and Lange-Bertalot 1997; **Ko98**: Kohly 1998; **Kw98**: Kawecka *et al*. 1998; **Le08**: Lee *et al*. 2008; **LK89**: Lange-Bertalot and Krammer 1989; **Lo04**: Lohne *et al*. 2004; **Lo07**: Lohne *et al*. 2007; **Oh06**: Ohtsuka *et al*. 2006; **Pa05**: Patterson *et al*. 2005; **PR66**: Patrick and Reimer 1966; **PR75**: Patrick and Reimer 1975; **Pz91**: Pienitz *et al*. 1991; **RM98**: Roberts and McMinn 1998; **RM99**: Roberts and McMinn 1999; **Ro04**: Roberts *et al*. 2004; **Sa03**: Sabbe *et al*. 2003; **Sc90**: Schmidt *et al*. 1990; **St09**: Sterken *et al*. 2009; **SV95**: Sabbe and Vyverman 1995; **Ta99**: Tatur *et al*. 1999; **UP00**: Underwood and Provot 2000; **VB96**: Van de Vijver and Beyens 1996; **VB97**: Van de Vijver and Beyens 1997; **VD94**: Van Dam *et al*. 1994; **Ve04**: Verleyen *et al*. 2004; **VU00**: Vinocur and Unrein 2000; **VV02**: Van de Vijver *et al*. 2002; **VV04**: Van de Vijver *et al*. 2004; **VV08**: Van de Vijver *et al*. 2008; **VV09**: Van de Vijver *et al*. 2009; **VW93**: Vos and de Wolf 1993; **Wa93**: Wasell 1993; **We02**: Westman and Hedenstrom 2002; **WH92**: Wasell and Hakansson 1992

Key to salinity: P: Polyhalobous (marine); **M**: Mesohalobous (brackish); **O-H**: Oligohalobous-halophilous (brackish-fresh); **O-I**: Oligohalobous-indifferent (fresh-brackish); **H**: Halophobous (fresh); **eury**: euryhalobous

Key to ecology: aero: aerophilic; **be**: benthic; **bryo**: bryophytic; **cryo**: cryophilic; **epi**: epiphytic; **epilit**: epilithic; **epipel**: epipelic; **epipsam**: epipsammic; **lit**: littoral; **peri**: periphytic; **pl**: planktonic; **tycho**: tychoplanktonic

Appendix 3. Diatom photos

Plate 1: Fig. 1: *Achnanthes* cf. *muelleri*, 2-3: *Achnanthes groenlandica*, 4-5: *Achnanthes delicatula*, 6: *Achnanthidium minutissimum* 7-8: *Planothidium delicatulum*, 9-10: *Planothidium lanceolatum*, 11-12: *Planothidium renei/quadripunctatum*, 13: *Psammothidium abundans*, 14-15: *Psammothidium investians*, 16: *Psammothidium metakryophilum*, 17: *Psammothidium subatomoides*, 18: *Psammothidium manguinii*, 19-21: *Psammothidium incognitum*, 22: *Psammothidium germainii*, 23: *Pinnularia borealis*, 24: *Pinnularia bottnica*, 25: *Pinnularia obscura*, 26: *Pinnularia microstauron*, 27: *Pinnularia gemella*, 28: *Pinnularia subantarctica* var. *elongata*, 29: *Pinnularia kolbei*, 30: *Pinnularia quadratarea*, 31-34: *Chamaepinnularia gerlachei*, 35: *Chamaepinnularia gracilistriata*, 36-37: *Chamaepinnularia australomediocris*, 38: *Chamaepinnularia krookii*, 39: *Chamaepinnularia krookiformis*, 40: *Gomphonema gracile*, 41: *Gomphonema angustatum/parvulum*, 42: *Gomphonena olivaceum*, 43: *Pseudogomphonema kamtschaticum*, 44: *Stauroneis latistauros*, 45: *Muelleria australoatlantica*, 46: *Amphora veneta*, 47: *Amphora coffeaeformis*, 48: *Amphora holsatica*, 49: *Amphora marina*, 50: *Encyonema minutum*.

Plate 2: Fig. 51: *Navicula australoshetlandica*, 52: *Navicula cincta*, 53: *Navicula veneta*, 54-55: *Navicula gregaria*, 56-57: *Navicula phyllepta*, 58: *Navicula senonquei*, 59: *Navicula criophila*, 60: *Navicula cancellata*, 61-62: *Navicula perminuta*, 63: *Hippodonta hungarica*, 64-66: *Naviculadicta seminulum*, 67: *Navicula halophila*, 68: *Navicula glaciei*, 69: *Navicula imperfecta* var. a*ntarctica*, 70: *Navicula directa*, 71: *Navicula directa* form 2, 72: *Craticula subpampeana*, 73: *Placoneis elginensis*, 74: *Caloneis bacillum*, 75-76: *Luticola mutica*, 77: *Luticola muticopsis*, 78-79: *Brachysira minor*, 80: *Diadesmis contenta*, 81: *Mayamaea atomus* var. *perminuta*, 82: *Fallacia marnierii*, 83: *Parlibellus delognei*, 84: *Petroneis plagiostoma*, 85: *Hantzschia amphioxys*, 86: *Nitzschia medioconstricta*, 87: *Nitzschia commutata*, 88: *Nitzschia australis*, 89: *Nitzschia lecointei*, 90-91: *Nitzschia gracilis*, 92: *Nitzschia frustulum/perminuta*, 93: *Nitzschia inconspicua*, 94: *Pseudonitzschia turgiduloides*, 95-96: *Entomoneis gigantea*, 97: *Aulacoseira distans*, 98: *Orthoseira roeseana*, 99: *Eunotia praerupta*, 100: *Surirella* sp. 1, 101: *Fragilaria capucina*, 102: *Fragilaria capucina* var. *vaucheriae*, 103: *Nanofrustulum shiloi*, 104: *Stauroforma exiguiformis*, 105: *Staurosirella pinnata*, 106: *Opephora naveana*, 107: *Pseudostaurosira* sp., 108: *Fragilariopsis curta*, 109:

Fragilariopsis rhombica, 110: *Fragilariopsis cylindriformis*, 111: *Fragilariopsis sublinearis*, 112: *Fragilariopsis ritscheri*.

Plate 3: Fig. 113-114: *Cocconeis costata/pinnata*, 115: *Cocconeis fasciolata*, 116: *Cocconeis schuetti*, 117: *Cocconeis californica* var. *kerguelensis*, 118: *Cocconeis* sp. 1, 119: *Cocconeis scutellum*, 120: *Actinocyclus actinochilus*, 121-122: *Actinocyclus curvatulus*, 123-124: *Porosira glacialis*, 125: *Odontella litigiosa*, 126-128: *Stellarima microtias*, 129: *Thalassiosira lentiginosa*, 130: *Thalassiosira antarctica*, 131: *Thalassiosira gracilis*, 132: *Thalassiosira tumida*, 133: *Stephanopyxis* sp., 134: *Asteromphalus hookeri*, 135: *Asteromphalus hyalinus*, 136-137: *Pleurosigma eudon* var. *kerguelensis*, 138-139: *Pleurosigma obscurum*, 140: *Gyrosigma fasciola*, 141: *Licmophora antarctica*, 142: *Licmophora decora*, 143: *Licmophora gracilis*, 144: *Synedra kerguelensis*, 145: *Synedropsis recta*, 146: *Thalassionema nitzschoides*, 147: *Thalassiothrix antarctica*, 148: *Rhizosolenia styliformis*, 149: *Trachyneis aspera*, 150: *Eucampia antarctica*, 151: *Distephanus speculum*.

Appendix 3

Plate 1

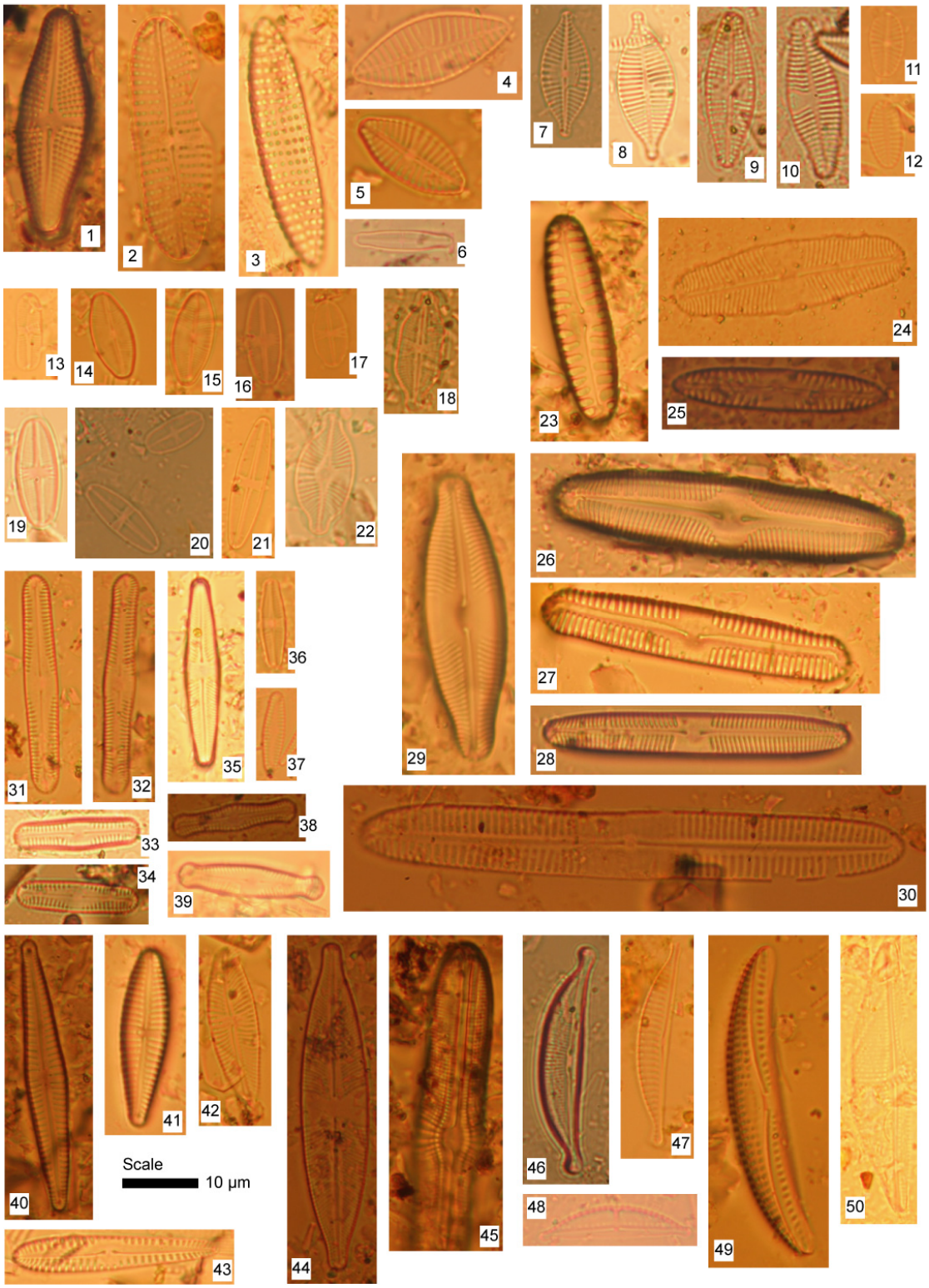

Appendix 3

Plate 2

Appendix 3

Plate 3

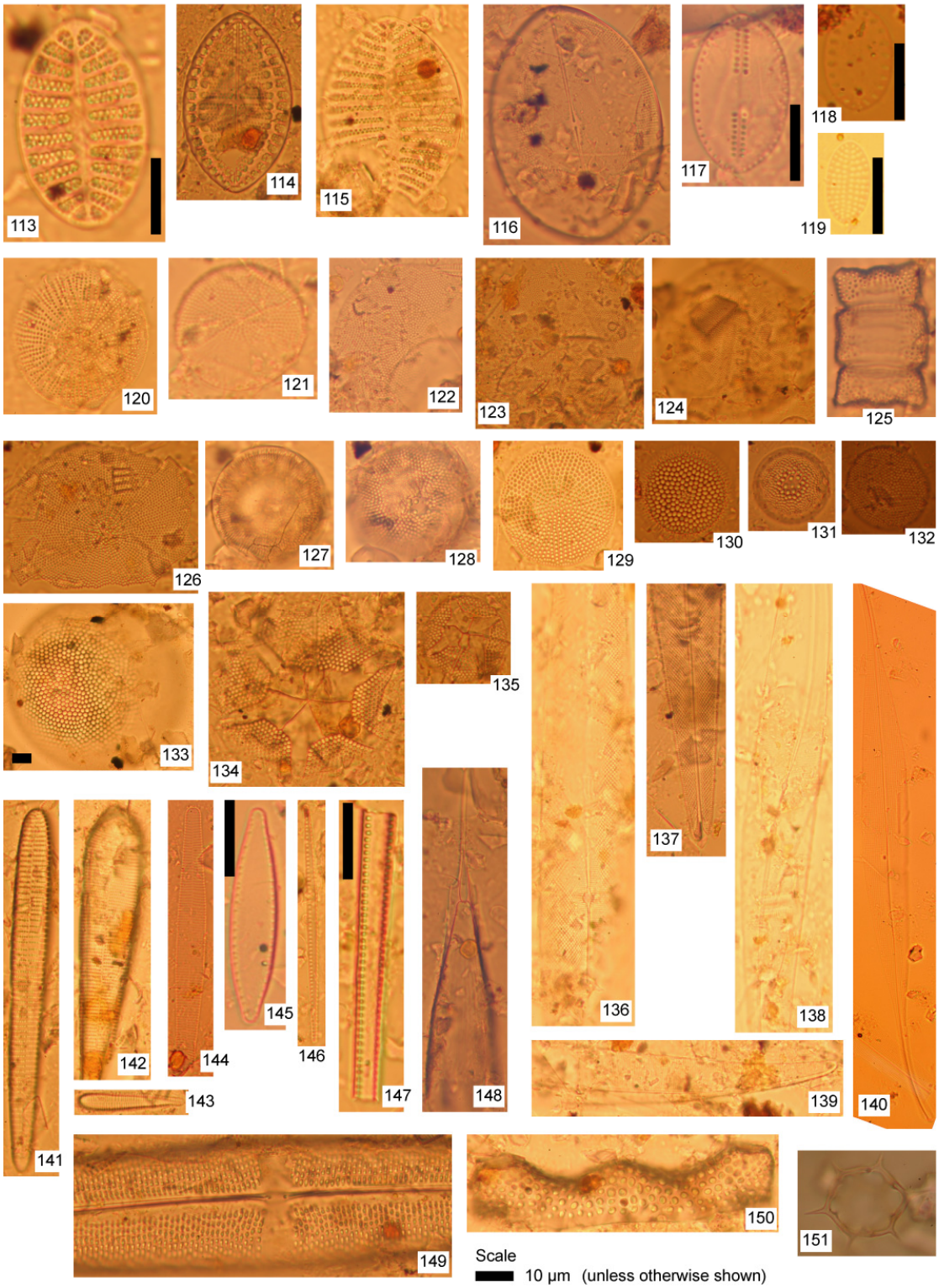

Appendix 4.1 Chlorine-36 exposure age determination

Sample NH1

1- Input	Symbol	Units	Calculations	Uncertainties	Ca	K	Ti	Fe	Cl	O, rock	Si	Na	Mg	Al	Mn	P	H	O, water	Li	B	Sm	Gd	Th	U	Be	Sc	Co	Rb	Sr	Zr	Cs	Ba
element concentration in bulk rock		ppm			54181	10128	3981	56429	46.2	448310	254817	26339	21406	93441	998.9	698.6	1500	12000	5	8.2	4.3	3.7	4.18	1.3	1	22	23	23	534	149	0.3	290
element concentration in dissolved sample (target fraction)		ppm			22087.17	10659.11	2237.59	215.82	46.19																								
uncertainty element concentration (target fraction)		ppm			447.6	289	73	881	2																								
atomic mass of element k	A_k	g*mol-1			40.08	39.10	47.90	55.85	35.45	16.00	28.09	22.99	24.31	26.98	54.94	30.97	1.01	16.00	6.94	10.81	150.40	157.25	232.00	238.03	9.01	44.96	58.93	85.47	87.62	91.22	132.91	137.33	
depth reference (surface or point under surface)		cm	0																													
sample thickness		cm	10																													
bulk rock density	rho	g cm^{-3}	2.6																													
mass depth reference	z	g cm^{-2}	0																													
mass thickness	z_s	g cm^{-2}	25																													
scaling factor for nucleonic production as a function of elevation, latitude (and geomagnetic variations)	$S_{el,s}$	-	1.4307	0.0715																												
scaling factor for muonic production as a function of elevation, latitude (and geomagnetic variations)	$S_{el,\mu}$	-	1.1869	0.0593																												
correction factor for shielding of a sample of arbitrary orientation by surrounding topography	S_T	-	0.992	0.0099																												
correction factor for geometry effects on spallogenic production	S_{shape}	-	1	0.03																												
correction factor for snow shielding for spallogenic production	S_{snow}	-	1	0.01																												
exposure duration (independently determined or estimated)	t_{expo}	yr	10000	3000																												
formation age of rock (independently determined or estimated) for radiogenic correction	t_{form}	yr	4.80E+07	3000000																												
erosion rate	ε	mm ka^{-1}	0	0.00E+00																												
total measured number of ^{36}Cl atoms in sample	N_{meas}	atoms ^{36}Cl g^{-1}	4.70E+04	4.82E+04																												

2- Output A: age of sample				
decay constant for ^{36}Cl	λ_{36}	yr^{-1}	2.30E-06	1.52E-08
scaled total sample specific ^{36}Cl production rate without radiogenic	P_{total}	atoms ^{36}Cl g^{-1} yr^{-1}	7.0182	0.6
time factor radiogenic	t_r		434216	2865.8
number of radiogenically produced ^{36}Cl atoms for estimated age	N_r	atoms ^{36}Cl g^{-1}	8617.5920	434.6
total measured number of ^{36}Cl atoms in sample without calculated radiogenic	$N_{m,r}$	atoms ^{36}Cl g^{-1}	3.83E+04	48233.1
age of sample	**t**	**yr**	**5497**	**6978.7**

3- Output B: calculated ^{36}Cl contributions from each production mechanism				
time factor cosmogenic without erosion	t_{coem}		9886	2931.6995
total calculated number of ^{36}Cl atoms for given time + radiogenic	$N_{calc,total}$	atoms ^{36}Cl g^{-1}	**7.80E+04**	21547
difference measured/calculated number of ^{36}Cl atoms in sample			**-66.12%**	
contribution from each production mechanism:				
number of atoms ^{36}Cl per g by spallation of Ca	$N_{x,Ca}$	atoms ^{36}Cl g^{-1}	19164.5153	**24.57%**
number of atoms ^{36}Cl per g by spallation of K	$N_{x,K}$	atoms ^{36}Cl g^{-1}	22429.3803	**28.76%**
number of atoms ^{36}Cl per g by spallation of Ti	$N_{x,Ti}$	atoms ^{36}Cl g^{-1}	377.8383	**0.48%**
number of atoms ^{36}Cl per g by spallation of Fe	$N_{x,Fe}$	atoms ^{36}Cl g^{-1}	5.3263	**0.01%**
number of atoms ^{36}Cl per g by spallation of target elements	N_s	atoms ^{36}Cl g^{-1}	41977.0603	**53.82%**
number of atoms ^{36}Cl per g by capture of thermal neutrons	N_{th}	atoms ^{36}Cl g^{-1}	21460.4719	**27.51%**
number of atoms ^{36}Cl per g by capture of epithermal neutrons	N_{eth}	atoms ^{36}Cl g^{-1}	3446.1014	**4.42%**
number of atoms ^{36}Cl per g by capture of thermal and epithermal neutrons	N_n	atoms ^{36}Cl g^{-1}	24906.5733	**31.93%**
number of atoms ^{36}Cl per g by capture of slow negative muons	N_μ	atoms ^{36}Cl g^{-1}	2496.2446	**3.20%**
number of atoms ^{36}Cl per g by radiogenic production	N_r	atoms ^{36}Cl g^{-1}	8617.5920	**11.05%**
				100%

4- Output C: calculated number of ^{36}Cl atoms and age of eroded sample				
total calculated number of ^{36}Cl atoms for approached estimated time in eroded sample	$N_{calc,total}$	atoms ^{36}Cl g^{-1}	**7.28E+04**	
difference measured/calculated number of ^{36}Cl atoms in eroded sample	$\Delta N_{meas-calc}$		**-55.12%**	
time factor with erosion for spallation reaction	$t_{coem,s}$		9886	2931.6995
time factor with erosion for capture of epithermal neutrons	$t_{coem,eth}$		9886	2931.6995
time factor with erosion for capture of thermal neutrons	$t_{coem,th}$		9886	2931.6995
time factor with erosion for capture of slow negative muons	$t_{coem,\mu}$		9886	2931.6995
depth reference factor for spallogenic reaction	d_s		1.000	
depth reference factor for capture of epithermal neutrons	d_{eth}		1.000	
depth reference factor for capture of thermal neutrons	d_{th}		1.000	
depth reference factor for capture of slow negative muons	d_μ		1.000	
production rate coefficient corrected for sample thickness for spallogenic reaction	$J_{Cl,s}$		7.67	
production rate coefficient corrected for sample thickness for capture of epithermal neutrons	$J_{Cl,eth}$		0.25	
production rate coefficient corrected for sample thickness for capture of thermal neutrons	$J_{Cl,th}$		-3.83	
production rate coefficient corrected for sample thickness for capture of slow negative muons	$J_{Cl,\mu}$		0.49	
production rate coefficient for spallogenic reaction	J_s		6.05	
production rate coefficient for capture of epithermal neutrons	J_{eth}		0.1291	
production rate coefficient for capture of thermal neutrons	J_{th}		-2.38	
production rate coefficient for capture of slow negative muons	J_μ		0.38	

5- Elemental parameters																																
avogadro			6.02E+23																													
atomic concentration of element k in **bulk rock**	N_k	atoms g^{-1}	2.87E+22		8.14E+20	1.56E+20	5.00E+19	6.08E+20	7.85E+17	1.69E+22	5.46E+21	6.90E+20	5.30E+20	2.09E+21	1.09E+19	1.36E+19	8.96E+20	4.52E+20	4.34E+17	4.57E+17	1.71E+16	1.43E+16	1.08E+16	3.29E+15	6.68E+16	2.95E+17	2.35E+17	1.62E+17	3.67E+18	9.84E+17	1.36E+15	1.27E+18
atomic concentration of element k in **target fraction**	N_{Cl}	atoms g^{-1}							7.8451E+17																							
dilute resonance integral for absorption of epithermal neutrons by element k (Fabryka-Martin, 1988)	$I_{0,k}$	E^{-24} cm^2			0.235	1	3.1	1.39	13.7	0.0004	0.127	0.311	0.038	0.17	14		0	0	1722	1400	390												
average log decrement of energy loss per collision for element k (Fabryka-Martin, 1988)	x_k	-			0.049	0.05	0.041	0.035	0.055	0.12	0.07	0.084	0.08	0.072	0.036		1	0.264	0.174	0.013	0.013											
neutron scattering cross ection of element k (Fabryka-Martin, 1988)	$\sigma_{sc,k}$	E^{-24} cm^2			2.93	2.04	4.09	11.35	15.8	3.76	2.04	3.025	3.42	1.41	2.2	5	20.5	0.95	4.27	38	172											
thermal neutron absorption cross section of element k (Fabryka-Martin, 1988)	$\sigma_{a,k}$	E^{-24} cm^2			0.43	2.15	6.1	2.56	33.5	0.0002	0.17	0.53	0.063	0.23	13.3	0.2	0.33	70.5	767	9640	41560											
proportion of muons stopped in element i that are captured by the nucleus (Fabryka-Martin, 1988)	$f_{i,k}$				0.864	0.83		0.906		0.223	0.671	0.432	0.538	0.582																		
average neutron yield per captured muon (Fabryka-Martin, 1988)	Y_n				0.75	1.25		1.125		0.8	0.86	1	0.6	1.26																		

6- Unscaled sample specific ^{36}Cl production rate by capture of epithermal neutrons																																
effective macroscopic resonance integral for absorption of epithermal neutrons	I_{eff}	cm^2 g^{-1}	0.0036		1.91E-04	1.56E-04	1.55E-04	8.46E-04	1.08E-05	6.75E-06	6.94E-04	2.15E-04	2.02E-05	3.55E-04	1.53E-04		0.00E+00	0.00E+00	7.87E-04	2.39E-05	5.57E-06											
fraction of epithermal neutrons absorbed by ^{35}Cl **(target fraction)**	f_{eth}	-	0.0030																													
neutron macroscopic scattering cross section in ss	Σ_{sc}	cm^2 g^{-1}	0.110		2.39E-03	3.18E-04	2.05E-04	6.91E-03	1.24E-05	6.34E-02	1.11E-02	2.09E-03	1.81E-03	2.94E-03	2.41E-05	6.79E-05	1.84E-02	0.00E+00	4.12E-07	1.95E-06	6.48E-07	2.46E-06	0.00E+00	0.00E+00	0.00E+00	0.00E+00	0.00E+00	0.00E+00	0.00E+00	0.00E+00	0.00E+00	0.00E+00	0.00E+00
scattering rate parameter	B		2.77E-02		1.17E-04	1.59E-05	8.39E-06	2.42E-04	6.82E-07	7.61E-03	7.80E-04	1.75E-04	1.45E-04	2.12E-04	8.67E-07	0.00E+00	1.84E-02	0.00E+00	1.09E-07	3.39E-07	8.43E-09	3.19E-08	0.00E+00	0.00E+00	0.00E+00	0.00E+00	0.00E+00	0.00E+00	0.00E+00	0.00E+00	0.00E+00	0.00E+00	0.00E+00
mean macroscopic log decrement of energy loss per collision in ss	X_{ss}		0.252																													
macroscopic absorption and moderation cross section for epithermal neutrons	Σ_{eth}	cm^2 g^{-1}	0.029																													
attenuation length for absorption and moderation of epithermal neutron flux	Λ_{eth}	g cm^{-2}	34.970																													
	$A_k * N_k$	atoms mol^{-1}	5.85E+23		3.26E+22	6.10E+21	2.40E+21	3.40E+22	2.78E+19	2.70E+23	1.53E+23	1.59E+22	1.29E+22	5.63E+22	6.02E+20		9.03E+20		3.01E+18	4.94E+18	2.57E+18	2.25E+18											
average atomic weight in subsurface	A_{ss}	g mol^{-1}	20.420																													

| | | |

result radiogenic sample specific ^{36}Cl production rate	P_r	atoms ^{36}Cl g^{-1} yr^{-1}	0.0198	0.0010

11- Thickness integration factors				
effective attenuation length for cosmic-ray flux through a surface of arbitrary orientation and shielding (Gosse and Phillips, 2001)	$\lambda_{e,e}$	g cm^{-2}	160	
ratio of production rate integrated over the thickness of a sample to the surface production rate, due to spallation	Q_s	-	0.9258	0.0185
ratio of production rate integrated over the thickness of a sample to the surface production rate, due to thermal neutron absorption	Q_{th}	-	1.6088	0.0322
ratio of production rate integrated over the thickness of a sample to the surface production rate, due to epithermal neutron absorption	Q_{eth}	-	1.146	0.0229
ratio of production rate integrated over the thickness of a sample to the surface production rate, due to muon absorption	Q_μ	-	0.992	0.0198

Notes
Spreadsheet from Schimmelpfennig *et al.*, 2009
Values input by user into black framed cells

Appendix 4.2 Chlorine-36 exposure age determination

Sample NH2

1- Input	Symbol	Units	Calculations	Uncertainties	Ca	K	Ti	Fe	Cl	O_rock	Si	Na	Mg	Al	Mn	P	H	O_water	Li	B	Sm	Gd	Th	U	Be	Sc	Co	Rb	Sr	Zr	Ba
element concentration in bulk rock		ppm			**31880**	**14694**	**4310**	**48108**	**38**	**457358**	**278802**	**32794**	**13929**	**88518**	**991**	**786**	**1356**	**10844**	**5**	**18.0**	**5.5**	**4.8**	**5.55**	**1.58**	**1**	**15**	**15**	**31**	**442**	**113**	**536**
element concentration in dissolved sample (target fraction)		ppm			**12264.11**	**22801.40**	**2389.33**	**186.77**	**38**																							
uncertainty element concentration (target fraction)		ppm			4470	290	73	886																							
atomic mass of element k	A_k	g*mol-1			40.08	39.10	47.90	55.85	35.45	16.00	28.09	22.99	24.31	26.98	54.94	30.97	1.01	16.00	6.94	10.81	150.40	157.25	232.00	238.03	9.01	44.96	58.93	85.47	87.62	91.22	137.33
depth reference (surface or point under surface)		cm	**0**																												
sample thickness		cm	**9**																												
bulk rock density	rho	g cm^{-3}	**2.5**																												
mass depth reference	z	g cm^{-2}	0																												
mass thickness	z_t	g cm^{-2}	22.5																												
scaling factor for nucleonic production as a function of elevation, latitude (and geomagnetic variations)	$S_{sl,s}$	-	**1.4307**	0.0715																											
scaling factor for muonic production as a function of elevation, latitude (and geomagnetic variations)	$S_{sl,\mu}$	-	**1.1869**	0.0593																											
correction factor for shielding of a sample of arbitrary orientation by surrounding topography	S_c	-	**0.9920**	0.0099																											
correction factor for geometry effects on spallogenic production	S_{shape}	-	**1**	0.03																											
correction factor for snow shielding for spallogenic production	S_{snow}	-	**1**	0.01																											
exposure duration (independently determined or estimated)	t_{expo}	yr	**10000**	3000																											
formation age of rock (independently determined or estimated) for radiogenic correction	t_{form}	yr	**4.80E+07**	3000000																											
erosion rate	ε	mm ka^{-1}	**0**	0.00E+00																											
total measured number of ^{36}Cl atoms in sample	N_{meas}	atoms ^{36}Cl g^{-1}	**5.15E+04**	9.49E+03																											

2- Output A: age of sample				
decay constant for ^{36}Cl	λ_{36}	yr^{-1}	2.30E-06	1.52E-08
scaled total sample specific ^{36}Cl production rate without radiogenic	P_{total}	atoms ^{36}Cl g^{-1} yr^{-1}	7.6757	0.9
time factor radiogenic	t_r		434216	2865.8
number of radiogenically produced ^{36}Cl atoms for estimated age	N_r	atoms ^{36}Cl g^{-1}	7582.2527	382.4
total measured number of ^{36}Cl atoms in sample without calculated radiogenic	$N_{m,r}$	atoms ^{36}Cl g^{-1}	4.39E+04	9502.0
age of sample	**t**	**yr**	**5764**	**1440.2**

3- Output B: calculated ^{36}Cl contributions from each production mechanism				
time factor cosmogenic without erosion	t_{coem}		9886	2931.6996
total calculated number of ^{36}Cl atoms for given time + radiogenic	$N_{calc,total}$	atoms ^{36}Cl g^{-1}	**8.35E+04**	24333
difference measured/calculated number of ^{36}Cl atoms in sample			**-61.97%**	
contribution from each production mechanism:				
number of atoms ^{36}Cl per g by spallation of Ca	$N_{s,Ca}$	atoms ^{36}Cl g^{-1}	7846.1013	**9.40%**
number of atoms ^{36}Cl per g by spallation of K	$N_{s,K}$	atoms ^{36}Cl g^{-1}	48346.7141	**57.93%**
number of atoms ^{36}Cl per g by spallation of Ti	$N_{s,Ti}$	atoms ^{36}Cl g^{-1}	406.5463	**0.49%**
number of atoms ^{36}Cl per g by spallation of Fe	$N_{s,Fe}$	atoms ^{36}Cl g^{-1}	4.6447	**0.01%**
number of atoms ^{36}Cl per g by spallation of target elements	N_s	atoms ^{36}Cl g^{-1}	56604.0064	**67.82%**
number of atoms ^{36}Cl per g by capture of thermal neutrons	N_{th}	atoms ^{36}Cl g^{-1}	14228.2217	**17.05%**
number of atoms ^{36}Cl per g by capture of epithermal neutrons	N_{eth}	atoms ^{36}Cl g^{-1}	2660.1265	**3.19%**
number of atoms ^{36}Cl per g by capture of thermal and epithermal neutrons	N_n	atoms ^{36}Cl g^{-1}	16888.3482	**20.23%**
number of atoms ^{36}Cl per g by capture of slow negative muons	N_μ	atoms ^{36}Cl g^{-1}	2387.5941	**2.86%**
number of atoms ^{36}Cl per g by radiogenic production	N_r	atoms ^{36}Cl g^{-1}	7582.2527	**9.08%**
				100%

4- Output C: calculated number of ^{36}Cl atoms and age of eroded sample				
total calculated number of ^{36}Cl atoms for approached estimated time in eroded sample	$N_{calc,total}$	atoms ^{36}Cl g^{-1}	**8.346E+04**	
difference measured/calculated number of ^{36}Cl atoms in eroded sample	$\Delta N_{meas-calc}$		**-61.97%**	
time factor with erosion for spallation reaction	$t_{coem,s}$		9886	2931.6995
time factor with erosion for capture of epithermal neutrons	$t_{coem,eth}$		9886	2931.6995
time factor with erosion for capture of thermal neutrons	$t_{coem,th}$		9886	2931.6995
time factor with erosion for capture of slow negative muons	$t_{coem,\mu}$		9886	2931.6995
depth reference factor for spallogenic reaction	d_s		1.000	
depth reference factor for capture of epithermal neutrons	d_{eth}		1.000	
depth reference factor for capture of thermal neutrons	d_{th}		1.000	
depth reference factor for capture of slow negative muons	d_μ		1.000	
production rate coefficient corrected for sample thickness for spallogenic reaction	J_{Cs}		7.25	
production rate coefficient corrected for sample thickness for capture of epithermal neutrons	J_{Ceth}		0.19	
production rate coefficient corrected for sample thickness for capture of thermal neutrons	J_{Cth}		-2.41	
production rate coefficient corrected for sample thickness for capture of slow negative muons	$J_{C\mu}$		0.38	
production rate coefficient for spallogenic reaction	J_s		6.48	
production rate coefficient for capture of epithermal neutrons	J_{eth}		0.1074	
production rate coefficient for capture of thermal neutrons	J_{th}		-1.57	
production rate coefficient for capture of slow negative muons	J_μ		0.31	

5- Elemental parameters																															
avogadro			6.02E+23																												
atomic concentration of element k in **bulk rock**	N_k	atoms g^{-1}	2.89E+22		4.79E+20	2.26E+20	5.42E+19	5.19E+20	5.95E+17	1.72E+22	5.98E+21	8.59E+20	3.45E+20	1.98E+21	1.09E+19	1.53E+19	8.10E+20	4.08E+20	4.34E+17	1.00E+18	2.21E+16	1.83E+16	1.44E+16	4.00E+15	6.68E+16	2.41E+17	1.53E+17	2.18E+17	3.04E+18	7.46E+17	2.36E+18
atomic concentration of element k in **target fraction**	N_{Cl}	atoms g^{-1}							5.92E+17																						
dilute resonance integral for absorption of epithermal neutrons by element k (Fabryka-Martin, 1988)	$I_{s,k}$	E^{-24} cm^2			0.235	1	3.1	1.39	13.7	0.0004	0.127	0.311	0.038	0.17	14		0	0	1722	1400	390										
average log decrement of energy loss per collision for element k (Fabryka-Martin, 1988)	x_k	-			0.049	0.05	0.041	0.035	0.055	0.12	0.07	0.084	0.08	0.072	0.036		1		0.264	0.174	0.013	0.013									
neutron scattering cross ection of element k (Fabryka-Martin, 1988)	$\sigma_{n,s,k}$	E^{-24} cm^2			2.93	2.04	4.09	11.35	15.8	3.76	2.04	3.025	3.42	1.41	2.2	5	20.5		0.95	4.27	38	172									
thermal neutron absorption cross section of element k (Fabryka-Martin, 1988)	$\sigma_{a,k}$	E^{-24} cm^2			0.43	2.15	6.1	2.56	33.5	0.0002	0.17	0.53	0.063	0.23	13.3	0.2	0.33		70.5	767	9640	41560									
proportion of muons stopped in element i that are captured by the nucleus (Fabryka-Martin, 1988)	$f_{\mu,k}$				0.864	0.83		0.906		0.223	0.671	0.432	0.538	0.582																	
average neutron yield per captured muon (Fabryka-Martin, 1988)	Y_n				0.75	1.25		1.125		0.8	0.86	1	0.6	1.26																	

6- Unscaled sample specific ^{36}Cl production rate by capture of epithermal neutrons																															
effective macroscopic resonance integral for absorption of epithermal neutrons	I_{eff}	cm^2 g^{-1}	0.004535		1.13E-04	2.26E-04	1.68E-04	7.21E-04	8.14E-06	6.89E-06	7.59E-04	2.67E-04	1.31E-05	3.36E-04	1.52E-04		0.00E+00		0.00E+00	1.73E-03	3.09E-05	7.15E-06									
fraction of epithermal neutrons absorbed by ^{36}Cl **(target fraction)**	f_{eth}	-	0.0018																												
neutron macroscopic scattering cross section in ss	Σ_{sc}	cm^2 g^{-1}	0.108		1.40E-03	4.62E-04	2.22E-04	5.89E-03	9.39E-06	6.47E-02	1.22E-02	2.60E-03	1.18E-03	2.79E-03	2.39E-05	7.64E-05	1.66E-02	0.00E+00	4.12E-07	4.28E-08	8.38E-07	3.16E-06	0.00E+00	0.00E+00	0.00E+00	0.00E+00	0.00E+00	0.00E+00	0.00E+00	0.00E+00	0.00E+00
scattering rate parameter	B		2.61E-02		6.88E-05	2.31E-05	9.09E-06	2.06E-04	5.17E-07	7.77E-03	8.54E-04	2.18E-04	9.44E-05	2.01E-04	8.60E-07	0.00E+00	1.66E-02	0.00E+00	1.09E-07	7.45E-07	1.09E-08	4.10E-08	0.00E+00	0.00E+00	0.00E+00	0.00E+00	0.00E+00	0.00E+00	0.00E+00	0.00E+00	0.00E+00
mean macroscopic log decrement of energy loss per collision in ss	X_{ss}		0.241																												
macroscopic absorption and moderation cross section for epithermal neutrons	Σ_{eth}	cm^2 g^{-1}	0.027																												
attenuation length for absorption and moderation of epithermal neutron flux	Λ_{eth}	g cm^{-2}	36.840																												
	$A_k * N_K$	atoms mol^{-1}	5.86E+23		1.92E+22	8.85E+21	2.60E+21	2.90E+22	2.11E+19	2.75E+23	1.68E+23	1.97E+22	8.39E+21	5.33E+22	5.97E+20		8.17E+20		3.01E+18	1.08E+19	3.32E+18	2.88E+18									

| | | |

neutron production by alpha,n-reactions	$P_{n,\alpha}$	n*g-1*yr-1	5.4630	
total radiogenic epithermal neutron production	$P_{eth,r}$	epithermal n/(g*yr)	0.9811	
total radiogenic thermal neutron production	$P_{th,r}$	thermal n/(g*yr)	5.1597	
result radiogenic sample specific ^{36}Cl production rate	**P_r**	**atoms ^{36}Cl g^{-1} yr^{-1}**	**0.0175**	0.0009

11- Thickness integration factors				
effective attenuation length for cosmic-ray flux through a surface of arbitrary orientation and shielding (Gosse and Phillips, 2001)	λ_{cr}	g cm^{-2}	160	
ratio of production rate integrated over the thickness of a sample to the surface production rate, due to spallation	Q_s	-	0.9329	0.0187
ratio of production rate integrated over the thickness of a sample to the surface production rate, due to thermal neutron absorption	Q_{th}	-	1.5327	0.0307
ratio of production rate integrated over the thickness of a sample to the surface production rate, due to epithermal neutron absorption	Q_{eth}	-	1.152	0.0230
ratio of production rate integrated over the thickness of a sample to the surface production rate, due to muon absorption	Q_μ	-	0.993	0.0199

Notes
Spreadsheet from Schimmelpfennig *et al*., 2009
Values input by user into black framed cells

Appendix 4.3 Chlorine-36 exposure age determination

Sample NH3

1- Input	Symbol	Units	Calculations	Uncertainties	Ca	K	Ti	Fe	Cl	O, rock	Si	Na	Mg	Al	Mn	P	H	O, water	Li	B	Sm	Gd	Th	U	Be	Sc	Co	Rb	Sr	Zr	Ba
element concentration in bulk rock		ppm			44246	873	4826	57478	41	454034	263841	30345	19597	90053	1154	873.2	1367	10933	5	11.4	4.7	4.1	4.45	1.38	1	22	16	30	508	150	370
element concentration in dissolved sample (target fraction)		ppm			20729.0553	19458.6837	2796.9925	257.7847	41																						
uncertainty element concentration (target fraction		ppm			4470	290	73	590	5																						
atomic mass of element k	A_k	g*mol-1			40.08	39.10	47.90	55.85	35.45	16.00	28.09	22.99	24.31	26.98	54.94	30.97	1.01	16.00	6.94	10.81	150.40	157.25	232.00	238.03	9.01	44.96	58.93	85.47	87.62	91.22	137.33
depth reference (surface or point under surface)		cm	0																												
sample thickness		cm	6																												
bulk rock density	rho	g cm^{-3}	2.5																												
mass depth reference	z	g cm^{-2}	0																												
mass thickness	z_k	g cm^{-2}	15																												
scaling factor for nucleonic production as a function of elevation, latitude (and geomagnetic variations)	$S_{e,s}$	-	1.4307	0.0715																											
scaling factor for muonic production as a function of elevation, latitude (and geomagnetic variations)	$S_{e,\mu}$	-	1.1869	0.0593																											
correction factor for shielding of a sample of arbitrary orientation by surrounding topography	S_T	-	0.992	0.0099																											
correction factor for geometry effects on spallogenic production	S_{shape}	-	1	0.03																											
correction factor for snow shielding for spallogenic production	S_{snow}	-	1	0.01																											
exposure duration (independently determined or estimated)	t_{expo}	yr	10000	3000																											
formation age of rock (independently determined or estimated) for radiogenic correction	t_{form}	yr	4.80E+07	3000000																											
erosion rate	ε	mm ka^{-1}	0	0.00E+00																											
total measured number of ^{36}Cl atoms in sample	N_{meas}	atoms ^{36}Cl g^{-1}	7.73E+04	8.41E+04																											

2- Output A: age of sample				
decay constant for ^{36}Cl	λ_{36}	yr^{-1}	2.30E-06	1.52E-08
scaled total sample specific ^{36}Cl production rate without radiogenic	P_{total}	atoms ^{36}Cl g^{-1} yr^{-1}	7.9624	0.9
time factor radiogenic	t_r		434216.2397	2865.8
number of radiogenically produced ^{36}Cl atoms for estimated age	N_r	atoms ^{36}Cl g^{-1}	8226.2458	414.9
total measured number of ^{36}Cl atoms in sample without calculated radiogenic	$N_{m,r}$	atoms ^{36}Cl g^{-1}	6.91E+04	84110.8
age of sample	**t**	**yr**	**8764**	**10822.5**

3- Output B: calculated ^{36}Cl contributions from each production mechanism				
time factor cosmogenic without erosion	t_{coem}		9886	2931.6995
total calculated number of ^{36}Cl atoms for given time + radiogenic	$N_{calc,total}$	atoms ^{36}Cl g^{-1}	**8.69E+04**	24904
difference measured/calculated number of ^{36}Cl atoms in sample			**-12.46%**	
contribution from each production mechanism:				
number of atoms ^{36}Cl per g by spallation of Ca	$N_{s,Ca}$	atoms ^{36}Cl g^{-1}	13547.8305	**15.58%**
number of atoms ^{36}Cl per g by spallation of K	$N_{s,K}$	atoms ^{36}Cl g^{-1}	42218.1206	**48.56%**
number of atoms ^{36}Cl per g by spallation of Ti	$N_{s,Ti}$	atoms ^{36}Cl g^{-1}	486.9732	**0.56%**
number of atoms ^{36}Cl per g by spallation of Fe	$N_{s,Fe}$	atoms ^{36}Cl g^{-1}	6.5597	**0.01%**
number of atoms ^{36}Cl per g by spallation of target elements	N_s	atoms ^{36}Cl g^{-1}	56259.4840	**64.71%**
number of atoms ^{36}Cl per g by capture of thermal neutrons	N_{th}	atoms ^{36}Cl g^{-1}	16431.5566	**18.90%**
number of atoms ^{36}Cl per g by capture of epithermal neutrons	N_{eth}	atoms ^{36}Cl g^{-1}	3097.1574	**3.56%**
number of atoms ^{36}Cl per g by capture of thermal and epithermal neutrons	N_n	atoms ^{36}Cl g^{-1}	19528.7140	**22.46%**
number of atoms ^{36}Cl per g by capture of slow negative muons	N_μ	atoms ^{36}Cl g^{-1}	2925.7267	**3.37%**
number of atoms ^{36}Cl per g by radiogenic production	N_r	atoms ^{36}Cl g^{-1}	8226.2458	**9.46%**
				100%

4- Output C: calculated number of ^{36}Cl atoms and age of eroded sample				
total calculated number of ^{36}Cl atoms for approached estimated time in eroded sample	$N_{calc,total}$	atoms ^{36}Cl g^{-1}	**8.69E+04**	
difference measured/calculated number of ^{36}Cl atoms in eroded sample	$\Delta N_{meas-calc}$		**-12.46%**	
time factor with erosion for spallation reaction	$t_{coem,s}$		9886	2931.6995
time factor with erosion for capture of epithermal neutrons	$t_{coem,eth}$		9886	2931.6995
time factor with erosion for capture of thermal neutrons	$t_{coem,th}$		9886	2931.6995
time factor with erosion for capture of slow negative muons	$t_{coem,\mu}$		9886	2931.6995
depth reference factor for spallogenic reaction	d_s		1.000	
depth reference factor for capture of epithermal neutrons	d_{eth}		1.000	
depth reference factor for capture of thermal neutrons	d_{th}		1.000	
depth reference factor for capture of slow negative muons	d_μ		1.000	
production rate coefficient corrected for sample thickness for spallogenic reaction	$J_{D,s}$		7.91	
production rate coefficient corrected for sample thickness for capture of epithermal neutrons	$J_{D,eth}$		0.20	
production rate coefficient corrected for sample thickness for capture of thermal neutrons	$J_{D,th}$		-2.95	
production rate coefficient corrected for sample thickness for capture of slow negative muons	$J_{D,\mu}$		0.45	
production rate coefficient for spallogenic reaction	J_s		7.01	
production rate coefficient for capture of epithermal neutrons	J_{eth}		0.1267	
production rate coefficient for capture of thermal neutrons	J_{th}		-2.09	
production rate coefficient for capture of slow negative muons	J_μ		0.39	

5- Elemental parameters																															
avogadro			6.02E+23																												
atomic concentration of element k in **bulk rock**	N_k	atoms g^{-1}	2.87E+22		6.65E+20	1.34E+19	6.07E+19	6.20E+20	6.96E+17	1.71E+22	5.66E+21	7.95E+20	4.86E+20	2.01E+21	1.26E+19	1.70E+19	8.17E+20	4.12E+20	4.34E+17	6.35E+17	1.87E+16	1.57E+16	1.16E+16	3.49E+15	6.68E+16	2.95E+17	1.63E+17	2.11E+17	3.49E+18	9.90E+17	1.62E+18
atomic concentration of element k in **target fraction**	N_{Cl}	atoms g^{-1}							6.95E+17																						
dilute resonance integral for absorption of epithermal neutrons by element k (Fabryka-Martin, 1988)	$I_{o,k}$	E^{-24} cm^2			0.235	1	3.1	1.39	13.7	0.0004	0.127	0.311	0.038	0.17	14		0		0	1722	1400	390										
average log decrement of energy loss per collision for element k (Fabryka-Martin, 1988)	x_k	-			0.049	0.05	0.041	0.035	0.055	0.12	0.07	0.084	0.08	0.072	0.036		1		0.264	0.174	0.013	0.013										
neutron scattering cross ection of element k (Fabryka-Martin, 1988)	$\sigma_{sc,k}$	E^{-24} cm^2			2.93	2.04	4.09	11.35	15.8	3.76	2.04	3.025	3.42	1.41	2.2	5	20.5		0.95	4.27	38	172										
thermal neutron absorption cross section of element k (Fabryka-Martin, 1988)	$\sigma_{a,k}$	E^{-24} cm^2			0.43	2.15	6.1	2.56	33.5	0.0002	0.17	0.53	0.063	0.23	13.3	0.2	0.33		70.5	767	9640	41560										
proportion of muons stopped in element i that are captured by the nucleus (Fabryka-Martin, 1988)	$f_{cl,k}$				0.864	0.83		0.906		0.223	0.671	0.432	0.538	0.582																	
average neutron yield per captured muon (Fabryka-Martin, 1988)	Y_n				0.75	1.25		1.125		0.8	0.86	1	0.6	1.26																	

6- Unscaled sample specific ^{36}Cl production rate by capture of epithermal neutrons																															
effective macroscopic resonance integral for absorption of epithermal neutrons	I_{eff}	cm^2 g^{-1}	0.0039		1.56E-04	1.34E-05	1.88E-04	8.62E-04	9.54E-06	6.84E-06	7.18E-04	2.47E-04	1.85E-05	3.42E-04	1.77E-04		0.00E+00		0.00E+00	1.09E-03	2.62E-05	6.14E-06									
fraction of epithermal neutrons absorbed by ^{35}Cl **(target fraction)**	f_{eth}	-	0.0025																												
neutron macroscopic scattering cross section in ss	$\sum_{sc}$	cm^2 g^{-1}	0.109		1.95E-03	2.74E-05	2.48E-04	7.03E-03	1.10E-05	6.43E-02	1.15E-02	2.40E-03	1.66E-03	2.83E-03	2.78E-05	8.49E-05	1.67E-02	0.00E+00	4.12E-07	2.71E-06	7.11E-07	2.71E-06	0.00E+00	0.00E+00	0.00E+00	0.00E+00	0.00E+00	0.00E+00	0.00E+00	0.00E+00	0.00E+00	0.00E+00
scattering rate parameter	B		2.62E-02		9.54E-05	1.37E-06	1.02E-05	2.46E-04	6.05E-07	7.71E-03	8.08E-04	2.02E-04	1.33E-04	2.04E-04	1.00E-06	0.00E+00	1.67E-02	0.00E+00	1.09E-07	4.72E-07	9.24E-09	3.52E-08	0.00E+00	0.00E+00	0.00E+00	0.00E+00	0.00E+00	0.00E+00	0.00E+00	0.00E+00	0.00E+00	0.00E+00
mean macroscopic log decrement of energy loss per collision in ss	X_{ss}		0.240																												
macroscopic absorption and moderation cross section for epithermal neutrons	$\sum_{eth}$	cm^2 g^{-1}	0.027																												
attenuation length for absorption and moderation of epithermal neutron flux	Λ_{eth}	g cm^{-2}	36.921																												
	$A_k * N_k$	atoms mol^{-1}	5.83E+23		2.66E+22	5.26E+20	2.91E+21	3.46E+22	2.47E+19	2.73E+23	1.59E+23	1.83E+22	1.18E+22	5.42E+22	6.95E+20		8.23E+20		3.01E+18	6.87E+18	2.81E+18	2.48E+18										
average atomic weight in subsurface	A_{ss}	g mol^{-1}	20.335																												

production rate of epithermal neutrons from fast neutrons in atm at land/atm interface (Gosse and Phillips, 2001)	$P_n(0)$	n cm^{-2} yr^{-1}	626	46
Ratio of epithermal neutron production in subsurface to that in atmosphere	R_{eth}	-	1.18	
epithermal neutron diffusion coefficient in ss	D_{eth}	g cm^{-2}	3.17	
apparent fast neutron attenuation coefficient (Gosse and Phillips, 2001)	Λ_f	g cm^{-2}	160	
epithermal neutron flux at land/atmosphere interface that would be observed in ss if interface was not present	Φ^*_{eth}	n cm^{-2} yr^{-1}	27496	
average neutron yield per stopped negative muon	Y_n		0.4109	
slow negative muon stopping rate at land surface SLHL (Heisinger*et al.*, 2002)	$\Psi_s(0)$	μ g^{-1} yr^{-1}	190	
fast muon flux at land surface SLHL (Gosse and Phillips, 2001)	ϕ_{sf0}	μ cm^{-2} yr^{-1}	7.90E+05	
total muon induced neutron production at land surface	P_{tu0}	μ cm^{-2} yr^{-1}	82.6464	
ratio of muon production rate to epithermal neutron production rate	R'_u	-	0.0925	
macroscopic neutron scattering cross section of atmosphere (Phillips and Plumber, 1996)	$\Sigma_{sc,a}$	cm^2 g^{-1}	0.3773	
thermal neutron diffusion coefficient in atmosphere	D_a	g cm^{-2}	0.9260	
macroscopic absorption and moderation cross section for epithermal neutrons in atm (Phillips and Plumber, 1996)	$\Sigma_{eth,a}$	cm^2 g^{-1}	0.0548	
epithermal neutron diffusion length in atm	$L_{eth,a}$	g cm^{-2}	4.015	
epithermal neutron flux at land/atmosphere interface that would be observed in atm if interface was not present	$\Phi^*_{eth,a}$	n cm^{-2} yr^{-1}	11431	
difference between hypothetical equilibrium epithermal neutron fluxes in atm and ss	$\Delta\Phi^*_{eth}$	n cm^{-2} yr^{-1}	-16065	
adjusted difference between hypothetical equilibrium epithermal neutron fluxes in atm and ss	$\Delta\Phi^{*a}_{eth,a}$	n cm^{-2} yr^{-1}	24154	
epithermal neutron diffusion length in ss	L_{eth}	g cm^{-2}	10.634	
difference between phi_star_eth,ss and actual epithermal neutron flux at land surface	$(F\Delta\phi)^*_{eth}$	-	-7917	
slow muon attenuation length (Heisinger*et al.*, 2002)	Λ_s	g cm^{-2}	1510	
epithermal neutron flux (concentration)	$\Phi_{eth,total}$	n cm^{-2} yr^{-1}	21256	
result unscaled sample specific ^{36}Cl production rate by capture of epithermal neutrons	$\mathbf{P_{eth}}$	**atoms ^{36}Cl g^{-1} yr^{-1}**	**0.1949**	0.0195

7- Unscaled sample specific ^{36}Cl production rate by capture of thermal neutrons																																
macroscopic thermal neutron absorption cross section for ss**(bulk rock)**	Σ_{th}	cm^2 g^{-1}	0.0060		2.86E-04	2.89E-05	3.70E-04	1.59E-03	2.33E-05	3.42E-06	9.62E-04	4.21E-04	3.06E-05	4.62E-04	1.68E-04	3.40E-06	2.70E-04	0.00E+00	3.06E-05	4.87E-04	1.80E-04	6.54E-04	0.00E+00	0.00E+00	0.00E+00	0.00E+00	0.00E+00	0.00E+00	0.00E+00	0.00E+00	0.00E+00	0.00E+00
fraction of thermal neutrons absorbed by elements that produce^{36}Cl **(target fraction)**	f_{th}	-	0.0039																													
attenuation length for absorption of thermal neutron flux	Λ_{th}	g cm^{-2}	1.68E+02																													
resonance escape probability of the atmosphere (Phillips and Plumber, 1996)	$p(E_{th})_a$	-	0.56																													
resonance escape probability of a neutron from the epithermal energy range in ss	$p(E_{th})$	-	0.8627																													
ratio of thermal neutron production in ss to that in atm	R_{th}	-	1.540																													
epithermal neutron diffusion coefficient in ss	D_{th}	g cm^{-2}	3.17																													
thermal neutron flux at land/atmosphere interface that would be observed in ss if interface was not present	Φ^*_{th}	n cm^{-2} yr^{-1}	1.10E+05																													
ratio of muon production rate to thermal neutron production rate	R'_u	-	0.0600																													
portion of difference between phi_star_eth,ss and actual flux due to epithermal flux profile	$(Im\Delta\phi)^*_{eth}$	-	8394.1																													
	$R_{th,a}$	-	1																													
macroscopic thermal neutron cross section of atm (Phillips and Plumber, 1996)	$\Sigma_{th,a}$	cm^2 g^{-1}	0.0602																													
thermal neutron flux at land/atmosphere interface that would be observed in atm if interface was not present	$\Phi^*_{th,a}$	n cm^{-2} yr^{-1}	5827																													
difference in equilibrium thermal neutron fluxes between atmosphere and ss	$\Delta\Phi^*_{th,a}$	n cm^{-2} yr^{-1}	1.04E+05																													
difference in equilibrium epithermal neutron fluxes between atm and ss	$\Delta\Phi^*_{eth,a}$	n cm^{-2} yr^{-1}	16065.4																													
parameter governing epithermal neutron flux near the land/atm interface	$(F\Delta\phi)^*_{eth,a}$	-	8148.8668																													
portion of difference between phi_star_eth,a and actual flux due to epithermal flux profile	$(Im\Delta\phi)^*_{eth,a}$		89310.4270																													
difference between (Im\phi)_star,eth,ss and (Im\phi)_star,eth,a	$\Delta(Im\Delta\phi)^*_{eth}$		8.09E+04																													
thermal neutron diffusion length in atm	$L_{th,a}$	g cm^{-2}	3.9208																													
difference between hypothetical equilibrium thermal neutron fluxes in atmosphere and ss	$\Delta\Phi^*_{th}$	n cm^{-2} yr^{-1}	-1.04E+05																													
thermal neutron diffusion length in ss	L_{th}	g cm^{-2}	23.0365																													
portion of difference betweeen phi_star_th,ss and actual flux due to thermal flux profile	$(Im\Delta\phi)^*_{th}$		-82211.6652																													
thermal neutron flux (concentration)	$\Phi_{th,total}$	n cm^{-2} yr^{-1}	3.56E+04																													
result unscaled sample specific ^{36}Cl production rate by capture of thermal neutrons	$\mathbf{P_{th}}$	**atoms ^{36}Cl g^{-1} yr^{-1}**	**0.8299**	0.0830																												

8- Unscaled sample specific ^{36}Cl production rate by capture of slow negative muons																																
		element			Ca	K	Ti	Fe	Cl	O	Si	Na	Mg	Al	Mn	P	H	O, water	Li	B	Sm	Gd	Th	U	Be	Sc	Co	Rb	Sr	Zr	Ba		
					40Ca	39K																												
atomic number	Z				20	19	22	26	17	8	14	11	12	13	25	15	1	8	3	5	62	64	90	92	4	21	27	37	38	40	56	
molar concentration **(bulk)**	$M_{k,bulk}$	mol g^{-1}			0.0011	2.23E-05	0.0001	0.0010	1.15E-06	0.0284	0.0094	0.0013	0.0008	0.0033	2.10E-05	2.82E-05	0.0014	0.0007	7.20E-07	1.05E-06	3.11E-08	2.61E-08	1.92E-08	5.80E-09	1.11E-07	4.89E-07	2.71E-07	3.51E-07	5.80E-06	1.64E-06	2.69E-06		
total cross-section for stopping negative muons**(bulk)**	$M_i Z_i$	mol e- g^{-1}	0.4859		0.0221	0.0004	0.0022	0.0268	1.96E-05	0.2270	0.1315	0.0145	0.0097	0.0434	0.0005	0.0004	0.0014	0.0055	2.16E-06	5.27E-06	1.93E-06	1.67E-06	1.73E-06	5.33E-07	4.44E-07	1.03E-05	7.33E-06	1.30E-05	0.0002	6.58E-05	0.0002		
fraction of stopped neg muons that are captured by element k**(bulk)**	$f_{cl,bulk}$				0.0454	0.0009		0.0551		0.4672	0.2707	0.0299	0.0199	0.0893																				
molar concentration**target fraction**	$M_{k,target}$				0.0005	0.0005																										
elemental cross section for stopping negative muons (?)**target fraction**	$M_k Z_k$				0.0103	0.0095																										
fraction of stopped neg muons that are captured by element k**target fraction**	$f_{cl,target}$				0.0213	0.0195																										
abundance of the isotope of element k that produces nuclide m subsequent to slow muon capture (Fabryka-Martin, 1988)	f_{ik}				0.969	0.933																										
fraction of slow muon captures by element k that produce nuclide m (Heisinger*et al.*, 2002)	f_{ck}				0.045	0.035																										
^{36}Cl production per stopped muon **target fraction**	$\sum Y_k$	atoms ^{36}Cl μ^{-1}	0.00133		0.0008	0.0005																										
slow negative muon stopping rate at land surface SLHL (Heisinger*et al.*, 2002)	$\Psi_s(0)$	μ g^{-1} yr^{-1}	190																													
result unscaled sample specific ^{36}Cl production rate by capture of slow negative muons	$\mathbf{P_\mu}$	**atoms ^{36}Cl g^{-1} yr^{-1}**	**0.2526**	0.0632																												

9- Unscaled sample specific ^{36}Cl production rate by spallation of target elements				
spallation production rate for Ca, SLHL: 66.8 ± 6.8 (Phillips*et al.*, 2001)	PR_{Ca}	atoms ^{36}Cl (g Ca)$^{-1}$ yr^{-1}	66.8	
spallation production rate for Ca, SLHL: 48.8 ± 3.4 (Stone*et al.*., 1996)	PR_{Ca}	atoms ^{36}Cl (g Ca)$^{-1}$ yr^{-1}	48.8	3.4
mass concentration of Ca**target fraction**	C_{Ca}	g Ca (g rock)$^{-1}$	0.0207	0.0045
result unscaled ^{36}Cl production by spallation of ^{40}Ca	$\mathbf{P_{sCa}}$	atoms ^{36}Cl (g Ca)$^{-1}$ yr^{-1}	**1.0116**	0.2292
spallation production rate for K, SLHL: 137 ± 9 (Phillips*et al.*, 2001)	PR_K	atoms ^{36}Cl (g K)$^{-1}$ yr^{-1}	137	
spallation production rate for K, SLHL: 162 ± 24 (Evans*et al.*., 1997)	PR_K	atoms ^{36}Cl (g K)$^{-1}$ yr^{-1}	162	25
mass concentration of K**target fraction**	C_K	g K (g rock)$^{-1}$	0.0195	0.0003
result unscaled ^{36}Cl production by spallation of ^{39}K	$\mathbf{P_{s,K}}$	atoms ^{36}Cl (g K)$^{-1}$ yr^{-1}	**3.1523**	0.4887
spallation production rate for Ti, SLHL: 13 ± 3 (Fink*et al.*., 2000)	PR_{Ti}	atoms ^{36}Cl (g Ti)$^{-1}$ yr^{-1}	13	3
mass concentration of Ti**target fraction**	C_{Ti}	g Ti (g rock)$^{-1}$	0.0028	0.0001
result unscaled ^{36}Cl production by spallation of Ti	$\mathbf{P_{sTi}}$	atoms ^{36}Cl (g Ti)$^{-1}$ yr^{-1}	**0.0364**	0.0084
spallation production rate for Fe, SLHL: 1.9 (Stone, 2005)	PR_{Fe}	atoms ^{36}Cl (g Fe)$^{-1}$ yr^{-1}	1.9	0.2
mass concentration of Fe**target fraction**	C_{Fe}	g Fe (g rock)$^{-1}$	0.0003	0.0006
result unscaled ^{36}Cl production by spallation of Fe	$\mathbf{P_{s,Fe}}$	atoms ^{36}Cl (g Fe)$^{-1}$ yr^{-1}	**0.0005**	0.0011
result unscaled sample specific ^{36}Cl production rate by spallation of target elements	$\mathbf{P_s}$	atoms ^{36}Cl (g)$^{-1}$ yr^{-1}	**4.2007**	0.4888

10- Radiogenic sample specific ^{36}Cl production rate																																
Mass stopping power of element k at 8.0 MeV (Fabryka-Martin, 1988)	S_k	MeV g^{-1} cm^{-2}			4.28E-04	4.14E-04	3.75E-04	3.51E-04		5.27E-04	4.54E-04	4.56E-04	4.61E-04	4.44E-04		4.33E-04			5.48E-04	5.27E-04												5.29E-04		
neutron yields or element k per ppm U (Fabryka-Martin, 1988)	Y_n^U	n (a g ppmU)$^{-1}$			0	0.45	0	0.19		0.23	0.69	14.5	5.8	5.1		0			21.1	62.3												265		
neutron yields or element k per ppm Th (Fabryka-Martin, 1988)	Y_n^{Th}	n (a g ppmTh)$^{-1}$			0	0.305	0	0.205		0.079	0.335	6.8	2.6	2.6		0			9.6	19.2												91.2		
weight factor	$S_k F_k$		4.64E+02		1.89E+01	3.61E-01	1.81E+00	2.02E+01	0.00E+00	2.39E+02	1.20E+02	1.38E+01	9.03E+00	4.00E+01	0.00E+00	3.78E-01		0.00E+00	2.74E-03	6.01E-03	0.00E+00	0.00E+00										5.29E-04		
	$S_k F_k Y_n^U$	n/(yr*g*ppmU)	5.99E+02		0.00E+00	1.63E-01	0.00E+00	3.83E+00	0.00E+00	5.50E+01	8.27E+01	2.01E+02	5.24E+01	2.04E+02	0.00E+00	0.00E+00		0.00E+00	5.78E-02	3.74E-01	0.00E+00	0.00E+00										1.40E-01		
	$S_k F_k Y_n^{Th}$	n/(yr*g*ppmTh)	2.85E+02		0.00E+00	1.10E-01	0.00E+00	4.14E+00	0.00E+00	1.89E+01	4.01E+01	9.41E+01	2.35E+01	1.04E+02	0.00E+00	0.00E+00		0.00E+00	2.63E-02	1.153E-01	0.00E+00	0.00E+00										4.82E-02		
neutron yield per ppm U	X	n/(g*yr*ppmU)	1.293																													
neutron yield per ppm Th	Y	n/(g*yr*ppmTh)	0.615																													
neutron production by spontaneous fission (Fabryka-Martin, 1988)	$P_{n,sf}$	n^g-1*yr-1	0.5920																													
neutron production by alpha,n-reactions	$P_{n,\alpha}$	n^g-1*yr-1	4.5195																													
total radiogenic epithermal neutron production	$P_{eth,r}$	epithermal n/(g*yr)	0.7021																													
total radiogenic thermal neutron production	$P_{th,r}$	thermal n/(g*yr)	4.4095																													

result radiogenic sample specific ^{36}Cl production rate	P_r	atoms ^{36}Cl g^{-1} yr^{-1}	**0.0189**	0.0009

11- Thickness integration factors				
effective attenuation length for cosmic-ray flux through a surface of arbitrary orientation and shielding (Gosse and Phillips, 2001)	$\lambda_{e,e}$	g cm^{-2}	160	
ratio of production rate integrated over the thickness of a sample to the surface production rate, due to spallation	Q_s	-	0.9546	0.0191
ratio of production rate integrated over the thickness of a sample to the surface production rate, due to thermal neutron absorption	Q_{th}	-	1.4112	0.0282
ratio of production rate integrated over the thickness of a sample to the surface production rate, due to epithermal neutron absorption	Q_{eth}	-	1.132	0.0226
ratio of production rate integrated over the thickness of a sample to the surface production rate, due to muon absorption	Q_μ	-	0.995	0.0199

Notes
Spreadsheet from Schimmelpfennig *et al.*, 2009
Values input by user into black framed cells

Appendix 4.4 Chlorine-36 exposure age determination

Sample NH8

1- Input	Symbol	Units	Calculations	Uncertainties	Ca	K	Ti	Fe	Cl	O, rock	Si	Na	Mg	Al	Mn	P	H	O, water	Li	B	Sm	Gd	Th	U	Be	Co	Rb	Sr	Zr	Cs	Ba
element concentration in bulk rock		ppm			19800	29553	2218	25522	50	470852	314383	26932	6462	81063	503.3	480.3	1489	11911	6	14.3	4.7	3.7	10.6	3.34	1	7	71	339	197	0.7	585
element concentration in dissolved sample (target fraction)		ppm			6361.66	35513.76	1538.35	353.70	50																						
uncertainty element concentration (target fraction		ppm			4470	290	73	388	1																						
atomic mass of element k	A_k	g*mol-1			40.08	39.10	47.90	55.85	35.45	16.00	28.09	22.99	24.31	26.98	54.94	30.97	1.01	16.00	6.94	10.81	150.40	157.25	232.00	238.03	9.01	58.93	85.47	87.62	91.22	132.91	137.33
depth reference (surface or point under surface)		cm	0																												
sample thickness		cm	6																												
bulk rock density	rho	g cm^{-3}	2.5																												
mass depth reference	z	g cm^{-2}	0																												
mass thickness	z_x	g cm^{-2}	15																												
scaling factor for nucleonic production as a function of elevation, latitude (and geomagnetic variations)	$S_{e,s}$	-	1.4307	0.0715																											
scaling factor for muonic production as a function of elevation, latitude (and geomagnetic variations)	$S_{e,\mu}$	-	1.1869	0.0593																											
correction factor for shielding of a sample of arbitrary orientation by surrounding topography	S_T	-	0.992	0.0099																											
correction factor for geometry effects on spallogenic production	S_{shape}	-	1	0.03																											
correction factor for snow shielding for spallogenic production	S_{snow}	-	1	0.01																											
exposure duration (independently determined or estimated)	t_{expo}	yr	10000	3000																											
formation age of rock (independently determined or estimated) for radiogenic correction	t_{form}	yr	4.80E+07	3000000																											
erosion rate	ε	mm ka^{-1}	0	0.00E+00																											
total measured number of ^{36}Cl atoms in sample	N_{meas}	atoms ^{36}Cl g^{-1}	1.08E+05	9.26E+03																											

2- Output A: age of sample				
decay constant for ^{36}Cl	λ_{36}	yr^{-1}	2.30E-06	1.51998E-08
scaled total sample specific ^{36}Cl production rate without radiogenic	P_{total}	atoms ^{36}Cl g^{-1} yr^{-1}	10.9580	1.4
time factor radiogenic	t_r		434216	2865.8
number of radiogenically produced ^{36}Cl atoms for estimated age	N_r	atoms ^{36}Cl g^{-1}	22536.6680	1136.6
total measured number of ^{36}Cl atoms in sample without calculated radiogenic	N_{m-r}	atoms ^{36}Cl g^{-1}	8.52E+04	9334.3
age of sample	**t**	**yr**	**7849**	**1337.2**

3- Output B: calculated ^{36}Cl contributions from each production mechanism				
time factor cosmogenic without erosion	t_{cosm}		9886	2931.6996
total calculated number of ^{36}Cl atoms for given time + radiogenic	$N_{calc,total}$	atoms ^{36}Cl g^{-1}	**1.31E+05**	35030
difference measured/calculated number of ^{36}Cl atoms in sample			**-21.42%**	
contribution from each production mechanism:				
number of atoms ^{36}Cl per g by spallation of Ca	$N_{s,Ca}$	atoms ^{36}Cl g^{-1}	4157.7825	**3.18%**
number of atoms ^{36}Cl per g by spallation of K	$N_{s,K}$	atoms ^{36}Cl g^{-1}	77051.6723	**58.88%**
number of atoms ^{36}Cl per g by spallation of Ti	$N_{s,Ti}$	atoms ^{36}Cl g^{-1}	267.8353	**0.20%**
number of atoms ^{36}Cl per g by spallation of Fe	$N_{s,Fe}$	atoms ^{36}Cl g^{-1}	9.0005	**0.01%**
number of atoms ^{36}Cl per g by spallation of target elements	N_s	atoms ^{36}Cl g^{-1}	81486.2905	**62.27%**
number of atoms ^{36}Cl per g by capture of thermal neutrons	N_{th}	atoms ^{36}Cl g^{-1}	20626.9055	**15.76%**
number of atoms ^{36}Cl per g by capture of epithermal neutrons	N_{eth}	atoms ^{36}Cl g^{-1}	3592.5625	**2.75%**
number of atoms ^{36}Cl per g by capture of thermal and epithermal neutrons	N_n	atoms ^{36}Cl g^{-1}	24219.4679	**18.51%**
number of atoms ^{36}Cl per g by capture of slow negative muons	N_μ	atoms ^{36}Cl g^{-1}	2622.4832	**2.00%**
number of atoms ^{36}Cl per g by radiogenic production	N_r	atoms ^{36}Cl g^{-1}	22536.6680	**17.22%**
				100%

4- Output C: calculated number of ^{36}Cl atoms and age of eroded sample				
total calculated number of ^{36}Cl atoms for approached estimated time in eroded sample	$N_{calc,total}$	atoms ^{36}Cl g^{-1}	**1.31E+05**	
difference measured/calculated number of ^{36}Cl atoms in eroded sample	$\Delta N_{meas-calc}$		**-21.42%**	
time factor with erosion for spallation reaction	$t_{cosm,s}$		9886	2931.699499
time factor with erosion for capture of epithermal neutrons	$t_{cosm,eth}$		9886	2931.699499
time factor with erosion for capture of thermal neutrons	$t_{cosm,th}$		9886	2931.699499
time factor with erosion for capture of slow negative muons	$t_{cosm,\mu}$		9886	2931.699499
depth reference factor for spallogenic reaction	d_s		1.000	
depth reference factor for capture of epithermal neutrons	d_{eth}		1.000	
depth reference factor for capture of thermal neutrons	d_{th}		1.000	
depth reference factor for capture of slow negative muons	d_μ		1.000	
production rate coefficient corrected for sample thickness for spallogenic reaction	$J_{O,s}$		10.73	
production rate coefficient corrected for sample thickness for capture of epithermal neutrons	$J_{O,eth}$		0.21	
production rate coefficient corrected for sample thickness for capture of thermal neutrons	$J_{O,th}$		-3.71	
production rate coefficient corrected for sample thickness for capture of slow negative muons	$J_{O,\mu}$		0.49	
production rate coefficient for spallogenic reaction	J_s		9.62	
production rate coefficient for capture of epithermal neutrons	J_{eth}		0.1305	
production rate coefficient for capture of thermal neutrons	J_{th}		-2.62	
production rate coefficient for capture of slow negative muons	J_μ		0.41	

5- Elemental parameters																															
avogadro			6.02E+23																												
atomic concentration of element k in **bulk rock**	N_k	atoms g^{-1}	2.96E+22		2.97E+20	4.55E+20	2.79E+19	2.75E+20	8.49E+17	1.77E+22	6.74E+21	7.05E+20	1.60E+20	1.81E+21	5.52E+18	9.34E+18	8.90E+20	4.48E+20	5.21E+17	7.97E+17	1.88E+16	1.41E+16	2.75E+16	8.45E+15	6.68E+16	7.15E+16	5.00E+17	2.33E+18	1.30E+18	3.17E+15	2.56E+18
atomic concentration of element k in **target fraction**	N_{Cl}	atoms g^{-1}							8.49E+17																						
dilute resonance integral for absorption of epithermal neutrons by element k (Fabryka-Martin, 1988)	$I_{o,k}$	E^{-24} cm^2			0.235	1	3.1	1.39	13.7	0.0004	0.127	0.311	0.038	0.17	14		0	0	1722	1400	390										
average log decrement of energy loss per collision for element k (Fabryka-Martin, 1988)	x_k	-			0.049	0.05	0.041	0.035	0.055	0.12	0.07	0.084	0.08	0.072	0.036		1	0.264	0.174	0.013	0.013										
neutron scattering cross ection of element k (Fabryka-Martin, 1988)	$\sigma_{sc,k}$	E^{-24} cm^2			2.93	2.04	4.09	11.35	15.8	3.76	2.04	3.025	3.42	1.41	2.2	5	20.5	0.95	4.27	38	172										
thermal neutron absorption cross section of element k (Fabryka-Martin, 1988)	$\sigma_{a,k}$	E^{-24} cm^2			0.43	2.15	6.1	2.56	33.5	0.0002	0.17	0.53	0.063	0.23	13.3	0.2	0.33	70.5	767	9640	41560										
proportion of muons stopped in element i that are captured by the nucleus (Fabryka-Martin, 1988)	$f_{\mu,k}$				0.864	0.83		0.906		0.223	0.671	0.432	0.538	0.582																	
average neutron yield per captured muon (Fabryka-Martin, 1988)	Y_n				0.75	1.25		1.125		0.8	0.86	1	0.6	1.26																	

6- Unscaled sample specific ^{36}Cl production rate by capture of epithermal neutrons																															
effective macroscopic resonance integral for absorption of epithermal neutrons	I_{eff}	cm^2 g^{-1}	0.0039		6.99E-05	4.55E-04	8.64E-05	3.83E-04	1.16E-05	7.09E-06	8.56E-04	2.19E-04	6.07E-06	3.08E-04	7.72E-05		0.00E+00	0.00E+00	1.37E-03	2.63E-05	5.50E-06										
fraction of epithermal neutrons absorbed by ^{35}Cl **(target fraction)**	f_{eth}	-	0.0030																												
neutron macroscopic scattering cross section in ss	Σ_{sc}	cm^2 g^{-1}	0.109		8.72E-04	9.29E-04	1.14E-04	3.12E-03	1.34E-05	6.66E-02	1.38E-02	2.13E-03	5.47E-04	2.55E-03	1.21E-05	4.67E-05	1.82E-02	0.00E+00	4.95E-07	3.40E-06	7.15E-07	2.42E-06	0.00E+00	0.00E+00	0.00E+00	0.00E+00	0.00E+00	0.00E+00	0.00E+00	0.00E+00	0.00E+00	0.00E+00
scattering rate parameter	B		2.78E-02		4.27E-05	4.64E-05	4.68E-06	1.09E-04	7.38E-07	8.00E-03	9.63E-04	1.79E-04	4.37E-05	1.84E-04	4.37E-07	0.00E+00	1.82E-02	0.00E+00	1.31E-07	5.92E-07	9.30E-09	3.15E-08	0.00E+00	0.00E+00	0.00E+00	0.00E+00	0.00E+00	0.00E+00	0.00E+00	0.00E+00	0.00E+00	0.00E+00
mean macroscopic log decrement of energy loss per collision in ss	X_{ss}		0.255																												
macroscopic absorption and moderation cross section for epithermal neutrons	Σ_{eth}	cm^2 g^{-1}	0.029																												
attenuation length for absorption and moderation of epithermal neutron flux	Λ_{eth}	g cm^{-2}	34.723																												
	$A_k * N_k$	atoms mol^{-1}	5.89E+23		1.19E+22	1.78E+22	1.34E+21	1.54E+22	3.01E+19	2.84E+23	1.89E+23	1.62E+22	3.89E+21	4.88E+22	3.03E+20		8.97E+20		3.61E+18	8.61E+18	2.83E+18	2.22E+18										
average atomic weight in subsurface	A_w	g mol^{-1}	19.944																												
production rate of epithermal neutrons from fast neutrons in atm at land/atm interface (Gosse and Phillips, 2001)	$P_f(0)$	n cm^{-2} yr^{-1}	626	46																											

| | | |

11- Thickness integration factors				
effective attenuation length for cosmic-ray flux through a surface of arbitrary orientation and shielding (Gosse and Phillips, 2001)	$\lambda_{e,e}$	g cm^{-2}	160	
ratio of production rate integrated over the thickness of a sample to the surface production rate, due to spallation	Q_s	-	0.9546	0.0191
ratio of production rate integrated over the thickness of a sample to the surface production rate, due to thermal neutron absorption	Q_{th}	-	1.4172	0.0283
ratio of production rate integrated over the thickness of a sample to the surface production rate, due to epithermal neutron absorption	Q_{eth}	-	1.120	0.0224
ratio of production rate integrated over the thickness of a sample to the surface production rate, due to muon absorption	Q_μ	-	0.995	0.0199

Notes
Spreadsheet from Schimmelpfennig *et al*., 2009
Values input by user into black framed cells